UNIVERSITÉ DE REIMS CHAMPAGNE-ARDENNE

ÉCOLE DOCTORALE SCIENCES DU NUMERIQUE ET DE L'INGENIEUR n°620

THÈSE

Pour obtenir le grade de

DOCTEUR DE L'UNIVERSITÉ DE REIMS CHAMPAGNE-ARDENNE

Discipline : ***GENIE DES PROCEDES***

Spécialité : Thermique et Énergétique

Présentée et soutenue publiquement par

MIRA ABOU RJEILY

Le 13 décembre 2022

Production de gaz de synthèse par pyrolyse de biomasse et reformage catalytique de volatils

---

Thèse dirigée par **JAONA RANDRIANALISOA** et co-dirigée par **Cédric GENNEQUIN**

JURY

M. Samer AOUAD,	Professeur,	University of Balamand, Liban,	**Président**
M. Jaona RANDRIANALISOA,	Maître de Conférences HDR,	URCA, ITheMM EA 7548,	**Directeur de thèse**
M. Cédric GENNEQUIN,	Professeur,	ULCO, UCEIV EA 4492,	**Co-Directeur de thèse**
M. Hervé PRON,	Professeur,	URCA, ITheMM EA 7548,	**Encadrant**
M. Bechara TAOUK,	Professeur,	INSA Rouen, LSPC, EA 4704,	**Rapporteur**
M. Anthony DUFOUR,	Directeur de recherche,	CNRS, LRGP, UMR 7274,	**Rapporteur**
Mme Gaëlle DUCOM,	Maîtresse de conférences,	INSA Lyon, DEEP EA 7429	**Examinatrice**
Mme Sylvie VALIN,	Chargée de recherche,	CEA Grenoble LITEN/DTCH/LRP,	**Examinatrice**

Remerciements

Tout d'abord, je voudrais remercier les membres du jury pour leur jugement professionnel. Merci beaucoup au président du jury monsieur Samer Aouad. Je remercie messieurs Bechara Taouk et Anthony Dufour d'avoir accepté d'être rapporteurs et de relire mon manuscrit de thèse. Je vous remercie pour vos retours positifs et remarques constructives. Je remercie également mesdames Gaëlle Ducom et Sylvie Valin d'avoir accepté d'être examinateurs. J'étends mes remerciements aux membres de mon comité de suivi de thèse, madame Gaëlle Ducom et monsieur Arnaud Haudrechy d'avoir évalué mon travail, de m'avoir prodigué des conseils et de m'avoir encouragée pour la poursuite de ma thèse. Je voudrais remercier le Grand Reims et l'Université de Reims Champagne-Ardenne pour le financement de ma thèse à travers l'allocation doctorale. Je remercie également la SFR Condorcet pour son financement de l'appel à projet RefCatPy 2021.

Je tiens à exprimer ma plus profonde reconnaissance à M. Jaona Randrianalisoa, mon directeur de thèse, Maitre de conférences HDR. Durant les années de doctorat vous m'avez guidé, accompagné et aidé à grandir au niveau personnel et professionnel. Je vous remercie pour votre disponibilité, votre suivi quotidien, votre réactivité, vos conseils et vos suggestions. Vous avez partagé vos connaissances et expertises pour la réussite de cette thèse. Je suis profondément reconnaissante pour vos critiques constructives qui m'ont encouragée à persévérer et améliorer mon travail et surtout pour les compliments, bien que rares, mais extrêmement précieux, venant de vous. Merci « Monsieur » d'être un exemple de professionnalisme, d'intégrité et curiosité scientifique, de rigueur et de persévérance. Je remercie énormément mon co-directeur de thèse, Professeur Cédric Gennequin, pour son accompagnement, même à distance, et pour son encouragement continu. Merci pour les précieux échanges et les mots de motivation. Je remercie également monsieur Hervé Pron, pour son encadrement de la thèse et de m'avoir confié, avec monsieur Jaona Randrianalisoa, des missions d'enseignement à l'ESI Reims.

Je remercie M. Edmond Abi Aad d'avoir facilité les collaborations entre les laboratoires de l'UCEIV et l'ITheMM. Mes remerciements vont aussi à M. François Delattre pour nous avoir procurer des échantillons d'anas de lin pour mes expériences. J'adresse également un grand merci à M. Fabrice Cazier ainsi que Madame Lucette Tidahy pour toutes les analyses effectuées sur les échantillons de charbons et de bio-huiles et sur les catalyseurs. J'adresse un remerciement immense à Dr. Muriel Chaghouri « Mumu, hey man ! », mon amie à l'UCEIV, qui a préparé les catalyseurs en poudre et en billes et les a caractérisés, mais qui a aussi enduré nos appels téléphoniques, parfois longs, pour discuter des résultats. Un grand merci à toi et à tous tes collègues à l'UCEIV de m'avoir bien reçue pendant mon séjour à Dunkerque.

Je remercie M. Thierry Duvaut, directeur du laboratoire ITheMM (Institut du Thermique, Mécanique, Matériaux) où les travaux de cette thèse ont été réalisé. Je vous remercie « Monsieur le Directeur » de m'avoir accueilli dans votre équipe, pour votre bienveillance, encouragement et présence quand on a besoin. Un remerciement spécial est dédié à M. Jean-François Henry pour sa gentillesse, ses bons conseils et ses mots réconfortants en moment de détresse. Je vous remercie « Chef » pour votre encouragement, votre humour et votre présence qui me rendait le courage et le sourire. Merci de m'avoir accordé de votre temps et effort afin de m'accompagner pour faire des analyses cruciales à un moment critique de ma thèse.

Je tiens à remercier notre technicien, maintenant retraité, M. Didier Caron, qui a monté la première version du montage expérimentale. Merci d'avoir établi la base fondamentale du dispositif expérimental sans laquelle je n'aurais pas pu commencer les expériences. J'adresse également un grand merci à notre informaticien Jonathan Lorentz qui n'a pas seulement sauvé mon travail informatique plusieurs fois mais qui a aussi accepté volontairement de travailler pour faire plusieurs modifications sur le montage expérimental. Il a fait appel à ses connaissances et ses passions pour effectuer un travail en dehors de ses responsabilités. Merci Jonathan d'être plus qu'un collègue mais aussi un ami qui m'a écouté et soutenu pendant les longues heures de manipulations et qui m'a aidé pendant les moments difficiles surtout face aux logiciels du microGC/MS. Un merci tout particulier à Valérie Mencier pour les petites discussions intéressantes. Je remercie les secrétaires Nathalie Humbert et surtout Naïma Baabouche pour leur aide administratif. Grand merci à M. Rabih Maamary pour son assistance technique et la gestion des commandes.

Un remerciement du fond du cœur est dédié à « Ing. Dr. Alexandre Briclot » avec qui j'ai eu l'honneur et le privilège de partager le bureau pendant trois années. Je te remercie pour tout ce que tu as fait pour moi, pour ton encouragement en moments de détresse et tes félicitations en moments de succès. Tu as partagé tes connaissances et tu m'as aidé à plusieurs reprises dans tous les domaines : scientifiques, administratifs et personnels. Merci beaucoup pour ta générosité, pour le covoiturage et en particulier pour ta patience (surtout les matins…). Merci pour les plus beaux moments de ma thèse, les rires et les petites taquineries qui ont rayonné sur mes journées et m'ont motivé constamment. Ma thèse n'aurait pas été pareil sans toi et c'était un vrai plaisir d'être ta collègue et ton amie. Merci « infiniment » Dr. Alexandre. À tous les « je serai en retard de 5 min » les matins. À tous les « je tarde à partir ce soir, je n'ai pas fini ma manip ». À tous les « le code Matlab bugue ». Je te dis 73 mercis et 286 choukran...

Je remercie tout spécialement mes chères amies Nathalie Chaaraoui « Nathy », ma compatriote et comme ma sœur, Céline Badouard, « Céliiine » la camarade du chemin depuis le début, ainsi que Quentin Pompidou, mon second collègue de bureau et ami. Merci beaucoup pour vos amitiés, aides, encouragements, pour toutes les belles discussions et les pauses agréables qui ont rendus les longues heures de travails plus tolérables. Je remercie également tous nos collègues Ghiwa, Pierre, Rim, Georges, Jesse, Maud, Maher, Raza, Adèle et Anthony ainsi que tous les membres de l'équipe thermique, pour la bonne ambiance et les moments conviviaux qu'on a partagés. Une petite réflexion et remerciement à mes amis, éparpillés entre le Liban et la France, en particulier Elyse et toute sa famille, Nour, Liza, Moe, Carla et Ahmad, qui m'ont bien encouragée.

J'exprime ma grande gratitude envers ma chère famille, ma mère Thérèse « Mamitii », ma sœur Leyla « Layouliii » et mon oncle Michel Sawaya « Khalo Micho » et sa famille pour leur amour et attention, pour leur support et encouragement au quotidien. Sans eux, je n'aurai pas pu arriver à ce stade de ma vie et je ne serai pas la personne qui je suis. Je vous remercie pour tout. Je m'excuse d'être absente ces dernières années et de ne pas pouvoir être à vos côtés pendant les moments difficiles. Je dédie ce travail à ma mère, qui a tout sacrifié au fil des années et n'a lésiné aucun effort pour subvenir à tous nos besoins, et pour me soutenir tout au long de mes études. J'espère qu'elle serait toujours fière de moi et que mon père, du ciel, le sois aussi.

Résumé

La demande massive en énergie et l'épuisement des combustibles fossiles nécessitent la production d'énergie « verte » pour répondre aux besoins globaux en électricité et en carburants. La biomasse, source d'énergie durable et renouvelable, est l'une des plus prometteuses pour atteindre ces objectifs. La pyrolyse de la biomasse produit majoritairement du monoxyde de carbone CO et du dioxyde de carbone CO_2 mais également du méthane CH_4 et de l'hydrogène H_2. Ce dernier est identifié comme vecteur énergétique de l'avenir pour le transport et la génération d'électricité. Il est donc nécessaire d'augmenter sa production. Traditionnellement, cela est réalisé à travers le reformage de gaz naturels.

Cette thèse vise à valoriser la biomasse en gaz de synthèse, et en hydrogène en particulier, tout en réduisant les émissions de CO_2. Un dispositif expérimental couplant la pyrolyse et le reformage catalytique a été développé. Dans le premier étage, la pyrolyse de biomasse (copeaux de chêne ou anas de lin) est réalisée. Dans le second, le reformage catalytique des hydrocarbures volatils et des gaz issus de la pyrolyse a lieu en présence d'un catalyseur**.** Les effets de divers paramètres ont été étudiés sur les produits de la pyrolyse (température, vitesse de chauffe et temps de séjour des composés volatils) et du reformage (température, phase active du catalyseur, sa charge métallique, vitesse horaire spatiale du gaz et le gaz vecteur). Les conditions opératoires favorisant respectivement la production de gaz biosourcés, de gaz de synthèse et d'hydrogène tout en réduisant les émissions de CO_2 par le biais du procédé couplé de pyrolyse et de reformage catalytique ont été révélées.

Mots clés : Biomasse, Gaz de synthèse, Hydrogène, Pyrolyse, Reformage catalytique, Catalyseur, Énergie, Environnement, micro-Chromatographie en phase gazeuse/Spectrométrie de masse

Abstract

The massive energy demand and the depletion of fossil fuels require the production of "green" energy to meet the global needs for electricity and fuels. Biomass, a renewable and sustainable energy source, is among the most promising resources to meet these objectives. Biomass pyrolysis mainly produces carbon monoxide CO and carbon dioxide CO_2, but also some methane CH_4 and hydrogen H_2. The latter has been identified as the energy carrier of the future for transportation and power generation. Therefore, it is of great importance to increase its production. Traditionally, H_2 is produced by natural gas reforming.

This thesis aims at valorizing biomass into syngas, and hydrogen in particular, while reducing CO_2 emissions. A two-stage experimental setup coupling the pyrolysis and the catalytic reforming processes has been developed. In the first stage, the pyrolysis of biomass (oak wood chips or flax shives) is performed. In the second one, the catalytic reforming of hydrocarbon volatiles and gases derived from biomass pyrolysis takes place in the presence of a catalyst. The effects of several parameters were studied on the products of pyrolysis (temperature, heating rate and residence time of volatile compounds) and the products of reforming (temperature, active phase of the catalyst, its metal loading, gas hourly space velocity and the nature of the carrier gas). The operating conditions favoring respectively the production of bio sourced gases, syngas, and hydrogen while reducing the CO_2 emissions via the process coupling the pyrolysis and the catalytic reforming were identified.

Keys words: Biomass, Syngas, Hydrogen, Pyrolysis, Catalytic reforming, Catalyst, Energy, Environment, micro-Gas chromatography/Mass spectrometry.

Table des matières

Table des figures

Liste des tableaux

Liste des symboles

Acronyme

µGC/MS	Micro Gas Chromatography/Mass Spectrometry
AP	Acidification Potential
BET	Brunauer–Emmett–Teller
BJH	Barrett, Joyner and Halenda
BTEX	Benzene, Toluene, Ethylbenzene and Xylene
CCS	Carbon Capture and Storage
CEV	Controlled Evaporator Mixer
DSC	Differential Scanning Calorimetry
DTA	Differential Thermal Analysis
DTG	Derivative Thermogravimetric
EDX	Energy-dispersive X-ray spectroscopy
GC/MS	Gas Chromatography/Mass Spectrometry
GHG	Greenhouse Gases
GHSV	Gas Hourly Space Velocity
GWP	Global Warming Potential
IEA	International Energy Agency
IPCC	Intergovernmental Panel on Climate Change
JCPDS	Joint Committee on Powder Diffraction Standards
LCA	Life Cycle Assessment
LDH	Layered Double Hydroxides
MIR	Mid Infrared
MW	Molecular weight
NIR	Near Infrared Reflectance
NMR	Nuclear Magnetic Resonance
PAH	Polycyclic Aromatic Hydrocarbons
PID	Proportional, Integral and Derivative
PSA	Pressure Swing Adsorption
RPM	Rotation per minute

SEM	Scanning Electron Microscopy
TCD	Thermal Conductivity Detector
TG	Thermogravimetry
TGA	Thermogravimetric Analysis
TPH	Temperature Programmed Hydrogenation
TPR	Temperature Programmed Reduction
TSA	Temperature Swing Adsorption
WGSR	Water-Gas Shift Reaction
XRD	X-ray Diffraction

Alphabet latin

m	Mass	[g]
C	Mass concentration	[$g/g_{dry\ wood}$]
X	Conversion rate	[%]

Alphabet grec

$\Delta H°_{298K}$	Standard formation enthalpy at 298 K	[kJ/mol]

Introduction générale

La croissance de la population mondiale entraîne incontestablement une augmentation de la demande énergétique globale. A l'heure actuelle, cette dernière est satisfaite par la consommation de combustibles fossiles qui sont à ce jour les principales ressources énergétiques. Malheureusement, leur combustion entraîne l'émission de particules nocives et de gaz à effet de serre (dioxyde de carbone CO_2, méthane CH_4...) contribuant au réchauffement climatique et à la pollution atmosphérique. Face à cette crise, le besoin d'alternatives renouvelables et durables s'avère primordial. Il s'agit notamment de ressources qui sont respectueuses de l'environnement, abondantes dans la nature et qui entraînent de faibles émissions de carbone. Parmi ces ressources énergétiques, la biomasse se présente comme l'une des plus prometteuses et respectueuses de l'environnement parmi les sources d'énergie renouvelables et la seule capable de fournir une puissance énergétique durable similaire à celle des combustibles fossiles. La biomasse est abondamment disponible dans le monde entier, ce qui lui permet d'être exploitée dans plusieurs filières énergétiques. De plus, sa combustion entraîne l'émission de gaz moins polluants que les combustibles fossiles traditionnels. D'autre part, la valorisation efficace de la biomasse en énergie s'inscrit dans le plan mondial de la réduction des émissions de gaz à effet de serre et de la réduction de l'impact dévastateur du réchauffement climatique sur la planète. Le gaz de synthèse est un mélange gazeux composé principalement de dihydrogène H_2, communément référé comme simplement hydrogène, et de monoxyde de carbone CO. Il est capable de générer de l'énergie en plus d'être largement utilisé pour de nombreuses synthèses chimiques. Le H_2, en tant que vecteur énergétique, est considéré comme l'avenir du transport et de la production d'énergie.

Plusieurs procédés permettent de convertir la biomasse en gaz de synthèse, à savoir la pyrolyse, la combustion et la gazéification, ainsi que l'hydrocraquage. C'est est un procédé de craquage catalytique à basse température (300 – 450°C) pour convertir les déchets en combustibles liquides de haute qualité mais il nécessite l'introduction d'hydrogène à haute pression pour casser le lien carbone-carbone et puisque la production d'hydrogène est un de nos objectifs, ce procédé apparaît pour nous plutôt comme un débouché et ne sera pas discuté dans cette thèse. La pyrolyse a été adoptée pour convertir la biomasse et les déchets en gaz, charbon et huile biosourcés. Cependant, l'huile biosourcée ou bio-huile et le gaz produits ne peuvent pas être utilisés directement et nécessitent d'autres processus d'amélioration avant d'être consommés comme carburant. Les procédés de traitement actuels comprennent la gazéification, la purification, la séparation et la pyrolyse catalytique. En même temps, la formation de goudron pendant la pyrolyse de la biomasse reste un problème technologique majeur dans la conception des réacteurs. Le reformage catalytique, traditionnellement connu pour convertir les hydrocarbures légers en gaz de synthèse, s'est avéré être une méthode attrayante et efficace pour éliminer le goudron par son oxydation en gaz valorisables. Plus important, des études récentes ont démontré que le reformage catalytique des produits volatils de la pyrolyse constitue une approche très prometteuse pour la conversion des goudrons et des gaz de pyrolyse en gaz de synthèse.

Deux types de reformage catalytique sont généralement appliqués pour la production de gaz de synthèse : le reformage à sec et le reformage à la vapeur. Lors du reformage à la vapeur, les hydrocarbures réagissent avec la vapeur d'eau afin de produire du gaz de synthèse, tandis que le reformage à sec se produit en présence de CO_2. Par conséquent, le reformage à sec est une approche attrayante qui non seulement transforme les hydrocarbures goudronneux en gaz de synthèse, mais consomme également le CO_2. Dans les procédés de reformage catalytique, l'adoption d'un catalyseur efficace est cruciale. Une large gamme de catalyseurs peut être utilisée pour le reformage à la vapeur et à sec de la bio-huile dérivée de la décomposition de la biomasse, y compris des catalyseurs alcalino-terreux, minéraux naturels et métalliques. La plupart des catalyseurs utilisés pour la valorisation du goudron sont des catalyseurs sur support, c'est-à-dire que le catalyseur est déposé sur un matériau différent tel que la silice, l'alumine et le carbone. La performance catalytique est fortement affectée par le choix du support du catalyseur.

Jusqu'à présent, les communautés scientifiques et plus spécifiquement françaises ont étudié séparément la pyrolyse et le reformage catalytique séparément, alors qu'il apparaît clairement important de les étudier conjointement. L'objectif de cette thèse est donc de montrer que cette approche combinée constitue la base d'une technologie innovante pour la valorisation de la biomasse ainsi que la production de gaz de synthèse. Le travail est réalisé à l'échelle du laboratoire, où plusieurs conditions et paramètres opératoires ont été modifiés pour évaluer leur effet sur l'efficacité du procédé et les rendements des produits, avec une attention particulière accordée à la production de gaz biosourcés, de gaz de synthèse et d'hydrogène.

Dans cette optique, ce manuscrit est organisé en cinq chapitres. Le premier chapitre sera consacré à une étude de l'état de l'art basée sur trois axes principaux : la pyrolyse de la biomasse, le reformage catalytique, et leur combinaison. La pyrolyse est abordée en termes de sa classification, de types de réacteurs couramment utilisés et de modèles cinétiques décrivant le processus. Les effets de la température et de la vitesse de chauffe sur les rendements des produits de certaines espèces de bois provenant d'études trouvées dans la littérature sont évalués. Le reformage catalytique est ensuite détaillé en donnant les principales réactions impliquées dans le processus et une liste des différents catalyseurs utilisés. Les effets de paramètres clés tels que la température, le rapport vapeur/carbone et les charges métalliques sont étudiés sur la composition des produits résultant du reformage catalytique de différents composés modèles de goudron et du gaz combustible dans son ensemble. Ensuite, l'approche pyrolyse-reformage catalytique est brièvement discutée à l'aide de quelques études récemment réalisées. Cette longue étude bibliographique a été valorisée à travers un article de synthèse publié en mars 2021 portant sur la pyrolyse catalytique et la pyrolyse combinée au reformage catalytique [1], un chapitre d'ouvrage publié en mars 2022 discutant du reformage catalytique et des catalyseurs utilisés [2], ainsi qu'un autre article de synthèse portant sur la pyrolyse seule, en cours de finalisation. Le premier chapitre présente donc un résumé de ces trois publications.

Le deuxième chapitre se focalise sur la pyrolyse de la biomasse réalisée dans le cadre de cette thèse. Nous considérons les copeaux de bois de chêne comme un échantillon de biomasse pour la réalisation d'une pyrolyse de référence servant de validation du procédé et pour la comparaison avec les travaux de la littérature. Nous réalisons la pyrolyse dans un réacteur tubulaire à lit fixe en variant les trois principaux paramètres influençant les produits : la température, la vitesse de chauffe et le temps de séjour des composés volatils. La composition des trois principaux produits formés, le charbon, la bio-huile et les gaz, a été analysée en détail

en fonction de ces paramètres. Pour toutes les expériences réalisées au cours de ce travail de thèse, les gaz produits ont été analysés à l'aide d'un micro-chromatographe en phase gazeuse couplé à un spectromètre de masse, appareil étalonné pour déterminer les concentrations des gaz principaux produits. La composition élémentaire du charbon produit a également été déterminée et les composés de la bio-huile ont été identifiés et quantifiés pour certaines expériences. Les résultats ont été publiés dans un article scientifique [3].

Le troisième chapitre présente la combinaison de la pyrolyse de la biomasse et du reformage catalytique réalisés dans un procédé à deux étages. La pyrolyse du bois de chêne a été réalisée dans un premier réacteur, le même que celui utilisé pour la pyrolyse seule dans le second chapitre, tandis que le reformage catalytique des composés volatils de la pyrolyse a été réalisé dans un second réacteur, également à lit fixe, en présence de catalyseurs massiques à base de nickel, de cobalt et de cobalt-nickel. De plus, les différents catalyseurs utilisés ont été caractérisés avant et après le reformage pour étudier leur évolution et évaluer le dépôt de carbone. Un article présentant et discutant les résultats obtenus a été publié [4].

Le quatrième chapitre discute l'application du procédé avec une autre variante de biomasse, l'anas de lin, et des catalyseurs supportés par des billes d'alumine, afin d'améliorer la production de gaz de synthèse. Dans ce but, les effets du type de catalyseur, de la charge métallique, de la température de reformage et de la vitesse spatiale horaire du gaz ont été étudiés sur les rendements des produits. Les catalyseurs ont également été analysés avant et après le reformage pour les caractériser et investiguer la formation de carbone sur leur surface.

Le cinquième chapitre examine plusieurs voies pour cibler davantage la production d'hydrogène. Tout d'abord, une série d'expériences de reformage des composés volatils de pyrolyse à la vapeur avec les catalyseurs nickel/alumine a été réalisée. En outre, le gaz vecteur est remplacé, passant de l'azote à l'air puis à la vapeur d'eau, afin d'étudier son effet sur la production de gaz de synthèse au cours d'une pyrolyse à une étape et du processus à deux étapes de pyrolyse/reformage. D'autre part, une étude technique, environnementale et économique des différentes voies de production d'hydrogène (gazéification, pyrolyse, reformage, électrolyse, fermentation etc.) a été réalisée.

Enfin, ce manuscrit se termine par les conclusions générales qui pourraient être retenues de ce travail de thèse ainsi qu'aux perspectives et futurs objectifs à envisager et à réaliser.

References

[1] M. Abou Rjeily, C. Gennequin, H. Pron, E. Abi-Aad, J.H. Randrianalisoa, Pyrolysis-catalytic upgrading of bio-oil and pyrolysis-catalytic steam reforming of biogas: a review, Environ. Chem. Lett. (2021) 48. https://doi.org/10.1007/s10311-021-01190-2.

[2] M. Abou Rjeily, C. Gennequin, H. Pron, E. Abi-Aad, J.H. Randrianalisoa, Chapter 9 - Catalysts for steam reforming of biomass tar and their effects on the products, in: M.R. Cesario, D.A. de Macedo (Eds.), Heterog. Catal., Elsevier, 2022: pp. 249–295. https://doi.org/10.1016/B978-0-323-85612-6.00009-7.

[3] M. Abou Rjeily, F. Cazier, C. Gennequin, J.H. Randrianalisoa, Detailed Analysis of Gas, Char and Bio-oil Products of Oak Wood Pyrolysis at Different Operating Conditions, Waste Biomass Valorization. (2022). https://doi.org/10.1007/s12649-022-01848-0.

[4] M. Abou Rjeily, M. Chaghouri, C. Gennequin, E. Abi Aad, H. Pron, J.H. Randrianalisoa, Biomass Pyrolysis Followed by Catalytic Hybrid Reforming for Syngas Production, Waste Biomass Valorization. (2023) 29. https://doi.org/10.1007/s12649-022-02012-4.

Chapter 1: State-of-the-art

Résumé

L'axe principal de la thèse se base sur deux procédés thermochimiques, la pyrolyse et le reformage catalytique ainsi que sur leur couplage. Il est donc crucial de comprendre ces trois procédés, en les définissant et en étudiant leurs mécanismes et les paramètres qui les influencent. Ce chapitre d'étude bibliographique est donc divisé en trois grandes parties : la première est consacrée à la pyrolyse de la biomasse, la deuxième est dédiée au reformage catalytique et la dernière se focalise sur leur couplage. Chacune des parties comprendra les aspects théoriques des procédés, les réacteurs généralement employés, les paramètres principaux dont ils dépendent ainsi que des résultats expérimentaux de quelques travaux sur ces sujets publiés dans la littérature.

La pyrolyse a été adoptée pour convertir la biomasse et les déchets en gaz (généralement CH_4 et CO_2), charbon et huile biosourcés. Cependant, la bio-huile et le gaz produits ne peuvent pas être utilisés directement et nécessitent des traitements et des filtrages supplémentaires. Les procédés de traitement actuels comprennent la gazéification, la purification, la séparation et la pyrolyse catalytique. En appliquant ces procédés, les rendements en gaz de synthèse restent faibles car ils favorisent la production de bio-huile ou de gaz. L'une des difficultés rencontrées lors de la pyrolyse et de la gazéification de la biomasse est la formation de goudron, qui pose d'obstacles techniques, comme l'encrassement des tuyaux et l'endommagement des composants en aval. Le reformage catalytique, traditionnellement connu pour convertir les hydrocarbures légers en gaz de synthèse (H_2 et CO principalement), s'est avéré être une méthode intéressante pour l'élimination des goudrons en les oxydant. Il conviendrait donc d'appliquer le reformage catalytique pour éliminer les goudrons et convertir le gaz de pyrolyse en gaz de synthèse. Jusqu'à présent, les communautés scientifiques étudient la pyrolyse et le reformage catalytique séparément où il manquait des travaux scientifiques notamment des papiers de revues qui les examinent conjointement. L'objectif de ce chapitre est donc de montrer que cette approche combinée constitue la base d'une technologie innovante pour la valorisation de la biomasse et la production de gaz de synthèse.

Dans la première section, la biomasse est définie en premier lieu en listant ses caractéristiques et sa composition élémentaire et chimique comprenant principalement la cellulose, l'hémicellulose et la linine. La composition typique du goudron dérivant de la pyrolyse de biomasse est détaillée ainsi que sa classification. La pyrolyse est abordée sous l'angle des paramètres qui l'impactent, de sa classification, et des types de réacteurs couramment utilisés pour ce processus. La température, la vitesse de chauffe et le temps de séjour des composés volatils sont les paramètres majeurs qui influencent le déroulement de la pyrolyse et impactent

la répartition des produits. La pyrolyse peut être classifiée comme lente, intermédiaire, rapide et flash, imposée en générale par la vitesse de chauffe de la biomasse ainsi que la température d'opération. Les réacteurs de pyrolyse les plus utilisés sont les réacteurs à lit fixe et fluidisés ainsi que ceux utilisés dans l'analyse thermogravimétrique (ATG).

En se basant sur des études expérimentales de la littérature, il a été montré que la température a un effet majeur sur les produits issus de la pyrolyse de bois de chêne. Il en a été déduit qu'en augmentant la température de 300°C à 900°C, la quantité de gaz augmente fortement et celles du charbon diminuent proportionnellement. La production de bio-huile atteint un maximum à 500°C.

Le reformage catalytique est ensuite détaillé en distinguant les deux types de reformage (à sec et à la vapeur, aussi appelé vaporeformage) en donnant les principales réactions impliquées, en partant du reformage du méthane qui est le plus courant, et en arrivant au reformage de goudron. Les paramètres opératoires caractéristiques du reformage sont la température, le rapport vapeur/biomasse et les charges métalliques des catalyseurs. Il a été retenu que les configurations de réacteur du reformage peuvent être regroupées en deux grandes catégories : les procédés à une étape, notamment les réacteurs à lit fixe, fluidisé et jaillissant, ainsi que les procédés à deux étapes, en particulier le réacteur à lit fixe à deux étages et le réacteur à lit fixe-fluidisé à deux étages. Une liste des différents catalyseurs et de leurs supports couramment utilisés pour le reformage est aussi fournie. Il a été remarqué que ce sont des métaux, comme le nickel, le cobalt et le fer, qui sont les plus employés grâce à leur bonne efficacité et à leur coût économique compétitif par rapport aux métaux nobles tels que le platine et le rhodium. Les supports les plus utilisés sont des particules à base d'alumine et de silice ainsi que des structures céramiques fortement poreuses sous forme de monolithe ou de mousses.

Les effets de paramètres clés sont étudiés sur la composition des produits résultant du vaporeformage catalytique des produits volatils de la pyrolyse de biomasse. L'étude bibliographique a montré que l'augmentation de la température de reformage de 550°C à 900°C réduit largement la formation de CH_4 et de CO_2. La concentration de H_2 augmente jusqu'à 700°C puis rediminue légèrement alors que celle de CO suit une tendance inverse et atteint un minimum à 700°C après lequel elle croît légèrement. En augmentant le rapport vapeur d'eau/carbone de 1 à 4, les quantités de H_2 et de CO_2 augmentent et celles de CO et de CH_4 diminuent. Le taux du catalyseur Ni a été varié de 1.36% à 5.96% ce qui a entrainé une diminution des concentrations de CH_4 et de CO_2 ainsi qu'une augmentation de celle de CO. La concentration de H_2 maximale a été atteinte à 2.5% de Ni.

Enfin, la combinaison de la pyrolyse et du reformage catalytique est discutée. Les réacteurs qui peuvent être employés pour ce procédé représentent une combinaison des réacteurs utilisés séparément pour la pyrolyse et le reformage. Les effets de quelques paramètres opératoires sur les produits issus du vaporeformage catalytique des composés de la pyrolyse de pin tirés de la littérature sont présentés pour illustrer la faisabilité de cette technique. Il a été observé que la présence de catalyseur permet d'obtenir des rendements de 70% d'H_2, là où le reformage sans catalyseur permet d'obtenir un rendement maximal de 10% d'H_2. La production d'H_2 est améliorée par l'augmentation de la température de 600°C à 800°C. Quand le rapport de vapeur

d'eau/carbone est augmenté de 1 à 15, les rendements de H_2 et de CO_2 augmentent et la production de CO diminue mais avec une variation moins importante à partir d'un rapport de vapeur d'eau/carbone de 5. Cette valeur a donc été choisie comme compromis afin de réduire les coûts énergétiques reliés à la production de la vapeur d'eau. Par ailleurs, une utilisation prolongée du catalyseur de 100 min entraine une désactivation partielle et une réduction dans son efficacité qui peut être attribuée au frittage du catalyseur et au dépôt de carbone sur sa surface.

Les conclusions tirées de cette étude bibliographique seront utilisées comme référence pour une comparaison avec les résultats expérimentaux obtenus dans cette thèse, afin de confirmer la viabilité de notre procédé de couplage de la pyrolyse et du reformage catalytique.

1.1. Biomass pyrolysis

1.1.1. Definition and background

Biomass pyrolysis has been attracting a lot of interest in the last few decades as one of the most technically and strategically advantageous thermo-conversion method to produce bio sourced char, oil and gas. These products are very promising energy resources that can be used as renewable and sustainable alternatives to the non-renewable fossil fuels which are in progressive depletion [1]. Biomass can be converted to energy via multiple thermal conversion processes such as fermentation, hydrocracking, anaerobic decomposition, pyrolysis, gasification and combustion. Among these, the pyrolysis stands out, given its numerous advantages, naming the lower emissions and the possibility of reusing all of the by-products. In short, pyrolysis represents the thermal degradation of the initial solid fuel, in an oxygen-devoid atmosphere or in the presence of an amount of oxygen lower than that required for a complete combustion [2]. It results in the production of solids (carbonized residue or the so-called char), liquids or condensable vapors (water, tars and bio-oils) and non-condensable gases (mixture containing mainly CO, CO_2, CH_4 and H_2). On the other hand, gasification consists of the reaction of the biomass with a gasifying agent which could be air, pure oxygen, carbon dioxide, or water vapor and produces mainly syngas (H_2 and CO), under high temperatures (above 800°C) and without combustion [3].

Pyrolysis owns its origin to the Greek words "pyro" which means fire and "lysis" referring to the breaking down or decomposition into constituents. Pyrolysis is an endothermic process, which allows the production of biofuel with elevated fuel-to-feed ratios in addition to its use to produce coke and charcoal as well as gas. Pyrolysis is the first stage of the gasification and combustion processes that are all applied to extract thermal and/or chemical energy from biomass. Therefore, the understanding of this process is essential, which justifies the abundance of the work and research in this field in the literature. Producing high-value bio-fuel is the ultimate purpose of the pyrolysis technology aiming to compete, and eventually replace, non-renewable fossil fuels [4]. Furthermore, pyrolysis leads to the production of the syngas including hydrogen H_2 and carbon monoxide CO [5]. Synthetic or synthesis gas (or simply syngas) is a mixture of gases including mainly hydrogen and carbon monoxide in addition to some carbon dioxide and water [6]. Syngas is perceived as one of the most encouraging alternative energy carrier, being an environmentally clean combustible and having the potential to diminish the greenhouse gas effect [7]. Hydrogen is regarded to become in the near future a very promising energy carrier [8]. Hydrogen yields three times more energy than gasoline for

the same mass. In addition, the combustion of hydrogen produces only water hence it is extremely eco-friendly [5].

Simultaneous and successive reactions are involved in the complex pyrolysis process of organic material where the heating of the organic matter is realized in a passive atmosphere. In the absence of air or oxygen, at 220°C begins the thermal degradation of the organic material present in the biomass and remains up to 700 – 800°C. Under pyrolysis conditions, the long chains of C, H and O compounds of the biomass decompose into shorter molecules of solid charcoal, condensable vapors (oils and tars) and gases. Several process parameters influence the extent and rate of the breaking down of every component such as the pyrolysis (reactor) temperature, the residence time, the pressure, the reactor configuration, the heating rate, the feedstock type, morphology and conditioning [4]. The yields and selectivity of the different pyrolysis products depend not only on the chemical parameters but also on the heat and mass transfer at the reactor level and/or at the particle level (wood pellets, chips and logs).

The pyrolysis has been the subject of investigations for a while now and a lot of progress have been made in the field. Some of the most important and global reviews discussing the pyrolysis include [3–5,9–13]. For instance, Jahirul *et al.* [4] provided a technological review on the biofuels production through biomass pyrolysis. Collard and Blin [10] addressed the pyrolysis of biomass constituents and detailed the mechanisms and composition of the products obtained from the conversion of cellulose, hemicelluloses and lignin. Sharma *et al.* [11] delivered a review of mathematical modelling of biomass pyrolysis, process parameters and catalytic studies. Dhyani and Bhaskar [12] elaborated a comprehensive review on the pyrolysis of lignocellulosic biomass.

Furthermore, pyrolysis can be also used as a preliminary step to other thermochemical processes such as combustion, gasification, and reforming. Therefore, to investigate the chemical modifications of the bio sourced materials, it becomes crucial to determine the composition of the different products formed during this pre-step. Additionally, understanding the effect of the parameters that impact the products distribution is extremely important in order to optimize the production of the desired species. In this perspective, the effect of the operating parameters has been the subject of researches and review papers [14,15] as well as multiple studies [16–22].

In this section, the biomass is first studied in terms of its elemental analysis and biochemical composition. Then, the tar classification and properties will be investigated. Moreover, the main parameters influencing the pyrolysis process will be discussed. Next, the pyrolysis classification and the reactor design will be described. Finally, some experimental studies will be presented as an illustrating example.

1.1.2. Characteristics of biomass

1.1.2.1. Elemental analysis of biomass

Biomass represents any material deriving from animal compost or growing plants, consisting mainly of carbon (C), hydrogen (H), oxygen (O), nitrogen (N), sulfur (S) and few mineral composites [23]. The biomass can be represented by the following general chemical formula: $C_xH_yO_zN_tS_u$. The wood and lignin biomass contains 0.01 to 0.42% of sulfur and 0.1 to 0.7% of nitrogen [24] hence these two elements have been neglected and the chemical formula of the biomass is generally reduced to: $C_xH_yO_z$. Experimentally, the ultimate elemental analysis can be retrieved using CHNS elemental analyzer. The oxygen content is determined at the end as a difference from 100% [25]. Moreover, intrinsic mineral materials can be naturally present in

biomass specially metals such as alkali and alkaline earth metal. In spite of their low concentrations, these metals can play the role of a catalyst that restricts the products yield and alter their distribution affecting subsequent processing [26].

The resources of biomass can be categorized into five main classes: (i) raw waste from wood such as tree branches, sawdust, wood chips etc.; (ii) energy crops obtained from energy applications such as Napier grass, hybrid eucalyptus; (iii) agricultural residues such as palm kernel shells, corn husks, coconut shell, sugarcane bagasse; (iv) food waste, animal wastes and municipal solid waste (MSW); (v) industrial waste derived from manufacturing industrial processes like demolition and construction activities [27,28].

1.1.2.2. Biochemical composition of biomass

Biomass is a complex material consisting mainly of a biopolymer mixture. The biochemical composition of the biomass differs from one type to another but shares same major chemical components: cellulose, hemicellulose and lignin in addition to the presence of some extractives. Their amounts vary significantly from one type of biomass to another. The wood structure is reported in **Figure 1.1.**

Each component has an unique structure and decomposes differently depending on temperature, heating rate and presence of contaminants [4]. Nevertheless, these components are understood to be closely associated and interconnected in the cell wall of the plants and are not just individual entities [29]. The products derived from the biomass pyrolysis represent a complex combination of the products obtained from the separate pyrolysis of each of the components with specific kinetic characteristics for each. Furthermore, due to the interactions between the primary pyrolysis products and the initial feedstock materials, there is formation of secondary reaction products [2].

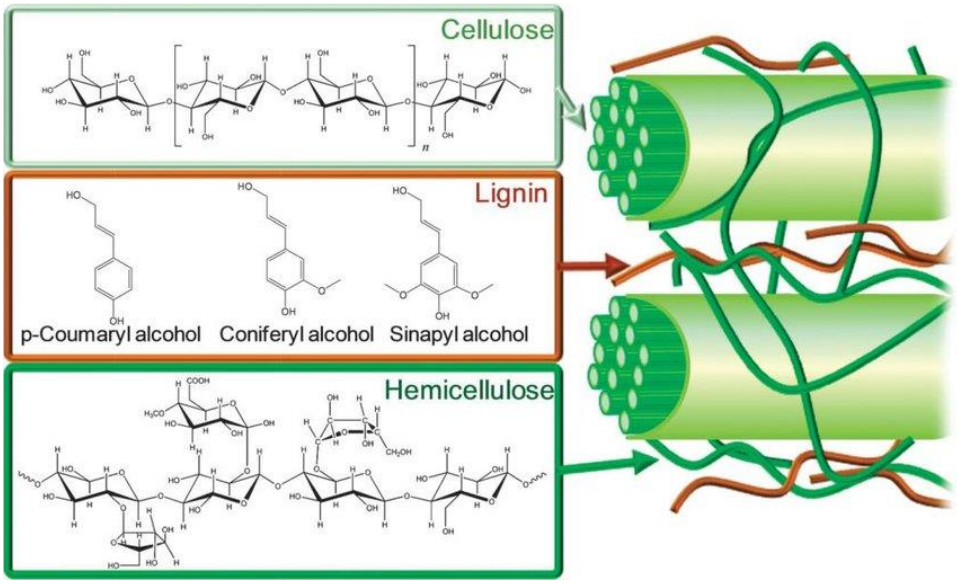

Figure 1.1 Structure of wood in terms of cellulose, hemicellulose and lignin [49]

Cellulose

Cellulose is the main wood component and one of the most abundant structural constituent present in biomass (from 20 to 60% of the total dry mass) [30] and can be mainly found in cell walls. It is a long chain linear polymer and has a high molecular weight (10^6 or more) [2]. Cellulose is characterized by its nearly totally crystalline structure thanks to the presence of

hydrogen bonds that keep the chains linked, in addition to some amorphous zones [30]. The fibers of the cellulose give the wood its strength. The degradation of cellulose takes place between 240°C and 350°C resulting in the formation of anhydrocellulose and levoglucosan. The crystalline structure of cellulose provides it with a high thermal decomposition resistance compared to hemicelluloses [2].

Hemicellulose

Hemicellulose, also known as polyose, is the second main wood structural component [2] and the third essential constituent of cell walls [31]. It typically represents 25% to 35% of dry wood mass with 35 % in hardwood and 28% in softwood. "Hardwood" is an imprecise term referring to the large class of angiospermae trees while "softwood" is used to identify the class of gymnospermae trees. The monomers forming the hemicellulose are either pentoses (5–C sugars) represented essentially by xylans ($C_5H_8O_4$) or hexoses (6–C sugars) whose main representative are the glucomannans. Hemicellulose has a much lower molecular weight than cellulose with around 150 saccharides monomers. Hemicellulose is characterized by the presence of branches, short sidechain pending from the main polymeric chain, which makes it amorphous and less thermally stable than cellulose and thereby it decomposes at lower temperatures. The decomposition of hemicellulose occurs at low temperatures of 200°C to 260°C leading to the production of more volatiles and chars but less tars than cellulose [2]. Commonly, cellulose and hemicellulose are combined and referred to as "holocellulose" [30].

Lignin

The third main wood component, lignin, is an amorphous, hetero-polymer, highly cross-linked resin with no specific structure. Hence, it is characterized by three different reference components: LIGC (rich in C), LIGH (rich in H) and LIGO (rich in O). The products of the lignin pyrolysis are assumed to be the linear combination of the reference components' pyrolysis products [30]. The stiffness and structural integrity of plant's cell walls is provided by the lignin. This latter is regarded as the most naturally present aromatic polymer contributing in around 30% of the total organic carbon in the biosphere. Lignin represents around 4% to 35% of the majority of biomass with 16 wt % to 25 wt.% of the hardwoods and 23 wt % to 35 wt.% of the softwoods. Huge amounts of lignin could be found as waste side products of the paper and pulp industry in addition to being a principal byproduct resulting from the second-generation biofuel production [32]. The lignin decomposition takes place between 280°C and 500°C [33].

Biochemical analysis: Van Soest's protocol

The most common method applied to determine the structural components of a plant cell is the Neutral detergent fiber (NDF). The detergent fiber analysis is based on the concept that the plant cells can be categorized into digestible cell contents including sugars and starch, and less digestible cell walls consisting of cellulose, hemicellulose and lignin. Van Soest used two types of detergents to separate these two groups of components. The neutral detergent used is Na-lauryl sulfate, EDTA having a pH of 7 while the acid detergent used was cetyl trimethyl ammonium bromide in H_2SO_4 solution with concentration 1N. The NDF consists of applying a neutral detergent which helps dissolve the proteins, lipids, sugars and pectins present in the plant. The fibrous parts of the plant including cellulose, hemicellulose and lignin are left behind [34].

The protocol of the Van Soest fiber analysis for the NDF is described briefly hereafter. First, a sample of 0.5-1 g is air-dried, weighted, and grounded to become able to pass 40 mesh into refluxing machine. Then, 100 ml of neutral-detergent solution is added, followed by the addition of 2 ml decahydronaphtalene and then 0.5g of sodium sulfite with some drops of n-octanol. The mixture is heated until boiling for around 5 to 10 minutes. As the boiling starts, the heating must be reduced to avoid the formation of foam. The boiling is next adjusted to a constant level and then the solution is refluxed for 60 minutes starting from onset of boiling. The beaker is swirled, and its content is emptied in a crucible previously tared. Vacuum is admitted until after the filling of the crucible.

Next, the sample in crucible is rinsed with minimum amount of hot water (80-90°C). Then the vacuum is removed, the mat is broken up and the crucible is filled with hot water. The liquid is filtered, and the washing procedure is repeated. In the same manner, washing with acetone is applied and then sucking until it dries. The crucible is then dried at 105°C for 8 hours. After that, the sample is cooled in a convenient desiccator and weighted. The yield of the recovered neutral-detergent fiber is reported as cell-wall constituents. The non-cell wall material is estimated by subtracting from 100 the yield previously determined. Next, the remaining is heated at 500-550°C in a muffle for 3 hours to determine the ash content. It is cooled in a desiccator and weighted and the ash content of neutral-detergent fiber is reported [35]. The same procedure is applied for the acid detergent fiber analysis.

1.1.3. Theoretical description of biomass decomposition

The biomass pyrolysis involves several chemical reactions occurring simultaneously, resulting from the strong interaction arising at the single particle levels and the surrounding environment between the physical and chemical processes. In order to understand this complex phenomenon, the biomass composition needs to be identified and the pyrolysis should be characterized.

Knowing that most of the biomass samples have a very heterogeneous nature, it can be arguably declared that the pyrolysis of any biomass feedstock will be realized in very distinct ways. Therefore, it is difficult to precisely define a generalized mechanism of pyrolysis. Instead, the term pyrolysis is used to refer to a complete set of diverse processes of thermal degradation taking place at different temperatures and rates while leading to the production of distinct products. That clarified, the simplified stages of the biomass pyrolysis, occurring consecutively with the temperature increase, can be identified as follows [36]:

1) Primary evaporation of the free moisture present in the biomass sample
2) A time interval of fast volatilization and depolymerization
3) A sustained slow period of decomposition during which the degradation of inorganic molecules and refractory stable organic compounds takes place along with the char generation as well as secondary and tertiary reactions occurring between the pyrolysis products.

The global mechanism of the biomass pyrolysis can be simplified by the reaction given in equation **(1.1)** where the biomass undergoes pyrolysis and decomposes to produce char (solid), bio-oil or tar (liquid) and non-condensable gases [37]:

$$\text{woody biomass} \rightarrow \text{char} + \text{tar} + \text{gases} \qquad \textbf{(1.1)}$$

Multiple homogeneous and mechanistic models have been elaborated to appropriately describe this process while relating to the transport phenomena and chemical kinetics. So far, the kinetic model established by Eliseo Ranzi and his colleagues [38] at the particle scale seems to be the most detailed and developed model to describe the main reactions involved in the decomposition of the three main biomass components: cellulose, hemicellulose and lignin. Ranzi's model is regarded as the most advanced scheme [39] describing the pyrolysis process in spite of some limitations [40]. The reaction rates and the heat transfer can both be influenced by the biomass properties which makes the operating conditions extremely variable [38].

1.1.4. Tar classification and properties

Tar is one of the products resulting from the pyrolysis of lignocellulosic biomass. It consists of multiple compounds that can affect the products of the pyrolysis or the combustion of biomass. Tar can be referred to as bio-oil, pyrolysis oil, bio-crude oil, pyrolytic oil, bio-fuel oil, liquid wood [41], liquid smoke, wood oil, wood distillate, pyroligneous acid and pyroligneous tar [42]. The pyrolytic oil comprises several oxygenated organic compounds such as alcohols, acids, furans, ketones, aldehydes, phenols in addition to complex oxygenates resulting from biomass lignin and carbohydrates [43]. Tars with diverse compositions and reactivity are formed depending on the thermal severity of the conversion of the vapor phase in the reactors, i.e. on the residence time and gas temperature [44].

The bio-oil content can be split into fractions: water and tar (bio-oil fraction without water). The major tar compounds produced are mainly oxygenated hydrocarbons. As the reaction temperature increases, the oxygenated hydrocarbons are converted into light hydrocarbons, olefins and aromatics, which are next transformed into higher hydrocarbons and larger polycyclic aromatic hydrocarbons (PAH). The organic compounds formed becomes more stable as the temperature increases [45]. Hence, tar can be considered as a mixture of the condensable organic compounds produced during pyrolysis process and consisting of aromatic hydrocarbons such as toluene, benzene, phenol, naphthalene and xylene [46].

Additionally, water accounts for around 15wt.% of the bio-oil and originates from dehydration reactions. The water present in the pyrolytic oil fraction is well dispersed. Therefore, the bio-oil is characterized by the hydrophilicity of its compounds derived from carbohydrates, representing the major fraction of the crude oil [43]. Bio-oil is miscible with water to an extent of 35 to 40%, which leads to the gradual aging of the liquid due to the polymerization of the polyphenols, resulting in a variable viscosity going from 10 to 10 000 cp [47]. Tars represent the leading contaminant in the gas produced with content varying from 5 to 100 g/Nm^3. Nevertheless, their maximum acceptable amount in the gas turbines is 5 mg/Nm^3 and in internal combustion engines, it is 100 g/Nm^3 [48]. The undesirable properties labeling the bio-oil include acidity, incomplete volatility and low heating value. These unfavorable characteristics urge the need to investigate alternative technologies for the use or upgrade of the bio-oil to yield high added-value species [47].

One of the ways of classifying the tar is based on its appearance and the products can be categorized in three major classes as detailed in the **Table 1.1**. **Figure 1.2** shows the typical composition of the biomass tar.

Table 1.1 Tar classification based on its appearance [44, 46, 49]

Tar class	Properties
Primary	Low molecular weight oxygenates generated at low thermal severity (400-700°C) (i.e. hydroxy acetaldehyde, furfural and levoglucosan)
Secondary	Olefins and phenolics, formed in a temperature range between 700°C and 850°C (i.e. xylene, cresol and phenol)
Tertiary	Complex polycyclic aromatic hydrocarbons (PAHs) formed between 850°C and 1000°C (i.e. benzene, toluene, pyrene and naphthalene)

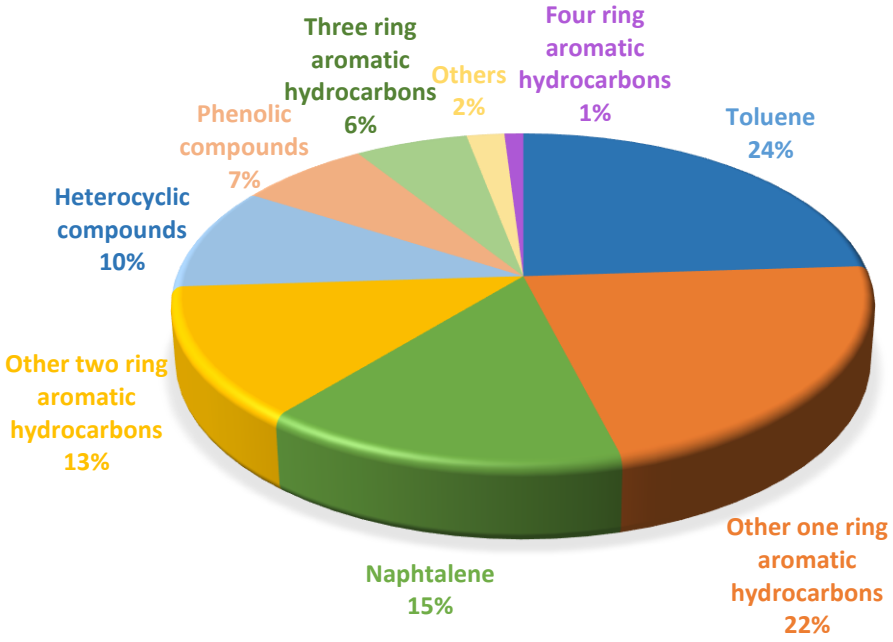

Figure 1.2 Typical composition of biomass tar [50]

1.1.5. Pyrolysis characteristic parameters

Among the major parameters that allow enhancing the pyrolysis efficiencies, the temperature, the heating rates, and the residence time remain the most effective and are described hereafter.

- ***Reactor's temperature***

The thermal degradation occurs sequentially depending on the temperature attained by the biomass particles. The first step, which takes place between 20°C and 120°C, is related to the water evaporation from the biomass. In the subsequent temperature range between 120°C and 300°C, the biomass weight loss is minimal where only small amounts of some light gases such as steam, carbon monoxide and dioxide are released resulting essentially from reactions of dehydration and decarboxylation from R-OH groups that belong to lignin and hemicellulose. Between 200°C and 350°C, the degradation of cellulose occurs where the depolymerization generates oligomers and anhydrous sugars of glucose, cellobiosan, cellotriosan, levoglucosan, etc. called "intermediary liquid compound" or "molten cellulose" or more commonly "active cellulose" [51]. Between 300°C and 400°C, the largest weight loss (about 80%) takes place, which corresponds to the volatiles emissions' maximum rate. In this stage, volatile products containing a high amount of oxygen is generated from the random decomposition of

hemicellulose and cellulose bonds along with the generation of carbonaceous residue commonly known as char. When the temperatures exceed 400°C, the depolymerization of lignin made of a rich aromatic carbonaceous matrix release CO and CO_2. With the increase of the temperature (between 580°C and 800°C), there is a decrease in the formation of volatile products such as acetone, paraffin, alcohols and aldehydes and a rise in the production of polyaromatic hydrocarbons (PAH), which are thermally more stable, like naphthalene, toluene, benzene, cresol and pyrene [52,53]. Unfortunately, the direct measurement of the biomass particles' temperature is difficult on both the lab and the industrial scale hence the temperature is in general assumed to be that of the pyrolysis reactor [54] or the biomass sample container even though they might be slightly different.

- ***Heating rate***

The heating rate is possibly the most essential parameter to differentiate between slow and fast pyrolysis. It represents the time needed to reach the temperature of the reaction. In general, slow pyrolysis is characterized by heating rates going from 1 to 100°C/min [53] and fast pyrolysis has heating rates surpassing 1000°C/min [55]. The depolymerization reactions of cellulose and hemicellulose are favored by high heating rates, which minimize the residence time of the volatiles inside the particles secondary reactions. In addition, high bio-oil yields and low char production are achieved due to the fast release of condensable gases. Furthermore, the heating rates affect the structure of the char obtained and the quality of the bio-oil. At higher heating rates, the bio-oils obtained can contain less moisture mainly because secondary reactions are inhibited. Additionally, the emissions of CO and CO_2 can also be enhanced with the increase of the heating rates. On the other side, elevated heating rates lead to the formation of biochar with smaller specific area and pores volume which will cause momentous pressure gradients between the outside and inside of the particles. This is the result of the rapid production of the volatiles without being able to be instantly evacuated leading to the cracking of few internal structures [54].

- ***Residence time***

In order to obtain high bio-oil yields, it is crucial to consider the solids and volatiles residence times within the reactor. The volatiles residence time has been generally adopted to be short consisting of a few seconds to reduce the cracking reactions [56]. The volatiles residence time is different than that of solids. The residence time of solid biomass must be high in order to reach a complete cracking and devolatilization whereas the residence time of the volatiles has to be as short as possible to avoid the undesirable secondary reactions [57]. These residence times are in direct relation with the operating conditions such as the flow of the carrier gas in addition to the technology implemented for the pyrolysis process. For example, in a fixed bed reactor, the solids residence time is long, tending to infinity, whereas in a fluidized bed reactor, both the solids and volatiles residence times are much shorter, in the order of a few seconds, according to the gas flow and the reactor's size. The flow of the carrier gas can be adjusted to reduce the condensable volatiles residence time thus minimizing the vapors' re-polymerization and cracking reactions [54]. Whereas, if longer residence times are adopted, the constituents of biomass benefit from bigger chances of undergoing re-polymerization and therefore the yield of bio-char increases. Moreover, elevating the residence time leads to a growth in the bio-char porosity. In addition to impacting the bio-char yield, the residence time greatly affects the quality and the composition of the liquid and the gaseous pyrolysis products [58]. Short volatiles residence time of lower than 2 seconds, elevated heating rates of higher than 1000 °C

/min and moderate reaction temperatures of around 500°C provide a suitable combination of operating parameters for maximizing the bio-oil yield by pyrolysis [54].

Nevertheless, applying short volatiles residence times in the reactor can be disadvantageous for multiple reasons. First, high carrier gas flow can entrain solids thus reducing the biomass conversion. This can further obstruct the cyclones and lead to the contamination of the bio-oil recovered from the condensation steps. Second, the cooling of the reactor by forced convection forbids the particles from achieving high heating rates [54]. Fassinou and his colleagues [59] demonstrated that there is an interactive effect between the residence time and the temperature on the bio-char yield. On one hand, high residence times and temperatures enhance the yield of bio-char. And on the other hand, decreasing the temperature and increasing the contact time leads to lower bio-char yields. Subsequently, making direct inferences concerning the link between the residence times and the bio-char production can be very difficult [58].

1.1.6. Pyrolysis classification

The pyrolysis classification depends on the operating conditions and thus can be divided into four categories according to the heating rate, process temperature, biomass particle size and solid residence time. The operating parameters also influence the relative composition of the pyrolysis products. Therefore, the pyrolysis can be classified into slow, conventional, fast and flash pyrolysis [36] as given in **Table 1.2.** It should be noted that the parameters values characterizing each type might be defined slightly differently depending on the references. Therefore, the values given here are a combination of the most encountered characteristic values.

Table 1.2 Pyrolysis classification into slow, intermediate, fast and flash pyrolysis along with approximate product yields

Pyrolysis process	Heating rate (°C/s)	Temperature (°C)	Residence time (sec)	Particle size (mm)	Product yield (%)			Ref
					Gas	Oil	Char	
Slow	0.1 - 1	300 - 700	300 - 550	5 - 50	35	30	35	[4,42, 60]
Intermediate	1 - 10	500 - 650	0.5 - 20	1-5	30	50	20	[36,61 ,62]
Fast	10 - 200	850 - 1250	0.5 - 10	< 1	30	50	20	[4,42, 60]
Flash	> 1000	900 - 1200	< 1	< 0.5	13	75	12	[4,42, 60]

- ***Slow pyrolysis***

For decades, slow pyrolysis has been implemented in the industrial sector for the char production which is favored at low heating rates and temperatures. During the slow (or commonly termed conventional pyrolysis [63]), the residence time of the vapor is very long going from 5 to 20 minutes, which allows the vapor components to keep interacting leading to the formation of other liquids and chars [4]. Slow pyrolysis is characterized by the slow heating rate of 0.1 to 1°C/s (6 to 60°C/min) and a solid residence time of 300 s to 550 s. To perform the slow pyrolysis at industrial scale, several configurations can be used such as screw pyrolyzers, rotary kilns, agitated drum kilns and batch or continuous large retorts [11]. Nevertheless, technological challenges limit the applicability of slow pyrolysis for the production of bio-oil

of a decent quality. For instance, the high residence time of the slow pyrolysis causes the primary products to crack, which might also have a negative impact on the quality and yield of the bio-oil. Furthermore, additional energy requirements are demanded due to the low heat transfer and the long residence time of the volatiles [64].

- ***Intermediate pyrolysis***

Intermediate pyrolysis is characterized by a relatively slow heating rate going from 0.1 to 10 °C/min at temperatures between 500°C and 650°C leading mainly to the formation of pyrolysis oil. The feedstock residence time is intermediate being between 5 to 10 minutes [36]. This type of pyrolysis is appropriate for several feedstock such as food and sewage sludge as well as waste wood [65]. Intermediate pyrolysis is generally applied to balance the production of solid char and liquid bio-oil. The conditions of intermediate pyrolysis hinder the formation of heavy tar molecules and encourage the formation of good quality bio-oil and dry biochar. The char formed has multiple applications such as agricultural fertilizer or fuel for the production of energy in thermal power plants via co-combustion [66].

- ***Fast pyrolysis***

In the fast pyrolysis, the biomass is heated in an oxygen-free atmosphere at a very rapid rate of 10 to 200°C /s (600 to 12000°C/min) and up to an elevated temperature (1250°C with a brief solid residence time of 0.5s to 10s and tiny particle size feedstock (<1mm). Biomass breaks down during the fast pyrolysis into char, aerosol and vapors. A dark brown oil is mainly produced after the cooling and condensation of aerosol and vapors [67]. In order to achieve fast pyrolysis, three major methods have been proposed. The first one is the ablative pyrolysis where the biomass is pushed over a heated area and then quickly removed. This allows the biomass to melt by the contact with the heated surface leaving an oil film which will be evaporated. The second one is by using a fluidized bed and a circulating fluidized bed where heat is transferred to the biomass mainly by convective heat transfer. The third method is the application of vacuum pyrolysis having a slow heating rate but a fast removal of the pyrolysis products as fast as in the pre-liquid product [68].

Fast pyrolysis favors the formation of liquid products and gases [63] derived from biomass due to short residence time, moderate temperatures and high heating rate. Around 60 % to 75 % of oil and liquids are produced along with 10 % to 20 % of gases and 15 % to 25 % of char [36]. The fast pyrolysis process is characterized by considerable heat transfer with good control of the reaction temperature in addition to fast cooling of aerosol and vapors. This technological process has been the center of attention for the production of liquid bio-oil and a series of commodities and specialty chemicals. Hence, the solid biomass can be decoupled from the application given that the liquid produced is subject to easy and economical transportation and storage. Moreover, this process is featured by an elevated energy efficiencies and low investment costs specifically at small scale [4]. Fast pyrolysis of biomass is also regarded as a viable route with which begins the hydrogen production from biomass. The progress realized in understanding the pyrolysis mechanisms and the technology demanded for achieving elevated heat-transfer rates to the particles, along with a firm control of the secondary cracking reactions leading to the production of char and gas, have allowed the developing of the fast pyrolysis. Thereby, high yields of biomass conversions (around 75 wt.% on dry biomass basis) into pyrolytic oil know as bio-oil were achieved [43].

- ***Flash pyrolysis***

Flash pyrolysis takes place at an extremely fast heating rate, superior to 1000°C/s (60 000°C/min) and appears a very promising process for the synthesis of gas, liquid and solid. Flash pyrolysis is sometimes referred to as very fast pyrolysis [36]. In this process, tremendously elevated temperatures falling between 750°C and 1000°C are imposed [67] and can sometimes go up to 1300°C [36]. In addition, a rapid devolatilization characterizes this process with a restricted residence time of less than 0.5s. Flash pyrolysis is applied to extremely small particles (lower than 0.2 mm diameter). The crude oil produced by the conversion of biomass in the flash pyrolysis has an efficiency of up to 70% [67] and a yield of around 75% [4]. However, some technological issues limit this process. These include the presence of solids in the oil, its corrosiveness, poor thermal stability, increase of the viscosity with time due to catalytic action of char. In addition, the flash pyrolysis leads to the production of pyrolytic water and alkali concentrated in the char which dissolves in the oil [4] in addition to the acidic nature of the oil, elevated viscosity, oxygen content, and water content [67].

The most common reactors used for performing a flash pyrolysis are fluidized-bed reactors via injection of the sample particles into a bed of solids previously heated. The evolving gases are swept out of the reactor using a fluidizing agent [69]. Moreover, entrainment reactors can be used to create ablative conditions and provoke flash pyrolysis. When individual particles are pneumatically conveyed, carried by an inert gas, they are exposed to an intensified radiant environment. The ablative states are created when these particles hit a heated surface and then slip over it at a large speed [26]. Other reactor types for the flash pyrolysis include rotating cone reactor where fast heating and short solid residence time can be maintained with a negligible char formation [70] as well as tubular reactor externally heated by an electrical furnace [71].

After describing the pyrolysis classification, it can be concluded that if high char yield is wanted then the slow or intermediate pyrolysis must be applied whereas if elevated bio-oil and/or gas yields are desired then fast or flash pyrolysis are more suitable. Therefore, the choice of the pyrolysis reactor holds a primary importance and thereby a description of the different reactors that can be involved in the pyrolysis process is realized next.

1.1.7. Pyrolysis reactors design

The heart of any chemical process and especially the pyrolysis is the reactor which has a critical influence on the efficiency and the products yields. Several research, development and innovative works were performed on the reactors, in order to enhance their primary characteristics including short vapors residence time, moderate temperatures and high heating rates. Aiming at the optimization of the pyrolysis performance and the production of high-quality bio-oil, multiple reactor designs were investigated with the continuous development of the pyrolysis technology. Nevertheless, every reactor type owns special characteristics, along with several advantages and drawbacks. Common reactors include: fixed bed reactor, fluidized-bed reactor, bubbling fluidized-bed reactors, ablative reactor, vortex reactor, rotating disk reactor, vacuum pyrolysis reactor, rotating cone reactor, auger reactor, microwave reactor and solar reactor [4]. It can be added to these, the use of thermogravimetric analysis (TGA) for the pyrolysis as well as the configuration of multi-stage reactor. Some of the most encountered and employed reactors will be described next.

- ***Thermogravimetric analysis TGA***

TGA is one of the most used techniques and one of the most powerful tools to investigate materials' decomposition by thermal process. It has emerged as a fast, easier, cheaper and an alternative technique [72] to those usually applied such as the empirical methods, statistical approaches, and spectroscopy techniques (Raman scattering spectroscopy, near infrared reflectance (NIR) spectroscopy and mid infrared (MIR) absorption as well as nuclear magnetic resonance (NMR) spectroscopy) [73]. In the framework of biomass analysis, TGA is utilized to specify the cellulose, hemicellulose and lignin content with improved accuracy when compared to the wet chemical methods commonly applied [72]. Moreover, TGA is considered extremely useful to comprehend the thermal behavior of small fuel samples and to learn about the thermal stability and chemical structure of several materials [74]. The coupling of the TGA to a mass spectrometer enhances the comprehension of the thermal degradation mechanisms [75,76]. Based on the studies previously done, it was proposed that the pyrolysis of biomass on a traditional TGA can be taken as the sum of the individual pyrolysis of the biomass main components (cellulose, hemicellulose and lignin), each done separately [77].

It also allows the estimation of the quantities of gas formed during the pyrolysis like H_2 and CH_4. TGA can analyze complex mixtures quantitatively knowing that each of the biomass components has a characteristic thermal decomposition temperature. Furthermore, the TGA allows the intrinsic kinetic study of the thermal decomposition of biomass in terms of decomposition temperature, velocity and species produced [77]. Given the few amounts of mass analyzed and the small size of sample container, this method is not influenced by heat transfer, mass diffusion, volumetric vs surface decomposition, and the possible recombination between the species… The beneficial aspect of TGA is its high-throughput nature (at-line) in addition to being perfect for polymers assessment such as lignin. However, TGA is a destructive method and some changes can take place in polymer analytes due to the temperature ramping [72].

Even though TGA is not a typical pyrolysis reactor, it is commonly applied to study the decomposition of the biomass and is therefore considered as a micro-pyrolizer. A powdered biomass sample of few milligrams encapsulated in a metallic or a ceramic container is subject to thermal decomposition during the typical TGA. As result, the sample is thermally thin ($Bi < 0.1$) so that heat transfer and gas flow within the sample container are insignificant and the chemical kinetics primarily control the process [74]. During thermogravimetric analysis, the evolution of the sample's mass and temperature with time is recorded. The mass loss data enables the identification of the characteristic temperatures of the sample decomposition. Indeed, the derivative thermogravimetric DTG curve, constructed from TGA data, exhibits one or several peaks corresponding to the maximum decomposition rates (in wt.% per °C). For a single wood component (cellulose, hemicellulose or lignin), the DTG curve presents one peak as shown in **Figure 1.3**. The abscissa and the width of the DTG curve peak give the temperature and the temperature interval of decomposition, respectively [78].

For the industrial scale applications, a larger amount of biomass with size up to multiple centimeters feeds the pyrolysis furnaces and as consequence, both heat transfer, gas flow and reaction kinetics prevail, simultaneously. Thereby, a lab scale macro-TGA of biomass thermal decomposition have been proposed by Onsree *et al.* [74]. It aims to overcome the limitations of classical TGA in reproducing combined kinetics and transport phenomena occurring in real pyrolysis reactors.

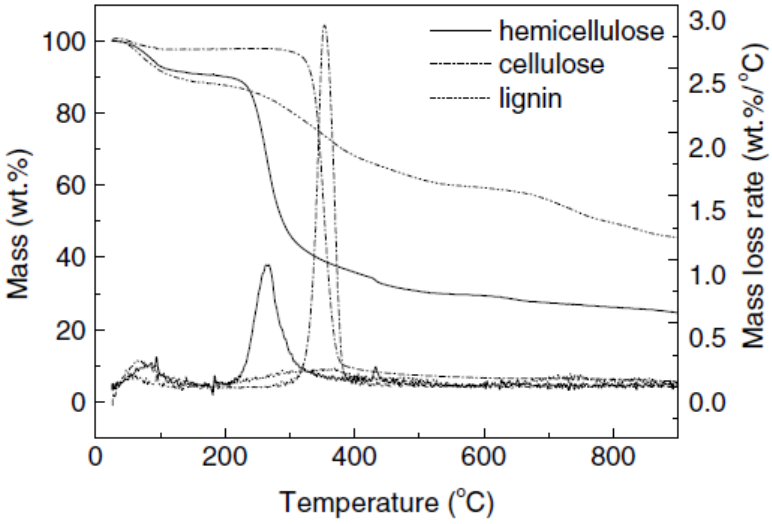

Figure 1.3 DT and DTG curves of the cellulose, hemicellulose and lignin [78]

- ***Fixed bed reactor***

The pyrolysis realized in fixed bed reactors includes a cooling system and gas cleaning. It is a reliable and simple technology that is established for solid fuels having a comparatively uniform size with a small number of fine particles. In counter-current (updraft) fixed bed reactors, the solids move downward through a vertical shaft and enter in contact with a gas stream moving upward. Whereas in co-current (downdraft) fixed-bed reactors, the solid fuels and gas stream are fed from above and then move downwards. These reactors operate generally with small gas velocity, long solid residence time, diminished ash carry over and elevated carbon conservation. Fixed bed reactors are applied for small-scale power and heat applications. The gas cleaning and cooling system are based on filtration through dry filters, wet scrubbers and cyclone [4].

Tar removal is the main limitation of fixed bed reactors but this drawback can be now overcome thanks to the recent progress in catalytic and thermal conversion of tar [4]. In the case of catalytic pyrolysis, the possibility of a quick and continuous regeneration of the catalyst is one of the main positive sides of the fixed bed reactors. If the catalyst is not continuously regenerated, the operation of the fixed bed will be constrained due to the fast deactivation of the catalyst, primarily through coking [79]. It should be noted that the fixed reactor of the pyrolysis or the gasification is different from the fixed bed reactor of the catalytic conversion of the pyrolysis gases.

- ***Fluidized bed reactor***

It contains a mixture of the solid biomass and a carrier fluid that exhibits fluid like properties where a pressurized fluid is injected through solid particles [4]. In these reactors, the feedstock is continuously introduced, and the bio-oil constantly produced which makes them more efficient. Small inorganic particles are used in the fluidized bed reactors as heat carriers since they provide efficient heat transfer along with uniform bed temperature distribution. The input particles are introduced at the bottom of the fluidized bed along with the pressurized gas, which will carry the feedstock particles via the heated mineral particles. The pressurized gas creates the movement of the feedstock and the inorganic particles through the reactor vertically forcing them to fluidize. The intimate contact between the feedstock particles and the tiny inorganic particles leads to an efficient heat transfer and results in elevated bio-oil yields [80].

The fluidized bed reactors are characterized by an elevated surface to volume ratio as well as high relative velocity between the solid and fluid. As common features of fluidized bed systems, they enable fast fluid-to-solid heat transfer and a good thermal transport through the system with a quasi-uniform temperature distribution provided by tiny mineral particles [4]. As a result, fluidized-bed reactors are commonly used for realizing fast pyrolysis since they allow good control of the pyrolysis reaction and the vapor residence time. Moreover, if the biomass particles have a narrow size distribution, fluidized bed reactors are considered "self-cleaning" reactors where the produced vapors and gases carry the by-product char formed out of the reactor [80]. Compared to fixed bed reactors, fluidized bed reactors are more efficient in terms of the heat transfer and offer a better control of the temperature thanks to the fast circulation and the turbulent gas flow[81]. However, the pyrolytic gas can be diluted by the large volumes of inert carrier gases used resulting in the reduction of the thermal efficiency [82].

- ***Multistage reactors***

The pyrolysis, although being an endothermic process in overall, it can be realized exothermically at its initial stage. The operating temperature and the heating rate strongly affect the products yield and quality as well as the overall energy consumption. This latter must be minimized for the pyrolysis to attain its potential of producing bio-oils. As a possible solution, it is perceived to trap the exothermic heat released at the initiation of the pyrolysis and to use it for the endothermic reactions taking place at the end of the pyrolysis. In that purpose, the pyrolysis can be better realized in multiple stages [83]. In a multi-stage reactor, the final target temperature is reached after passing by intermediate temperature stages each reached at different heating rates. This approach has been proven to save up to 30% of the total energy consumption and to reduce the processing time [84].

1.1.8. Experimental studies on the pyrolysis of some typical wood biomass

The forests of the Grand-Est region in France comprise several wood species that are distributed between 79% for the surfaces in hardwood and 21% for the surfaces in softwood. The main wood species in the region are oak (27% of the forest areas), beech (18%), charm (11%), pectin fir (7%), common epicea (7%) and scots pine (3%). The regional commercial harvesting is distributed between the three major uses of the wood in the following proportions: 42% for the lumber (sawing, peeling), 33% for the industrial wood (trituration for panels and paper) and 25% wood energy (logs, chips, granules) [85]. The oak wood pyrolysis is treated as an example hereafter.

For clarification, in the results given for the pyrolysis products, the gases composition in % refers to ratio of one of the gas species to the sum of all the gases at a certain operating condition. The yield represents an indication of the part of the original biomass that was converted into a certain product (gas, liquid or solid). The gas composition is generally determined using the gas chromatography whereas the gases yields are specified from the gasifying medium flow rate and the biomass flow rate.

Oak wood pyrolysis

- **Elemental and biochemical compositions of oak**

Schmidt and his colleagues investigated elemental and biochemical compositions of oak wood among others (fir and beech) while they focused on their combustion and their gaseous emissions and particulate products [86]. Biochemical composition was analyzed according to Van Soest's protocols, described in section 1.1.2.2. The analysis results are reported in **Table**

1.3, for the elemental composition, and in **Figure 1.4**, for the biochemical composition. It can be remarked that oak is made almost in half of cellulose (45 wt.%) with 34.7wt.% of hemicellulose and the rest is lignin.

Table 1.3 Elemental analysis of raw oak [86]

Element	wt %
C	46.3
H	5.7
N	<0.1
S	<0.03
O	40.9

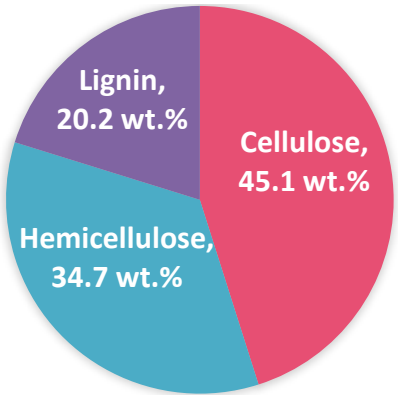

Figure 1.4 Biochemical composition of raw oak [86]

- **Pyrolysis results**

Main products distribution

Figueiredo *et al.* [87] studied the influence of temperature and particle size on the pyrolysis of holm-oak. In that purpose, they realized the pyrolysis under atmospheric pressure, in a cylindrical stainless-steel reactor with 200 $cm^3.min^{-1}$ nitrogen flowrate. The temperature ranged from 300°C to 900°C with 100°C increment and the particle size was varied from 0.4 to 2 mm diameter. The evolution of the pyrolysis yield was determined in function of temperature. It was reported that as the temperature increases, the pyrolysis yield decreased from 57.4 wt.% at 300°C to stabilize above 600°C where the same yield of 18.4 wt.% was obtained at 800 and 900°C. It was suggested that the pyrolysis was practically complete at around 400°C above which there was only a loss of the volatile matter as the temperature was increased along with an enhancement in the charcoal quality.

The variation of the mass yields of the different fractions of oak pyrolysis products with the temperature for particle diameter of 0.62–1 mm is summarized in **Figure 1.5**. It can be clearly noticed that as the temperature increases, the gas yields keep increasing while the solid yields decrease to stabilize above 600°C. The liquid yield increases to reach a maximum at 500°C and then decreases meaning that the gas portion increases above this temperature at the expense of that of the liquid. One can say that as the temperature rises, the oak wood volatilizes with an important fraction of tar formed. Above 600°C, the devolatilization becomes almost total and the tar is subjected to secondary cracking reactions which is noticed by the remarkable increase in the non-condensable gases yield.

Comparing to the results obtained by Ansari *et al.* [22] who realized the pyrolysis of the biomass main components separately, it was remarked that the tar yield increased as well with the temperature up until 500°C for cellulose, hemicellulose and lignin. This corresponds to the increase in the liquid yield reported by Figueiredo *et al.* [87].

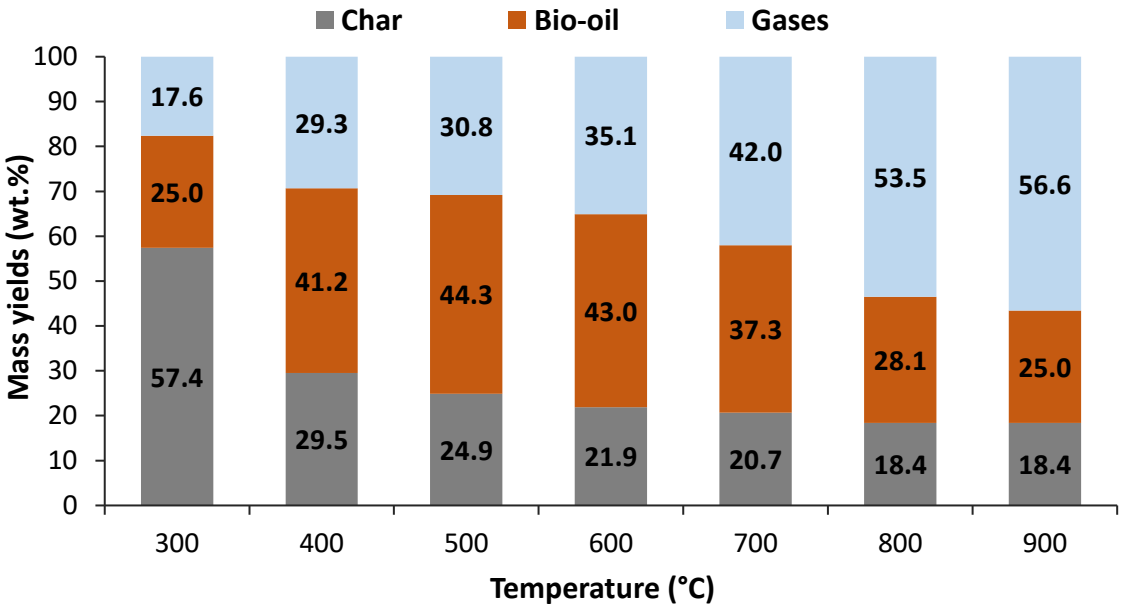

Figure 1.5 Variation of the mass yields of the different fractions of oak pyrolysis products with the temperature [87]

Non-condensable gases composition

The gas products resulting from the pyrolysis realized by [87] were also analyzed using a gas chromatograph linked to a thermal conductivity detector. It was shown that the major pyrolysis products are carbon monoxide CO, carbon dioxide CO_2, methane CH_4 and hydrogen H_2, with traces of oxygen and some hydrocarbons such as acetylene and ethylene C_2H_4. The variation of the molar concentrations of the main gases at 700°C with time was studied. We extracted the maximum amounts and converted them into weight percent. The results are shown in **Figure 1.6** where the mass yield of the CO is the highest, followed by that of CO_2 then CH_4 while H_2 has the lowest mass yield at 700°C.

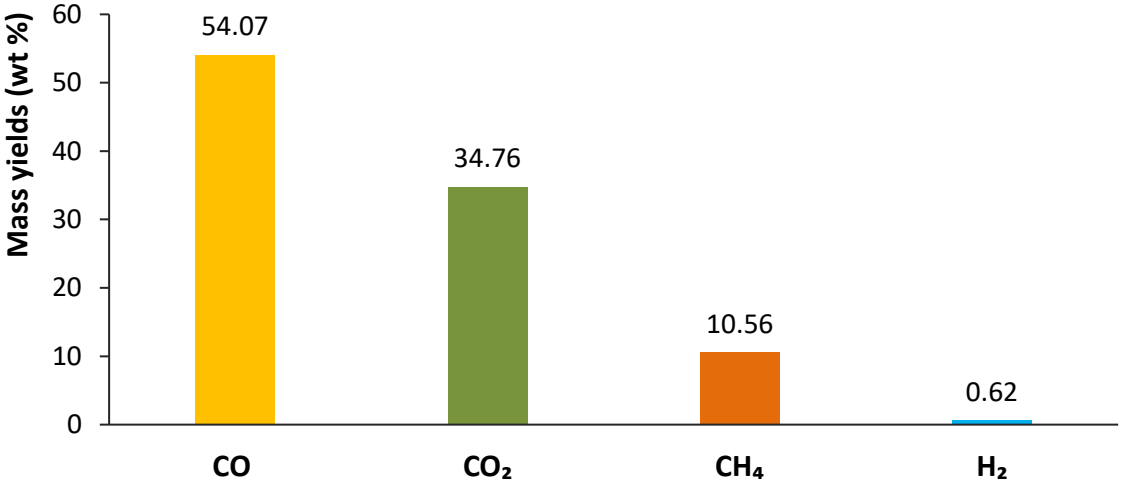

Figure 1.6 Composition of non-condensable gases of pyrolysis of oak at 700°C [87]

More recently, Amini *et al.* [88] investigated the slow pyrolysis of live and dead vegetation considering two sets of experiments under nitrogen atmosphere. The first set of experiments aimed to study the effect of temperature on the pyrolysis products yield. The pyrolysis tests were carried out in a pyrolyzer at temperatures 400, 500, 600, 700 to 800°C with a heating rate of 30°C.min^{-1} under constant nitrogen flow rate of 100 mL.min^{-1}. The second set of experiments analyzed the effect of heating rate on the pyrolysis products yield by considered several heating rates of 5, 10, 15, 20, 25 and 30°C.min^{-1} at a reactor temperature of 500°C. The furnace temperature was held constant in each experiment at the final temperature for 1 hour until there was no further gas release. They concluded that the optimum operating conditions in terms of the highest tar yield consists of a heating rate of 30°C.min^{-1} and a temperature of 500°C under constant nitrogen flow rate of 100 mL.min^{-1}. Under these optimal conditions, 14 plants species (dead and live) coming from the forests in the southern United States were studied, among which live oak and water oak for which the composition of light gases obtained from the pyrolysis under the optimal conditions is realized. The repartition of the produced gases' mass yields is presented in **Figure 1.7**.

It is noticed again that the tendency of the mass yields found by the study of Amini *et al.*[88] confirms that obtained by the work of Figueiredo *et al.* [87] where the mass yield decreases going from that of CO being the highest to H_2 the lowest. The gases yields in **Figure 1.7** correspond to oak wood samples having completely distinct origins and possibly different elemental and biochemical compositions than those previously reported.

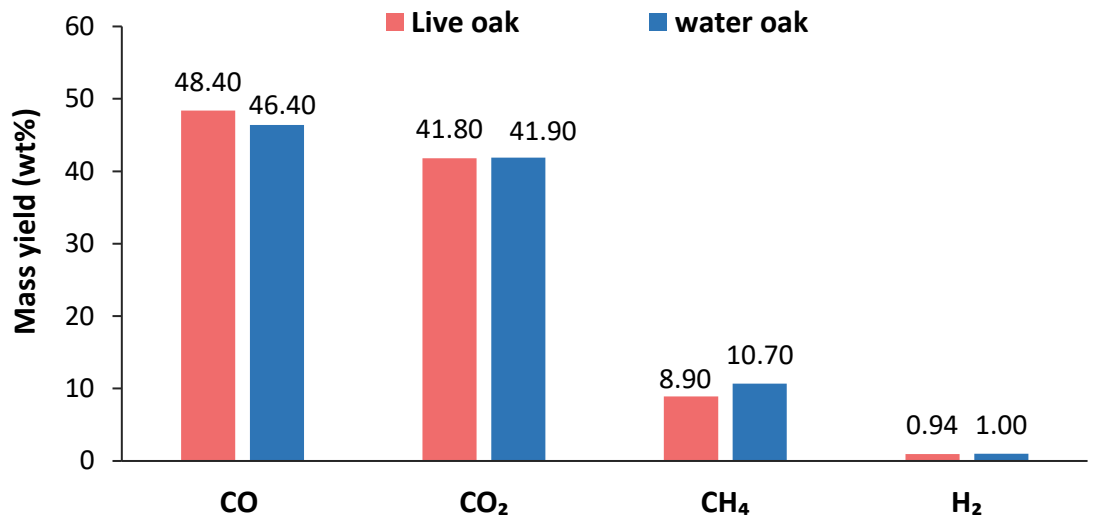

Figure 1.7 Composition of light gases obtained from the pyrolysis of dead oak at 500 °C with a heating rate of 30°C.min^{-1} and sweep gas flowrate of 100 ml.min^{-1} [88]

Bio-oil composition

Amini *et al.* [88] worked as well on the analysis of the tar characterization derived from the slow pyrolysis of the different plant species (live and dead) using a typical GC-MS chromatogram. The tars formed represent a complex mixture consisting of organic aromatic (C_5-C_{20}), oxygenated aromatic, non-aromatic and some nitrogen containing components. They identified more than 200 compounds in the tars. The tar species obtained appear to be the products of primary pyrolysis since a moderate temperature of 500°C was applied, which corresponded to the maximum tar yield. Thereby, the tar species were not affected by secondary pyrolysis reactions further occurring in the gas phase. From the tar analysis, it was remarked that the tar composition was not the same for the distinct plant species [88].

A large number of the tar components are primary products derived from lignin degradation taking place during the pyrolysis between 280°C and 500°C [89]. Lignin is highly reactive since its chemical structure contains phenolic methoxyl and hydroxyl groups. The lignin degradation leads to the formation of mainly phenols and aromatic carbons, while the cellulose and hemicellulose degradation result in the production of carboxylic acids, ketones and furans [20,89]. In thermal decomposition, hemicellulose is highly activated given its random amorphous structure and its low strength. Its pyrolysis, occurring between 200°C and 280°C, results in the production of furfural and acids mainly [20,89]. In contrast, cellulose is thermally stable given its finely ordered structure containing long glucose polymer chain. High tar yields are obtained from the pyrolysis of cellulose, but it is not restricted to the aromatic compounds. The degradation of active cellulose, taking place between 240°C and 350°C, produces linear carbonyls, cyclopentanone and furans [20].

For instance, the tar composition derived from the pyrolysis of live water oak (live and dead) are detailed in the **Figure 1.8**. It should be noted that some of the values in **Figure 1.8** differ from the original figure by [88] since they were adapted from the corresponding text. In the tars formed by the pyrolysis of live water oak, several compounds were present such as furfural (8 mol%), 2-methoxy 5-methyl phenol (2.8 mol%), 2-methyl phenol (1.4 mol%) and maltol (larixic acid) (1.5 mol%) which were not observed in the tars from the dead water oak. Other compounds were found in the dead water oak such as 2,3-dihydrobenzofuran (3.1 mol%) and 1,2,3-benzenetriol (1.1 mol%). Less oxygenated aromatic compounds were obtained from the pyrolysis of dead water oak samples than from live samples [88].

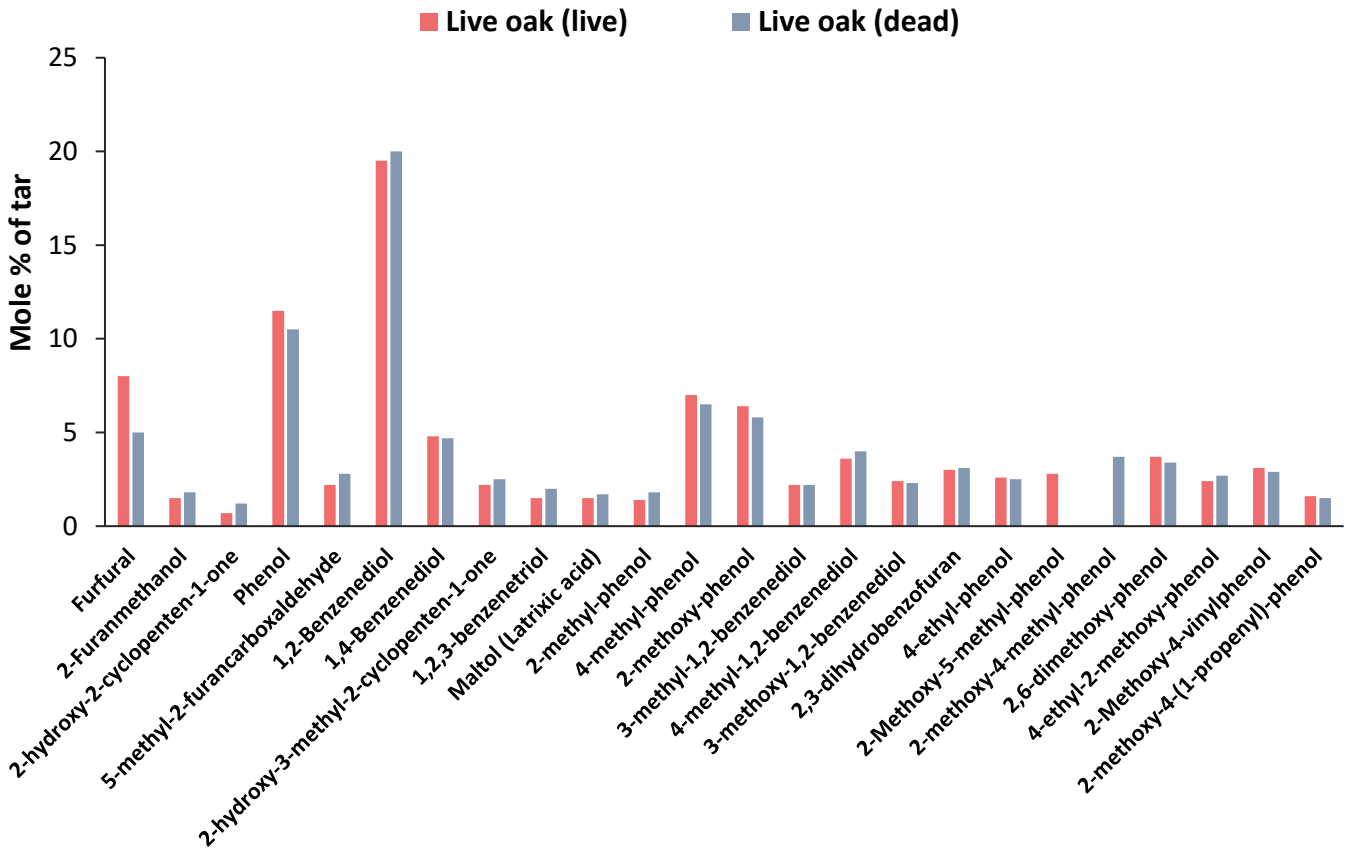

Figure 1.8 Tar composition derived from the slow pyrolysis of water oak wood (live and dead) (adapted from Amini *et al.* [88])

1.2. Catalytic reforming

1.2.1. Definition and background

Aware of the rising demand on fuels for the energy supply and after the depletion of the fossil resources with the population increase, intensive research works are elaborated around the world to innovate the production of fuels deriving from renewable resources. As an alternative for fossil fuels, biomass has been emerging as a sustainable renewable resource for the production of biofuels having similar energy power to that of fossil fuels [45]. Four major routes are adopted for the conversion of the biomass into multiple energy forms (such as gaseous, liquid, solid fuels and heat) which are: physical conversion, thermochemical and biochemical conversions, and direct combustion. The biomass is converted in the thermochemical process by one of the four followings ways: direct liquefaction, torrefaction, gasification and pyrolysis [45,90].

The pyrolysis of biomass has been wildly exploited for the production of useful products by thermochemically converting lignocellulosic biomass [47]. Along the production of biochar and numerous gases (methane, hydrogen, carbon monoxide and dioxide etc…), the biomass pyrolysis results in the formation of a dark, viscous, complex liquid called tar. It is made of more than 300 compounds which can cause major issues during the process operation. Being a sticky material, it condenses usually in the low-temperature parts of the downstream process plugging narrow pipelines, corroding the metals, clogging the filters, polymerizing into more complex molecules and deposing coke on the catalyst [48]. Moreover, elevated tar concentrations lead to intolerable need for engines' and turbines' maintenance. Additionally, tar is especially harmful for human health given its carcinogenic character [91].

Several techniques are envisaged as possible solutions for the tar removal, classified into: physical methods using wet scrubbers or ceramic candle filters, thermochemical conversion technologies applying elevated temperatures and catalytic reforming with the use of catalyst in order to transform the tar into syngas [91]. During the physical processes, the tar is removed from the produced gas through liquid/gas or solid/gas interactions. This is an efficient method with relatively easy maintenance. However, the problem is persistent since there is no destruction of the tar. In addition, it is difficult to dispose of the filter loaded with tar in an environmentally responsible way. Thermochemical process relies on the considerable increase of the produced gas temperature where heavy aromatic compounds forming the tar are cracked into lighter species such as H_2, CO and CH_4 causing less problems than tar. In order to effectively remove the tar, extremely elevated temperatures surpassing 1000°C are demanded for the thermal cracking which might be challenging to attain in biomass thermochemical processes [92].

Catalytic reforming is regarded as a viable route to valorize the tar into syngas. It was introduced initially in 1940 by Universal Oil Products and since then, multiple reforming process types were developed [93]. It can be operated at considerably lower temperatures of around 600°C to 800°C, when compared to the thermochemical processes, which eliminates the requirement of expensive alloys needed for the construction of the reactors. Moreover, in contrast to the physical processes, catalytic reforming helps destroying completely the tar and thereby removes the waste disposal issue. Two types of catalytic reforming exist: steam reforming and dry reforming. Water vapor and carbon dioxide are employed as oxidizing agents in steam and dry reforming, respectively. In both cases, the reforming reactions serve the aim of transforming the hydrocarbons into valuable gases, mainly syngas rich in hydrogen and

carbon monoxide. It is realized by applying heat in the presence of an appropriate catalyst that lowers the reforming temperature and allows the production of selective products [94].

Catalytic steam reforming has been widely applied for the generation of hydrogen H_2 and syngas which are used to produce methanol, ammonia or to directly generate energy. Hydrogen is characterized by being very abundant, nontoxic, nonpolluting and having a high energy density [95]. H_2 is very reactive and largely valuable. It interferes in numerous and important industrial processes such as the synthesis of ammonia, which is the first consumer of hydrogen at the global level. This gas is also used during the petroleum reforming in the steps of hydrotreatment and hydrocracking, and for the hydrocarbon synthesis by the Fisher-Tropsh process [96]. Nowadays, hydrogen is perceived as an alternative fuel with a special interest for fuel cells, which are able to provide a clean energy source for automotive applications replacing diesel and gasoline engines [97]. The fuel cell plays the role of a direct converter of the hydrogen chemical energy into electrical energy and is usually referred to as continuously operating batteries [98].

The production of syngas and hydrogen is most commonly ensured via the catalytic steam reforming of methane (SRM). The methane steam reforming is a strongly endothermic process that is generally operated at above 800°C [99]. It is an industrial cost-effective process that provides around 50% of the hydrogen global demand [100]. Methane is the most abundant natural gas. It is a very stable gas requiring a considerable amount of energy input to be used as a renewable energy source [99]. The steam reforming of methane was firstly used in the United States given the abundant availability of the natural gas as feedstock. In 1930, Standard Oil of New Jersey was the first to implement the SRM for the industrial application [101]. Even though the steam reforming of methane is a well-established process, it suffers from some drawbacks on which multiple research works are still being performed. These studies are dedicated to improve the performance of the catalyst to produce more hydrogen, reduce the carbon deposition and resist to sintering [100].

In this section, the catalytic steam reforming of the biomass tar is the main topic discussed. The steam and dry reforming of methane are first introduced followed by the catalytic tar reforming. Next, the reactor characteristics are defined in terms of the tar reforming parameters and the reactor design. Furthermore, the catalysts used for the tar reforming as well as the catalyst supports are detailed. Following the theoretical section, the experimental results obtained from the catalytic steam reforming of tar products are presented. The effects of the temperature, the catalyst loading and the steam to carbon S/C ratio are investigated on the biomass tar.

1.2.2. Theoretical approach of biomass tar reforming

1.2.2.1. Catalytic steam reforming of methane

During the methane steam reforming process, the methane reacts with the water vapor (as a principal oxidizing agent), with a contact time of several seconds, over a catalyst following the reaction equations **(1.2)** and **(1.3)** in order to produce hydrogen and carbon monoxide. When the reaction is driven in the stoichiometric conditions, the ratio H_2/CO equals 3. If an excess of steam is supplied, the water-gas-shift-reaction (WGSR) (equation **(1.4)**) can take place despite its moderately exothermic nature. This reaction increases the hydrogen production resulting from the oxidation of CO into CO_2 [99] while simultaneously reducing the CO formation. This can be regarded as an advantage given its hazardous impact on human health and environment

[102]. The reactions involved in the catalytic steam reforming process are stated as follows [99]:

Steam reforming of methane SRM 1: $CH_4 + H_2O \leftrightarrow 3H_2 + CO$ $\Delta H°_{298K} = +205.9\ kJ/mol$ **(1.2)**

Steam reforming of methane SRM 2: $CH_4 + 2H_2O \leftrightarrow 4H_2 + CO_2$ $\Delta H°_{298K} = +164.7\ kJ/mol$ **(1.3)**

Water-gas shift reaction WGSR: $CO + H_2O \leftrightarrow H_2 + CO_2$ $\Delta H°_{298K} = -41.1 kJ/mol$ **(1.4)**

Reverse WGSR: $H_2 + CO_2 \leftrightarrow CO + H_2O$ $\Delta H°_{298K} = +41.1 kJ/mol$ **(1.5)**

Boudouard reaction (BR): $CO_2 + C \leftrightarrow 2CO$ $\Delta H°_{298K} = +172\ kJ/mol$ **(1.6)**

As shown from equations **(1.2)** and **(1.3)**, the steam reforming of methane (SRM) reactions represents volumetric expansion reactions and hence the steam reforming is usually operated at low pressure, making it more thermodynamically favorable. Nevertheless, in order to facilitate the overall operation and reduce the reactor size, an operating pressure above 0.5 MPa is adopted in the reactor. Hence, the optimal operating conditions are to be chosen depending on the process scale, the quantity of the desired product and the composition. Additionally, due to the presence of carbon dioxide generated in the process, the dry reforming of methane, described hereafter, might also take place [99].

1.2.2.2. *Catalytic dry reforming of methane*

In this process, carbon dioxide is used as an oxidizing gas of methane instead of the steam according to the reaction in equation **(1.7)** [95]:

Dry reforming reaction: $CH_4 + CO_2 \leftrightarrow 2H_2 + 2CO$ $\Delta H°_{298K} = +247\ kJ/mol$ **(1.7)**

This process is not deprived of interest since, on one hand, it gives a ratio of H_2/CO close to one, useful in processes such as hydroformylation and the reactions of carbonylation and on the other hand, it consumes two greenhouse gases (CO_2 and CH_4). However, this reaction is more endothermic than the steam reforming and requires higher reaction temperatures resulting in the deactivation of the catalyst by sintering of the active phase and by coke deposition. In addition, simultaneously to the basic WGSR, equation **(1.4)**, the reverse WGSR, equation **(1.5)**, takes place, which translates in the conversion of CO_2 being always more important than the conversion of CH_4 but with a H_2/CO ratio inferior to 1 [103].

1.2.2.3. Catalytic tar reforming

The biomass pyrolysis produces, along with char and non-condensable gases, a complex liquid formed by more than 300 compounds. In order to represent the tar as a single product and to integrate it into the chemical reactions involved during the reforming process, the tar chemical formula was simplified by the scientific community of the catalytic reforming. The tar was therefore considered a single hydrocarbon compound having C_nH_x as a general chemical formula. The steam and dry reforming of tar entails the conversion of tar generating several non-condensable gases such as H_2, CO, CO_2… along with other hydrocarbons. The latter can also interact with steam producing additional syngas and other non-condensable gases [104].
During this process, several reactions occur simultaneously and the competition between them leads to the distribution of the products. The reactions are listed as follows [45,104,105]:

Thermal tar cracking: $pC_nH_x(tar) \rightarrow qC_mH_y(smaller\ tar) + rH_2$ $\Delta H > 0$ **(1.8)**

Steam tar reforming: $C_nH_x(tar) + nH_2O \rightarrow (n + \frac{x}{2})H_2 + nCO$ $\Delta H > 0$ **(1.9)**

Dry tar reforming: $C_nH_x(tar) + nCO_2 \rightarrow (\frac{x}{2})H_2 + 2nCO$ $\Delta H > 0$ **(1.10)**

Hydrocarbons (HC) reforming: $HC + H_2O \rightarrow H_2 + CO + CO_2$ $\Delta H > 0$ **(1.11)**

Carbon formation: $C_nH_x(tar) \rightarrow nC + \left(\frac{x}{2}\right)H_2$ $\Delta H > 0$ **(1.12)**

During the catalytic reforming process, these reactions are expected to co-exist. Nonetheless, the reaction conditions as well as the type of catalyst used determine the dominant reaction based on the promoting or inhibiting interactions among the different compounds. According to the catalytic tar-reforming described by equations **(1.8)** to **(1.12)**, it is considered that all tar is expected to be transformed into lighter and simpler molecules like CO and H_2 by steam and dry reforming [45]. Therefore, catalytic reforming presents itself as a promising economical and technical alternative process where gas with a considerably high purity can be obtained in addition to the increase in the heating value of the gas product [48].

1.2.2.4. Carbon formation

One of the major issues faced during the catalytic reforming is the catalyst deactivation, which could be triggered by multiple mechanisms and numerous causes. In reforming reactions, the deposition of carbon or hydrocarbons (also referred to as coking), oxidation, poisoning and sintering are the main causes behind the deactivation of the catalyst. In addition, the carbon formation can lead to technical issues such as increase of pressure drop and blocking of the reactor [106].

It is important to make a distinction between the terms “carbon” and “coke”. Although both terms are sometimes used interchangeably, by default their definition is related to their origin. Carbon is considered the product of CO disproportionation as in the Boudouard reaction (equation **(1.6)**), whereas the term coke refers to the material that originates from the decomposition or condensation of hydrocarbons. Coke usually consists of polymerized heavy hydrocarbons. However, the composition of coke could vary from high molecular weight hydrocarbons to primary carbons such as graphite depending on reaction conditions [104]. Carbon formation results from unfavorable reactions. It appears mainly during the reaction of tar steam and dry reforming according to the equation **(1.12)** [45]. In the case of the methane steam reforming, the carbon deposition produced by the methane decomposition, equation **(1.13)**, and the reverse Boudouard reaction, equation **(1.14)**, [107] is to be avoided.

Methane decomposition (MD): $CH_4 \leftrightarrow C + 2H_2$ $\Delta H°_{298K} = +75\ kJ/mol$ **(1.13)**

Boudouard reaction (BR): $2\ CO \leftrightarrow C + CO_2$ $\Delta H°_{298K} = -172\ kJ/mol$ **(1.14)**

The formation of carbon during the methane reforming can depend on numerous factors and the most important are the following [108]:

- The reaction conditions:
  - Temperature
  - Steam to carbon ratio
- The nature of catalysts:
  - Nature and morphological structure of the catalyst
  - Nature of support
  - Metal-support interaction

To prevent carbon deposition, two approaches have been adopted. The first approach consists in enhancing the steam adsorption on the catalyst surface by using carbon precursors [109]. The steam plays a favorable role via the reactions in equations **(1.15)** and **(1.16)** that express the gasification potential of the carbon deposited on the catalyst by the steam [107].

$$C + H_2O \leftrightarrow CO + H_2 \qquad \Delta H°_{298K} = +131 kJ/mol \quad \textbf{(1.15)}$$

$$CO + H_2O \leftrightarrow H_2 + CO_2 \qquad \Delta H°_{298K} = -41\ kJ/mol \quad \textbf{(1.16)}$$

The second method is by modifying the catalyst by adding other metal additives [109] such as CaO, MgO, K_2O and La_2O_3. The use of these basic promoters helps adsorbing and dissociating CO_2, which is acid, and thus results in reducing the carbon formation rate on the catalyst surface. Moreover, carbon can be oxidized by adding oxygen carriers such as La_2O_3, CeO_2, ZrO_2 thereby decreasing its formation [106]. The use of bimetallic (or trimetallic) active phase systems was suggested by some researchers instead of monometallic ones. They investigated the use of several metals such as Cu, Co, Fe, V, Cr, Rh, Mo, Mn and Sn [107,110]. It was also proposed to add some quantities of noble metals such as Ru and Rh to the transition metals like Co or Ni [111]. Moreover, it was demonstrated that less carbon can be formed when the particle size is smaller [112].

1.2.3. Characteristic parameters of the steam reforming of methane

1.2.3.1. Effect of temperature

The reaction's temperature greatly affects the composition of the methane or tar reforming gaseous products. Knowing that higher temperatures are in favor of endothermic reactions, the temperature augmentation profoundly affects the production of CO, CO_2 and H_2 and strengthens the tar cracking. It is proposed that tars decompose more easily into small molecules such as CO, CO_2 and H_2 with the temperature increase. Regarding the Water Gas Shift Reaction, given its exothermic nature, the temperature elevation becomes adverse for the production of H_2. Due to Le Chatelier's principle, the tendency is directed towards the reactants with the temperature increase. To improve the hydrogen yield efficiency, the temperature must be balanced between the tar conversion and the energy consumption [105].

Several side reactions occur with the dry reforming of methane (DRM), equation **(1.7)**, such as the steam reforming of methane (SRM), equation **(1.2)**, Boudouard reaction (BR), equation **(1.6)**, reverse water-gas shift reaction (RWGSR), equation **(1.5)**, carbon dioxide methanation (CDM), equation **(1.17)**, carbon monoxide hydrogenation (CMH), equation **(1.18)**, and methane decomposition (MD), equation **(1.13)** [106].

Carbon dioxide methanation (CDM):

$$CO_2 + 4H_2 \leftrightarrow CH_4 + 2H_2O \qquad \Delta H°_{298K} = -164.7\ kJ/mol \quad \textbf{(1.17)}$$

Carbon monoxide hydrogenation (CMH):

$$CO + H_2 \rightarrow C + H_2O \qquad \Delta H°_{298K} = -131.3\ kJ/mol \quad \textbf{(1.18)}$$

Practically, the residence time in the reactor is smaller than the interval of time required to attain the theoretical equilibrium. Hence, a catalyst is required to reduce the activation energy and to favor the DRM reaction over the other reactions. As a consequence, the methane dry reforming process is made more economical with the use of a catalyst [106].

Park and colleagues [99] worked on the steam reforming of methane at the lab scale and on the bench-scale using powder- and pellet-type commercial Ni-based catalysts, respectively. The

effect of the temperature on the SRM was evaluated at a pressure of 1 MPa, a gas-hourly space velocity (GHSV) fixed at 4.8 L CH_4/(h.gcat) and a steam/methane ratio equaling to 3, as shown in the **Figure 1.9**. It indicates that the methane conversion increases with the temperature, the expected behavior from the highly endothermic methane steam reforming reactions, equation **(1.2)** and **(1.3)** [99].

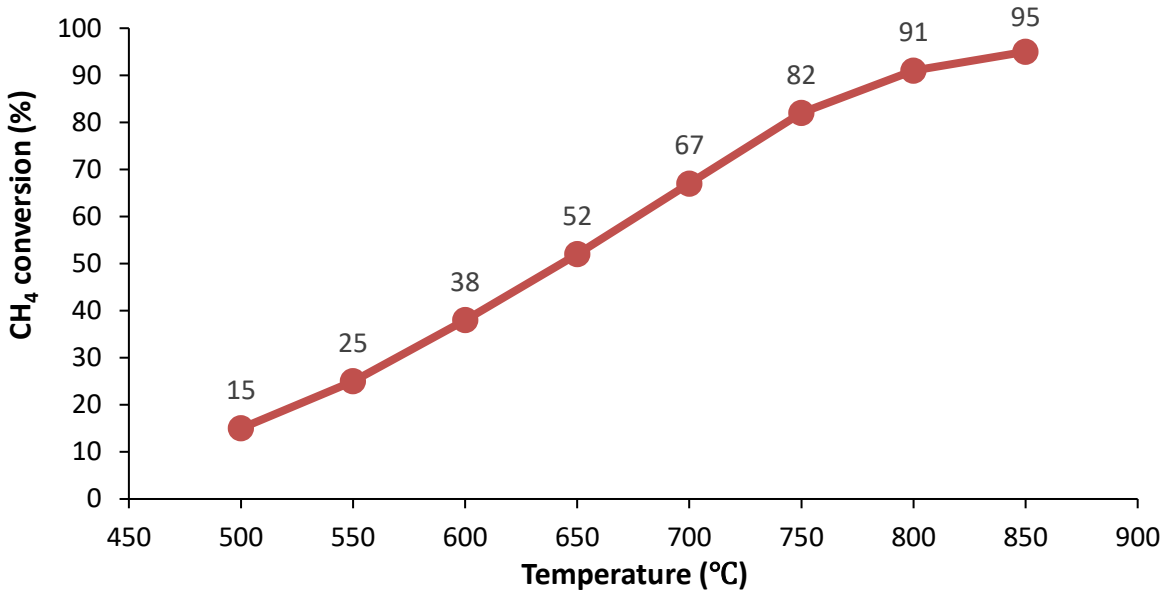

Figure 1.9 Effect of temperature on the methane steam reforming [99]

1.2.3.2. Effect of steam to carbon S/C ratio

The steam to carbon S/C ratio is defined as the ratio between the feed rate of steam for the tar reforming over the feed rate of tar containing carbon. It plays a crucial role in the tar reforming process and its value usually ranges between 0 and 4. It is noteworthy to mention that the increase of the steam supply tends to favor the equilibrium of the tar reforming reaction and WGSR [105]. With a S/C ratio equaling to 1, the steam quantity would be insufficient to ensure the reforming of methane SRM 2 (equation **(1.3))** and the WGSR (equation **(1.4)**). The increase of the S/C ratio helps improve the intensity of these reactions since it greatly affects them. An elevated steam partial pressure ameliorates the steam reforming reaction and the WGSR to increase the formation of hydrogen. This can explain the fact that the increase of the S/C ratio to 2 results generally in a remarkable increase in H_2 and CO_2 yields in opposition to a significant decrease in CO and CH_4 yields. By further increasing the S/C ratio, a huge amount of heat for the reforming is absorbed by the water evaporation into steam, which negatively impacts the hydrogen production in the reforming reactions. Moreover, the active sites present on the surface of the catalyst would be saturated by the excess of water molecules, increasing the reactants partial pressure in the gas stream thus reducing the efficiency of the catalysis [113].

Practically, two issues are usually encountered in the real reforming reactions. On one hand, insufficient steam (i.e. low S/C) can lead to a low hydrogen yield and concentration resulting from incomplete reactions occurring during the reforming. Consequently, the reforming reactions and the WGSR become unable to reach the complete reaction state. When high S/C ratio is applied, sufficient steam can be utilized to drive reforming and cracking of tar with

consequently more elevated hydrogen and gas yields. Moreover, the equilibrium of the WGSR is shifted toward the hydrogen production with higher water partial pressure. In addition, the gasification of carbonaceous intermediates is promoted, reducing the coke formation and deposition on the catalyst. One the other hand, excessive steam has several undesirable effects. Firstly, supplementary energy consumption results from the excessive water, due to the separation of steam and the dryness of formed gas and in the condensation process. Secondly, the excess of steam leads to the absorption of the heat, thus decreasing the reforming temperature resulting in a drop of the tar decomposition. Therefore, an optimal steam to carbon ratio might exist at the different operating conditions [105].

The effect of the S/C ratio on the SRM was determined by Park *et al.* [99] at the reaction temperature of 830°C, a GHSV of 4.8 L CH_4/(h.gcat) and a pressure of 1 MPa, as demonstrated in the **Figure 1.10**. If the SRM was the only involved reaction, the excess of steam would moderately affect the methane conversion, as shown in the equation **(1.2)**. Nevertheless, since the increase of S/C ratio increases the methane conversion as seen in the **Figure 1.10**, then an additional reaction could have occurred which is the WGSR, equation **(1.4)**. It shifts the equilibrium of the SRM in a way that the methane consumption accelerates as the S/C ratio is elevated [99].

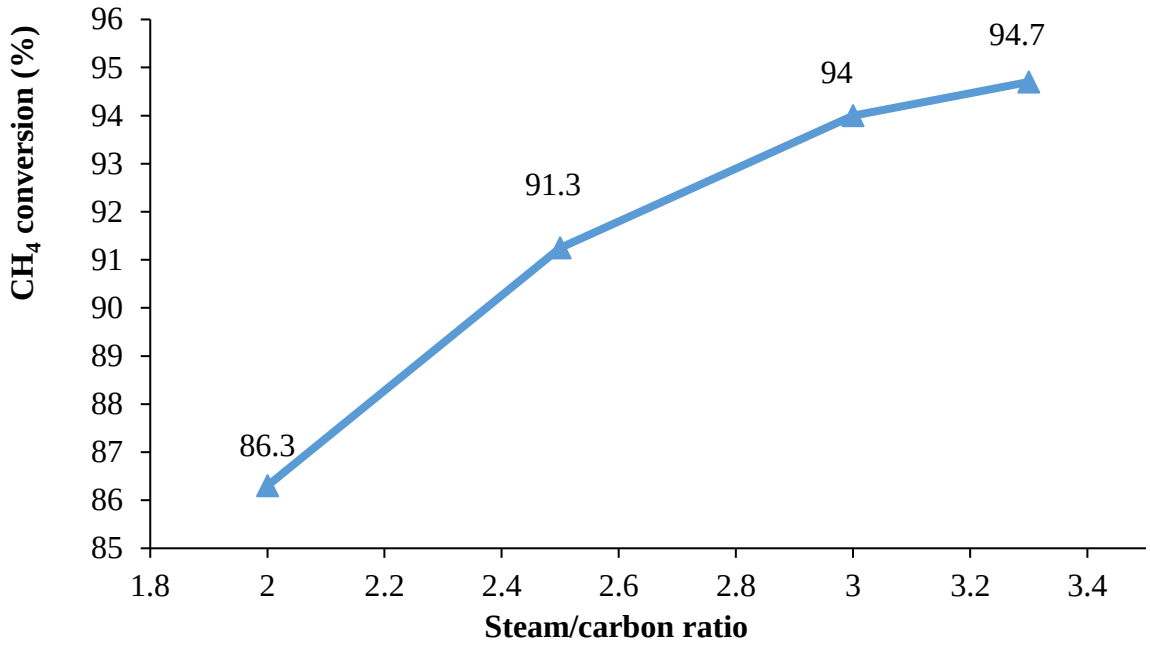

Figure 1.10 Effect of steam/methane ratio on the methane steam reforming [99]

1.2.4. Steam reforming reactor design

Various designs of reactors have been adopted for the steam reforming. Nevertheless, the reactors are mainly classified according to the catalyst bed [114]. The reactor configurations for the steam reforming can be grouped under two main categories: (i) one-step processes including fixed bed, fluidized bed and spouted bed reactors; (ii) two-step processes including two-stage fixed bed reactor and two-stage fixed-fluidized bed reactor [115]. Fluidized and fixed bed reactors have been both used to conduct several studies with both resulting in good yields and high hydrogen selectivity [114]. The five steam reforming reactor configurations are presented in the **Figure 1.11**.

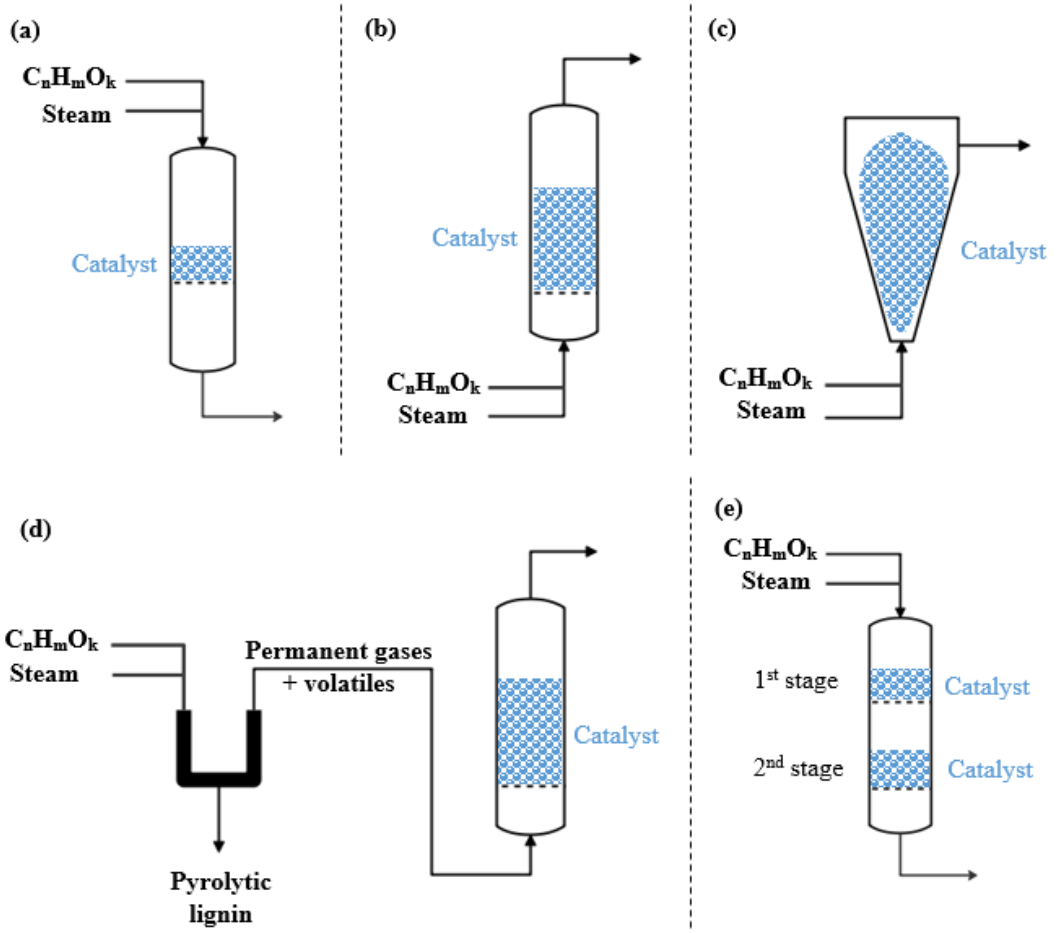

Figure 1.11 Different configurations for the reactors of the steam reforming of biomass-derived oxygenates: (a) fixed bed reactor, (b) fluidized bed reactor, (c) spouted bed reactor, (d) two-stage fixed-fluidized bed reactor, and (e) two-stage fixed bed reactor reproduced from Arregi *et al.* [90]

1.2.5. One-step processes

1.2.5.1. Fixed bed

Methane steam reforming is conventionally realized in a fixed bed reactor (**Figure 1.11** a). Several tubes are used into which the catalyst is loaded and are introduced in a furnace whose operating temperature can go from 527°C up to 807°C. An efficient heat transfer and distribution is required for the extremely endothermic reversible reaction of the steam reforming and hence the process is very challenging and expensive. Furthermore, the effectiveness factor is very low being in the order of 10^{-3} to 10^{-2} hence the limitations of diffusion are very severe. The effectiveness factor is defined as the ratio between the actual reaction rate of the catalyst particles to the calculated rate that would exist in the absence of diffusion limitations [116–118]. Additionally, several drawbacks exist for the fixed bed reactor including huge temperature gradients, small heat transfer rates, limited mass transfer and strong resistance to diffusion in the pores of the catalyst. It should be noted that the heat input efficiency strongly affects the highly endothermic steam methane reforming process [119].

1.2.5.2. Fluidized bed

The fluidized bed (**Figure 1.11** b) represents a bubbling design operating at atmospheric pressure. Pressure taps and thermocouples are inserted along the axis of the fluidized bed

reactor to ensure the measurement of the pressures and the temperatures respectively [120]. Fluidizing the reforming catalyst is possible if the particle size falls into the proper range and if the catalyst is strong enough to endure the mechanical environment inside the fluidized bed reactor. Successful use of the catalyst particles was achieved for average diameters of around 170 to 200 μm and size ranges between 90 to 355 μm. The fluidized bed thermal uniformity was reached at a velocity five times higher than the minimum fluidization velocity [119].

Fluidized bed are characterized by their outstanding mass and heat transfer properties, large variety of operating conditions, excellent gas/solid contact, uniformity of the catalyst bed, and capability of producing elevated efficiencies [119,121]. In addition, it has the ability of shifting the thermodynamic equilibrium of the steam reforming reactions as well as realizing the reaction and the product separation simultaneously. The fluidized bed reactor has a more compact design in comparison to the fixed bed reactor and it can virtually eliminate the limitations of diffusion along with enhancing the selectivity and conversion [122]. Furthermore, fluidized bed processes have a strong ability to mitigate the deactivation of the catalyst which is especially motivating for feeds heavier than methanol, ethanol, butanol and bio-oil. These products are more susceptible to the thermal degradation and lead to high amounts of coke deposition on the catalyst [123]. Thereby, fluidized bed reactors are acquiring increasing attention and their field of application is extending specially in the industrial, chemical and environmental processes [121].

Despite the fluidized bed ability to produce high H_2 yields (more than 80% of the maximum stoichiometric) and to perform a full conversion in the steam reforming of oxygenates (including biomass), the coke deposition and thus the catalyst deactivation remains a severe drawback of the fluidized bed [123].

1.2.5.3. Spouted bed reactor

The spouted bed reactor (**Figure 1.11** c) was developed to mitigate the problem of coke deposition encountered with the use of fluidized bed. No coke was deposited when this reactor was evaluated for the steam reforming of the aqueous fraction of bio-oil [124]. It was implemented after modifying the reactor by using an injection nozzle specially designed [125]. This reactor was demonstrated to be very successful leading to a competent processing of ethylene glycol, chosen as a bio-oil model component. It was noticed that the coke formation is drastically low for three types of material tested (olivine, Ni/olivine catalyst and sand). The coke deposition is minimized in a spouted bed reactor thanks to advantageous hydrodynamics particularly in the catalyst continuous recirculation where the catalyst is exposed to changing reaction atmospheres [124].

1.2.6. Two-step processes

In the purpose of avoiding the issue of carbon formation and coke deposition in the bio-oil steam reforming processes, thereby leading to the deactivation of the catalyst, some works included the use of two-stage reactor configurations.

1.2.6.1. Two-stage fixed-fluidized bed reactor

A two-stage thermal-catalytic system (**Figure 1.11** d). was used to study the steam reforming of raw bio-oil [126–128], bio-oil/ethanol mixtures [129,130] and bio-oil aqueous fraction [131–133]. In this system, some bio-oil compounds were repolymerized in the first stage leading to the deposition of “pyrolytic lignin”. The second stage consisting of a fluidized bed was

dedicated for the in-line reforming of gases produced in the first reactor along with the treated bio-oil.

1.2.6.2. Two-stage fixed bed reactor

Several authors have performed the steam reforming in a two-stage fixed bed reactor (**Figure 1.11** e). Yao *et al.* [134] firstly volatilized the bio-oil aqueous fraction at 400°C in a first fixed bed rector and then performed the reforming in a second fixed bed reactor over modified Ni/Al catalysts. Wu *et al.* [135] aimed at avoiding the direct contact between the catalyst and the bio-oil and therefore they relied on a two-stage fixed bed reactor system. In a first stage, dolomite was employed as catalyst for the reforming of bio-oil and in the second stage, the purification of the volatiles was realized using Ni/MgO catalyst.

1.2.7. Catalysts and their supports for the catalytic steam reforming

1.2.7.1. Catalysts for steam reforming

The key to the success of the catalytic steam reforming is the choice of an effective catalyst. For this purpose, a wide selection of catalyst has been adopted going from natural minerals and alkaline earth to metal catalysts [105]. For an efficient steam reforming, various metals can be employed counting noble metals (rhodium Rh, palladium Pd, platinum Pt), base metals (cobalt Co, iron Fe, nickel Ni) or their combination forming the so-called transition metals. For instance, although Rh is highly active and resistant to carbon deposition, it is rarely used at the industrial scale given its high cost, which is the case of all noble metals [8]. On the other hand, a particular attention has been attributed to nickel-based systems among the transition metals. Compared to noble metals, nickel-based catalysts are less expensive and more available which attract their application on the industrial scale. However, their major drawback resides in their deactivation resulting from the coke deposition and the metallic phase sintering under certain operating conditions [104].

To improve the coke resistance of Ni-based catalysts, multiple parameters can be adjusted including the catalyst preparation method, the insertion of promoters into the catalyst structure, the support characteristics and its metal concentration. In fact, adding some metals such as magnesium in the support structure creates basic oxides which enable Ni catalysts to chemisorb oxidants like CO_2 and H_2O, thereby decreasing the coking [111]. Modifiers such as Fe, Pt, Cu, CaO, ZrO_2, CeO_2 and MnO_x are also adopted to enhance the Ni catalysts [8].

Based on the catalyst properties, the most convenient catalyst can be chosen according to several criteria [45,104]:

- The catalyst stability and reusability
- Moderate pressure drops during operation
- The catalyst efficacy of tar reforming
- The catalyst mechanical and thermal strength
- The economic cost and availability for industrial deployment
- The capability of the catalyst to deliver suitable syngas ratio for a specified application
- Efficiency in reforming of aromatic compounds and heavy hydrocarbons
- Resistance to deactivation caused by impurity coking, sintering and fouling.

1.2.7.2. Bimetallic catalysts for steam reforming

Improving the metal dispersion is an essential feature in order to limit the catalyst fouling, taking place at high temperatures in general. Interestingly, the use of bimetallic catalyst entails higher activities than monometallic catalysts due to the co-existence and good dispersion of the

metals [136]. The alloys of Ni, Co and Fe have been commonly adopted and proven to be very promising for the catalyst steam reforming of tar [137]. The important catalytic activity and the resistance to coking characterize these alloys.

- **Nickel-Iron bimetallic catalysts**

Amongst the numerous bimetallic catalysts used for the steam reforming of biomass tar and its model compounds, the nickel-iron Ni-Fe bimetallic catalyst has been largely explored. The synergistic effect between Ni and Fe during tar reforming strongly impacts the catalyst performance. Water molecules are activated by the Fe sites which produces adsorbed oxygen while C–C and C–H linkages are activated in the hydrocarbons by the Ni sites. Incorporating iron to nickel increases the coverage of oxygen compounds due to the stronger iron-oxygen affinity than nickel-oxygen. Therefore, the formation of coke can be restrained by the rapid reaction of the carbonaceous products existing on the neighboring Ni sites and the oxygen atoms available. The uniformity of the Ni-Fe alloy structure is a key factor needed to improve the catalyst selectivity to produce the wanted products as well as to minimize the carbon formation [104,137].

- **Nickel-Cobalt bimetallic catalysts**

The alloy of cobalt with nickel presents itself as an alternative effective catalyst for the tar removal. The similarity in the Ni and Co atomic radius favors the creation of Ni-Co alloy nanoparticles generating a synergistic effect between these two metals. The Co sites can efficiently restrict the reactions of tar decomposition and CO disproportionation causing the coke formation. Unfortunately, the oxidation of cobalt species produced Co oxides which leads to deactivation of the Ni-Co alloy catalyst. Subsequently, the exact amount of cobalt doping over nickel is crucial to reach a steady catalytic activity along with suppressed coke deposition. The synthesis method also impacts the uniformity of the nickel-cobalt bimetallic catalyst similar to the nickel-iron alloy [104,137].

1.2.7.3. Catalysts supports for catalytic reforming

In the tar steam reforming, both reactants, the tar and the steam, must be activated by the catalyst used. The balance between the reactants strongly controls the activity and stability of the catalyst [137]. In general, a support is employed for the catalysts used for the tar removal where the cost-effective material such as silica, carbon or alumina is adopted to disperse the metal catalyst. The catalyst support provides a strong linkage with the catalyst inhibiting the leaching out of the active metal. It also delivers acidic and basic centers, oxygen vacancy and enhance the performance of the catalyst [137]. The nature of the catalyst and its support significantly affect the performance of the steam reforming process, along with reaction conditions. It also has a strong impact over the conversion of the raw materials and the influence the selectivity of the products [138]. In addition, the mechanisms of the steam reforming are markedly determined by the surface properties of the catalyst support [139,140]. In some cases, the support itself might act as a catalyst such as the zeolites [45]. The following parts describe some supports and identify the impact of their properties on overcoming these drawbacks.

- **Particle bed supports**

Small particles have been employed as catalyst support given their ability to expand the active sites' density [113]. The good activity and stability of the particle catalysts make them one of the most widely used catalyst supports for the steam reforming of not only methane but also tar and aromatic products (benzene, toluene, naphta…). The most common Ni-based catalyst

supports are particles of minerals (MgO, ZrO_2 and olivine), alumina (Al_2O_3) and alumina modifiers (α-Al_2O_3 and γ-Al_2O_3) [141].

1) Al_2O_3 based support

Alumina Al_2O_3 is extensively used for the tar reforming as Ni-based catalyst support, being available, mechanically strong, and chemically/physically stable, with a considerable ability to disperse the active metal phase. Alumina modifiers α- and γ-Al_2O_3 are often exploited for toluene steam reforming [142]. The use of alumina alone as support leads to coke deposition over its surface, sintering the metal catalyst. The surface properties of inorganic substance such as zeolites, silica and alumina can be adjusted by applying silylation on the metal oxide surface which improves the hydrothermal stability of the support during the steam reforming process [143]. Another alternative solution to improve the thermal stability is to dope Al_2O_3 in SiO_2 or Fe_2O_3 whose presence generates strong acids. These latter promote the tar cracking and the conversion reactivity of the different compounds reformed (toluene …) [144]. Furthermore, redox metal oxides including ZrO_2 or CeO_2 can also be used to dope alumina. Zr and Ce presence cover the acidic sites and lower their densities [145]. A substitute method to the modification of the alumina support can be the use of Ca, La and La/Ce hexa-aluminates based supports [146]. They are distinguished by their large surface area, good metal dispersion and favor the synergistic effect between the metal catalyst and its oxide support [147].

2) Silica based catalyst support

For high reforming temperatures, Silica SiO_2 is one of the most commonly employed support given its large availability, high thermal stability, big surface area and good resistance to metal sintering. Unfortunately, in environments of high steam reaction produced at elevated steam reforming temperatures, silica supports can leak. Thus, for commercial applications, the use of silica is limited to minimal amounts [137]. SBA-15 mesoporous silica has also been largely employed due to its big surface area and hexagonal, uniform and ordered pores. SBA-15 can be modified as well with La and Ce which improves the support's stability and the oxygen mobility in addition to inhibiting cracking of big molecules [148]. Despite of these ameliorations, Silica-based catalyst supports are still less implied in the biomass tar reforming than alumina supports.

3) Biochar based support

Biochar is one of the products formed during the biomass gasification and pyrolysis. Thanks to its thermal stability, big surface area, large pore volume and the availability of its surface active sites, biochar has been investigated as catalyst for tar reforming [149]. Biochar is therefore the cheapest product employed as catalyst support. Char can be activated into carbon and used as catalyst support given the stability of the activated carbon formed under basic and acid environments [150,151]. Lately, biochar is being assessed by numerous researchers mostly for biomass pyrolysis and gasification for commercial applications [152] and for producing biodiesel [153].

4) Other supports

Numerous different catalyst supports are applied for the tar steam reforming including mixed oxide, natural minerals, perovskite and core-shell among others [137]. The $NiTiO_3$ mixed oxide permits the co-existence of smaller particles since it is very active and more resisting to sintering and catalyst deactivation during the ethanol steam reforming [154]. Olivine, $(Mg_xFe_{1-x})SiO_4$, a mineral present in nature, is a support largely used in the biomass steam reforming

[155]. Oxides derived from perovskite have lattice oxygen and many oxygen vacancies useful for the steam activation thus improving the hydrocarbons oxidation, the thermal stability and the redox property [156]. Core shell catalysts such as Ni@ZrO_2 help increase the number of surface-active oxygens, reduce the metal sintering and extend the interfacial perimeter of the metal-support. This facilitates the carbon deposit removal during the steam reforming of ethanol [157].

- **Monolithic catalyst support**

The Ni-based monolithic catalyst is as innovative catalyst characterized by its excellent resistance to coke deposition. It is prepared by impregnation of MgO and NiO over cordierite catalyst support. Its advantageous features include large surface area, smaller pressure drops pellets catalyst used in fixed bed-reactors [158] as well as being mechanically strong and highly efficient for catalyst recycle. Moreover, monoliths can withstand elevated temperatures, be effortlessly oriented in a reactor with numerous design options [159].

- **Ceramic foam as catalyst support**

Ceramic foams as catalyst carrier are a three-dimensional cellular lightweight solid with a network of ceramic interconnected ligaments. They are known for their large porosity, robust thermal stability at high temperatures, moderate pressure drop, high specific heat capacity, strong ability for thermal isolation and dual scale specific surface area [46]. Thanks to all these favorable physical properties, ceramic foam can be used as monolithic catalyst support for tar reforming. The tar removal rate can be potentially increased and the production of hydrogen largely enhanced [105].

Additional descriptions of the numerous catalyst supports introduced previously are present in the review papers of Abou Rjeily *et al.* [104] and Ashok *et al.* [137] and book chapter by Abou Rjeily *et al.* [160]. An overview of the main catalysts and their supports applied for the catalytic steam reforming of methane and tar compounds as well as their advantages and drawbacks can be found in form of a summary table in Abou Rjeily *et al.* [104].

1.2.8. Experimental studies for catalytic reforming

1.2.8.1. Biomass fuel gas reforming over NiO/ceramic foam catalyst

Quan *et al*. [113] studied the catalytic steam reforming over monolithic NiO/porous ceramic catalyst for the production of high-quality syngas from biomass fuel gas in a fixed-bed reactor. They investigated the influence of the temperature, the S/C ratio and the nickel loading on the catalyst performance. Usually, nickel is loaded on powder- or pellet- type catalyst support. Recently, monolithic catalyst has emerged as an interesting catalytic type given its strong resistance to coke deposition, high mechanical strength and elevated effectiveness for catalyst recycling. Porous ceramic, one of the monolithic catalyst supports, is loaded with NiO and employed for the reforming and upgrading of mixed model compounds of syngas. The composition of the model biomass fuel used for their study is as follows: 40 vol% CO_2, 30 vol% CO, 20 vol% H_2 and 10 vol% CH_4 [113].

1.2.8.2. Effect of reaction temperature on the steam reforming of biomass fuel gas

The effect of temperature on gas composition using the NiO/monolithic porous ceramic catalyst was evaluated in the presence of steam by varying the temperature from 550°C to 900°C while fixing the S/C ratio at 2 with 2.5% metal loading, as shown in **Figure 1.12**. It is remarked that the temperature modifies the gas compositions. For instance, H_2 yield increased when the

temperature was raised from 550°C to 700°C where it reached a peak of 42.2% after which it decreased with the further increase of the temperature. Controversially, CO displays an opposite trend to that of H_2 where it reached a minimum at 700°C. On the other hand, the CO_2 decreased as the temperature increased from 550°C to 900°C. The CH_4 yield decreased drastically from 11.5 to 0.2% from 550°C to 900°C indicating that the CH_4 was remarkably converted by the NiO/monolithic porous ceramic catalyst through the reforming of the model biomass fuel.

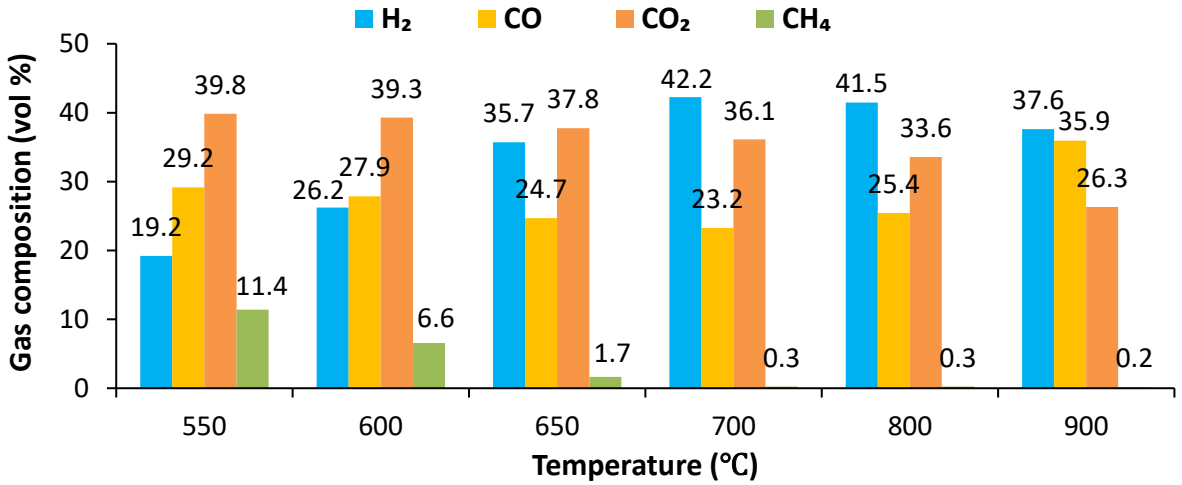

Figure 1.12 Effect of reaction temperature on the gas composition from the steam reforming of bio-fuel gas at S/C =2 and 2.5% metal loading [113]

The main reactions involved in the catalytic steam reforming of the mixed bio-fuel gas are those previously stated in equations **(1.2)** to **(1.4)** and equation **(1.7)**. The fact that the H_2 yield increased while that of CO and CH_4 decreased when the temperature was raised from 550°C to 700°C, reveals that the steam reforming reaction and WGSR are dominant for this temperature range when the reforming is done over NiO/monolithic porous ceramic catalyst. The CO_2 decrease can be rooted to the fact that the amount of CO_2 generated during the steam reforming reaction and the WGSR is inferior to its consumption by the dry reforming reaction. Regarding the results obtained between 700°C and 900°C, it can be deduced that the reverse water gas shift reaction was promoted which is thermodynamically favorable at high temperatures [113].

1.2.8.3. Effect of S/C ratio on the steam reforming of biomass fuel gas

The effect of the S/C ratio was studied at 700°C using 2.5% NiO/monolithic porous ceramic catalyst. The S/C ratio was regulated by modifying the steam amounts. The variation of the gas composition in function of the S/C ratio is demonstrated in **Figure 1.13**. H_2 yield increased from 28.1 to 40.2% with the increase of S/C ratio from 1 to 2, but it remained almost constant with the further increase of the S/C ratio. The CO_2 yield increased from 25.1% to 40% when the S/C ratio was raised from 0 to 3, while the CO yield dropped down from 44.8% to 18.6%. CH_4 yield slightly decreased from 2.1 to 0.3% when the S/C ratio increased from 1 to 2, after which it remained almost stable. Further increasing the S/C ratio from 3 to 4 slightly impacted the variations of the different gases.

At S/C ratio of 1, the water steam amount is inadequate for the steam reforming and water-gas shift reactions. The intensity of these latter reactions can be enhanced with the increase of the S/C ratio. Consequently, the increase of the S/C ratio from 1 to 2 leads to a remarkable elevation of the concentrations of CO_2 and H_2 on one hand and a dramatic decrease of CH_4 and CO on the other hand. In fact, a very high S/C ratio results in the absorption of a big amount of heat

for the evaporation of water into steam for the evaporation, badly affecting the hydrogen production through the reforming reactions. Moreover, the active sites present on the catalyst surface would be occupied by the excess of H_2O molecules reducing the catalysis efficiency [113].

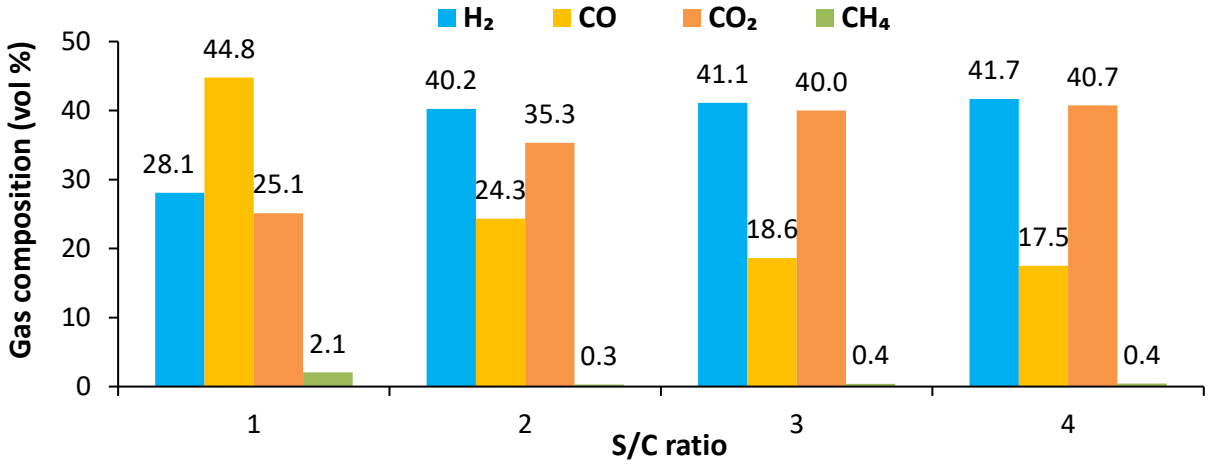

Figure 1.13 Effect of S/C ratio on the gas composition from the steam reforming of bio-fuel gas at 700°C and 2.5% metal loading [113]

1.2.8.4. Effect of metal loading on the steam reforming of biomass fuel gas

The influence of the metal loading on the gas yields from the seam reforming of model biomass fuel gas was investigated at 700°C and S/C ratio of 2 as demonstrated in **Figure 1.14**. Significant changes in gas composition can be noticed after the augmentation of NiO loading. Generally, an increasing trend was demonstrated by the CO concentration whereas a decreasing tendency was remarked for the CH_4 and CO_2. The H_2 content went through an increase and peaked at a metal loading of 2.5% followed by a decrease as the metal loading was further increased. When a high loading of NiO is applied, the dispersion of metal can be attenuated, and active sites would be more aggregated reducing the catalyst efficiency. Hence, for the steam reforming of bio-oil or biofuel, the more suitable is to apply a lower metal loading amount. The major reason behind the decrease of the CH_4 and CO_2 yields can be speculated to be the occurrence of the dry reforming reaction [113].

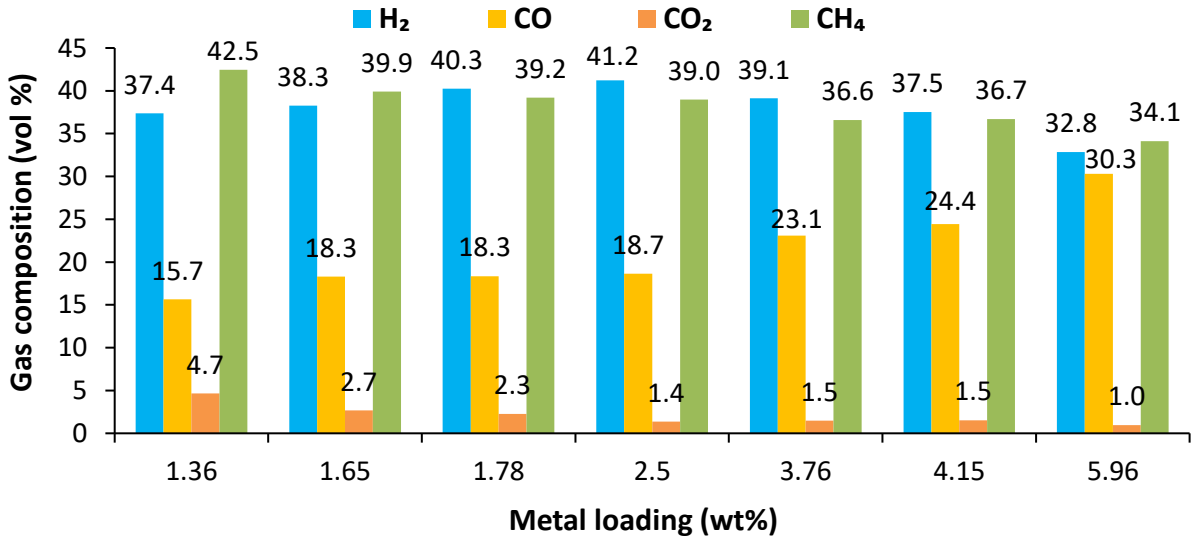

Figure 1.14 Effect of metal loading on gas composition from steam reforming of bio-fuel gas at 700°C and S/C =2 [113]

1.3. Coupling of Biomass Pyrolysis and Catalytic Reforming

1.3.1. Definition and background

Several well-established processes exist to produce syngas involving solid fuels' gasification, heavy oil residues' partial oxidation, hydrocarbons' steam reforming [161]. The gasification consists on converting the biomass or any solid fuel such as charcoal, to syngas via a partial oxidation at high temperatures [162]. For syngas production by gasification, renewable lignocellulosic biomass has been considered. However, the use of inexpensive coal and other hydrocarbons such as C_2-C_5, naphtha, and natural gas have been favored due to the lower cost of the processes. Pyrolysis, on the other hand, has been identified as one of the most promising thermochemical conversion technologies capable of converting local, abundant and inexpensive lignocellulosic biomass into useful products with a low capital investment [47]. A lot of work has been realized to improve the properties of the bio-oil derived from the biomass pyrolysis through catalysis [163]. However, in most applications, the bio-oil effectiveness has been hampered by the presence of water and oxygenated organic compounds [164]. Thus, the pyrolytic oil must be chemically modified by removing and modifying the undesired products, mainly those containing oxygen. This aims at reaching a high hydrogen-to-carbon (H/C) ratio and low oxygen-to-carbon (O/C) ratio which indicate a higher quality liquid product [47].

Catalytic steam reforming is touted as an attractive method for not only tar cracking but syngas production as well. It removes the tar by converting it simultaneously to valuable gases by tar oxidation in the presence of steam. The use of a catalyst lowers the operating temperatures compared to those applied for non-catalytic reforming [94]. Based on the deep studies performed on the subjects of pyrolysis from one side and catalytic reforming on the other side, it can be stated that despite the multiple advantages of these processes and their high productivity, areas of improvement still exist in order to ameliorate the yield of biomass conversion and the production of syngas.

One promising route for the syngas production from the biomass would be the combination of the biomass pyrolysis with the catalytic reforming of the pyrolysis volatile products in a two or multi-stage reactor. The pyrolysis taking place in the first stage yields a set of hydrocarbon gases, oxygenates and tar that will be catalytically reformed subsequently in the second stage [165,166]. Thereby, the coupling of the pyrolysis with the catalytic reforming is a relatively young technology that has been demonstrating good performance in terms of tar removal and syngas production.

The combination of the pyrolyzer to a catalytic converter termed "Pyrocat" was first developed by Parker in 1988 [167] to determine the heat of the volatiles combustion and to evaluate the kinetic parameters of the combined process. The coupling of the pyrolysis with the catalytic reforming, also referred to as "pyrolysis-catalytic reforming", is therefore a relatively recently emerging approach that has been adopted in several applications. For instance, the field of the bio-oil production from the biomass via the coupling of the catalytic reforming to the pyrolysis has been considered few decades ago [168]. It was first investigated theoretically by simulation and has been tested experimentally, then proven to be highly effective and was put into application.

Wang and fellows [161] considered the process combining the lignocellulosic biomass pyrolysis to the pyrolytic oil reforming as a cost competitive strategy for the production of hydrogen when compared to conventional methods. They performed thermodynamic modelling

and simulation on Aspen Plus software of the main bio-oil model compounds. It has shown the possibility of the reforming for a large range of operating temperatures and steam to carbon S/C ratios. Moreover, screening tests were realized to catalytically reform model compounds of the bio-oil into hydrogen. The experiments were realized over Ni-based catalysts in a vertical dual-bed quartz reactor connected to a molecular beam mass spectrometer (MBMS). They demonstrated a capacity of a total conversion into hydrogen [161].

For biomass, the process of pyrolysis-catalytic steam reforming is realized in a two-stage reactor. The biomass hydrocarbons are cracked during the pyrolysis process in the first stage and the products are subsequently subject to the steam reforming over a an appropriate catalyst in the second stage [169]. For instance, Al-Rahbi and Williams [170] investigated the pyrolysis-catalytic steam reforming of biomass waste for the production of a hydrogen-rich gas. They used ashes derived from the combustion of waste tires, coal and refuse-derived fuel as catalysts since they are rich in minerals (Zn, Na, K, Fe, Cu, Mg, Ca and Al). In addition, the ashes were impregnated with 10 wt.% Nickel in order to test its impact on the hydrogen production.

The main gases produced consisted of CO, H_2, CO_2, CH_4 and C_2H_4. It was found that the presence of the ash samples increases considerably the total gas yield and the hydrogen yield. In the presence of coal ash, the total gas yield increased to 50.3 wt.% from 39.9 wt.% in the presence of clean quartz sand. With refuse-derived ash, the total gas yield augmented to 59.5 wt.% for which the highest hydrogen yield was produced and was equal to 7.9 mmol/g biomass which corresponds to 29.73 vol.%. Adding Nickel to the combustion ash samples enhances catalytic steam reforming of hydrocarbons such as methane and ethylene and the hydrogen yield was further increased by around 20 % [170].

The topic of pyrolysis has been largely evaluated and deeply studied since decades and some important reviews have been reported [171–174]. The catalytic reforming is a more recent subject that has been attracting the attention in the last decades with some reviews published [175–179]. Nevertheless, the reviews that address both the biomass pyrolysis and the catalytic reforming are missing from the literature. So far, the scientific communities study pyrolysis and catalytic reforming separately whereas it appears clearly important to investigate them jointly. Furthermore, in general, the reviews on the discussed topics covered essentially the state of the art for the theoretical aspects of these processes, their operation conditions, the development of the reactors and the optimization procedures. However, rare are the reviews that report the experimental results obtained and the influence of the operating parameters on the products' distribution. We realized a review paper on the subject [104].

The ultimate purpose of this thesis is the production of high added value products, mainly syngas, through the combination of the biomass pyrolysis and the catalytic reforming of the pyrolysis hydrocarbon volatiles, with the principle illustrated in the schematic representation in **Figure 1.15**. This section aims at discussing the reactors design for the process combining the biomass pyrolysis and catalytic reforming followed by an analysis of some experimental results obtained on the subject.

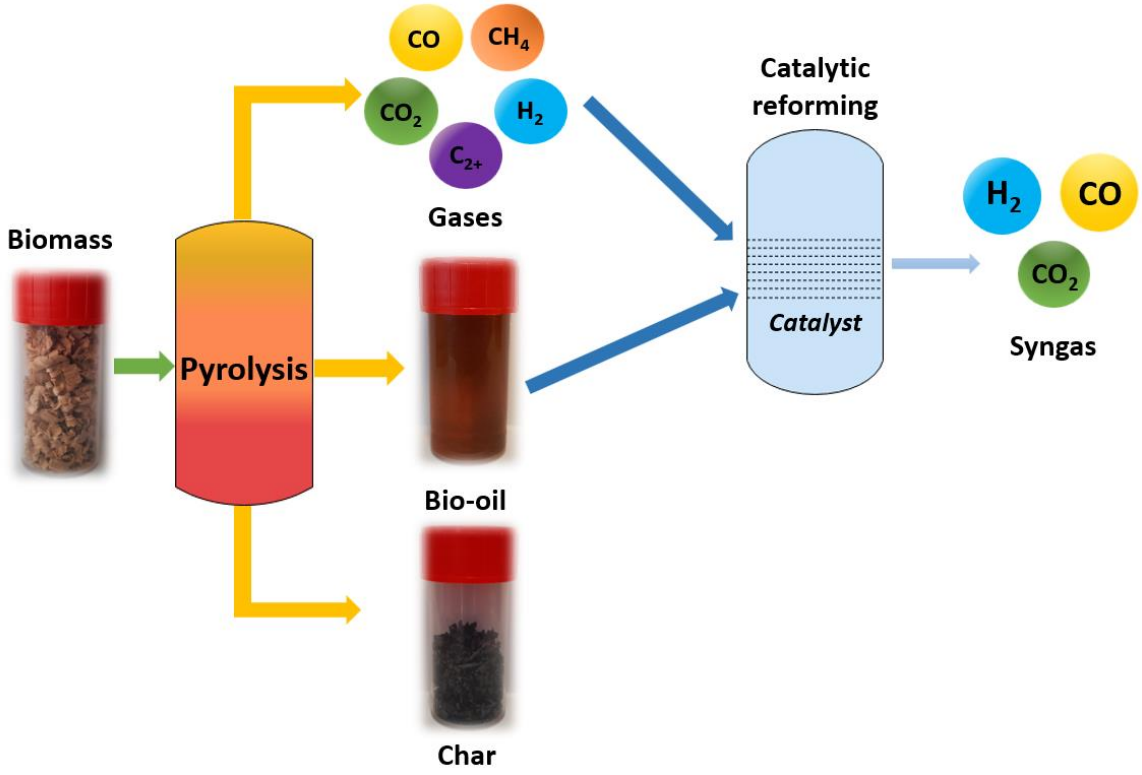

Figure 1.15 Schematic representation of the combination of the pyrolysis and catalytic reforming process. Pyrolysis of biomass produces char (a black solid), bio-oil (a viscous dark liquid) and multiple non-condensable gases: CO_2, CO, CH_4, H_2 and C_{2+} (hydrocarbons with more than 2 carbons in their chemical structure). These gases and the bio-oil hydrocarbon molecules can undergo catalytic reforming in the presence of a catalyst. This process leads to the production of syngas (H_2, CO, and CO_2)

1.3.2. Reactor design of the pyrolysis-catalytic reforming process

A two stage in-line pyrolysis-reforming process has been envisaged as an appropriate configuration for the production of hydrogen through valorizing the biomass. This design is characterized by the two separated stage reactors offering a higher versatility and a recently increasing interest [90,180]. Different configurations of the two-stage reactors are presented in **Figure 1.16**.

The two-stage fixed bed (or fixed-fixed bed) reactor (**Figure 1.16** a) was operated for the pyrolysis and reforming of biomass and plastics mixtures [181,182], in a discontinuous operation mode. It was also employed in a continuous mode for the pyrolysis-reforming of cellulose [183], wheat straw and sugar can bagasse [184], biomass feedstock, wood sawdust primarily [185,186] and rice husk [187,188]. The second configuration is a fluidized–fixed bed reactor (**Figure 1.16** b) that is designed for improving the heat and mass transfer during the pyrolysis. The bed in the pyrolysis step was fluidized by silica sand and was continuously fed with the biomass sample from the lower part of the system. The tar reforming step took place in the upper stage fixed bed with a commercial catalyst (Ni/Al_2O_3) and a recently prepared catalyst of Ni-loaded brown coal char [189,190]. A screw-kiln reactor was used in another innovated configuration for the continuous pyrolysis of biomass while the reforming was maintained in a fixed bed reactor **Figure 1.16** c). This configuration was functioned for both biomass [191] and municipal solid waste [192]. An intermediate entrained flow gasification step was introduced between the initial fluidized bed of the pyrolysis and the final fixed bed of the reforming to enhance the two-step configuration [193] as shown in the **Figure 1.16** d).

As discussed previously, one of the main drawbacks of the fixed bed reactor is the coke deposition leading to the bed blockage, which might lead to a severe limitation in the scaling up of the reactor [194]. To mitigate these operational issues, the fixed bed reactor was replaced by a fluidized bed reactor for the reforming step. Czernik and French [195] were among the pioneers to operate with continuous fluidized bed reactors for both the pyrolysis and the reforming steps of polypropylene. Several works were subsequent to improve the performance of the system. For the pyrolysis step, a conical spouted bed reactor (**Figure 1.16** e) was employed given its enhanced heat and mass transfer properties. It also allows avoiding the defluidization of the bed by the vigorous cyclic movement. Succeeding, a fluidized bed was used for the catalytic reforming which was applied for the biomass [196,197], plastics [198,199] and mixtures of biomass and plastic [200]. The conical spouted bed reactor is convenient for operating with particles of fine size, irregular texture, or even solids of sticky nature or having a large size distribution. This generates a vigorous contact between the gas and solid ameliorating the mass and heat transfers among the phases thus reducing the gas residence time to the order of some milliseconds. In addition, continuous operation is facilitated by the conical spouted bed reactor which is particularly interesting for large scale operation of the biomass pyrolysis [201]. Thanks to this design, the continuous operation of the process is possible for extended durations and without functional issues, thereby a significant enhancement was realized allowing a scaling up in the near future [90]. Nevertheless, the spouted bed reactor faces some limitations such as small volatiles residence time, high capital cost, difficulties in the catalyst's feeding and entraining as well as complicated retrieving of the products.

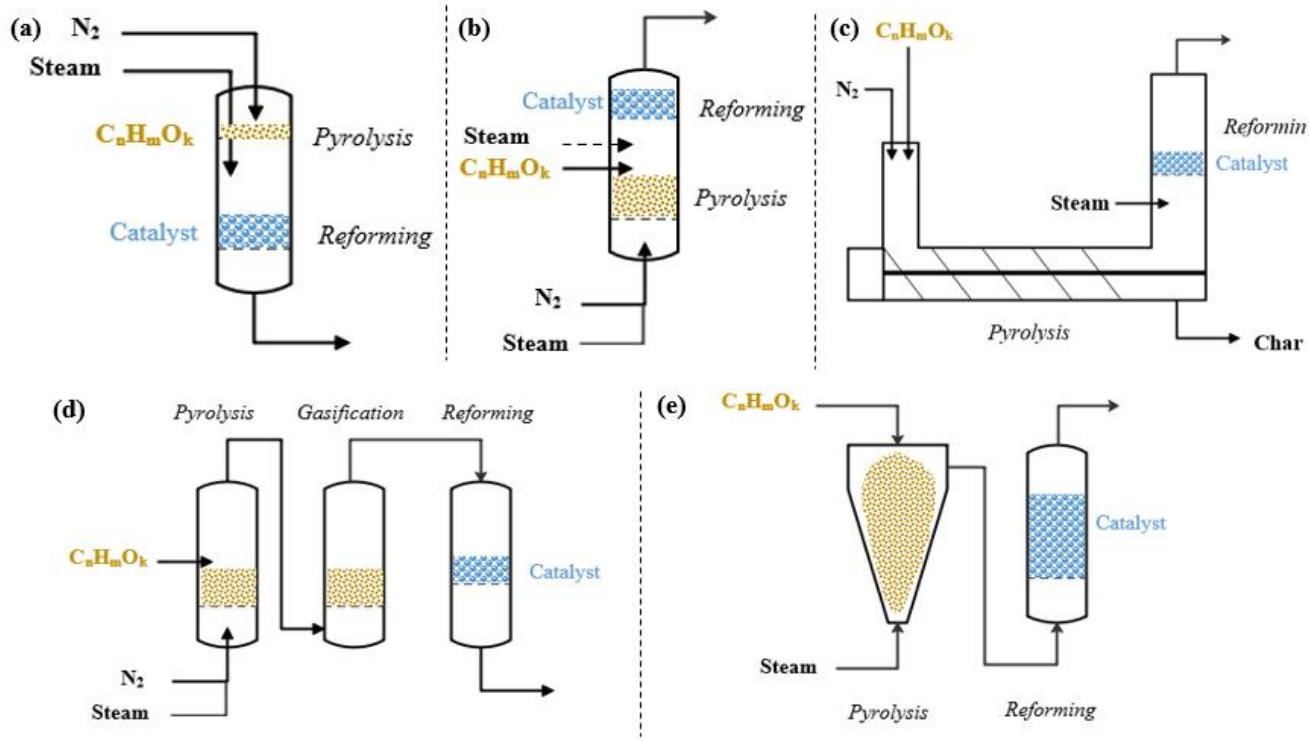

Figure 1.16 Several designs for the reactors of the in-line pyrolysis and catalytic reforming of biomass which represented by $C_nH_mO_k$ (a) two-stage fixed bed reactor, (b) fluidized – fixed bed reactor, (c) screw-kiln – fixed bed reactor, (d) fluidized bed, entrained flow gasification and fixed bed reactor, and (e) spouted bed – fluidized bed reactor (adapted from [90,180])

Table 1.4 summarizes some applications of the pyrolysis-catalytic reforming approach with the reactors used as well as the operating temperatures and hydrogen yields. The classification is made by increasing order of the hydrogen yield. As remarked, the highest hydrogen yield was

obtained for the pyrolysis of pine wood in a spouted bed reactor at 500°C while the reforming of the pyrolysis vapors was performed in a fluidized bed reactor at 600°C using Ni commercial as catalyst.

Table 1.4 Review of works on the coupling of the pyrolysis and the catalytic reforming with the relative feeds and temperatures as well as the reforming catalyst and the hydrogen yield.

Pyrolysis			Reforming			Reforming catalyst	H_2 yield (g/kg)	Ref
Reactor	Feed	Temperature (°C)	Reactor	Feed	Temperature (°C)			
Fixed bed	Wood sawdust	500	Fixed bed	Pyrolysis volatiles	800	Ni-Ca-AlO_x	31	[186]
Fixed bed	Pine wood	700	Fixed bed	Pyrolysis volatiles	650	Ni-coal char	52	[202]
Fluidized bed	Timber wood	600	Fixed bed	Pyrolysis volatiles	850	Ni-MgO commercial	76	[193]
Fixed bed	Pine wood	650	Fixed bed	Pyrolysis volatiles	650	Ni-coal char	100	[190]
Spouted bed	Pine wood	500	Fluidized bed	Pyrolysis volatiles	600	Ni commercial	110	[196]

1.3.3. Experimental studies for combination of pyrolysis and catalytic reforming

Remiro and colleagues [203] studied the effect of several operating conditions including steam/carbon ratio, hourly space velocity and temperature on the steam reforming of raw bio-fuel derived from the flash pyrolysis of pine sawdust in a two stage reactor (pyrolyzer-reformer) in continuous regime. The flash pyrolysis of pine sawdust was made at 480°C. The pyrolytic lignin (carbonaceous solid), produced in the first step by repolymerization of some tar oxygenates, was separated and excluded from the other volatiles. This was done prior to the feeding into the second stage where the catalytic steam reforming occurs in a fluidized bed reactor. Moreover, dolomite was incorporated into the reformer to increase the hydrogen yield thanks to carbon dioxide capture. The catalyst used was Nickel catalyst supported on lanthana-alumina Ni/La_2O_3-αAl_2O_3 with 10 wt.% Ni and 9 wt.% La_2O_3. The thermal treatment step occurring at 500°C resulted in the formation of treated tar and led to the deposition of 23 wt.% of the raw tar oxygenates as pyrolytic lignin. The tar flow rate was set at 0.1 mL/min.

1.3.3.1. Effect of temperature on the catalytic reforming of raw tar from pine sawdust

In a first set of runs, the variation of the tar conversion and the different product yields with the operating temperature was elaborated at the "zero" time corresponding to the initial analysis made with the fresh catalyst and after 100 min of the reaction. Furthermore, experiments were performed without a catalyst and for that purpose an inert solid (silicon carbide CSi) was used. The steam to carbon S/C ratio was fixed at 9 and the space velocity 155 000 h^{-1}. The effects of the temperature on the tar conversion and the product yields are investigated in the **Figure 1.17** and **Figure 1.18**. Without a catalyst, the tar conversion becomes significant (0.81) only at 800°C with major compounds consisting of carbon monoxide, methane and hydrocarbons. The

catalytic reforming clearly enhances the tar conversion and plays an important role in modifying the product distribution where the major compounds formed were H_2 and CO_2 in the presence of the catalyst due to the methane and hydrocarbons reforming [203].

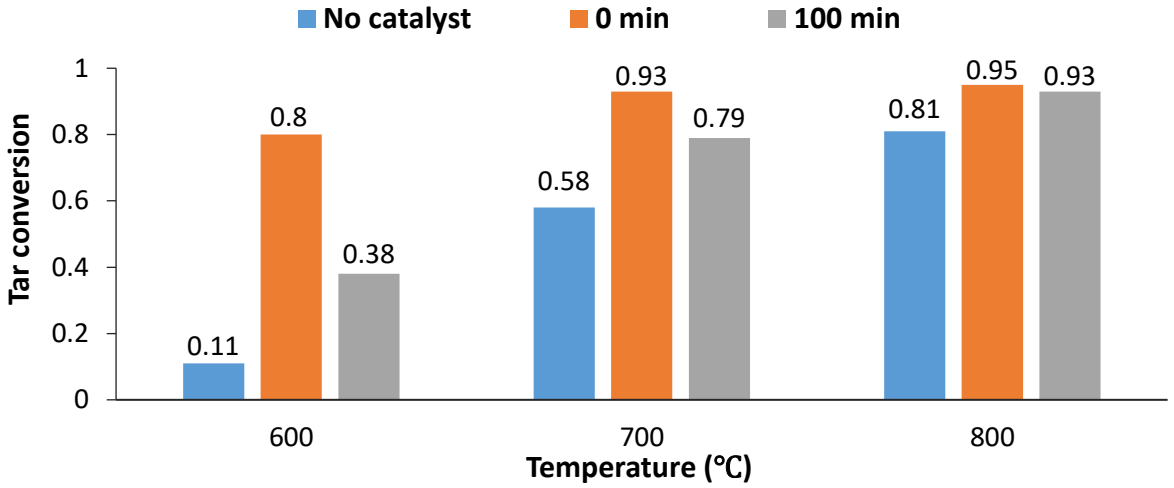

Figure 1.17 Evolution of the tar conversion in function of temperature without catalyst and at 0- and 100-min time of the catalyst freshness in the steam reforming of raw tar (catalyst Ni/La_2O_3-αAl_2O_3, S/C =9 and GHSV=155 000 h^{-1}) [203]

Looking at **Figure 1.17**, it can be noticed that with the fresh catalyst (zero time), important tar conversion of above 0.8 is obtained for all the temperatures and keeps growing with the temperature increase. After 100 min, it is remarked that the tar conversion is attenuated at 600°C in comparison to the zero time, is a bit lower at 700°C and is almost the same at 800°C. In fact, the temperature increase weakens the deactivation of the catalyst with time as explained hereafter.

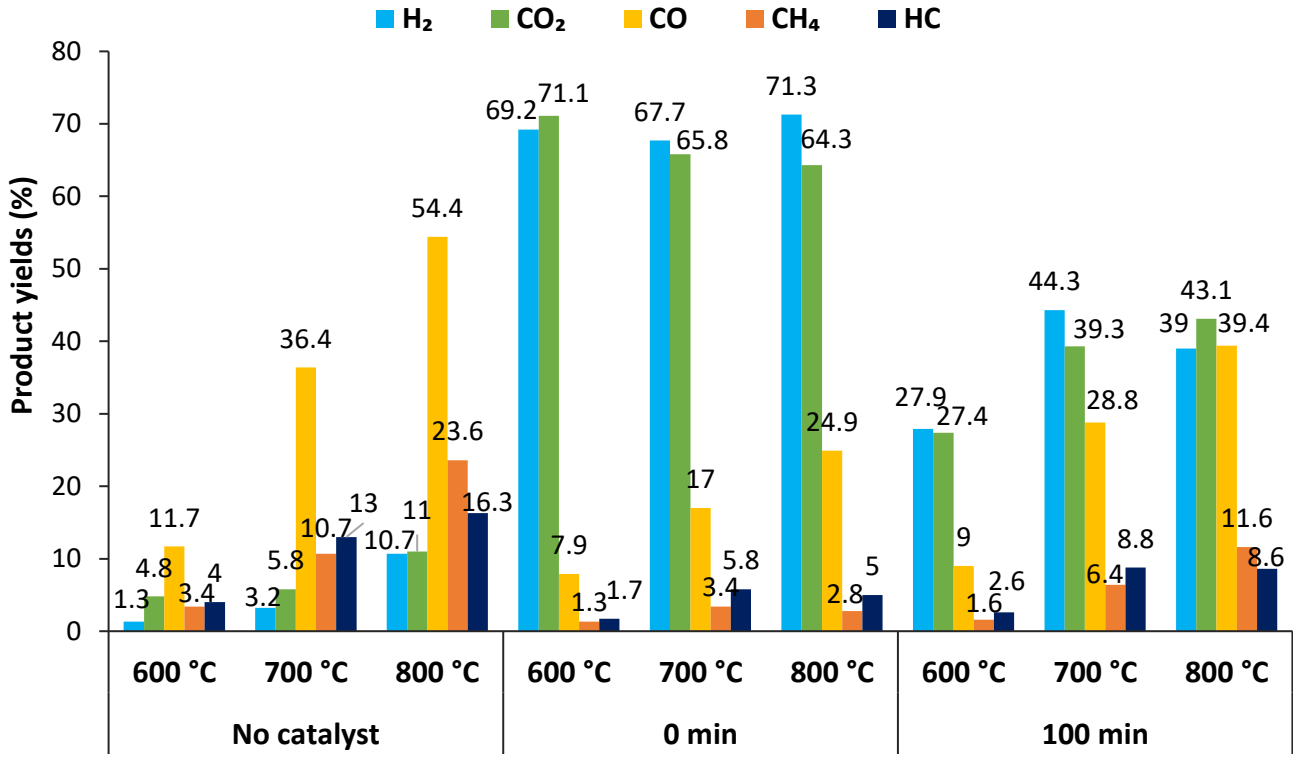

Figure 1.18 Evolution of the product yields in function of temperature at 0- and 100-min time and without catalyst in the steam reforming of raw tar (catalyst Ni/La_2O_3-αAl_2O_3, S/C =9 and GHSV=155 000 h^{-1} [203]

Based on **Figure 1.18**, regarding the hydrogen yield, without a catalyst, it reaches a maximum of 10% at 800°C revealing a poor selectivity from the tar thermal decomposition. H_2 yield fluctuates around 70% at zero time for the different temperatures. At 100 min, the H_2 yield remarkably decreases in comparison to the zero time with the maximum yield of 44% reached at 700°C. At this temperature, the deactivation of the catalyst was the least important. This could be explained by the large gas hourly space velocity GHSV that was applied for these runs (155 000 h^{-1}). Such large GHSV value causes a fast deactivation of the catalyst for the reforming and the water-gas-shift reactions (WGSR). With the fresh catalyst at zero time, the CO_2 yield slightly decreases with the temperature while the CO yield increases due to the disfavor of the WGSR. The methane and hydrocarbon yields are less affected by the temperature with the fresh catalyst and peak at 700°C.

Without a catalyst, the CO_2 yield slowly increases with the temperature while having very low values (between 4.8 and 11%) in contrast to those with the fresh catalyst (between 64.3% and 71%). Whereas the yield of the CO significantly rises with the temperature and reaches the maximum value of 54.4% at 800°C, which is the highest among all the CO yields obtained at the different temperatures. It should be noted that the CO yields without a catalyst are always higher than those with the fresh catalyst and the catalyst after 100 min, at the three temperatures tested. The yields of CO, CO_2 and CH_4 are more remarkable without a catalyst and increase with the temperature. Methane and hydrocarbons are reformed more efficiently at elevated temperatures.

After 100 min of the reaction, the catalyst became partially deactivated. This led to a decrease in the H_2 and CO_2 yields in opposite to the higher values reached with the fresh catalyst. Additionally, an increase in the CH_4, CO and hydrocarbons yields was observed in contrast to the lower values obtained with the fresh catalyst for the different temperatures evaluated. These conditions emphasize the thermal cracking of the tar oxygenates, equation **(1.19)**, which becomes more pronounced with the elevation of the temperature. It thereby leads to an increase in the yields of CH_4 and CO with a smaller effect on the hydrocarbons yield. Therefore, it can be deduced that the catalytic reactions including the reforming and the water gas shift are strongly dependent on the thermal cracking reactions, whose products are converted by the catalysts. In order to balance between the sharp decrease of the tar conversion obtained at 600°C and the elevated yields of carbon monoxide, methane and hydrocarbons at 800°C, the optimum temperature is suggested to be 700°C.

The coke formation described by equation **(1.20)** highly affects the catalyst deactivation. As the temperature increases, the coke formation amplifies until a certain high temperature is reached above which the gasification of coke and its precursors (aromatics and olefins) through reverse reactions, equations **(1.20)** and **(1.21)**, becomes considerable. It was proven that at 700°C, the coke precursors responsible for the catalyst deactivation are gasified, therefore the coke deposition was limited. In addition, the sintering of Ni/La_2O_3-αAl_2O_3 catalyst was reduced to a minimum at 700°C [203].

Thermal cracking: $C_nH_mO_k \rightarrow C_xH_yO_z + \text{gas}\ (H_2, CO, CO_2, CH_4, H_xC) + \text{coke}$ **(1.19)**

Cracking reaction of hydrocarbons: $H_xC \leftrightarrow \text{coke precursors (aromatics + olefins)}$

$$\rightarrow C + \frac{x}{2}H_2 \quad \textbf{(1.20)}$$

Cracking reaction of CH_4: $CH_4 \leftrightarrow C + 2H_2$ **(1.21)**

1.3.3.2. *Effect of the S/C ratio on the catalytic reforming of raw tar from pine sawdust*

The impact that the steam to carbon S/C ratio has over the tar conversion and the product yields of gases was evaluated (**Figure 1.19**). The steam flow rate was varied in the range of 0 and 0.3 cm^3/min at the optimum temperature of 700°C and for a space velocity of 32 500 h^{-1}. Thus, the steam to carbon ratio was varied from 1 to 15. The variation of the tar conversion in function of the S/C ratio showed an almost complete conversion of the tar for the whole range of the S/C ratio fluctuating around 0.99. This is due to the negligible deactivation of the catalyst given that a low space velocity was applied.

The yields of methane and hydrocarbons were very low and were not represented. From **Figure 1.19**, it is remarked that the S/C ratio markedly affects the product yields where the H_2 and CO_2 yields significantly increase when the S/C ratio is increased up to 5. At S/C ratios higher than 5, the variations of these yields become less pertinent. The highest H_2 yield of 95% was reached at S/C equal to 15. In contrast, the CO yield remarkably decreases as the S/C ratio increases bringing a higher water content that enhances the WGSR.

Careful must be accorded to the increasing energy cost resulting from the increase of the S/C ratio due to water evaporation. Therefore, the optimum S/C ratio is chosen to be around 5 which is sufficient to reach elevated tar conversion and hydrogen yield while avoiding excessive energy cost [203]. Consequently, the optimal operational conditions of the steam reforming of raw biofuel derived from the flash pyrolysis of pine sawdust can be chosen as follows: 480°C for pyrolysis temperature, 700°C for reforming temperature, S/C ratio equal to 5, GHSV equal to 32 500 h^{-1} and Ni/La_2O_3-αAl_2O_3 as catalyst with 10 wt.% Ni and 9 wt.% La_2O_3. These conditions lead to achieving a high hydrogen yield (above 90%) and tar conversion (above 98%) while reducing the CO yield to below 22%.

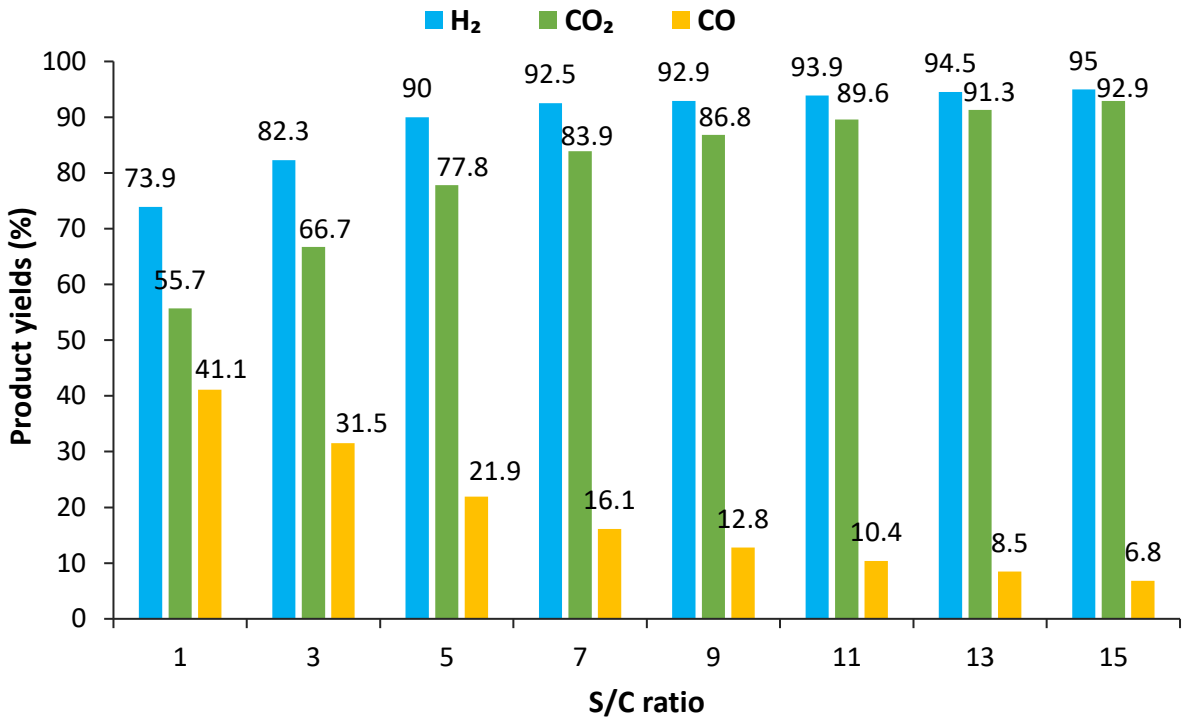

Figure 1.19 Evolution of the product yields with the S/C ratio at 700°C and GHSV = 32 500 h^{-1}. The gases yield are strongly affected by the increase of the S/C ratio up to 5 after which the effect becomes less significant [203]

1.4. Conclusion

In this chapter, three main axes were addressed: (i) biomass pyrolysis, (ii) catalytic reforming and (iii) coupling of the biomass pyrolysis and the catalytic reforming of the volatiles. First, the pyrolysis process, in which lignocellulosic biomass thermally decomposes into char, bio-oil and non-condensable gases, was largely studied. The biomass was characterized in terms of its elemental analysis and its biochemical composition. Biomass is a complex mixture of multiple components that differ from one type of biomass to another. However, common structures exist among the different biomass species which constitute the biomass main components, and they include: cellulose, hemicellulose and lignin. Tar, one of the major biomass pyrolysis products, is an extremely complex mixture of organic and inorganic compounds. The determination of all the components of the tar is practically very challenging given the large number of species it contains. Tar contains among others: benzene, toluene, m- and o-xylene, phenols, indene and naphthalene.

The main parameters strongly influencing the biomass pyrolysis are the reactor's temperature, its heating rate and the solids and volatiles residence time. Each one has a distinct impact on the pyrolysis products distribution and gases compositions. Based on different values attributed to these parameters, the pyrolysis process can be classified into slow, intermediate, fast and flash with the heating rate being the key parameter distinguishing the four classes. Moreover, the pyrolysis reactor's configuration has a great influence on the process efficiency and the products formation. Several reactors are suitable for the pyrolysis including thermogravimetric analyzer (TGA), fixed or fluidized bed reactor as well as a multistage reactor. The TGA allows the analysis of multiple species produced by the pyrolysis which can be realized at very high temperatures but operates with very small amounts of the biomass. Fixed bed reactors are generally used as small-scale heat applications, since they allow large solid residence time and can be operated with small gas velocities. Fluidized bed reactors have the advantages of increasing the heat and mass transfer as well as allowing better control over the reactor's temperature and the pyrolysis reaction thus improving the process efficiency.

Next, experimental studies focusing on the pyrolysis of oak wood were presented. The effect of temperature on the products' yields was evaluated. In terms of the product distribution, it was seen that in general as the temperature increases, the gases yield increases whereas that of the char decreases. The bio-oil yield undergoes an increase to reach a maximum at a certain temperature above which the yield starts decreasing. As for the yield of non-condensable gases, generally the yields of H_2, CO and CH_4 increase with the temperature while that of CO_2 decreases.

The second part on this chapter discussed the catalytic steam reforming process applied for the removal of the tar produced during the biomass pyrolysis. A description of the different catalytic reforming types including steam and dry reforming was detailed along with a description of the main parameters influencing the reforming and the design of the reactors involved. In addition, a list of the main catalysts utilized for these processes with their advantages and drawbacks was elaborated. Coke formation and deposition on the catalyst surface is one of the main downsides encountered while operating a catalytic steam reforming process. Several reactions take place simultaneously during the catalytic reforming including the steam reforming, water-gas shift reaction, dry reforming and Boudouard reaction. However,

the dominant reaction might change with different catalyst and different reaction conditions due to the promoting or inhibiting interactions among different compositions.

It should be noted that the tar compositions vary depending on the biomass pyrolyzed. The tar is a complex mixture of hydrocarbons, and it would be unreasonable to represent the tar by one compound. The study of the evolution of all of the tar compounds formed is technically very challenging. Therefore, in most studies, a model compound is chosen to characterize the tar and to study its catalytic reforming.

Essentially, it was found that nickel-based catalysts are the most widely investigated catalysts for tar removal given their low cost, large availability and effectiveness in catalytic cracking of aromatic hydrocarbons. Alumina (Al_2O_3) has been largely used as a Ni-based catalyst support. However, Ni/Al_2O_3 catalyst is known to be rapidly deactivated by carbon deposition on the surface of the catalyst, which can block the active sites, and result in the deactivation of catalyst. One possible solution would be the alloy of Ni with Co which can significantly reduce the carbon deposition over the catalyst surface. In addition, ceramic foam has high porosity, large specific surface area and good isolation properties making it an attractive catalyst support.

Following the theoretical background, the experimental results of the catalytic steam reforming of some tar model compounds were displayed. The effects of temperature, steam to carbon (S/C) ratio and metal loadings on the gas yields produced from the steam reforming were largely investigated. Concerning the temperature's effect, it was demonstrated that for a temperature falling between 500°C and 700°C, the H_2 yield increases and CO yield decreases, while for temperature exceeding 700°C and going up to 900°C, the opposite trends were obtained for both gases. On the other hand, for the temperature range going from 500°C to 900°C, the trend of variation of CO_2 and CH_4 was almost always decreasing. The hydrocarbon conversion was enhanced by the increase of the temperature. While investigating the effect of the steam to carbon S/C ratio on the steam reforming, it was found that when the S/C ratio goes from 1 to 4, H_2 and CO_2 concentrations increase while those of CH_4 and CO drop. Analyzing the effect of the metal loading, with the NiO used for the catalytic steam reforming of bio-fuel gas, increasing the loading from 1.36 % to 6% results in an increase in the CO concentration and a decrease in those of CO_2 and CH_4. The H_2 concentration was increased when the metal loading was raised from 1.36 % to 2.5 % but it dropped when the metal loading was further elevated to 6%.

Although the values varied from one study to another, but it can be deduced that the optimal operating temperature is between 700°C and 750°C. The most convenient steam to carbon ratio can be chosen to be around 2. The best metal loading was considered to be 2.5% NiO when tested for a mixture of several tar model compounds. Operating above these values will lead to a decrease in the steam reforming efficiency mainly caused by coke deposition on the catalyst surface.

The third section was devoted to the feasibility of coupling both thermochemical processes, the biomass pyrolysis and the catalytic reforming of the pyrolysis tar hydrocarbons, for the potential amelioration in the production of syngas. Hydrogen has been regarded as an energy carrier that is expected to be highly demanded in the near future given its clean combustion and elevated

energy density. It is currently mainly produced from natural gas, crude oil and fossil fuel. While gasification has been widely investigated for hydrogen production, it was found to face multiple challenges regarding the syngas quality. This is mainly due to its tar content that is responsible for the fouling and subsequently blocking of the process equipment. An indirect route for producing hydrogen from biomass is the biomass pyrolysis followed by an in-line bio-oil reforming which holds several advantages in comparison to the direct gasification. It is operated at significantly lower temperatures thus requiring less energy and lower material costs. In addition, the transportation costs are lowered due to the high bio-oil energy density in contrast to biomass. This method helps avoiding the issues of handling the bio-oil and its vaporization. Moreover, during this process the totality of the hydrocarbon gases produced from the pyrolysis are reformed which ameliorates the process yield.

The steam reforming of the raw bio-oil derived from the pine sawdust pyrolysis revealed the efficiency of this technology. When a fresh Ni/La_2O_3-αAl_2O_3 catalyst was used, these yields were clearly enhanced. An optimum temperature of 700°C was chosen where a significant H_2 yield was obtained due to the relevant bio-oil reforming as well as the reduction of the coke deposition and catalyst deactivation. The optimum steam to carbon ratio was selected to be around 5 where the yields of H_2 and CO_2 increased importantly. Above this S/C ratio, their increase became less pronounced, and the CO yield decreased since the water gas shift reaction (WGSR) was favored.

As demonstrated in this chapter, the coupling of the biomass pyrolysis with the catalytic reforming has been recently emerging and developing with several works already put into action. Therefore, it would be of a great interest and significant efficiency to couple these processes to valorize the gas produced and crack the tar formed into generating gases of high value and wide application such as hydrogen. Nevertheless, the application of this novel technology to biomass is still at its dawn and further studies need to be performed in order to investigate even more the applicability and efficiency of this process for the production of syngas. This specially concerns woody biomass such as oak among other wood types, as well as different biomass types such as flax shives and potentially other wastes such bio-composite based waste. These will be the objectives of this thesis work.

References

[1] T. Fahmy, Y. Fahmy, F. Mobarak, M. El-Sakhawy, R. Abouzeid, Biomass pyrolysis: past, present, and future, Environ. Dev. Sustain. (2018) 1–16. https://doi.org/10.1007/s10668-018-0200-5.

[2] D. Mohan, C. Pittman, P. Steele, Pyrolysis of Wood/Biomass for Bio-Oil: A Critical Review, Energy. 20 (2006) 848. https://doi.org/10.1021/ef0502397.

[3] M.N. Uddin, K. Techato, J. Taweekun, M.M. Rahman, M.G. Rasul, T.M.I. Mahlia, S.M. Ashrafur, An Overview of Recent Developments in Biomass Pyrolysis Technologies, Energies. 11 (2018) 3115. https://doi.org/10.3390/en11113115.

[4] M.I. Jahirul, M. Rasul, A. Chowdhury, N. Ashwath, Biofuels Production through Biomass Pyrolysis —A Technological Review, Energies. 5 (2012) 4952–5001. https://doi.org/10.3390/en5124952.

[5] T. Fahmy, Y. Fahmy, F. Mobarak, M. El-Sakhawy, R. Abouzeid, Biomass pyrolysis: past, present, and future, Environ. Dev. Sustain. (2018) 1–16. https://doi.org/10.1007/s10668-018-0200-5.
[6] L. Yang, X. Ge, Chapter Three - Biogas and Syngas Upgrading, in: Y. Li, X. Ge (Eds.), Adv. Bioenergy, Elsevier, 2016: pp. 125–188. https://doi.org/10.1016/bs.aibe.2016.09.003.
[7] J. Fu, C. Tang, W. Jin, L.D. Thi, Z. Huang, Y. Zhang, Study on laminar flame speed and flame structure of syngas with varied compositions using OH-PLIF and spectrograph, Int. J. Hydrog. Energy. 38 (2013) 1636–1643. https://doi.org/10.1016/j.ijhydene.2012.11.023.
[8] N. Gao, Y. Han, C. Quan, Study on steam reforming of coal tar over NiCo/ceramic foam catalyst for hydrogen production: Effect of Ni/Co ratio, Int. J. Hydrog. Energy. 43 (2018) 22170–22186. https://doi.org/10.1016/j.ijhydene.2018.10.119.
[9] R.H. Venderbosch, W. Prins, Fast pyrolysis technology development, Biofuels Bioprod. Biorefining. 4 (2010) 178–208. https://doi.org/10.1002/bbb.205.
[10] F.-X. Collard, J. Blin, A review on pyrolysis of biomass constituents: Mechanisms and composition of the products obtained from the conversion of cellulose, hemicelluloses and lignin, Renew. Sustain. Energy Rev. 38 (2014) 594–608. https://doi.org/10.1016/j.rser.2014.06.013.
[11] A. Sharma, V. Pareek, D. Zhang, Biomass pyrolysis—A review of modelling, process parameters and catalytic studies, Renew. Sustain. Energy Rev. 50 (2015) 1081–1096. https://doi.org/10.1016/j.rser.2015.04.193.
[12] V. Dhyani, T. Bhaskar, A comprehensive review on the pyrolysis of lignocellulosic biomass, Renew. Energy. 129 (2018) 695–716. https://doi.org/10.1016/j.renene.2017.04.035.
[13] G. Wang, Y. Dai, H. Yang, Q. Xiong, K. Wang, J. Zhou, Y. Li, S. Wang, A Review of Recent Advances in Biomass Pyrolysis, Energy Fuels. 34 (2020) 15557–15578. https://doi.org/10.1021/acs.energyfuels.0c03107.
[14] M. Tripathi, J.N. Sahu, P. Ganesan, Effect of process parameters on production of biochar from biomass waste through pyrolysis: A review, Renew. Sustain. Energy Rev. 55 (2016) 467–481. https://doi.org/10.1016/j.rser.2015.10.122.
[15] A. Verma, R. Shankar, P. Mondal, A Review on Pyrolysis of Biomass and the Impacts of Operating Conditions on Product Yield, Quality, and Upgradation, in: Recent Adv. Biofuels Bioenergy Util., 2018: pp. 227–259. https://doi.org/10.1007/978-981-13-1307-3_10.
[16] P.T. Williams, S. Besler, The influence of temperature and heating rate on the slow pyrolysis of biomass, Renew. Energy. 7 (1996) 233–250. https://doi.org/10.1016/0960-1481(96)00006-7.
[17] R.J.M. Westerhof, D.W.F. (Wim) Brilman, W.P.M. van Swaaij, S.R.A. Kersten, Effect of Temperature in Fluidized Bed Fast Pyrolysis of Biomass: Oil Quality Assessment in Test Units, Ind. Eng. Chem. Res. 49 (2010) 1160–1168. https://doi.org/10.1021/ie900885c.
[18] K. Norinaga, T. Shoji, S. Kudo, J. Hayashi, Detailed chemical kinetic modelling of vapour-phase cracking of multi-component molecular mixtures derived from the fast pyrolysis of cellulose, Fuel. 103 (2013) 141–150. https://doi.org/10.1016/j.fuel.2011.07.045.
[19] A. Fukutome, H. Kawamoto, S. Saka, Processes forming Gas, Tar, and Coke in Cellulose Gasification from Gas-Phase Reactions of Levoglucosan as Intermediate, ChemSusChem. 8 (2015) 2240–2249. https://doi.org/10.1002/cssc.201500275.
[20] D. Chen, X. Chen, J. Sun, Z. Zheng, K. Fu, Pyrolysis polygeneration of pine nut shell: Quality of pyrolysis products and study on the preparation of activated carbon from biochar, Bioresour. Technol. 216 (2016) 629–636. https://doi.org/10.1016/j.biortech.2016.05.107.
[21] K. Zeng, D. Gauthier, D.P. Minh, E. Weiss-Hortala, A. Nzihou, G. Flamant, Characterization of solar fuels obtained from beech wood solar pyrolysis, Fuel. 188 (2017) 285–293. https://doi.org/10.1016/j.fuel.2016.10.036.
[22] K.B. Ansari, J.S. Arora, J.W. Chew, P.J. Dauenhauer, S.H. Mushrif, Fast Pyrolysis of Cellulose, Hemicellulose, and Lignin: Effect of Operating Temperature on Bio-oil Yield and Composition and Insights into the Intrinsic Pyrolysis Chemistry, Ind. Eng. Chem. Res. 58 (2019) 15838–15852. https://doi.org/10.1021/acs.iecr.9b00920.
[23] T. Cornelissen, J. Yperman, G. Reggers, S. Schreurs, R. Carleer, Flash co-pyrolysis of biomass with polylactic acid. Part 1: Influence on bio-oil yield and heating value, Fuel. 87 (2008) 1031–1041. https://doi.org/10.1016/j.fuel.2007.07.019.
[24] S.V. Vassilev, D. Baxter, L.K. Andersen, C.G. Vassileva, An overview of the chemical composition of biomass, Fuel. 89 (2010) 913–933. https://doi.org/10.1016/j.fuel.2009.10.022.

[25] G. Özbay, Pyrolysis of Firwood (Abies bornmüllerianaMattf.) Sawdust: Characterization of Bio-Oil and Bio-Char, Drv. Ind. 66 (2015) 105–114. https://doi.org/10.5552/drind.2015.1359.
[26] A. Nzihou, B. Stanmore, N. Lyczko, D.P. Minh, The catalytic effect of inherent and adsorbed metals on the fast/flash pyrolysis of biomass: A review, Energy. 170 (2019) 326–337. https://doi.org/10.1016/j.energy.2018.12.174.
[27] A.A. Ahmad, N.A. Zawawi, F.H. Kasim, A. Inayat, A. Khasri, Assessing the gasification performance of biomass: A review on biomass gasification process conditions, optimization and economic evaluation, Renew. Sustain. Energy Rev. 53 (2016) 1333–1347. https://doi.org/10.1016/j.rser.2015.09.030.
[28] R.A. Jansen, Second Generation Biofuels and Biomass: Essential Guide for Investors, Scientists and Decision Makers, John Wiley & Sons, 2012.
[29] D. Laskar, B. Yang, H. Wang, J. Lee, Pathways for biomass-derived lignin to hydrocarbon fuels, Biofuels. 7 (2013). https://doi.org/10.1002/bbb.1422.
[30] P. Debiagi, C. Pecchi, G. Gentile, A. Frassoldati, A. Cuoci, T. Faravelli, E. Ranzi, Extractives Extend the Applicability of Multistep Kinetic Scheme of Biomass Pyrolysis, Energy Fuels. In press (2016). https://doi.org/10.1021/acs.energyfuels.5b01753.
[31] I. Haberle, Ø. Skreiberg, J. Łazar, N.E.L. Haugen, Numerical models for thermochemical degradation of thermally thick woody biomass, and their application in domestic wood heating appliances and grate furnaces, Prog. Energy Combust. Sci. 63 (2017) 204–252. https://doi.org/10.1016/j.pecs.2017.07.004.
[32] M. Brebu, G. Cazacu, O. Chirila, Pyrolysis of lignin - A potential method for obtaining chemicals and/or fuels, ResearchGate. 45 (2011) 43–50.
[33] C.D. Blasi, Kinetic and Heat Transfer Control in the Slow and Flash Pyrolysis of Solids, (1996). https://doi.org/10.1021/IE950243D.
[34] P.J. Van Soest, J.B. Robertson, B.A. Lewis, Methods for Dietary Fiber, Neutral Detergent Fiber, and Nonstarch Polysaccharides in Relation to Animal Nutrition, J. Dairy Sci. 74 (1991) 3583–3597. https://doi.org/10.3168/jds.S0022-0302(91)78551-2.
[35] P.J.V. Soest, R.H. Wine, Use of Detergents in the Analysis of Fibrous Feeds. IV. Determination of Plant Cell-Wall Constituents, J. AOAC Int. 50 (1967) 50–55. https://doi.org/10.1093/jaoac/50.1.50.
[36] L. Li, J. Rowbotham, C. Greenwell, P. Dyer, An Introduction to Pyrolysis and Catalytic Pyrolysis: Versatile Techniques for Biomass Conversion, New Future Dev. Catal. Catal. Biomass Convers. (2013) 173–208. https://doi.org/10.1016/B978-0-444-53878-9.00009-6.
[37] A. Demirbaş, Current Technologies for the Thermo-Conversion of Biomass into Fuels and Chemicals, Energy Sources - ENERG SOURCE. 26 (2004) 715–730. https://doi.org/10.1080/00908310490445562.
[38] E. Ranzi, A. Cuoci, T. Faravelli, A. Frassoldati, G. Migliavacca, S. Pierucci, S. Sommariva, Chemical Kinetics of Biomass Pyrolysis, Energy Fuels. 22 (2008) 4292–4300. https://doi.org/10.1021/ef800551t.
[39] G. Mauviel, Y. Le Brech, O. Authier, Ranzi detailed kinetic scheme predictions vs. detailed experimental results | Request PDF, ResearchGate. (2014). https://www.researchgate.net/publication/281992437_Ranzi_detailed_kinetic_scheme_predictions_vs_detailed_experimental_results (accessed February 14, 2020).
[40] J. Blondeau, H. Jeanmart, Biomass pyrolysis at high temperatures: Prediction of gaseous species yields from an anisotropic particle, Biomass Bioenergy. 41 (2012) 107–121. https://doi.org/10.1016/j.biombioe.2012.02.016.
[41] W.N.R.W. Isahak, M.W.M. Hisham, M.A. Yarmo, T. Yun Hin, A review on bio-oil production from biomass by using pyrolysis method, Renew. Sustain. Energy Rev. 16 (2012) 5910–5923. https://doi.org/10.1016/j.rser.2012.05.039.
[42] M. Balat, M. Balat, E. Kırtay, H. Balat, Main routes for the thermo-conversion of biomass into fuels and chemicals. Part 1: Pyrolysis systems, Energy Convers. Manag. 50 (2009) 3147–3157. https://doi.org/10.1016/j.enconman.2009.08.014.
[43] D. Wang, S. Czernik, D. Montané, M. Mann, E. Chornet, Biomass to Hydrogen via Fast Pyrolysis and Catalytic Steam Reforming of the Pyrolysis Oil or Its Fractions, Ind. Eng. Chem. Res. 36 (1997) 1507–1518. https://doi.org/10.1021/ie960396g.

[44] A. Dufour, E. Masson, P. Girods, Y. Rogaume, A. Zoulalian, Evolution of Aromatic Tar Composition in Relation to Methane and Ethylene from Biomass Pyrolysis-Gasification, Energy Fuels. 25 (2011) 4182–4189. https://doi.org/10.1021/ef200846g.
[45] G. Guan, M. Kaewpanha, X. Hao, A. Abudula, Catalytic steam reforming of biomass tar: Prospects and challenges, Renew. Sustain. Energy Rev. 58 (2016) 450–461. https://doi.org/10.1016/j.rser.2015.12.316.
[46] N. Gao, X. Wang, A. Li, C. Wu, Z. Yin, Hydrogen production from catalytic steam reforming of benzene as tar model compound of biomass gasification, Fuel Process. Technol. 148 (2016) 380–387. https://doi.org/10.1016/j.fuproc.2016.03.019.
[47] T. Dickerson, J. Soria, Catalytic Fast Pyrolysis: A Review, Energies. 6 (2013) 514–538. https://doi.org/10.3390/en6010514.
[48] M. Artetxe, J. Alvarez, M.A. Nahil, M. Olazar, P.T. Williams, Steam reforming of different biomass tar model compounds over Ni/Al2O3 catalysts, Energy Convers. Manag. 136 (2017) 119–126. https://doi.org/10.1016/j.enconman.2016.12.092.
[49] L. Devi, K.J. Ptasinski, F.J.J.G. Janssen, S.V.B. van Paasen, P.C.A. Bergman, J.H.A. Kiel, Catalytic decomposition of biomass tars: use of dolomite and untreated olivine, Renew. Energy. 30 (2005) 565–587. https://doi.org/10.1016/j.renene.2004.07.014.
[50] R. Coll, J. Salvadó, X. Farriol, D. Montané, Steam reforming model compounds of biomass gasification tars: conversion at different operating conditions and tendency towards coke formation, Fuel Process. Technol. 74 (2001) 19–31. https://doi.org/10.1016/S0378-3820(01)00214-4.
[51] Y.-C. Lin, J. Cho, G. Tompsett, P. Westmoreland, G. Huber, Kinetics and Mechanism of Cellulose Pyrolysis, J. Phys. Chem. C. 113 (2009) 20097–20107. https://doi.org/10.1021/jp906702p.
[52] M. Garcia-Perez, The Formation of Polyaromatic Hydrocarbons and Dioxins During Pyrolysis: A Review of the Literature with Descriptions of Biomass Composition, Fast Pyrolysis Technologies and Thermochemical Reactions, (2008).
[53] J. Akhtar, N. Saidina Amin, A review on operating parameters for optimum liquid oil yield in biomass pyrolysis, Renew. Sustain. Energy Rev. 16 (2012) 5101–5109. https://doi.org/10.1016/j.rser.2012.05.033.
[54] J. Montoya, F. Chejne Janna, M. Garcia-Perez, Fast pyrolysis of biomass: A review of relevant aspects. Part I: Parametric study, DYNA. 82 (2015) 239–248. https://doi.org/10.15446/dyna.v82n192.44701.
[55] A.S. Kalgo, The development and optimisation of a fast pyrolysis process for bio-oil production, Undefined. (2011). /paper/The-development-and-optimisation-of-a-fast-process-Kalgo/89b3fbef6865a9172c5b9c0d859c8e7d73975bfe (accessed October 12, 2020).
[56] D. Meier, B. van de Beld, A.V. Bridgwater, D.C. Elliott, A. Oasmaa, F. Preto, State-of-the-art of fast pyrolysis in IEA bioenergy member countries, Renew. Sustain. Energy Rev. 20 (2013) 619–641. https://doi.org/10.1016/j.rser.2012.11.061.
[57] F.-X. Collard, J. Blin, A. Bensakhria, J. Valette, Influence of impregnated metal on the pyrolysis conversion of biomass constituents, J. Anal. Appl. Pyrolysis. 95 (2012) 213–226. https://doi.org/10.1016/j.jaap.2012.02.009.
[58] K. Yadav, S. Jagadevan, Influence of Process Parameters on Synthesis of Biochar by Pyrolysis of Biomass: An Alternative Source of Energy, in: 2019. https://doi.org/10.5772/intechopen.88204.
[59] W.F. Fassinou, L. Van de Steene, S. Toure, G. Volle, P. Girard, Pyrolysis of Pinus pinaster in a two-stage gasifier: Influence of processing parameters and thermal cracking of tar, Fuel Process. Technol. 90 (2009) 75–90. https://doi.org/10.1016/j.fuproc.2008.07.016.
[60] M.-K. Bahng, C. Mukarakate, D.J. Robichaud, M.R. Nimlos, Current technologies for analysis of biomass thermochemical processing: A review, Anal. Chim. Acta. 651 (2009) 117–138. https://doi.org/10.1016/j.aca.2009.08.016.
[61] L. Zhang, C. (Charles) Xu, P. Champagne, Overview of recent advances in thermo-chemical conversion of biomass, Energy Convers. Manag. 51 (2010) 969–982. https://doi.org/10.1016/j.enconman.2009.11.038.
[62] K. Kebelmann, A. Hornung, U. Karsten, G. Griffiths, Intermediate pyrolysis and product identification by TGA and Py-GC/MS of green microalgae and their extracted protein and lipid components, Biomass Bioenergy. 49 (2013) 38–48. https://doi.org/10.1016/j.biombioe.2012.12.006.

[63] S. Al Arni, Comparison of slow and fast pyrolysis for converting biomass into fuel, Renew. Energy. 124 (2018) 197–201. https://doi.org/10.1016/j.renene.2017.04.060.
[64] N. Tippayawong, J. Kinorn, S. Thavornun, Yields and Gaseous Composition from Slow Pyrolysis of Refuse-derived Fuels, Energy Sources. Part A (2008) 1572–1580. https://doi.org/10.1080/15567030701258550.
[65] Y. Yang, J.G. Brammer, M. Ouadi, J. Samanya, A. Hornung, H.M. Xu, Y. Li, Characterisation of waste derived intermediate pyrolysis oils for use as diesel engine fuels, Fuel. 103 (2013) 247–257. https://doi.org/10.1016/j.fuel.2012.07.014.
[66] A. Hornung, A. Apfelbacher, S. Sagi, Intermediate pyrolysis: A sustainable biomass-to-energy concept – Biothermal valorisation of biomass (BtVB) process, J. Sci. Ind. Res. 70 (2011).
[67] D. Barik, Chapter 3 - Energy Extraction From Toxic Waste Originating From Food Processing Industries, in: D. Barik (Ed.), Energy Toxic Org. Waste Heat Power Gener., Woodhead Publishing, 2019: pp. 17–42. https://doi.org/10.1016/B978-0-08-102528-4.00003-1.
[68] A.V. Bridgwater, D. Meier, D. Radlein, An overview of fast pyrolysis of biomass - ScienceDirect, Org. Geochem. 30 (1999) 1479–1493. https://doi.org/10.1016/S0146-6380(99)00120-5.
[69] R. Kandiyoti, A. Herod, K. Bartle, T. Morgan, 3 - Pyrolysis of solid fuels: Experimental design and applications, in: R. Kandiyoti, A. Herod, K. Bartle, T. Morgan (Eds.), Solid Fuels Heavy Hydrocarb. Liq. Second Ed., Elsevier, 2017: pp. 25–123. https://doi.org/10.1016/B978-0-08-100784-6.00003-5.
[70] B.M. Wagenaar, J.A.M. Kuipers, W. Prins, W.P.M. van Swaaij, The Rotating Cone Flash Pyrolysis Reactor, in: A.V. Bridgwater (Ed.), Adv. Thermochem. Biomass Convers., Springer Netherlands, Dordrecht, 1993: pp. 1122–1133. https://doi.org/10.1007/978-94-011-1336-6_87.
[71] O. Onay, O.M. Kockar, Slow, fast and flash pyrolysis of rapeseed, Renew. Energy. 28 (2003) 2417–2433. https://doi.org/10.1016/S0960-1481(03)00137-X.
[72] J. Gomes, J. Batra, V.R. Chopda, P. Kathiresan, A.S. Rathore, Chapter 25 - Monitoring and Control of Bioethanol Production From Lignocellulosic Biomass, in: T. Bhaskar, A. Pandey, S.V. Mohan, D.-J. Lee, S.K. Khanal (Eds.), Waste Biorefinery, Elsevier, 2018: pp. 727–749. https://doi.org/10.1016/B978-0-444-63992-9.00025-2.
[73] D. Krasznai, R. Hartley, H. Roy, M. Cunningham, Compositional analysis of lignocellulosic biomass: conventional methodologies and future outlook, Crit. Rev. Biotechnol. 38 (2017). https://doi.org/10.1080/07388551.2017.1331336.
[74] T. Onsree, N. Tippayawong, A. Zheng, H. Li, Pyrolysis behavior and kinetics of corn residue pellets and eucalyptus wood chips in a macro thermogravimetric analyzer, Case Stud. Therm. Eng. 12 (2018) 546–556. https://doi.org/10.1016/j.csite.2018.07.011.
[75] G. Varhegyi, E. Jakab, F. Till, T. Szekely, Thermogravimetric-mass spectrometric characterization of the thermal decomposition of sunflower stem, Energy Fuels. 3 (1989) 755–760. https://doi.org/10.1021/ef00018a017.
[76] E. Mészáros, E. Jakab, G. Várhegyi, P. Tóvári, Thermogravimetry/mass spectrometry analysis of energy crops, J. Therm. Anal. Calorim. 88 (2007). https://doi.org/10.1007/s10973-006-8102-4.
[77] M. Carrier, A. Loppinet-Serani, D. Denux, J.-M. Lasnier, F. Ham-Pichavant, F. Cansell, C. Aymonier, Thermogravimetric analysis as a new method to determine the lignocellulosic composition of biomass - ScienceDirect, 35 (2011) 298–307.
[78] H. Yang, R. Yan, H. Chen, D.H. Lee, C. Zheng, Characteristics of hemicellulose, cellulose and lignin pyrolysis, Fuel. 86 (2007) 1781–1788. https://doi.org/10.1016/j.fuel.2006.12.013.
[79] A. Dutta, J. Schaidle, D. Humbird, F. Baddour, A. Sahir, Conceptual Process Design and Techno-Economic Assessment of Ex Situ Catalytic Fast Pyrolysis of Biomass: A Fixed Bed Reactor Implementation Scenario for Future Feasibility, Top. Catal. 59 (2015). https://doi.org/10.1007/s11244-015-0500-z.
[80] V.K. Guda, P.H. Steele, V.K. Penmetsa, Q. Li, Chapter 7 - Fast Pyrolysis of Biomass: Recent Advances in Fast Pyrolysis Technology, in: A. Pandey, T. Bhaskar, M. Stöcker, R.K. Sukumaran (Eds.), Recent Adv. Thermo-Chem. Convers. Biomass, Elsevier, Boston, 2015: pp. 177–211. https://doi.org/10.1016/B978-0-444-63289-0.00007-7.
[81] A. Lappas, E. Heracleous, 18 - Production of biofuels via Fischer–Tropsch synthesis: Biomass-to-liquids, in: R. Luque, C.S.K. Lin, K. Wilson, J. Clark (Eds.), Handb. Biofuels Prod. Second Ed., Woodhead Publishing, 2016: pp. 549–593. https://doi.org/10.1016/B978-0-08-100455-5.00018-7.

[82] S.-S. Liaw, Z. Wang, P. Ndegwa, C. Frear, S. Ha, C.-Z. Li, M. Garcia-Perez, Effect of pyrolysis temperature on the yield and properties of bio-oils obtained from the auger pyrolysis of Douglas Fir wood, J. Anal. Appl. Pyrolysis. 93 (2012) 52–62. https://doi.org/10.1016/j.jaap.2011.09.011.

[83] K.-Y. Cheung, K.-L. Lee, K.L. Lam, T.-Y. Chan, C.-W. Lee, D. Hui, Operation strategy for multi-stage pyrolysis, J. Anal. Appl. Pyrolysis - J ANAL APPL PYROL. 91 (2011) 165–182. https://doi.org/10.1016/j.jaap.2011.02.004.

[84] A.O. Oyedun, K.L. Lam, C.W. Hui, Charcoal Production via Multistage Pyrolysis, Chin. J. Chem. Eng. 20 (2012) 455–460. https://doi.org/10.1016/S1004-9541(11)60206-1.

[85] de l'Agriculture et de la F. région G.E. Direction régionale de l'Alimentation, Commission régionale de la forêt et du bois - PRFB, (2016). http://draaf.grand-est.agriculture.gouv.fr/Commission-regionale-de-la-foret (accessed November 5, 2019).

[86] G. Schmidt, G. Trouvé, G. Leyssens, C. Schönnenbeck, P. Genevray, F. Cazier, D. Dewaele, C. Vandenbilcke, E. Faivre, Y. Denance, C. Le Dreff-Lorimier, Wood washing: Influence on gaseous and particulate emissions during wood combustion in a domestic pellet stove, Fuel Process. Technol. 174 (2018) 104–117. https://doi.org/10.1016/j.fuproc.2018.02.020.

[87] J.L. Figueiredo, C. Valenzuela, A. Bernalte, J.M. Encinar, Pyrolysis of holm-oak wood: influence of temperature and particle size, Fuel. 68 (1989) 1012–1016. https://doi.org/10.1016/0016-2361(89)90067-7.

[88] E. Amini, M.-S. Safdari, J.T. DeYoung, D.R. Weise, T.H. Fletcher, Characterization of pyrolysis products from slow pyrolysis of live and dead vegetation native to the southern United States, Fuel. 235 (2019) 1475–1491. https://doi.org/10.1016/j.fuel.2018.08.112.

[89] T. Aysu, M.M. Küçük, Biomass pyrolysis in a fixed-bed reactor: Effects of pyrolysis parameters on product yields and characterization of products, Energy. 64 (2014) 1002–1025. https://doi.org/10.1016/j.energy.2013.11.053.

[90] A. Arregi, M. Amutio, G. Lopez, J. Bilbao, M. Olazar, Evaluation of thermochemical routes for hydrogen production from biomass: A review, Energy Convers. Manag. 165 (2018) 696–719. https://doi.org/10.1016/j.enconman.2018.03.089.

[91] C. Li, K. Suzuki, Tar property, analysis, reforming mechanism and model for biomass gasification—An overview, Renew. Sustain. Energy Rev. 13 (2009) 594–604. https://doi.org/10.1016/j.rser.2008.01.009.

[92] T.A. Milne, R.J. Evans, N. Abatzaglou, Biomass Gasifier "'Tars'": Their Nature, Formation, and Conversion, National Renewable Energy Laboratory, Golden, CO (US), 1998. https://doi.org/10.2172/3726.

[93] B.S. Babaqi, M.S. Takriff, S.K. Kamarudin, N.T.B.A. Othman, M.M. Ba-Abbad, Comparison of Catalytic Reforming Processes for Process Integration Opportunities: Brief Review, in: Adv. Eng. Res. Appl., Research India Publications, 2017: pp. 1–11. https://www.researchgate.net/publication/309411348_Comparison_of_Catalytic_Reforming_Processes_for_Process_Integration_Opportunities_Brief_Review (accessed August 31, 2020).

[94] G. Guan, M. Kaewpanha, X. Hao, A. Zhu, Y. Kasai, S. Kakuta, K. Kusakabe, A. Abudula, Steam reforming of tar derived from lignin over pompom-like potassium-promoted iron-based catalysts formed on calcined scallop shell, Bioresour. Technol. 139 (2013) 280–284. https://doi.org/10.1016/j.biortech.2013.04.007.

[95] N. Gao, Y. Han, C. Quan, Study on steam reforming of coal tar over NiCo/ceramic foam catalyst for hydrogen production: Effect of Ni/Co ratio, Int. J. Hydrog. Energy. 43 (2018) 22170–22186. https://doi.org/10.1016/j.ijhydene.2018.10.119.

[96] J.R. Rostrup-Nielsen, New aspects of syngas production and use, Catal. Today. 63 (2000) 159–164. https://doi.org/10.1016/S0920-5861(00)00455-7.

[97] H.V. Fajardo, L.F.D. Probst, Production of hydrogen by steam reforming of ethanol over Ni/Al2O3 spherical catalysts, Appl. Catal. Gen. 306 (2006) 134–141. https://doi.org/10.1016/j.apcata.2006.03.043.

[98] O. Vozniuk, N. Tanchoux, J.-M. Millet, S. Albonetti, F. Di Renzo, F. Cavani, Chapter 14 - Spinel Mixed Oxides for Chemical-Loop Reforming: From Solid State to Potential Application, in: S. Albonetti, S. Perathoner, E.A. Quadrelli (Eds.), Stud. Surf. Sci. Catal., Elsevier, 2019: pp. 281–302. https://doi.org/10.1016/B978-0-444-64127-4.00014-8.

[99] H.-G. Park, S. Han, K.-W. Jun, Y. Woo, M.-J. Park, S. Kim, Bench-Scale Steam Reforming of Methane for Hydrogen Production, Catalysts. 9 (2019) 615. https://doi.org/10.3390/catal9070615.
[100] A. Basile, S. Liguori, A. Iulianelli, 2 - Membrane reactors for methane steam reforming (MSR), in: A. Basile, L. Di Paola, F. l. Hai, V. Piemonte (Eds.), Membr. React. Energy Appl. Basic Chem. Prod., Woodhead Publishing, 2015: pp. 31–59. https://doi.org/10.1016/B978-1-78242-223-5.00002-9.
[101] J.R. Rostrup-Nielsen, Catalytic Steam Reforming, in: Adv. Comp. Environ. Physiol., Springer Berlin Heidelberg, Berlin, Heidelberg, 1984: pp. 1–130. https://doi.org/10.1007/978-3-642-93247-2_1.
[102] B.G. Miller, 4 - The Effect of Coal Usage on Human Health and the Environment, in: B.G. Miller (Ed.), Clean Coal Eng. Technol., Butterworth-Heinemann, Boston, 2011: pp. 85–132. https://doi.org/10.1016/B978-1-85617-710-8.00004-2.
[103] J. Guo, H. Lou, H. Zhao, D. Chai, X. Zheng, Dry Reforming of Methane over Nickel Catalysts Supported on Magnesium Aluminate Spinels, Appl. Catal. Gen. 273 (2004) 75–82. https://doi.org/10.1016/j.apcata.2004.06.014.
[104] M. Abou Rjeily, C. Gennequin, H. Pron, E. Abi-Aad, J.H. Randrianalisoa, Pyrolysis-catalytic upgrading of bio-oil and pyrolysis-catalytic steam reforming of biogas: a review, Environ. Chem. Lett. (2021) 48. https://doi.org/10.1007/s10311-021-01190-2.
[105] N. Gao, S. Liu, Y. Han, C. Xing, A. Li, Steam reforming of biomass tar for hydrogen production over NiO/ceramic foam catalyst, Int. J. Hydrog. Energy. 40 (2015) 7983–7990. https://doi.org/10.1016/j.ijhydene.2015.04.050.
[106] S. Aouad, M. Labaki, S. Ojala, P.K. Seelam, E. Turpeinen, C. Gennequin, J. Estephane, E. Abi-Aad, A Review on the Dry Reforming Processes for Hydrogen Production: Catalytic Materials and Technologies, in: 2018: pp. 60–128. https://doi.org/10.2174/9781681087580118020007.
[107] J. Zhang, H. Wang, A.K. Dalai, Development of stable bimetallic catalysts for carbon dioxide reforming of methane, J. Catal. 249 (2007) 300–310. https://doi.org/10.1016/j.jcat.2007.05.004.
[108] H.M. Swaan, V.C.H. Kroll, G.A. Martin, C. Mirodatos, Deactivation of supported nickel catalysts during the reforming of methane by carbon dioxide, Catal. Today. 21 (1994) 571–578. https://doi.org/10.1016/0920-5861(94)80181-9.
[109] D. Swierczynski, C. Courson, A. Kiennemann, Study of steam reforming of toluene used as model compound of tar produced by biomass gasification, Chem. Eng. Process. Process Intensif. 47 (2008) 508–513. https://doi.org/10.1016/j.cep.2007.01.012.
[110] J. Estephane, S. Aouad, S. Hany, B. El Khoury, C. Gennequin, H. El Zakhem, J. El Nakat, A. Aboukaïs, E. Abi Aad, CO2 reforming of methane over Ni–Co/ZSM5 catalysts. Aging and carbon deposition study, Int. J. Hydrog. Energy. 40 (2015) 9201–9208. https://doi.org/10.1016/j.ijhydene.2015.05.147.
[111] C. Gennequin, S. Hany, H. Tidahy, S. Aouad, J. Estephane, A. Aboukaïs, E. Abi-Aad, Influence of the presence of ruthenium on the activity and stability of Co–Mg–Al-based catalysts in CO2 reforming of methane for syngas production, Environ. Sci. Pollut. Res. 23 (2016). https://doi.org/10.1007/s11356-016-7453-z.
[112] O.W. Perez-Lopez, A. Senger, N.R. Marcilio, M.A. Lansarin, Effect of composition and thermal pretreatment on properties of Ni–Mg–Al catalysts for CO2 reforming of methane, Appl. Catal. Gen. 303 (2006) 234–244. https://doi.org/10.1016/j.apcata.2006.02.024.
[113] C. Quan, N. Gao, C. Wu, Utilization of NiO/porous ceramic monolithic catalyst for upgrading biomass fuel gas, J. Energy Inst. 91 (2018) 331–338. https://doi.org/10.1016/j.joei.2017.02.008.
[114] A. Adeniyi, K. Otoikhian, J. O. Ighalo, Steam Reforming of Biomass Pyrolysis Oil: A Review, Int. J. Chem. React. Eng. (2019). https://doi.org/10.1515/ijcre-2018-0328.
[115] A. Ochoa, J. Bilbao, A.G. Gayubo, P. Castaño, Coke formation and deactivation during catalytic reforming of biomass and waste pyrolysis products: A review, Renew. Sustain. Energy Rev. 119 (2020) 109600. https://doi.org/10.1016/j.rser.2019.109600.
[116] S.S.E.H. Elnashaie, M.E.E. Abashar, Steam reforming and methanation effectiveness factors using the dusty gas model under industrial conditions, Chem. Eng. Process. Process Intensif. 32 (1993) 177–189. https://doi.org/10.1016/0255-2701(93)80014-8.

[117] J.C. DE DEKEN, E.F. DEVOS, G.F. FROMENT, Steam Reforming of Natural Gas: Intrinsic Kinetics, Diffusional Influences, and Reactor Design, in: Chem. React. Eng., AMERICAN CHEMICAL SOCIETY, 1982: pp. 181–197. https://doi.org/10.1021/bk-1982-0196.ch016.

[118] A.M. Adris, S.S.E.H. Elnashaie, R. Hughes, A fluidized bed membrane reactor for the steam reforming of methane, Can. J. Chem. Eng. 69 (1991) 1061–1070. https://doi.org/10.1002/cjce.5450690504.

[119] S. Roy, B.B. Pruden, A.M. Adris, J.R. Grace, C.J. Lim, Fluidized-bed steam methane reforming with oxygen input, Chem. Eng. Sci. 54 (1999) 2095–2102. https://doi.org/10.1016/S0009-2509(98)00300-5.

[120] R.C. Brown, Biomass-Derived Hydrogen from a Thermally Ballasted Gasifier, in: 2007. https://doi.org/10.2172/901792.

[121] F. Winter, B. Schratzer, 23 - Applications of fluidized bed technology in processes other than combustion and gasification, in: F. Scala (Ed.), Fluid. Bed Technol. -Zero Emiss. Combust. Gasif., Woodhead Publishing, 2013: pp. 1005–1033. https://doi.org/10.1533/9780857098801.5.1005.

[122] M.E.E. Abashar, K.I. Alhumaizi, A.M. Adris, Investigation of Methane–Steam Reforming in Fluidized Bed Membrane Reactors, Chem. Eng. Res. Des. 81 (2003) 251–258. https://doi.org/10.1205/026387603762878719.

[123] R. Trane, S. Dahl, M.S. Skjøth-Rasmussen, A.D. Jensen, Catalytic steam reforming of bio-oil, Int. J. Hydrog. Energy. 37 (2012) 6447–6472. https://doi.org/10.1016/j.ijhydene.2012.01.023.

[124] P.N. Kechagiopoulos, S.S. Voutetakis, A.A. Lemonidou, I.A. Vasalos, Hydrogen Production via Reforming of the Aqueous Phase of Bio-Oil over Ni/Olivine Catalysts in a Spouted Bed Reactor, Ind. Eng. Chem. Res. 48 (2009) 1400–1408. https://doi.org/10.1021/ie8013378.

[125] P.N. Kechagiopoulos, S.S. Voutetakis, A.A. Lemonidou, I.A. Vasalos, Sustainable hydrogen production via reforming of ethylene glycol using a novel spouted bed reactor, Catal. Today. 127 (2007) 246–255. https://doi.org/10.1016/j.cattod.2007.05.018.

[126] A. Remiro, B. Valle, A.T. Aguayo, J. Bilbao, A.G. Gayubo, Steam Reforming of Raw Bio-oil in a Fluidized Bed Reactor with Prior Separation of Pyrolytic Lignin, Energy Fuels. 27 (2013) 7549–7559. https://doi.org/10.1021/ef401835s.

[127] B. Valle, B. Aramburu, P.L. Benito, J. Bilbao, A.G. Gayubo, Biomass to hydrogen-rich gas via steam reforming of raw bio-oil over Ni/La2O3-αAl2O3 catalyst: Effect of space-time and steam-to-carbon ratio, Fuel. 216 (2018) 445–455. https://doi.org/10.1016/j.fuel.2017.11.151.

[128] B. Valle, B. Aramburu, M. Olazar, J. Bilbao, A.G. Gayubo, Steam reforming of raw bio-oil over Ni/La2O3-αAl2O3: Influence of temperature on product yields and catalyst deactivation, Fuel. 216 (2018) 463–474. https://doi.org/10.1016/j.fuel.2017.11.149.

[129] A. Remiro, B. Valle, L. Oar-Arteta, A.T. Aguayo, J. Bilbao, A.G. Gayubo, Hydrogen production by steam reforming of bio-oil/bio-ethanol mixtures in a continuous thermal-catalytic process, Int. J. Hydrog. Energy. 39 (2014) 6889–6898. https://doi.org/10.1016/j.ijhydene.2014.02.137.

[130] B. Valle, B. Aramburu, A. Remiro, J. Bilbao, A.G. Gayubo, Effect of calcination/reduction conditions of Ni/La2O3–αAl2O3 catalyst on its activity and stability for hydrogen production by steam reforming of raw bio-oil/ethanol, Appl. Catal. B Environ. 147 (2014) 402–410. https://doi.org/10.1016/j.apcatb.2013.09.022.

[131] A. Remiro, B. Valle, B. Aramburu, A.T. Aguayo, J. Bilbao, A.G. Gayubo, Steam Reforming of the Bio-Oil Aqueous Fraction in a Fluidized Bed Reactor with in Situ CO2 Capture, Ind. Eng. Chem. Res. 52 (2013) 17087–17098. https://doi.org/10.1021/ie4021705.

[132] A. Remiro, B. Valle, A.T. Aguayo, J. Bilbao, A.G. Gayubo, Operating conditions for attenuating Ni/La2O3–αAl2O3 catalyst deactivation in the steam reforming of bio-oil aqueous fraction, Fuel Process. Technol. 115 (2013) 222–232. https://doi.org/10.1016/j.fuproc.2013.06.003.

[133] B. Valle, A. Remiro, A.T. Aguayo, J. Bilbao, A.G. Gayubo, Catalysts of Ni/α-Al2O3 and Ni/La2O3-αAl2O3 for hydrogen production by steam reforming of bio-oil aqueous fraction with pyrolytic lignin retention, Int. J. Hydrog. Energy. 38 (2013) 1307–1318. https://doi.org/10.1016/j.ijhydene.2012.11.014.

[134] D. Yao, C. Wu, H. Yang, Q. Hu, M.A. Nahil, H. Chen, P.T. Williams, Hydrogen production from catalytic reforming of the aqueous fraction of pyrolysis bio-oil with modified Ni–Al catalysts, Int. J. Hydrog. Energy. 39 (2014) 14642–14652. https://doi.org/10.1016/j.ijhydene.2014.07.077.

[135] C. Wu, Q. Huang, M. Sui, Y. Yan, F. Wang, Hydrogen production via catalytic steam reforming of fast pyrolysis bio-oil in a two-stage fixed bed reactor system, Fuel Process. Technol. 89 (2008) 1306–1316. https://doi.org/10.1016/j.fuproc.2008.05.018.

[136] E.T. Saw, U. Oemar, M.L. Ang, K. Hidajat, S. Kawi, Highly Active and Stable Bimetallic Nickel-Copper Core-Ceria Shell Catalyst for High-Temperature Water-Gas Shift Reaction, ChemCatChem. 7 (2015) n/a-n/a. https://doi.org/10.1002/cctc.201500481.

[137] J. Ashok, N. Dewangan, S. Das, P. Hongmanorom, M.H. Wai, K. Tomishige, S. Kawi, Recent progress in the development of catalysts for steam reforming of biomass tar model reaction, Fuel Process. Technol. 199 (2020) 106252. https://doi.org/10.1016/j.fuproc.2019.106252.

[138] H.V. Fajardo, E. Longo, D.Z. Mezalira, G.B. Nuernberg, G.I. Almerindo, A. Collasiol, L.F.D. Probst, I.T.S. Garcia, N.L.V. Carreño, Influence of support on catalytic behavior of nickel catalysts in the steam reforming of ethanol for hydrogen production, Environ. Chem. Lett. 8 (2008) 79–85. https://doi.org/10.1007/s10311-008-0195-5.

[139] S. Li, J. Gong, Strategies for improving the performance and stability of Ni-based catalysts for reforming reactions, Chem. Soc. Rev. 43 (2014) 7245–7256. https://doi.org/10.1039/C4CS00223G.

[140] Z. Li, M. Li, Z. Bian, Y. Kathiraser, S. Kawi, Design of highly stable and selective core/yolk–shell nanocatalysts—A review, Appl. Catal. B Environ. 188 (2016) 324–341. https://doi.org/10.1016/j.apcatb.2016.01.067.

[141] M. Kong, J. Fei, S. Wang, W. Lu, X. Zheng, Influence of supports on catalytic behavior of nickel catalysts in carbon dioxide reforming of toluene as a model compound of tar from biomass gasification, Bioresour. Technol. 102 (2011) 2004–2008. https://doi.org/10.1016/j.biortech.2010.09.054.

[142] L. He, S. Hu, L. Jiang, G. Liao, X. Chen, H. Han, L. Xiao, Q. Ren, Y. Wang, S. Su, J. Xiang, Carbon nanotubes formation and its influence on steam reforming of toluene over Ni/Al2O3 catalysts: Roles of catalyst supports, Fuel Process. Technol. 176 (2018) 7–14. https://doi.org/10.1016/j.fuproc.2018.03.007.

[143] A.M. Fidalgo, L.M. Ilharco, Tailoring the structure and hydrophobic properties of amorphous silica by silylation, Microporous Mesoporous Mater. 158 (2012) 39–46. https://doi.org/10.1016/j.micromeso.2012.03.009.

[144] M.A. Adnan, O. Muraza, S.A. Razzak, M.M. Hossain, H.I. de Lasa, Iron Oxide over Silica-Doped Alumina Catalyst for Catalytic Steam Reforming of Toluene as a Surrogate Tar Biomass Species, Energy Fuels. 31 (2017) 7471–7481. https://doi.org/10.1021/acs.energyfuels.7b01301.

[145] T. Castro, R. Peguin, R. Rabelo Neto, L. Borges, F. Noronha, Steam Reforming of Toluene Over Pt/CexZr1−xO2/Al2O3 Catalysts, Top. Catal. 59 (2016) 292. https://doi.org/10.1007/s11244-015-0443-4.

[146] C.P.B. Quitete, R.C.P. Bittencourt, M.M.V.M. Souza, Steam Reforming of Tar Model Compounds Over Nickel Catalysts Supported on Barium Hexaaluminate, Catal. Lett. 145 (2015) 541–548. https://doi.org/10.1007/s10562-014-1405-3.

[147] V. Nichele, M. Signoretto, F. Pinna, F. Menegazzo, I. Rossetti, G. Cruciani, G. Cerrato, A. Di Michele, Ni/ZrO2 catalysts in ethanol steam reforming: Inhibition of coke formation by CaO-doping, Appl. Catal. B Environ. 150–151 (2014) 12–20. https://doi.org/10.1016/j.apcatb.2013.11.037.

[148] U. Oemar, Y. Kathiraser, M.L. Ang, K. Hidajat, S. Kawi, Catalytic Biomass Gasification to Syngas Over Highly Dispersed Lanthanum-Doped Nickel on SBA-15, ChemCatChem. 7 (2015). https://doi.org/10.1002/cctc.201500482.

[149] Y. Shen, Y. Fu, Advances in in situ and ex situ tar reforming with biochar catalysts for clean energy production, Sustain. Energy Fuels. 2 (2018) 326–344. https://doi.org/10.1039/C7SE00553A.

[150] J.-P. Cao, J. Ren, X.-Y. Zhao, X.-Y. Wei, T. Takarada, Effect of atmosphere on carbon deposition of Ni/Al2O3 and Ni-loaded on lignite char during reforming of toluene as a biomass tar model compound, Fuel. 217 (2018) 515–521. https://doi.org/10.1016/j.fuel.2017.12.121.

[151] F. Guo, X. Li, Y. Liu, K. Peng, C. Guo, Z. Rao, Catalytic cracking of biomass pyrolysis tar over char-supported catalysts, Energy Convers. Manag. 167 (2018) 81–90. https://doi.org/10.1016/j.enconman.2018.04.094.

[152] V. Gunarathne, A. Ashiq, S. Ramanayaka, P. Wijekoon, M. Vithanage, Biochar from municipal solid waste for resource recovery and pollution remediation, Environ. Chem. Lett. 17 (2019). https://doi.org/10.1007/s10311-019-00866-0.
[153] M. Balajii, S. Niju, Biochar-derived heterogeneous catalysts for biodiesel production, Environ. Chem. Lett. 17 (2019) 1447–1469. https://doi.org/10.1007/s10311-019-00885-x.
[154] Z. Yaakob, A. Bshish, A. Ebshish, S.M. Tasirin, F.H. Alhasan, Hydrogen Production by Steam Reforming of Ethanol over Nickel Catalysts Supported on Sol Gel Made Alumina: Influence of Calcination Temperature on Supports, Mater. Basel Switz. 6 (2013) 2229–2239. https://doi.org/10.3390/ma6062229.
[155] C. Pfeifer, H. Hofbauer, Development of catalytic tar decomposition downstream from a dual fluidized bed biomass steam gasifier, Powder Technol. 180 (2008) 9–16. https://doi.org/10.1016/j.powtec.2007.03.008.
[156] U. Oemar, Z. Bian, K. Hidajat, S. Kawi, Sulfur resistant LaxCe1−xNi0.5Cu0.5O3 catalysts for an ultra-high temperature water gas shift reaction, Catal. Sci. Technol. 6 (2016) 6569–6580. https://doi.org/10.1039/C6CY00635C.
[157] Z. Li, B. Jiang, Z. Wang, S. Kawi, High carbon resistant Ni@Ni phyllosilicate@SiO2 core shell hollow sphere catalysts for low temperature CH4 dry reforming, J. CO2 Util. 27 (2018) 238–246. https://doi.org/10.1016/j.jcou.2018.07.017.
[158] F. Lónyi, J. Valyon, E. Someus, J. Hancsók, Steam reforming of bio-oil from pyrolysis of MBM over particulate and monolith supported Ni/γ-Al2O3 catalysts, Fuel. 112 (2013) 23–30. https://doi.org/10.1016/j.fuel.2013.05.010.
[159] C. Wang, T. Wang, L. Ma, Y. Gao, C. Wu, Steam reforming of biomass raw fuel gas over NiO–MgO solid solution cordierite monolith catalyst, Energy Convers. Manag. 51 (2010) 446–451. https://doi.org/10.1016/j.enconman.2009.10.006.
[160] M. Abou Rjeily, C. Gennequin, H. Pron, E. Abi-Aad, J.H. Randrianalisoa, Chapter 9 - Catalysts for steam reforming of biomass tar and their effects on the products, in: M.R. Cesario, D.A. de Macedo (Eds.), Heterog. Catal., Elsevier, 2022: pp. 249–295. https://doi.org/10.1016/B978-0-323-85612-6.00009-7.
[161] D. Wang, S. Czernik, D. Montané, M. Mann, E. Chornet, Biomass to Hydrogen via Fast Pyrolysis and Catalytic Steam Reforming of the Pyrolysis Oil or Its Fractions, Ind. Eng. Chem. Res. 36 (1997) 1507–1518. https://doi.org/10.1021/ie960396g.
[162] L. Dong, M. Asadullah, S. Zhang, X.-S. Wang, H. Wu, C.-Z. Li, An advanced biomass gasification technology with integrated catalytic hot gas cleaning: Part I. Technology and initial experimental results in a lab-scale facility, Fuel. 108 (2013) 409–416. https://doi.org/10.1016/j.fuel.2012.11.043.
[163] S. Zarnegar, A review on catalytic-pyrolysis of coal and biomass for value-added fuel and chemicals, Energy Sources Part Recovery Util. Environ. Eff. 40 (2018) 1–7. https://doi.org/10.1080/15567036.2018.1472680.
[164] R. Trane, S. Dahl, M.S. Skjøth-Rasmussen, A.D. Jensen, Catalytic steam reforming of bio-oil, Int. J. Hydrog. Energy. 37 (2012) 6447–6472. https://doi.org/10.1016/j.ijhydene.2012.01.023.
[165] S. Luo, B. Xiao, X. Guo, Z. Hu, S. Liu, M. He, Hydrogen-rich gas from catalytic steam gasification of biomass in a fixed bed reactor: Influence of particle size on gasification performance, Int. J. Hydrog. Energy. 34 (2009) 1260–1264. https://doi.org/10.1016/j.ijhydene.2008.10.088.
[166] Q.M.K. Waheed, P.T. Williams, Hydrogen Production from High Temperature Pyrolysis/Steam Reforming of Waste Biomass: Rice Husk, Sugar Cane Bagasse, and Wheat Straw, Energy Fuels. 27 (2013) 6695–6704. https://doi.org/10.1021/ef401145w.
[167] W.J. Parker, Determination of the Input Data for a Model of the Heat Release Rate of Wood, Math. Model. Fires. (1988). https://doi.org/10.1520/STP26220S.
[168] D. Wang, D. Montané, E. Chornet, Catalytic steam reforming of biomass-derived oxygenates: acetic acid and hydroxyacetaldehyde, Appl. Catal. Gen. 143 (1996) 245–270. https://doi.org/10.1016/0926-860X(96)00093-2.
[169] K. Akubo, M.A. Nahil, P.T. Williams, Pyrolysis-catalytic steam reforming of agricultural biomass wastes and biomass components for production of hydrogen/syngas, J. Energy Inst. 92 (2019) 1987–1996. https://doi.org/10.1016/j.joei.2018.10.013.

[170] A. Al-Rahbi, P. Williams, Waste ashes as catalysts for the pyrolysis–catalytic steam reforming of biomass for hydrogen-rich gas production, J. Mater. Cycles Waste Manag. (2019). https://doi.org/10.1007/s10163-019-00876-8.
[171] M.I. Jahirul, M.G. Rasul, A.A. Chowdhury, N. Ashwath, Biofuels Production through Biomass Pyrolysis —A Technological Review, Energies. 5 (2012) 4952–5001. https://doi.org/10.3390/en5124952.
[172] F.-X. Collard, J. Blin, A review on pyrolysis of biomass constituents: Mechanisms and composition of the products obtained from the conversion of cellulose, hemicelluloses and lignin, Renew. Sustain. Energy Rev. 38 (2014) 594–608. https://doi.org/10.1016/j.rser.2014.06.013.
[173] A. Sharma, V. Pareek, D. Zhang, Biomass pyrolysis—A review of modelling, process parameters and catalytic studies, Renew. Sustain. Energy Rev. 50 (2015) 1081–1096. https://doi.org/wang.
[174] V. Dhyani, T. Bhaskar, A comprehensive review on the pyrolysis of lignocellulosic biomass, Renew. Energy. 129 (2018) 695–716. https://doi.org/10.1016/j.renene.2017.04.035.
[175] D. Li, X. Li, J. Long, Catalytic Reforming of Oxygenates: State of the Art and Future Prospects, Chem. Rev. 116 (2016). https://doi.org/10.1021/acs.chemrev.6b00099.
[176] J. Chen, J. Sun, Y. Wang, Catalysts for Steam Reforming of Bio-oil: A Review, Ind. Eng. Chem. Res. 56 (2017). https://doi.org/10.1021/acs.iecr.7b00600.
[177] S. Aouad, M. Labaki, S. Ojala, P.K. Seelam, E. Turpeinen, C. Gennequin, J. Estephane, E. Abi-Aad, A Review on the Dry Reforming Processes for Hydrogen Production: Catalytic Materials and Technologies, in: 2018: pp. 60–128. https://doi.org/10.2174/9781681087580118020007.
[178] A. Adeniyi, K. Otoikhian, J. O. Ighalo, Steam Reforming of Biomass Pyrolysis Oil: A Review, Int. J. Chem. React. Eng. (2019). https://doi.org/10.1515/ijcre-2018-0328.
[179] T.T.P. Pham, K.S. Ro, L. Chen, D. Mahajan, T.J. Siang, U.P.M. Ashik, J. Hayashi, D. Pham Minh, D.-V.N. Vo, Microwave-assisted dry reforming of methane for syngas production: a review, Environ. Chem. Lett. 18 (2020) 1987–2019. https://doi.org/10.1007/s10311-020-01055-0.
[180] G. Lopez, M. Artetxe, M. Amutio, J. Alvarez, J. Bilbao, M. Olazar, Recent advances in the gasification of waste plastics. A critical overview, Renew. Sustain. Energy Rev. 82 (2018) 576–596. https://doi.org/10.1016/j.rser.2017.09.032.
[181] J. Alvarez, S. Kumagai, C. Wu, T. Yoshioka, J. Bilbao, M. Olazar, P.T. Williams, Hydrogen production from biomass and plastic mixtures by pyrolysis-gasification, Int. J. Hydrog. Energy. 39 (2014) 10883–10891. https://doi.org/10.1016/j.ijhydene.2014.04.189.
[182] S. Kumagai, J. Alvarez, P.H. Blanco, C. Wu, T. Yoshioka, M. Olazar, P.T. Williams, Novel Ni–Mg–Al–Ca catalyst for enhanced hydrogen production for the pyrolysis–gasification of a biomass/plastic mixture, J. Anal. Appl. Pyrolysis. 113 (2015) 15–21. https://doi.org/10.1016/j.jaap.2014.09.012.
[183] J. Zou, H. Yang, Z. Zeng, C. Wu, P.T. Williams, H. Chen, Hydrogen production from pyrolysis catalytic reforming of cellulose in the presence of K alkali metal, Int. J. Hydrog. Energy. 41 (2016) 10598–10607. https://doi.org/10.1016/j.ijhydene.2016.04.207.
[184] Q.M.K. Waheed, P.T. Williams, Hydrogen Production from High Temperature Pyrolysis/Steam Reforming of Waste Biomass: Rice Husk, Sugar Cane Bagasse, and Wheat Straw, Energy Fuels. 27 (2013) 6695–6704. https://doi.org/10.1021/ef401145w.
[185] A.K. Olaleye, K.J. Adedayo, C. Wu, M.A. Nahil, M. Wang, P.T. Williams, Experimental study, dynamic modelling, validation and analysis of hydrogen production from biomass pyrolysis/gasification of biomass in a two-stage fixed bed reaction system, Fuel. 137 (2014) 364–374. https://doi.org/10.1016/j.fuel.2014.07.076.
[186] F. Chen, C. Wu, L. Dong, A. Vassallo, P.T. Williams, J. Huang, Characteristics and catalytic properties of Ni/CaAlOx catalyst for hydrogen-enriched syngas production from pyrolysis-steam reforming of biomass sawdust, Appl. Catal. B Environ. 183 (2016) 168–175. https://doi.org/10.1016/j.apcatb.2015.10.028.
[187] Y. Shen, C. Areeprasert, B. Prabowo, F. Takahashi, K. Yoshikawa, Metal nickel nanoparticles in situ generated in rice husk char for catalytic reformation of tar and syngas from biomass pyrolytic gasification, RSC Adv. 4 (2014) 40651–40664. https://doi.org/10.1039/C4RA07760A.

[188] Y. Shen, P. Zhao, Q. Shao, D. Ma, F. Takahashi, K. Yoshikawa, In-situ catalytic conversion of tar using rice husk char-supported nickel-iron catalysts for biomass pyrolysis/gasification, Appl. Catal. B Environ. 152–153 (2014) 140–151. https://doi.org/10.1016/j.apcatb.2014.01.032.

[189] Y. Wang, X. Hu, Y. Song, Z. Min, D. Mourant, T. Li, R. Gunawan, C.-Z. Li, Catalytic steam reforming of cellulose-derived compounds using a char-supported iron catalyst, Fuel Process. Technol. 116 (2013) 234–240. https://doi.org/10.1016/j.fuproc.2013.07.014.

[190] X. Xiao, X. Meng, D.D. Le, T. Takarada, Two-stage steam gasification of waste biomass in fluidized bed at low temperature: Parametric investigations and performance optimization, Bioresour. Technol. 102 (2011) 1975–1981. https://doi.org/10.1016/j.biortech.2010.09.016.

[191] C.E. Efika, C. Wu, P.T. Williams, Syngas production from pyrolysis–catalytic steam reforming of waste biomass in a continuous screw kiln reactor, J. Anal. Appl. Pyrolysis. 95 (2012) 87–94. https://doi.org/10.1016/j.jaap.2012.01.010.

[192] M. Ouadi, N. Jaeger, C. Greenhalf, J. Santos, R. Conti, A. Hornung, Thermo-Catalytic Reforming of municipal solid waste, Waste Manag. 68 (2017) 198–206. https://doi.org/10.1016/j.wasman.2017.06.044.

[193] Z. Ma, S. Zhang, D. Xie, Y. Yan, A novel integrated process for hydrogen production from biomass, Int. J. Hydrog. Energy. 39 (2014) 1274–1279. https://doi.org/10.1016/j.ijhydene.2013.10.146.

[194] A. Erkiaga, G. Lopez, I. Barbarias, M. Artetxe, M. Amutio, J. Bilbao, M. Olazar, HDPE pyrolysis-steam reforming in a tandem spouted bed-fixed bed reactor for H2 production, J. Anal. Appl. Pyrolysis. 116 (2015) 34–41. https://doi.org/10.1016/j.jaap.2015.10.010.

[195] S. Czernik, R.J. French, Production of Hydrogen from Plastics by Pyrolysis and Catalytic Steam Reform, Energy Fuels. 20 (2006) 754–758. https://doi.org/10.1021/ef050354h.

[196] A. Arregi, G. Lopez, M. Amutio, I. Barbarias, J. Bilbao, M. Olazar, Hydrogen production from biomass by continuous fast pyrolysis and in-line steam reforming, RSC Adv. 6 (2016). https://doi.org/10.1039/C6RA01657J.

[197] A. Arregi, G. Lopez, M. Amutio, M. Artetxe, I. Barbarias, J. Bilbao, M. Olazar, Role of operating conditions in the catalyst deactivation in the in-line steam reforming of volatiles from biomass fast pyrolysis, Fuel. 216 (2018) 233–244. https://doi.org/10.1016/j.fuel.2017.12.002.

[198] I. Barbarias, G. Lopez, J. Alvarez, M. Artetxe, A. Arregi, J. Bilbao, M. Olazar, A sequential process for hydrogen production based on continuous HDPE fast pyrolysis and in-line steam reforming, Chem. Eng. J. 296 (2016) 191–198. https://doi.org/10.1016/j.cej.2016.03.091.

[199] I. Barbarias, G. Lopez, M. Artetxe, A. Arregi, L. Santamaria, J. Bilbao, M. Olazar, Pyrolysis and in-line catalytic steam reforming of polystyrene through a two-step reaction system, J. Anal. Appl. Pyrolysis. 122 (2016) 502–510. https://doi.org/10.1016/j.jaap.2016.10.006.

[200] A. Arregi, M. Amutio, G. Lopez, M. Artetxe, J. Alvarez, J. Bilbao, M. Olazar, Hydrogen-rich gas production by continuous pyrolysis and in-line catalytic reforming of pine wood waste and HDPE mixtures, Energy Convers. Manag. 136 (2017) 192–201. https://doi.org/10.1016/j.enconman.2017.01.008.

[201] M. Amutio, G. Lopez, M. Artetxe, G. Elordi, M. Olazar, J. Bilbao, Influence of temperature on biomass pyrolysis in a conical spouted bed reactor, Resour. Conserv. Recycl. 59 (2012) 23–31. https://doi.org/10.1016/j.resconrec.2011.04.002.

[202] X. Xiao, J. Cao, X. Meng, D.D. Le, L. Li, Y. Ogawa, K. Sato, T. Takarada, Synthesis gas production from catalytic gasification of waste biomass using nickel-loaded brown coal char, Fuel. 103 (2013) 135–140. https://doi.org/10.1016/j.fuel.2011.06.077.

[203] A. Remiro, B. Valle, A.T. Aguayo, J. Bilbao, A.G. Gayubo, Steam Reforming of Raw Bio-oil in a Fluidized Bed Reactor with Prior Separation of Pyrolytic Lignin, Energy Fuels. 27 (2013) 7549–7559. https://doi.org/10.1021/ef401835s.

Chapter 2: Detailed analysis of gas, char and bio-oil products of oak wood pyrolysis at different operating conditions

Résumé

Ce chapitre est issu dans son intégralité de l'article publié en juillet 2022 dans le journal « *Waste and Biomass Valorization* » [1].

L'objectif ultime de la thèse étant le couplage des procédés de la pyrolyse de la biomasse et du reformage catalytique, il s'avère nécessaire de commencer par étudier la pyrolyse de la biomasse seule afin de mieux comprendre les produits et les analyser en fonction des paramètres opératoires. Ceci permettra de déterminer les conditions optimales pour une production maximisée des espèces d'intérêts tels que les gaz biosourcés.

Les concentrations et compositions de ces produits dépendent fortement des conditions opératoires et de la nature de la biomasse. Ce chapitre présente une étude complète et détaillée de la composition chimique du gaz, de la bio-huile et du charbon dérivés de la pyrolyse des copeaux de bois de chêne en fonction de la température, de la vitesse de chauffe et du temps de séjour des composés volatils. La chromatographie en phase gazeuse et la spectrométrie de masse ont été utilisées pour déterminer les concentrations de dix gaz et de plusieurs composés de la bio-huile. L'analyse élémentaire a été appliquée pour analyser le charbon produit lors de chaque essai.

Nous montrons que lorsque la température augmente de 400°C à 800°C, les rendements en charbon et en bio-huile diminuent alors que les quantités de gaz augmentent. Les concentrations de H_2, CO et CH_4 ont augmenté tandis que celle de CO_2 a diminué avec la température. La vitesse de chauffe étudiée pendant la pyrolyse (5 à 100°C/min) a eu un impact moins important sur la distribution des gaz contrairement à la température. Néanmoins, lorsque la vitesse de chauffe augmente, le CH_4, et le CO augmentent alors que l'H_2 et le CO_2 diminuent. Il convient de noter que l'effet du temps de séjour a été examiné de deux façons : en faisant varier le volume disponible pour les réactions des composés volatils en modifiant l'emplacement de la biomasse dans le réacteur et en modifiant le débit du gaz vecteur. L'allongement du temps de séjour en réduisant le débit d'azote, le gaz vecteur, augmente les concentrations de CH_4, et de CO mais diminue celles de H_2 et de CO_2, de manière similaire à l'effet de l'accélération de la vitesse de chauffe. En plaçant l'échantillon au fond du réacteur, ce qui allonge le temps de séjour des produits volatiles, les concentrations de H_2 et de CO sont plus faibles tandis que celles de CH_4 et de CO_2 sont plus importantes que lorsque l'échantillon est placé au sommet du réacteur, proche de la sortie des gaz.

La composition de la bio-huile comprenait : benzène, toluène, éthylbenzène, xylène, naphtalène et phénol, entre autres. L'analyse élémentaire du charbon a montré une baisse de la teneur en hydrogène et en oxygène et une augmentation de la teneur en carbone à la suite du processus de volatilisation, par rapport aux teneurs en biomasse initiale. Cette étude a permis l'identification des paramètres adaptés demandés pour les applications des post-processus de pyrolyse (combustion, gazéification, ou pyrolyse catalytique) et ceux nécessaires pour favoriser la formation des produits désirés (charbon, bio-huile, gaz de synthèse) avec des compositions et des concentrations significatives.

2.1. Introduction

In the midst of the global energy crisis with the massive increase in the energy demand, the need for renewable and sustainable alternatives has been urging for a while now. Among the multiple solutions available, biomass presents itself as one of the most promising and environmentally friendly ultimate renewable sources of energy. Biomass is plentifully available all around the world which allows it to be exploited in several mainstreams of energy. Its biochemical composition consists of cellulose, hemicellulose and lignin with some extractives. Its combustion leads to the production of less pollutant gases than traditional fossil fuels. It also leads to lower emissions of Sulphur dioxide (SO_2), nitrogen oxides (NO_x) and carbon dioxide (CO_2) [2]. The effective valorization of biomass into energy falls in the world's planning for the mitigation of the greenhouse gas emissions and for the reduction of the global warming devastating impact on the Planet.

Biomass can be converted to energy via multiple conversion processes such as fermentation, anaerobic decomposition, pyrolysis, gasification, and combustion. Among these, the pyrolysis stands out given its numerous advantages naming the lower emissions and the possibility of reusing all the by-products. The pyrolysis takes place in an inert atmosphere in the absence of air, oxygen or any oxidizing agent. It results in the production of solids (carbonized products), liquids (water, tars and bio-oils) and syngas (mixture of gases containing mainly CO, CO_2, CH_4 and H_2) [3]. The biochar has multiple industrial, agricultural, and environmental applications such as catalytic reforming, fertilizer, and contaminants removal [4]. The bio-oil is a complex viscous liquid mixture and can be composed of more than 300 hydrocarbons and organic compounds [5]. Its composition is highly influenced by the nature of the biomass feedstock and the operating conditions of the pyrolysis [6]. H_2 and CO rich syngas is of special interest given its numerous fields of applications. While hydrogen is an energy carrier considered as a clean fuel and building block for several chemical activities, CO is also an important industrial species used as a reducing agent in metallurgy and as a water or producer gas. Together, H_2 and CO produced frequently by gasification can be applied to produce hydrocarbons and their oxygenated derivatives in the Fischer-Tropsch process [7].

Biomass pyrolysis has been drawing a lot of attention in the last few decades as one of the most technically and strategically advantageous thermal conversion methods to produce biochar, biofuel, and syngas. These products are very promising energy resources as they can be used as renewable and sustainable alternatives to the non-renewable and unsustainable fossil fuels [8]. Specifically, they can be a suitable replacement for the fossil fuels in the transportation and power generation fields. Nonetheless, the pyrolysis process is not restricted to the main decomposition of the biomass since secondary reactions such as tar cracking or bio-oil pyrolysis can take place between the volatile species at high temperatures [9–11].

The pyrolysis has been the subject of investigations for a while now and a lot of progress have been made in the field. Some of the most important and global reviews discussing the pyrolysis are available elsewhere [12–14]. The study of the effect of the operating parameters has been also the subject of researches and review papers [15,16]. Pyrolysis has been also employed as a preliminary step to other thermochemical processes such as combustion, gasification, and reforming. Therefore, it is of primary importance to know the composition of the different products formed during this pre-step since it may have a strong influence on the overall process results.

Additionally, several factors and operating parameters have been identified to play a key role on the distribution of the volatile compounds. They include the reactor temperature, the heating rate, the residence time, the operating pressure, the biomass type and structure, the particle size and shape… Understanding the effect of these parameters is extremely important to optimize the production of the desired species. In this perspective, multiple studies have been conducted. For instance, the effect of the temperature on the main products and the gas composition derived from the pyrolysis has been studied for the biomass main components (cellulose, hemicellulose or lignin) and typical wood species [17–19]. The effect of heating rate on the biomass primary pyrolysis products distribution has also been considered in the literature [20–22]. While the residence time is known to have a great influence on pyrolysis, studies reporting its influence on the process products are limited [23–25]. Although the composition of the biomass and the main pyrolysis gases has been frequently investigated [26–28], a detailed analysis of all the pyrolysis products (gases, bio-oil and char) compositions is less frequent, and will only be in function of one or few parameters only [29–31].

The purpose of this work is twofold: (i) to investigate the effect of main and most influencing operating parameters namely temperature, heating rate and residence time on the wood biomass pyrolysis; and (ii) to realize a detailed analysis of chemical composition of the gas, liquid and solid pyrolysis products. Oak wood chips are selected as biomass sample. The effect of temperature will be studied by varying the reactor temperature from 400°C to 800°C. The influence of the heating rate on the primary pyrolysis will be considered by working at rates going from 5°C/min to 100°C/min. It is worthy to note that the effect of residence time will also be examined in two ways: by varying the available volume for volatile reactions downward the sample within the reactor and by changing the flowrate of the carrier gas. The composition of the gases, the bio-oil and the char formed during the pyrolysis at the different operating conditions will be determined and the optimal parameters favoring the formation of selective products will be determined.

2.2. Materials and methods

2.2.1. Materials and characterization

2.2.1.1. Materials

The biomass investigated is oak wood chips, one of the most abundant wood species in France (27% of the forest area). Oak is a hard wood used for decades given its large applications and its high content of tannin. It provides bark for tanning leather, timber for construction, acorns to feed livestock in addition to the possibility of burning wood to produce fuel. Moreover, oak wood is characterized by its high-quality hardwood allowing its use in construction and furniture manufacture. Thereby, oak is economically one of the most remarkable deciduous tree in the European forest [32].

For the different pyrolysis tests, a constant amount of oak wood chips of around 3.5 g was taken from the feedstock as received. The wood chips are placed in a porous cylindrical container (diameter 4 cm and height 10.2 cm) made of nickel wires. For our experiments, the sample container is filled up to a height around 5 cm which is equivalent to an approximate oak chips volume of 60 cm^3 and a bed density of 0.059 g/cm^3. **Figure 2.1** shows the photographs of: (a) the biomass sample (3.5 g of oak wood chips) before pyrolysis; (b) the corresponding char sample obtained after a pyrolysis experiment realized at 700°C, a heating rate of 80°C/min and a nitrogen flow rate of 100 mL_n/min; and (c) the related bio-oil sample obtained after the pyrolysis under the same experimental conditions.

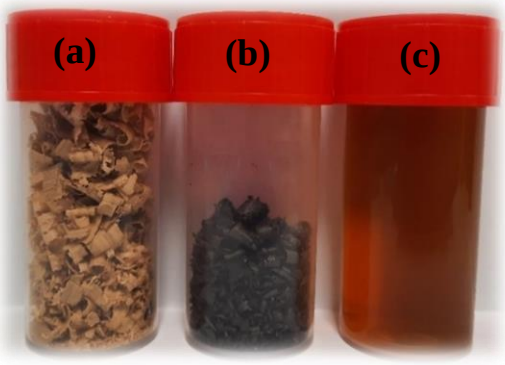

Figure 2.1 Photograph of typical biomass sample with the pyrolysis char and bio-oil products. (a) the initial oak wood chips (3.5g); (b) corresponding char sample after pyrolysis at 700°C, a heating rate of 80°C/min and a nitrogen flow rate of 100 mL_n/min; (c) a bio-oil sample diluted with pure acetone after pyrolysis in the same conditions

2.2.1.2. Characterization of oak wood

Moisture content of oak wood

The moisture content of the oak wood chips was determined by drying the wood at 100°C for 35 min in the pyrolysis furnace. The water content was estimated as the difference between the initial and the final weights after 35 min of drying. The experiment was realized in five replicates and the average moisture content was determined to be around 7.5 wt.%.

Physical characteristics of oak wood

Some of the basic physical characteristic of the oak wood chips such as the thickness, characteristic length and the density are summarized in the **Table 2.1**. The thickness of the wood chips was measured using a micrometer. The characteristic length was quantified using a Vernier caliper. The density was determined based on a block of the same oak wood from which the chips were cut. It had a regular shape for which the volume was calculated, and the mass was weighed.

Table 2.1 Physical characteristics of the oak wood chips

Physical characteristics	Value
Thickness (mm)	0.3 – 0.4
Characteristic length (mm)	8
Density (kg/m^3)	806

Composition of the oak wood

The elemental and proximate analyses of the oak wood chips as well as their chemical composition in terms of cellulose, hemicellulose, and lignin (the wood main components) were

determined. The results of these analyses are listed in the **Table 2.2**. The elemental analysis was realized following the method described in the section 2.2.5. The proximate analysis was performed according to analytical methods using a micro pyrolyzer, while the chemical composition was retrieved following the Van Soest's protocol [34]. For the chemical composition, other compounds were detected in the oak wood, in addition to the cellulose, hemicellulose, and lignin. They include nitrogenous compounds and phenolic extractables. Both the elemental and proximate analyses of the oak wood can be considered relatively close to that found in the literature [35] whereas the chemical composition appears distinct. The differences could be related to the diverse origins of the initial samples between our study and that in the literature even though the samples both originate from France but come from different regions.

Table 2.2 Oak wood detailed composition

Elemental analysis (%)		***Proximate analysis (%)***		***Chemical composition (%)***	
Carbon	46.52	**Volatile matter**	82.4	**Cellulose**	37.85
Hydrogen	6.03	**Fixed carbon**	17.2	**Hemicellulose**	21.22
Oxygen	47.13	**Ash**	0.4	**Lignin**	25.41
Nitrogen	0.21			**Other**	15.52
Sulphur	0.11				

2.2.2. Methods

2.2.2.1. Pyrolysis setup

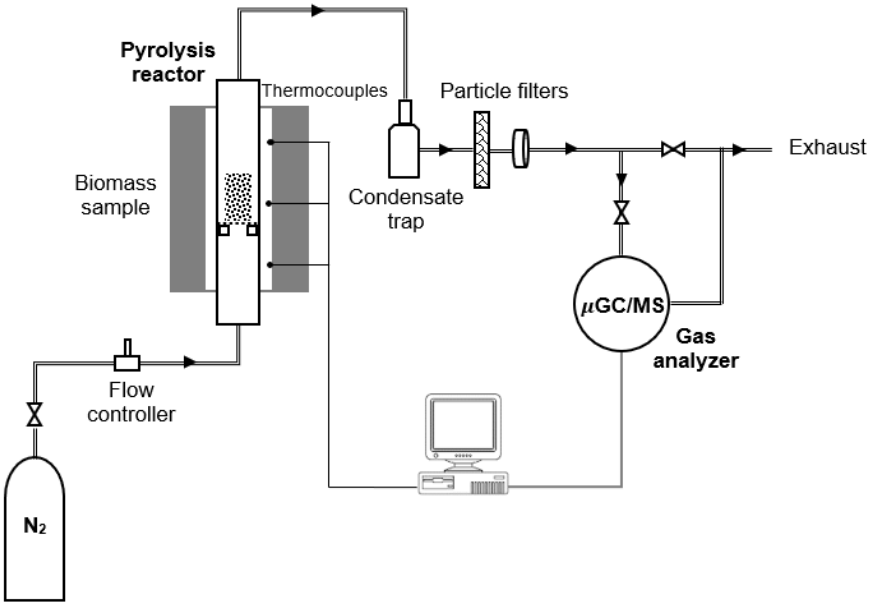

Figure 2.2 Experimental set up for the pyrolysis study of wood coupled with the gas analyzer

The biomass pyrolysis was realized in a lab-scale cylindrical pyrolyzer which is a three-zone compact vertical split tube furnace (model EVZ12/600b-Carbolite Gero 30-3000C) (**Figure 2.2**). It uses free radiating wire elements which are embedded within the insulation of the furnace body. It has an electric power of 2.5 kW with a heated length of 600 mm. The furnace is equipped with three K-type thermocouples which are inserted at three levels: top, center and bottom with the furnace placed vertically. The effective temperature of the sample was taken

as the temperature given by thermocouple located in its vicinity. The reactor is a cylindrical quartz tube having a diameter of 45 mm and a height of 600 mm. Inlet and outlet gas flanges, made of stainless steel, close the two ends of the quartz tube.

High purity nitrogen (about 99.996%) was employed as gas carrier of the vapors formed during the pyrolysis. It also avoided oxidation and combustion phenomena within the reactor. The nitrogen flow rate was controlled by a flow meter of capacity ranging from 0 to 500 mL_n/min, with mL_n/min defined at the normal conditions of temperature and pressure (20°C and 1 atm). Before each pyrolysis test, a continuous nitrogen flow rate of 100 mL_n/min during 20 min was applied to purge the reactor of oxidizing gases such air and steam. Unless otherwise stated, this gas flow rate was kept constant at 100 mL_n/min during the entire operation.

The vapors residence time has an undeniably crucial role in the pyrolysis process since a long residence time favors the tar cracking and allows gaseous secondary reactions to take place. It is important to differentiate between the solid and the vapors residence times. The solid residence time refers to the duration of the solid sample staying in the pyrolysis furnace while it is heated. It is imposed by the reactor type (fixed bed, fluidized bed, spouted bed reactors …). For instance, the solids residence time in a fixed bed reactor is very long, whereas in a fluidized bed reactor, both the solids and volatiles residence times are much shorter (about few seconds). The solid residence time must be long (in the order of minutes or hours) if complete cracking and devolatilization are needed [36].

The vapor residence time is directly related to the operating conditions such as the carrier gas flow rate and the reactor volume. A low carrier gas flow rate implies a long vapor residence time whereas a large flow rate reduces the volatiles residing time in the reactor to the order of few seconds. When longer residence times are applied, the biomass constituents have more opportunities to be repolymerized which increases the biochar yield. Likewise, if the biomass is positioned in the bottom of a vertical furnace, the vapors ascending the heated furnace take more time to reach the reactor's exit. Thereby, they are exposed to additional heating as they travel through the furnace and might be subject to secondary reactions. When the biomass is placed at the top of the furnace, i.e., close to the exit of the reactor, the vapors leave rapidly. They have less residence time in the reactor to be exposed to more heating and thus are less influenced by secondary reactions. The vapor residence time must be as short as possible if the secondary reactions are undesired [37].

To study the effect of the residence time on the pyrolysis, two approaches were adopted. The first consists of varying the position of the sample container between the bottom and the top of the furnace (**Figure 2.3**) thereby changing the volume of the reaction zone during the pyrolysis. This approach is rarely encountered in the literature. When the sample container is placed at the top (**Figure 2.3** (a) zone A), the distance between the top end of the tube and the top surface of the sample equals 17 cm, corresponding to a volatiles volume of 270.4 cm^3 above it. Given the small volume, the pyrolysis vapors rapidly exit the reactor so that they are fairly subject to secondary reactions. When the container is placed at the bottom (**Figure 2.3** (b) zone C), the distance between the top end of tube and the top surface of the sample equals 47 cm, corresponding to a volatiles volume of 747.5 cm^3 above it. The pyrolysis vapors travel the long heating zone of the reactor. This can lead to the potential occurrence of secondary tar cracking reactions. The sample can be also placed in the center of the furnace in the zone B at a distance of 32 cm from the top end of the tube, which corresponds to a volatile volume of 508.9 cm^3.

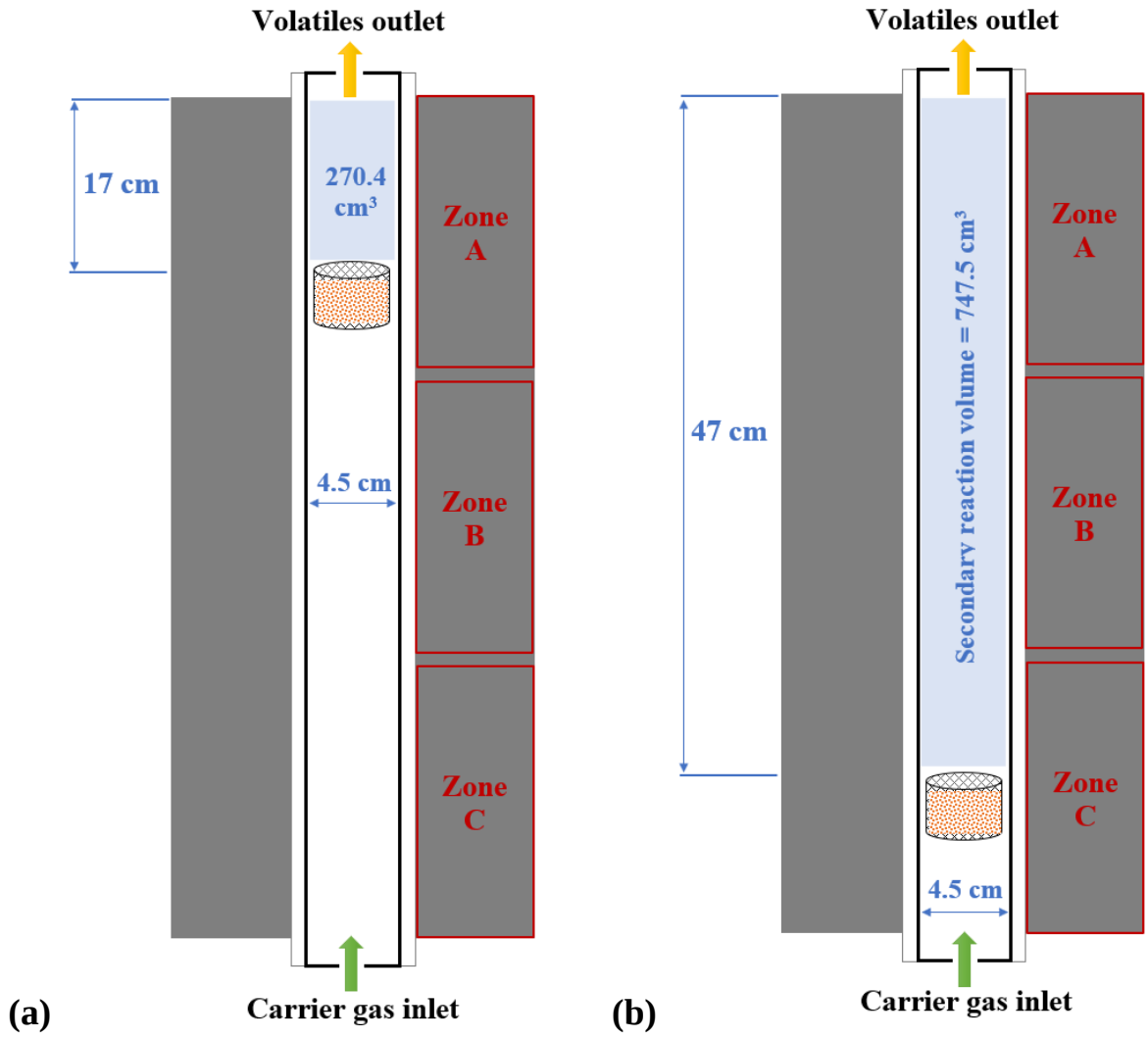

Figure 2.3 Representation of the furnace used for the pyrolysis with the three heating zones referred to as A, B and C. The heights of the reaction zones are linked to sample positions in zones A, B and C, respectively. (a) The sample is placed at the top of the furnace, in Zone A, with a volume of potential secondary reactions equals to 270.4 cm^3 above it. (b) The sample is placed at the bottom of the furnace, in Zone C, with a volume of potential secondary reactions equals to 747.5 cm^3 above it

The second approach of varying the residence time consists of applying different flow rates of the carrier gas. For this purpose, the nitrogen flow rate was varied from 50 to 300 mL_n/min and the estimates of the corresponding residence times in function of the position in the furnace are summarized in **Table 2.3**. With a low flow rate (50 mL_n/min), the residence time can be reasonably considered as the longest (around 630s with sample at the bottom and 250s at top), since the gases have a long path of flow throughout the reactor. Whereas, with a high flow rate of 300 mL_n /min, the gases produced will be forced to leave the reactor rapidly and the residence time is the lowest (around 140s at the bottom and 50s at the top).

Table 2.3 Estimation of the vapor residence time in the furnace with varying nitrogen flow rate with the wood basket at top and bottom of the furnace

Nitrogen flow rate (mL_n/min)	Estimated residence time at top (s)	Estimated residence time at bottom (s)
300	50	140
100	140	390
50	250	630

The bio-oil, i.e., the condensable pyrolysis vapors, was filtered with a condensate trap, installed downstream of the furnace. It consists of a beaker filled with ice cooled water and aims to liquefy the steam as well as the majority of the condensable gases. For further removal of bio-oil residues and solid particles, which can plug the flowmeters and harm the gas analyzer [38], additional filters are needed. Therefore, a 10 cm tube filled with cotton, followed by a particle filter consisting of an 8 µm membrane, were positioned after the condensate trap. A heating wire attaining 100°C is wrapped around the volatiles conducting tubes from the furnace until the gas analyzer, to avoid the condensations of the unfiltered heavy hydrocarbons. A flowmeter of capacity ranging from 0 to 500 mL_n/min was placed after the two filters to measure the overall gas flow leaving the pyrolysis reactor.

All the experiments began with the drying phase of the sample as received. The furnace was programmed to heat from room temperature to 100°C, at a heating rate of 10°C/min and to dwell at this temperature for 35 min. This duration was found to be the one required to complete the drying phase, based on additional weight loss experiments. After this duration, the weight loss becomes negligible. Next, the pyrolysis phase was started from 100°C by applying a temperature ramp (e.g., 5, 30, 80 and 100°C/min) to the target temperature of pyrolysis (400, 500, 600, 700 and 800°C). The set point temperature is maintained constant for 1 hour, after which the pyrolysis tests were ended. Under these operating conditions, the pyrolysis process has been categorized as slow and intermediate pyrolysis [15].

2.2.2.2. Main products distribution

The products of the pyrolysis have been divided into three categories based on their phases under normal conditions: char (black solid), gases (non-condensable volatiles) and bio-oil (liquid or condensable vapors). Char or biochar is a carbon-rich solid residue, which might also contain some impurities like aromatic species. The gases include mainly hydrogen, carbon monoxide, carbon dioxide, and methane. They have been classified industrially as syngas. At the same time, the gases contain short hydrocarbon chain gases such as ethane and propane… The liquid products consist of aromatic and aliphatic compounds, aldehydes, levoglucosan, phenols, other hydrocarbon chain compounds and water. It is worth noting that there is a difference between tar and bio-oil. While tar is a dark brown or black liquid with high viscosity containing free carbon and hydrocarbons, bio-oil is a less viscous liquid composed of lighter organic compounds than tar [8]. With the absence of a stiff scientific definition of the tar, it has been a common practice to define tar as all the products of pyrolysis having a molecular weight superior to that of benzene [39].

2.2.2.3. Gas analysis

A micro–Gas Chromatography/Mass Spectrometry (µGC/MS, Agilent Single quad MSD 5977B and SOLIA 490 microGC) was used to analyze the non-condensable gases produced by the pyrolysis. The analyzer, equipped with a pump, sucks a gas sample of 50 mL_n/min flowrate. The µGC used included three analytical modules equipped with micro TCD (thermal conductivity detector). The first column is a molecular sieve MS5A column and separates hydrogen H_2, oxygen O_2, nitrogen N_2, methane CH_4 and carbon monoxide CO from the gas sample. The second, a PPU column, is able of separating carbon dioxide CO_2 as well as C_2 and C_3 hydrocarbons (ethylene C_2H_4, ethane C_2H_6, acetylene C_2H_2, propane C_3H_8, propylene C_3H_6…). Whereas the third column, made of 13CB, detects H_2O molecules and heavy hydrocarbons (benzene C_6H_6, toluene C_7H_8, furan, furfural, ethylbenzene, m-, p- and o-xylene among many others). The carrier gases of the analyzer were helium and argon.

For the quantification purpose, the analyzer was calibrated by using standard gas samples with known concentrations. Details on the standard gas samples used for the calibration are provided in **Table S2.6** in the supplementary information. Quantitative analysis of all produced gas molecules during the pyrolysis is fastidious given the large number of required reference gases. Therefore, we quantified only main interest molecules in the wood biomass pyrolysis field such as H_2, CO, CH_4 and CO_2 as well as C_2H_4, C_2H_6, C_6H_6 and C_7H_8.

Based on the literature reviewed and the experiments realized, it is noticed that the pyrolysis initiates at around 240°C. Indeed, this is known as the onset temperature of hemicellulose decomposition [5]. This was also confirmed by the major weight loss that begins at 240°C. Therefore, the sequences of analysis in the µGC/MS were launched when the temperature of the reactor reaches 200°C. This avoids aspirating water during the pre-pyrolysis drying phase, which may damage the analyzer columns. Each analysis took around 90s and for each experiment 36 analysis were made to cover the phase of heating and dwelling at the constant temperature of pyrolysis.

2.2.2.4. Bio-oil analysis

The condensable gases produced during the pyrolysis form the so-called bio-oil. Its composition is analyzed using a gas chromatography/mass spectrometry (GC/MS/MS Varian 1200 Single Quadrupole with Varian CP 3800 GC) for some pyrolysis experiments. The analyzed bio-oil was produced during pyrolysis experiments realized at several temperatures, heating rates and vapor residence time. The volatiles forming the bio-oil were condensed in 100 mL of pure acetone in an ice-cooled beaker positioned at the outlet of the furnace. Knowing that the bio-oil compounds are numerous and can go up to 300 [38], several methods were applied for the analysis with the GC/MS in order to identify a wide range of the bio-oil species:

- A method with a slow heating rate program to elute the lightest compounds, in particular the BTEX (benzene, toluene, ethylbenzene and xylene).
- A method with a split was also applied to quantify the benzene.
- A method with a higher heating rate program at the beginning was adapted for the heavier compounds and specifically the PAHs (polycyclic aromatic hydrocarbons).
- Seeing that the amounts of the PAHs detected were very small, the samples were reanalyzed with mass detection in SIM mode.

The slow, fast and split programs are summarized in the **Table S2.1, Table S2.2 and Table S2.3** reported in the supplementary information. From these methods, qualitative analysis was performed which allowed the identification of multiple compounds, partially by comparison to the spectra libraries of Nist and Wiley. The quantification of numerous bio-oil compounds was also realized based on a previous calibration of the GC/MS apparatus. Some of the bio-oil samples are shown in **Figure S2.9** in supplementary information. The color difference visible between the samples reveals the effect of two operating parameters: the heating rate and the residence time as it will be discussed in the results section.

2.2.2.5. Characterization of the char formed

The elemental analysis was also performed on the char produced during some pyrolysis experiments in terms of the chemical elements content: Carbon C, Hydrogen H, Oxygen O and Nitrogen N. These elements were measured using a CHNS/O Thermo Electron Flash. Portions of the grinded samples were weighed in a tin (for C, N and H) or silver (for O) capsule with a mass of approximately 1 mg (± 0.2 mg). Capsules were then closed, placed onto the apparatus holder, and dropped periodically into a vertical combustion tube where pyrolysis takes place at

1000°C. The compounds produced by pyrolysis are separated on a poraplot Q column and detected by a thermal conductivity detector. The four compounds were previously calibrated using a cysteine standard. The analyses were performed in three replicates and the averages will be given in a summary table along with uncertainty in the results section. A selection of the biochar formed is given in the **Figure S2.8** (supplementary information). The difference in the char volume exposes the influence of the temperature and the heating rate as it will be explained in the results section.

2.2.2.6. Mass balance

At the beginning of the pyrolysis experiments, the biomass sample container was filled with around 3.5 g of oak wood chips. This weight represents the initial amount of wood biomass (m_{wood}). This sample contains 7.5 wt.% of moisture and therefore, the dry wood weight was determined ($m_{\text{dry wood}}$). At the end of the experiment, the container filled with the char was extracted from the reactor and weighed to obtain an approximate mass of the char produced (m_{char}). The mass concentration of char produced was calculated on a dry basis (equation **(2.1)**):

$$C_{\text{char}} = 100 \times \frac{m_{char}}{m_{dry\ wood}} \quad \textbf{(2.1)}$$

The gases exiting the pyrolysis reactors were cooled by the condensate trap to the ambient temperature (20°C). From the gas analysis, the volume concentrations (in vol.%) of the main compounds quantified were measured each 90s. Knowing the volume flow rate for each analysis and the density of each gas at normal conditions (20°C and 1 atm), the mass of each gas produced was calculated and integrated over the pyrolysis experiment duration. The mass concentration of gas produced was calculated (equation **(2.2)**):

$$C_{\text{gas}} = 100 \times \frac{\sum m_{\text{gases}} - m_{\text{N}_2}}{m_{\text{dry wood}}} \quad \textbf{(2.2)}$$

Given the bio-oil filtration steps previously described, the weight of the bio-oil was determined from the global mass balance. The mass concentration of bio-oil produced was estimated (equation **(2.3)**):

$$C_{\text{bio-oil}} = 100 - (C_{\text{char}} + C_{\text{gas}}) \quad \textbf{(2.3)}$$

2.2.2.7. Reproducibility analysis

In order to analysis the reproducibility of our experiments, a pyrolysis experiment was repeated five times in the same operating conditions: 3.5 g of oak wood chips, heating rate of 30°C/min, nitrogen flow rate of 100 mL_n/min, and temperature of 500°C maintained for 30 min. The uncertainties were determined following the equation **(S2.1)** [40], described in section 1 in the supplementary information, with the relative explanation. Knowing the uncertainty related to each concentration, the relative uncertainty can be also determined and is represented in **Figure S2.1** in the supplementary information. It can be stated that for low concentration ranges (less than 1%, corresponding to the light and heavy hydrocarbons representing our minor products), the relative uncertainties fall between 8% and 17%. Whereas for high concentration ranges (above 30%, related to the permanent gases corresponding to our major products), the relative uncertainties drop down to between 3 and 4%. The uncertainties will be represented as error bars on some of the results graphs.

2.3. Results and discussions

2.3.1. Effect of temperature on biomass pyrolysis

2.3.1.1. Main products distribution

The temperature, and more precisely heat, is the most critical parameter influencing the pyrolysis being an endothermal process. In order to investigate the effect of temperature on the oak pyrolysis, we began our study by realizing multiple pyrolysis tests while varying the temperature from 400°C to 800°C with 100°C increment. The container holding the biomass sample was placed at the bottom of the pyrolysis furnace (see **Figure 2.4**). The heating applied to reach the target temperature was accomplished at a rate of 30°C/min. An inert environment was created by applying a nitrogen flow rate of 100 mL_n/min during the entire experiment. In this first set of experiments, the temperature was maintained constant at the target set point for around 30 minutes. The effect of temperature on the main products of the oak pyrolysis is illustrated in the **Figure 2.4**.

As the temperature was raised from 400°C to 800°C, the gas yield remarkably increased whereas the char yield dropped until 700°C then slightly increased as the temperature was further elevated to 800°C.the increase in the char yield could be the results of the carbon deposition over the char surface resulting from the cracking of the hydrocarbons into carbon and hydrogen, as explained later. Interestingly, the drop in the char yield can be visualized from **Figure S2.8** (supplementary information) between the experiment (a) at 500°C and (b) at 700°C, with a remarkable weight decrease from 0.92 g to 0.82 g, respectively. The bio-oil yield increased at first to reach a maximum around 500°C above which it started decreasing. The gas yield made a high leap when the temperature was increased from 500°C to 600°C. This means that the gas fraction starts increasing at the expense of the liquid fraction above 500°C.

These results are in accordance with several other works [41,42]. Thereby, as the temperature increases, the oak wood starts devolatilizing with a considerable formation of bio-oil. Nonetheless, the highest jump in the gas yield was observed between 700°C and 800°C. and was accompanied by a large drop in the bio-oil yield It can be concluded that above 700°C, the bio-oil undergoes secondary cracking reactions followed by the undeniably important rise in the gases yield. *Therefore, it can be concluded that to produce a high gas yield and to reduce the bio-oil formation, the pyrolysis must be realized at high temperatures (above 700°C).*

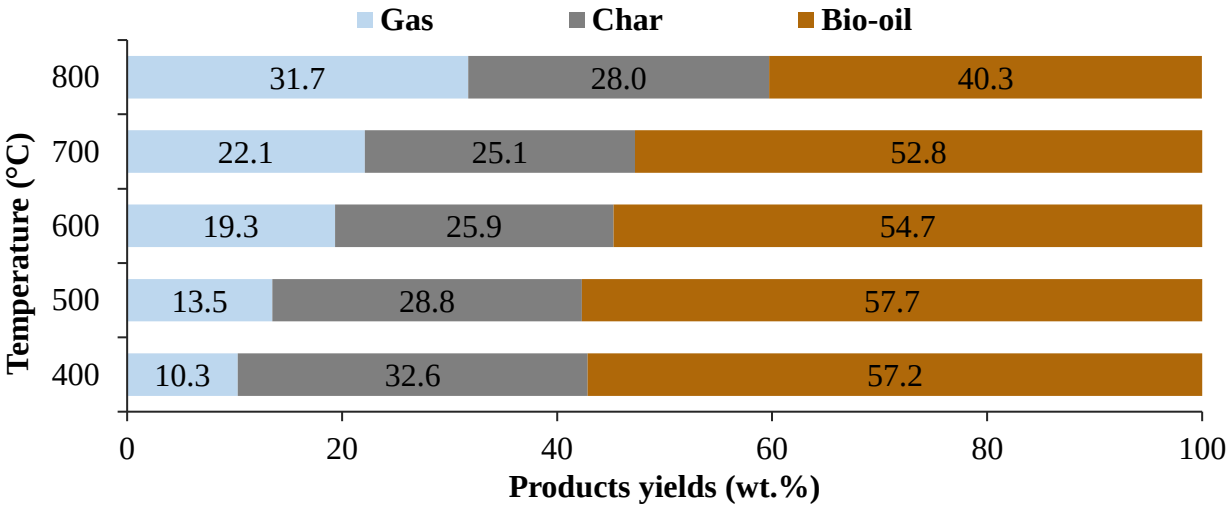

Figure 2.4 Effect of temperature on the main products of the pyrolysis of oak wood chips (heating rate = 30°C/min, nitrogen flow rate=100mL/min, reactor at bottom, duration of constant temperature = 30 min)

It should be noted that the volatile's residence time varies with the temperature due to the gas expansion. In fact, increasing the temperature from 400°C to 800°C, decreases the residence time from 415s to 363s when the biomass sample is placed at the bottom of the pyrolysis reactor. Given the relatively small gap (52s) between the two extreme residence times, its influence on the pyrolysis products is expected to be minimal. The effect of the residence time will be investigated in depth with larger intervals of residence time values in section 3.3. of the results.

2.3.1.2. Gas' concentrations

Ten of the gases produced by the pyrolysis are quantified by the μGC/MS. The gaseous products are subdivided into three categories: permanent gases composed of H_2, CO, CO_2 and CH_4 (forming the major pyrolysis gases); light hydrocarbons such as ethane and ethylene; and heavier hydrocarbons including benzene, toluene, ethylbenzene and m,p-xylene. The light and heavy hydrocarbons are detected in small amounts since these are the traces of condensable gases that remain after the filters and the condensate trap. They are therefore categorized as minor products and therefore their concentrations will be presented in the supplementary information document. In addition to water vapor, other hydrocarbons were also produced in small quantities and have been identified but not quantified by the μGC/MS including propene, furan, 1,3-cyclopentadiene, 2-butene, 2-methylfurane, 2,5-dimethylfurane, phenol, 2-ethyl-5-methylfurane.

Figure 2.5, **Figure S2.2** and **Figure S2.3** (supplementary information) depict the evolution in function of temperature of the volume concentrations of the quantified gases produced during the pyrolysis of oak wood chips. It can be noticed that temperature's increase entails an abrupt increase in the hydrogen yield from 0.6 vol.% at 400°C to 24.16 vol.% at 800°C. It is worth mentioning that the hydrogen formation begins intensely at high temperatures (above 500°C). Methane increased to reach a maximum at 700°C. The carbon monoxide peaked at 600°C. The increase in the concentrations of CO and CH_4 can be considered linear with the increasing temperature. When the temperature is further increased to 800°C, the concentrations of both CH_4 and CO dropped. CO_2 had a monotone decreasing evolution from 400°C to 800°C.

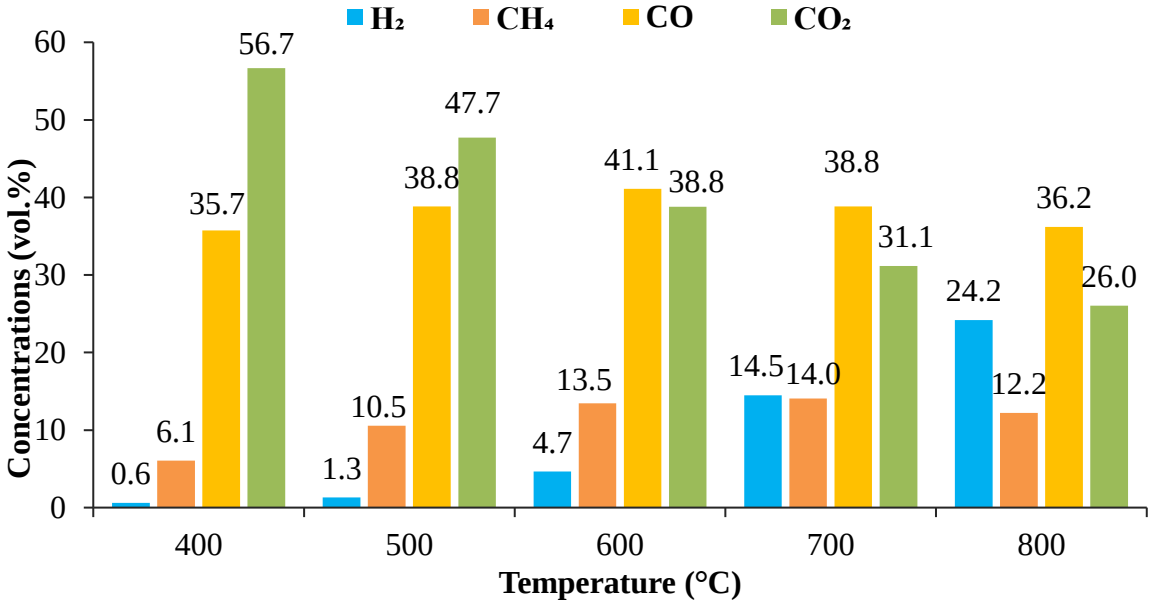

Figure 2.5 Effect of temperature on the volume concentrations of the major gases produced from the pyrolysis of oak wood chips (heating rate = 30°C/min, nitrogen flow rate = 100 mL_n/min, reactor at bottom, duration of constant temperature = 30 min)

Interestingly, for temperatures lower than 500°C, with a slow heating rate, the dominant gas produced in terms of volume concentrations is the CO_2, followed by CO and then CH_4 and H_2. However, as the temperature is further increased above 500°C, the CO becomes the main gas produced with the highest volume concentrations. The increase in the CO concentrations can be attributed to homogeneous secondary reactions which potentially take place at temperatures surpassing 500°C producing primarily CO [43]. These results are in accordance with the works of Xin *et al.* [44] who performed the pyrolysis of the three main components of the biomass and studied the variation of the products in function of the temperature varied from 350°C to 850°C. They found similar gases evolution mainly with the cellulose pyrolysis, which is compatible with our findings given that cellulose is the major biomass component of our oak wood.

The difference in the gases released at the different temperatures can be attributed to the distinct chemical structures of the main components forming the biomass: cellulose, hemicellulose and lignin. Cellulose is made of a long glucose polymer without ramifications, with a well-ordered robust structure and a high thermal stability. The high CO concentrations can be originated from the decomposition of cellulose due to the thermal cracking of carboxyl (C=O) and carbonyl (C−O−C) [26]. The CO_2 concentration was the highest at 400°C, since the degradation of hemicellulose, having a high carboxyl content, begins at low temperatures with CO_2 as a main degradation product [45]. In fact, hemicellulose involves several sugar molecules such as galactose, glucose, mannose… with an amorphous random structure exhibiting numerous ramifications. These branches can be easily detached from the core stem at low temperatures and are degraded into volatiles including CO, CO_2 and other hydrocarbons. H_2 and CH_4 are mainly released from the deformation and cracking of lignin, containing methoxyl-O-CH_3 and aromatic rings with several branches, which take place within a large temperature range (200-900°C) [26].

Ethylene and ethane followed the same trend as CO where it increased from 400°C to 600°C and then it decreased. In fact, at high temperatures (above 500°C), the lignin degradation occurs which leads to the formation of more CO, H_2, CH_4, C_2H_4 and C_2H_6 gases. These gases can also be the products of some other reactions such as vapor cracking, water gas-shift reaction and reforming [5].

Regarding heavier hydrocarbons, it can be noted that the benzene concentration began by increasing with the rise of temperature to 500°C but then quickly changed its evolution by descending when the temperature increased up to 800°C. Toluene also behaved similarly to CH_4 and CO where it peaked at 700°C above which it dropped. It is worth noting that the ethylbenzene made its appearance only at the highest temperature of 800°C with a very small concentration of 0.03 vol.%.

It is important to mention that benzene, toluene, ethylbenzene and m,p-xylene, which are referred to as BTEX, are considered in the literature as secondary tar compounds [46]. They are produced essentially from phenolics (aromatic compounds containing a phenyl group), originating from lignin. BTEX are also produced, in lower amounts, from cellulose and hemicellulose [47]. This confirms that secondary reactions take place especially at high temperatures, knowing that the biomass sample was positioned at the bottom of the reactor, extending the residence time of the vapors, as it will be discussed later.

Some of possible gaseous phase reactions that can occur during the pyrolysis are summarized by the following equations [48]:

$$C + CO_2 \leftrightarrow 2CO \qquad \Delta H^0_{298} = +168\ MJ/kmol \qquad \textbf{(2.4)}$$
$$C + H_2O \leftrightarrow CO + H_2 \qquad \Delta H^0_{298} = +175\ MJ/kmol \qquad \textbf{(2.5)}$$
$$CH_4 + H_2O \leftrightarrow CO + 3\,H_2 \qquad \Delta H^0_{298} = +206\ MJ/kmol \qquad \textbf{(2.6)}$$
$$CH_4 + 2H_2O \leftrightarrow CO_2 + 4\,H_2 \qquad \Delta H^0_{298} = +165\ MJ/kmol \qquad \textbf{(2.7)}$$
$$CO + H_2O \leftrightarrow CO_2 + H_2 \qquad \Delta H^0_{298} = -41\ MJ/kmol \qquad \textbf{(2.8)}$$
$$C + 2H_2 \leftrightarrow CH_4 \qquad \Delta H^0_{298} = -75\ MJ/kmol \qquad \textbf{(2.9)}$$
$$[C_xH_yO_z] \rightarrow C + Tar + CO + H_2 + CH_4 + C_nH_m \qquad \textbf{(2.10)}$$
$$[C_xH_yO_z] + H_2O \rightarrow CO + H_2 + Tar \qquad \textbf{(2.11)}$$
$$[C_xH_yO_z] + CO_2 \rightarrow CO + H_2O + Tar \qquad \textbf{(2.12)}$$

C is used for the char or coke formed (solid product), tar represents the secondary tar formed (liquid product) and $[C_xH_yO_z]$ indicates the intermediate tar phase while ΔH^0_{298} is the standard formation enthalpy at 298 K.

It can be concluded that the major product of the oak pyrolysis at low temperatures is the CO_2 followed by CO, CH_4 and H_2. These results are contradictory with those obtained by Amini *et al.* [22] where the pyrolysis of live and water oak wood was performed at 500°C, with same operational conditions (30°C/min heating rate and 100 mL_n/min). They found that the major gas was CO followed by CO_2. In our experiments, at 600°C and above, CO becomes the dominant product instead of CO_2. This result is in accordance with the one found by Figueiredo *et al.* [41] who also performed the pyrolysis of oak wood at 700°C. Interestingly, we found that the hydrogen yield (24.16 vol.%) surpasses that of methane (12.21 vol.%) at 800°C. The rest of the gases are in minor amounts and can be considered as part of the bio-oil products along with the other condensable vapors.

The largest gas yield is obtained at the highest pyrolysis temperature of 800°C. However, the evolution's tendency of gas concentrations started changing at 800°C especially for the CO, CH_4, ethane and toluene which started to decrease. *Being aware of the larger power requirement to reach higher temperatures, and in the goal of reducing the energy consumption, 700°C will be considered as a compromise temperature for the pyrolysis in terms of high gas production (including syngas) and low bio-oil formation with an inferior energy consumption, simultaneously*. This temperature will be adapted for the following experiments when the temperature is required to be constant.

2.3.2. Effect of heating rate on biomass pyrolysis

2.3.2.1. Main products distribution

The heating rate is the second most important parameter affecting the pyrolysis. It influences not only the products distribution and the gas composition but also the char structure and the bio-oil quality, as well as the char specific area and the pores volume. The heating rate reflects the time required to attain the pyrolysis target temperature. In our study, four values of heating rates (5, 30, 80 and 100°C/min) were applied to reach the target set point temperature of pyrolysis (700°C). This set point temperature was then fixed for 1 hour, as for all the experiments realized here after. The nitrogen flow rate was fixed at 100 mL_n/min over the experiment duration. The container filled with 3.5 g of oak wood chips was placed at the top of

the pyrolysis furnace. The impact of the heating rate on the main products distribution of the pyrolysis is elaborated in **Figure 2.6**.

It can be noticed that the heating rate has a smaller effect on the main product distribution than the temperature, since the heating rate was changed from 5 to 100°C/min for which the pyrolysis can be categorized as slow and intermediate pyrolysis [15]. Thereby, the heating rate change cannot be considered drastic, and its effect is minimal on the pyrolysis products. The uncertainties of the experiments based on their repeatability are shown as error bars on the graph in **Figure 2.6**. The gas yield fluctuated as the heating rate increases but has an ascending global tendency Similarly, the bio-oil does not follow a single tendency of variation, but a general increasing trend can be retained from 5°C/min to 100°C/min. On the other hand, the char yield has a monotone variation where it decreases from 5°C/min to 100°C/min. This variation can be noticed from the change in the weight of the char samples as given in **Figure S2.8** (supplementary information). Even though the variation is not visibly clear from the char volumes, nonetheless it can be deduced from the final weight of the char samples. The char weight drops from 0.82 g obtained at a heating rate of 30°C/min (**Figure S2.8** (b)), to 0.75 g at a heating rate of 80°C/min (**Figure S2.8** (c)).

When the heating is slow, it inhibits biomass thermal cracking which increases the formation of biochar. In addition, secondary pyrolysis reactions are less likely to take place at low heating rates. Increasing the heating rate helps extracting more gases from the wood sample by backing the biomass fragmentation which ameliorates the gaseous and liquid products yields and narrow the chances of biochar formation [15]. At elevated heating rates, the biomass is likely depolymerized into primary volatiles retarding the formation of char at the end [49]. *In brief, if a high gas concentration and a low char yield are desired, the pyrolysis temperature must be achieved with a high heating rate (80°C/min and above).*

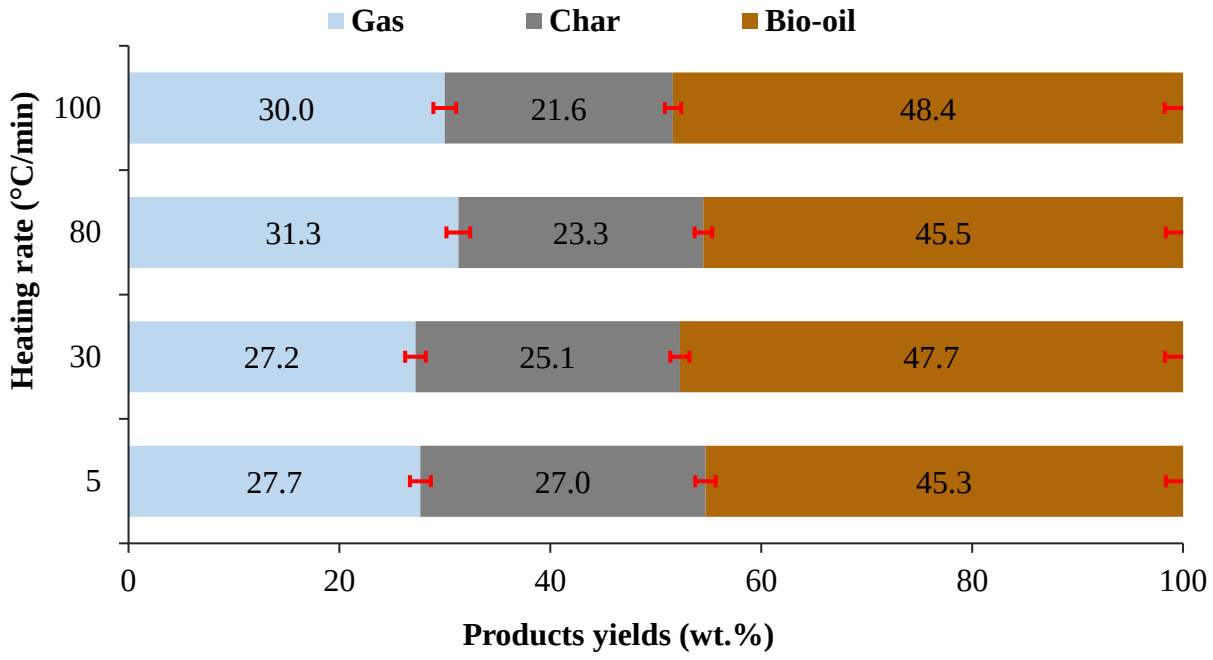

Figure 2.6 Effect of heating rate on the main products of the pyrolysis of oak wood chips (pyrolysis temperature = 700°C, nitrogen flow rate = 100 mL_n/min, reactor at top, duration of constant temperature = 60 min)

2.3.2.2. *Gases' concentrations*

The volume concentrations of the pyrolysis gases are detailed in the **Figure 2.7**, **Figure S2.4 and Figure S2.5** (supplementary information) in function of the heating rate. It is noticed that the higher the heating rate, the lower the H_2 and CO_2 concentrations are and the higher CH_4 and CO concentrations are. The ethane and ethylene concentrations also grow with the increase in the heating rate from 5 to 100°C/min except for ethylene which started decreasing above 80°C/min. The benzene and toluene concentrations fluctuate around 0.1 vol.% and 0.04 vol.%, respectively, for the different heating rates. Secondary pyrolysis reactions become dominant at high heating rates which produce more gases [49]. *But, if a high hydrogen production is required, the heating rate must remain relatively low (around 30°C/min).*

The effect of the heating rate over the bio-oil composition is clearly noticeable by comparing the three bio-oil samples at the left of the **Figure S2.9** (supplementary information). Interestingly, the bio-oil has a darker color at the higher heating rate. It is especially discerned when contrasting the light-colored bio-oil sample (**Figure S2.9** (d)) obtained at a 5°C/min heating rate to the dark colored sample (**Figure S2.9** (e)) at 80°C/min. This observation reflects the presence of heavier hydrocarbons formed at the higher heating rates, favored by the secondary pyrolysis reactions. The color of the bio-oil sample in **Figure S2.9** (f) at a heating rate of 100°C/min is slightly lighter than that at 80°C/min (**Figure S2.9** (e)), reflecting the decrease in some of the hydrocarbons' concentrations obtained at 100°C/min such as ethylene in **Figure S2.4** and benzene and toluene in **Figure S2.5** (supplementary information).

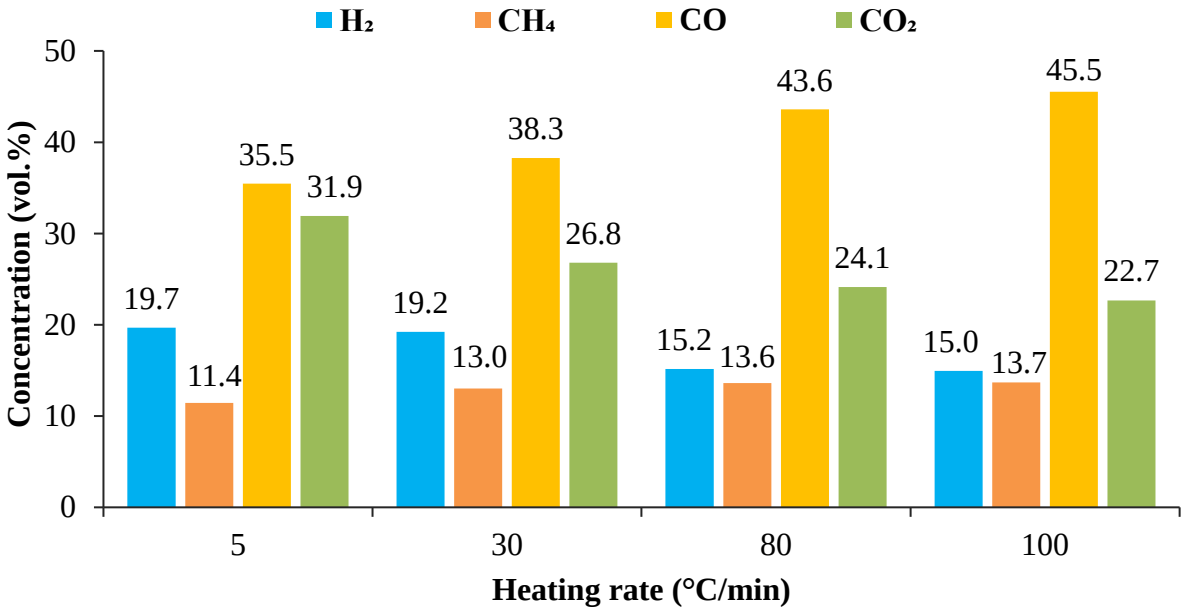

Figure 2.7 Effect of heating rate on the volume concentrations of the major gases produced from the pyrolysis of oak wood chips (pyrolysis temperature = 700°C, nitrogen flow rate = 100 mL_n/min, reactor at top, duration of constant temperature = 60 min)

2.3.3. Effect of residence time on biomass pyrolysis

The residence time markedly influences not only the char, bio-oil and gases yields but also their quality. In order to study the effect of the vapor residence time over the pyrolysis products, a series of experiments was realized. In a first set, the residence time was changed by varying the nitrogen flow rate from 50 to 100 to 300 mL_n/min. The other conditions were fixed as follow: the sample container was placed at the bottom of the pyrolysis and the reactor temperature was

fixed at 700°C reached at a 30°C/min rate. In a second set of tests, the influence of residence time was studied by changing the position of the biomass container in the reactor: top and bottom. The reactor temperature, the heating rate, and the carrier gas flow rate were fixed at 700°C, 30°C/min, and 100 mL_n/min. The results of both sets of the experiments will be presented together in the following sections but will be discussed separately.

First, the effect of the residence time is studied by changing the nitrogen flow rate. The lowest nitrogen flow rate tested for the primary pyrolysis was 50 mL_n/min which corresponds to a long residence time. The largest nitrogen flow rate was 300 mL_n/min corresponding to a short residence time. "Bottom" refers to the sample placed at the bottom and "top" is when the sample is placed at top of the furnace. Therefore, when the sample is placed at top and the nitrogen flow rate is set to its maximum (300 mL_n/min), the residence time is the shortest (50s) between the different cases of experiments. When the sample is placed at bottom and the nitrogen flow rate is set to its minimum (50 mL_n/min), the residence time is the longest (630s) among the different experiments.

2.3.3.1. Main products distribution

The products distribution of oak wood chips pyrolysis influenced by different residence times is represented in the **Figure 2.8**.

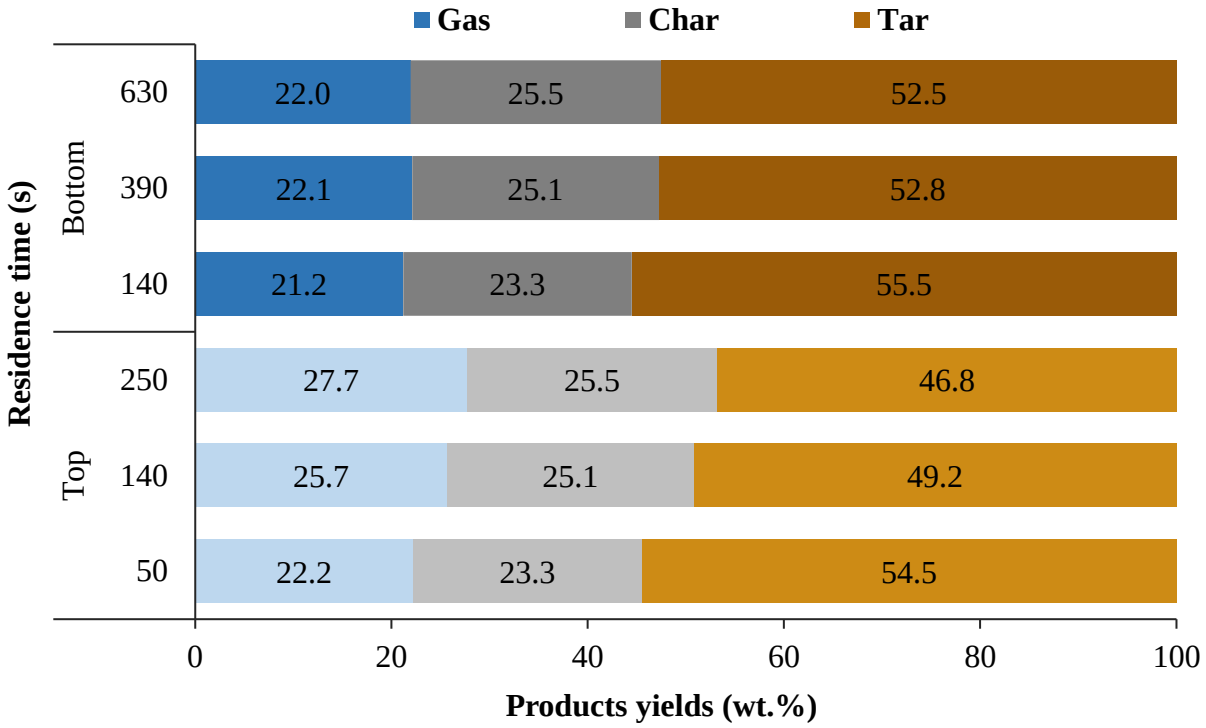

Figure 2.8 Effect of residence time on the main products of the pyrolysis of oak wood chips (pyrolysis temperature = 700°C, heating rate = 30°C/min) with the light shading referring to the positioning of the sample container at the top and the dark shadings for the positioning at the bottom

- **Changing the sample location in the reactor**

Comparing the products distribution at the same nitrogen flow rate and for the two sample positions, it is noticed that by moving the sample from the bottom of the reactor to its top, and thus reducing the vapors residence time to almost the third, the gas yield increases at the expense of the bio-oil yield which decreases. The char yield remains constant whether the wood sample is placed at the top or the bottom of the reactor when the nitrogen flow rate is the same.

The contact time between the hot char formed during the pyrolysis and the initial vapors produced is strongly influenced by the residence time. Consequently, the severity of the secondary reactions as well as the properties of the volatiles produced are greatly impacted. Thereby, placing the biomass sample at the top of the pyrolysis furnace, and thereby dividing the volatiles residence time by three, strongly increases the gas production and decreases that of bio-oil.

- **Changing the carrier gas flow rate**

During the phase of pyrolysis, moderate to elevated amounts of vapors were produced. If these vapors are not evacuated rapidly from the reactor, they can be subjected to secondary reactions which alter the composition and nature of the products [15]. Therefore, controlling the carrier gas flow rate plays a major role in the pyrolysis. From **Figure 2.8**, the effect of the residence time modified by the carrier gas flow rate can also be observed by fixing the sample position in the furnace. Reducing the nitrogen flow rate from 300 to 50 mL_n/min, increases the vapor residence time by five times when the biomass is placed at the top of the furnace and by 4.5 times when it is at the bottom, which enhances the yield of the gaseous products to the detriment of the bio-oil yield.

This is more significantly remarked with the wood sample placed at the top of the reactor where the gas yields pass from 22.2 wt.% to 27.7 wt.% by extending the residence time from 50s to 250s. The char yield slightly increases to reach a maximum of 25.5 wt.% with the increase of the residence time. The decline in the bio-oil yield can be observed in **Figure S2.9** (supplementary information) by opposing the bio-oil sample derived from the pyrolysis at a nitrogen flow rate of 300 mL_n/min (**Figure S2.9** (h)) with the biomass sample at the top of the furnace (corresponding to a residence time of 50s) and the bio-oil sample with a 50 mL_n/min nitrogen flow rate (residence time of 250s) (**Figure S2.9** (g)). The color shade becomes significantly lighter at the highest residence time. Thus, to obtain elevated gas and char yields with diminished bio-oil yields, the vapor residence time must be extended.

Secondary reactions are favored by a long residence time of volatiles in the furnace. These reactions can be catalyzed by the char formed which reduces the formation of the organic compounds constituting the bio-oil by transforming them into gases [25]. When the residence time is short, the biomass constituents are not completely repolymerized, which reduces the biochar yield. On the other hand, it was observed that at high temperature (700°C) and for long residence times, the biochar yield increases. In fact, other parameters such as the heating rate and the temperature dominate the influence of the residence time. Thereby, it is very challenging to formulate a clear idea on the impact of the residence time on the biochar production. And yet, the vapors residence time is considered a critical parameter influencing the char yield [43].

2.3.3.2. Gases' concentrations

The volume concentrations of non-condensable gases produced from pyrolysis of the oak wood chips at different residence times are represented in **Figure 2.9**, **Figure S2.6** and **Figure S2.7** (supplementary information).

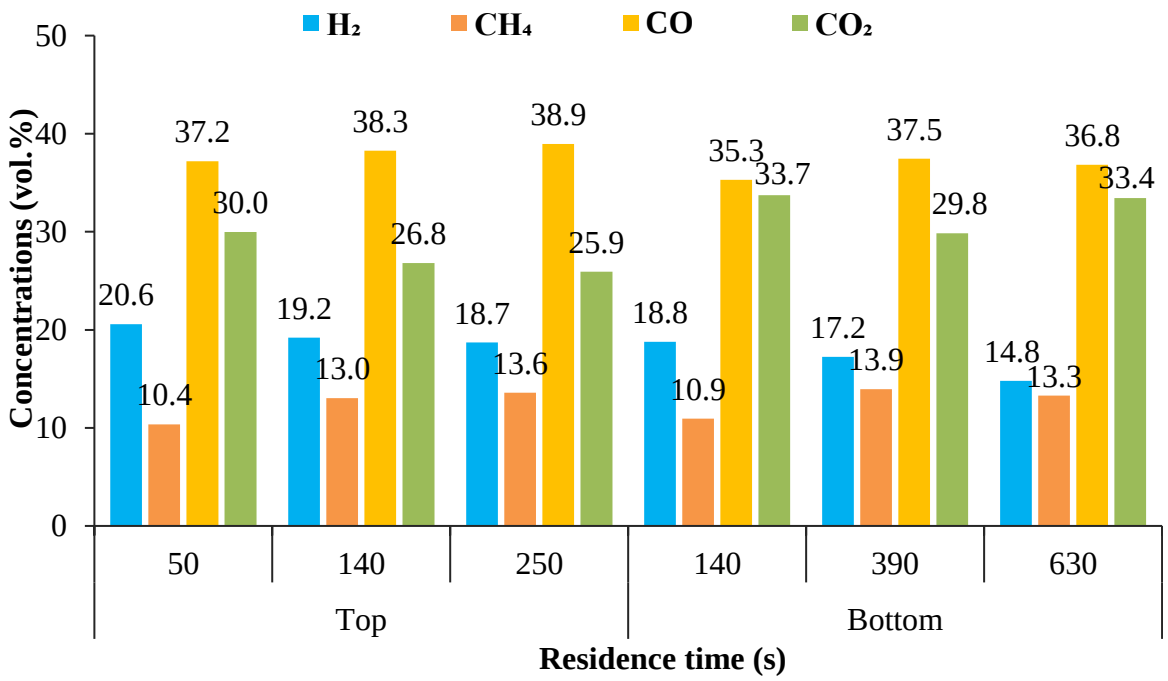

Figure 2.9 Effect of residence time on the volume concentrations of the major gases produced from the pyrolysis of oak wood chips (pyrolysis temperature = 700°C, heating rate = 30°C/min)

- **Changing the sample location in the reactor**

It is remarked that for the same nitrogen flow rate, placing the sample at the top of the reactor, which reduces the residence time to almost the third, improves the production of syngas (H_2 and CO). The hydrogen yield reaches a maximum of 20.6 vol.% when the reactor is placed at top while the residence time is reduced to the shortest (50s). CO, a primary pyrolysis product, is the major gas produced at each residence time, and its concentration is increased when the residence time is reduced by placing the reactor at the top of the furnace. CH_4 was slightly reduced by placing the reactor at the top (**Figure 2.9**). However, when the sample is positioned at the bottom of the reactor, which almost triples the vapors residence time, the CO_2 concentrations are much higher in contrast to when it is placed at the top, for each nitrogen flow rate. Even though CO_2 is a primary pyrolysis product, its production can be improved by heterogeneous char-forming secondary reactions whose by-products are water and CO_2 along with aromatic compounds [43]. *Therefore, placing the biomass sample at the top of the pyrolysis furnace, reduces the residence time and hence increases the production of syngas and reduces that of CO_2.*

Ethylene was markedly increased whereas ethane was a bit augmented by the elevation of the sample position in the reactor from bottom to top. As for the heavy hydrocarbons' evolution, it can be noticed that reducing the residence time by changing the sample position has a smaller impact on the heavy hydrocarbons.

- **Changing the carrier gas flow rate**

Globally, fixing the biomass position in the reactor and increasing the residence time from 50s to 250s (furnace at top) and from 140s to 630s (furnace at bottom) leads to a drop of the H_2 and CO_2 concentrations and a rise in the CO and CH_4 concentrations (**Figure 2.9**). Both ethane and ethylene concentrations were enhanced by the extension of the residence time while benzene and toluene dropped. Ethylbenzene was only observed with a medium flow rate and was

improved with the increase of the residence time. *It can be concluded that a residence time of 140s represents a compromise solution to optimize the production of H_2, CO and CH_4 simultaneously, while reducing CO_2.*

Increasing the gas flow rates drives the vapors produced rapidly out of the reactor leading to shorter vapor residence times. This inhibits the volatiles from initiating the repolymerization process [15]. On the other hand, when slow pyrolysis is applied with the slow heating rate (30°C/min) and long residence times, sufficient time and a suitable ambience is created to complete secondary reactions. Furthermore, the vapors formed during the secondary reactions are transformed by the long vapor residence time which ultimately leads to the production of solid biochar [15]. Even though the residence time has a significant influence on the composition of the gaseous and liquid products, it slightly affects the char yield. But even at low carrier gas flow rates, almost all the vapors are purged out of the reacting zone leading to higher biochar yield.

2.3.4. Analysis of the bio-oil compounds

2.3.4.1. Qualitative analysis

A list of the identified compounds from the different bio-oil samples is presented in **Table S2.4** (supplementary information) along with the percentage of the chromatographic area for each compound in relative to the total area of all the compounds detected. The compounds identified belong to the chemical groups of alkanes, anhydrosugars, esters, acids, alcohols, phenols and PAHs. These observations were confirmed by previous works that analyze the pyrolysis products from cellulose, hemicellulose and lignin [19,50–52] as well as some wood species such as fir [53], pine [54], beech [55] and oak [56], among others. In fact, the products derived from the biomass pyrolysis represent a complex combination of the products obtained from the separate pyrolysis of each component with specific kinetic characteristics for each.

The chromatographic surface area of each compound is proportional to its concentration. Therefore, this table reflects the amount of the species. It can be noticed that, globally, the most abundant compounds from the different samples are furfural, styrene, toluene, m- and o-xylene. Furfural has the highest surface area (47.2 %) reflecting its high concentration at 800°C. Furfural is considered an effective organic reactant utilized for the productions of resins, medicines and additives for food and fuels [57]. The low molecular weight oxygenates such as levoglucosan and furfural are in general generated at moderate temperatures (400°C-700°C) and are classified as primary tar. Olefins and phenolic species such as xylene and phenol are produced between 700°C and 850°C, and are referred to as secondary tar [51,58].

A more detailed table obtained with the fast heating rate method of the GC/MS is given in the **Table S2.5** (supplementary information) (the lighter compounds are not detected by the fast method; they are masked partially by the delay of the solvent).

2.3.4.2. Quantitative analysis

The bio-oil compounds derived from the biomass pyrolysis can be categorized into several main groups. The species quantified in our case are divided into three main classes: BTEX, PAHs and phenols. Their concentrations are detailed in **Table 2.4 and Table 2.5.** Among the phenols, the species searched for were guaiacol, phenol and syringol, but only the latter was detected and quantified as given in **Table 2.6**.

Table 2.4 Concentrations of the BTEX compounds from the different bio-oil samples

Temperature (°C)	**700**	**700**	**700**	**700**	**800**
Heating rate (°C/min)	**5**	**30**	**30**	**100**	**30**
Residence time (s)	**140**	**50**	**250**	**140**	**140**
Compounds (BTEX)	**Concentration (mg/L)**				
Benzene	9.05	11.25	36.87	9.3	0.00
Toluene	69.04	82.23	81.78	69.77	47.95
Ethylbenzene	69.53	74.73	59.71	57.62	51.86
m-xylene	180.57	213.65	156.89	142.48	96.23
p-xylene	42.72	55.66	38.85	39.7	29.62
o-xylene	51.64	58.46	46.36	40.38	34.29

Table 2.5 Concentrations of the PAHs compounds from the different bio-oil samples using the SIM method given their low amounts

Temperature (°C)	**700**	**700**	**700**	**700**	**800**
Heating rate (°C/min)	**5**	**30**	**30**	**100**	**30**
Residence time (s)	**140**	**50**	**250**	**140**	**140**
Compounds (PAHs)	**Concentration (mg/L)**				
Naphthalene	0.432	0.417	0.089	0.165	0.322
Phenanthrene	0.081	0.064	0.110	0.086	0.587
Anthracene	0.025	0.019	0.033	0.024	0.208
Fluoranthene	0.018	0.016	0.030	0.026	0.182
Pyrene	0.015	0.008	0.027	0.026	0.169
Benzo(a)anthracene	nd*	0.019	nd	nd	0.244
Chrysene	nd	0.012	nd	nd	0.092

*Not determined

Table 2.6 Concentrations of the phenol compounds from the different bio-oil samples

Temperature (°C)	**700**	**700**	**700**	**700**	**800**
Heating rate (°C/min)	**5**	**30**	**30**	**100**	**30**
Residence time (s)	**140**	**50**	**250**	**140**	**140**
Compounds (phenols)	**Concentration (mg/L)**				
Syringol (mg/l)	4.88	5.14	nd*	nd	46.24

*Not determined

Looking at these tables, it can be noticed that the BTEX represent the major bio-oil compounds with the highest concentrations for each sample, followed by the phenols and the PAHs. The BTEX are monocyclic aromatic hydrocarbons with massive market demands and a large contribution in the petrochemical and fine particles industries [59,60]. Xylene, for instance, is hugely used for the cleaning of circuit board, clothing of polyester and manufacturing of plastic

bottles [59]. The phenols produced during the pyrolysis are regarded as high-value products used in multiple synthesis processes such as polymers, pharmaceutical and adhesives [57]. Furans and ketones derive in general from the decomposition of cellulose. The hemicellulose's pyrolysis produces acetic acids and aldehydes such as furfural. While methoxy groups, phenols and BTEX are considered the products of the lignin's decomposition [61,62].

From these tables, the effects of the different operating parameters over the bio-oil compounds can be evaluated. Regarding the influence of the temperature, it can be noticed that as the temperature increases while fixing the heating rate and the residence time, the concentrations of the different BTEX species drop while that of the PAHs and the phenols rise. In fact, at 700°C and above, the lignin (one of the biomass main components), consisting of a rich aromatic carbonaceous matrix is depolymerized. This decreases the concentrations of the volatile products like alcohols, paraffin and aldehydes and upsurges the production of phenols and PAHs such as pyrene, syringol, and naphthalene which are more thermally stable [63,64]. Elevated temperatures favor the secondary cracking reactions of ketones and aldehydes and contribute in the condensation of molecules with unsaturated bonds [54].

Fixing the temperature at 700°C and the residence time at 140s, while varying the heating rate from 5 to 100°C/min has a minor effect on the bio-oil compounds' concentration, as previously demonstrated. The BTEX species slightly dropped with the heating rate increase whereas the phenols increased faintly at the exception of naphthalene which decreased. It is known that high heating rates favors the depolymerization reactions of cellulose and hemicellulose. This results in high bio-oil yields due to the rapid release of the condensable gases [65].

The residence time effect was investigated by maintaining the temperature at 700°C and the heating rate at 30°C/min while increasing the residence time from 50s to 250s. It can be remarked that all the BTEX species, except the benzene, strongly decrease with the increase of the residence time. The phenols, on the other hand, at the exception of naphthalene, increase remarkably with the extension of the residence time. These conclusions are compatible with the observations made on the bio-oil samples shown in **Figure S2.9** (g) and (h) with the bio-oil appearance getting lighter with the increase of the residence time, as previously discussed. The high presence of aromatics was also noticed by the strong smell. Similar results were obtained by other works such as Gao *et al.* [54]. Adjusting the carrier gas flow rate to increase the volatiles' residence time maximizes the re-polymerization of the vapors and their cracking reactions [65] resulting in higher phenols and aldehydes and lower BTEX concentrations.

To sum up, in order to produce a bio-oil rich in BTEX, the pyrolysis must be realized at high temperature (700°C), a relatively slow heating rate (30°C/min) and a small vapor residence time (50s). On the other hand, to reduce the BTEX content of the bio-oil, the pyrolysis temperature must be augmented to 800°C, a heating rate of 30°C/min, with an adequate residence time (around 140s).

2.3.5. Elemental analysis of char produced

A summary of the elemental analyses of the char produced from several pyrolysis experiments are presented in **Table 2.7** along with the experimental conditions applied. The uncertainties given after the ± symbol were determined following the equation S1 as described in section 1 of the supplementary information. In this case, α equals 0.05 and n (the number of replicates) is 3. It is known that carbon is the main element composing the char, while the ash and moisture are present in minor amounts [66]. Referring to the elemental analysis of the initial oak wood

chips re-given in the first row of **Table 2.7**, it can be noticed that the carbon content has significantly increased from 46.5% in the raw wood chips to reach more than 90% in the char produced at 700°C. On the other hand, the hydrogen content has dropped from around 6% in the raw oak chips to less than 3.3% in the char produced and decreased even to below 1.5% at pyrolysis temperatures of 700°C and above. Similarly, the oxygen content has been hugely reduced in the char formed from almost 47% in the raw wood chips to below 3% at high temperatures.

Regarding the effect of the different parameters, starting with the temperature while fixing the heating rate at 30°C/min and the residence time at 140s, it can be noticed that the carbon content increases, the hydrogen content decreases, and the oxygen content strongly drops with the temperature rise from 400°C to 800°C. As a matter of fact, looking at the previous results obtained (**Figure 2.5**, **Figure S2.2** and **Figure S2.3** (supplementary information)), the reduction of the hydrogen content in the char can be explained by the production of H_2, as well as CH_4, C_2H_6 and C_2H_4 along with the heavier hydrocarbons. The concentrations of these compounds strongly increased with the temperature. As the temperature increases, it was noticed that the production of CO increased marginally while that of CO_2 decreased significantly, shifting the balance toward the increase in the carbon content in the char formed. The drop in the oxygen content can be attributed to the drying step performed prior to the pyrolysis where the water vapor H_2O is extracted from the wood sample.

Increasing the heating rate from 5 to 100°C/min while maintaining the temperature at 700°C and the residence time at 140s, contributes to the small drop in the carbon content in contrast to the slight increase in the hydrogen and oxygen contents in the char formed. These variations are the result of the balance between the decrease in the H_2 and CO_2 concentrations and the surge in those of CH_4 and CO with the increase of the heating rate as noticed from **Figure 2.7**.

Extending the residence time from 50s to 250s while keeping the sample at the top of the furnace and conserving a fixed temperature of 700°C and a heating rate of 30°C/min, had a smaller impact on the different elements content in the char produced. For instance, the carbon and the hydrogen content remained almost constant whereas the oxygen content dropped marginally. As it can be noted from **Figure 2.9**, the H_2 and CO_2 concentrations diminished faintly while CH_4 and CO increased with the increase of the residence time, resulting in the small variations observed in the char content. On the other hand, moving the sample from top to bottom while maintaining the carrier gas flow rate at 100 mL_n/min, thereby increasing the residence time from 140s to 390s, led to a slight drop in the carbon and hydrogen contents while the oxygen remained increased slightly. The small changes can also be remarked from **Figure 2.9**, where the H_2 and CO concentrations faintly decrease while the CH_4 and CO_2 marginally escalate.
The nitrogen content in the char produced is, in most of the cases, higher than the original content in the raw biomass (0.21%) but remains lower than 1%. This can be attributed to the use of nitrogen as carrier gas which might have slightly penetrated the char molecules during the heating phase of the pyrolysis. It is interesting to notice that a considerable percentage of other compounds is present in the char formed reaching around 10% in contrast to 0.11% in the raw oak wood chips. This is another indication of the secondary reactions taking place and forming the bio-oil which can condense over the char surface. The elevated C content of the char allows it be applied as an adsorbent or a solid fuel [66]. *Therefore, in order to obtain a carbon-rich char, the pyrolysis temperature must be 700°C and the heating rate relatively slow (30°C/min) with a high residence time (250s or 390s).*

Table 2.7 Elemental analyses of the char produced from several pyrolysis experiments. The first raw in italic corresponds to the oak wood chips elemental analysis. The variation of the temperature is notified in bold, the heating rate in bold italic and the residence time in bold underlined

Temperature (°C)	**Heating rate (°C/min)**	**Residence time (s)**	**Sample position**	**N_2 flow rate (mL_n/min)**	**Carbon (%)**	**Hydrogen (%)**	**Oxygen (%)**	**Nitrogen (%)**	**Others (%)**
20	-	-	-	-	*46.52*	*6.03*	*47.13*	*0.21*	*0.11*
400	30	140	Top	100	73.65 ± 0.94	3.26 ± 0.33	13.93 ± 1.10	0.37 ± 0.12	8.79 ± 0.62
500	30	140	Top	100	82.10 ± 1.26	3.02 ± 0.24	8.58 ± 0.33	0.44 ± 0.04	5.86 ± 1.67
700	***5***	140	Top	100	87.78 ± 2.93	1.18 ± 0.10	2.51 ± 0.45	0.65 ± 0.19	7.88 ± 3.08
700	30	**50**	Top	300	93.03 ± 2.82	1.10 ± 0.05	2.39 ± 0.14	0.67 ± 0.20	2.81 ± 2.84
700	***30***	**140**	Top	100	90.28 ± 0.80	1.48 ± 0.01	2.27 ± 0.11	0.36 ± 0.21	5.97 ± 1.04
700	30	**250**	Top	50	93.84 ±12.40	1.11 ± 0.15	2.15 ± 0.15	0.91 ± 0.17	4.33 ± 1.03
700	30	**390**	**Bottom**	100	88.28 ±1.14	1.43 ± 0.15	3.54 ± 0.14	0.54 ± 0.08	6.21 ± 1.13
700	***100***	140	Top	100	85.31 ±13.52	1.47 ± 0.19	2.65 ± 0.87	0.21 ± 0.51	10.36 ± 1.43
800	30	140	Top	100	84.81 ±5.630	1.27 ± 0.80	1.95 ± 0.74	0.06 ± 0.14	11.96 ± 5.27

2.4. Conclusion

Based on the results obtained from the evaluation of the effects of the different parameters over the pyrolysis of the oak wood chips, some approaches can be retained to improve the yields of the products. For instance, to obtain a high char yield, the pyrolysis needs to be operated at a low temperature, with a slow heating rate and a long residence time. To increase the bio-oil yield, a low temperature, a high heating rate along with a moderate residence time should be imposed. To enhance the gases yields, a high temperature and slow heating rate with a long residence time are of interest.

The gas yield is highly improved by the temperature rise (400°C to 800°C) where H_2, CH_4 and CO markedly increase while CO_2 drops. The heating rate studied during the pyrolysis (5 to 100°C/min) has a limited effect on the gases distribution in contrast to the temperature. Nonetheless, as the heating rate rises, CH_4, and CO increase whereas H_2 and CO_2 decrease. Extending the residence time by reducing the nitrogen flow rate enhances the concentrations of CH_4, and CO but decreases those of H_2 and CO_2, similarly to the effect of the acceleration of the heating rate. By positioning the sample container at the bottom of the reactor, which prolongs the residence time, the concentrations of H_2 and CO are smaller while those of CH_4 and CO_2 are larger than when the sample is placed at top of the reactor.

The bio-oil analysis revealed the presence of multiple components that were identified with some species quantified and categorized into three main classes: BTEX, PAHs and phenols. Their concentrations were the most affected by the temperature variation followed by the residence time modification, but less impacted by the heating rate alteration. The char elemental analysis was also performed and demonstrated a huge increase in the carbon content accompanied by a remarkable fall in the oxygen and hydrogen concentrations for the different parameters studied.

To sum up, studying the effect of the different parameters allows the identification of the optimal operating conditions in order to maximize the syngas formation. This implies working at a high temperature (700°C), a moderate heating rate (about 30°C/min) with a short residence time (about 140s). The composition of the biomass also strongly affects the concentrations of the different products formed given its distinct content of cellulose, hemicellulose and lignin. Thereby, it appears interesting to extend the study of the influence of the operating parameters on the pyrolysis of several wood species such as beech, fir and pine as well as other biomass compounds like flax shives and composite based on waste coffee grounds**.** Moreover, the differences observed in the products and gases distribution by varying the residence time led to question if a second pyrolysis is more effective. In that purpose, a secondary reactor can be connected to the biomass pyrolysis reactor to realize distinctly a second pyrolysis and to study the products formed in function of the different operating parameters.

References

[1] M. Abou Rjeily, F. Cazier, C. Gennequin, J.H. Randrianalisoa, Detailed Analysis of Gas, Char and Bio-oil Products of Oak Wood Pyrolysis at Different Operating Conditions, Waste Biomass Valorization. (2022). https://doi.org/10.1007/s12649-022-01848-0.

[2] M.I. Jahirul, M. Rasul, A. Chowdhury, N. Ashwath, Biofuels Production through Biomass Pyrolysis —A Technological Review, Energies. 5 (2012) 4952–5001. https://doi.org/10.3390/en5124952.

[3] M.N. Uddin, K. Techato, J. Taweekun, M.M. Rahman, M.G. Rasul, T.M.I. Mahlia, S.M. Ashrafur, An Overview of Recent Developments in Biomass Pyrolysis Technologies, Energies. 11 (2018) 3115. https://doi.org/10.3390/en11113115.

[4] N. Bolan, S.A. Hoang, J. Beiyuan, S. Gupta, D. Hou, A. Karakoti, S. Joseph, S. Jung, K.-H. Kim, M.B. Kirkham, H.W. Kua, M. Kumar, E.E. Kwon, Y.S. Ok, V. Perera, J. Rinklebe, S.M. Shaheen, B. Sarkar, A.K. Sarmah, B.P. Singh, G. Singh, D.C.W. Tsang, K. Vikrant, M. Vithanage, A. Vinu, H. Wang, H. Wijesekara, Y. Yan, S.A. Younis, L. Van Zwieten, Multifunctional applications of biochar beyond carbon storage, Int. Mater. Rev. 0 (2021) 1–51. https://doi.org/10.1080/09506608.2021.1922047.

[5] D. Mohan, C. Pittman, P. Steele, Pyrolysis of Wood/Biomass for Bio-Oil: A Critical Review, Energy. 20 (2006) 848. https://doi.org/10.1021/ef0502397.

[6] M. Abou Rjeily, C. Gennequin, H. Pron, E. Abi-Aad, J.H. Randrianalisoa, Pyrolysis-catalytic upgrading of bio-oil and pyrolysis-catalytic steam reforming of biogas: a review, Environ. Chem. Lett. (2021) 48. https://doi.org/10.1007/s10311-021-01190-2.

[7] P. Baredar, V. Khare, S. Nema, Chapter 6 - Biomass liquefaction, in: P. Baredar, V. Khare, S. Nema (Eds.), Des. Optim. Biogas Energy Syst., Academic Press, 2020: pp. 231–266. https://doi.org/10.1016/B978-0-12-822718-3.00006-X.
[8] T. Fahmy, Y. Fahmy, F. Mobarak, M. El-Sakhawy, R. Abouzeid, Biomass pyrolysis: past, present, and future, Environ. Dev. Sustain. (2018) 1–16. https://doi.org/10.1007/s10668-018-0200-5.
[9] P. Morf, P. Hasler, T. Nussbaumer, Mechanisms and kinetics of homogeneous secondary reactions of tar from continuous pyrolysis of wood chips, Fuel. 81 (2002) 843–853. https://doi.org/10.1016/S0016-2361(01)00216-2.
[10] M. Asmadi, H. Kawamoto, S. Saka, Pyrolysis reactions of Japanese cedar and Japanese beech woods in a closed ampoule reactor, J. Wood Sci. 56 (2010) 319–330. https://doi.org/10.1007/s10086-009-1097-2.
[11] P.R. Patwardhan, D.L. Dalluge, B.H. Shanks, R.C. Brown, Distinguishing primary and secondary reactions of cellulose pyrolysis, Bioresour. Technol. 102 (2011) 5265–5269. https://doi.org/10.1016/j.biortech.2011.02.018.
[12] M.I. Jahirul, M.G. Rasul, A.A. Chowdhury, N. Ashwath, Biofuels Production through Biomass Pyrolysis —A Technological Review, Energies. 5 (2012) 4952–5001. https://doi.org/10.3390/en5124952.
[13] A. Sharma, V. Pareek, D. Zhang, Biomass pyrolysis—A review of modelling, process parameters and catalytic studies, Renew. Sustain. Energy Rev. 50 (2015) 1081–1096. https://doi.org/wang.
[14] G. Wang, Y. Dai, H. Yang, Q. Xiong, K. Wang, J. Zhou, Y. Li, S. Wang, A Review of Recent Advances in Biomass Pyrolysis, Energy Fuels. 34 (2020) 15557–15578. https://doi.org/10.1021/acs.energyfuels.0c03107.
[15] M. Tripathi, J.N. Sahu, P. Ganesan, Effect of process parameters on production of biochar from biomass waste through pyrolysis: A review, Renew. Sustain. Energy Rev. 55 (2016) 467–481. https://doi.org/10.1016/j.rser.2015.10.122.
[16] A. Verma, R. Shankar, P. Mondal, A Review on Pyrolysis of Biomass and the Impacts of Operating Conditions on Product Yield, Quality, and Upgradation, in: Recent Adv. Biofuels Bioenergy Util., 2018: pp. 227–259. https://doi.org/10.1007/978-981-13-1307-3_10.
[17] P.T. Williams, S. Besler, The influence of temperature and heating rate on the slow pyrolysis of biomass, Renew. Energy. 7 (1996) 233–250. https://doi.org/10.1016/0960-1481(96)00006-7.
[18] A. Fukutome, H. Kawamoto, S. Saka, Processes forming Gas, Tar, and Coke in Cellulose Gasification from Gas-Phase Reactions of Levoglucosan as Intermediate, ChemSusChem. 8 (2015) 2240–2249. https://doi.org/10.1002/cssc.201500275.
[19] K.B. Ansari, J.S. Arora, J.W. Chew, P.J. Dauenhauer, S.H. Mushrif, Fast Pyrolysis of Cellulose, Hemicellulose, and Lignin: Effect of Operating Temperature on Bio-oil Yield and Composition and Insights into the Intrinsic Pyrolysis Chemistry, Ind. Eng. Chem. Res. 58 (2019) 15838–15852. https://doi.org/10.1021/acs.iecr.9b00920.
[20] D. Chen, X. Chen, J. Sun, Z. Zheng, K. Fu, Pyrolysis polygeneration of pine nut shell: Quality of pyrolysis products and study on the preparation of activated carbon from biochar, Bioresour. Technol. 216 (2016) 629–636. https://doi.org/10.1016/j.biortech.2016.05.107.
[21] S. Zhou, B. Pecha, M. van Kuppevelt, A.G. McDonald, M. Garcia-Perez, Slow and fast pyrolysis of Douglas-fir lignin: Importance of liquid-intermediate formation on the distribution of products, Biomass Bioenergy. 66 (2014) 398–409. https://doi.org/10.1016/j.biombioe.2014.03.064.
[22] E. Amini, M.-S. Safdari, J.T. DeYoung, D.R. Weise, T.H. Fletcher, Characterization of pyrolysis products from slow pyrolysis of live and dead vegetation native to the southern United States, Fuel. 235 (2019) 1475–1491. https://doi.org/10.1016/j.fuel.2018.08.112.
[23] W.F. Fassinou, L. Van de Steene, S. Toure, G. Volle, P. Girard, Pyrolysis of Pinus pinaster in a two-stage gasifier: Influence of processing parameters and thermal cracking of tar, Fuel Process. Technol. 90 (2009) 75–90. https://doi.org/10.1016/j.fuproc.2008.07.016.
[24] K. Norinaga, T. Shoji, S. Kudo, J. Hayashi, Detailed chemical kinetic modelling of vapour-phase cracking of multi-component molecular mixtures derived from the fast pyrolysis of cellulose, Fuel. 103 (2013) 141–150. https://doi.org/10.1016/j.fuel.2011.07.045.
[25] J. Solar, I. de Marco, B.M. Caballero, A. Lopez-Urionabarrenechea, N. Rodriguez, I. Agirre, A. Adrados, Influence of temperature and residence time in the pyrolysis of woody biomass waste in

a continuous screw reactor, Biomass Bioenergy. 95 (2016) 416–423. https://doi.org/10.1016/j.biombioe.2016.07.004.
[26] H. Yang, R. Yan, H. Chen, D.H. Lee, C. Zheng, Characteristics of hemicellulose, cellulose and lignin pyrolysis, Fuel. 86 (2007) 1781–1788. https://doi.org/10.1016/j.fuel.2006.12.013.
[27] R.J.M. Westerhof, D.W.F. (Wim) Brilman, W.P.M. van Swaaij, S.R.A. Kersten, Effect of Temperature in Fluidized Bed Fast Pyrolysis of Biomass: Oil Quality Assessment in Test Units, Ind. Eng. Chem. Res. 49 (2010) 1160–1168. https://doi.org/10.1021/ie900885c.
[28] G. Ningbo, L. Baoling, L. Aimin, L. Juanjuan, Continuous pyrolysis of pine sawdust at different pyrolysis temperatures and solid residence times, J. Anal. Appl. Pyrolysis. 114 (2015) 155–162. https://doi.org/10.1016/j.jaap.2015.05.011.
[29] N. Mahinpey, P. Murugan, T. Mani, R. Raina-Fulton (Bailey), Analysis of Bio-Oil, Biogas, and Biochar from Pressurized Pyrolysis of Wheat Straw Using a Tubular Reactor, Energy Fuels - ENERG FUEL. 23 (2009). https://doi.org/10.1021/ef8010959.
[30] T. Imam, S. Capareda, Characterization of bio-oil, syn-gas and bio-char from switchgrass pyrolysis at various temperatures, J. Anal. Appl. Pyrolysis. 93 (2012) 170–177. https://doi.org/10.1016/j.jaap.2011.11.010.
[31] A. Mlonka-Mędrala, P. Evangelopoulos, M. Sieradzka, M. Zajemska, A. Magdziarz, Pyrolysis of agricultural waste biomass towards production of gas fuel and high-quality char: Experimental and numerical investigations, Fuel. 296 (2021) 120611. https://doi.org/10.1016/j.fuel.2021.120611.
[32] T. Lange, Pedunculate oak, EU Sci. Hub - Eur. Comm. (2017). https://ec.europa.eu/jrc/en/research-topic/forestry/qr-tree-project/pedunculate-oak (accessed May 4, 2021).
[33] C. Lorreyte, Etudes numérique et expérimentale de la synthèse de biogaz : vers la transformation thermochimique solaire de copeaux de bois, These de doctorat, Reims, 2017. http://www.theses.fr/2017REIMS033 (accessed May 5, 2021).
[34] P.J. Van Soest, J.B. Robertson, B.A. Lewis, Methods for Dietary Fiber, Neutral Detergent Fiber, and Nonstarch Polysaccharides in Relation to Animal Nutrition, J. Dairy Sci. 74 (1991) 3583–3597. https://doi.org/10.3168/jds.S0022-0302(91)78551-2.
[35] G. Schmidt, G. Trouvé, G. Leyssens, C. Schönnenbeck, P. Genevray, F. Cazier, D. Dewaele, C. Vandenbilcke, E. Faivre, Y. Denance, C. Le Dreff-Lorimier, Wood washing: Influence on gaseous and particulate emissions during wood combustion in a domestic pellet stove, Fuel Process. Technol. 174 (2018) 104–117. https://doi.org/10.1016/j.fuproc.2018.02.020.
[36] F.-X. Collard, J. Blin, A. Bensakhria, J. Valette, Influence of impregnated metal on the pyrolysis conversion of biomass constituents, J. Anal. Appl. Pyrolysis. 95 (2012) 213–226. https://doi.org/10.1016/j.jaap.2012.02.009.
[37] D. Meier, B. van de Beld, A.V. Bridgwater, D.C. Elliott, A. Oasmaa, F. Preto, State-of-the-art of fast pyrolysis in IEA bioenergy member countries, Renew. Sustain. Energy Rev. 20 (2013) 619–641. https://doi.org/10.1016/j.rser.2012.11.061.
[38] M. Abou Rjeily, C. Gennequin, H. Pron, E. Abi-Aad, J.H. Randrianalisoa, Chapter 9 - Catalysts for steam reforming of biomass tar and their effects on the products, in: M.R. Cesario, D.A. de Macedo (Eds.), Heterog. Catal., Elsevier, 2022: pp. 249–295. https://doi.org/10.1016/B978-0-323-85612-6.00009-7.
[39] J.H.A. Kiel, S.V.B. Van Paasen, J.P.A. Neeft, L. Devi, K.J. Ptasinski, F.J.J.G. Janssen, R. Meijer, R.H. Berends, H.M.G. Temmink, G. Brem, N. Padban, E.A. Bramer, Primary measures to reduce tar formation in fluidised-bed biomass gasifiers. Final report SDE project P1999-012, (2004). https://www.osti.gov/etdeweb/biblio/20464070 (accessed May 7, 2021).
[40] J.R. Taylor, An Introduction to Error Analysis: The Study of Uncertainties in Physical Measurements, University Science Books, 1997.
[41] J.L. Figueiredo, C. Valenzuela, A. Bernalte, J.M. Encinar, Pyrolysis of holm-oak wood: influence of temperature and particle size, Fuel. 68 (1989) 1012–1016. https://doi.org/10.1016/0016-2361(89)90067-7.
[42] G. Özbay, Pyrolysis of Firwood (Abies bornmüllerianaMattf.) Sawdust: Characterization of Bio-Oil and Bio-Char, Drv. Ind. 66 (2015) 105–114. https://doi.org/10.5552/drind.2015.1359.
[43] A. Dieguez-Alonso, A. Anca-Couce, N. Zobel, F. Behrendt, Understanding the primary and secondary slow pyrolysis mechanisms of holocellulose, lignin and wood with laser-induced fluorescence, Fuel. 153 (2015) 102–109. https://doi.org/10.1016/j.fuel.2015.02.097.

[44] S. Xin, H. Yang, Y. Chen, X. Wang, H. Chen, Assessment of pyrolysis polygeneration of biomass based on major components: Product characterization and elucidation of degradation pathways, Fuel. 113 (2013) 266–273. https://doi.org/10.1016/j.fuel.2013.05.061.
[45] T.G. Bridgeman, J.M. Jones, I. Shield, P.T. Williams, Torrefaction of reed canary grass, wheat straw and willow to enhance solid fuel qualities and combustion properties, Fuel. 87 (2008) 844–856. https://doi.org/10.1016/j.fuel.2007.05.041.
[46] T.A. Milne, R.J. Evans, N. Abatzaglou, Biomass Gasifier "'Tars'": Their Nature, Formation, and Conversion, National Renewable Energy Laboratory, Golden, CO (US), 1998. https://doi.org/10.2172/3726.
[47] A. Anca-Couce, Reaction mechanisms and multi-scale modelling of lignocellulosic biomass pyrolysis, Prog. Energy Combust. Sci. 53 (2016) 41–79. https://doi.org/10.1016/j.pecs.2015.10.002.
[48] K. Zeng, D. Gauthier, D.P. Minh, E. Weiss-Hortala, A. Nzihou, G. Flamant, Characterization of solar fuels obtained from beech wood solar pyrolysis, Fuel. 188 (2017) 285–293. https://doi.org/10.1016/j.fuel.2016.10.036.
[49] F. Ateş, E. Pütün, A.E. Pütün, Fast pyrolysis of sesame stalk: yields and structural analysis of bio-oil, J. Anal. Appl. Pyrolysis. 71 (2004) 779–790. https://doi.org/10.1016/j.jaap.2003.11.001.
[50] D. Wang, S. Czernik, D. Montané, M. Mann, E. Chornet, Biomass to Hydrogen via Fast Pyrolysis and Catalytic Steam Reforming of the Pyrolysis Oil or Its Fractions, Ind. Eng. Chem. Res. 36 (1997) 1507–1518. https://doi.org/10.1021/ie960396g.
[51] A. Dufour, E. Masson, P. Girods, Y. Rogaume, A. Zoulalian, Evolution of Aromatic Tar Composition in Relation to Methane and Ethylene from Biomass Pyrolysis-Gasification, Energy Fuels. 25 (2011) 4182–4189. https://doi.org/10.1021/ef200846g.
[52] E. Ranzi, M. Corbetta, F. Manenti, S. Pierucci, Kinetic modeling of the thermal degradation and combustion of biomass, Chem. Eng. Sci. 110 (2014) 2–12. https://doi.org/10.1016/j.ces.2013.08.014.
[53] G. Özbay, Pyrolysis of Firwood (Abies bornmüllerianaMattf.) Sawdust: Characterization of Bio-Oil and Bio-Char, Drv. Ind. 66 (2015) 105–114. https://doi.org/10.5552/drind.2015.1359.
[54] N. Gao, L. Baoling, A. Li, L. Juanjuan, Continuous pyrolysis of pine sawdust at different pyrolysis temperatures and solid residence times, J. Anal. Appl. Pyrolysis. 114 (2015). https://doi.org/10.1016/j.jaap.2015.05.011.
[55] B. Martin, Pyrolysis of woody material, Pet. Coal. 52 (2010).
[56] E. Amini, M.-S. Safdari, J.T. DeYoung, D.R. Weise, T.H. Fletcher, Characterization of pyrolysis products from slow pyrolysis of live and dead vegetation native to the southern United States, Fuel. 235 (2019) 1475–1491. https://doi.org/10.1016/j.fuel.2018.08.112.
[57] L. Fele Žilnik, A. Jazbinšek, Recovery of renewable phenolic fraction from pyrolysis oil, Sep. Purif. Technol. 86 (2012) 157–170. https://doi.org/10.1016/j.seppur.2011.10.040.
[58] L. Devi, K.J. Ptasinski, F.J.J.G. Janssen, S.V.B. van Paasen, P.C.A. Bergman, J.H.A. Kiel, Catalytic decomposition of biomass tars: use of dolomite and untreated olivine, Renew. Energy. 30 (2005) 565–587. https://doi.org/10.1016/j.renene.2004.07.014.
[59] P. Gaurh, H. Pramanik, Production of benzene/toluene/ethyl benzene/xylene (BTEX) via multiphase catalytic pyrolysis of hazardous waste polyethylene using low cost fly ash synthesized natural catalyst, Waste Manag. 77 (2018) 114–130. https://doi.org/10.1016/j.wasman.2018.05.013.
[60] C. Zhang, G. Kwak, H.-G. Park, K.-W. Jun, Y.-J. Lee, S.C. Kang, S. Kim, Light hydrocarbons to BTEX aromatics over hierarchical HZSM-5: Effects of alkali treatment on catalytic performance, Microporous Mesoporous Mater. 276 (2019) 292–301. https://doi.org/10.1016/j.micromeso.2018.10.005.
[61] S. Karagöz, Catalytic pyrolysis of waste melamine coated chipboard, Environ. Prog. Sustain. Energy. 32 (2013) 156–161.
[62] Q. Meng, J. Yan, R. Wu, H. Liu, Y. Sun, N. Wu, J. Xiang, L. Zheng, J. Zhang, B. Han, Sustainable production of benzene from lignin, Nat. Commun. 12 (2021) 4534. https://doi.org/10.1038/s41467-021-24780-8.
[63] M. Garcia-Perez, The Formation of Polyaromatic Hydrocarbons and Dioxins During Pyrolysis: A Review of the Literature with Descriptions of Biomass Composition, Fast Pyrolysis Technologies and Thermochemical Reactions, (2008).

[64] J. Akhtar, N. Saidina Amin, A review on operating parameters for optimum liquid oil yield in biomass pyrolysis, Renew. Sustain. Energy Rev. 16 (2012) 5101–5109. https://doi.org/10.1016/j.rser.2012.05.033.

[65] J. Montoya, F. Chejne Janna, M. Garcia-Perez, Fast pyrolysis of biomass: A review of relevant aspects. Part I: Parametric study, DYNA. 82 (2015) 239–248. https://doi.org/10.15446/dyna.v82n192.44701.

[66] S.A. Salaudeen, P. Arku, A. Dutta, 10 - Gasification of Plastic Solid Waste and Competitive Technologies, in: S.M. Al-Salem (Ed.), Plast. Energy, William Andrew Publishing, 2019: pp. 269–293. https://doi.org/10.1016/B978-0-12-813140-4.00010-8.

2.5. SUPPLEMEMTARY INFORMATION

1. Reproducibility analysis

In order to analysis the reproducibility of our experiments, a pyrolysis experiment was repeated five times in the same operating conditions: 3.5 g of oak wood chips mass, heating rate of 30 °C/min, nitrogen flow rate of 100 mL_n/min, and temperature of 500°C maintained for 30 min. The different gases concentrations are an average of the concentrations obtained from the five experiments. The uncertainty δ was determined according to the equation **(S2.1)** [40]:

$$\delta = t_{1-\alpha,v}\frac{S_n}{\sqrt{n}} \quad \textbf{(S2.1)}$$

With S_n as the standard deviation, n is the number of replicates (5 in our case), $1-\alpha$ reflects the confidence level (α is chosen to be 0.05 which corresponds to 95% of confidence level), v is the degree of freedom (equals to $n-1$ so 4 in our case) and $t_{\alpha,v}$ is the value of Student t-distribution (equal to 2.776 for $v = 4$ and $\alpha = 0.05$) [40].

Knowing the uncertainty related to each concentration, the relative uncertainty can be determined by dividing the uncertainty by the corresponding concentration. The variation of the relative uncertainty in function of the volume concentrations is demonstrated in **Figure S2.1**.

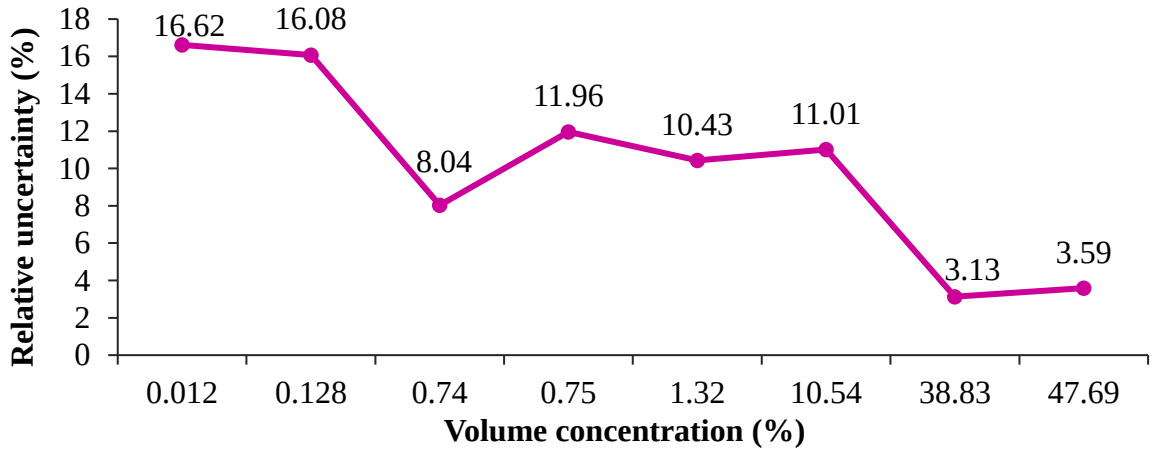

Figure S2.1 Variation of the relative uncertainty in function of the volume concentration of the compounds produced during the pyrolysis at 500°C with a heating rate of 30°C/min and 100 mL_n/min nitrogen flow rate

2. Programs of the methods applied for the bio-oil analysis with the GC/MS

Table S2.1 Slow program for the GC/MS analysis of the light species of the pyrolysis bio-oil

Slow program			
Temperature (°C)	**Heating rate (°C/min)**	**Hold time (min)**	**Total time (min)**
40	0	5	5
310	5	1	60

Table S2.2 Fast program for the GC/MS analysis of the heavy species of the pyrolysis bio-oil

Fast program			
Temperature (°C)	**Heating rate (°C/min)**	**Hold time (min)**	**Total time (min)**
70	0	2	2
150	30	0	4.67
200	5	0	14.67
310	4	3	45.17

Table S2.3 Method with a split for the GC/MS analysis of benzene

Time (min)	**Split state**		**Split Ratio**
Initial	ON		20
0	ON		100
1	ON		20
Temperature (°C)	**Heating rate (°C/min)**	**Hold time (min)**	**Total time (min)**
40	0	5	5
115	5	0	20

3. Effect of temperature on biomass pyrolysis

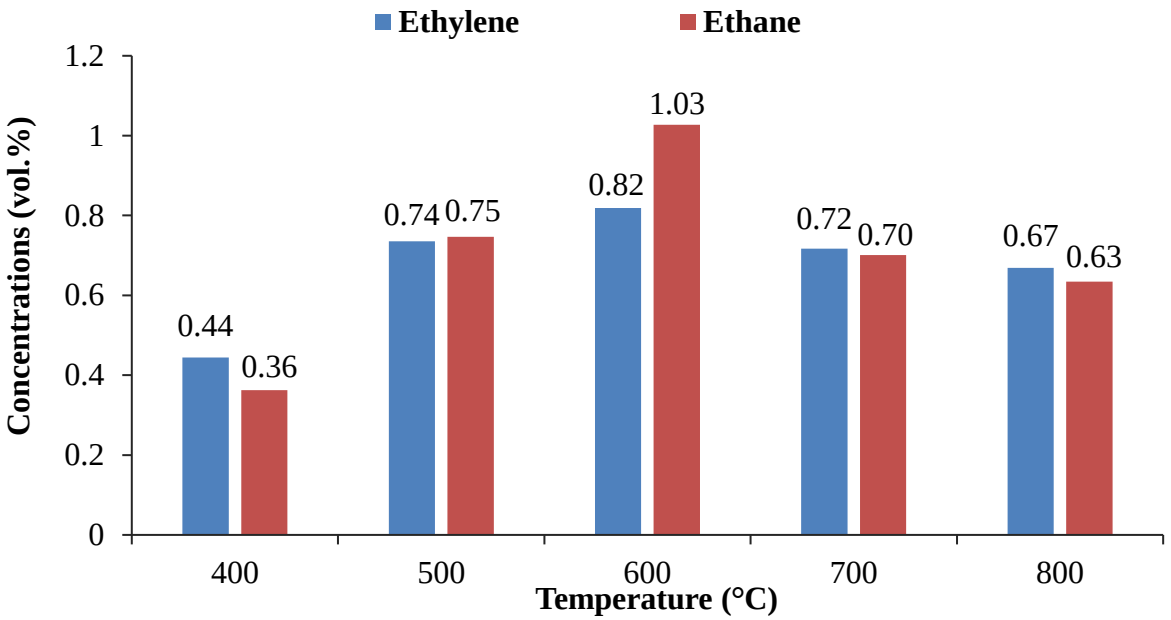

Figure S2.2 Effect of temperature on the volume yields of the light hydrocarbon gases produced from the pyrolysis of oak wood chips (heating rate = 30°C/min, nitrogen flow rate = 100mL/min, reactor at bottom, duration of constant temperature =20min)

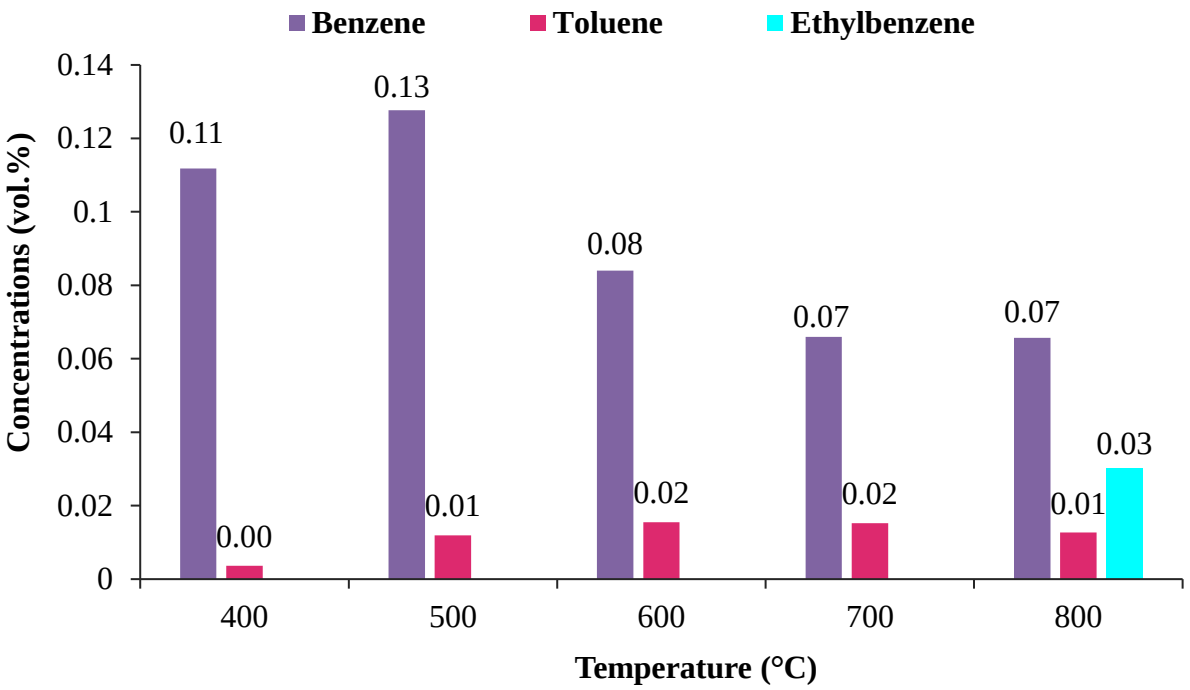

Figure S2.3 Effect of temperature on the volume yields of the heavy hydrocarbon gases produced from the pyrolysis of oak wood chips (heating rate = 30°C/min, nitrogen flow rate = 100mL/min, reactor at bottom, duration of constant temperature = 20min)

4. Effect of heating rate on biomass pyrolysis

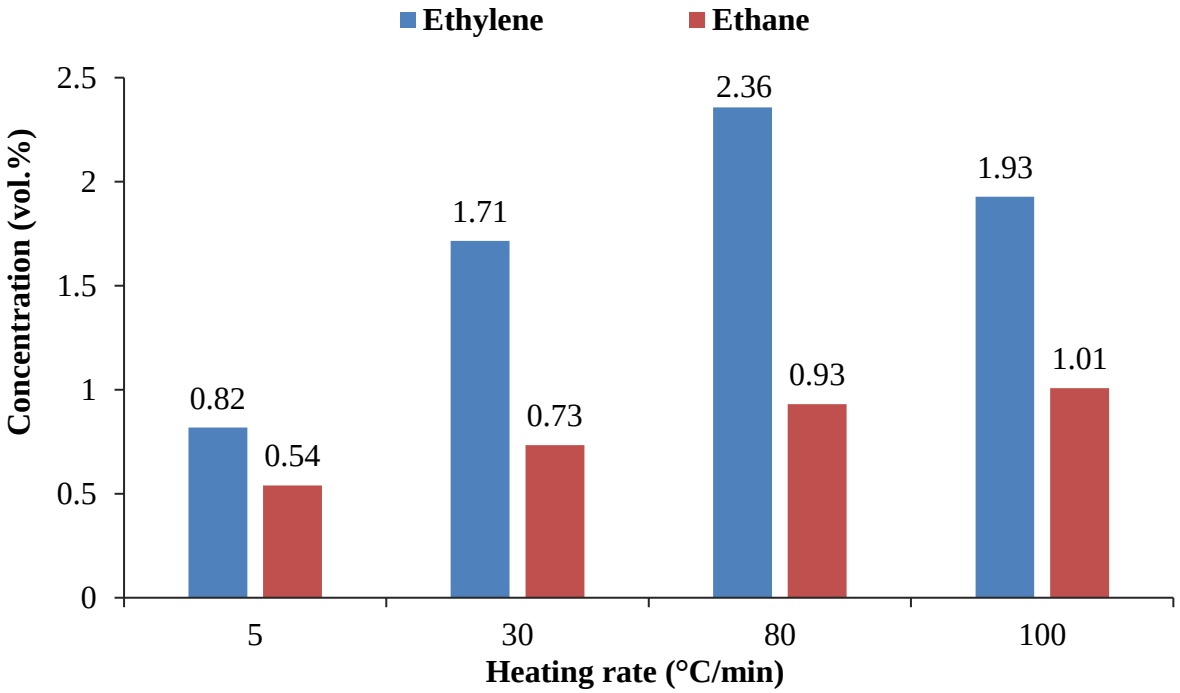

Figure S2.4 Effect of heating rate on the volume yields of the light hydrocarbon gases produced from the pyrolysis of oak wood chips (pyrolysis temperature = 700°C, nitrogen flow rate = 100mL/min, reactor at top, duration of constant temperature = 60 min)

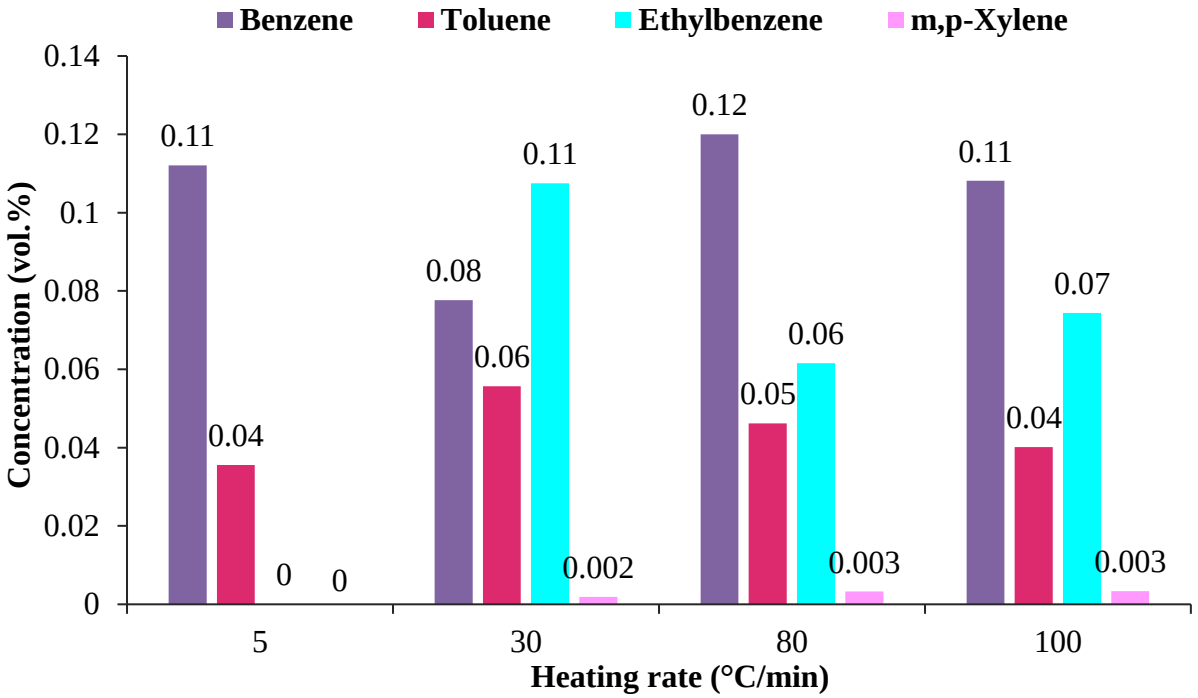

Figure S2.5 Effect of heating rate on the volume yields of the heavy hydrocarbon gases produced from the pyrolysis of oak wood chips (pyrolysis temperature= 700°C, nitrogen flow rate=100mL/min, reactor at top, duration of constant temperature = 60 min)

5. Effect of residence time on biomass pyrolysis

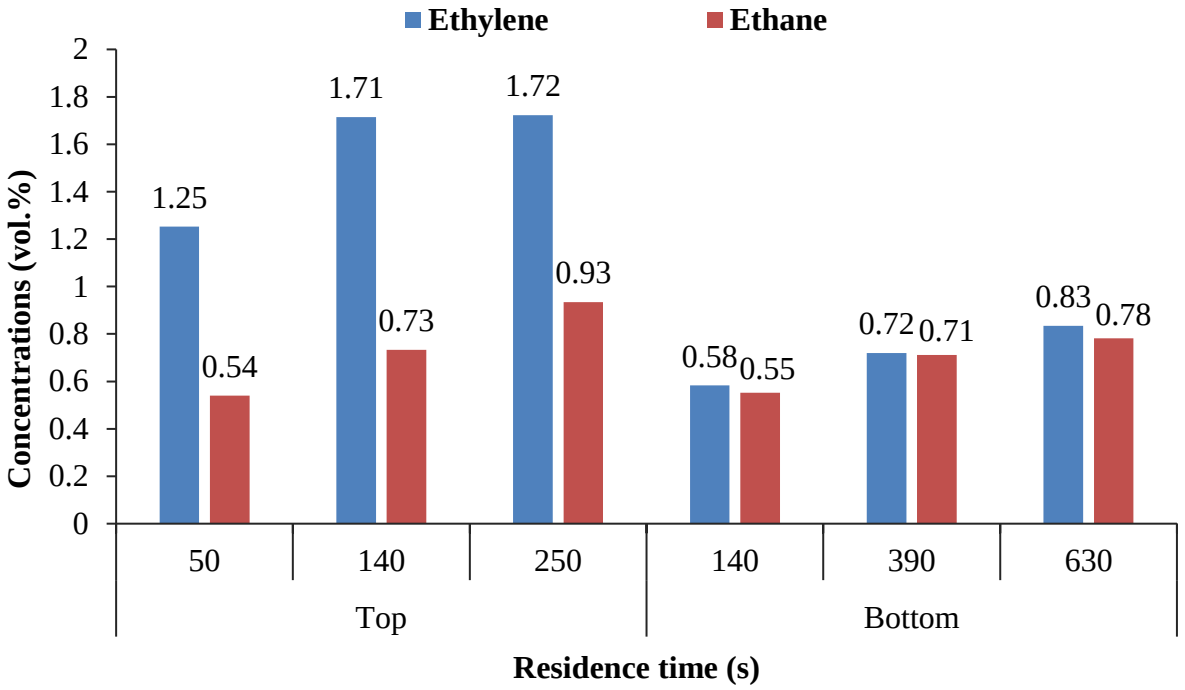

Figure S2.6 Effect of residence time on the volume yields of the light hydrocarbons gases produced from the pyrolysis of oak wood chips (pyrolysis temperature= 700°C, heating rate=30°C/min)

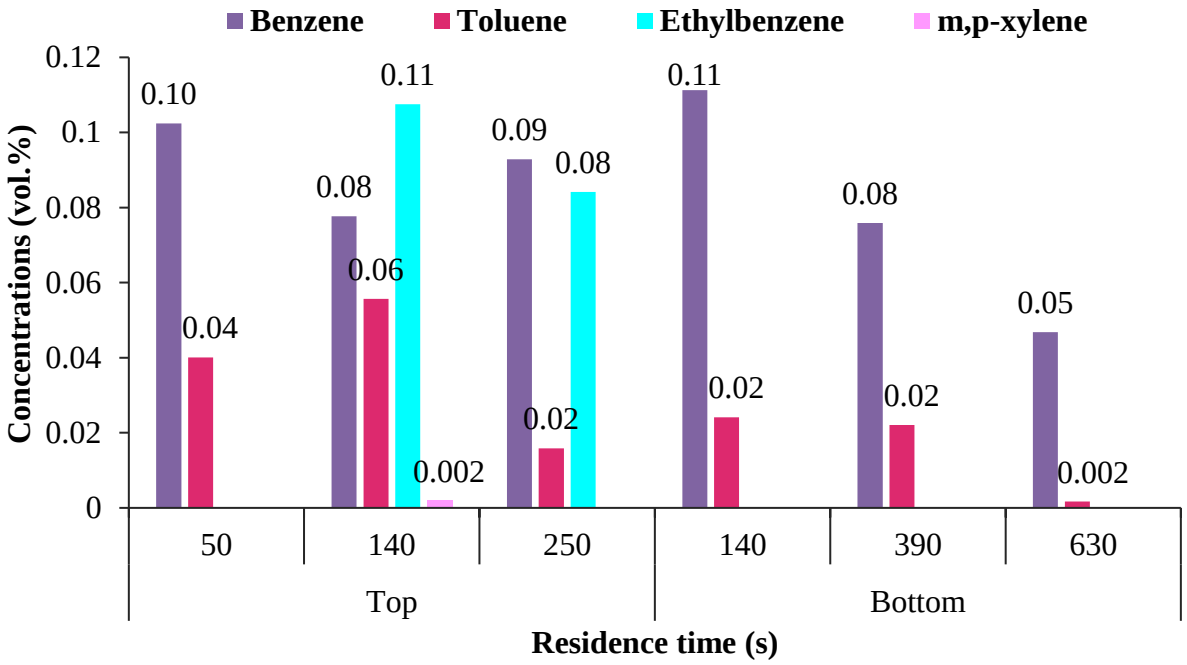

Figure S2.7 Effect of residence time on the volume yields of the heavy hydrocarbons gases produced from the pyrolysis of oak wood chips (pyrolysis temperature= 700°C, heating rate=30°C/min)

6. Qualitative analysis of the minor bio-oil compounds

Table S2.4 Qualitative analysis of the main bio-oil compounds

Temperature (°C)	**700**	**700**	**700**	**700**	**800**
Heating rate (°C/min)	**5**	**30**	**30**	**100**	**30**
Residence time (s)	**140**	**50**	**250**	**140**	**140**
Compounds	**Chromatographic surface area (%)**				
1,6-Anhydro-beta-D-glucopyranose (levoglucosan)	0.066	nd*	nd	nd	nd
2,5-Dimethoxybenzyl alcohol	1.947	3.299	nd	nd	11.640
2,6-Dimethoxy-phenol	2.533	2.854	nd	nd	28.100
2,6-Dimethyl undecane	2.439	0.945	nd	nd	nd
2.6-Dimethoxy-4-(2-propenyl)-phenol	nd	2.146	nd	nd	nd
3-Hexen-2-one	11.280	0.506	2.372	0.980	nd
4-Hydroxy-4-methyl-2-pentanone	0.935	0.484	1.866	1.299	nd
4-Methoxy-3-methyl-phenol	nd	0.376	nd	nd	nd
5-Tert-butylpyrogallol	nd	1.267	nd	nd	nd
Acetic acid, butyl ester	2.009	3.335	4.503	5.163	nd
Ethylbenzene	5.538	5.577	8.526	9.372	nd
Furfural	14.970	21.290	0.358	nd	47.270
Nonane	0.958	nd	1.478	nd	nd
Pentadecane	3.285	1.509	3.472	1.741	nd
Pentadecane	2.741	2.871	2.712	1.673	nd
Styrene	11.630	12.460	15.200	18.920	nd

Toluene	11.680	12.430	18.610	21.160	5.395
m-Xylene	8.020	8.125	10.550	6.872	nd
o-Xylene	15.690	16.300	21.130	25.200	nd
p-Xylene	0.279	0.169	1.142	4.015	nd

*Not determined

Table S2.5 Qualitative analysis of some minor bio-oil compounds

Temperature (°C)	**700**	**700**	**700**	**700**	**800**
Heating rate (°C/min)	**5**	**30**	**30**	**100**	**30**
Residence time (s)	**140**	**50**	**250**	**140**	**140**
Compounds	**Chromatographic surface area (%)**				
2-Cyclopenten-1-one. 2-hydroxy-3-methyl-					0.78
2-methylphenol					0.84
Phenol. 3-methyl- or 4-methylphénol	0.63				1.18
2-cyclopentene-1-one	2.81	8.4			2.6
Alkane	7.53		14.91	13.89	
Maltol					1.1
Phenol. 2.4-dimethyl-					1.23
Phenol. 3.5-dimethyl-					0.73
Alkane	12.03	9.77	11.37	12.32	
Phenol. 2-methoxy-4-methyl-					3.48
Alkane	0.77	0.28	10.89	4.38	
1.2-Benzenediol					5.9
2-Furancarboxaldehyde. 5-(hydroxymethyl)	4.06	4.77	0.78	3.8	
Benzene. 1-ethyl-4-methoxy-					0.14
Cyclohexane derived		0.26	0.97	0.65	
1.2-Benzenediol. 4-methyl- (or 3-methyl)	6.59	1.66		3.1	
1.2-Benzenediol. 3-methoxy-	4.97	4.01	0.84	0.71	10.14
Phenol. 4-ethyl-2-methoxy-	0.64	0.5	0.2		
1.2-Benzenediol. 4-methyl-	0.54	0.61		0.64	
Heptadecane			1.11		
Ethanone. 1-(2-hydroxy-5-methylphenyl)- or 4-hydroxy-3-methylacetophenone	0.71	1.35	0.34	0.14	4.59
Phenol. 2.6-dimethoxy-	7.1	6.05	1.35	0.75	6.49
Phenol. 3.4-dimethoxy-	0.74	0.62			2.7

4-Ethylcatechol	0.13	0.29		0.23	2.28
4-hydroxy-2-methoxybenzaldehyde or 3-hydroxy-4-methoxybenzaldehyde	0.33	0.4			
1.2.4-Trimethoxybenzene	5.86	4.72	1.2	0.7	5.19
Phenol. 2-methoxy-4-(1-propenyl)-. (Z)-	0.92	0.86	0.7	0.41	2.59
Phenol. 2-methoxy-4-propyl-	0.13	0.32	0.06	0.1	
4-Acetoxy-3-methoxyacetophenone				0.12	0.1
4-Acetoxy-3-methoxyacetophenone or Ethanone. 1-(4-hydroxy-3-methoxyphenyl)-	0.38	0.32			0.38
D-Allose or 1.6-Anhydro-.beta.-D-glucopyranose (levo)	2.04	2.19	2.93	12.84	
5-tert-Butylpyrogallol	5.37	9.28	0.63		3.12
2-propanone-1(4-ydroxy-3-methoxyphenyl)	1.79	0.74	0.4		1.94
Ethanone. 1-(3.4-dimethoxyphenyl)-	0.51	3.58	0.46	0.58	2.55
Naphthalene. 2.3.6-trimethyl-	0.22	0.23		0.18	0.38
Phenol. 2.6-dimethoxy-4-(2-propenyl)-	0.73	0.47	0.24	0.19	1.14
Phenol. 2.6-dimethoxy-4-(2-propenyl)-	0.33	0.41	0.11	0.13	0.64
Benzaldehyde. 4-hydroxy-3.5-dimethoxy-	0.51	0.77	0.26	0.26	1.6
Isomer Phenol. 2.6-dimethoxy-4-(2-propenyl)-	1.86	3.35	1.1	0.71	2.7
Ethanone. 1-(4-hydroxy-3.5-dimethoxyphen	0.86	0.79	0.25	0.24	0.98
4-Hydroxy-2-methoxycinnamaldehyde	0.23	0.67	0.11	0.15	0.68
2-Pentanone. 1-(2.4.6-trihydroxyphenyl) or 1-Butanone. 1-(2.4.6-trihydroxy-3-methyl	1.81	2.01	0.9	0.47	3.81
Phenanthrene			0.22	0.14	0.5
Anthracene					0.17

4'-Phenylpropiophenone	0.47	0.5	0.05	0.05	1.15
3.5-Dimethoxy-4-hydroxycinnamaldehyde	0.19	1.57	0.19		1.46
Fluoranthene					0.37
Pyrene					0.23
Phenol. 4.4'-(1-methylethylidene)bis-	0.05	0.2			0.24
benzene acetic acid. 4-hydroxy-3-methoxy					0.11
Hexadecanoic acid. 2-hydroxy-1-(hydroxymethyl)ethyl ester					0.58
Heptane. 1.1-diphenyl-		0.18			0.48

7. Effects of temperature and heating rate on the char

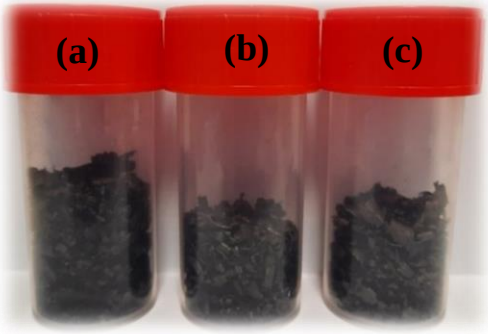

Figure S2.8 Char samples derived from three different pyrolysis experiments: (a) Pyrolysis temperature = 500°C, heating rate = 30°C/min, nitrogen flow rate = 100mL/min, char weight = 0.92 g. (b) Pyrolysis temperature = 700°C, heating rate = 30°C/min, nitrogen flow rate = 100mL/min, char weight = 0.82 g. (c) Pyrolysis temperature = 700°C, heating rate = 80°C/min, nitrogen flow rate = 100mL/min, char weight = 0.75 g. Comparing the two samples at the left demonstrates the effect of the temperature on the char while the two samples at the right shows the impact of the heating rate

8. Effects of heating rate and residence time on the bio-oil

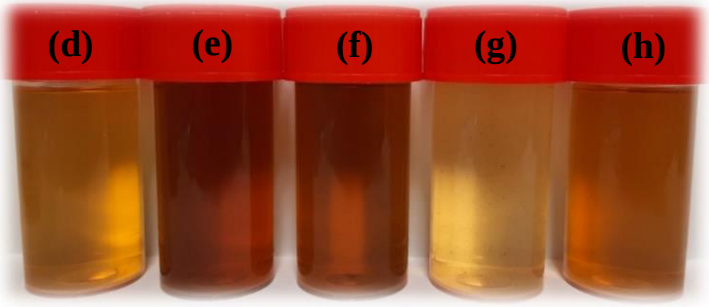

Figure S2.9 Bio-oil samples diluted with pure acetone derived from five different pyrolysis experiments at same temperature of 700°C with the biomass sample at the top of the furnace: (d) heating rate = 5°C/min, nitrogen flow rate = 100mL/min. (e) heating rate = 80°C/min, nitrogen flow rate = 100mL/min. (f) heating rate = 100°C/min, nitrogen flow rate = 100mL/min. (g) heating rate = 30°C/min, nitrogen flow rate = 50mL/min. (h) heating rate = 30°C/min, nitrogen flow rate = 300mL/min. Comparing the three samples at the left elaborates the impact of the heating rate on the bio-oil whereas the two samples on the right gives the influence of the residence time.

9. Calibration of the µGC/MS analyzer using standard gas bottles

For the quantification purpose, the µGC/MS analyzer was calibrated by using standard gas samples with known concentrations. Quantitative analysis of all produced gas molecules during the pyrolysis is fastidious given the large number of required reference gases. Therefore, only molecules of interest in the wood biomass pyrolysis field were quantified. **Table S2.6** reports the details of standard gas bottles used for the calibration, their composition as well as the relative uncertainty in their preparations.

Table S2.6 Gas bottles used for calibration of the µGC/MS

Calibration gas	Compounds	Concentration C effective	Uncertainty $(\pm \Delta C/C \times 100)$	Commercial supplier
Methane	CH_4	12.9 vol.%	± 2 %	SOL France
	N_2	87.1 vol.%		
Hydrogen	H_2	10.1 vol.%	± 2 %	SOL France
	N_2	89.9 vol.%		
Carbon monoxide	CO	11.9 vol.%	± 2 %	SOL France
	N_2	88.1 vol.%		
Carbone dioxide	CO_2	30 vol.%	± 2 %	
	N_2	70 vol.%		
BTEX	Benzene	10 ppm		Air Liquide
	Toluene	10 ppm		
	Ethylbenzene	10 ppm		
	m-xylene	10 ppm		
	p-xylene	10 ppm		
	o-xylene	10 ppm		
	N_2	99.94 vol%		
Mix	CH_4	7.035 vol.%	± 0.141%	SOL France
	H_2	2.013 vol.%	± 0.041%	
	CO	46.014 vol%		
	CO_2	41.91 vol.%	± 0.84%	
	C_2H_4	1.526 vol.%	± 0.031%	
	C_2H_6	1.502 vol.%	± 0.031%	

Chapter 3: Biomass Pyrolysis Followed by Catalytic Hybrid Reforming for Syngas Production Over Bulk Catalysts

Résumé

Ce chapitre, rédigé en anglais, est issu dans son intégralité de l'article publié en janvier 2023 dans le journal « *Waste and Biomass Valorization* » [1].

L'objectif principal de la thèse étant la valorisation de la biomasse au travers du couplage de deux procédés de pyrolyse et de reformage, ce chapitre est consacré aux premiers résultats expérimentaux obtenus par ce processus. Dans ce but, la biomasse étudiée est identique à celle du chapitre précédent, à savoir des copeaux de chêne. La pyrolyse est réalisée dans le même four à une température fixe de 700°C, à une vitesse de chauffe égale à 30°C/min et un débit d'azote de 100mL/min, choisis comme paramètres optimaux de pyrolyse produisant le maximum de volatils selon le chapitre précédent. La méthode appliquée est brièvement réexpliquée dans ce chapitre.

La composition des gaz obtenus à l'issue de cette pyrolyse est utilisée pour analyser l'efficacité du reformage réalisé en aval. Pour ce faire, un second four est employé pour le reformage avec un réacteur en quartz en forme de U d'une hauteur de 25 cm et de diamètre interne de 6 mm. Dans cette seconde étape, les composés volatils produits par la pyrolyse de biomasse subissent des réactions de craquage thermique et de reformage catalytique par le biais d'un reformage hybride (combinaison du reformage à sec et à la vapeur d'eau en consommant le CO_2 et la vapeur d'eau produits par la pyrolyse). Des catalyseurs massiques (c.à.d. sous forme de poudre) à base de nickel $Ni_2Mg_4Al_2$, Cobalt $Co_2Mg_4Al_2$ et Cobalt-Nickel $Co_1Ni_1Mg_4Al_2$ y sont utilisés. Différentes températures de reformage allant de 700°C à 800°C ont été testés.

Les résultats montrent qu'avec un procédé couplé, l'augmentation de la température améliore la production de gaz et réduit la formation de la bio-huile. Les taux de conversion de la bio-huile, du méthane et du dioxyde de carbone ont augmenté avec la température, ce qui a amélioré la formation de gaz de synthèse. Néanmoins, l'augmentation considérable de la température du processus accroîtra de manière significative les coûts opérationnels de la production de chaleur. Ainsi, une température optimale de 750°C est suggérée comme étant un compromis convenable entre l'amélioration de la production de gaz de synthèse d'une part et la réduction de la consommation d'énergie d'autre part.

Parmi les catalyseurs évalués, il a été constaté que le reformage en présence de Co-Ni à une température d'opération de 800°C donne lieu à une production maximale de gaz (43 wt.%) et à une formation minimale de bio-huile (32,4 wt.%). En ce qui concerne les concentrations de gaz, le catalyseur Ni a montré de meilleures performances que les autres en produisant la

concentration la plus élevée en gaz de synthèse (82,1 vol.% ou 16,8 mmol/g de biomasse sèche) après le reformage à 750°C. Cela peut être le résultat des conversions de méthane de 68,2% et de CO_2 de 52,6% atteinte avec le Ni à 750°C. Le catalyseur à base de Co s'est montré le moins performant et, en général, il est rarement utilisé seul mais plutôt allié au Ni pour réduire la formation de carbone.

D'autre part, les analyses DRX, ATD et ATG des catalyseurs post-reformage ont révélé la formation de plusieurs types de carbone déposés sur la surface des différents catalyseurs, y compris le Cα formé en dessous de 400°C, le C_β apparaissant autour de 460°C et le C_γ autour de 500°C ainsi que du carbone inerte formé à des températures plus élevées. La formation du carbone à une température plus élevée reflète une stabilité plus importante et donc une difficulté plus grande pour oxyder le carbone et l'éliminer. En comparant les trois catalyseurs, il a été constaté que l'utilisation du Co-Ni permettait le plus faible dépôt de carbone grâce à la présence du Co qui améliore la résistance du Ni à la formation de carbone.

Le test de vieillissement du catalyseur réalisé, sans aucun prétraitement, a révélé une diminution de l'activité du catalyseur avec le temps, qui a été associée au dépôt de carbone sur la surface du catalyseur comme démontré par les analyses ATG. D'autres problèmes peuvent également être rencontrés avec le catalyseur, notamment sa désactivation due à l'oxydation de ses sites métalliques actifs. Pour les réactiver, une régénération peut être appliquée en réduisant le catalyseur usé en présence d'un agent réducteur tel que l'hydrogène. Cette méthode a donc été testée sur nos catalyseurs, sans amélioration notable de leurs performances. Ceci a permis de déduire que les sites métalliques de notre catalyseur n'ont pas été oxydés pendant l'expérience de reformage. La régénération du catalyseur a alors été tentée par d'autres approches, à savoir l'oxydation à l'air du catalyseur et une combinaison de réduction et d'oxydation. L'oxydation à l'air à 800°C s'est avérée être un moyen efficace permettant d'oxyder le carbone déposé sur le catalyseur et a conduit à sa réactivation. Par conséquent, le test de vieillissement du catalyseur a été répété mais avec une étape de prétraitement par oxydation. Une amélioration de l'activité du catalyseur a été observée avec une stabilité dans le temps.

Pour permettre un meilleur référencement, les équations des réactions de pyrolyse et de reformage sont rementionnées dans ce chapitre puisqu'elles sont cruciales pour les interprétations et les explications des résultats.

Référence

[1] M. Abou Rjeily, M. Chaghouri, C. Gennequin, E. Abi Aad, H. Pron, J.H. Randrianalisoa, Biomass Pyrolysis Followed by Catalytic Hybrid Reforming for Syngas Production, Waste Biomass Valorization. (2023) 29. https://doi.org/10.1007/s12649-022-02012-4.

3.1. Introduction

Traditionally, fossil fuels were the main combustible generating power and feeding several chemical and petrochemical industries [1]. Nonetheless, their continuous depletion has triggered the researchers and engineers to investigate alternative energy sources. The use of renewable and sustainable sources of energy becomes a necessity in order to provide the global energy demand for electricity and fuels [2]. Hydrogen requirement has been remarkably escalading in the last decades to produce energy, electricity and for multiple industrial applications, being used as raw material and fuel [3]. Thereby, hydrogen, as an energy carrier, has been identified as the future of transportation and power generation [4]. Despite its abundance in nature, hydrogen is generally found associated to other elements in multiple molecules such as water, hydrocarbons (fossil fuels) or biomass. To dissociate the hydrogen molecule (H_2) from these primary sources, several processes exist, namely electrolysis of water (requiring electricity itself), steam reforming of fossil fuels (emitting carbon dioxide), and biomass gasification (soliciting a further step for products purification) [3]. Nowadays, multiple technics are applied to produce hydrogen from biomass namely thermochemical processes (liquefaction, combustion, gasification, pyrolysis…) as well as biological processes (fermentation, photolysis…).

The pyrolysis decomposes thermally the biomass into several products grouped into three main classes according to their physical state: gases (incondensable vapors: H_2, CO, CO_2 and CH_4), liquid (condensable hydrocarbon volatiles known as bio-oil or tar) and solid (carbonaceous residues or char) [5]. Bio-oil is a viscous brown liquid whom yield can reach 75 wt.% in the case of biomass fast pyrolysis [6]. The bio-oil reforming presented itself in the recent years as an alternative and indirect route for the production of syngas (mix of hydrogen H_2 and carbon monoxide CO) from biomass [7]. Two types of reforming are generally distinguished: dry reforming as the reaction of hydrocarbons with carbon dioxide CO_2 to produce H_2 and CO and the steam reforming taking place in presence of water vapor, with methane being the most commonly encountered hydrocarbon [8]. In contrast to the direct gasification, the bio-oil reforming can be performed at noticeably lower temperatures leading to inferior material costs and power consumption [9]. Nonetheless, this strategy is held back by the inconvenient physical properties of the bio-oil, its instability and polymerization during the storage, which makes it heavier and more viscous [10]. Moreover, the bio-oil composition is very complex and comprises more than three hundred different oxygenated compounds including ethanol, phenols, aldehydes, ketones and carboxylic acids [11,12]. Therefore, the majority of the studies found in the literature were realized not with the multicomponent features of the bio-oil but rather with single bio-oil model compounds such as ethanol [13,14], acetic acid [15–17], benzene [18], toluene [19], a synthetic mixture formed by blending these compounds in various ratios [20,21] or even with the aqueous fraction of the bio-oil [22–24]. Scarce are the studies dealing with the complex bio-oil composition during its catalytic reforming for the syngas production [25].

Coupling the biomass pyrolysis in-line with the catalytic reforming of the pyrolysis volatiles to produce hydrogen is a solution enabling to overcome the problems associated to the handling of the bio-oil [25], which is a relatively new approach dating from two decades. It was first envisaged by the US renewable Energy Laboratory in 1997 who proposed the production of hydrogen through the fast pyrolysis of biomass followed by the catalytic steam reforming of the bio-oil [26]. This method allows the cracking and reforming of the pyrolysis volatile

hydrocarbons which enhances the process gas yield and remarkably boosts the H_2 production [4]. It also helps avoiding the issues associated with the bio-oil such as vaporization, condensation and storage since the totality of the pyrolysis gases and bio-oil volatiles are directly fed to the second reforming reactor [27]. Moreover, an interesting aspect of combining the biomass pyrolysis to the dry reforming of the volatiles produced is that it produces syngas while consuming the greenhouse gases, namely carbon dioxide and methane [28], known for their devastating impact on the environment (air pollution, climate change, global warming... [29,30]).

This recently emerging technology has been also applied as a thermochemical recycling approach of plastic waste for the syngas production given their fossil fuels origin and high content of Carbon and Hydrogen elements. For instance, Younis *et al.* [31] realized the catalytic dry reforming of polypropylene derived from the pyrolysis of domestic waste plastics for the syngas production. In spite of the scarce studies on this approach for the hydrogen production from biomass, it has been considered as an achievable route for the small scale H_2 production [32] as highlighted by several recent works [33–37]. For instance, some researchers investigated the biomass pyrolysis and volatiles reforming in two in-line fixed bed reactors [38–40]. Wang *et al.* [41], studied the syngas production via the reforming of the bio-oil derived from the in-line pyrolysis of poplar wood while using the char formed as a catalyst and a support for the nickel catalyst.

Several catalysts can be used to realize a successful and efficient tar reforming including alkaline earth, metal catalysts and natural minerals [42]. Base metal such as Nickel Ni, Cobalt Co and Iron Fe, are more commonly encountered than noble metals, especially on the industrial level, thanks to their higher availability and lower cost [43,44]. The Nickel catalyst has been attracting a lot of attention for the dry and steam reforming of tar and bio-oil. It is characterized by its strong activity and high selectivity toward syngas production during the reforming reactions [45]. Moreover, the alloy of Nickel with Cobalt has been identified as an efficient catalyst for the bio-oil reforming [46]. Nonetheless, Nickel-based catalysts suffer from fast deactivation caused by sintering of the metallic phase and carbon formation over their surface [30,47]. This is considered as a major challenge of the bio-oil reforming process which is mainly caused by the presence of insoluble water and non-volatile species. The reforming of these compounds is very difficult which tends to produce carbon over the catalyst's surface resulting in its deactivation as well as the fouling of the reaction bed [35].

The catalyst support plays equally an important role in improving the catalyst activity and reducing the carbon deposition over its surface [48]. In addition, basic supports have a particular interest for the dry reforming given the acidic nature of the CO_2 [49]. Alumina Al_2O_3 has been the most employed as a Nickel support for tar reforming due to its high mechanical strength, chemical/physical stability and good dispersion of the metal active phase [50].

Aware that the biomass is one of the most promising eco-friendly renewable energy sources, its valorization into syngas (H_2 mainly and CO) through a two-stage process is our chief objective. Specifically, the biomass pyrolysis takes place in the first stage reactor. The volatiles produced undergo reactions of thermal cracking and catalytic reforming, in the second stage, through a hybrid reforming (combination of dry and steam ~~and dry~~ reforming by consuming respectively the CO_2 and water vapor produced by the pyrolysis). Interestingly, this presents one of the innovative sides of this work since the reforming of pyrolysis products is usually

realized in the presence of CO_2 (dry reforming) [51,49,52,53] or water vapor (steam reforming) [13,54–56]. However, realizing a hybrid reforming combining both the dry and the steam reforming is extremely rare in the literature [57]. Furthermore, the reforming of the bio-oil hydrocarbons produced from the biomass pyrolysis will be realized in this work and not some model compounds, which is less frequent in the literature.

Even though the combination of pyrolysis and catalytic reforming is a promising methodology for the syngas and hydrogen production, it still faces several challenges before being able to be extrapolated to the industrial level. These include the high operating temperatures and the catalyst deactivation caused by the carbon deposition and active phase sintering [30]. In this work, these difficulties are aborded by studying the effects of temperature and catalyst active phase over the products distribution and the gas composition to determine the optimal operating conditions to maximize the production of syngas, in particularly hydrogen, while reducing the formation of methane and carbon dioxide. For this purpose, three bulk catalysts are used for the catalytic reforming on bases of Nickel, Cobalt and Cobalt-Nickel Co-Ni. The post-reforming catalysts will be characterized to understand the origin of the catalyst deactivation. The optimal catalyst will be identified to maximize the hydrogen production. In addition, an aging test will be realized on the Cobalt-Nickel catalyst for five consecutive cycles to determine its stability. Furthermore, different pre-treatments tests will be performed on this catalyst to study its potential regeneration post-reforming.

3.2. Materials and methods

3.2.1. Biomass

To evaluate the efficiency of coupling the pyrolysis to the reforming process, a well-studied biomass type was chosen to be tested, the oak wood chips. It is one of the most abundant wood types in the Grand-Est region of France, where the studies were realized. Its moisture content is 7.5 wt.%. Its characterization was realized in **chapter 2 subsection 2.2.1.** and in the published work [58]. **Figure 3.1** represents the oak wood chips before the pyrolysis (a), the char (b) and the bio-oil (c) products formed after a pyrolysis step realized at 700°C with a 30°C/min heating rate, and the bio-oil (d) produced after the catalytic reforming at 700°C in presence of Nickel based catalyst. Both bio-oil samples were diluted with pure acetone.

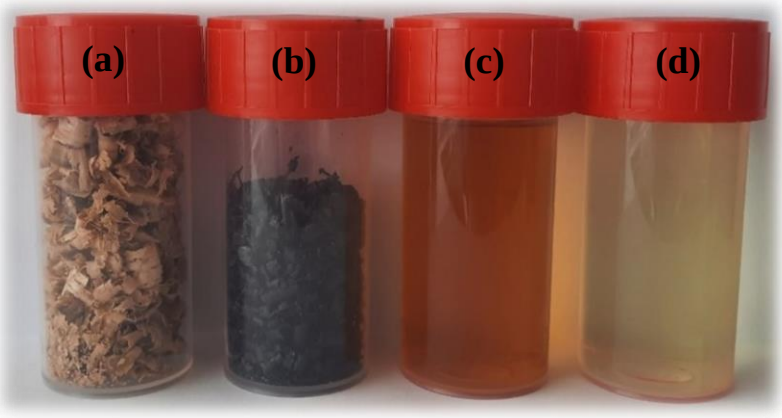

Figure 3.1 Photography of tested biomass along with its pyrolysis products: (a) oak wood chips before pyrolysis (b) char formed after the pyrolysis realized at 700°C with a heating rate of 30°C/min; (c) bio-oil sample produced by the pyrolysis performed under these conditions (diluted with pure acetone); (d) bio-oil sample produced after catalytic reforming at 700°C with Nickel (diluted with pure acetone)

3.2.2. Catalyst's synthesis

The hydrotalcite route is applied to synthesize Ni, Co, Al and Mg based mixed oxides with a molar ratio $(Mg^{2+} + Ni^{2+} + Co^{2+})/Al^{3+} = 3$. The catalysts were prepared following the protocol applied in the works of Tanios *et al.* [59,60]. This protocol is briefly recapitulated hereafter. An aqueous solution of Na_2CO_3 (1 M) and NaOH (2 M) was prepared to which drops of a solution containing relative amounts of $Al(NO_3)_3.9H_2O$, $Mg(NO_3)_2.6H_2O$, $Ni(NO_3)_2.6H_2O$ and $Co(NO_3)_2.6H_2O$, were added under vigorous mixing. A temperature of 60°C and a final pH of 9 were maintained. To crystallize the hydrotalcite phase slowly, the formed slurry was heated for 18 hours at 60°C through the maturation step. Next, a filtration of the precipitate was realized followed by a repetitive washing with a hot (60°C) deionized water until a pH of 7 was obtained. Then, a drying of the precipitate was realized for 48 hours at 60°C. To obtain fine powders, a grounding of the precipitate was done with a subsequent calcination for 4 hours at 800°C reached at a heating rate of $1°C.min^{-1}$ and under an air flow rate of $2L.h^{-1}$, to produce the oxide forms of the catalysts. Therefore, the catalysts obtained are Nickel $Ni_2Mg_4Al_2$, Cobalt $Co_2Mg_4Al_2$ and Cobalt-Nickel $Co_1Ni_1Mg_4Al_2$.

3.2.3. Pyrolysis-catalytic reforming

A two-stage reactor system for the pyrolysis-catalytic reforming has been proven more favorable than a single stage reactor where the catalyst and the biomass are blended. The process conditions of the pyrolysis and the catalytic reforming (temperature, inputs flow rate, residence times, etc.) can be more efficiently controlled when separated in a two-stage reactor [61]. The biomass pyrolysis alone produces a large amount of CO_2 and water vapor [8]. Consequently, it was envisaged to use the CO_2 and water vapor produced during the pyrolysis, as reactants for the dry and steam catalytic reforming reactions. The reforming that takes place is therefore referred to as "hybrid reforming" since it might combine the dry and steam reforming. In this way, not only the syngas (H_2 and CO) production is enriched but also the CO_2 emission is reduced, knowing its undesirable greenhouse effect and air pollution [29].

Figure 3.2 illustrates the experimental set up of the coupled pyrolysis-reforming process connected with the gas analyzer. For the biomass pyrolysis, the same reactor used in the previous chapter was also used here with the detailed description provided in **chapter 2 subsection 2.2.2.** The reforming reactor consists of a U-shaped quartz tube with an inner diameter of 0.006m and a total height of 0.25m introduced in a cylindrical tubular furnace **(**Thermolyne 21100). The catalyst is deposited over a sintered quartz support at the bottom of one side of the reactor. A thermally insulated stainless-steel pipe connects the two reactors. Moreover, the pipes connecting the different elements of the experimental set up are heated to 100°C by a heating cable (Vulcanic Silicon self-regulating heating cable 26175-00) to avoid the condensation of the volatiles flowing inside the tubes.

For the biomass pyrolysis, 3.5g of oak wood chips were introduced in a porous cylindrical nickel basket placed at the top of the furnace. Prior to the pyrolysis tests, the biomass was dried at 100°C for 35 min under an inert atmosphere ensured by 100 mL_n/min N_2 flow rate (99.996% purity). At the same time, the second furnace was preheated to reach the target reforming temperature (700, 750 or 800°C). Next, the dried biomass was heated in the first pyrolysis furnace at 700°C reached with a heating rate of 30°C/min and maintained for 1h, after which the biomass pyrolysis was finished. The volatiles produced during the pyrolysis were continuously fed to the second reactor where they undergo catalytic reforming reactions. The carrier gas flow rate (100 mln/min N_2) was maintained through the entire process and allows

an average volatiles residence time of 140s in the pyrolysis reactor and 9s in the reforming reactor.

The vapors exiting the reforming process were passed through a condensate trap filled with ice-cooled acetone, which condensed the heavy volatiles forming the bio-oil. The uncondensed gases are then filtered through a cotton filter and a membrane of 8µm of porosity. A similar pyrolysis procedure was applied by Cheng *et al.* [62] in their work on the pyrolysis of poplar waste. The gas stream is then measured by a flowmeter (Bronkhorst F-201CV-500-RAD-22-V) having a range from 0 to 500 ml_n/min. The vapors were then analyzed by the micro–Gas Chromatography/Mass Spectrometry (µGC/MS, Agilent Single quad MSD 5977B and SOLIA 490 microGC). Some of the main gases produced such as H_2, CO, CO_2 and CH_4, along with some minor gases formed like ethane C_2H_6, ethylene C_2H_4, benzene C_6H_6 and toluene C_7H_8 were quantified thanks to a previous calibration of the µGC/MS. Concerning the quantitative analysis of the gases formed, the calibration of the µGC/MS analyzer was realized based on external standard method using standard gas samples provided by commercial suppliers (Air Liquid and SOL France companies). The software used for the gases analyses was Soprane Solia (CP 490 LAN), provided with the µGC/MS which allows the identification and quantification of the gases produced and provides their instantaneous volume concentrations thanks to its prior calibration.

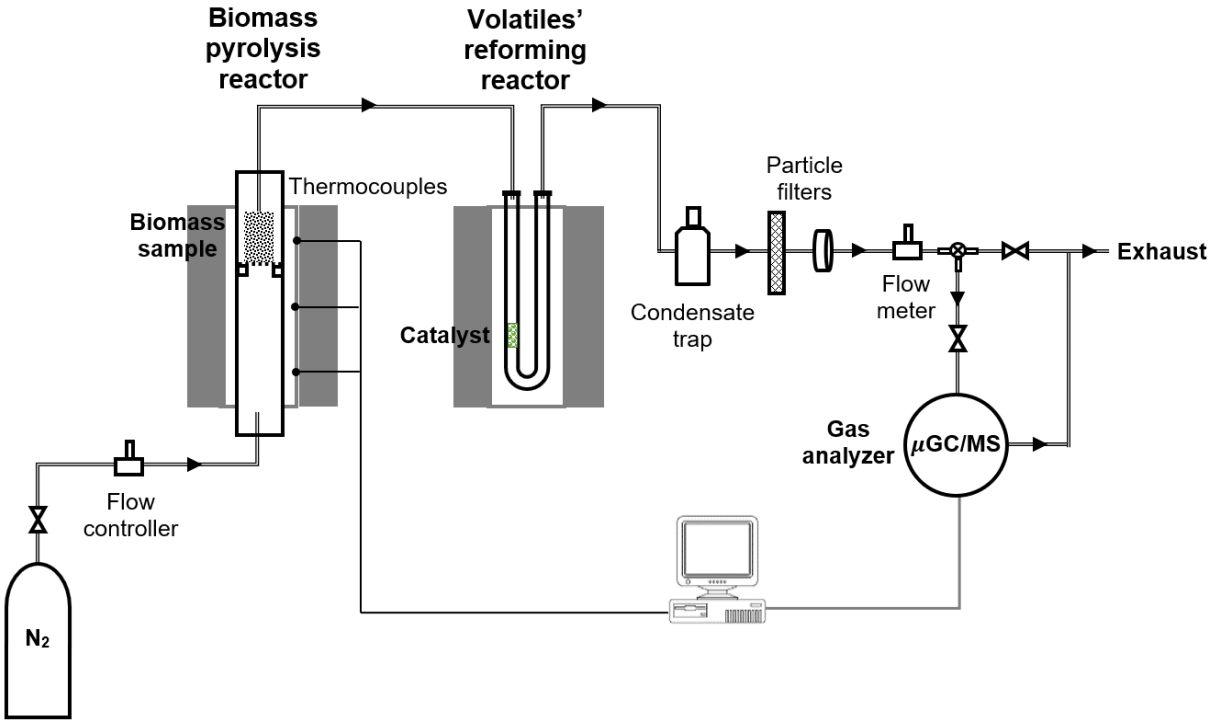

Figure 3.2 Experimental set up for the pyrolysis-reforming process with the gas analyzer. The first stage reactor is devoted to the biomass pyrolysis while the second stage reactor aims to ensure the volatiles reforming in presence of a catalyst

For each experiment, 100 mg of bulk catalyst was used corresponding to a gas hourly space velocity (GHSV) of 32 000 h^{-1}. A pre-treatment step was applied to clean the catalyst surface by heating the catalyst at 800°C for 3 h at a constant pure nitrogen flow rate of 100 mln/min. It should be noted that the catalysts are in their oxidized form. To be active, they need to be reduced using a reduction agent such as hydrogen H_2. Our catalysts were activated with the H_2 produced by the pyrolysis-reforming which eliminates the need for an external H_2 inlet. This

procedure was proven efficient by Chen *et al.* who demonstrated that the syngas formed during the reforming was sufficient for the reduction of the catalysts [63].

It is worth mentioning that this same experimental set up allows the realization of a classical one-stage pyrolysis without passing by the second furnace. Thereby, a one-stage pyrolysis test was performed, under the same conditions (700°C, heating rate of 30°C/min, 100 mln/min N_2 and 3.5g of biomass). The products were similarly analyzed to obtain the composition of the volatiles that are ultimately fed to the reforming reactor. Additionally, a two-stage pyrolysis can be realized by sending the pyrolysis volatiles to the second reactor used without a catalyst, which allows their thermal cracking. Thus, a two-stage pyrolysis was realized by setting the temperatures of both reactors at 700°C, under the same conditions. These two experiments were performed for the comparison purpose with the pyrolysis-catalytic reforming.

3.2.4. Catalyst aging test

An aging test was carried out on the powder catalysts during five consecutive experiments. For the first experiment, the same protocol followed for the previously described pyrolysis-reforming was applied with $Co_1Ni_1Mg_4Al_2$ catalyst and the reforming temperature sets to 750°C. This is defined as cycle 1 as shown in **Figure 3.3**.

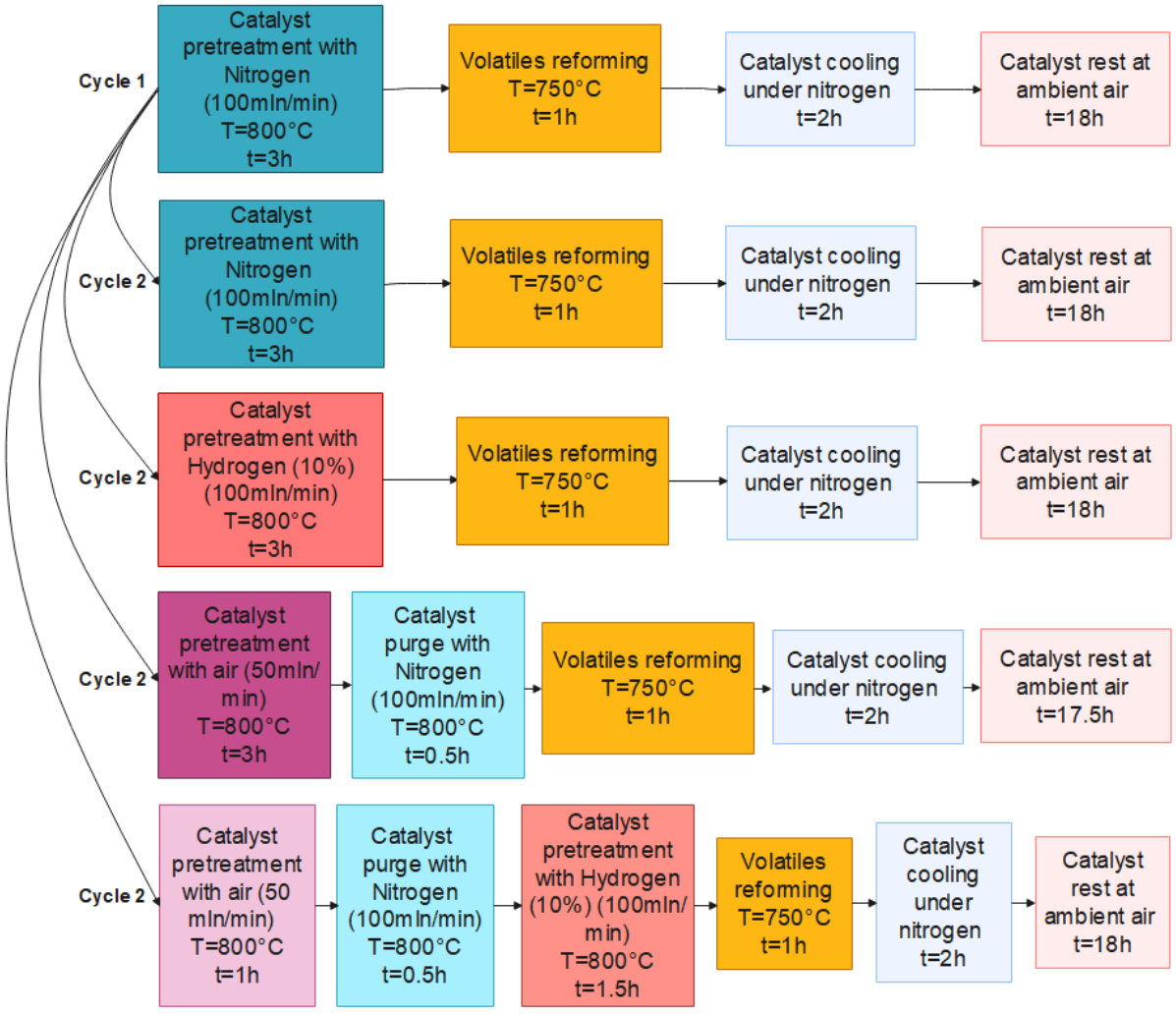

Figure 3.3 Steps of catalytic reforming experiments with the cycle 1 for the protocol followed for the first trial and cycle 2 referring to the different pretreating methods applied to the catalyst for the second trial of the aging test

For the other experiments, the same protocol was followed without a pretreatment step, thereby after the biomass drying phase, the pyrolysis volatiles were directly fed to the second furnace preheated at 750°C. This experiment was repeated four times and thereby the aging test was realized over five consecutive experiments. The catalyst was not changed during these five consecutive tests which implies five cycles of catalyst operation.

3.2.5. Pretreatment of spent catalyst with different gases

Several gases (N_2, H_2 and air, i.e. O_2) were used to pretreat the catalyst. In this purpose, experiments were realized over two trials with the $Co_1Ni_1Mg_4Al_2$. Cycle 1 was applied for the first trial. For the second trial, several approaches were applied but are referred to as cycle 2 in **Figure 3.3** where only the first step of pretreatment differs for the several gases tested (N_2, H_2, air and combination of air and H_2). Given that the best catalyst performance was obtained after the oxidation with air, the aging test was repeated over 5 experiments with the same catalyst $Co_1Ni_1Mg_4Al_2$ under GHSV=32 000h^{-1}. For each experiment, the catalyst was oxidized under 50 ml_n/min flow rate of air at 800°C for 1h followed by a purge under 100 ml_n/min flow rate of nitrogen for 0.5h, prior to the reforming at 750°C of the pyrolysis volatiles. The outcomes will be displayed in the results section.

3.2.6. Characterization of the spent catalysts

X-ray diffraction (XRD) was employed to determine the crystallographic structure of the catalysts at room temperature. In that purpose, a Bruker D8 advance diffractometer equipped with a copper anode (λ=1.5406 Å) was used. An angular range of $20° < 2\theta < 80°$ was applied to measure the scattering intensities with 2θ=0.02° for a step-size and 2s for the counting time. An index of the diffraction patters was realized by comparison to the files of joint committee on powder diffraction standards (JCPDS) thanks to EVA software.

Differential scanning calorimetry-thermogravimetry (DSC-TG) analyses were simultaneously realized by a NETZSCH STA 409 apparatus furnished with a gas inlet system, a differential scanning calorimetry for DSC and a microbalance for TG. In a furnace, two alumina crucibles are introduced and symmetrically placed on a support. One of these crucibles is kept empty and used as a reference while the second one is for the catalysts. The temperature inside the furnace is increased from room temperature to 900°C at 5°C/min heating rate with an air flow rate of 75 ml_n/min. The temperature of the sample is controlled and measured by a thermocouple system. The temperature difference between the sample and the reference allows the determination of the differential thermal analysis (DTA) while the weight differences (gain or loss) give the thermogravimetric analysis (TGA).

3.3. Theory/Calculation

3.3.1. Pyrolysis and reforming reactions

The pyrolysis involves numerous chemical reactions occurring simultaneously, resulting from the strong interactions between the single particle and the surrounding environment [64]. Several models exist to describe in details the reactions involved during the pyrolysis such as Ranzi's [65] and Di Blasi models [66,67], however one global reaction model (equation **(3.1**) can be used to simplify the process [68]:

$$\text{Biomass pyrolysis: Biomass} \rightarrow \text{char} + \text{hydrocarbon volatiles} + H_2 + CO + CO_2 + H_2O \quad \textbf{(3.1)}$$

Multiple reactions interfere in the catalytic reforming process of the pyrolysis volatiles. Two types of reforming are generally distinguished: steam and dry reforming. During the steam

reforming, the tar, the hydrocarbon volatiles or the methane CH_4 react with the water vapor to produce syngas (H_2 and CO) (equations **(3.2), (3.3)** and **(3.4)**), respectively) with an H_2/CO ratio superior to 1 (equals to 3 in the case of methane steam reforming). Whereas, for the dry reforming, the carbon dioxide CO_2 ensures the role of oxidizing gas [30] (equations **(3.5)**, **(3.6)** and **(3.7)**. The dry reforming of methane has the quality of consuming two greenhouse gases, CH_4 and CO_2, which is of critical importance nowadays to deal with the global warming, climate change and air pollution issues the world is facing [29,69]. For the dry reforming of methane, the ratio of H_2/CO is around 1, thereby the syngas produced is a key in the chemical industry. It is used for numerous types of highly selective synthesis, in order to produce a wide range of chemical compounds such as acetic acid, formaldehyde and liquid hydrocarbons [70]. The reactions of the steam and dry reforming of methane and tar, responsible for the production of hydrogen enriched syngas, can be summarized as follows [42,47,68,71]:

Steam tar reforming: $C_xH_yO_z(\text{tar}) + (x-z)H_2O \rightarrow \left(x + \frac{y}{2} - z\right)H_2 + xCO \quad \Delta H > 0$ **(3.2)**

Hydrocarbon volatiles steam reforming: $C_mH_n + mH_2O \rightarrow (m + \frac{n}{2})H_2 + mCO \quad \Delta H > 0$ **(3.3)**

Steam reforming of methane SRM: $CH_4 + H_2O \leftrightarrow 3H_2 + CO \quad \Delta H°_{298K} = +205.9\ kJ/mol$ **(3.4)**

Dry tar reforming: $C_xH_yO_z(\text{tar}) + (x-z)CO_2 \rightarrow \frac{y}{2}H_2 + (2x-z)CO \quad \Delta H > 0$ **(3.5)**

Hydrocarbon volatiles dry reforming: $C_mH_n + mCO_2 \rightarrow \frac{n}{2}H_2 + 2mCO \quad \Delta H > 0$ **(3.6)**

Dry reforming of methane: $CH_4 + CO_2 \leftrightarrow 2H_2 + 2CO \quad \Delta H°_{298K} = +247\ kJ/mol$ **(3.7)**

In addition to the main reforming reactions, and given their endothermic nature, some secondary reactions can potentially take place simultaneously [42,47,68,71]. They include:

Water-gas shift reaction WGSR: $CO + H_2O \leftrightarrow H_2 + CO_2 \quad \Delta H°_{298K} = -41.1 kJ/mol$ **(3.8)**

Reverse WGSR: $H_2 + CO_2 \leftrightarrow CO + H_2O \quad \Delta H°_{298K} = +41.1 kJ/mol$ **(3.9)**

Boudouard reaction: $2CO \leftrightarrow CO_2 + C \quad \Delta H°_{298K} = -172\ kJ/mol$ **(3.10)**

Reverse water-gas reaction: $CO + H_2 \rightarrow H_2O + C \quad \Delta H°_{298K} = -131 kJ/mol$ **(3.11)**

Thermal tar cracking: $pC_nH_x(\text{tar}) \rightarrow qC_mH_y(\text{smaller tar}) + rH_2 \quad \Delta H > 0$ **(3.12)**

Tar decomposition: $C_nH_x(\text{tar}) \rightarrow nC + \left(\frac{x}{2}\right)H_2 \quad \Delta H > 0$ **(3.13)**

Hydrocarbons steam reforming: $HC + H_2O \rightarrow H_2 + CO + CO_2 \quad \Delta H > 0$ **(3.14)**

The products' formation and distribution are therefore the results of the combination of these competitive reactions. With the endothermic character of the reforming reactions, the use of a catalyst is necessary to avoid operating at much higher temperatures and to facilitate the process feasibility. The major problem associated to the reforming process remains, however, the carbon deposition on the catalytic system, occurring as a result of the Boudouard reaction **(3.10)**, the reverse water-gas reaction **(3.11)** and the tar decomposition **(3.13)**. This carbon acts as poison to the catalyst and leads to its deactivation [72].

3.3.2. Characteristic parameters

3.3.2.1. Global mass balance

The biomass pyrolysis results in the production of multiple products which can be grouped according to their physical state under normal conditions. The three main categories are: char, bio-oil, and gas. Char is a dark solid composed mainly of Carbon with some Oxygen and Hydrogen and traces of nitrogen and sulfur depending on the nature of the biomass [73]. The bio-oil is a brown to black viscous liquid containing more than 300 hydrocarbons grouped mainly under polyaromatic hydrocarbons (PAHs), aldehydes, aliphatic species, phenols, levoglucosan, BTEX (benzene, toluene, ethylbenzene and xylene) along with some other hydrocarbons and water. Gas includes a mixture of several incondensable gases consisting primarily of carbon monoxide and dioxide, hydrogen (industrially grouped under the label "syngas") and some light hydrocarbons such as methane, ethane and propane [30,58].

From previous drying experiments, it was found that the moisture content of the biomass sample was around 7.5 wt.% [58]. A global mass balance was realized to determine the concentrations of the major biomass pyrolysis products: char, bio-oil and gases. More details on the calculations are provided in **chapter 2 subsection 2.2.2.**

3.3.2.2. Reproducibility analysis

To determine the reproducibility of our experiments, a pyrolysis-reforming experiment was repeated six times in the same operating conditions. For the pyrolysis, the operating conditions were as follows: 3.5 g of oak wood chips, a heating rate of 30°C/min, a nitrogen flow rate of 100 mL_n/min, and a temperature of 700°C maintained for 2h. For the reforming, a temperature of 750°C was applied with the Cobalt-Nickel as catalyst. The concentrations of the different gases as well as those of the main products are an average of the concentrations obtained from the six experiments. The uncertainty δ was calculated according to the **equation (3.15).**

$$\delta = t_{1-\alpha,v}\frac{S_n}{\sqrt{n}} \quad \textbf{(3.15)}$$

With S_n as the standard deviation, n is the number of replicates (6 in our case), $1-\alpha$ reflects the confidence level (α is chosen to be 0.05 which corresponds to 95% of confidence level), v is the degree of freedom (equals to $n-1$ so 6 in our case) and $t_{\alpha,v}$ is the value of Student t-distribution (equal to 2.015 for $v=5$ and α = 0.05).

The relative uncertainty was determined as well by dividing each uncertainty by the corresponding concentration and it is illustrated in **Figure 3.4.** It can be remarked that as the concentration increases, the relative uncertainty decreases globally. For concentrations lower than 5%, corresponding in general to the minor products formed such as the light and heavy hydrocarbons, the relative uncertainty is around 7.7%. Whereas when the concentrations are between 5% and 15%, the relative uncertainty is around 6%. For higher concentrations (above 20%) corresponding to the major gases produced, the relative uncertainty becomes considerably small with values between 2% and 3%. Next, the uncertainties of the different concentrations were determined from the relative uncertainties and are illustrated as error bars on the graphs of the results.

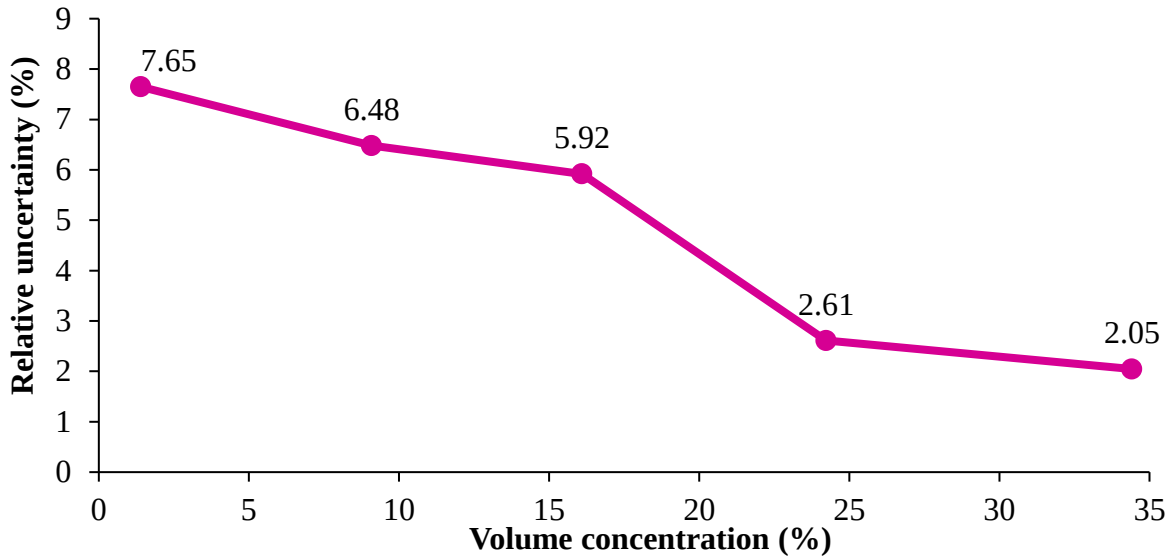

Figure 3.4 Variation of the relative uncertainty in function of the volume concentration of the compounds produced during the pyrolysis at 700°C with a heating rate of 30°C/min and 100 mL_n/min nitrogen flow rate followed by the catalytic reforming at 750°C with the cobalt-Nickel catalyst

3.3.2.3. Conversion rates and syngas concentration

The conversion rates of our main reactants: bio-oil, methane and carbon dioxide are determined according to equations **(3.16)**-**(3.18)**, where X stands for the conversion rate. The pyrolysis refers to the products obtained by a simple pyrolysis, supposed to be the inlet stream to the reforming reactor, while pyrolysis/reforming is for the products obtained after the pyrolysis coupled to the reforming process i.e., the outlet stream of the reforming reactor.

$$\text{Conversion rate of bio} - \text{oil } (X_{\text{bio-oil}})\ (\%) = \frac{\text{moles of bio} - \text{oil(pyrolysis)} - \text{moles of bio} - \text{oil (pyrolysis/reforming)}}{\text{moles of bio} - \text{oil(pyrolysis)}} \times 100 \quad \textbf{(3.16)}$$

$$\text{Conversion rate of } CH_4\ (X_{CH_4})\ (\%) = \frac{\text{moles of } CH_4\text{(pyrolysis)} - \text{moles of } CH_4\text{(pyrolysis/reforming)}}{\text{moles of } CH_4\text{(pyrolysis)}} \times 100 \quad \textbf{(3.17)}$$

$$\text{Conversion rate of } CO_2\ (X_{CO_2})\ (\%) = \frac{\text{moles of } CO_2\text{(pyrolysis)} - \text{moles of } CO_2\text{(pyrolysis/reforming)}}{\text{moles of } CO_2\text{(pyrolysis)}} \times 100 \quad \textbf{(3.18)}$$

Since the production of syngas is of major interest, its concentration was calculated in terms of mmol/g of dry biomass, along with the ratio of hydrogen to carbon monoxide, according to equations **(3.19)** and **(3.20)**, respectively.

$$\text{Syngas concentration } (H_2 + CO)\ (\text{mmol/g dry biomass}) = \frac{\text{number of moles of } H_2 + \text{number of moles of CO}}{\text{dry weight of biomass}} \quad \textbf{(3.19)}$$

$$\text{Ratio } H_2/CO = \frac{\text{number of moles of } H_2}{\text{number of moles of CO}} \quad \textbf{(3.20)}$$

3.4. Results and discussion

3.4.1. Reforming of pyrolysis volatiles over bulk catalysts

3.4.1.1. Products distribution

The results of the pyrolysis realized in a one-stage reactor at 700°C and in two-stage reactors with both stages' temperatures set at 700°C are given in **Figure 3.5** (a). The one-stage pyrolysis thermally decomposes the biomass in an inert atmosphere which results in the formation of three main products: 49.2 wt.% of bio-oil, 25.7 wt.% of gas and 25.1 wt.% of char. From our previous work focalized on the chemical analysis of the oak wood pyrolysis products [58], the composition of these products was determined. It revealed that the char derived from the oak wood pyrolysis at 700°C, at a heating rate of 30°C/min and 100 ml_n/min nitrogen flow rate, is a black solid, rich in Carbon (90%), with some traces of Oxygen (2.27%) and Hydrogen (1.48%). The bio-oil is a liquid formed by the condensation of multiple volatiles consisting mainly of BTEX (around 500 mg/L) followed by phenols (5 mg/L) and few traces of PAHs compounds (around 0.6 mg/L) [58,74]. The gas is a mixture of several incondensable gases composed mainly of CO (38.3 vol.%) and CO_2 (26.8 vol.%) along with H_2 (19.2 vol.%) and CH_4 (13 vol.%) [58]. The results of a one-stage pyrolysis are used as basis for the calculations and as reference for comparison with the pyrolysis-reforming results. It can be noticed that realizing a two-stage pyrolysis enhances moderately the gases yield which increases from 25.1 wt.% to 28.4 wt.% and drops that of bio-oil from 49.2 wt.% to 46.5 wt.%. The bio-oil volatiles fed to the second reactor are subject to some secondary thermal cracking reactions where they are decomposed and fragmented into lighter species [5].

The temperature remains one of the key parameters influencing the catalytic reforming process. Varying the temperature of the reforming allows studying the efficiency of the catalyst and its selectivity towards the syngas formation. The active phase of the catalyst also influences greatly the reforming and the products distribution, in a way of favoring the formation of some selected compounds [53]. In these perspectives, the efficiency of the pyrolysis coupled to the reforming process was studied by testing the three bulk catalysts on bases of Nickel, Cobalt and Cobalt-Nickel and by varying the reforming temperature from 700°C to 800°C while fixing the pyrolysis temperature at 700°C. The distributions of the main products in terms of gas, char and bio-oil in function of the temperature and the catalysts active phase are demonstrated in **Figure 3.5** (b, c and d).

Regarding the impact of the temperature, it can be noticed that for the different catalysts, the gases yields enhance at the expense of the bio-oil yields which drop with the temperature rise. The yields of gas are significantly higher and those of bio-oil markedly lower when coupling the pyrolysis to the reforming process, in contrast to the one-stage and two-stage pyrolysis processes. This proves that the hydrocarbon volatiles forming the bio-oil produced by the biomass pyrolysis are effectively converted in the second reforming reactor. In fact, when the volatiles enter the second reactor, secondary tar cracking reactions can take place before contact with the catalyst. This means that the bio-oil is subject to some decomposition reactions producing lighter hydrocarbons [75] (equations **(3.12**) and **(3.13)** or to other repolymerization reactions forming higher molecular weight molecules [76]. The newly emitted gases as well as the remaining bio-oil hydrocarbons are then reformed over the catalyst surface and release additional gases. The catalytic reforming can be therefore considered as a purification step downward the pyrolysis since it helps cracking most of the tar and transforms it into a valuable product such as the syngas. This can be noticeably observed from the **Figure 3.1** with the color

of the tar becoming much clearer after the reforming step compared to the tar obtained by a pyrolysis alone. The char yields fluctuate around 25wt.% since the char is produced in the pyrolysis reactor where the pyrolysis was realized under the same conditions for the different experiments.

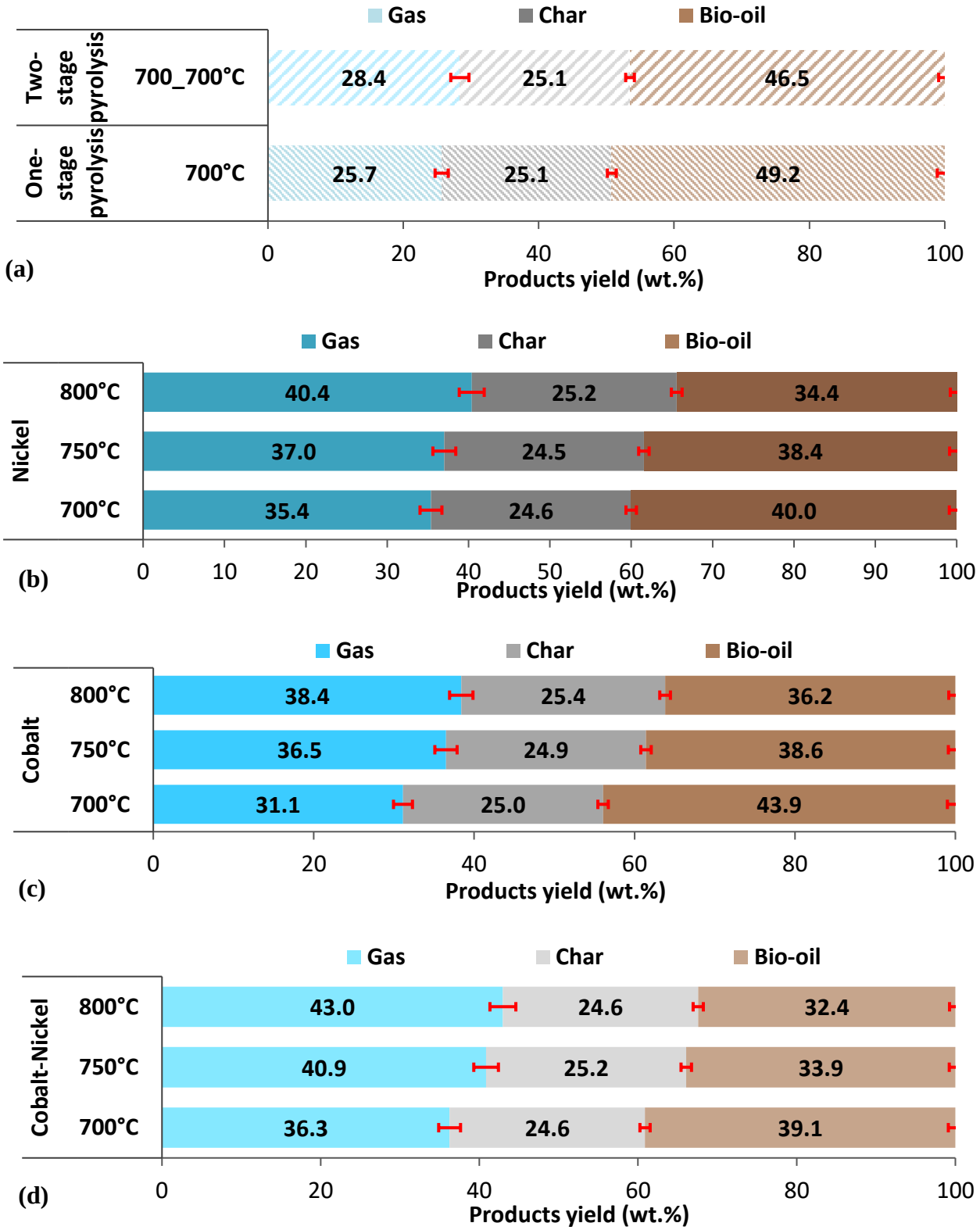

Figure 3.5 Distribution of the products derived from: (a) one-stage pyrolysis at 700°C and two-stage pyrolysis at 700°C for both stages; the combined pyrolysis-catalytic reforming at different temperatures (700, 750 and 800°C) over three catalysts: (b) Nickel, (c) Cobalt and (d) Cobalt-Nickel

Comparing the three catalysts, it can be noticed that the Co-Ni produces the highest gas yield with a maximum of 43wt.% reached at 800°C, followed by a gas yield of 40.9wt.% at 750°C, in contrast to the 25.7wt.% of gas yield obtained with the one-stage pyrolysis and 28.4wt.% with the two-stage pyrolysis at 700°C. Simultaneously, the bio-oil formation was significantly reduced by the catalytic reforming. The lowest bio-oil yield of 32.4wt.% was achieved with the Co-Ni at 800°C and 33.9wt.% at 750°C, in comparison to the 49.2wt.% of bio-oil formed with the one-stage pyrolysis and 46.5wt.% with the two-stage pyrolysis at 700°C. Moreover, it can be stated that the catalytic reforming with Co exhibits the lowest reforming efficiency among the three catalysts tested.

Several research groups reported the higher activity of Co-Ni based catalysts over those of Co or Ni alone. Zhang *et al.* [77] compared the bimetallic Ni-Co catalyst to the Co and Ni monometallic catalysts. They found that Ni-Co had higher activity, stronger carbon resistance and outstanding stability due to the synergetic effect created between the Co and Ni, the large metallic surface, and the good metal dispersion. Takanabe *et al.* [78] also investigated the catalytic behavior of bimetallic Co-Ni over TiO_2 for the methane dry reforming and showed that the catalyst with optimal Co/Ni ratio demonstrated elevated catalytic stability and minimal amount of carbon deposits over the catalyst surface at a large range of temperature (500-850°C). This was attributed to the homogeneous alloy formed between the Ni and Co at the appropriate ratios of the active metals.

3.4.1.2. Gases' concentrations

The major gases produced by the biomass pyrolysis process include CO, CO_2, CH_4 and H_2 as seen in **Figure 3.6** (a). It can be observed that the two-stage pyrolysis produces less H_2 and CO_2 and more CH_4 and CO than the one-stage pyrolysis, due to the cracking of the heavy hydrocarbons within the secondary reactor [5]. The dry reforming reactions imply that the CO_2 and CH_4, along with the hydrocarbons are the main reactants. In this purpose, the concentrations of these gases are studied in function of the reforming temperature and the catalyst active phase, as demonstrated in **Figure 3.6** (b, c and d). Referring to the results of the one-stage pyrolysis at 700°C, it can be noticed that, for the three catalysts and the different temperatures, the catalytic reforming markedly enhances the production of H_2 and CO and reduces that of CH_4 and CO_2. For instance, the hydrogen production was more than doubled with the catalytic reforming with the Ni catalyst at 750°C (41.7vol%) and 800°C (40.4vol%) relative to the one-stage pyrolysis (19.2vol%). The CH_4 concentration is generally lowered by the catalytic reforming in contrast to the pyrolysis, and it reached its lowest at a reforming temperature of 750°C, for the different catalysts.

Concerning the temperature effect, the gases evolutions differ between the three catalysts. For instance, the CO concentrations decreased with the Co catalyst, whereas with the Co-Ni, it increased with the temperature and in contrast to the pyrolysis alone. For the catalytic reforming with Ni, CO increased with the temperature and peaked at 750°C with 40.4vol% concentration, then slightly decreased at 800°C to 39vol%. Hydrogen, on the other hand, was increased with the Co, with the temperature increase from 700 to 800°C, whereas with the Ni and Co-Ni, hydrogen peaked at 750°C. CH_4 behaved similarly for the three catalysts with the temperature variation where it decreased from 700°C to 750°C then it augmented faintly at 800°C. CO_2 generally diminished with the temperature for the three catalysts except for the Ni where the CO_2 slightly increased from 750°C to 800°C, which can be disregarded considering the relative uncertainties.

Similar gases evolutions were observed in the work of Remiro *et al.* [79]. They realized the flash pyrolysis of pine sawdust and the tar produced was reformed in fluidized bed reactor in the presence of Ni catalyst supported on lanthana-alumina Ni/La_2O_3-αAl_2O_3. They also found that when the catalyst is fresh, the H_2 and CO concentrations increase when the temperature is raised from 600°C to 800°C while those of CH_4 and CO_2 drop.

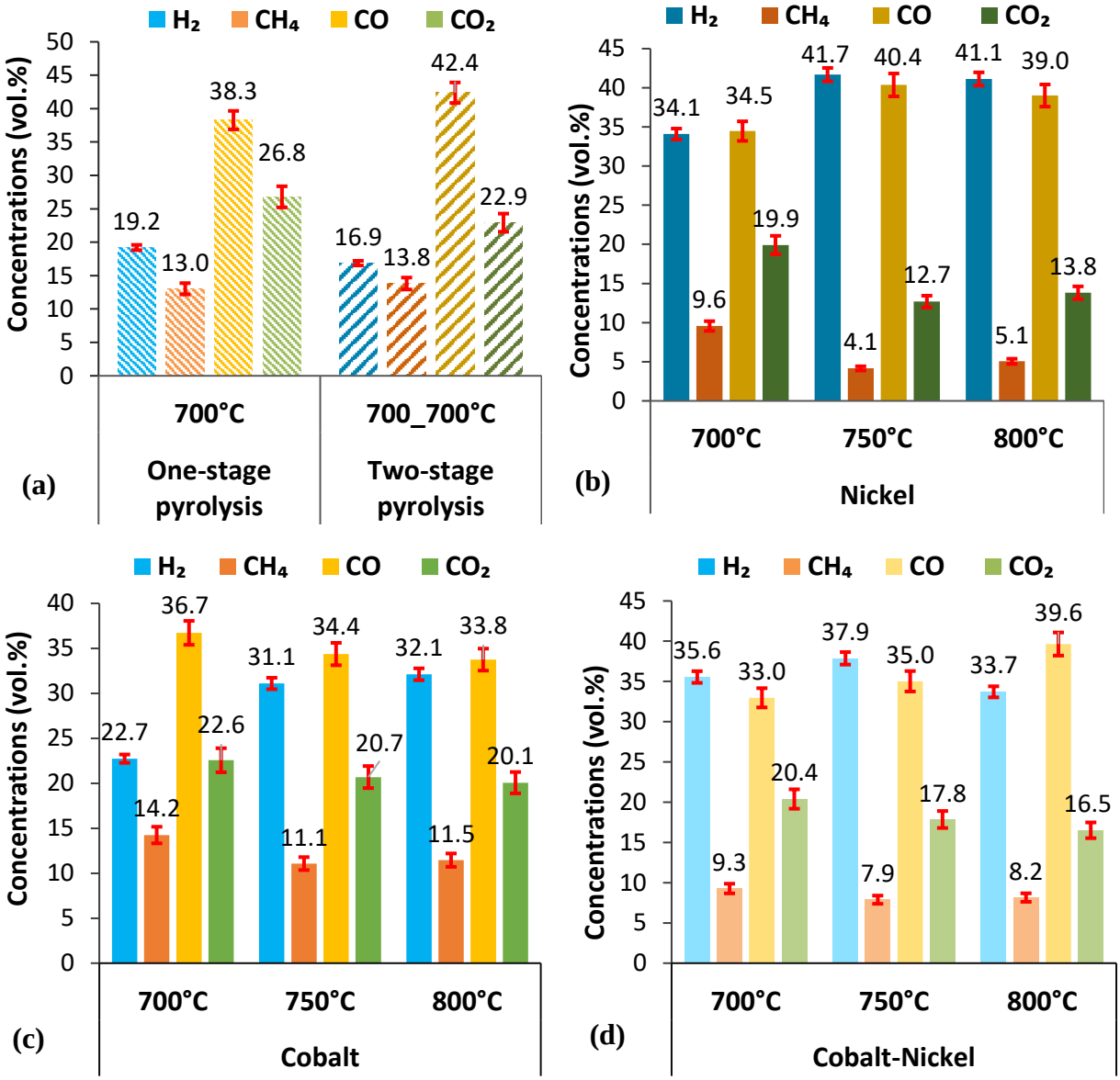

Figure 3.6 Variation of the volume concentrations of the major gases derived from: (a) one-stage pyrolysis at 700°C and two-stage pyrolysis at 700°C for both stages; the combined pyrolysis-catalytic reforming at different temperatures (700, 750 and 800°C) over three catalysts: (b) Nickel, (c) Cobalt and (d) Cobalt-Nickel

Comparing the three catalysts, it can be stated that the highest H_2 and CO concentrations and the lowest CH_4 and CO_2 concentrations are obtained with the Ni catalyst at 750°C. The greater activity noticed with the Ni is related to its potential to dissociate the C-H bonds and to activate the CH_4 [80]. Indeed, due to their low cost, large accessibility and high catalytic efficiency for the aromatic hydrocarbons cracking, Ni based catalysts have been broadly considered for the bio-oil conversion [18,81,82]. The increase in the H_2 and CO production with the simultaneous drop in the concentrations of CH_4 and CO_2 represent a proof of the occurrence of the dry

reforming of tar (reaction **(3.4)**, or the dry reforming of methane (reaction **(3.7)**, previously introduced.

Given the endothermic nature of these reactions, they are favored by the rise of the temperature which swings the reactions toward the formation of the products, leading to stronger consumptions of CO_2 and CH_4 as reactants and higher production of CO and H_2 [83]. However, it can be remarked that the steepest changes occur between 700 and 750°C, with modest variations occurring between 750 and 800°C. Nonetheless, the heat power consumption for the temperature increase is significantly large. *Thus, the optimal reforming temperature would be between 700°C and 750°C to boost the syngas production while maintaining an economical efficiency.* This similar conclusion was made by Xu *et al.* (2015) [84] who realized the dry and steam reforming of biomass pyrolysis gases over Ni/Fe/Ce/Al_2O_3 catalysts and studied the effect of several parameters, including the temperature, on the efficiency of the process. They obtained concentrations increasing from 3.49 vol.% to 31 vol.% for H_2 and from 36.99 vol.% to 60.94vol.% for CO by increasing the temperature from 500°C to 800°C. On the other hand, the concentrations of CH_4 dropped from 19.47 vol.% to 0.24 vol.% and for CO_2 from 37.04 vol.% to 6.63 vol.%. They also suggest the optimal reactor reforming temperature to be between 700 and 750°C.

Moreover, the concentrations of minor volatiles such as few light hydrocarbons (C_2H_4 and C_2H_6) as well as some heavy hydrocarbons (benzene, toluene, ethylbenzene and m,p-xylene) are given in **Figure 3.7** and **Figure 3.8**, respectively. The poor activity of the Co catalyst can be again noticed in **Figure 3.7** (c) and **Figure 3.8** (c) where the concentrations obtained with the Co catalyst surpass those obtained with the two other catalysts. This indicates a weaker tar reforming capacity of the Co confirmed by its negligible activity, observed by numerous researchers [85–87]. Furthermore, the concentrations of these bio-oil compounds were, globally, lower with the Ni than with the Co-Ni and the concentrations were further reduced by the temperature increase. *This reflects the strong Ni performance in converting the pyrolysis bio-oil into syngas through the catalytic reforming* [88], *which is particularly enhanced at high temperatures (750°C and above).*

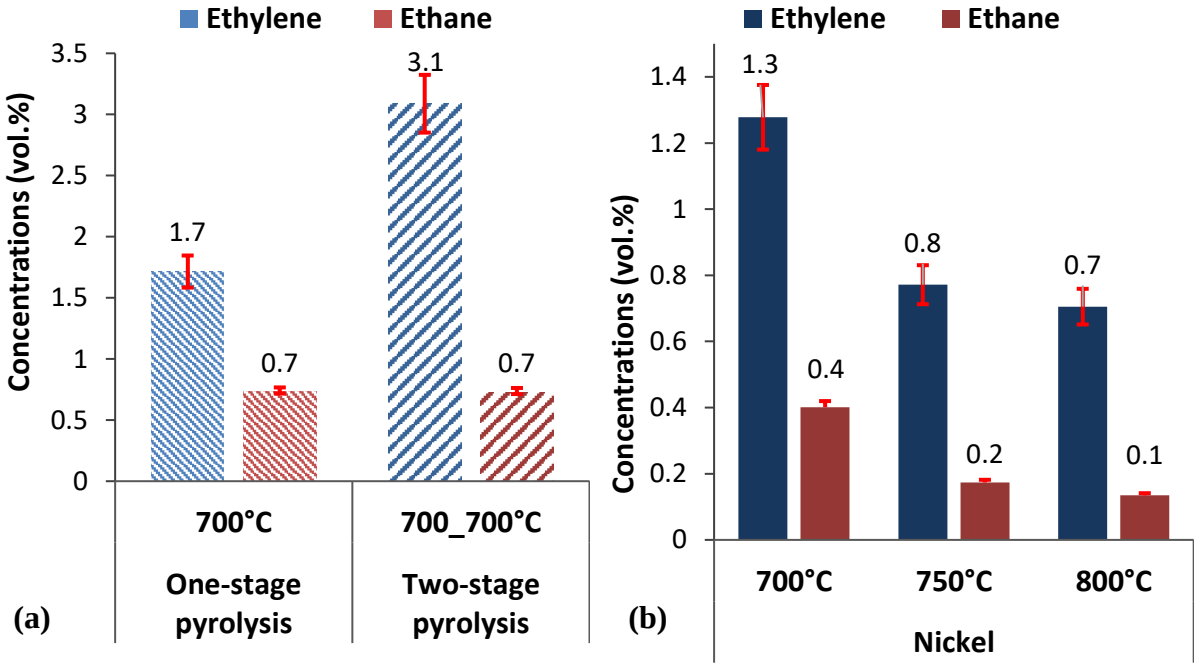

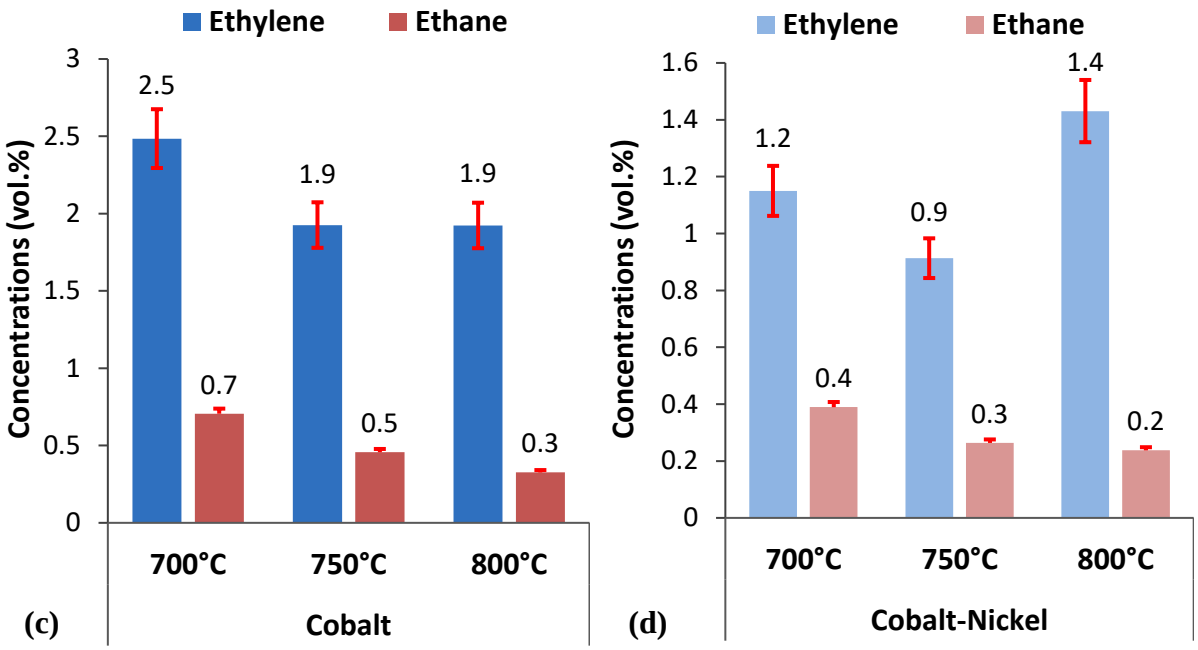

Figure 3.7 Variation of the volume concentrations of the minor light hydrocarbon gases derived from: (a) one-stage pyrolysis at 700°C and two-stage pyrolysis at 700°C for both stages; the combined pyrolysis-catalytic reforming at different temperatures (700, 750 and 800°C) over three catalysts: (b) Nickel, (c) Cobalt and (d) Cobalt-Nickel

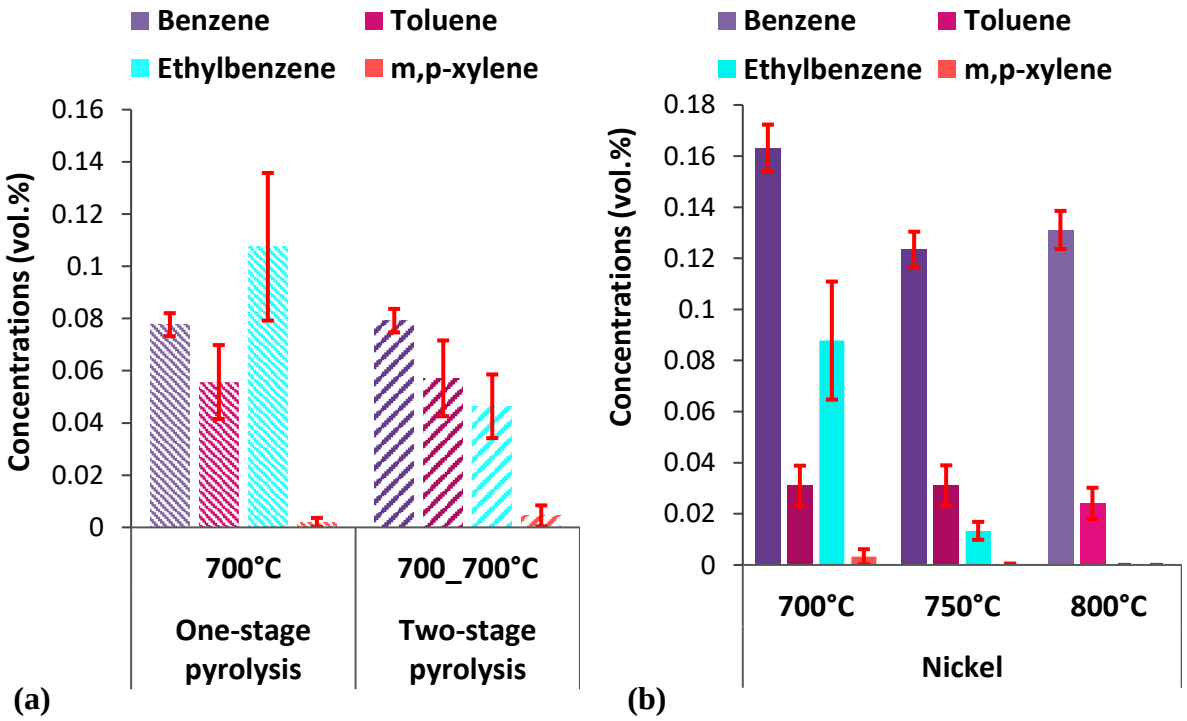

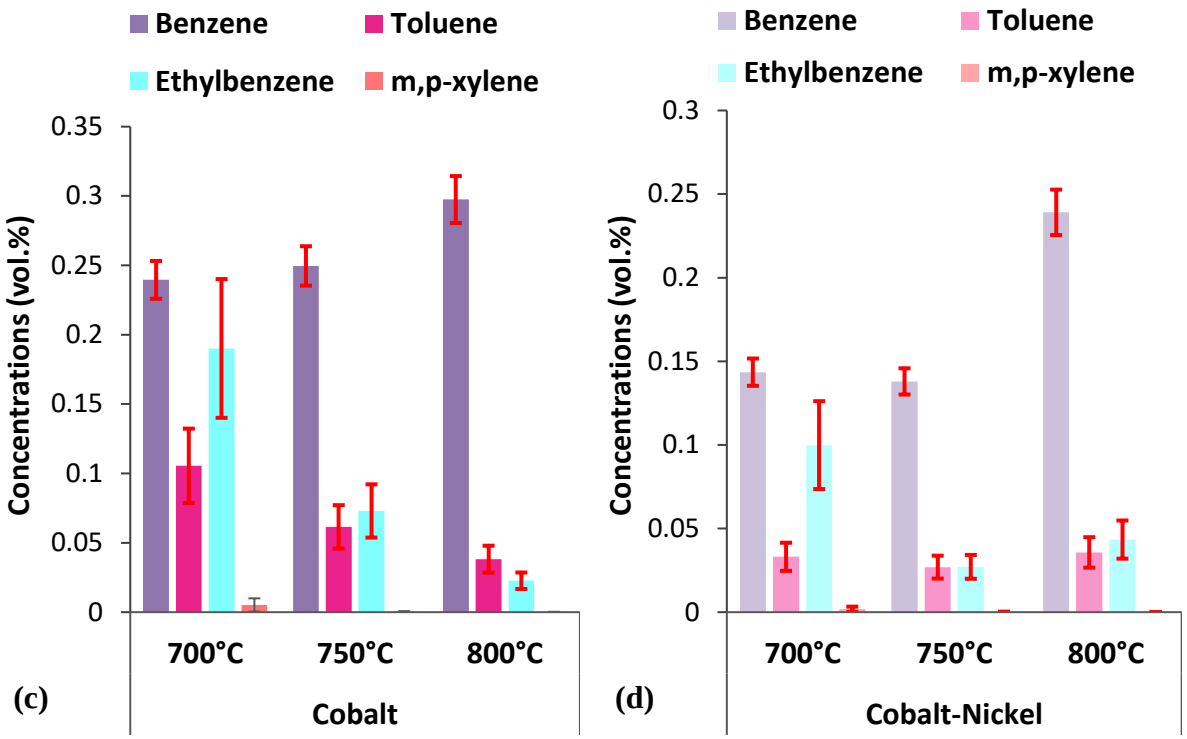

Figure 3.8 Variation of the volume concentrations of the minor heavy hydrocarbon gases derived from: (a) one-stage pyrolysis at 700°C and two-stage pyrolysis at 700°C for both stages; the combined pyrolysis-catalytic reforming at different temperatures (700, 750 and 800°C) over three catalysts: (b) Nickel, (c) Cobalt and (d) Cobalt-Nickel

3.4.1.3. Conversion rates of main reactants

The conversion rates of the bio-oil as well as the CH_4 and CO_2 produced by the pyrolysis-catalytic reforming with the three bulk catalysts at the different temperatures are depicted in **Figure 3.9**. As the gases concentrations revealed previously, a similar behavior of the conversion rates is observed with the different catalysts. The bio-oil conversion rate remarkably increases when the temperature is raised from 700°C to 800°C, for the three catalysts. The lowest bio-oil yield obtained with the catalytic reforming in presence of the Co-Ni at 800°C is translated by the highest bio-oil conversion rate of 34.1%. The increase of the bio-oil conversion with the temperature was proven by other researches [79,84]. Similarly, the tendency of evolution of the CH_4 previously observed, is also expressed by the CH_4 conversion rate which increases by rising the temperature from 700°C to 750°C, and then slightly drops when the temperature reaches 800°C, for the three catalysts. The CO_2 conversion rate, on the other hand, increased with the temperature for the catalytic reforming with Co and Co-Ni, with higher conversion rates reached with Co-Ni. As for the Ni catalyst, the CO_2 conversion rate peaked at 750°C, with values greatly surpassing those for the catalytic reforming with Co and Co-Ni. Remarkably, the highest conversion rates of CO_2 (52.6%) and CH_4 (68.2%) are reached with the Ni at 750°C.

Surprisingly, the CH_4 conversion surpasses that of CO_2 for the two catalysts Ni and Co-Ni. This can be attributed to the CH_4 cracking reaction through equation **(3.21)**, (spontaneous between 600°C and 800°C), on one hand, and the WGSR through equation **(3.8)**, on the other hand, which produces CO_2, in competition with the dry methane reforming reaction which consumes CO_2 (reaction expressed by equation **(3.7)** [89]. Similar tendencies were obtained by Tanios *et al.* [59,60] who realized the dry reforming of methane over the same catalysts.

CH_4 cracking: $CH_4 \rightarrow C + 2H_2$ $\Delta H°_{298K} = +75\ kJ/mol$ **(3.21)**

These observations are contradictory with the ones found generally in the literature [53,84] which are in accordance with the ones observed in our case only with the Co catalyst. The CO_2 conversion markedly surpasses that of CH_4 which is accentuated with the temperature augmentation with the Co based catalysts. These variations are due to the occurrence of the reverse WGS reaction, equation **(3.9)**, which consumes the CO_2 [84], while the dry methane reforming reaction is attenuated at temperatures higher than 700°C [53], which explains the higher CO_2 consumptions than those of CH_4.

It should be noted that the Co is the least performant among the catalysts tested and the negative conversion rate of CH_4 obtained at 700°C reflects the poor, almost null activity of the Co at this temperature. In fact, Co has been rarely used alone for the tar reforming and is generally coupled with other more active catalysts [53]. Its strength resides mainly in its ability to reduce the carbon deposition on the catalyst and thus avoiding its deactivation [49]. *Ni is thereby more efficient than Co for the bio-oil hydrocarbons reforming while Co is suitable for the reforming of oxygenates such as methanol and ethano*l [88]. The Co is frequently combined with the Ni to create a more efficient, stable and carbon resistant catalyst as demonstrated by several works [85–87].

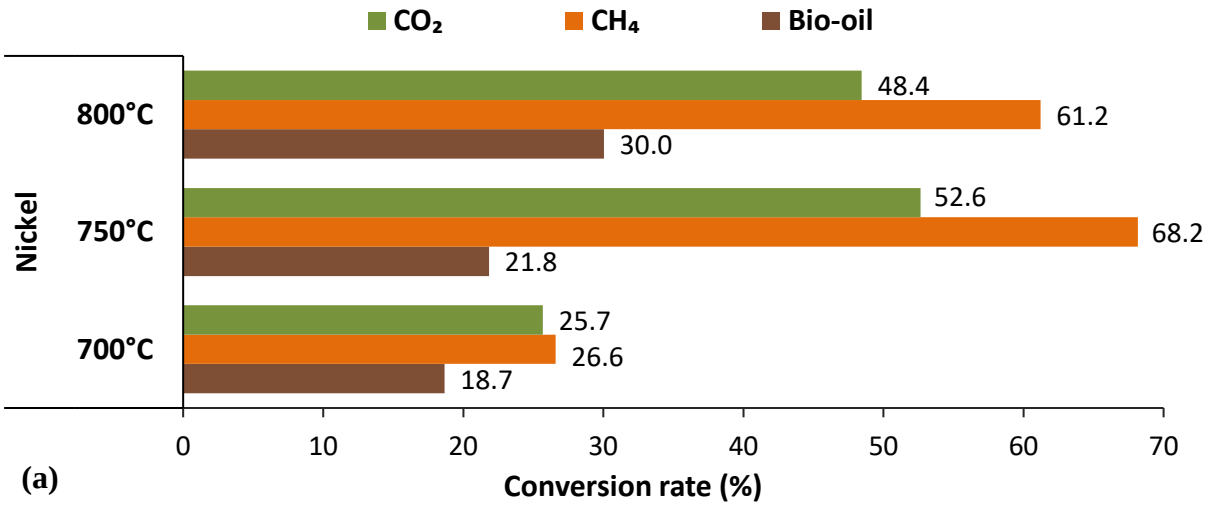

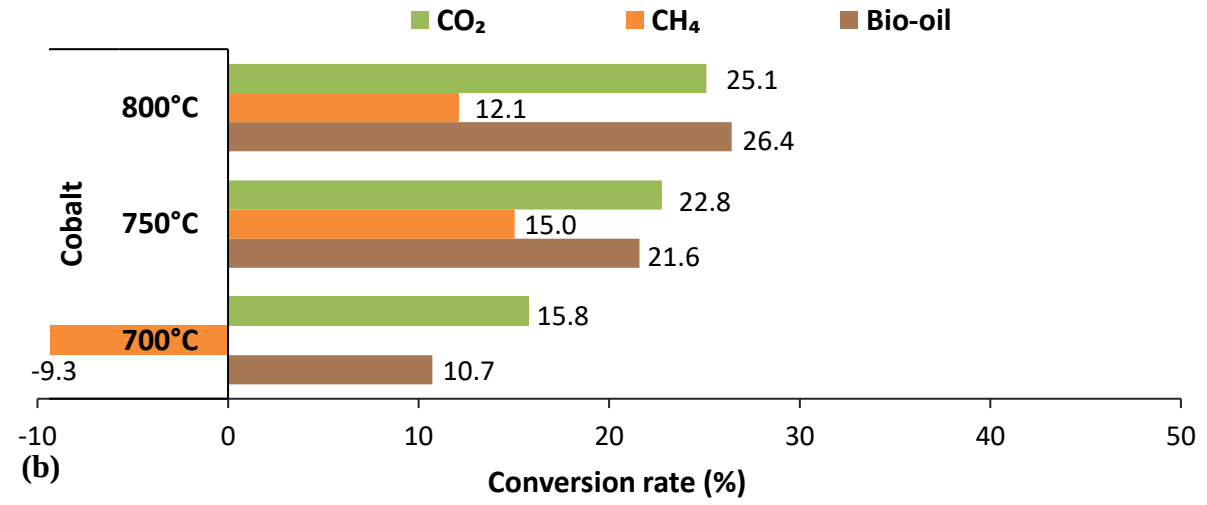

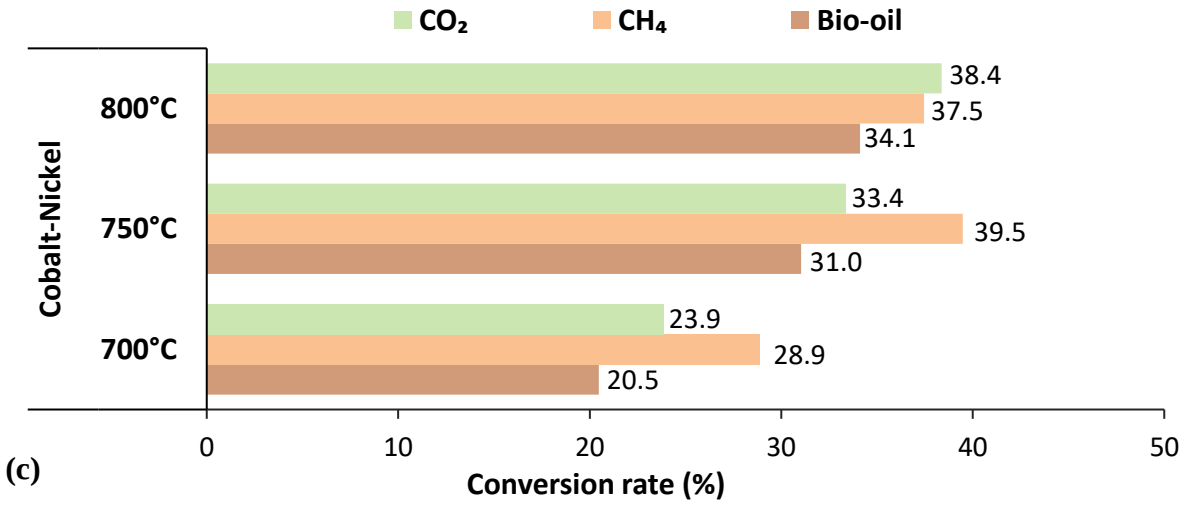

Figure 3.9 Variation of the conversion rates of bio-oil, CH_4 and CO_2 during the combined pyrolysis-catalytic reforming at different temperatures (700, 750 and 800°C) over three catalysts: (a) Nickel, (b) Cobalt and (c) Cobalt-Nickel)

3.4.1.4. Syngas concentration

Being the main interest of the pyrolysis-reforming process, and in the perspective of extrapolating the applicability of this process on the industrial level, the syngas concentrations was determined in mmol/g dry biomass along with the hydrogen to carbon monoxide H_2/CO ratio. Their evolutions were studied for the one-stage and two-stage pyrolysis as well as for the pyrolysis-reforming in function of the temperature and the catalyst active phase as demonstrated in **Figure 3.10**.

From **Figure 3.10** (a), it can be noticed that the two-stage pyrolysis produces more syngas but with a lower H_2/CO ratio than the one-stage pyrolysis. As for the effect of temperature over the combined pyrolysis and reforming, it is remarked that the syngas production is improved with the temperature increase of the catalytic reforming for the different catalysts and largely surpasses that of the pyrolysis. Comparing the three catalysts, it can be observed that with the Nickel catalyst, the largest syngas concentration is produced with 16.8 mmol/g dry biomass at 800°C followed by 16 mmol/g dry biomass at 750°C. The Co-Ni follows next with 14.8 mmol/g dry biomass of syngas at 800°C while the highest syngas production reached by the Co catalyst was only 11.5 mmol/g dry biomass at 800°C.

The H_2/CO ratio increases with the temperature for the Ni catalyst, to reach 1.05 at 800°C. As for the Co, the H_2/CO ratio strongly escalated from 0.62 at 700°C to 0.95 at 800°C. The largest H_2/CO ratio of 1.08 was however obtained with the Co-Ni at 700°C and 750°C. Nevertheless, it dropped to 0.85 when the reforming temperature was increased to 800°C. The higher activity of the Co-Ni was also observed in the work of Wang *et al.* [88], along with a lower carbon deposition. They tested the steam reforming of the tar derived from the pyrolysis of cedar wood over Ni, Co and Co-Ni based catalysts and found the highest activity and coke deposition resistance with the Co-Ni catalyst with a Co/Ni ratio equal to 0.25 in contrast to the monometallic catalysts.

As remarked from the dry reforming reactions, equations **(3.4)** and **(3.7)**, the H_2/CO ratio is around 1, specially for the methane. Whereas for the steam reforming reactions, the H_2/CO ratio is around 3 or even higher. Looking at **Figure 3.10**, it can be noticed that for Ni and Co-Ni based catalysts, the H_2/CO ratio is close to 1. Thereby, it can be deduced that the dry reforming

reactions dominate over the steam reforming reactions in our process. This could be most conveniently explained by the relatively high CO_2 concentrations produced by the pyrolysis (around 27%), which certainly surpasses that of water vapor emitted. Without an external feed of CO_2 or steam, the main reactant for our reforming reactions remains the CO_2 emitted by the biomass pyrolysis in the first reactor. Moreover, an H_2/CO ratio close to unity and CO_2 conversions lower than those of CH_4, implies that the Boudouard reaction, equation **(3.10)**, and the methane cracking reaction, equation **(3.21)**, predominate over the methane steam reforming, equation **(3.4)**, and the RWGS reaction, equation **(3.9)** [59].

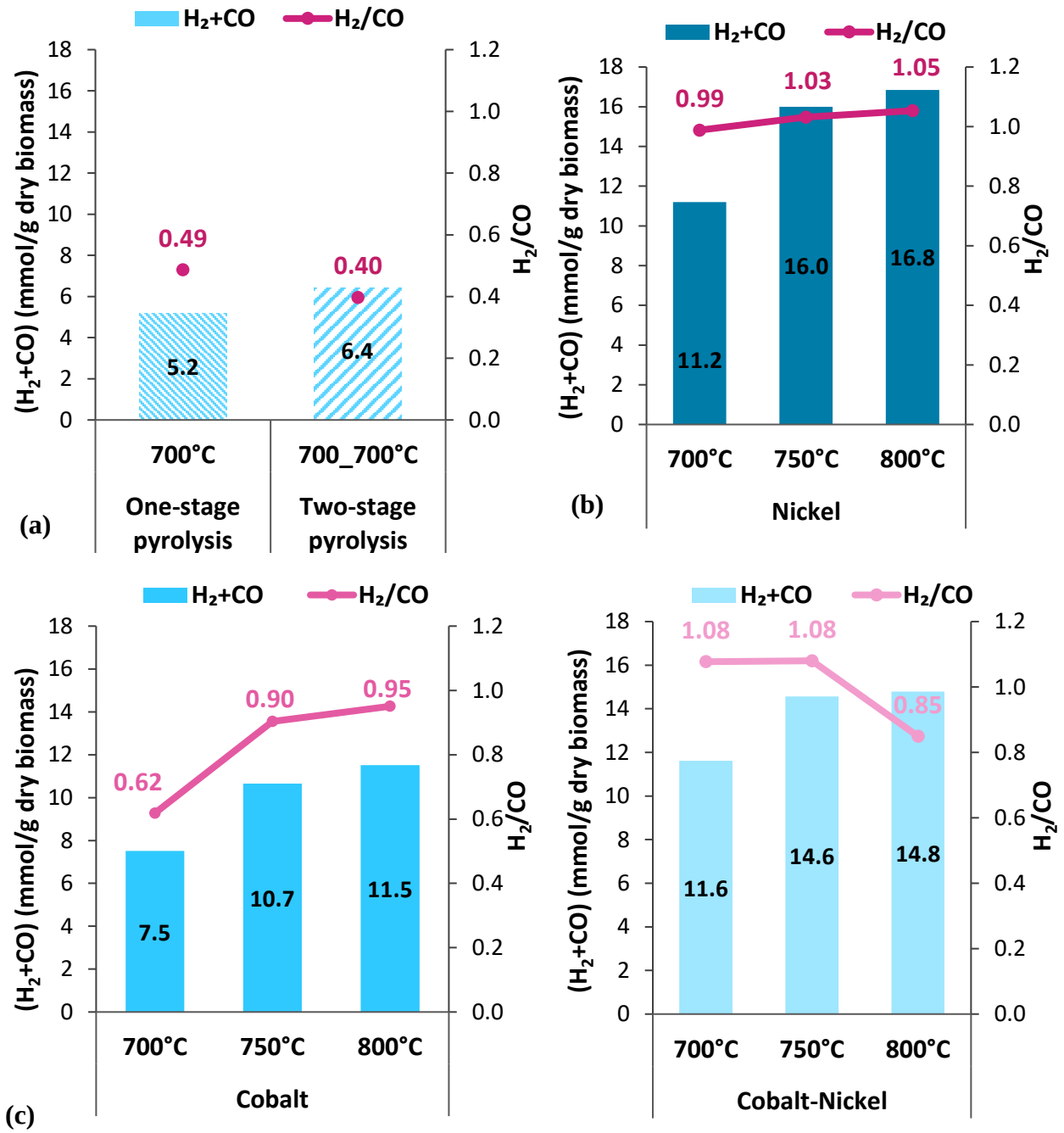

Figure 3.10 Variation of the syngas concentration in mmol/g dry biomass and the H_2/CO ratio at: (a) one-stage pyrolysis at 700°C and two-stage pyrolysis at 700°C for both stages; the combined pyrolysis-catalytic reforming at different temperatures (700, 750 and 800°C) over three catalysts: (b) Nickel, (c) Cobalt and (d) Cobalt-Nickel

Nevertheless, the H_2/CO ratio is not always equal to 1. This infers the occurrence of some secondary reactions such as reverse of carbon gasification (equation **(3.22)** [90]) which consumes equal quantities of CO and H_2 and produces water which can further react with CO in the WGSR (equation **(3.8)**). With the Co catalyst, the H_2/CO ratio is lower than 1 and the CO_2 conversion rates surpass those of CH_4, which suggests the occurrence of a methanation reaction, equation **(3.23)**, (favorable below 750°C [60]) where the CO_2 reacts with the H_2 to form CH_4 and H_2O, in parallel to the dry reforming reaction (equation **(3.7)**). Referring to this reaction to explain these observations is rarely done in the literature even though similar results were obtained by several studies [83,91,92] but were interpreted by the other secondary reactions previously stated. Nonetheless, the methanation reactions was evaluated over the Ni and Co based catalysts by several works [93,94]. The Boudouard reaction also takes place but at an inferior extent [59].

Reverse of carbon gasification: $CO + H_2 \rightarrow C + H_2O$ $\quad \Delta H°_{298K} = +31.4 kJ/mol$ **(3.22)**

Methanation: $CO_2 + 4H_2 \rightarrow CH_4 + 2\ H_2O$ $\quad \Delta H°_{298K} = -164\ kJ/mol$ **(3.23)**

3.4.2. Characterization of the spent catalysts after reforming

The catalysts used in this study were previously used in other research works for the dry reforming of methane. Their characteristics such as the specific surface area and the analyses (XRD, DTA and TGA) realized on them prior to the reforming can be found in the works of Tanios et *al.* [59,60]. The catalysts used for this study are layered double hydroxides (LDHs) with a structure analogous to that of natural hydrotalcite ($Mg_6Al_2(OH)_{16}CO_3.4H_2O$) [95]. When the LDHs catalysts are calcinated, the precursors are decomposed and produce oxidized forms, having outstanding catalytic specifications required for heterogeneous reactions. These include high specific surface area, large dispersion, basic nature and small crystal size [96]. Among these LDHs, Nickel and Cobalt based catalysts are broadly employed for their excellent catalytic performance [97].

To examine the status of the catalysts after the reforming process, some analytical analyses (XRD, DTA and TGA) were performed on the three catalysts after the tests of pyrolysis-reforming at 700°C, 750°C and 800°C. The XRD patterns obtained are given in **Figure 3.11**, the DTA graphs are shown in **Figure 3.12** (a, b and c) and the TGA curves are illustrated in **Figure 3.12** (d, e and f). Evaluating the XRD patterns and considering the Nickel catalyst first (**Figure 3.11** (a)), five main compounds can be detected, which were numbered and labeled on the plots. The extensiveness of the diffraction peaks detected can be ascribed to the existence of a mixture of oxide phases, which are extremely challenging to be distinguished by the XRD given their adjacent intensities and 2θ values.

After the reforming at 700°C and 750°C, it can be noticed that some of the Ni metal have been oxidized into NiO. Whereas after the reforming at 800°C, peaks of the metal Ni are observed at 2θ = 44° and 2θ = 52°, which suggests that the oxidized Ni is reduced [98,99] due to the high presence of hydrogen produced by the biomass pyrolysis. *This reveals the presence of Ni metal sites still active and available for additional reforming reactions, especially post the reforming at 800°C.*

Moreover, the presence of carbon peaks on the XRD profiles of all the catalysts can be remarked. It indicates the crystalline graphitic and cubic natures of the carbon deposited over

these catalysts [100]. However, the intensity of the carbon diffraction peaks is different for each catalyst, reflecting the distinct quantities of carbon deposited during the reforming at the different temperatures. For instance, the highest carbon peak is observed after the reforming at 800°C at 2θ=26° revealing that the carbon deposition is the most expressed on this catalyst. It indicates that the cracking reactions are favored over the reforming reactions at 800°C.

The carbon formation derives mainly from an imbalance between the kinetics of the decomposition of CH_4 and CO_2. When the CH_4 decomposition is faster than that of CO_2, the carbon formed is no longer gasified and accumulates over the catalyst surface provoking its deactivation. The gasification of the surface carbon might take place during its reaction with the remaining unreacted CO_2 (reverse Boudouard reaction, equation **(3.10)**). The carbon formed can take several forms through the reactions of methane decomposition, equation **(3.21)**, Boudouard, equation **(3.10)**), and carbon gasification (reverse reaction of equation **(3.22)**), mainly in the form of carbon filaments (also known as whiskers [87]) or carbon encapsulating the metallic particles. Among the several types of carbon deposits, the ones reported include crystalline graphitic, amorphous carbon and adsorbed atomic carbon [101,102].

The carbon formed can also be a result of the hydrocarbon cracking through the tar decomposition reaction **(3.13)** ($C_nH_x(\text{tar}) \rightarrow nC + (\frac{x}{2})H_2$). As previously shown, the pyrolysis produces a large quantity of heavy hydrocarbons forming the tar. These aromatic volatiles fed to the reforming reactor are carbon precursors [103,104]. For instance, the toluene decomposition follows the reaction: $C_7H_8 \rightarrow 7C + 4H_2$, favorable at the whole range of temperature tested (700 – 800°C). Even for low toluene concentrations, this reaction can take place in addition to the secondary undesirable reactions **(3.8)** – **(3.14)**, greatly influencing the performance of the main reforming reactions **(3.2)** – **(3.7)**.

Similar analyses can be applied to the XRD plots of Co (**Figure 3.11** (b)). It can be noticed that at 700°C and 750°C, the Co is oxidized into CoO [105] where large CoO peaks are observed at 2θ=37° for the catalysts after reforming at 700°C and 750°C, in contrast to the small peak at 800°C [106,107]. Moreover, after the reforming at 750°C, the peak of metal Co observed at 2θ=44° is the highest, pointing that part of the oxidized CoO is reduced into Co by the hydrogen produced by the biomass pyrolysis [106,108]. Interestingly, after the reforming at 800°C, the peaks of the distinct phases become almost flat, which reflects the partial degradation of the Co based catalyst at 800°C due to the favoring of the cracking reactions.

While for the Co-Ni, the different peaks identified for the Ni and Co based catalysts are also detected for the Co-Ni catalyst on the XRD profiles. As the temperature increases, the peaks intensities of the active metallic phases of Ni and Co detected at 2θ=44° and 2θ=52°, become larger. This is due to the reduction of the oxidized NiO and CoO phases, by the reducing effect of H_2 produced by the pyrolysis. In contrast to the Ni based catalysts, the intensities of the carbon peaks are smaller with the Co-Ni based catalysts which can be attributed to the presence of Co and the synergistic effect between Co and Ni which helps reducing the carbon formation [30,109]. Several researches obtained similar results where the carbon deposition is significantly minimized by the alloy of Co to Ni [60,78,110].

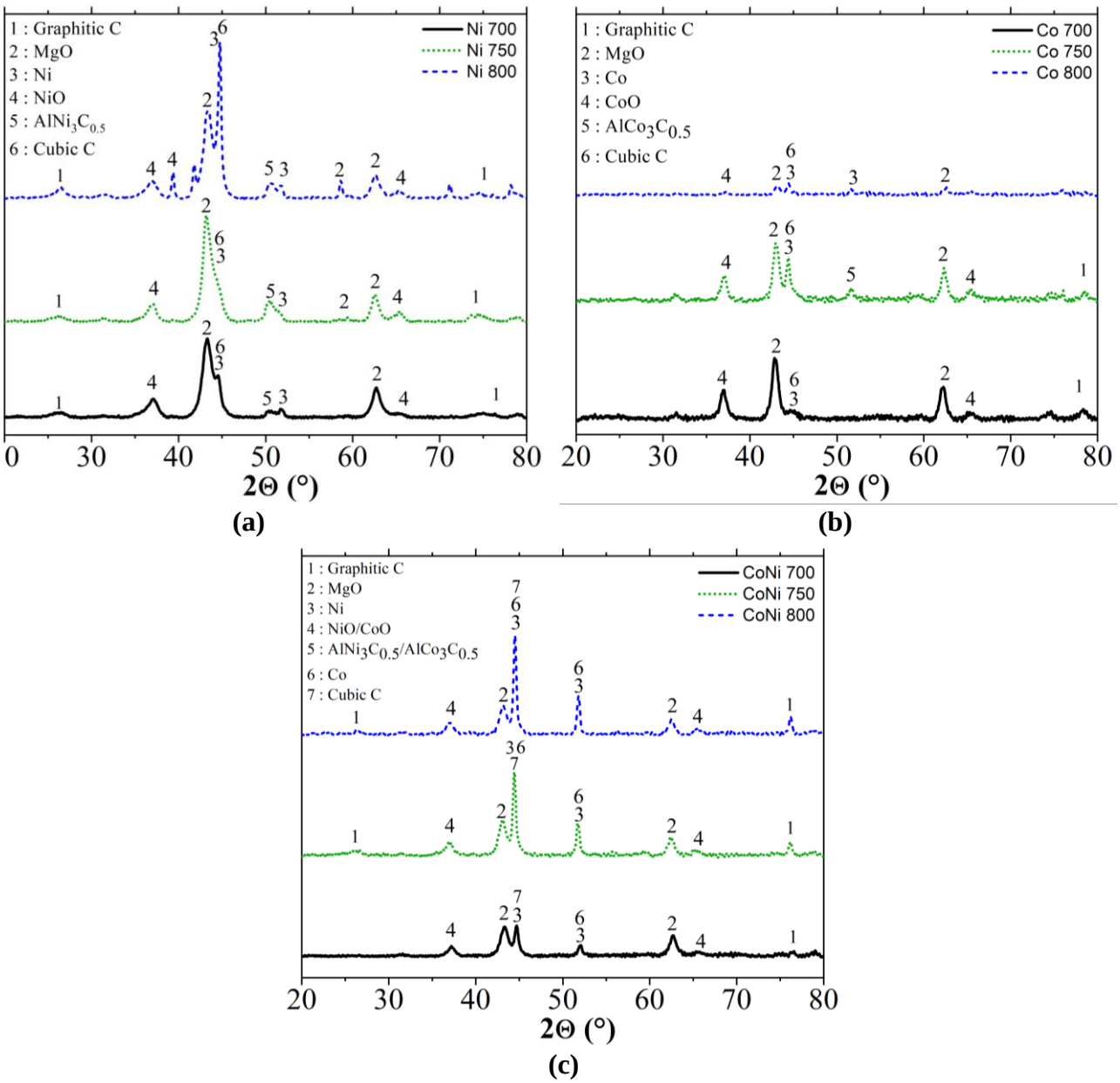

Figure 3.11 XRD patterns of the bulk catalysts after the reforming at three tested temperatures (700, 750 and 800°C) for the three catalysts: (a) Nickel Ni, (b) Cobalt Co and (c) Cobalt-Nickel Co-Ni

The DTA analyses illustrated in **Figure 3.12** (a, b and c) can be associated to the TGA (or weight loss) analysis given in **Figure 3.12** (d, e and f) for each of the catalyst respectively. Considering first the Ni catalyst, it can be stated that for temperatures inferior to 250°C, a weight loss of around 10% occurred for the Ni catalyst after reforming at 700°C, 12% for the reforming at 750°C and 8% for the reforming at 800°C. It is mainly related to the evaporation of physiosorbed water and the elimination of the interlayer water [111]. Thereby, these percentages correspond to the moisture content in the nickel catalysts, accordingly, with an average of 10%. It is followed by small endothermic peaks appearing around 280°C, which correspond to the three exothermic peaks observed at 280°C on the DTA graph.

Moreover, a small weight gain is observed on the weight loss graph between 300°C and 400°C for the Ni after reforming at 750°C and 800°C, corresponding to the small exothermic peaks observed on the DTA graphs at 360°C, which could be attributed to the oxidation of Ni, as previously deduced from the XRD analysis. This uncovers the presence of active Ni sites after

reforming at 750°C and 800°C. A second weight loss of 8% approximately followed the weight gain for the Ni after the reforming at 800°C. The weight losses for Ni after reforming at 700°C and 750°C were 16% and 13%, respectively. This can be explained by the carbon oxidation into CO or CO_2 (volatiles) [112–114].

Given that the highest weight loss occurred for the catalyst after reforming at 700°C, it can be concluded that the carbon formation and deposition was most significant after the reforming at 700°C. Whereas the least carbon deposition is obtained after reforming at 800°C. In fact, at high temperatures (above 700°C), the reactions forming the carbon (Boudouard reaction, equation **(3.10)**, reverse water-gas reaction, equation **(3.11)**, and methane cracking, equation **(3.21)** are repressed, leading to a drop in the carbon formation and increase in the carbon balance [53]. Therefore, it can be deduced that at 800°C, the main dry reforming reactions are favored over these secondary reactions which reduce the carbon deposition. Indeed, other research groups also state that lower carbon deposition is formed by the increase of the reforming temperature [53].

Looking at the DTA curves for the Ni, some main exothermic peaks can be detected for each of the catalysts at three to four distinct temperatures of oxidation marked on the DTA plots. These peaks correspond to the inflection points observed on the weight loss curves. This allowed the identification of three to four types of carbon deposited over the catalyst surface.

An analogous reasoning can be applied to the two other catalysts. For the Co catalysts, looking at the weight loss graph on **Figure 3.12** (e), it can be noticed that the largest weight loss of 22% is obtained with the Co catalyst after reforming at 700°C, among the other catalysts, reflecting the highest carbon deposition over the Co surface. As the reforming temperature increases, the weight loss of the catalyst drops (13% at 750°C and 5% at 800°C), confirming the previous conclusion made where the increase of the reforming temperature helps reduce the carbon deposition. It is worth noticing the absence of weight gain for the Co catalyst at the different reforming temperatures, revealing the absence of Co active sites after the reforming reactions. Looking at the DTA curves of the Co on **Figure 3.12** (b), fewer peaks are obtained and at lower temperatures than with the Ni catalysts. Only two peaks are formed for each reforming temperature. These endothermic peaks reflect the formation of two types of carbon over the Co surface.

The Co-Ni behavior is between those of Ni and Co. The weight loss graphs on **Figure 3.12** (f) consolidate the previous observations where the weight loss, and therefore the carbon deposition, diminish as the reforming temperature increases, with 16% of weight loss obtained at 700°C, 13% at 750°C and 8% at 800°C. Interestingly, small weight gain curves are observed prior to the large weight losses which can be attributed to the presence of active Co-Ni sites available for additional reforming reactions. The DTA curves of the Co-Ni on **Figure 3.12** (c), reveal four endothermic peaks for each of the catalyst at the different reforming temperatures, indicating the deposition of four types of carbon over the Co-Ni surface, similarly to the Ni catalyst but obtained at slightly lower temperatures.

It can be deduced that in spite of the good efficiency of Ni, the drop in its activity due to carbon deposition remains one of its major inconvenient [30,47]. *Co alone was less active than Ni but showed better carbon resistant capacities. Interestingly, the alloy of Ni to Co appears to be an effective compromise to obtain high catalyst activity provided by the Ni and a strong resistance to carbon formation ensured by the Co.* Several works [60,77,78] confirmed this observation

where the addition of Co to other catalysts improves the resistance to carbon formation, which can justify the drop in the quantity of carbon deposits on our Ni-Co catalysts. In fact, Co, in spite of its alloy with Ni, undergoes redox reactions where the Co oxides contribute markedly to the carbon oxidation, preventing the carbon formation and deposition [115].

Nonetheless, Co exhibited the fewest types of carbon deposited which were formed at lower temperatures than with the Ni and Co-Ni, revealing their less stable nature. As the reforming temperature increased, the temperature of the exothermic peaks decreased with the Co catalyst. When the exothermic peak temperatures are low, the carbon formed is unstable and can be easily oxidized, and thus removed. Whereas the higher the peak temperatures, the more stable the carbon formed is, making its oxidation harder.

Thereby, for the Co, the highest peak temperature was observed for the reforming at 700°C revealing that the most stable carbon is formed at 700°C. On the other hand, for Ni and Co-Ni based catalysts, the exothermic peak temperatures increase with the reforming temperature while the weight loss decreases. Therefore, the amount of carbon formed at low reforming temperatures (700°C), is bigger but more easily oxidized than at higher reforming temperature, where fewer quantity of carbon is formed yet it is more stable and harder to be oxidized.

The carbon deposited during the catalytic reforming reactions was categorized in the literature into three major classes: pyrolytic coke, filamentous coke (whiskers) and gum coke (also known as soft coke) [85,87,116]. If the Boudouard reaction predominates, the formation of carbonous filaments can be favored during the methane cracking reaction occurring at high temperatures [117]. Gum coke is generally formed at relatively low temperatures whereas the two other carbon types are formed at higher temperatures. The carbon deposition leads to a total encapsulation of the catalyst particles resulting in the deactivation of the catalyst and in the augmentation of the pressure drop throughout the reforming reactor [87,118].

Furthermore, the surface coke species have been classified into different types using temperature programmed hydrogenation (TPH): C_α known as "methynic or atomic" carbon, C_β identified as "naphthalenic or polyaromatic" carbon [119], and graphite carbon C_γ [120]. While C_α is easily oxidized, C_β and C_γ are much harder to be oxidized being more stable leading consequently to the deactivation of the catalyst [121–123]. Therefore, the exothermic peaks detected on the DTA graphs of the different catalysts allow the identification of the types of carbon deposited over their surface.

Thereby, the peaks appearing below 400°C, are attributed to the amorphous, very reactive and unstable C_α carbon species [100]. Some research assigned these peaks to the oxidation of the metal particles available over the surface of the catalyst [124]. The peaks present at around 460°C are assigned to the carbon species of type C_β oxidized near the metal sites eliminated under oxidative atmosphere at low temperatures [100]. The peaks around 500°C can be ascribed to graphitic carbon type C_γ stable and hard to be gasified and removed [125]. The peaks appearing at temperatures above 550°C are more challenging to be assigned but occur potentially as a result of the oxidation of relatively inert carbon species being extremely stable and requires higher temperatures to be oxidized [60,126].

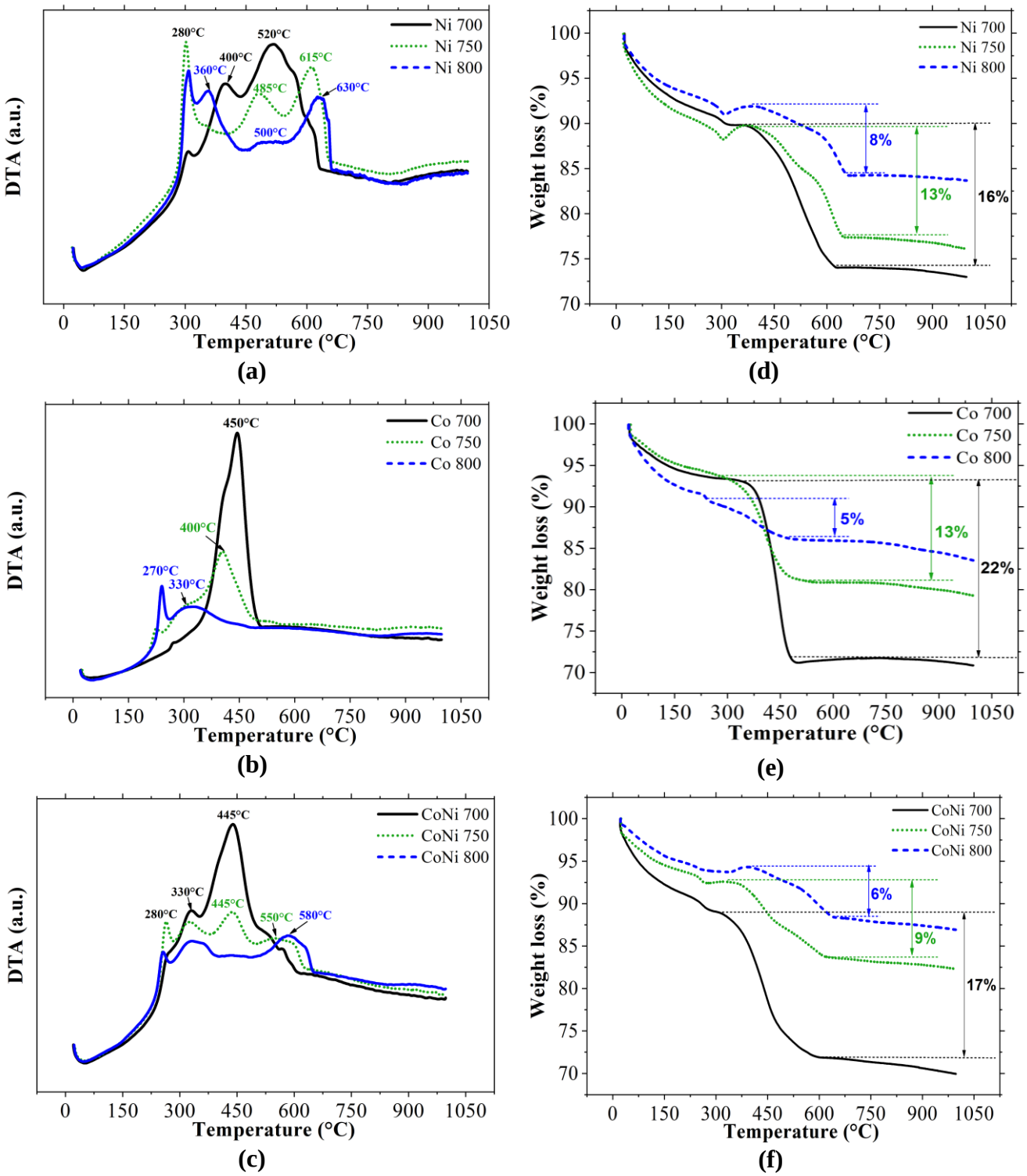

Figure 3.12 DTA analyses of the bulk catalysts after the reforming at three tested temperatures (700, 750 and 800°C) for the three catalysts: (a) DTA of Nickel Ni, (b) DTA of Cobalt Co and (c) DTA of Cobalt-Nickel CoNi; along with weight loss (TGA) analyses of the same catalysts under the same conditions: (d) weight loss of Ni, (e) weight loss of Co and (f) weight loss of CoNi

3.4.3. Catalyst aging test without pretreatment

The results of the catalyst aging test over 5 cycles without a prior treatment of the catalyst are presented in **Figure 3.13** to **Figure 3.16**. They revealed a decreasing of the catalyst efficiency over the time starting from the second cycle of operation. The yields of gases and syngas in particular drop, while the bio-oil yield rises along with the concentrations of CH_4 and CO_2.

From the third cycle, a certain catalyst stability is observed where similar values are obtained for the third, fourth and fifth cycles, revealing the partial deactivation of the catalyst. *Between the first and fifth cycles of reforming, the catalyst activity deteriorated* where the conversion rates of bio-oil, CH_4 and CO_2 dropped by 21.49%, 135.76% and 62.14%, respectively while the syngas concentration and the H_2/CO ratio decreased by 20.49% and 32.25%, correspondingly.

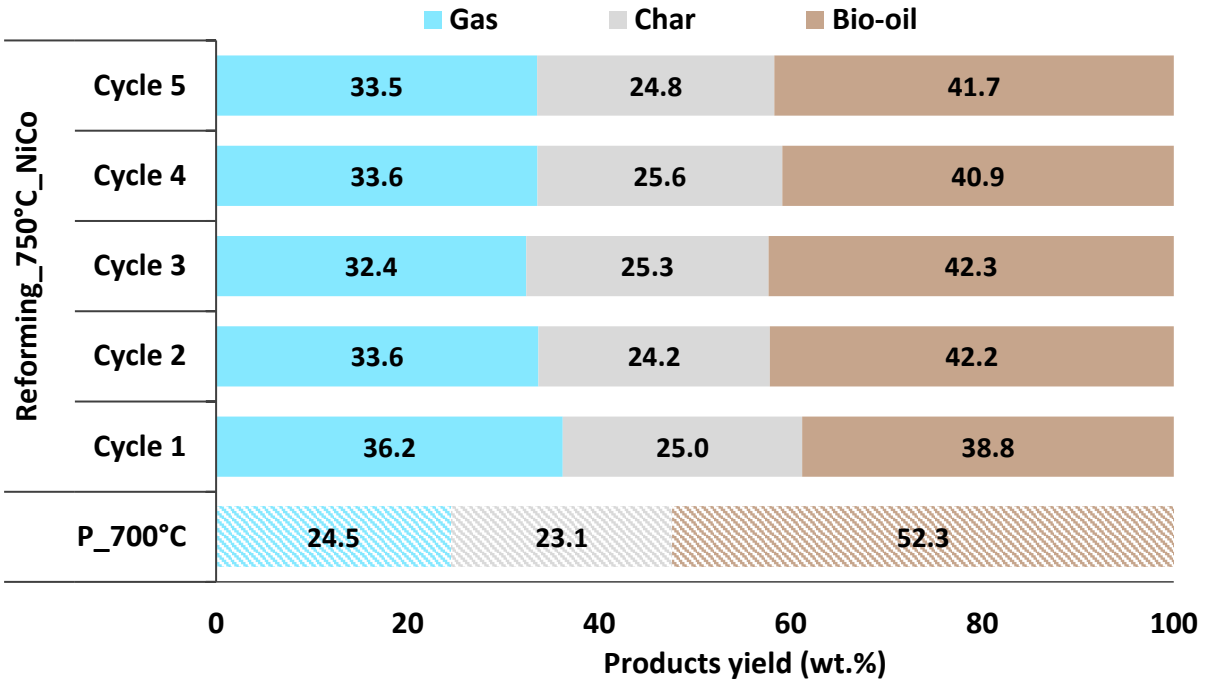

Figure 3.13 Distribution of the products derived from the combined pyrolysis-catalytic reforming at 750°C over CoNi catalyst during its aging test, with the pyrolysis alone at 700°C as the base reference

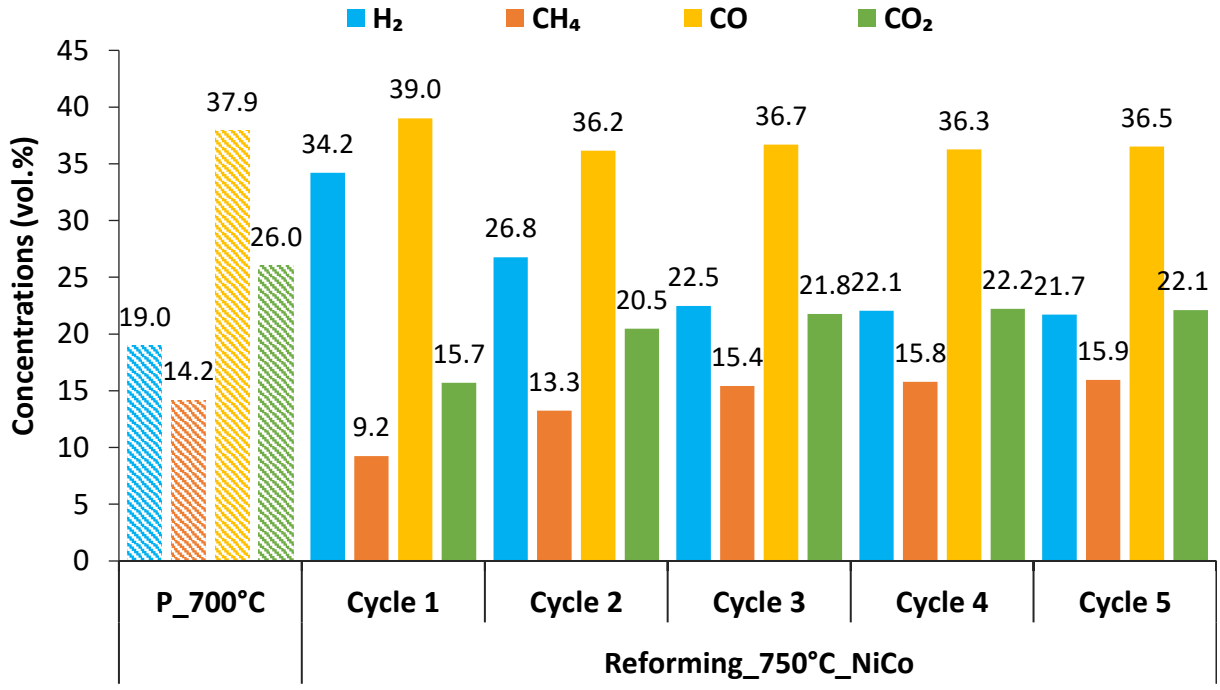

Figure 3.14 Variation of the volume concentrations of the major gases derived from the combined pyrolysis-catalytic reforming at 750°C over CoNi catalyst during its aging test, with the pyrolysis alone at 700°C as the base reference

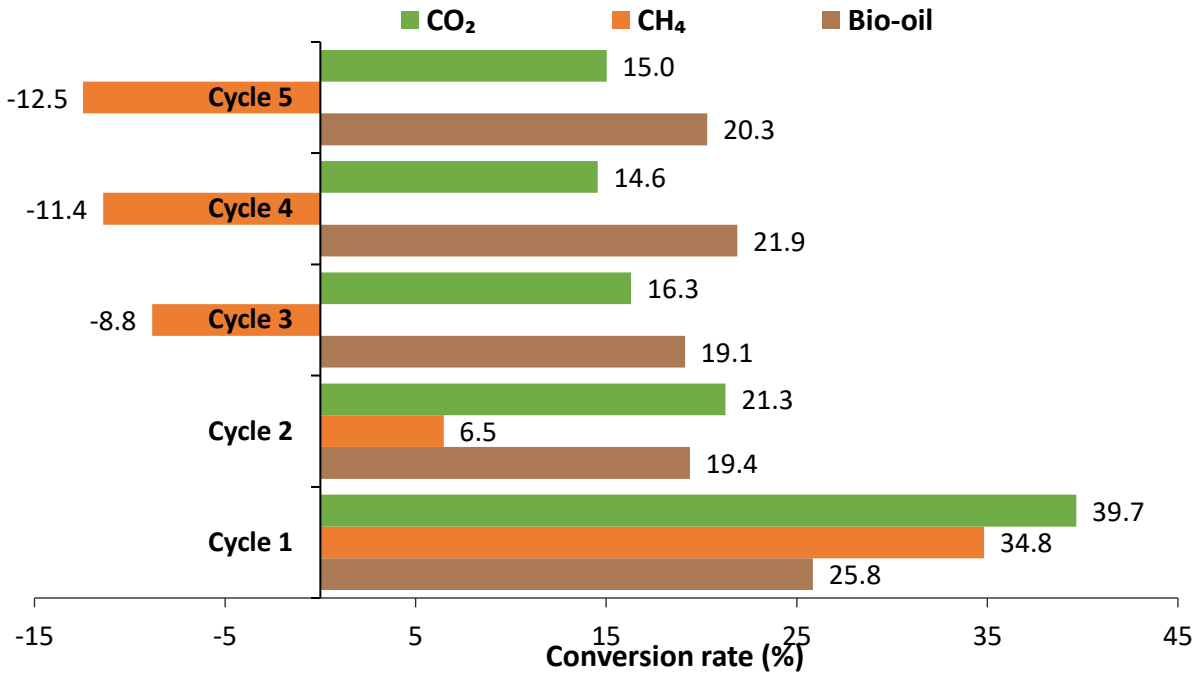

Figure 3.15 Variation of the conversion rates of bio-oil, CH_4 and CO_2 during the combined pyrolysis-catalytic reforming at 750°C over CoNi catalyst during its aging test, with the pyrolysis alone at 700°C as the base reference

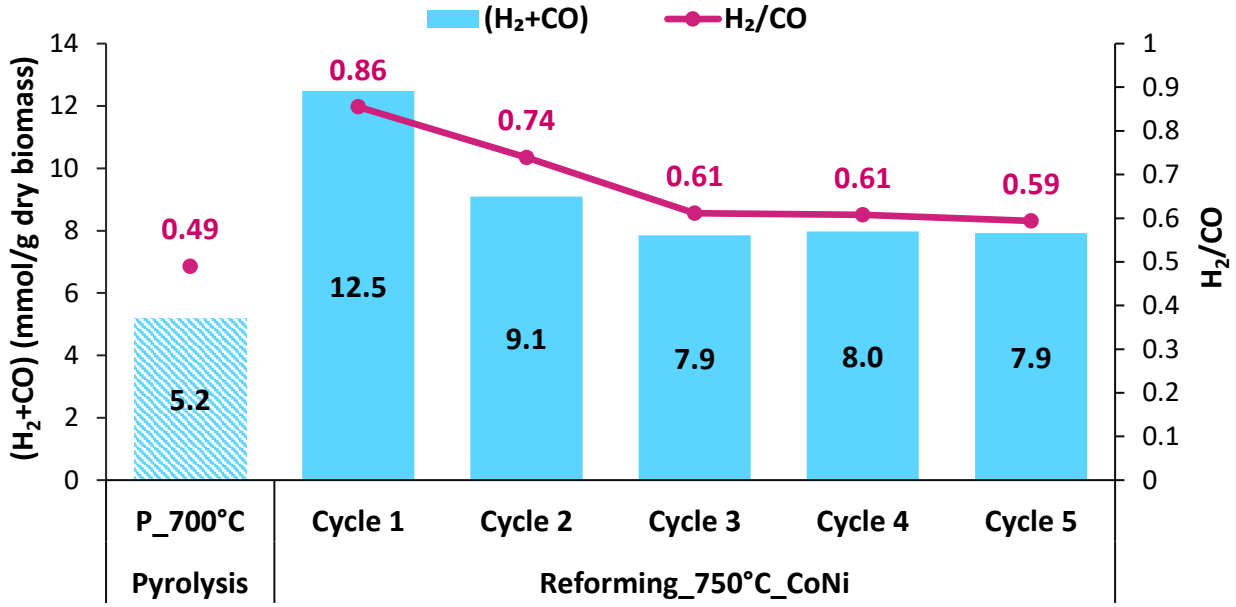

Figure 3.16 Variation of the syngas concentration and the H_2/CO ratio from the combined pyrolysis-catalytic reforming at 750°C over CoNi catalyst during its aging test, with the pyrolysis alone at 700°C as the base reference

The catalyst deactivation can be attributed to several reasons mainly sintering, poisoning, fouling, oxidation of the active metal sites and carbon deposition over the catalyst surface [127]. They lead to a degradation in the catalyst performance and efficiency as well as its selectivity. The catalyst's sintering is an irreversible physical process which leads to a reduction of the active surface area of the catalyst. It is due to the migration and agglomeration of small metallic crystals to form larger crystals reducing the dispersion and specific surface [128]. High temperatures significantly increase the sintering mechanism [129]. Poisoning is caused by the presence of impurities in the feedstock (sulfureous compounds…) which decreases the catalyst

activity by being adsorbed over its surface [129]. The poison can have solely a geometric effect by blocking the active sites or an electronic effect by modifying the catalyst capacity to adsorb other species (i.e., the reactants) [130]. Nonetheless, the poisoned catalyst can be regenerated by increasing the temperature which favors the kinetics of the desorption of the sulfur species adsorbed [131].

The fouling consists of a physical blocking of the metal sites due to the deposition of dust or carbonaceous residues known as "coke". These deposits can either cover the active sites or block the pores which limits the mass transfer and leads to a drop of the catalyst activity and selectivity [129]. The catalyst activity which disintegrated due to the carbon deposition can be restored by burning the carbon formed through oxidation; this is known as the "regeneration" of the catalyst [132,133]. Other deactivation sources are due to the loss of the active species by vaporization into volatiles metal carbonyls, under high temperatures. The active species can also be converted into other less active or less selective species. If the active phase of the catalyst is based on transition metal, the oxidation of the metal sites is also a reason behind the catalyst deactivation. This phenomenon is generally observed for the catalysts at low temperatures given the small particles size, their high mobility and the porous nature of the catalyst support [134].

The deactivation of the catalyst by the carbon formation remains the major issue related to the reforming. This phenomenon is very common during the dry reforming since it is a strongly endothermic process requiring relatively high temperatures to reach important conversion rates of the reactants. However, these high temperatures favor, in parallel, the occurrence of secondary reactions of carbon formation such as the methane decomposition (equation **(3.21)**) and CO disproportionation known as the Boudouard reaction (equation **(3.10)**), favored between 550°C and 800°C [135,136].

3.4.4. Characterization of the spent catalysts after aging test without pretreatment

DTA and TGA analyses were realized on the catalysts employed for the Co-Ni aging test without the pretreatment steps, after the first and fifth cycles of operation and the results are illustrated in **Figure 3.17** (a) and (b), respectively. Considering the Ni-Co after cycle 1 of reforming at 750°C, it can be noticed that the results obtained here are similar to those previously found (**Figure 3.12** (b) and (e)) with a 9% weight loss corresponding to the carbon deposition over the catalyst surface and three exothermic peaks identified on the DTA plot at 280, 330 and 540°C related to different types of carbon.

Now looking at the DTA plot on **Figure 3.17** (a) for Ni-Co after the cycle 5 of reforming at 750°C, three exothermic peaks can also be identified with the first one similar for both cycles 1 and 5 but the two remaining peaks are obtained at higher temperatures (405°C and 595°C) with larger intensities for the Ni-Co after cycle 5 than after cycle 1 of reforming. This implies that higher amounts and different types of carbon are deposited over the catalyst surface after cycle 5. The higher peaks' temperatures suggest that the carbon deposit is more stable and harder to be oxidized. The carbon formed at 405°C can be considered of type C_β [100] while that at 595°C would be an inert very stable carbon [60,126].

These observations are confirmed by the weight loss analysis presented in **Figure 3.17** (b). The first weight losses observed below 250°C for Ni-Co after cycles 1 and 5 of around 5% correspond to the relative moisture content of the catalysts. The following weight gain between

300 and 400°C can be associated to the oxidation of the Co-Ni catalyst as previously discussed. Above 400°C, some huge weight losses are observed for both catalysts. The higher weight loss of 19% observed for the Ni-Co after cycle 5 of reforming reflects a large carbon deposition over the catalyst surface which is formed after five consecutive cycles of reforming without regeneration. *This proves the results obtained where the catalyst's activity remarkably dropped by the end of the fifth cycle of operation, due to the partial deactivation of the catalyst* caused by the fouling and carbon deposition [129].

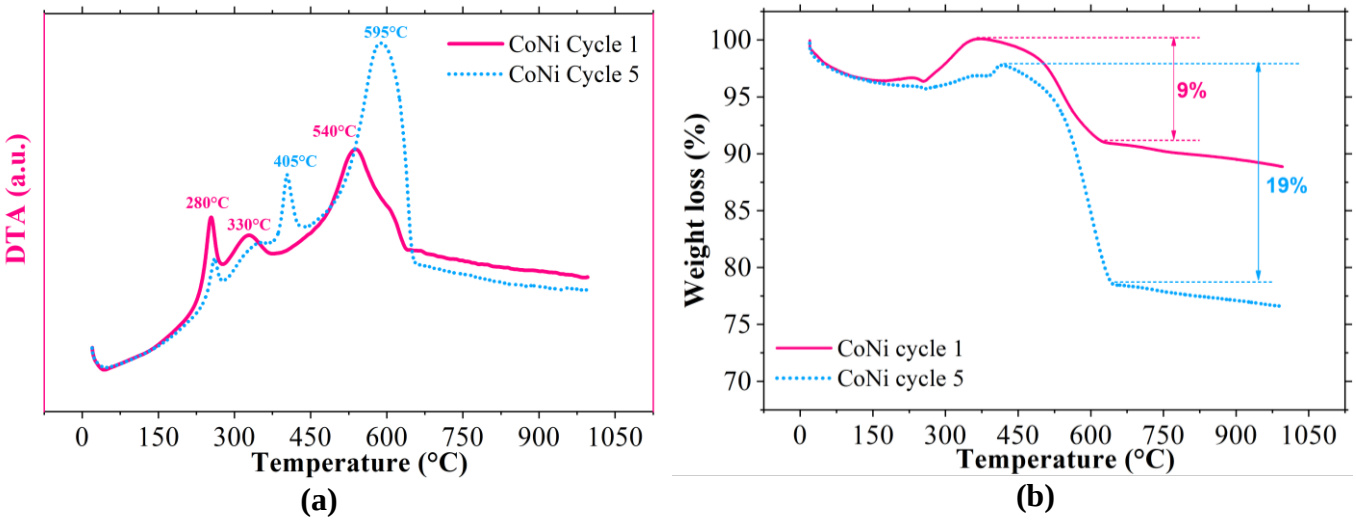

Figure 3.17 DTA (a) and weight loss (b) analyses for the Ni-Co catalyst during its aging test without pretreatment steps after cycle 1 and cycle 5 with the reforming realized at 700°C

3.4.5. Pretreatment of spent catalyst with different gases

The catalyst deactivation issues were addressed in the literature by several methods. For instance, regeneration by hydrogen has been applied to potentially reactivate the catalyst through reduction of the oxidized catalyst [137,138]. The air or O_2 oxidation has been used to remove the carbon which might form over the catalyst surface [88,139]. The pretreatment experiments of the catalyst Co-Ni with different gases (N_2, H_2 and air) prior to the second cycle of reforming operation are detailed in **Figure 3.18** to **Figure 3.21**. *The figures demonstrate that the oxidation under air was the most efficient method.* In fact, the conversion rates of CH_4, CO_2 and bio-oil were enhanced by 11.8%, 32% and 18.5%, respectively. The syngas concentration and the H_2/CO ratio were also ameliorated by 5.6% and 9.6%, correspondingly.

Similar results were obtained by the pretreatment with both H_2 and air. On the other hand, *the pretreatment with N_2 and H_2 alone led to a further decrease in the catalyst activity.* For the pretreatment with N_2, the conversion rates of CH_4, CO_2 and bio-oil dropped by 35.7%, 99.4% and 36.1%, respectively, while the syngas concentration decreased by 13% and H_2/CO ratio fell by 28%. Whereas for the pretreatment with H_2, the conversion rates of CH_4, CO_2 and bio-oil dropped by 40.6%, 67.4% and 17.4%, respectively while the syngas decreased by 8% and H_2/CO ratio reduced by 18.6%. The most common potential solutions attributed to the catalyst deactivation issues are the regeneration of the catalyst by a reduction agent such as hydrogen to restore the active sites, and the removal of the carbon formed by oxidation (reaction **(3.24)**) [114].

Carbon oxidation: $C + O_2 \rightarrow CO_2$ $\qquad \Delta H°_{298K} = -394\ kJ/mol$ **(3.24)**

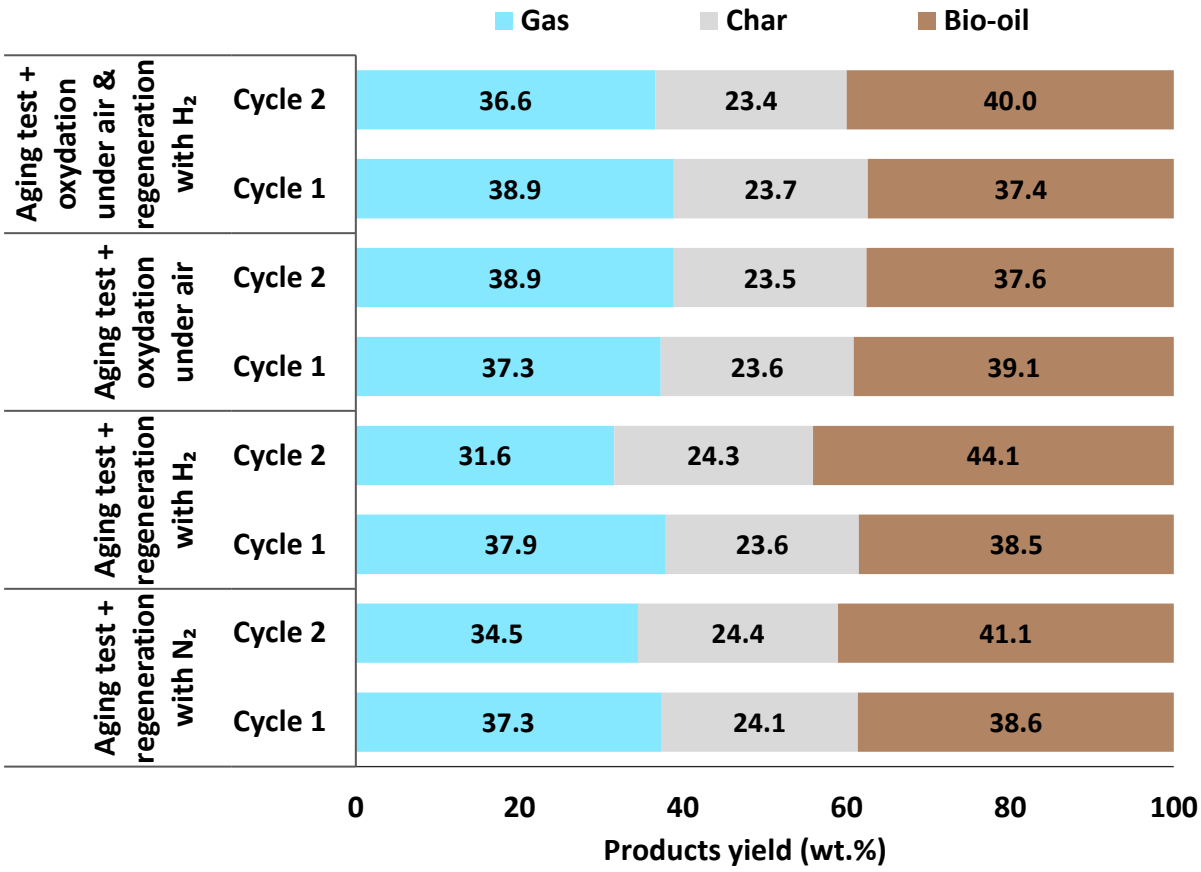

Figure 3.18 Distribution of the products derived from the combined pyrolysis-catalytic reforming over CoNi catalyst during the aging test and the pretreatment step with different gases prior to the second cycle

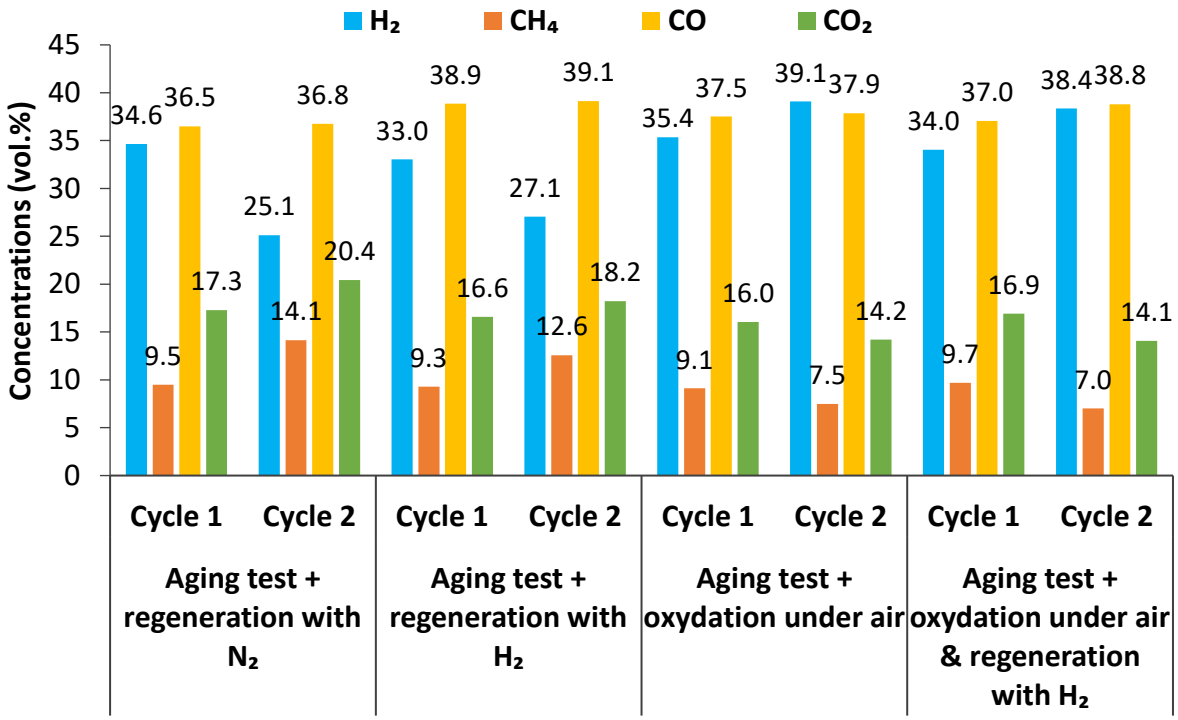

Figure 3.19 Variation of the volume concentrations of the major gases derived from the combined pyrolysis-catalytic reforming over CoNi catalyst during the aging test and the pretreatment step with different gases prior to the second cycle

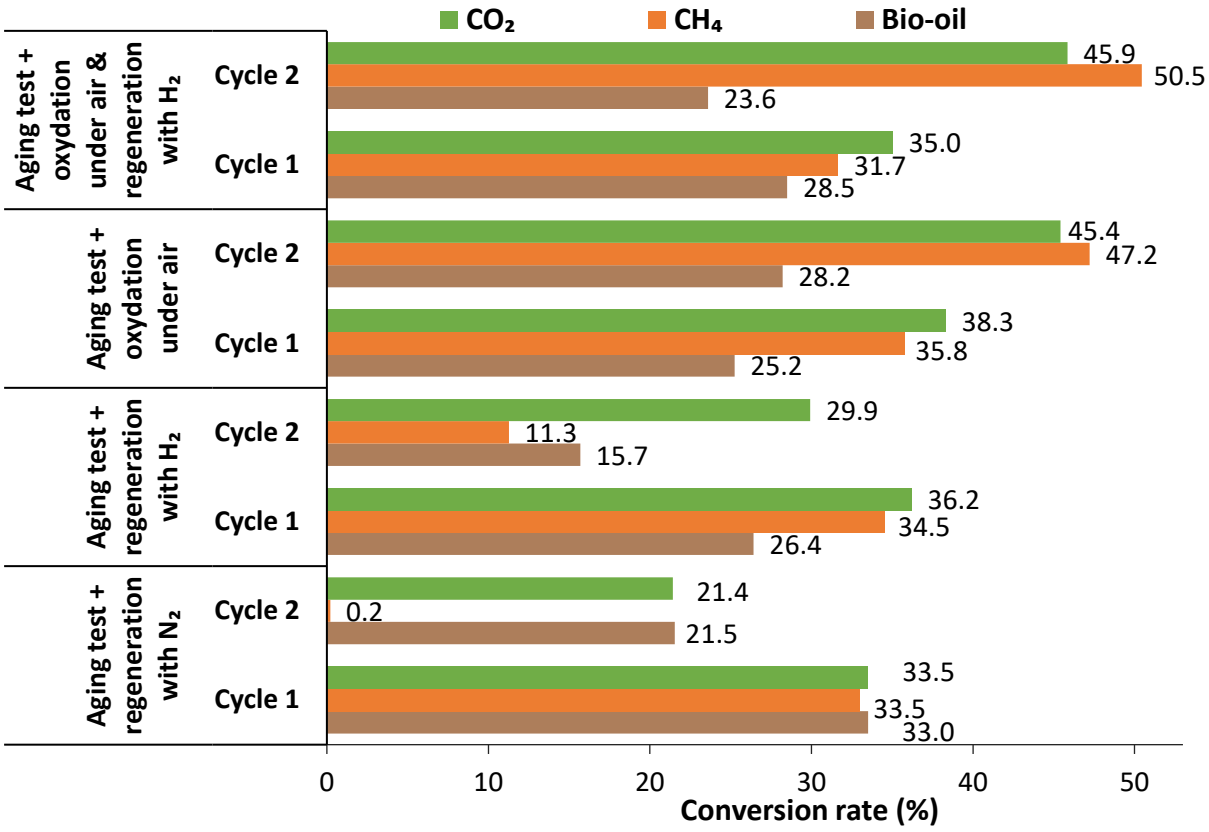

Figure 3.20 Variation of the conversion rates of bio-oil, CH_4 and CO_2 from the combined pyrolysis-catalytic reforming over CoNi catalyst during the aging test and the pretreatment step with different gases prior to the second cycle

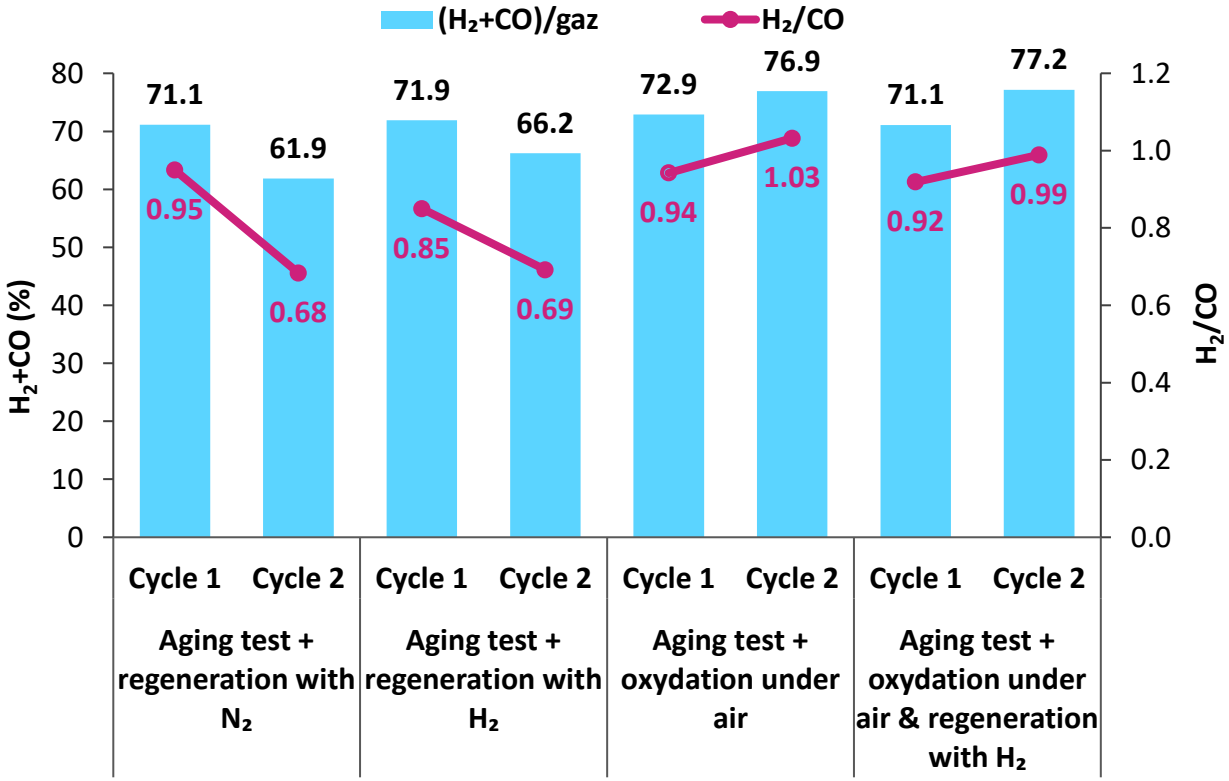

Figure 3.21 Variation of the syngas concentration and the H_2/CO ratio from the combined pyrolysis-catalytic reforming over CoNi catalyst during the aging test and the pretreatment step with different gases prior to the second cycle

The fact that there was no amelioration in the Co-Ni activity by the regeneration with H_2, implies that the catalyst sites were not oxidized, otherwise their reduction was not effective. On the other hand, the enhancement in the catalyst efficiency after the oxidation with air is potentially due to the oxidation of the carbon deposited over the catalyst surface which leads to the formation of carbon dioxide as shown in equation **(3.24)**. The gases emitted during the oxidation step were in fact analyzed by the μGC/MS and demonstrated a production of more than 90% of CO_2 which confirms the occurring of the oxidation reaction and the presence of carbon on the catalyst surface.

3.4.6. Catalyst aging tests after oxidation with air

The remarkable amelioration in the catalyst Co-Ni with the pretreatment by oxidation, led to realizing the aging tests through another series of experiments over five tests by applying air oxidation of the catalyst prior to each pyrolysis-catalytic reforming for each test. The results obtained are displayed in the following sections.

3.4.6.1. Products distribution

The evolution of the main products formed by the reforming of the biomass pyrolysis volatiles in function of time with a pretreatment by air oxidation of the Co-Ni catalyst is depicted in **Figure 3.22**. Taking the repeatability uncertainties into consideration, it can be noticed that the gas and bio-oil yields are almost steady for the first two cycles of operation. Interestingly, the gas formation enhances and that of bio-oil drops from the third cycle of aging and remains almost constant for the following cycles. This reflects an amelioration in the Co-Ni activity with time (or cycle), which was not present in the first aging test. *The oxidation pretreatment did not only remove the carbon deposited over the catalyst surface but potentially liberated more active sites of the catalyst which significantly improved its activity.*

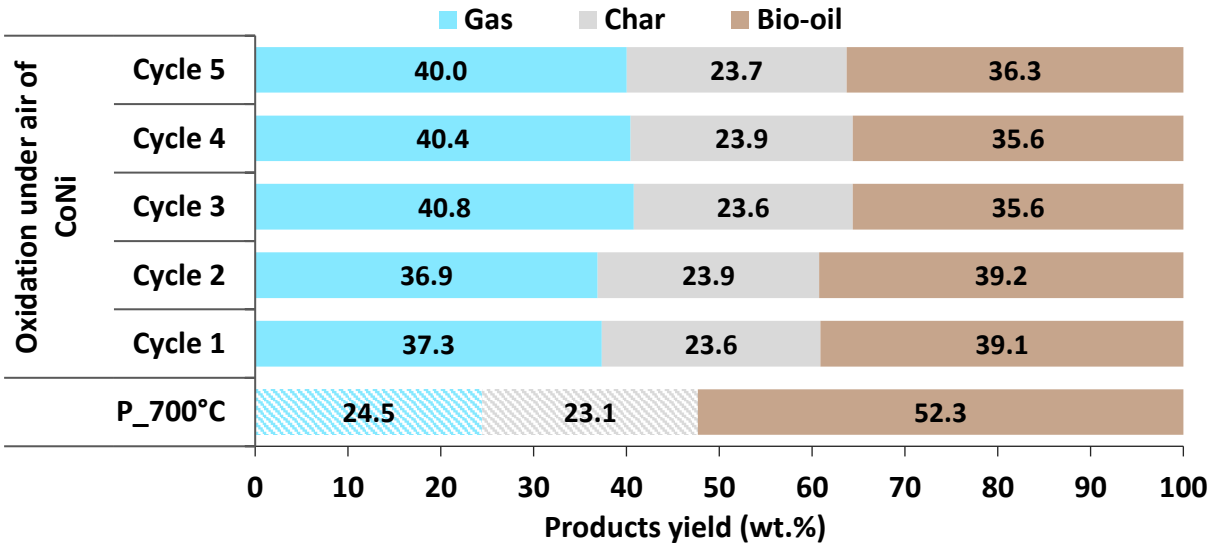

Figure 3.22 Distribution of the products derived from the pyrolysis at 700°C coupled to catalytic reforming at 750°C, over CoNi catalyst during its aging test after oxidation under air before each cycle

3.4.6.2. Gases' concentrations

The concentrations of the major gases produced during the aging test with the oxidation pretreatment step are represented in function of time in **Figure 3.23**. After the second cycle of experiment, the concentrations of H_2 and CO were superior and those of CH_4 and CO_2 were inferior to those obtained after only one hour. This shows again an amelioration of the catalyst

performance thanks to the oxidation step which removed the carbon deposited over the catalyst surface after the first cycle of catalytic reforming and freed some additional active sites. The concentrations of H_2 and CO then slightly decreased as from the third cycle and those of CH_4 and CO_2 faintly increased. *The values remained almost constant for the following cycles and approached those of the first cycle, which implies a good activity maintained over time.*

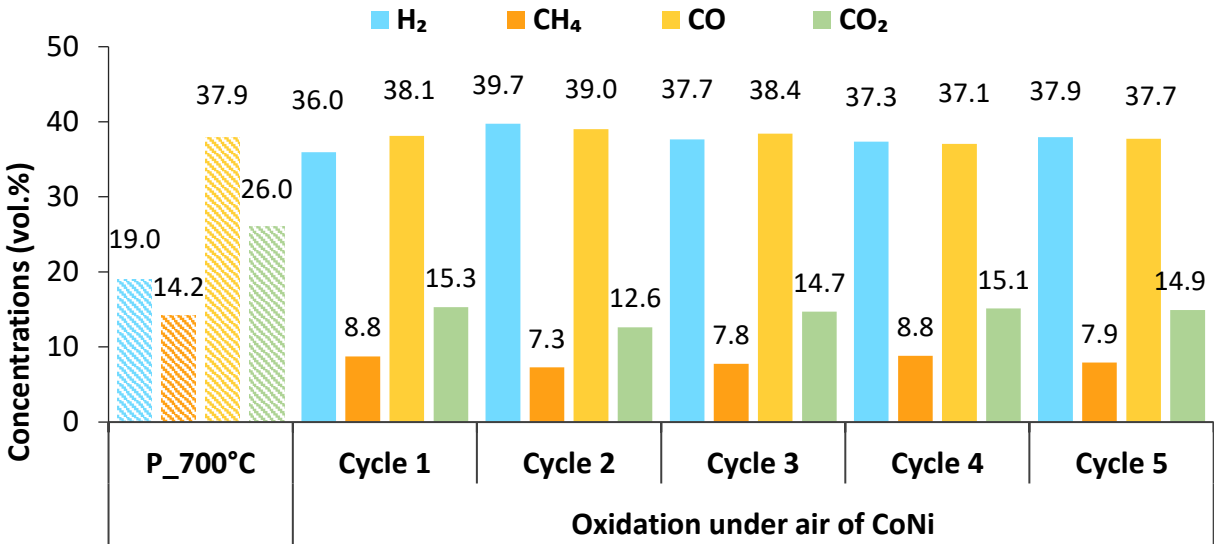

Figure 3.23 Variation of the volume concentrations of the major gases derived from the pyrolysis at 700°C coupled to catalytic reforming at 750°C, over CoNi catalyst during its aging test after oxidation under air before each cycle

3.4.6.3. Conversion rates of main reactants

Figure 3.24 illustrating the conversion rates of the main reactants after the oxidation and the aging test confirms the observations previously made. The conversions of CH_4 and CO_2 markedly increase after the second cycle of operation and oxidation whereas the bio-oil conversion remains almost the same. After the second cycle, the CH_4 and CO_2 conversions drop and approach those obtained after the first cycle, while the bio-oil conversion is remarkably improved as it was seen with the reduction in the bio-oil yields.

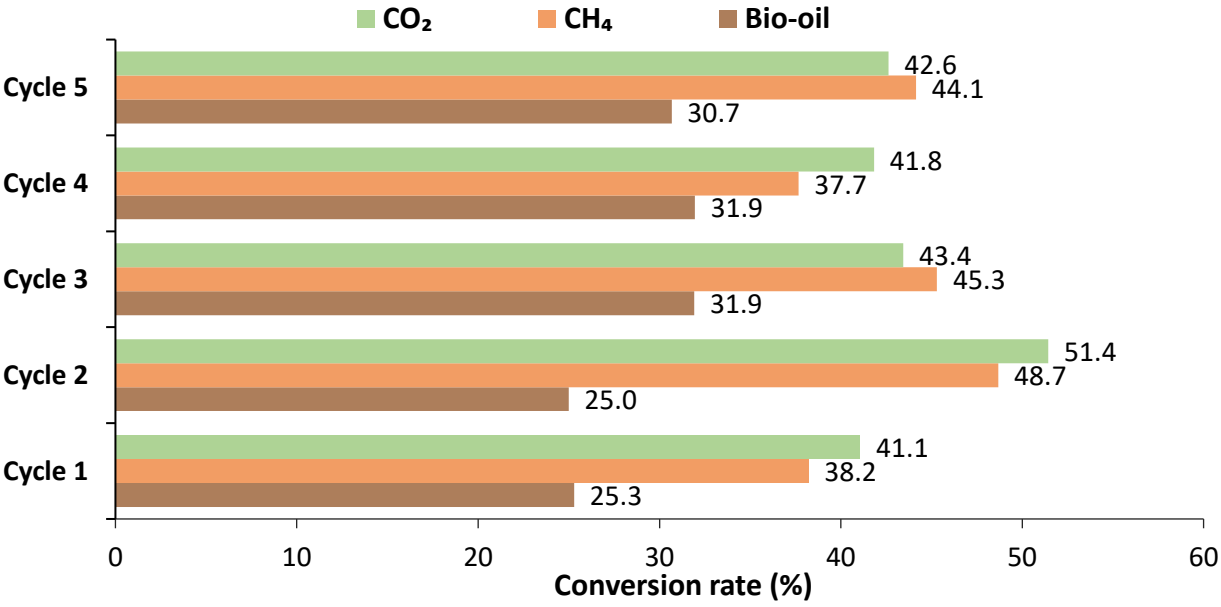

Figure 3.24 Variation of the conversion rates of bio-oil, CH_4 and CO_2 during the pyrolysis at 700°C coupled to catalytic reforming at 750°C, over CoNi catalyst during its aging test after oxidation under air before each cycle

3.4.6.4. Syngas concentration

The syngas concentration presented in **Figure 3.25** is similarly enhanced after the second and third cycles of oxidation and operation as previously noted, and then slightly decreases after the third cycle, to remain always higher than the syngas concentration obtained after the first hour. The H_2/CO ratio peaks at 1.02 after the second cycle by increasing from 0.94 after the first cycle of operation. It then slightly decreases from the third cycle and fluctuates around 1 for the rest of the aging test, *thereby reflecting the strong performance of the Cobalt-Nickel catalyst with time if it is well oxidized prior to the next reforming test.*

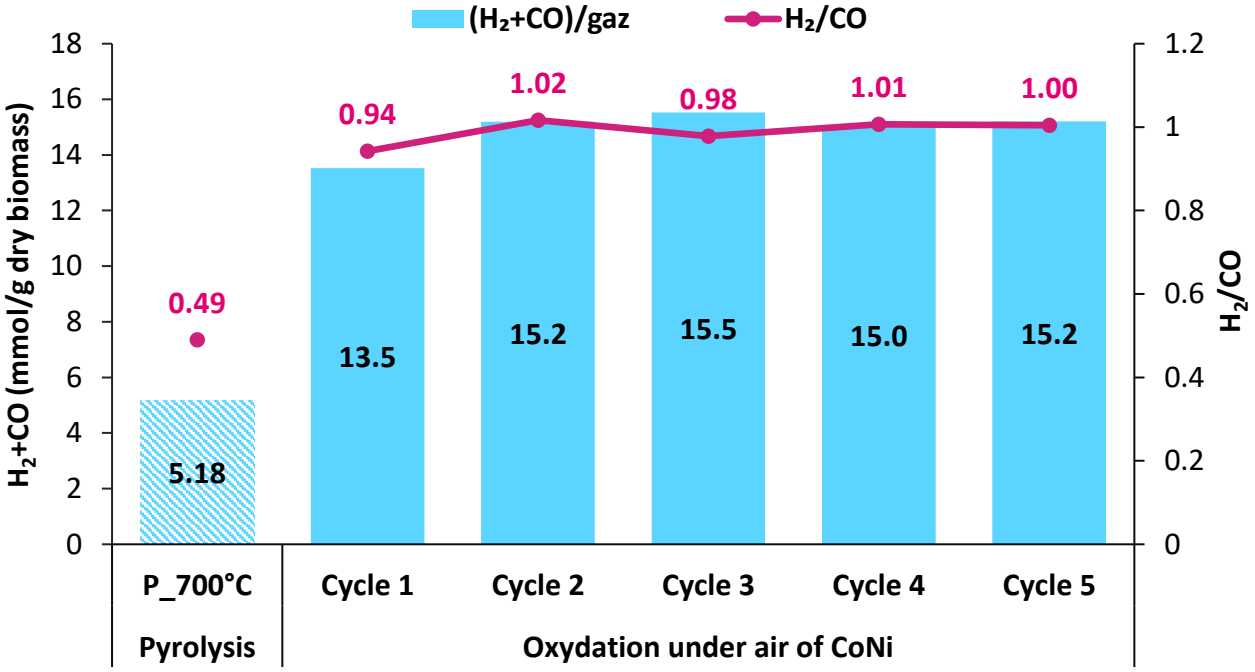

Figure 3.25 Variation of the syngas concentration and the H_2/CO ratio from the pyrolysis at 700°C coupled to catalytic reforming at 750°C, over CoNi catalyst during its aging test after oxidation under air before each cycle

3.5. Conclusion

In this work, the process coupling the biomass pyrolysis to the catalytic reforming of the pyrolysis volatiles was investigated, for the hydrogen enriched syngas production. Several conclusions can be made from the study of the different parameters:

- Higher gas yields with larger H_2 concentrations and smaller CH_4 and CO_2 concentrations are obtained with the pyrolysis-catalytic reforming in comparison to pyrolysis alone.
- For the pyrolysis-catalytic reforming process, the increase of the temperature improves the gases production and reduces the bio-oil formation. The conversion rates of the bio-oil, CH_4 and CO_2 were enhanced with the temperature which increased the syngas formation.
- An optimal temperature of 750°C is suggested to be a suitable compromise between the improved syngas production and the reduced energy consumption.

- Among the catalyst evaluated, the reforming in the presence of Co-Ni at 800°C results in the maximum gases production (43 wt.%) and minimum bio-oil formation (32.4 wt.%).
- The Ni catalyst outranged the other catalysts by producing the highest syngas concentration (82.1 vol.% or 16.8 mmol/g dry biomass) after reforming at 750°C. It is due to the highest conversion of CH_4 (68.2%) and CO_2 (52.6%) reached with the Ni at 750°C.
- XRD, DTA and TGA analyses of the post-reforming catalysts revealed the formation of several types of carbon including C_α formed below 400°C, C_β appearing around 460°C and C_γ around 500°C as well as some inert carbon formed at higher temperatures.
- Co-Ni had the lowest carbon deposition due to the presence of Co which increases the Ni resistance to carbon formation.
- The catalyst aging test realized without any pretreatment revealed a decrease in the catalyst activity with time, which was associated to the carbon deposition over the catalyst surface.
- To regenerate and reactivate the catalyst, the oxidation under air was the most effective way which oxidized the carbon deposited over the catalyst. The catalyst aging test was repeated with an oxidation pre-step, which improved the catalyst activity and stability with time.

Several additional parameters including the nature of biomass, the catalyst type, the nature of its support, the GHSV can also affect the catalyst performance in addition to the temperature, the catalyst active phase and the pretreatment methods. It appears necessary to study the influence of each of these parameters on the biomass pyrolysis-catalytic reforming process, to determine the most optimized process conditions which maximize the CO and H_2 production. These are the objectives of the following chapter.

References

[1] İ. Yıldız, 1.12 Fossil Fuels, in: I. Dincer (Ed.), Compr. Energy Syst., Elsevier, Oxford, 2018: pp. 521–567. https://doi.org/10.1016/B978-0-12-809597-3.00111-5.

[2] E. Tzimas, A. Georgakaki, A long-term view of fossil-fuelled power generation in Europe, Energy Policy. 38 (2010) 4252–4264. https://doi.org/10.1016/j.enpol.2010.03.055.

[3] J. Manna, P. Jha, R. Sarkhel, C. Banerjee, A.K. Tripathi, M.R. Nouni, Opportunities for green hydrogen production in petroleum refining and ammonia synthesis industries in India, Int. J. Hydrog. Energy. 46 (2021) 38212–38231. https://doi.org/10.1016/j.ijhydene.2021.09.064.

[4] A. Arregi, G. Lopez, M. Amutio, I. Barbarias, J. Bilbao, M. Olazar, Hydrogen production from biomass by continuous fast pyrolysis and in-line steam reforming, RSC Adv. 6 (2016) 25975–25985. https://doi.org/10.1039/C6RA01657J.

[5] M.N. Uddin, K. Techato, J. Taweekun, M.M. Rahman, M.G. Rasul, T.M.I. Mahlia, S.M. Ashrafur, An Overview of Recent Developments in Biomass Pyrolysis Technologies, Energies. 11 (2018) 3115. https://doi.org/10.3390/en11113115.

[6] Z. Ma, L. Wei, W. Zhou, L. Jia, B. Hou, D. Li, Y. Zhao, Overview of catalyst application in petroleum refinery for biomass catalytic pyrolysis and bio-oil upgrading, RSC Adv. 5 (2015) 88287–88297. https://doi.org/10.1039/C5RA17241A.

[7] R. Trane, S. Dahl, M.S. Skjøth-Rasmussen, A.D. Jensen, Catalytic steam reforming of bio-oil, Int. J. Hydrog. Energy. 37 (2012) 6447–6472. https://doi.org/10.1016/j.ijhydene.2012.01.023.
[8] M.I. Jahirul, M.G. Rasul, A.A. Chowdhury, N. Ashwath, Biofuels Production through Biomass Pyrolysis —A Technological Review, Energies. 5 (2012) 4952–5001. https://doi.org/10.3390/en5124952.
[9] A.A. Lemonidou, P. Kechagiopoulos, E. Heracleous, S. Voutetakis, Chapter 14 - Steam Reforming of Bio-oils to Hydrogen, in: K.S. Triantafyllidis, A.A. Lappas, M. Stöcker (Eds.), Role Catal. Sustain. Prod. Bio-Fuels Bio-Chem., Elsevier, Amsterdam, 2013: pp. 467–493. https://doi.org/10.1016/B978-0-444-56330-9.00014-0.
[10] A. Demirbas, Competitive liquid biofuels from biomass, Appl. Energy. 88 (2011) 17–28. https://doi.org/10.1016/j.apenergy.2010.07.016.
[11] D. Wang, D. Montané, E. Chornet, Catalytic steam reforming of biomass-derived oxygenates: acetic acid and hydroxyacetaldehyde, Appl. Catal. Gen. 143 (1996) 245–270. https://doi.org/10.1016/0926-860X(96)00093-2.
[12] A. Haryanto, S. Fernando, N. Murali, S. Adhikari, Current Status of Hydrogen Production Techniques by Steam Reforming of Ethanol: A Review, Energy Fuels. 19 (2005) 2098–2106. https://doi.org/10.1021/ef0500538.
[13] L. Santamaria, G. Lopez, A. Arregi, M. Artetxe, M. Amutio, J. Bilbao, M. Olazar, Catalytic steam reforming of biomass fast pyrolysis volatiles over Ni–Co bimetallic catalysts, J. Ind. Eng. Chem. 91 (2020) 167–181. https://doi.org/10.1016/j.jiec.2020.07.050.
[14] M.A. Elharati, K.-M. Lee, S. Hwang, A. Mohammed Hussain, Y. Miura, S. Dong, Y. Fukuyama, N. Dale, S. Saunders, T. Kim, S. Ha, The effect of silica oxide support on the catalytic activity of nickel-molybdenum bimetallic catalyst toward ethanol steam reforming for hydrogen production, Chem. Eng. J. 441 (2022) 135916. https://doi.org/10.1016/j.cej.2022.135916.
[15] F. Bimbela, M. Oliva, J. Ruiz, L. García, J. Arauzo, Hydrogen production by catalytic steam reforming of acetic acid, a model compound of biomass pyrolysis liquids, J. Anal. Appl. Pyrolysis. 79 (2007) 112–120. https://doi.org/10.1016/j.jaap.2006.11.006.
[16] E.Ch. Vagia, A.A. Lemonidou, Thermodynamic analysis of hydrogen production via autothermal steam reforming of selected components of aqueous bio-oil fraction, Int. J. Hydrog. Energy. 33 (2008) 2489–2500. https://doi.org/10.1016/j.ijhydene.2008.02.057.
[17] I.-H. Choi, K.-R. Hwang, K.-Y. Lee, I.-G. Lee, Catalytic steam reforming of biomass-derived acetic acid over modified Ni/γ-Al2O3 for sustainable hydrogen production, Int. J. Hydrog. Energy. 44 (2019) 180–190. https://doi.org/10.1016/j.ijhydene.2018.04.192.
[18] N. Gao, X. Wang, A. Li, C. Wu, Z. Yin, Hydrogen production from catalytic steam reforming of benzene as tar model compound of biomass gasification, Fuel Process. Technol. 148 (2016) 380–387. https://doi.org/10.1016/j.fuproc.2016.03.019.
[19] J. Tao, L. Zhao, C. Dong, Q. Lu, X. Du, E. Dahlquist, Catalytic Steam Reforming of Toluene as a Model Compound of Biomass Gasification Tar Using Ni-CeO2/SBA-15 Catalysts, Energies. 6 (2013) 3284–3296. https://doi.org/10.3390/en6073284.
[20] Q. Xu, P. Lan, B. Zhang, Z. Ren, Y. Yan, Hydrogen Production via Catalytic Steam Reforming of Fast Pyrolysis Bio-oil in a Fluidized-Bed Reactor, Energy Fuels. 24 (2010) 6456–6462. https://doi.org/10.1021/ef1010995.
[21] M. Artetxe, J. Alvarez, M.A. Nahil, M. Olazar, P.T. Williams, Steam reforming of different biomass tar model compounds over Ni/Al2O3 catalysts, Energy Convers. Manag. 136 (2017) 119–126. https://doi.org/10.1016/j.enconman.2016.12.092.
[22] P.N. Kechagiopoulos, S.S. Voutetakis, A.A. Lemonidou, I.A. Vasalos, Hydrogen Production via Reforming of the Aqueous Phase of Bio-Oil over Ni/Olivine Catalysts in a Spouted Bed Reactor, Ind. Eng. Chem. Res. 48 (2009) 1400–1408. https://doi.org/10.1021/ie8013378.
[23] B. Valle, A. Remiro, A.T. Aguayo, J. Bilbao, A.G. Gayubo, Catalysts of Ni/α-Al2O3 and Ni/La2O3-αAl2O3 for hydrogen production by steam reforming of bio-oil aqueous fraction with pyrolytic lignin retention, Int. J. Hydrog. Energy. 38 (2013) 1307–1318. https://doi.org/10.1016/j.ijhydene.2012.11.014.
[24] F. Bimbela, M. Oliva, J. Ruiz, L. García, J. Arauzo, Hydrogen production via catalytic steam reforming of the aqueous fraction of bio-oil using nickel-based coprecipitated catalysts, Int. J. Hydrog. Energy. 38 (2013) 14476–14487. https://doi.org/10.1016/j.ijhydene.2013.09.038.

[25] C. Zhang, Review of catalytic reforming of biomass pyrolysis oil for hydrogen production, Front. Chem. 10 (2022) 962587. https://doi.org/10.3389/fchem.2022.962587.
[26] D. Wang, S. Czernik, D. Montané, M. Mann, E. Chornet, Biomass to Hydrogen via Fast Pyrolysis and Catalytic Steam Reforming of the Pyrolysis Oil or Its Fractions, Ind. Eng. Chem. Res. 36 (1997) 1507–1518. https://doi.org/10.1021/ie960396g.
[27] G. Lopez, L. Santamaria, A. Lemonidou, S. Zhang, C. Wu, A.T. Sipra, N. Gao, Hydrogen generation from biomass by pyrolysis, Nat. Rev. Methods Primer. 2 (2022) 1–13. https://doi.org/10.1038/s43586-022-00097-8.
[28] A. Pietraszek, B. Koubaissy, A.-C. Roger, A. Kiennemann, The influence of the support modification over Ni-based catalysts for dry reforming of methane reaction, Catal. Today. 176 (2011) 267–271. https://doi.org/10.1016/j.cattod.2010.12.015.
[29] Z. Qin, J. Chen, X. Xie, X. Luo, T. Su, H. Ji, CO2 reforming of CH4 to syngas over nickel-based catalysts, Environ. Chem. Lett. 18 (2020) 997–1017. https://doi.org/10.1007/s10311-020-00996-w.
[30] M. Abou Rjeily, C. Gennequin, H. Pron, E. Abi-Aad, J.H. Randrianalisoa, Pyrolysis-catalytic upgrading of bio-oil and pyrolysis-catalytic steam reforming of biogas: a review, Environ. Chem. Lett. (2021) 48. https://doi.org/10.1007/s10311-021-01190-2.
[31] A. Younis, J. Estephane, C. Gennequin, L. Tidahy, B. El Khoury, S. Aouad, E. Abi Aad, Influence of promoting Ni-based catalysts with ruthenium in the dry reforming of polypropylene plastics for syngas production, Int. J. Hydrog. Energy. (2022). https://doi.org/10.1016/j.ijhydene.2022.07.156.
[32] T. Namioka, A. Saito, Y. Inoue, Y. Park, T. Min, S. Roh, K. Yoshikawa, Hydrogen-rich gas production from waste plastics by pyrolysis and low-temperature steam reforming over a ruthenium catalyst, Appl. Energy. 88 (2011) 2019–2026. https://doi.org/10.1016/j.apenergy.2010.12.053.
[33] C. Mukarakate, R.J. Evans, S. Deutch, T. Evans, A.K. Starace, J. ten Dam, M.J. Watson, K. Magrini, Reforming Biomass Derived Pyrolysis Bio-oil Aqueous Phase to Fuels, Energy Fuels. 31 (2017) 1600–1607. https://doi.org/10.1021/acs.energyfuels.6b02463.
[34] F. Bimbela, J. Ábrego, R. Puerta, L. García, J. Arauzo, Catalytic steam reforming of the aqueous fraction of bio-oil using Ni-Ce/Mg-Al catalysts, Appl. Catal. B Environ. 209 (2017) 346–357. https://doi.org/10.1016/j.apcatb.2017.03.009.
[35] P. Fu, Z. Andong, S. Luo, W. Yi, Y. Zhang, Comparative study on the catalytic steam reforming of biomass pyrolysis oil and its derivatives for hydrogen production, RSC Adv. 10 (2020) 12721–12729. https://doi.org/10.1039/D0RA01409E.
[36] C. Liu, D. Chen, Y. Cao, T. zhang, Y. Mao, W. Wang, Z. Wang, S. Kawi, Catalytic steam reforming of in-situ tar from rice husk over MCM-41 supported LaNiO3 to produce hydrogen rich syngas, Renew. Energy. 161 (2020) 408–418. https://doi.org/10.1016/j.renene.2020.07.089.
[37] J. Hu, Z. Jia, S. Zhao, W. Wang, Q. Zhang, R. Liu, Z. Huang, Activated char supported Fe-Ni catalyst for syngas production from catalytic gasification of pine wood, Bioresour. Technol. 340 (2021) 125600. https://doi.org/10.1016/j.biortech.2021.125600.
[38] S. Luo, B. Xiao, X. Guo, Z. Hu, S. Liu, M. He, Hydrogen-rich gas from catalytic steam gasification of biomass in a fixed bed reactor: Influence of particle size on gasification performance, Int. J. Hydrog. Energy. 34 (2009) 1260–1264. https://doi.org/10.1016/j.ijhydene.2008.10.088.
[39] Q.M.K. Waheed, P.T. Williams, Hydrogen Production from High Temperature Pyrolysis/Steam Reforming of Waste Biomass: Rice Husk, Sugar Cane Bagasse, and Wheat Straw, Energy Fuels. 27 (2013) 6695–6704. https://doi.org/10.1021/ef401145w.
[40] K. Akubo, M.A. Nahil, P.T. Williams, Pyrolysis-catalytic steam reforming of agricultural biomass wastes and biomass components for production of hydrogen/syngas, J. Energy Inst. 92 (2019) 1987–1996. https://doi.org/10.1016/j.joei.2018.10.013.
[41] Y. Wang, L. Huang, T. Zhang, Q. Wang, Hydrogen-rich syngas production from biomass pyrolysis and catalytic reforming using biochar-based catalysts, Fuel. 313 (2022) 123006. https://doi.org/10.1016/j.fuel.2021.123006.
[42] N. Gao, S. Liu, Y. Han, C. Xing, A. Li, Steam reforming of biomass tar for hydrogen production over NiO/ceramic foam catalyst, Int. J. Hydrog. Energy. 40 (2015) 7983–7990. https://doi.org/10.1016/j.ijhydene.2015.04.050.
[43] N. Gao, Y. Han, C. Quan, Study on steam reforming of coal tar over NiCo/ceramic foam catalyst for hydrogen production: Effect of Ni/Co ratio, Int. J. Hydrog. Energy. 43 (2018) 22170–22186. https://doi.org/10.1016/j.ijhydene.2018.10.119.

[44] L. Zhao, T. Han, H. Wang, L. Zhang, Y. Liu, Ni-Co alloy catalyst from LaNi1−xCoxO3 perovskite supported on zirconia for steam reforming of ethanol, Appl. Catal. B Environ. 187 (2016) 19–29. https://doi.org/10.1016/j.apcatb.2016.01.007.
[45] M.M. Barroso-Quiroga, A.E. Castro-Luna, Catalytic activity and effect of modifiers on Ni-based catalysts for the dry reforming of methane, Int. J. Hydrog. Energy. 35 (2010) 6052–6056. https://doi.org/10.1016/j.ijhydene.2009.12.073.
[46] J. Ashok, N. Dewangan, S. Das, P. Hongmanorom, M.H. Wai, K. Tomishige, S. Kawi, Recent progress in the development of catalysts for steam reforming of biomass tar model reaction, Fuel Process. Technol. 199 (2020) 106252. https://doi.org/10.1016/j.fuproc.2019.106252.
[47] G. Guan, M. Kaewpanha, X. Hao, A. Abudula, Catalytic steam reforming of biomass tar: Prospects and challenges, Renew. Sustain. Energy Rev. 58 (2016) 450–461. https://doi.org/10.1016/j.rser.2015.12.316.
[48] M.C.J. Bradford, M.A. Vannice, CO2 Reforming of CH4, Catal. Rev. 41 (1999) 1–42. https://doi.org/10.1081/CR-100101948.
[49] S. Aouad, M. Labaki, S. Ojala, P.K. Seelam, E. Turpeinen, C. Gennequin, J. Estephane, E. Abi-Aad, A Review on the Dry Reforming Processes for Hydrogen Production: Catalytic Materials and Technologies, in: 2018: pp. 60–128. https://doi.org/10.2174/9781681087580118020007.
[50] L. He, S. Hu, L. Jiang, G. Liao, X. Chen, H. Han, L. Xiao, Q. Ren, Y. Wang, S. Su, J. Xiang, Carbon nanotubes formation and its influence on steam reforming of toluene over Ni/Al2O3 catalysts: Roles of catalyst supports, Fuel Process. Technol. 176 (2018) 7–14. https://doi.org/10.1016/j.fuproc.2018.03.007.
[51] D. Pakhare, J. Spivey, A review of dry (CO2) reforming of methane over noble metal catalysts, Chem. Soc. Rev. 43 (2014) 7813–7837. https://doi.org/10.1039/C3CS60395D.
[52] W.-J. Jang, J.-O. Shim, H.-M. Kim, S.-Y. Yoo, H.-S. Roh, A review on dry reforming of methane in aspect of catalytic properties, Catal. Today. 324 (2019) 15–26. https://doi.org/10.1016/j.cattod.2018.07.032.
[53] M. Chaghouri, S. Hany, H.L. Tidahy, F. Cazier, C. Gennequin, E. Abi-Aad, Chapter 8 - Dry reforming of methane for catalytic valorization of biogas, in: M.R. Cesario, D.A. de Macedo (Eds.), Heterog. Catal., Elsevier, 2022: pp. 207–248. https://doi.org/10.1016/B978-0-323-85612-6.00008-5.
[54] J. Chen, J. Sun, Y. Wang, Catalysts for Steam Reforming of Bio-oil: A Review, Ind. Eng. Chem. Res. 56 (2017). https://doi.org/10.1021/acs.iecr.7b00600.
[55] A. Adeniyi, K. Otoikhian, J. O. Ighalo, Steam Reforming of Biomass Pyrolysis Oil: A Review, Int. J. Chem. React. Eng. (2019). https://doi.org/10.1515/ijcre-2018-0328.
[56] H.D. Setiabudi, M.A.A. Aziz, S. Abdullah, L.P. Teh, R. Jusoh, Hydrogen production from catalytic steam reforming of biomass pyrolysis oil or bio-oil derivatives: A review, Int. J. Hydrog. Energy. (2019). https://doi.org/10.1016/j.ijhydene.2019.10.141.
[57] H. Xie, R. Li, Z. Yu, Z. Wang, Q. Yu, Q. Qin, Combined steam/dry reforming of bio-oil for H2/CO syngas production with blast furnace slag as heat carrier, Energy. 200 (2020) 117481. https://doi.org/10.1016/j.energy.2020.117481.
[58] M. Abou Rjeily, F. Cazier, C. Gennequin, J.H. Randrianalisoa, Detailed Analysis of Gas, Char and Bio-oil Products of Oak Wood Pyrolysis at Different Operating Conditions, Waste Biomass Valorization. (2022). https://doi.org/10.1007/s12649-022-01848-0.
[59] C. Tanios, S. Bsaibes, M. Nawfal, C. Gennequin, H.L. Tidahy, A. Aboukais, E. Abi-aad, M. Labaki, B. Nsouli, Preparation and characterization of Ni-Co-Mg-Al mixed oxides derived from layered double hydroxides and their performance in the dry reforming of methane, 2016 3rd Int. Conf. Renew. Energ. Dev. Ctries. REDEC. (2016). https://doi.org/10.1109/REDEC.2016.7577544.
[60] C. Tanios, S. Bsaibes, C. Gennequin, M. Labaki, F. Cazier, S. Billet, H. Tidahy, B. Nsouli, A. Aboukaïs, E. Abi-Aad, Syngas production by the CO2 reforming of CH4 over Ni–Co–Mg–Al catalysts obtained from hydrotalcite precursors, Int. J. Hydrog. Energy. (2017). https://doi.org/10.1016/j.ijhydene.2017.01.120.
[61] C. Wu, L. Wang, P.T. Williams, J. Shi, J. Huang, Hydrogen production from biomass gasification with Ni/MCM-41 catalysts: Influence of Ni content, Appl. Catal. B Environ. 108–109 (2011) 6–13. https://doi.org/10.1016/j.apcatb.2011.07.023.

[62] S. Cheng, M. Meng, B. Xing, C. Shi, Y. Nie, D. Xia, G. Yi, C. Zhang, H. Xia, Preparation of valuable pyrolysis products from poplar waste under different temperatures by pyrolysis: Evaluation of pyrolysis products, Bioresour. Technol. 364 (2022) 128011. https://doi.org/10.1016/j.biortech.2022.128011.

[63] Y. Chen, J. Ren, Conversion of methane and carbon dioxide into synthesis gas over alumina-supported nickel catalysts. Effect of Ni-Al2O3 interactions, Catal. Lett. 29 (1994) 39–48. https://doi.org/10.1007/BF00814250.

[64] L. Li, J.S. Rowbotham, H. Christopher Greenwell, P.W. Dyer, Chapter 8 - An Introduction to Pyrolysis and Catalytic Pyrolysis: Versatile Techniques for Biomass Conversion, in: S.L. Suib (Ed.), New Future Dev. Catal., Elsevier, Amsterdam, 2013: pp. 173–208. https://doi.org/10.1016/B978-0-444-53878-9.00009-6.

[65] E. Ranzi, A. Cuoci, T. Faravelli, A. Frassoldati, G. Migliavacca, S. Pierucci, S. Sommariva, Chemical Kinetics of Biomass Pyrolysis, Energy Fuels. 22 (2008) 4292–4300. https://doi.org/10.1021/ef800551t.

[66] C. Branca, C. Di Blasi, Kinetics of the isothermal degradation of wood in the temperature range 528–708 K, J. Anal. Appl. Pyrolysis. 67 (2003) 207–219. https://doi.org/10.1016/S0165-2370(02)00062-1.

[67] C. Di Blasi, Modeling chemical and physical processes of wood and biomass pyrolysis, Prog. Energy Combust. Sci. 34 (2008) 47–90. https://doi.org/10.1016/j.pecs.2006.12.001.

[68] L. Dong, C. Wu, H. Ling, J. Shi, P.T. Williams, J. Huang, Promoting hydrogen production and minimizing catalyst deactivation from the pyrolysis-catalytic steam reforming of biomass on nanosized NiZnAlOx catalysts, Fuel. 188 (2017) 610–620. https://doi.org/10.1016/j.fuel.2016.10.072.

[69] S.K. Chauhan, S. Gangopadhyay, N. Singh, Environmental aspects of biofuels in road transportation, Environ. Chem. Lett. 7 (2009) 289–299. https://doi.org/10.1007/s10311-008-0185-7.

[70] S. Sumrunronnasak, S. Tantayanon, S. Kiatgamolchai, T. Sukonket, Improved hydrogen production from dry reforming reaction using a catalytic packed-bed membrane reactor with Ni-based catalyst and dense PdAgCu alloy membrane, Int. J. Hydrog. Energy. 41 (2016). https://doi.org/10.1016/j.ijhydene.2015.10.129.

[71] H.-G. Park, S. Han, K.-W. Jun, Y. Woo, M.-J. Park, S. Kim, Bench-Scale Steam Reforming of Methane for Hydrogen Production, Catalysts. 9 (2019) 615. https://doi.org/10.3390/catal9070615.

[72] M.A. Soria, C. Mateos-Pedrero, A. Guerrero-Ruiz, I. Rodríguez-Ramos, Thermodynamic and experimental study of combined dry and steam reforming of methane on Ru/ ZrO2-La2O3 catalyst at low temperature, Int. J. Hydrog. Energy. 36 (2011) 15212–15220. https://doi.org/10.1016/j.ijhydene.2011.08.117.

[73] S. Cheng, Y. Liu, B. Xing, X. Qin, C. Zhang, H. Xia, Lead and cadmium clean removal from wastewater by sustainable biochar derived from poplar saw dust, J. Clean. Prod. 314 (2021) 128074. https://doi.org/10.1016/j.jclepro.2021.128074.

[74] M. Meng, W. Meng, S. Cheng, B. Xing, G. Yi, C. Zhang, Effect of pyrolysis temperature on pyrolysis of Camellia oleifera shell, Biomass Convers. Biorefinery. (2022). https://doi.org/10.1007/s13399-022-03317-z.

[75] M. Van de Velden, J. Baeyens, A. Brems, B. Janssens, R. Dewil, Fundamentals, kinetics and endothermicity of the biomass pyrolysis reaction, Renew. Energy. 35 (2010) 232–242. https://doi.org/10.1016/j.renene.2009.04.019.

[76] P. Morf, P. Hasler, T. Nussbaumer, Mechanisms and kinetics of homogeneous secondary reactions of tar from continuous pyrolysis of wood chips, Fuel. 81 (2002) 843–853. https://doi.org/10.1016/S0016-2361(01)00216-2.

[77] J. Zhang, H. Wang, A.K. Dalai, Development of stable bimetallic catalysts for carbon dioxide reforming of methane, J. Catal. 249 (2007) 300–310. https://doi.org/10.1016/j.jcat.2007.05.004.

[78] K. Takanabe, K. Nagaoka, K. Aika, Improved resistance against coke deposition of titania supported cobalt and nickel bimetallic catalysts for carbon dioxide reforming of methane, Catal. Lett. 102 (2005) 153–157. https://doi.org/10.1007/s10562-005-5848-4.

[79] A. Remiro, B. Valle, A.T. Aguayo, J. Bilbao, A.G. Gayubo, Steam Reforming of Raw Bio-oil in a Fluidized Bed Reactor with Prior Separation of Pyrolytic Lignin, Energy Fuels. 27 (2013) 7549–7559. https://doi.org/10.1021/ef401835s.
[80] Y. Li, D. Li, G. Wang, Methane decomposition to COx-free hydrogen and nano-carbon material on group 8–10 base metal catalysts: A review, Catal. Today. 162 (2011) 1–48. https://doi.org/10.1016/j.cattod.2010.12.042.
[81] D. Świerczyński, S. Libs, C. Courson, A. Kiennemann, Steam reforming of tar from a biomass gasification process over Ni/olivine catalyst using toluene as a model compound, Appl. Catal. B Environ. 74 (2007) 211–222. https://doi.org/10.1016/j.apcatb.2007.01.017.
[82] J. Ashok, S. Kawi, Steam reforming of toluene as a biomass tar model compound over CeO2 promoted Ni/CaO–Al2O3 catalytic systems, Int. J. Hydrog. Energy. 38 (2013) 13938–13949. https://doi.org/10.1016/j.ijhydene.2013.08.029.
[83] J. Xu, W. Zhou, Z. Li, J. Wang, J. Ma, Biogas reforming for hydrogen production over a Ni–Co bimetallic catalyst: Effect of operating conditions, Int. J. Hydrog. Energy. 35 (2010) 13013–13020. https://doi.org/10.1016/j.ijhydene.2010.04.075.
[84] X. Xu, E. Jiang, M. Wang, Y. Xu, Dry and steam reforming of biomass pyrolysis gas for rich hydrogen gas, Biomass Bioenergy. 78 (2015) 6–16. https://doi.org/10.1016/j.biombioe.2015.03.015.
[85] M. Usman, W.M.A. Wan Daud, H.F. Abbas, Dry reforming of methane: Influence of process parameters—A review, Renew. Sustain. Energy Rev. 45 (2015) 710–744. https://doi.org/10.1016/j.rser.2015.02.026.
[86] Z. Bao, F. Yu, Chapter Two - Catalytic Conversion of Biogas to Syngas via Dry Reforming Process, in: Y. Li, X. Ge (Eds.), Adv. Bioenergy, Elsevier, 2018: pp. 43–76. https://doi.org/10.1016/bs.aibe.2018.02.002.
[87] N.A.K. Aramouni, J.G. Touma, B.A. Tarboush, J. Zeaiter, M.N. Ahmad, Catalyst design for dry reforming of methane: Analysis review, Renew. Sustain. Energy Rev. 82 (2018) 2570–2585. https://doi.org/10.1016/j.rser.2017.09.076.
[88] L. Wang, D. Li, M. Koike, H. Watanabe, Y. Xu, Y. Nakagawa, K. Tomishige, Catalytic performance and characterization of Ni–Co catalysts for the steam reforming of biomass tar to synthesis gas, Fuel. 112 (2013) 654–661. https://doi.org/10.1016/j.fuel.2012.01.073.
[89] C. Tanios, C. Gennequin, H.L. Tidahy, A. Aboukaïs, E. Abi-Aad, F. Cazier, C. Tanios, M. Labaki, C. Tanios, B. Nsouli, H2 production by dry reforming of biogas over Ni-Co-Mg-Al mixed oxides prepared via hydrotalcite route, in: 2016 7th Int. Renew. Energy Congr. IREC, 2016: pp. 1–6. https://doi.org/10.1109/IREC.2016.7478866.
[90] D. Kunii, T. Chisaki, 3 - Conversion of Solids with Gaseous Reactant, in: D. Kunii, T. Chisaki (Eds.), Rotary React. Eng., Elsevier, Amsterdam, 2008: pp. 27–46. https://doi.org/10.1016/B978-044453026-4.50005-0.
[91] J. Zhao, W. Zhou, J. Ma, Effects of pretreatment on performance and structure of Ni-Co bimetallic catalyst for biogas reforming to hydrogen, Chin. J. Catal. 34 (2013) 1826–1832. https://doi.org/10.1016/S1872-2067(12)60648-2.
[92] M. Abdollahifar, M. Haghighi, A.A. Babaluo, S.K. Talkhoncheh, Sono-synthesis and characterization of bimetallic Ni–Co/Al2O3–MgO nanocatalyst: Effects of metal content on catalytic properties and activity for hydrogen production via CO2 reforming of CH4, Ultrason. Sonochem. 31 (2016) 173–183. https://doi.org/10.1016/j.ultsonch.2015.12.010.
[93] G. Zhou, H. Liu, K. Cui, A. Jia, G. Hu, Z. Jiao, Y. Liu, X. Zhang, Role of surface Ni and Ce species of Ni/CeO2 catalyst in CO2 methanation, Appl. Surf. Sci. 383 (2016) 248–252. https://doi.org/10.1016/j.apsusc.2016.04.180.
[94] P. Dumrongbunditkul, T. Witoon, M. Chareonpanich, T. Mungcharoen, Preparation and characterization of Co–Cu–ZrO2 nanomaterials and their catalytic activity in CO2 methanation, Ceram. Int. 42 (2016) 10444–10451. https://doi.org/10.1016/j.ceramint.2016.03.193.
[95] F. Basile, P. Benito, G. Fornasari, A. Vaccari, Hydrotalcite-type precursors of active catalysts for hydrogen production, Appl. Clay Sci. 1–2 (2010) 250–259. https://doi.org/10.1016/j.clay.2009.11.027.

[96] H. Long, Y. Xu, X. Zhang, S. Hu, S. Shang, Y. Yin, X. Dai, Ni-Co/Mg-Al catalyst derived from hydrotalcite-like compound prepared by plasma for dry reforming of methane, J. Energy Chem. 22 (2013) 733–739. https://doi.org/10.1016/S2095-4956(13)60097-2.

[97] M. Muñoz, S. Moreno, R. Molina, Synthesis of Ce and Pr-promoted Ni and Co catalysts from hydrotalcite type precursors by reconstruction method, Int. J. Hydrog. Energy. 37 (2012) 18827–18842. https://doi.org/10.1016/j.ijhydene.2012.09.132.

[98] D. Homsi, S. Aouad, C. Gennequin, A. Aboukaïs, E. Abi-Aad, A highly reactive and stable Ru/Co6−xMgxAl2 catalyst for hydrogen production via methane steam reforming, Int. J. Hydrog. Energy. 39 (2014). https://doi.org/10.1016/j.ijhydene.2014.04.151.

[99] C.K. Cheng, S.Y. Foo, A.A. Adesina, Carbon deposition on bimetallic Co–Ni/Al2O3 catalyst during steam reforming of glycerol, Catal. Today. 164 (2011) 268–274. https://doi.org/10.1016/j.cattod.2010.10.040.

[100] J. Estephane, S. Aouad, S. Hany, B. El Khoury, C. Gennequin, H. El Zakhem, J. El Nakat, A. Aboukaïs, E. Abi Aad, CO2 reforming of methane over Ni–Co/ZSM5 catalysts. Aging and carbon deposition study, Int. J. Hydrog. Energy. 40 (2015) 9201–9208. https://doi.org/10.1016/j.ijhydene.2015.05.147.

[101] C. Gennequin, M. Safariamin, S. Siffert, A. Aboukaïs, E. Abi-Aad, CO2 reforming of CH4 over Co–Mg–Al mixed oxides prepared via hydrotalcite like precursors, Catal. Today. 176 (2011) 139–143. https://doi.org/10.1016/j.cattod.2011.01.029.

[102] P. Tan, Z. Gao, C. Shen, Y. Du, X. Li, W. Huang, Ni-Mg-Al solid basic layered double oxide catalysts prepared using surfactant-assisted coprecipitation method for CO2 reforming of CH4, Chin. J. Catal. 35 (2014) 1955–1971. https://doi.org/10.1016/S1872-2067(14)60171-6.

[103] V. Chiodo, S. Maisano, G. Zafarana, F. Urbani, Effect of pollutants on biogas steam reforming, Int. J. Hydrog. Energy. (2016). https://doi.org/10.1016/j.ijhydene.2016.07.251.

[104] D. Laprune, C. Theodoridi, A. Tuel, D. Farrusseng, F.C. Meunier, Effect of polyaromatic tars on the activity for methane steam reforming of nickel particles embedded in silicalite-1, Appl. Catal. B Environ. 204 (2017) 515–524. https://doi.org/10.1016/j.apcatb.2016.12.004.

[105] A. Al-Fatesh, Suppression of carbon formation in CH4–CO2 reforming by addition of Sr into bimetallic Ni–Co/γ-Al2O3 catalyst, J. King Saud Univ. - Eng. Sci. 27 (2015) 101–107. https://doi.org/10.1016/j.jksues.2013.09.006.

[106] S.I. Garcés-Polo, J. Villarroel-Rocha, K. Sapag, S.A. Korili, A. Gil, Adsorption of CO2 on mixed oxides derived from hydrotalcites at several temperatures and high pressures, Chem. Eng. J. 332 (2018) 24–32. https://doi.org/10.1016/j.cej.2017.09.056.

[107] C. Gennequin, T. Barakat, H.L. Tidahy, R. Cousin, J.-F. Lamonier, A. Aboukaïs, S. Siffert, Use and observation of the hydrotalcite "memory effect" for VOC oxidation, Catal. Today. 157 (2010) 191–197. https://doi.org/10.1016/j.cattod.2010.03.012.

[108] A. Machocki, T. Ioannides, E. Papadopoulou, B. Banach, Hydrogen-rich gas generation from alcohols over cobalt-based catalysts for fuel cell feeding, Fuel Process. Technol. 148 (2016) 341–349. https://doi.org/10.1016/j.fuproc.2016.03.015.

[109] M. Abou Rjeily, C. Gennequin, H. Pron, E. Abi-Aad, J.H. Randrianalisoa, Chapter 9 - Catalysts for steam reforming of biomass tar and their effects on the products, in: M.R. Cesario, D.A. de Macedo (Eds.), Heterog. Catal., Elsevier, 2022: pp. 249–295. https://doi.org/10.1016/B978-0-323-85612-6.00009-7.

[110] C.B. Grzona, I.D. Lick, E.R. Castellón, M.I. Ponzi, E.N. Ponzi, Cobalt and KNO3 supported on alumina catalysts for diesel soot combustion, Mater. Chem. Phys. 123 (2010) 557–562. https://doi.org/10.1016/j.matchemphys.2010.05.014.

[111] L. Chmielarz, M. Rutkowska, P. Kuśtrowski, M. Drozdek, Z. Piwowarska, B. Dudek, R. Dziembaj, M. Michalik, An influence of thermal treatment conditions of hydrotalcite-like materials on their catalytic activity in the process of N 2 O decomposition, J. Therm. Anal. Calorim. - J THERM ANAL CALORIM. 105 (2011) 161–170. https://doi.org/10.1007/s10973-011-1284-4.

[112] S.-J. Park, M.-K. Seo, Chapter 7 - Types of Composites, in: S.-J. Park, M.-K. Seo (Eds.), Interface Sci. Technol., Elsevier, 2011: pp. 501–629. https://doi.org/10.1016/B978-0-12-375049-5.00007-4.

[113] L. Zhou, Chapter 3 - Fundamentals of Combustion Theory, in: L. Zhou (Ed.), Theory Model. Dispersed Multiph. Turbul. React. Flows, Butterworth-Heinemann, 2018: pp. 15–70. https://doi.org/10.1016/B978-0-12-813465-8.00003-X.
[114] Y. Cui, J. Liang, Z. Wang, X. Zhang, C. Fan, D. Liang, X. Wang, Forward and reverse combustion gasification of coal with production of high-quality syngas in a simulated pilot system for in situ gasification, Appl. Energy. 131 (2014) 9–19. https://doi.org/10.1016/j.apenergy.2014.06.001.
[115] I. Luisetto, S. Tuti, E. Di Bartolomeo, Co and Ni supported on CeO2 as selective bimetallic catalyst for dry reforming of methane, Int. J. Hydrog. Energy. 37 (2012) 15992–15999. https://doi.org/10.1016/j.ijhydene.2012.08.006.
[116] J. Sehested, Four challenges for nickel steam-reforming catalysts, Catal. Today. 111 (2006) 103–110. https://doi.org/10.1016/j.cattod.2005.10.002.
[117] J. Snoeck, G. Froment, Steam/CO2 Reforming of Methane. Carbon Formation and Gasification on Catalysts with Various Potassium Contents, Ind. Eng. Chem. Res. - IND ENG CHEM RES. 41 (2002). https://doi.org/10.1021/ie010665p.
[118] J.R. Rostrup-Nielsen, Production of synthesis gas, Catal. Today. 18 (1993) 305–324. https://doi.org/10.1016/0920-5861(93)80059-A.
[119] K.M. Hardiman, C.G. Cooper, A.A. Adesina, R. Lange, Post-mortem characterization of coke-induced deactivated alumina-supported Co–Ni catalysts, Chem. Eng. Sci. 61 (2006) 2565–2573. https://doi.org/10.1016/j.ces.2005.11.021.
[120] D. Swierczynski, C. Courson, A. Kiennemann, Study of steam reforming of toluene used as model compound of tar produced by biomass gasification, Chem. Eng. Process. Process Intensif. 47 (2008) 508–513. https://doi.org/10.1016/j.cep.2007.01.012.
[121] N. Charisiou, S. Douvartzides, G.I. Siakavelas, L. Tzounis, V. Sebastian, V. Stolojan, S. Hinder, M. Baker, K. Polychronopoulou, M. Goula, The Relationship between Reaction Temperature and Carbon Deposition on Nickel Catalysts Based on Al2O3, ZrO2 or SiO2 Supports during the Biogas Dry Reforming Reaction, Catalysts. 9 (2019) 676. https://doi.org/10.3390/catal9080676.
[122] Z.L. Zhang, X.E. Verykios, Carbon dioxide reforming of methane to synthesis gas over supported Ni catalysts, Catal. Today. 21 (1994) 589–595. https://doi.org/10.1016/0920-5861(94)80183-5.
[123] M.A. Goula, A.A. Lemonidou, A.M. Efstathiou, Characterization of Carbonaceous Species Formed during Reforming of CH4with CO2over Ni/CaO–Al2O3Catalysts Studied by Various Transient Techniques, J. Catal. 161 (1996) 626–640. https://doi.org/10.1006/jcat.1996.0225.
[124] Y. Zhang, W. Wang, Z. Wang, X. Zhou, Z. Wang, C.-J. Liu, Steam reforming of methane over Ni/SiO2 catalyst with enhanced coke resistance at low steam to methane ratio, Catal. Today. 256 (2015) 130–136. https://doi.org/10.1016/j.cattod.2015.01.016.
[125] J. Zhang, F. Li, Coke-resistant Ni@SiO2 catalyst for dry reforming of methane, Appl. Catal. B Environ. 176–177 (2015) 513–521. https://doi.org/10.1016/j.apcatb.2015.04.039.
[126] X. Yu, N. Wang, W. Chu, M. Liu, Carbon dioxide reforming of methane for syngas production over La-promoted NiMgAl catalysts derived from hydrotalcites, Chem. Eng. J. 209 (2012) 623–632. https://doi.org/10.1016/j.cej.2012.08.037.
[127] M.H. Aboonasr Shiraz, M. Rezaei, F. Meshkani, Microemulsion synthesis method for preparation of mesoporous nanocrystalline γ-Al2O3 powders as catalyst carrier for nickel catalyst in dry reforming reaction, Int. J. Hydrog. Energy. 41 (2016) 6353–6361. https://doi.org/10.1016/j.ijhydene.2016.03.017.
[128] J. Ducamp, A. Bengaouer, P. Baurens, I. Fechete, P. Turek, F. Garin, Statu quo sur la méthanation du dioxyde de carbone : une revue de la littérature, Comptes Rendus Chim. 21 (2018) 427–469. https://doi.org/10.1016/j.crci.2017.07.005.
[129] L. da R. Novaes, M.E. Pacheco, V.M.M. Salim, N.S. de Resende, Accelerated deactivation studies of hydrotreating catalysts in pilot unit, Appl. Catal. Gen. 548 (2017) 114–121. https://doi.org/10.1016/j.apcata.2017.06.040.
[130] C.H. Bartholomew, Mechanisms of catalyst deactivation, Appl. Catal. Gen. 212 (2001) 17–60. https://doi.org/10.1016/S0926-860X(00)00843-7.

[131] A. Srinivas, V. Janardhanan, R. Bauri, S. Jayanti, Deactivation and regeneration of Ni catalyst during steam reforming of model biogas: An experimental investigation, Int J Hydrog. Energy. (2013). https://doi.org/10.1016/j.ijhydene.2013.10.056.

[132] J.R. Rostrupnielsen, J.H.B. Hansen, CO2-Reforming of Methane over Transition Metals, J. Catal. 144 (1993) 38–49. https://doi.org/10.1006/jcat.1993.1312.

[133] G. SCACCHI, M. BOUCHY, J.-F. FOUCAUT, O. ZAHRAA, R. FOURNET, Cinétique et catalyse, Lavoisier, 2011. http://www.lavoisier.eu/books/chemistry/cinetique-et-catalyse-2-ed/scacchi/description-9782743013929 (accessed March 25, 2022).

[134] K. Kumbilieva, L. Petrov, Y. Alhamed, A. Alzahrani, Reaction Mechanism and Deactivation Modes of Heterogeneous Catalytic Systems, Chin. J. Catal. 32 (2011) 387–404. https://doi.org/10.1016/S1872-2067(10)60181-7.

[135] Ş. Özkara-Aydınoğlu, Thermodynamic equilibrium analysis of combined carbon dioxide reforming with steam reforming of methane to synthesis gas, Int. J. Hydrog. Energy. 35 (2010) 12821–12828. https://doi.org/10.1016/j.ijhydene.2010.08.134.

[136] B. Abdullah, N.A. Abd Ghani, D.-V.N. Vo, Recent advances in dry reforming of methane over Ni-based catalysts, J. Clean. Prod. 162 (2017) 170–185. https://doi.org/10.1016/j.jclepro.2017.05.176.

[137] P. Marecot, S. Peyrovi, D. Bahloul, J. Barbier, Regeneration by hydrogen treatment of bifunctional catalysts deactivated by coke deposition I. Regeneration of precoked catalysts, (n.d.) 10.

[138] R. Koc, E. Alper, E. Croiset, A. Elkamel, Partial Regeneration of Ni-Based Catalysts for Hydrogen Production via Methane Cracking, (2017) 157–168. https://dergipark.org.tr/tr/download/article-file/123826.

[139] B. Rego de Vasconcelos, D. Pham Minh, P. Sharrock, A. Nzihou, Regeneration study of Ni/hydroxyapatite spent catalyst from dry reforming, Catal. Today. 310 (2018) 107–115. https://doi.org/10.1016/j.cattod.2017.05.092.

Chapter 4: Syngas Production by Catalytic Reforming of Biomass Pyrolysis Volatiles Over Supported Catalysts: Effects of Operating Parameters

Résumé

Ce chapitre est issu dans son intégralité du manuscrit en cours de finalisation pour soumission dans le journal « Energy and Fuels ».

Dans ce chapitre, le procédé couplé de pyrolyse et de reformage est exploité pour valider sa compatibilité et son efficacité avec une biomasse différente et un autre type de catalyseurs. Pour cela, les anas de lin, matériaux abondants dans le nord de la France et peu valorisés, ont été sélectionnés comme échantillon de biomasse, tandis que des catalyseurs de Nickel, de Cobalt et de Cobalt-Nickel supportés sur des billes d'alumine (Al_2O_3) ont été choisis pour le reformage catalytique.

Le même dispositif précédemment décrit au chapitre 3 a été utilisé et par conséquent, sa description sera brève dans ce chapitre. Pour la pyrolyse des anas de lin, plusieurs températures, vitesses de chauffe et débits d'azote ont été testés. Cela a permis de déterminer les conditions opératoires suivantes qui maximisent la production de gaz : température de 700°C, vitesse de chauffe de 80°C/min et débit d'azote (le gaz vecteur) de 25 mL/min. La pyrolyse d'anas de lin a donc été réalisée dans ces conditions pour analyser ses produits et déterminer la concentration des composés volatils créés qui seront envoyés pour le reformage. Le réacteur de reformage utilisé avec les catalyseurs supportés est un tube de quartz en forme de U également mais ayant une hauteur totale de 30 cm et deux côtés de diamètres intérieurs différents (0,6 et 2,2 cm). Le catalyseur est introduit sur le support en quartz fritté placé au fond du côté le plus large du réacteur en U. Le reformage est aussi qualifié d'"hybride" dans ce chapitre, et il est réalisé sans une alimentation externe de vapeur d'eau. De nombreux paramètres opératoires ont été variés et leurs effets ont été étudiés sur les principaux produits, les concentrations de gaz majeurs et le gaz de synthèse, en particulier.

Dans un premier temps, trois types de phase active de catalyseurs ont été testés : Cobalt, Nickel et Cobalt-Nickel pour réaliser le reformage à 800°C. Il a été constaté que le catalyseur à base de nickel était le plus performant parmi les trois catalyseurs, notamment en ce qui concerne le rendement en gaz de synthèse et le reformage du méthane. Le catalyseur à base de Co s'est révélé être le moins performant tandis que le Co-Ni a eu une activité intermédiaire. Le nickel a donc été adopté pour la suite des expérimentations.

En second lieu, la charge métallique de Ni sur les billes d'alumine a été modifiée de 0 à 25% avec un incrément de 5%. L'augmentation de la charge métallique à 20% a considérablement amélioré la production de gaz, en particulier le gaz de synthèse, a augmenté la conversion de la bio-huile et a réduit les émissions de CH_4 et de CO_2. Cependant, une augmentation supplémentaire de la charge de Ni au-delà de 20% a eu des effets opposés et par conséquent, la valeur de 20% de Ni a été considérée comme la charge métallique optimale pour un reformage catalytique efficace sur ce type de support.

La température de reformage a ensuite été modifiée de 650°C à 800°C avec une incrémentation de 50°C tout en gardant la température de pyrolyse à 700°C. L'augmentation de la température a tendance à produire plus de gaz avec une augmentation marquée de H_2 et de CO, et à améliorer les conversions de la bio-huile, de CH_4 et de CO_2. Une quantité maximale de gaz de synthèse d'une valeur de 22,55 mmol/g de biomasse sèche a été atteinte avec 20% de Ni et une température de 800°C. Néanmoins, atteindre cette température peut s'avérer fortement énergivore avec un impact économique important. Par conséquent, une température de 750°C, permettant une efficacité satisfaisante a été sélectionnée.

Par la suite, l'impact de la vitesse spatiale horaire du gaz (VSHG) a été étudié en changeant la hauteur du lit de catalyseur, ce qui a conduit à une variation de la VSHG de 900 à 4500 h^{-1}. L'augmentation de la VSHG de 1125 à 4500 h^{-1} a eu un impact positif, bien que relativement faible, sur la distribution des produits permettant une augmentation de la production de gaz et la diminution de celle de la bio-huile. Cependant, les concentrations de gaz de synthèse et les conversions de CH_4 et de CO_2 ont chuté. Il est important de noter que la valeur la plus basse du VSHG, 900 h^{-1}, a eu l'impact le plus prononcé où les concentrations de gaz, et en particulier celles de synthèse, et les taux de conversions de réactifs les plus élevés ont été atteints. Néanmoins, travailler avec un VSHG aussi faible entraîne la consommation d'une grande quantité de catalyseur, ce qui peut être économiquement peu rentable à grande échelle. Par conséquent, une valeur de VSHG autour de 4500 h^{-1} est considérée comme satisfaisante.

Enfin, un test de vieillissement du catalyseur a été réalisé sur le catalyseur à 20% de Ni avec un reformage à 750°C sur cinq cycles consécutifs. Il a révélé une baisse de l'activité du catalyseur du cycle 1 au cycle 3, avec une diminution de la formation des gaz et des taux de conversion. Il est intéressant de noter que l'activité du catalyseur a été restaurée à la fin du troisième cycle entrainant une amélioration des concentrations de gaz et de la conversion de la bio-huile au quatrième cycle, suivie d'une stabilisation au cours du cinquième cycle.

Des tests analytiques ont été effectués sur les catalyseurs avant et après reformage afin de les caractériser. Ils comprennent la détermination de la surface spécifique des catalyseurs, du volume total des pores et du diamètre des pores, ainsi que la réalisation d'images MEB avec cartographie chimique EDX et de courbes d'ATG. Ils ont démontré qu'une couche de carbone s'était déposée sur la surface du catalyseur, ce qui se traduit par une diminution de la surface spécifique et du volume des pores et une augmentation du diamètre des pores à cause du frittage du catalyseur. Les images MEB ont également montré la formation de carbone filamenteux qui est l'un des types de carbone les plus défavorables pour le reformage en réduisant considérablement la performance du catalyseur. Les courbes d'ATG ont confirmé ces observations et ont aidé à quantifier la quantité de carbone déposée qui était de 9% sur le catalyseur 20% Ni après le reformage à 700°C et réduite à 6% lorsque la température de reformage a été augmentée à 800°C.

Pour permettre un meilleur référencement, les équations des réactions de pyrolyse et de reformage sont rementionnées aussi dans ce chapitre puisqu'elles sont cruciales pour les interprétations et les explications des résultats.

4.1. Introduction

Syngas is a gas mixture consisting primarily of hydrogen (H_2), carbon monoxide (CO), and some carbon dioxide (CO_2). It can be used as feedstock or as an intermediate for the production of solvents, fertilizers, pharmaceutical, chemicals or chemical intermediates (NH_3, CH_3OH…) and plastics [1]. A particular syngas ratio is needed in practice for the divers subsequent applications of the production process [2]. For instance, for the synthesis of methanol, a suitable H_2/CO ratio is 2:1. Whereas an H_2/CO ratio between 0.3 and 4 is required for an effective Fischer-Tropsch process [3,4]. Syngas can be produced from multiple raw materials, conventionally divided into three main classes depending on their existing states: solid (biomass, petroleum coke, coal …), liquid (oil) and gaseous (natural gases). These products are then consumed as feedstock for several processes for the syngas production, including endothermic steam gasification, exothermic oxidation reaction, oxidative steam reforming or steam reforming [1].

The hydrogen role as a medium for energy storage has been increasingly acknowledged in order to balance the power systems, especially with the increase in the introduction of electricity generated from renewable and sustainable energy sources (solar, wind…) [5]. "Green hydrogen" refers in general to the hydrogen produced based on renewable energy sources, without an universally admitted definition [6]. Nevertheless, the global hydrogen production using the renewable energy sources remains mediocre where it stabilized around 0.36 MT per year between 2015 and 2019 [7].

For the hydrogen production, the most widespread method applied nowadays is the steam reforming of fossil fuels or natural gas [8]. Currently, 96% of the hydrogen produced derive from fossil fuels including coal, petroleum products and natural gas [9]. Moreover, partial oxidation and pyrolysis of fossil fuels are also applied to generate hydrogen, but also produce large quantities of carbon dioxide CO_2 [10]. Nevertheless, a more promising technology for the hydrogen production for the long term is based on biomass derivatives or renewable sources. Relying on waste organic materials for the production of syngas is an eco-friendly approach since it helps reducing the organic content in the waste products as well as minimizing the greenhouse gases emissions [8]. If biomass is used to generate hydrogen, it is labeled as "green hydrogen" since the CO_2 emitted by the process is considered almost compensated by the quantity of CO_2 absorbed by the biomass during its growth [10].

Therefore, realizing a two-stage process where the biomass pyrolysis takes place in the first stage and the catalytic reforming of the pyrolysis volatile hydrocarbons in a second one, presents itself as a viable solution to produce syngas, in particular hydrogen, while valorizing the biomass and reducing the CO_2 emissions [11,12]. In fact, two categories of reforming prevail: dry and steam reforming. The dry reforming is the reaction of carbon dioxide with hydrocarbons to generate syngas while the steam reforming involves operating with water vapor [13–15]. Thereby, the dry reforming allows on one side the consumption of the CO_2 emitted by the pyrolysis and on the other side enables the cracking and transformation of the heavy hydrocarbons forming the pyrolysis tar, into high added value products such as the

syngas. This approach can be regarded as a purification method of the pyrolysis tar [16] while producing hydrogen, among other valuable compounds. On the other hand, the catalytic steam reforming is regarded as an efficient strategy for the tar removal from the gas thereby elevating the degree of purity of the gas and increasing its heating value, simultaneously [17,18]. This process uses steam to oxidize the tar species into useful products (mainly syngas). The catalyst's presence enables the tar removal at relatively inferior temperatures than those required for the non-catalytic bio-oil conversion [16]. Furthermore, the gas derived from the catalytic reforming following the pyrolysis, can be used for hydrogen production or even as a direct feedstock for fuel cells [19]. In addition to the syngas and up-graded tar, this process allows the co-production of char which allows its valorization into biodiesel [20], solid fuel, adsorbent [21], fertilizers [22], activated carbon or catalyst support [12,23], in contrast to the gasification which produces mainly syngas.

For an efficient catalytic tar reforming, multiple catalysts can be employed naming natural minerals, alkaline earth and metal catalysts [15]. Among the metals, noble metals such as rhodium, ruthenium and palladium demonstrate a considerable activity with durable stability and high carbon deposition resistance. But noble metals are rarely employed at the large-scale tar reforming due to their expensiveness [24]. Base metals like nickel Ni, cobalt Co and iron Fe or their combination forming the transition metals, exhibit remarkable activities and are more widely used given their large availability and accessibility [12,24]. Ni-based catalysts with 10 to 20 wt.% loadings are the most broadly adopted catalysts for the steam and dry reforming of tar, thanks to their elevated efficiency and selectivity for the syngas production [25], due to their capacity of rupturing the C−C and O−H bonds [16]. Unfortunately, these catalysts are subject to carbon deposition over their surfaces and sintering of the metal phase leading to their partial deactivation [14,26].

The catalyst support plays a crucial role in dispersing the catalyst, providing acidic and basic centers as well as oxygen vacancies and enhancing the catalyst activity [11,27]. Alumina Al_2O_3 has been extensively used as Nickel-based support for tar reforming given its availability, thermomechanical strength, physical/chemical stability and high ability for metal dispersion given its high surface area [28]. Nonetheless, alumina can also suffer from sintering and carbon deposition when it is used alone as support due to it mild acidity [26,29,30]. Minimizing the deactivation of the catalyst can be realized following multiple strategies suggested in the literature. They include adjusting the process configuration into one or two stages [31], optimizing the operational parameters (temperature, steam to carbon ratio or the gas hourly space velocity) [32,33] as well as ameliorating the catalyst stability and selectivity by adjusting the nickel metal loading or using additives [34].

Pre-treatment steps of oxidation and reduction were applied on all the catalysts used. These steps have frequently been applied to modify the catalyst's structure[35] thereby enhancing its activity [35,36]. The oxidation pretreatment using air is an efficient pretreatment which provides a cleaner catalyst surface [37]. The reduction pretreatment with H_2 has also been proven effective to improve the catalytic activity due to the cleaning of the catalyst's surface [38]. In addition, the combination of the reduction and oxidation processes as a pretreatment steps was demonstrated to reconstruct the catalyst's surface creating a catalyst with a higher activity [35,39]. Therefore, the performance of the metal oxide catalyst is greatly affected by the oxidation reduction pretreatment steps [36].

To realize the pyrolysis, flax shives are used as the biomass to be valorized. Shives are the vascular tissues of the flax plant. The linen textile culture produces at the same time the tall fibers and the shives. The tall fiber is particularly demanded by the textile industry for its comfort and lightness. Whereas the flax shives are used in chipboard panels, for animal bedding (equine), as horticultural mulch or even as fuel. These applications have very low added value (0.15 euros/kg) [40]. The production of linen textiles is majorly localized (80%) in the North of France in the regions situated along La Manche, from Normandy to the Netherlands. 50% of the cultured surface of Normandy is devoted for flax, making France a world leader in the production of linen textile. Some research works determined their composition, most commonly by sequential extraction [41–43]. The main compound of the flax shives is cellulose (34-53 %), along with lignin (23-31%), hemicellulose (13-26%), as well as other minor compounds such as ashes, wax, and easily extractable phenolic compounds [44], but the composition might be different accordingly to the plant's age [45]. Flax shives were the subject of very few scientific studies. Thereby, it would be of great interest to valorize this biomass into high added value products.

In this work, the syngas production will be realized through a two-stage process consisting of a reactor for the biomass pyrolysis and a second for the catalytic reforming of the pyrolysis volatile products. The process is termed hybrid reforming since it combines both the steam and dry reforming where the water vapor and the CO_2 produced by the pyrolysis in the first stage react with the bio-oil hydrocarbons reformed in the second stage. In this purpose, alumina Al_2O_3 beads are used as support for three catalysts Nickel, Cobalt and Cobalt-Nickel for the catalytic reforming. To favorize the gases formation, hydrogen in particular, high pyrolysis and reforming temperatures should be imposed, with a high heating rate and long volatiles residence time [46–48], which will be applied in this work. Even though the valorization of the co-products (char and bio-oil) is not the main objective of this work, the elemental composition of the char formed by the pyrolysis, and the chemical composition of the bio-oil produced before and after the reforming were analyzed. Several reforming parameters were varied, including catalyst active phase type, catalytic metal loading, reforming temperature, and gas hourly space velocity (GHSV). Their effects were examined over the main products distribution, the gases composition as well as the conversion rates of the main reactants and the syngas concentrations. The catalysts are characterized pre and post reforming to evaluate the carbon deposition, by determining their physical properties as well as by realizing Scanning Electron Microscopy (SEM) images, Energy-dispersive X-ray (EDX) spectroscopy mapping and thermogravimetric analysis (TGA).

4.2. Materials and methods

4.2.1. Characterization of biomass

Flax shives are used as the biomass to be valorized. The elemental analysis of the flax shives and the char produced is determined using a CHNS/O Thermo Electron Flash. 1mg of the grinded sample was weighed in a silver capsule (for oxygen) or a tin capsule (for carbon, hydrogen, and nitrogen). The capsules were pyrolyzed at 1000°C in a vertical combustion tube. The elements formed are separated on a poraplot Q column and detected using a TCD (thermal conductivity detector). The analyses are realized in three replicates and the average values as well as the corresponding uncertainties will be presented in the results section**.** More details on the protocol followed can be found in our previous work [46].

To determine the moisture content of the flax shives, a sample of 3.5g was dried for 1h at 100°C in the pyrolysis reactor. The moisture content was evaluated as the difference between the initial weight of the raw flax shives (i.e. as received) and their final dry weight. The experiment was repeated five times to ensure the repeatability and the average moisture content was found to be 8.16 wt.%. Three main physical characteristics of the flax shives were determined and listed in the **Table 4.1**. A micrometer was used to assess the thickness of the flax shives. A Vernier caliper was utilized to quantify the characteristic length. A Gay-Lussac pycnometer with a volume capacity precisely determined by the manufacturer to be 25.053 mL, was used to determine the density of the flax shives.

Table 4.1 Physical characteristics of the flax shives

Physical characteristics	**Thickness (mm)**	**Characteristic length (mm)**	**Density (kg/m^3)**
Value	0.20 – 2.4	0.5 – 1.5	537

4.2.2. Bio-oil chemical composition

A gas chromatography/mass spectrometry (GC/MS/MS Varian 1200 Single Quadrupole with Varian CP 3800 GC) is used to analyze the chemical composition of the bio-oil derived from the biomass pyrolysis experiments at 400°C and 700°C as well as from the coupling of the biomass pyrolysis at 700°C and the catalytic reforming at 800°C with 20%Ni/Al_2O_3. The nitrogen flowrate applied for these tests was 25 mL_n/min (normal millimeter per minute defined at 0°C and 1 atm). The pyrolysis temperature is reached at 80°C/min heating rate. The bio-oil was obtained by condensing the volatiles produced in 100 mL of pure acetone filled in an ice-cooled beaker placed at the exit of the pyrolysis or the reforming reactors. The bio-oil consists of more than 300 species belonging to several chemical groups. The major ones produced by our process were identified and quantified in terms of µg/mL and were grouped into four main categories: BTEX (benzene, toluene, ethylbenzene and xylene), PAHs (polycyclic aromatic hydrocarbons), phenols and others. The details of the methods followed for the analysis of the bio-oil are explained in our previous work [46].

4.2.3. Catalyst's synthesis

An optimized protocol was established for the preparation of the nickel, cobalt and nickel-cobalt catalysts supported on γ-Al_2O_3 (alumina) beads. The wet impregnation method was used for the synthesis of these catalysts. Specific quantities of cobalt ($Co(NO_3)_2.6H_2O$, 97.7%, Alfa Aesar) and nickel ($Ni(NO_3)_2.6H_2O$, 98%, Alfa Aesar) nitrates were dissolved in a solution of pure ethanol (Carlo Erbe) at ambient temperature. 10g of 1.6 mm γ-Al_2O_3 beads (Strem Chemicals) are added to the ethanol solution and mixed at 40°C in a rotary evaporator (BUCHI B-300 Base) at atmospheric pressure for 24 h at 150 rpm (rotation per minute). After the impregnation step, the solvent is slowly evaporated at 40°C, 150 rpm and 150 mBar. The beads are then dried at 60°C for 24h in a fixed oven. The calcination step takes place at 800°C, reached at a heating rate of 1°C.min^{-1}, for 4 h in a Nabertherm muffle furnace. Therefore, three classes of catalysts were prepared: 10% Cobalt, 10% Cobalt-Nickel (Ratio of Cobalt/Nickel equals 1) and Nickel with metal loading ranging between 5 to 25%.

4.2.4. Characterization of the fresh and spent catalysts

4.2.4.1. Porosity and BET surface area (nitrogen adsorption-desorption)

In order to characterize the freshly synthesized and the spent catalyst beads by determining their catalytic surface area as well as their porosity, the nitrogen adsorption-desorption method was applied. The samples were first pretreated at 90°C for 1h under vacuum then at 350°C for 4h in order to clean the impurities and water molecules accumulated at ambient temperature over the sample's surface. A Micrometrics 3 flex surface characterization analyzer (Micrometrics, Norcoss, GA, USA, 3 Flex Version 5.03) was used to carry out the measurements over 150 mg of the catalyst sample. The static volumetric method is used by the Accelerated Surface Area and Porosimetry (ASAP) to evaluate the catalyst surface area while using nitrogen physisorption isotherms at −196°C. The instrument records the volume of the nitrogen absorbed and draws the adsorption and desorption curves. The BET (Brunauer–Emmett–Teller) surface area can then be calculated in function of the experimental data collected. The pore volume is determined based on the single point desorption total pore volume of pores less than 40.3122 nm width at p/p° = 0.95. The pore diameter is given as the average pore width of the majority of the pores on the BJH (Barrett, Joyner and Halenda) desorption curves.

4.2.4.2. Scanning Electron Microscopy and Energy-dispersive X-ray spectroscopy

Scanning Electron Microscopy (SEM) micrographs were realized for some of the fresh and spent beads catalysts using a microscope JEOL, JSM-7900F, with a low vacuum mode for sample insulation and a LED detector. The accelerating voltage is set to 10kV, the working distance is varied from 4 mm to 10 mm, to modify the quality of the images. Different magnifications were applied to have distinct imaging scales (10,000 and 50,000 times). It should be noted that for each catalyst, one bead was selected randomly to be examined as a representative of the corresponding catalyst's sample. At a magnification of 60 times, the average diameter of the beads before and after reforming was approximated which allows the estimation of the thickness of the carbon layer. The SEM is coupled to an Energy-dispersive X-ray spectroscopy (EDX) detector which allows an elemental mapping. It provides the elemental composition of the sample analyzed which allows the identification of the carbon deposition over the catalyst surface. The working distance is set at 10 mm for the EDX elemental mapping.

4.2.4.3. Thermogravimetry Analysis

NETZSCH TG 209 F3 Tarsus apparatus was employed for the Thermogravimetry Analysis (TGA). It is equipped with a microbalance with a 0.1µg resolution for the thermogravimetry analyses. The catalyst sample of around 20 mg was heated in an alumina crucible at a 5°C/min heating rate from room temperature to 922°C under air flow rate (1.2 bar pressure). This allowed the removal of the carbon deposited over the catalyst surface by oxidation under air.

4.2.5. Pyrolysis-catalytic reforming process

The same experimental methodology applied previously for the pyrolysis coupled to the catalytic reforming was also adopted here. A schematic of the experimental set up is given in **Figure 4.1** showing the two-stage reactor system. The first reactor is devoted for the biomass pyrolysis while the second one is for the volatiles catalytic reforming. The pyrolysis reactor and furnace as well as the reforming furnace are the same ones used in the previous chapters and were described earlier. The reforming reactor is changed to a quartz tube in the shape of U having a total height of 30 cm and two sides with different inner diameters (0.6 and 2.2 cm), resulting in a total inner volume of 88.3 cm^3. The catalyst is introduced over the sintered quartz support placed at the bottom of the larger side of the U-tube reactor.

3.5 g of flax shives were fed in a nickel porous basket and introduced at the top of the pyrolysis furnace. First, the flax shives were dried at 100°C for 1h under 50 mL_n/min of nitrogen flow rate (99.996% purity), creating an inert atmosphere. The reforming reactor was simultaneously heated to attain the reforming temperature desired (800°C). Then, the pyrolysis reactor was heated at 80°C/min heating rate to 700°C, maintained for 2 h under a nitrogen flow rate of 25 mL_n/min. Other operating conditions for the pyrolysis were tested as well, including a 50 mL_n/min of nitrogen flow rate for a temperature of 700°C as well as a temperature of 400°C with a heating rate of 30°C/min and a nitrogen flow rate of 300 mL_n/min. The volatiles produced by the biomass pyrolysis are continuously fed to the reforming reactor preheated at 800°C and containing the catalyst. This is regarded as a hybrid reforming process where the CO_2 and water vapor produced by the pyrolysis are consumed for the dry and steam reforming. The average volatiles residence time in the pyrolysis reactor was estimated to be around 400 s while in the reforming reactor it was found to be around 128 s. The remaining parts of the experimental setup are unchanged with their description given in chapter **2 subsection 2.2.2** and **chapter 3 subsection 3.2.3**.

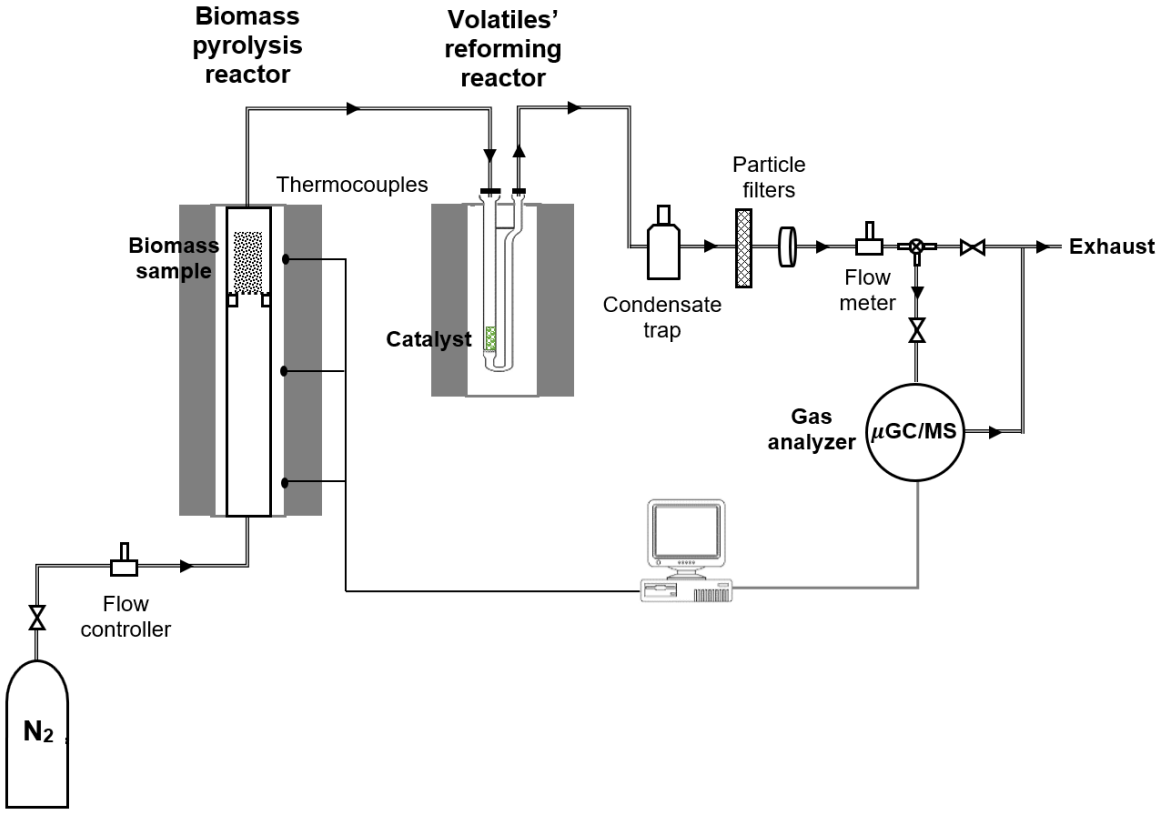

Figure 4.1 Schematic of the experimental set up used for the pyrolysis coupled in-line with the catalytic reforming. It consists of a two-stage reactor with the first one devoted for the biomass pyrolysis and the second one is for the catalytic reforming of the pyrolysis volatiles

A one-stage pyrolysis was realized under the same conditions stated previously (700°C, 80°C/min and 25 mL_n/min) and the gases produced were analyzed, which gives the composition of the volatiles eventually fed to the reforming reactor. These concentrations will be used to evaluate the efficiency of the reforming step. The catalysts were pretreated by applying oxidation and reduction steps prior to the reforming. For the first step of oxidation, an air flow rate of 30 mL_n/min (normal millimeter per minute defined at 0°C and 1 atm) was applied during 1 h over the catalyst heated from ambient temperature to 800°C. Next, a purge step was applied

using 50 mL_n/min of nitrogen flow rate for 30 min with the temperature maintained at 800°C. Then, the reduction of the catalyst is realized by injecting 50 mL_n/min flow rate of a mixture of 10% hydrogen and 90% nitrogen, for 1.5 h at 800°C.

The stability of the catalyst was studied by realizing an aging test over five consecutives experiences. The first one follows the same protocol described previously. The catalyst chosen for the test was the 20% Ni/Al_2O_3 with a GHSV of 4500 h^{-1} and it was pretreated at 800°C by the oxidation and reduction steps previously introduced. The pyrolysis temperature was set to 700°C, while the reforming was realized at 750°C (chosen as an intermediate reforming temperature) with 25 mL_n/min of nitrogen flow rate to realize a hybrid dry reforming (without an external steam feed). This experiment is labeled cycle 1. For the following experiments, the spent catalyst obtained after cycle 1 is used without renewal and without the pretreatment steps, applying the same operating conditions as cycle 1. This test was repeated four times and the experiments are then numbered from cycle 2 to cycle 5. The catalyst was then operated for 5 consecutive cycles for a total of 10 hours of reforming.

4.3. Theory/Calculation

4.3.1. Pyrolysis and reforming reactions

During the pyrolysis, several reactions can take place simultaneously during the thermal decomposition of the feedstock [50]. Describing these reactions involves setting up models which cite the detailed reactions of the disintegration of the biomass main components as was done by the models of Ranzi [51] and Di Blasi [52,53]. Not being the main objective of this work, a single simplified reaction can be used to describe the biomass pyrolysis consisting on the decomposition of the biomass to char (solid), hydrocarbon volatiles (condensable into the bio-oil) and the incondensable gases (H_2, CO, CO_2 …) [54], as given by equation **(4.1)**.

Biomass pyrolysis: $\text{Biomass} \rightarrow \text{char} + \text{hydrocarbon volatiles} + H_2 + CO + CO_2 + H_2O$ **(4.1)**

The steam reforming reactions are detailed in equations **(4.2**), **(4.3**) and **(4.4**), and the dry reforming in equations **(4.5**), **(4.6**) and **(4.7**) with hydrogen enriched syngas as main product [14,15,54,55].

Steam tar reforming: $C_xH_yO_z(\text{tar}) + (x-z)H_2O \rightarrow \left(x + \frac{y}{2} - z\right)H_2 + xCO \qquad \Delta H > 0$ **(4.2)**

Hydrocarbon volatiles steam reforming: $C_mH_n + mH_2O \rightarrow (m + \frac{n}{2})H_2 + mCO \qquad \Delta H > 0$ **(4.3)**

Steam reforming of methane SRM: $CH_4 + H_2O \leftrightarrow 3H_2 + CO \;\; \Delta H°_{298K} = +205.9\ \text{kJ/mol}$ **(4.4)**

Dry tar reforming: $C_xH_yO_z(\text{tar}) + (x-z)CO_2 \rightarrow \frac{y}{2}H_2 + (2x-z)CO \qquad \Delta H > 0$ **(4.5)**

Hydrocarbon volatiles dry reforming: $C_mH_n + mCO_2 \rightarrow \frac{n}{2}H_2 + 2mCO \qquad \Delta H > 0$ **(4.6)**

Dry reforming of methane: $CH_4 + CO_2 \leftrightarrow 2H_2 + 2CO \qquad \Delta H°_{298K} = +247\ \text{kJ/mol}$ **(4.7)**

The endothermic nature of the reforming reactions leaves space for numerous secondary reactions to occur simultaneously [14,15,54,55] given in equations **(4.8**) to **(4.14**). Thereby, the generally products formed during the reforming process will result from the combination of these different competing reactions. The endothermic nature of the reforming reactions would imply operating at excessively high temperatures. The addition of a catalyst to the process aims to reduce significantly the operating temperatures and increase the process feasibility.

Nevertheless, the catalytic reforming process endures a major drawback where the catalyst suffers from partial deactivation resulting from the carbon deposition over its surface due to several reactions such as Boudouard (equation **(4.10)**), the reverse water-gas (equation **(4.11)**) and the tar decomposition (equation **(4.13)**) [59].

Water-gas shift reaction WGSR: $CO + H_2O \leftrightarrow H_2 + CO_2$ $\Delta H°_{298K} = -41.1 kJ/mol$ **(4.8)**

Reverse WGSR: $H_2 + CO_2 \leftrightarrow CO + H_2O$ $\Delta H°_{298K} = +41.1 kJ/mol$ **(4.9)**

Boudouard reaction: $2CO \leftrightarrow CO_2 + C$ $\Delta H°_{298K} = -172\ kJ/mol$ **(4.10)**

Reverse water-gas reaction: $CO + H_2 \rightarrow H_2O + C$ $\Delta H°_{298K} = -131 kJ/mol$ **(4.11)**

Thermal tar cracking: $pC_nH_x(tar) \rightarrow qC_mH_y(\text{smaller tar}) + rH_2$ $\Delta H > 0$ **(4.12)**

Tar decomposition: $C_nH_x(tar) \rightarrow \text{coke precursors (aromatics + olefins)} \rightarrow nC + \left(\frac{x}{2}\right)H_2$ $\Delta H > 0$ **(4.13)**

Hydrocarbons (HC) steam reforming: $HC + H_2O \rightarrow H_2 + CO + CO_2$ $\Delta H > 0$ **(4.14)**

4.3.2. Characteristic parameters

4.3.2.1. Global mass balance

The relative humidity of the flax shives was previously determined to be approximately 8.16wt.% which allows the calculation of the dry biomass weight. The concentrations of the gases, bio-oil and char produced by the process were determined after realizing a global mass balance as described in chapter **2 subsection 2.2.2**. The equations used for the different concentrations' calculations can be found in our previous published work [46].

4.3.2.2. Conversion rates and syngas concentration

The main reactants involved in our reforming process are the CO_2, CH_4 and bio-oil and their conversion rates are evaluated according to equations **(4.15)**-**(4.17)**, respectively, with X referring to the conversion rate. The inlet of the reforming process is the volatiles stream derived from the first pyrolysis reactor and referred to by "pyrolysis". The outlet of the process is the stream of volatiles produced by the pyrolysis coupled to the reforming process labeled as "pyrolysis/reforming" in the equations.

$$\text{Conversion rate of } CO_2 \left(X_{CO_2}\right)(\%) = \frac{\text{moles of } CO_2(\text{pyrolysis}) - \text{moles of } CO_2(\text{pyrolysis/reforming})}{\text{moles of } CO_2(\text{pyrolysis})} \times 100 \quad \textbf{(4.15)}$$

$$\text{Conversion rate of } CH_4 \left(X_{CH_4}\right)(\%) = \frac{\text{moles of } CH_4(\text{pyrolysis}) - \text{moles of } CH_4(\text{pyrolysis/reforming})}{\text{moles of } CH_4(\text{pyrolysis})} \times 100 \quad \textbf{(4.16)}$$

$$\text{Conversion rate of bio} - \text{oil } (X_{bio-oil})(\%) = \frac{\text{moles of bio} - \text{oil(pyrolysis)} - \text{moles of bio} - \text{oil (pyrolysis/reforming)}}{\text{moles of bio} - \text{oil(pyrolysis)}} \times 100 \quad \textbf{(4.17)}$$

The syngas concentration is determined in terms of mmol/g dry biomass (equation **(4.18)**) along with the hydrogen to carbon monoxide (H_2/CO) ratio (equation **(4.19)**).

$$\text{Syngas concentration } (H_2 + CO)\ (\text{mmol/g dry biomass}) = \frac{\text{number of moles of } H_2 + \text{number of moles of } CO}{\text{dry weight of biomass}} \quad \textbf{(4.18)}$$

$$\text{Ratio } H_2/CO = \frac{\text{number of moles of } H_2}{\text{number of moles of } CO} \quad \textbf{(4.19)}$$

4.3.2.3. GHSV

The gas hourly space velocity was determined for the supported catalysts used by applying the equation **(4.20)**):

$$\text{GHSV } (h^{-1}) = \frac{N_2 \text{ flow rate}}{\text{Volume of catalytic bed}} = \frac{N_2 \text{ flow rate}}{\text{Height of catalytic bed} \times \text{Reactor's surface}} \quad \textbf{(4.20)}$$

The flow rate of nitrogen, used as carrier gas, was fixed at 25 mL_n/min for all the experiments. The internal diameter of the reforming reactor was 0.022 m. The height of the catalytic bed was varied from 1.6 mm to 8 mm, corresponding to a catalyst weight going from 0.32 g to 1.7g. The void fraction between the catalyst beads is assumed to be 0.55 maximum [60]. Therefore, the GHSV was modified from 900 h^{-1} to 4500 h^{-1} as given in **Table 4.2**.

Table 4.2 Variation of the GHSV in function of the catalyst height in the reactor

Catalyst height (mm)	GHSV (h^{-1})
1.6	4500
3.2	2250
6.4	1125
8	900

4.4. Results and discussion

4.4.1. Characterization of biomass

The elemental analysis of the flax shives char produced by few pyrolysis experiments realized at different operating conditions is given in the **Table 4.3**. Compared to the elemental analysis of the initial flax shives given in the first raw, it can be noticed that with the pyrolysis realized at 400°C, the carbon content of char passes to 75.16% from 46.09% in the initial flax shives, while the hydrogen decreases from 6.07% to 3.97%. As the temperature of the pyrolysis rises from 400°C to 700°C, the carbon content in the char augments whereas the hydrogen and the oxygen decreases. The content of the other elements increases. These observations are associated with the decomposition of the initial biomass which releases a significant quantity of gases and volatiles such as H_2, CH_4, C_2H_4, C_2H_6 among others, which explains the drop in the hydrogen content in the solid residue. In addition, the increase of the temperature leads to a huge drop in the CO_2 concentration produced by the pyrolysis in contrast to the small increase in the CO [46], which shift the total balance of carbon towards its appearance in the char formed. Similar results were obtained in our previous work on the pyrolysis of oak wood chips [46]. Fixing the pyrolysis temperature at 700°C while increasing the volatiles residence time from 225 s to 400 s, had a smaller impact on the char elemental composition where the carbon slightly increased, while the hydrogen and the oxygen faintly decreased. *Nonetheless, the pyrolysis at 700°C, with a heating rate of 80°C/min and a residence time of 400 s corresponding to a*

nitrogen flow rate of 25 mL_n/min, produced the highest gases and bio-oil concentrations, which are needed for the subsequent reforming step and are therefore the optimal operating conditions chosen for the pyrolysis.

Table 4.3 Elemental analysis of char produced by some pyrolysis experiments

Temperature (°C)	Heating rate (°C/min)	Residence time (s)	Carbon (%)	Hydrogen (%)	Nitrogen (%)	Oxygen (%)	Others (%)
20	-	-	46.09 ± 1.35	6.07 ± 0.22	0.47 ± 0.13	nd*	47.37 ± 1.20
400	**30**	**50**	75.16 ± 0.58	3.97 ± 0.49	0.84 ± 0.12	14.39 ± 0.60	5.64 ± 0.41
700	**80**	**225**	82.90 ± 3.68	1.45 ± 0.35	0.59 ± 0.17	5.04 ± 1.52	10.02 ± 2.42
700	**80**	**400**	84.26 ± 1.10	1.35 ± 0.07	0.43 ± 0.09	4.95 ± 1.78	9.00 ± 1.80

nd* not determined

Figure 4.2 illustrates the raw flax shives before the pyrolysis (a), the char formed after pyrolysis at 700°C reached at 80°C/min heating rate (b), the bio-oil sample produced by the pyrolysis realized under the same conditions (c) and bio-oil sample resulting from the reforming process at 800°C with 20% Ni based catalyst supported on alumina beads (d).

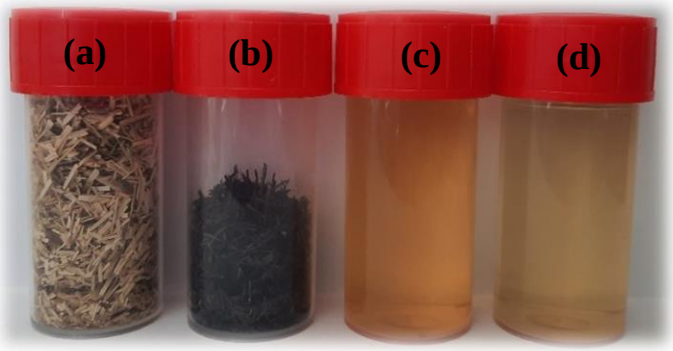

Figure 4.2 Photo of the biomass tested with the products resulted from the pyrolysis-reforming process: (a) raw flax shives; (b) char formed after pyrolysis at 700°C reached at 80°C.min^{-1} heating rate; (c) bio-oil sample produced by the pyrolysis realized under the same conditions; (d) bio-oil sample resulting from the reforming process at 800°C with 20% Ni supported on alumina beads. (Both bio-oil samples are diluted with pure acetone)

4.4.2. Bio-oil chemical composition

Table 4.4 demonstrates the chemical composition of the bio-oil produced by the biomass pyrolysis at 400°C and 700°C as well as after the pyrolysis at 700°C coupled to the reforming at 800°C realized with 20%Ni/Al_2O_3 (GHSV of 4500 h^{-1}). The bio-oil analysis showed that it consists mainly of BTEX, followed by phenols, PAHs and some other products such as furfural. For the bio-oil derived from the pyrolysis, it can be noticed that as the pyrolysis temperature increases from 400°C to 700°C, the concentrations of the majority of the bio-oil compounds dropped significantly except those of ethylbenzene and o-xylene as well as guaiacol. This is a

significant indication of the thermal cracking of the bio-oil species by the pyrolysis specially with the increase in the temperature as shown in equations **(4.13)** and **(4.13)**. Similar results were obtained in our previous work [46] where we studied the composition of the bio-oil issued from the biomass pyrolysis. In fact, secondary decomposition reactions of molecules such as aldehydes and ketones are favored at high pyrolysis temperatures while other molecules with unsaturated bonds are condensed [61].

Table 4.4 Chemical composition of bio-oil produced by pyrolysis at 400°C and 700°C and after reforming at 800°C with 20%Ni/Al_2O_3

	Compounds (µg/mL)	Pyrolysis at 400°C	Pyrolysis at 700°C	Pyrolysis at 700°C + Reforming at 800°C
BTEX	benzene	326	145	7,4
	toluene	1 805	1 097	1 273
	ethylbenzene	1,5	5,1	5,1
	m-, p-xylenes	4,9	4,0	3,5
	o-xylene	1,2	2,1	1,9
Phenols	phenol	65,1	31,6	8,1
	guaiacol	-	373	114
	syringol	181	181	45,4
PAHs	naphtalene	15,7	0,13	0,08
	acenaphtylene	4,28	0,33	0,10
	acenaphtene	0,70	0,16	-
	fluorene	2,78	0,16	-
	phenanthrene	3,67	0,60	0,04
	anthracene	0,84	0,41	0,01
	fluoranthene	0,79	0,24	0,01
	pyrene	1,51	0,22	0,01
	benzo(a)anthracene	0,48	0,17	-
	chrysene	0,18	0,05	-
	benzo(b)fluoranthene	0,22	0,07	-
	benzo(k)fluoranthene	0,09	0,02	-
	benzo(a)pyrene	0,35	0,07	-
	indeno(1,2,3,cd)pyrene	0,09	0,02	-
	dibenzo(ah)anthracene	0,05	0,01	-
	benzo(ghi)perylene	0,04	0,02	-
Other	furfural	-	319	266

Remarkably, the concentrations of the different bio-oil compounds strongly dropped after the catalytic reforming in comparison to the composition of the pyrolysis bio-oil. Interestingly, this huge reduction in the amount of the bio-oil species is a proof of their degradation and transformation into lighter species as it can be seen in the different reforming reactions (equations **(4.2)**, **(4.7)** and **(4.14)**) [11,12,49].

Interestingly, this can be noticed through the change of the color of the bio-oil samples represented in **Figure 4.2.** The bio-oil sample obtained after the reforming is much lighter than that formed by the pyrolysis alone which reveals the transformation of a considerable part of the "dark" heavy bio-oil hydrocarbons and oxygenated species into lighter compounds. This demonstrates that the coupling of the biomass pyrolysis to the catalytic reforming is an efficient way to upgrade the quality of the bio-oil produced by the pyrolysis, which increases its efficiency and its industrial applications [17,18].

4.4.3. Hybrid reforming of pyrolysis volatiles over supported catalysts

4.4.2.1. Effect of catalyst active phase

4.4.2.1.1. Main products concentrations

The success of the catalytic reforming relies on the choice of an appropriate and efficient catalyst. Thereby, the effect of the catalyst active phase was first studied on the products distribution by evaluating the catalytic reforming with three catalysts based on Ni, Co and Co-Ni with a fixed metal loading of 10%, supported on alumina beads, as shown in **Figure 4.3**. They are labeled by "10% Metal" with "metal corresponding to the catalyst active phase. In addition, an experiment was realized with the alumina beads without catalyst and is referred to as "0%". For these tests, the pyrolysis temperature was realized at 700°C reached at a heating rate of 80°C/min while the reforming was performed at 800°C, and they are grouped under the label "Ref_800". The nitrogen flowrate was fixed at 25 mL_n/min. A classical one-stage pyrolysis was also performed under the same conditions but without the reforming step and is referred to as "Pyro_700".

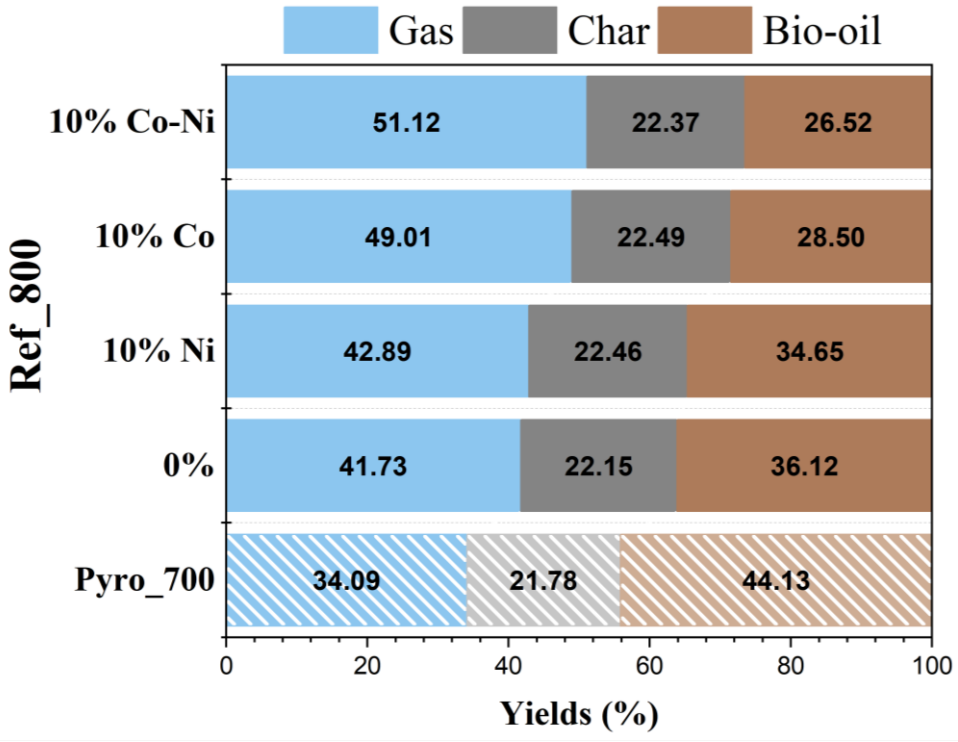

Figure 4.3 Distribution of the products derived from the pyrolysis-reforming process realized with the three catalysts based on Ni, Co and Co-Ni supported over alumina beads with 10% loadings each as well as on alumina beads with 0% catalyst loading. The pyrolysis was realized at 700°C while the reforming at 800°C denoted as "Ref_800". A one-stage pyrolysis was realized alone under the same conditions (temperature: 700°C, heating rate: 80°C/min and 25 mL_n/min nitrogen flowrate) referred to by "Pyro_700"

It can be noticed that combining the catalytic reforming with the pyrolysis strongly enhances the gas production and reduces that of bio-oil, with each catalyst type, in contrast to a one-stage pyrolysis alone. In particular, even with the alumina beads with 0% of catalyst deposition, the gas yield obtained (41.73wt.%) was higher and the bio-oil yield (36.12 wt.%) lower than that with the pyrolysis alone (34.09 wt.% gas and 44.13 wt.% bio-oil). This case can be seen as a two-stage pyrolysis which allows the thermal cracking in the second reactor of the volatiles produced by the biomass pyrolysis in the first reactor. The additional gas produced results from the decomposition of the bio-oil compounds into lower molecular weight hydrocarbons liberating some lighter gases [62] or the repolymerization leading to the formation of heavier hydrocarbons [63].

The deposition of an active phase over the alumina beads enables the catalytic reforming reactions to take place which further improves the transformation of the bio-oil volatiles produced by the biomass pyrolysis into incondensable gases such as syngas [11,12]. It has significantly increased the gases yields to around 50 wt.% and lowered the bio-oil yields to around 30 wt.% in opposite to the 34 wt.% gases and 44 wt.% bio-oil formed with the pyrolysis alone. Comparing the three catalysts, it can be remarked that the highest gas yields (around 51 wt.%) and the lowest bio-oil yield (26.5 wt.%) were produced with the reforming in the presence of the 10% Co-Ni/Al_2O_3 catalyst. On the other hand, the reforming with the 10% Ni/Al_2O_3 revealed the lowest catalytic activity with the smallest gas yield (around 43 wt.%) and largest bio-oil yield (34.7 wt.%) among the catalysts tested. The reforming with Co produces intermediary gas and bio-oil yields.

Therefore, it can be deduced that with alumina beads as catalyst support, the Co-Ni appears to be the most efficient for the tar reduction and conversion into gas. However, in the chapter 3, it was seen that for the bulk catalysts, the nickel was the most convenient for the bio-oil reforming. This can be explained by the better metal dispersion of the Co and Ni particles over the alumina beads which allows a better selectivity towards the bio-oil reforming provided by the Ni active sites and a reduction of the carbon deposition partially responsible for the catalyst deactivation, ensured by the Co presence. The Ni alone supported on the alumina beads suffers from more sintering and carbon deposition which reduces its selectivity and efficiency for the tar reduction and therefore leads to lower gases production.

It should be noted that the char formation was around 22.5 wt.% for the different experiments realized since the char is formed in the first reactor where the biomass pyrolysis was realized at 700°C for the different set of experiences.

4.4.2.1.2. Major gases' concentrations

The concentrations of the major gases produced by the pyrolysis-reforming over the catalysts with the different active phase are represented in **Figure 4.4**, with the same labels defined in the previous sub-section. It can be noticed that compared to pyrolysis alone, the reforming with the 0% catalyst over alumina beads produces slightly higher H_2 and CH_4 concentrations and lower CO and CO_2 concentrations. This behavior can be mostly related to a second stage pyrolysis where the heavy hydrocarbons are cracked into lighter ones resulting in the liberation of H_2 molecules and formation of CH_4 and other light molecules [62]. Realizing a catalytic reforming step after the pyrolysis allows an increase in the H_2 and CO concentrations and a reduction in those of CH_4 and CO_2 which corresponds to the reforming reactions equations **(4.2)** to **(4.7)**.

Comparing the reforming with the three catalysts, it can be observed that the most improved H_2 and CO formations and the most reduced CH_4 and CO_2 concentrations in contrast to the pyrolysis alone are obtained with the 10% Ni/Al_2O_3 catalyst. This can be related to the large thermal stability of the Ni/Al_2O_3 catalyst as well as its large metal surface area resulting in its strong activity [64]. The catalytic reforming with the Co and Co-Ni supported on alumina beads proved to be much less effective than with the Ni. *This proves the efficiency of the Ni/Al_2O_3 catalyst in the catalytic reforming of light hydrocarbons such as methane towards the formation of syngas (H_2 and CO).* It is routed to the capacity of Ni catalyst to break the carbon-hydrogen links and to activate the methane [65].

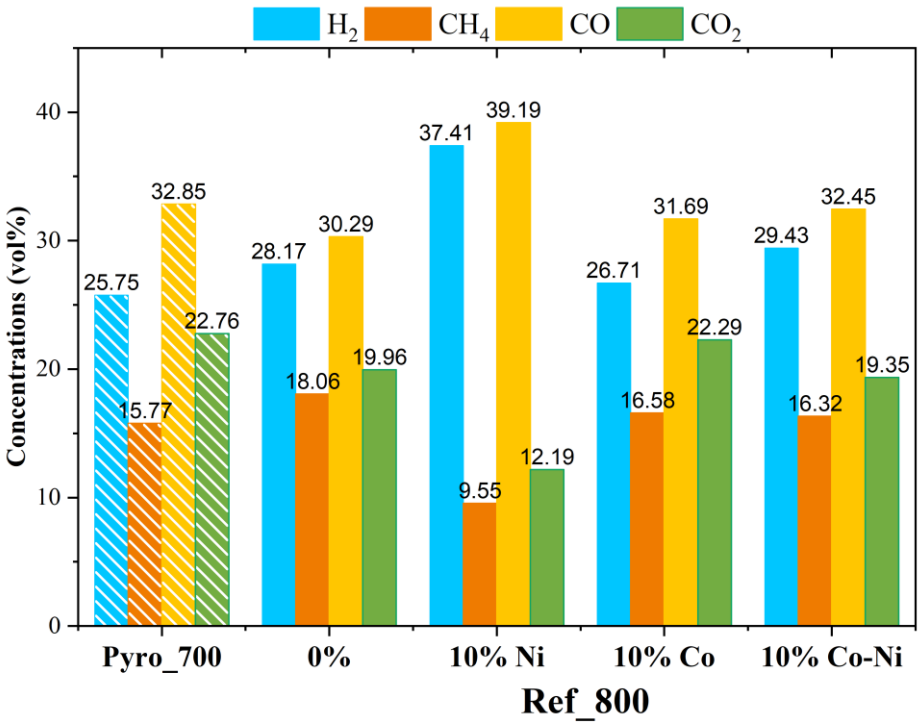

Figure 4.4 Concentrations of the major gases produced by the pyrolysis-reforming process realized with the three catalysts based on Ni, Co and Co-Ni supported over alumina beads with 10% loadings each as well as on alumina beads with 0% catalyst loading

4.4.2.1.3. Main reactants' conversion rates

The chief reactants in the pyrolysis volatiles reforming process are the bio-oil hydrocarbons, along with methane and carbon dioxide. Their conversion rates are studied for the catalytic reforming with the catalysts having different active phases as shown in **Figure 4.5**. The 10% Ni catalyst surpasses the other catalysts in the values of conversion rates reached for CH_4 (39.5%) and CO_2 (46.5%). The conversion rates of the CO_2 and CH_4 were far behind for the Co and Co-Ni with Co suffering from the poorest activity. Small particles used as catalysts' support increase the density of the active sites [66].

Thanks to the high activity and stability of the nickel supported catalysts, they are one of the most extensively employed for the steam reforming of methane as well as tar and aromatics, with alumina and its modifiers (α- and γ-Al_2O_3) being the most commonly encountered catalyst support [12,67]. γ-Al_2O_3 is known for its ability to stimulate the catalytic activity and to restrain the carbon formation [68]. As for the bio-oil conversion, the highest rate was reached with the Co-Ni followed by the Co, whereas Ni had the lowest bio-oil conversion rate.

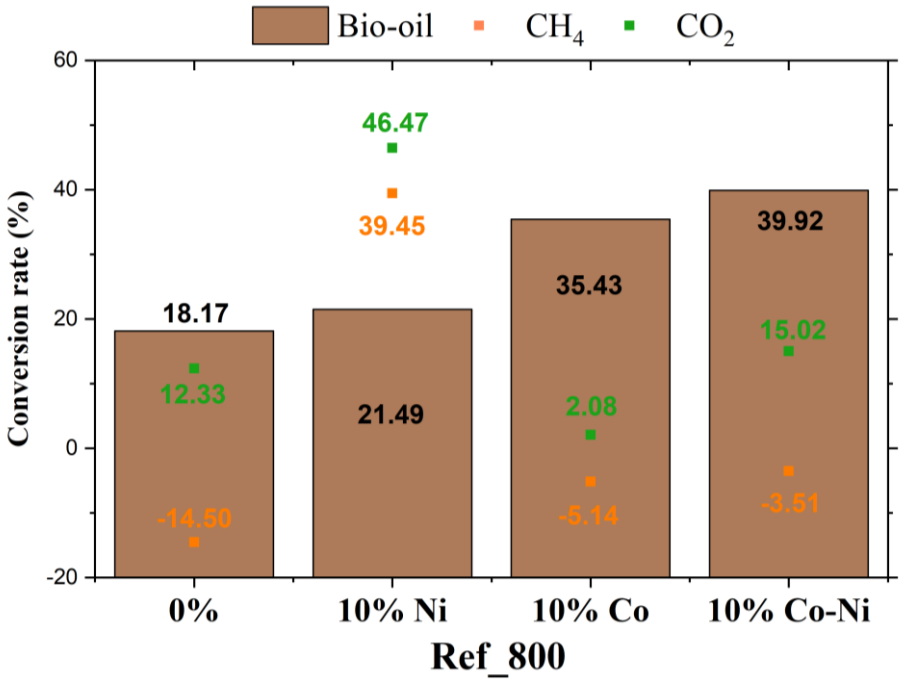

Figure 4.5 Conversion rates of the main reactants involved in the pyrolysis-reforming process realized with the three catalysts based on Ni, Co and Co-Ni supported over alumina beads with 10% loadings each as well as on alumina beads with 0% catalyst loading

4.4.2.1.4. Syngas production

To focus on the syngas production during the pyrolysis-catalytic reforming process, the H_2/CO ratio and the syngas concentration in terms of mmol/dry biomass weight were determined to evaluate the hydrogen formation. The impact of the active phase of the catalysts over the syngas production is depicted in **Figure 4.6**. Realizing a catalytic reforming post the pyrolysis markedly enhances the syngas production and improves the H_2 formation relatively to the CO. Moreover, the catalytic reforming with the Ni was the most efficient for the syngas production among the other catalysts where it almost doubled the syngas production from 8.5 mmol/g dry biomass with the pyrolysis alone to 16.9 mmol/g dry biomass obtained with the pyrolysis-reforming with the Ni. The H_2/CO ratio was also the highest with 0.95 when the Ni was used in contrast to the 0.78 for the pyrolysis alone. On the other hand, the Co and Co-Ni slightly improve the syngas production relative to the pyrolysis alone or to the 0% catalyst with the Co-Ni performing faintly better than the Co alone.

The reason behind these results can be the occurrence of the secondary reactions such as the reverse WGSR (equation **(4.9)**), the Boudouard reaction (equation **(4.10)**) and the reverse water-gas reaction (equation **(4.11)**) which counterbalance the syngas production and prevent the hydrogen formation which reduces the H_2/CO ratio. An H_2/CO ratio around 1 is the case for an ideal stochiometric methane dry reforming reaction (equation **(4.7)**) and is thereby a sign of the good activity and performance of the catalyst [28]. An H_2/CO ratio of 1 is particularly useful for multiple selective chemical syntheses such as liquid hydrocarbons, formaldehyde and acetic acid [58].

The Ni/Al_2O_3 catalyst has been largely investigated for the methane reforming due to its high availability and low cost and was proven to have high catalytic activity and remarkable performance [69–71]. Supported nickel catalysts have been used commercially for the reforming for over 40 years [72]. The design of these catalysts allows their good functioning

under extreme temperatures going from 700°C to 1000°C as well as severe pressure going up to 30 bar [73]. The Co on the other hand has been scarcely used alone for the bio-oil reforming and is commonly alloyed with more efficient catalysts such as Ni and Fe [74]. The addition of Co to other catalyst derives from its capacity to minimize the carbon formation and deposition over the catalyst surface which reduces the chances of the catalyst deactivation [75]. *Therefore, for the remaining catalytic reforming experiments realized in this work, the catalyst used will be Ni supported on alumina beads.*

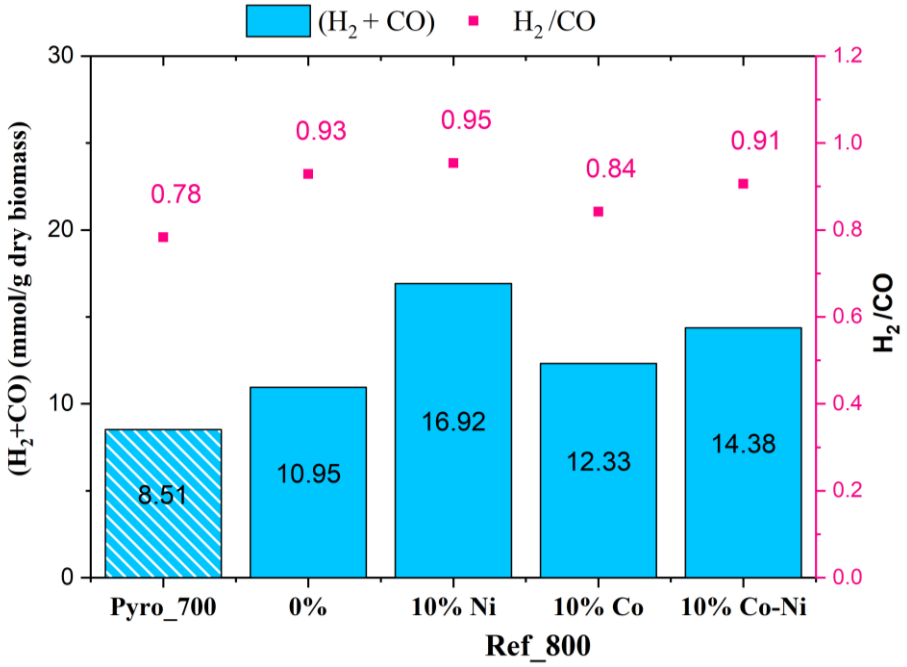

Figure 4.6 Syngas concentrations and H_2/CO ratio of the pyrolysis-reforming process realized with the three catalysts based on Ni, Co and Co-Ni supported over alumina beads with 10% loadings each as well as on alumina beads with 0% catalyst loading

4.4.4. Effect of metal loading

4.4.4.1. Main products concentrations

Given that the Ni catalyst was proven the most efficient for the syngas production, it was chosen for the next series of experiments. The metal loading effect on the reforming efficiency was studied by varying the loading of the Ni metal over the alumina beads from 0% to 25%. The pyrolysis was realized at 700°C, while the reforming temperature was fixed at 800°C for this series of tests. The Ni metal loading impact on the products distribution of the pyrolysis-reforming is investigated in **Figure 4.7**. It can be remarked that increasing the Ni metal loading from 0 to 20% improves the gas production at the expense of the bio-oil which decreases with a maximum of gas production (around 53 wt.%) and a minimum of bio-oil formation (around 24.3wt.%) reached with the 20% Ni/Al_2O_3. At 25% Ni, the gases production dropped to 40.5 wt.% (the lowest gas yield attained among the different loading percentages) and that of bio-oil increased to around 37 wt.% (the highest bio-oil yield attained among the different loading percentages).

The nickel-based catalysts consisting mainly of NiO dispersed on Al_2O_3 supports are the non-promoted Ni catalysts usually used [76–78] since they render the catalyst appropriate for reaction requiring high temperatures (superior to 800°C) [79]. The Ni-based catalyst activity highly depends on the Ni dispersion which is linked to the metal loading as well as the surface

area of the support [80,81]. Moreover, at reaction temperatures higher than 650°C, the Ni-based catalysts are subject to sintering and carbon deposition which inhibit the active metal sites from performing the catalytic surface reactions, rendering the catalysts partially deactivated [82,83]. Ni catalysts are known to be easily deactivated by the Ni sintering and coking [84]. Nonetheless, a solution to this issue would be the optimization of the Ni loading levels according to the operating conditions [85]. The methane catalytic reforming reaction occurs on the catalyst's surface, thereby the increase of the catalyst surface area by augmenting the active Ni loading amounts strongly improves the activity and performance of the reforming process. Increasing the Ni loading above 20% drops the catalyst activity per unit metal surface area. Thus, using a Ni loading above 20% reduces the dispersion of the additional amounts of the metal and drops the catalyst activity [86–88], mainly caused by the limited mass and heat transfers.

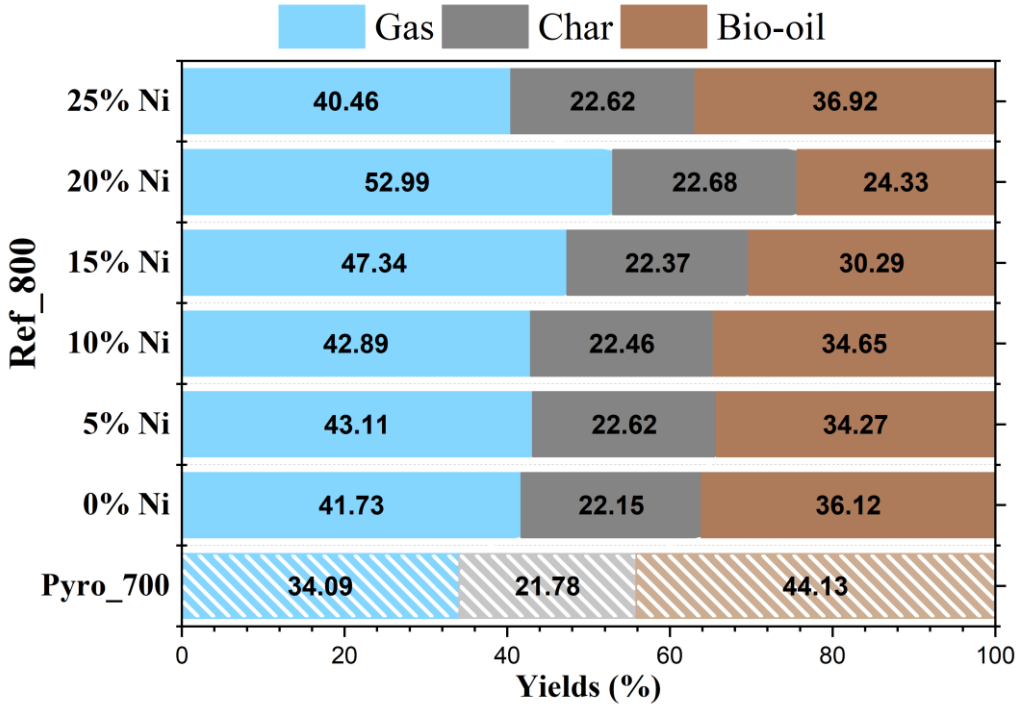

Figure 4.7 Effect of metal loading on the distribution of the products derived from the pyrolysis-reforming process realized with the Ni/Al_2O_3 beads. The pyrolysis was realized at 700°C while the reforming at 800°C, referred to by "Ref_800". A one-stage pyrolysis was realized alone under the same conditions (temperature: 700°C, heating rate: 80°C/min and 25 mL_n/min nitrogen flowrate) referred to by "Pyro_700"

4.4.4.2. Major gases' concentrations

The effect of the Ni metal loading on the major gases' concentrations derived from the pyrolysis-reforming under the same operating conditions previously described is illustrated in **Figure 4.8**. Increasing the Ni metal loading contributed to the amelioration of the H_2 and CO concentrations and a reduction of those of CH_4 and CO_2 up to 20% of Ni deposition. Above 20% Ni, the CO started decreasing and the CH_4 increasing, while CO_2 continued decreasing to 9.7 vol% and H_2 reached its maximum of 43.3 vol.% at 25% Ni. This might lead to think that a small addition of the Ni loading amount can contribute to an increase in the H_2 production and CO_2 conversion. However, the variations can be considered relatively small in comparison to the higher cost implied by increasing the metal deposition level.

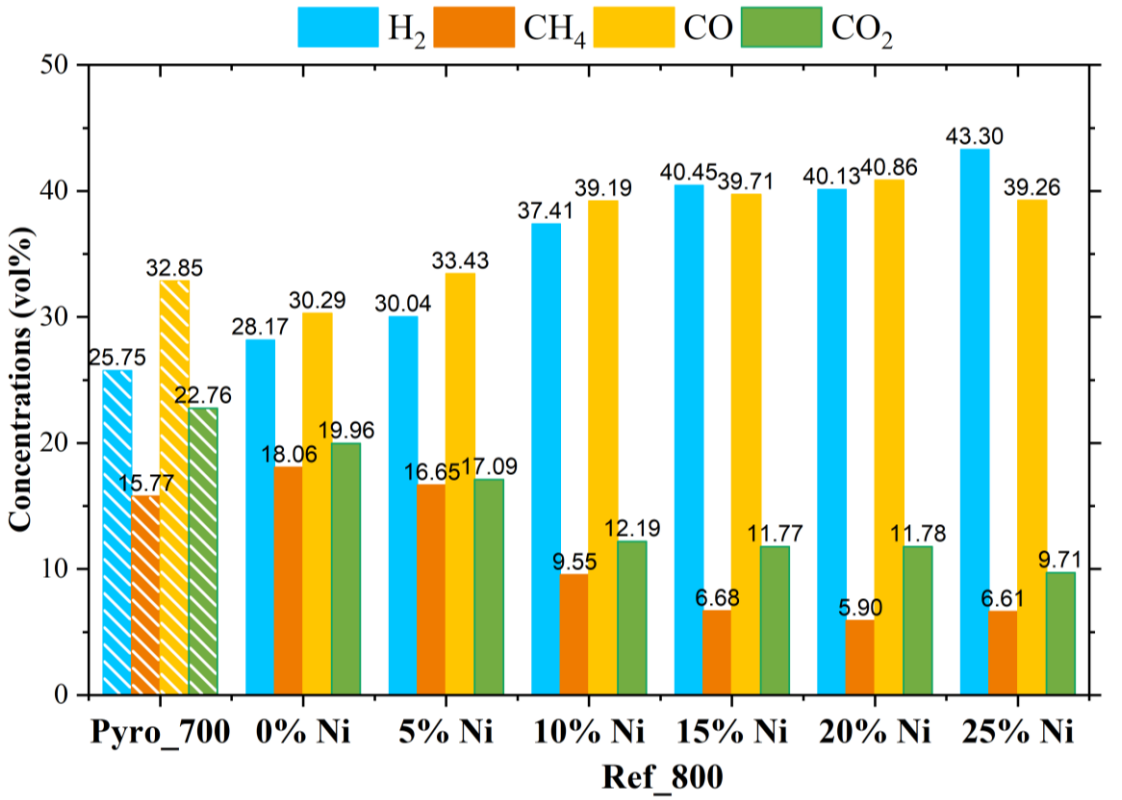

Figure 4.8 Effect of metal loading on the concentrations of major gases produced by the pyrolysis-reforming process realized with the Ni/Al_2O_3 beads

4.4.4.3. Main reactants' conversion rates

The variations of the conversion rates of the chief reactants of the pyrolysis-reforming process in function of the Ni metal loading is demonstrated in **Figure 4.9**. The evolution of the bio-oil yields and the concentrations of CO_2 and CH_4 previously observed are reflected on their conversion rates. For instance, the bio-oil conversion rates increased with the augmentation of the Ni loading to peak at 44.87% with the 20%Ni above which it dropped to 16.34%. the CH_4 conversion was maximized at 62.57% with the 20% Ni but slightly dropped to 58.07% with the 25% Ni. On the other hand, the CO_2 conversion rate maintained a monotone increasing tendency and peaked at 57.35% with the 25% Ni. Increasing the metal loading is believed to improve the reforming capacity, but to a certain limit [87,88]. As remarked, a 25% loading might have enhanced the H_2 production and the CO_2 conversions but led to a drop in those of bio-oil and CH_4, revealing the limited capacity of the catalyst, overcharged by the Ni molecules [81,85].

The increase of the syngas production with the metal loading was also proven by Younis *et al.* [81] who worked on the syngas production from the pyrolysis of polypropylene plastic in one stage and the dry reforming over Ni/Al_2O_3 catalyst in a second stage at 800°C. They found that increasing the Ni metal loading from 5 wt.% to 50 wt.%, strongly enhances the syngas production from 76.5 mmol/g polypropylene to 170 mmol/g polypropylene. This was attributed to the improvement of the catalytic performance during the reforming of the pyrolysis volatiles by the addition of the Ni active phase.

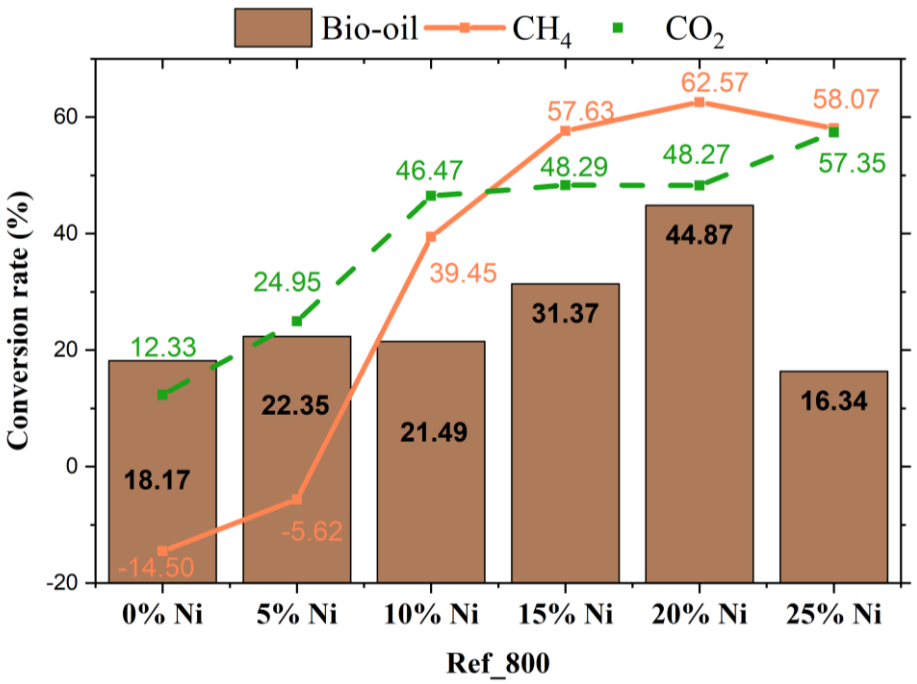

Figure 4.9 Effect of metal loading on the conversion rates of the main reactants involved in the pyrolysis-reforming process realized with the Ni/Al_2O_3 beads

4.4.4.4. Syngas production

The influence of the Ni metal loading over the syngas concentration and the H_2/CO ratio obtained from the pyrolysis-reforming process is presented in **Figure 4.10**. The syngas production also followed the H_2 and CO variations where the highest syngas production of 22.55 mmol/g dry biomass was attained with the 20% Ni above which it diminishes again. The slight decrease in the CO concentration observed with the 25% Ni accompanied with the maximum H_2 concentration, led to the highest H_2/CO ratio of 1.10 reached with 25% Ni.

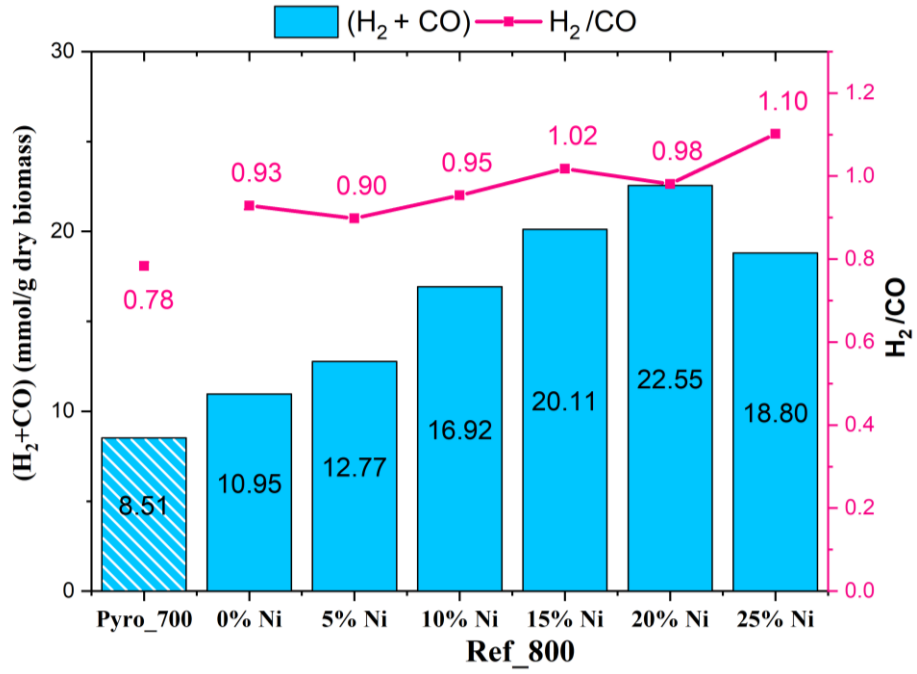

Figure 4.10 Effect of metal loading on syngas concentration and H_2/CO ratio produced by the pyrolysis-reforming process realized with the Ni/Al_2O_3 beads

The metal loading has a crucial role on the catalyst activity since a high metal loading might lessens the good metal dispersion and intensify the active sites' aggregation thus reducing the catalyst's efficiency [11]. Therefore, for the bio-oil reforming a lower metal loading can be generally found convenient [66]. *For our experiments, the 20% Ni loading is considered to be the most appropriate for the bio-oil reforming and syngas production and will be chosen for the following catalytic reforming experiments.* This conclusion was also made by some other research. For instance, Artetxe *et al.* [16] realized the steam reforming of a mixture of model bio-oil compounds over Ni/Al_2O_3 catalyst and studied the effect of the Ni loading on the major gases yields by considering loadings going from 5 to 40%. They also found that a 20% Ni loading was the optimal loading for the carbon conversion and the gases formation.

4.4.5. Effect of reforming temperature

4.4.5.1. Main products concentrations

Having a major influence on the reforming reactions, the temperature of the reforming reactor was varied from 650°C to 800°C to study its effect on the reforming efficiency. The pyrolysis temperature was maintained at 700°C. The catalyst used for this series of experiment and all the following was 20% Ni supported on the alumina beads with a GHSV set at 4500 h^{-1}. The influence of the reforming temperature on the products distribution is revealed in **Figure 4.11**.

It can be observed that the increase of the reforming temperature from 650°C to 800°C entails an augmentation of the gases production coupled with a simultaneous drop in the bio-oil formation. It represents tangible evidence that the bio-oil hydrocarbons formed in the first pyrolysis reactor are effectively transformed in the second reforming reactor into gases and lighter hydrocarbons. It is worth noting that even the pyrolysis at 700°C coupled to the reforming realized at a lower temperature of 650°C produces significantly higher gas yields and lower bio-oil yields than a single stage pyrolysis. This reflects the importance of realizing a second step of reforming for the increase of the gases production resulting from the main and secondary reactions.

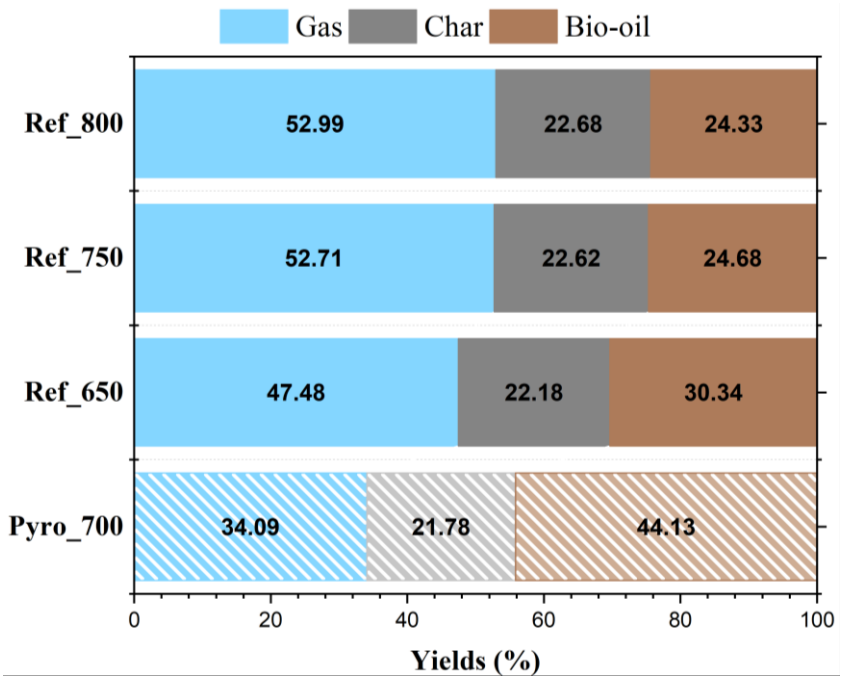

Figure 4.11 Effect of reforming temperature on the distribution of the products derived from the pyrolysis-reforming process realized with the 20% Ni/Al_2O_3 beads (GHSV=4500h^{-1}). The pyrolysis was realized at 700°C. A one-stage pyrolysis was realized alone under the same conditions (temperature: 700°C, heating rate: 80°C/min and 25 mL_n/min nitrogen flowrate)

When the pyrolysis volatiles penetrate the reforming reactor, they are subject to the tar cracking reactions prior to the contact with the catalyst. These reactions consist of either decomposing the heavy bio-oil hydrocarbons into lighters compounds [62] (equations **(4.12)** and **(4.13)**) or to repolymerizing the small molecular weight species into heavier ones [63]. The unreacted bio-oil hydrocarbons along with the newly formed gases react over the catalyst surface to produce other gases and low molecular weight molecules according to the equations **(4.2)−(4.7)** previously introduced. The reforming is hereby regarded as a purification method which helps in removing the tar from the pyrolysis gases while converting it into products of interest such as syngas. These results are illustrated in **Figure 4.2** showing the lightening of the bio-oil color before and after the reforming as well as the analysis of the bio-oil composition given in **Table 4.4**.

4.4.5.2. Major gases' concentrations

The evolution of the major gases' concentrations derived from the pyrolysis-reforming process in function of the reforming temperature is depicted in **Figure 4.12**. Globally, as the reforming temperature augments from 650°C to 800°C, the concentrations of H_2 and CO augment while those of CO_2 and CH_4 drop. These observations support the endothermic nature of the dry and steam reforming reactions which are accentuated at high temperatures [90]. They are also an explicit proof of the occurrence of the dry reforming reactions of tar (equation **(4.5)**), hydrocarbon volatiles (equation **(4.6)**) and methane (equation **(4.7)**) where these products are transformed by reacting with the CO_2 to produce H_2 and CO.

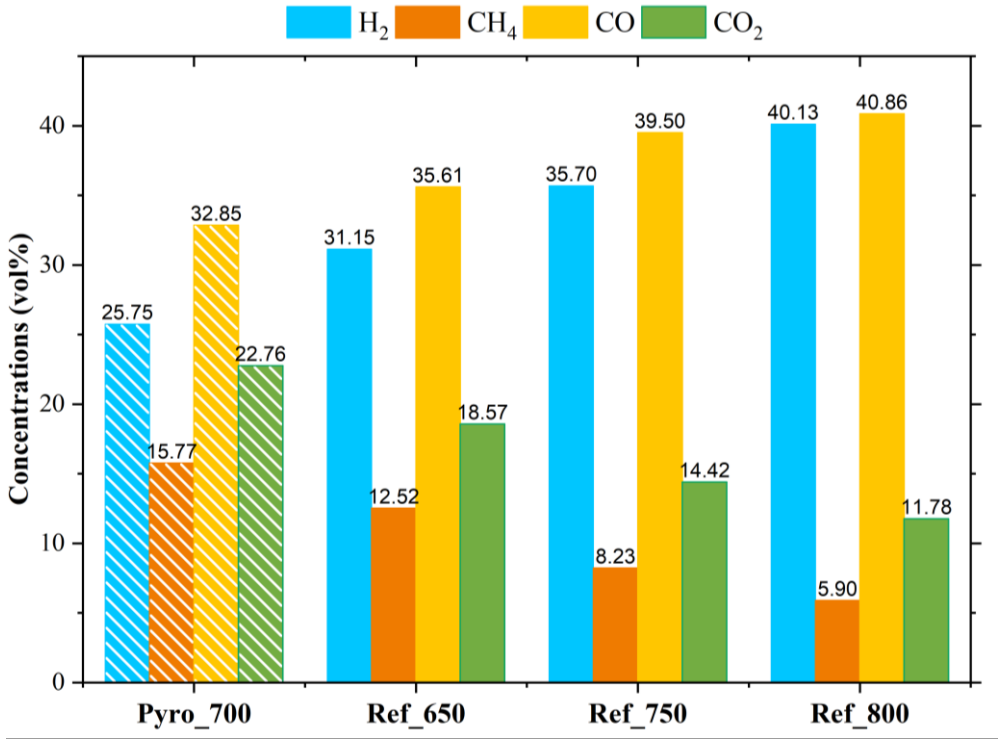

Figure 4.12 Effect of reforming temperature on the concentrations of major gases produced by the pyrolysis-reforming process realized with 20% Ni/Al_2O_3 beads (GHSV=4500h^{-1}). The pyrolysis was realized at 700°C. A one-stage pyrolysis was realized alone under the same conditions (temperature: 700°C, heating rate: 80°C/min and 25 mL_n/min nitrogen flowrate)

4.4.5.3. Main reactants' conversion rates

The effect of the reforming temperature on the conversion rates of the bio-oil, CH_4 and CO_2 involved in the pyrolysis-reforming reactions is represented in **Figure 4.13**. The variations of the conversion rates of bio-oil, methane and carbon dioxide mirror the evolutions in their

respective concentrations. For instance, the bio-oil conversion rate increased from 650°C to 750°C then remained almost steady at 800°C. The CO_2 conversion rate has a general increasing tendency at the exception of a faint fall at 750°C. The CH_4 conversion maintained an increasing tendency from 650°C to 800°C.

Interestingly, the methane conversion exceeds that of carbon dioxide at the different temperatures. It can be related to the methane cracking reactions which is spontaneous at temperatures going from 600°C to 800°C (equation **(4.21)**) consuming the CH_4 and to the WGSR (equation **(4.8))** resulting in the production of CO_2. These reactions enter in competition with the main dry methane reforming (equation **(4.7)**) where the CO_2 is consumed [91].

CH_4 cracking: $CH_4 \rightarrow C + 2H_2$ $\Delta H°_{298K} = +75$ kJ/mol **(4.21)**

These tendencies were also found by other research works such as those of Tanios *et al.* [92,93] who studied the methane dry reforming over Ni based bulk catalysts. Nevertheless, these observations contradict with the results generally encountered in the literature [19,74] where the CO_2 conversion are higher than that of CH_4. Therefore, when the CH_4 conversion surpasses that of CO_2, secondary reactions have potentially occurred, influencing the reforming performance, which shall be confirmed by the catalyst's characterization analyses after the reforming.

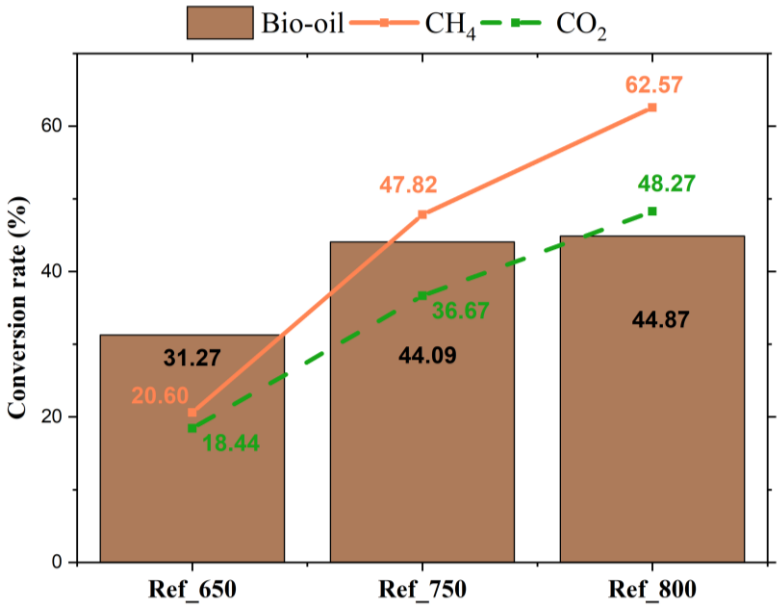

Figure 4.13 Effect of reforming temperature on the conversion rates of the main reactants involved in the pyrolysis-reforming process realized with 20% Ni/Al_2O_3 beads (GHSV=4500h^{-1}). The pyrolysis was realized at 700°C. A one-stage pyrolysis was realized alone under the same conditions (temperature: 700°C, heating rate: 80°C/min and 25 mL_n/min nitrogen flowrate)

4.4.5.4. Syngas production

The syngas production and the H_2/CO ratio evolutions with the temperature of reforming process are illustrated in **Figure 4.14**. The temperature rise leads to a major enhancement in syngas production where it rises from 14.52 mmol/g dry biomass to 22.55 mmol/g dry biomass when the temperature passes from 650°C to 800°C. The H_2/CO ratio followed also an increasing tendency from 0.87 at 650°C to 0.98 at 800°C.

Looking at the methane dry reforming reaction presented in equation **(4.7)**, it can be deduced from the stoichiometry that the H_2/CO ratio is equal to 1. On the other hand, for the methane

steam reforming given in equation **(4.4)**, the H_2/CO ratio equals 3. From **Figure 4.14** it can be remarked that the H_2/CO ratio approaches the value 1. Given the absence of an external steam feed applied for this series of experiments, it can be presumed that the dry reforming reactions are more significant than the steam reforming reactions. It can be associated with the higher production of CO_2 (around 23%) than that of water vapor emitted by the biomass pyrolysis. With the absence of an external water vapor feed or an additional CO_2 inlet, the chief reactant of the current reforming process is more likely to be the CO_2 produced by the pyrolysis of biomass in the first stage. Furthermore, given that the CO_2 conversions were lower than those of CH_4 and the H_2/CO ratio was close to 1, it can be presumed that the Boudouard reaction (equation **(4.10)**) and the CH_4 cracking reaction (equation **(4.21)**) take over the CH_4 steam reforming (equation **(4.4)**) and the reverse water-gas shift reaction (equation **(4.9)**) [92].

Nonetheless, the H_2/CO ratio takes sometimes values different than 1 which reveals that other secondary reactions take place. These include the reverse of carbon gasification (equation **(4.22**) [94] involving the consumption of equal amounts of CO and H_2 and the production of H_2O, which can undergo the WGSR (equation **(4.9)**) with the CO.

Reverse of carbon gasification: $CO + H_2 \rightarrow C + H_2O \quad \Delta H°_{298K} = +31.4 kJ/mol$ **(4.22)**

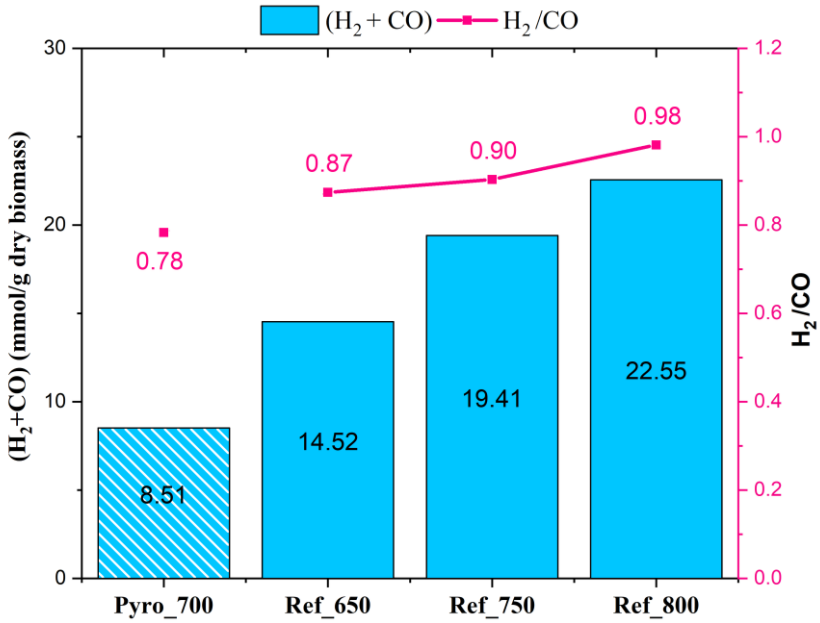

Figure 4.14 Effect of reforming temperature on syngas concentration and H_2/CO ratio produced by the pyrolysis-reforming process realized with 20% Ni/Al_2O_3 beads (GHSV=4500h^{-1})

It was remarked that the difference in the products' yields can be assessed relatively slight between 750°C and 800°C, which suggests that *the reforming can be as effective at a lower temperature like 750°C rather than 800°C for the gas formation which can be very interesting in terms of economy and energy efficiency*. In the literature, a catalytic reforming temperature between 650°C and 750°C is considered favorable [15,95].

4.4.6. Effect of GHSV

4.4.6.1. Main products concentrations

The gas hourly space velocity (GHSV) plays an important role in the catalytic reforming process and therefore its effect was studied with 20% Ni/Al_2O_3 beads. For this set of experiments, the temperatures of both the pyrolysis and the reforming were fixed at 700°C, in

order to attenuate the effect of high temperature on the process efficiency, in a way that the effect of GHSV is not covered by that of temperature. The GHSV was varied from 900 to 4500 h^{-1} by changing the height of the catalyst in the reforming reactor as explained previously in **Table 4.2**. Its influence on the products distribution is shown in **Figure 4.15**. At a GHSV of 900 h^{-1}, the gas yield is at its highest with 52.61 wt.% and the bio-oil at its lowest with 24.86 wt.%. Nonetheless, increasing the GHSV to 1125 h^{-1} led to a remarkable drop in the gas yield to 41.68 wt.% and a considerable increase in the bio-oil formation to 35.83 wt.%. further increasing the GHSV had a relatively negligible impact on the gases and bio-oil productions, where the gases slightly increase to 43.52 wt.% while the bio-oil remained almost constant at a GHSV of 2250 h^{-1} to then dropping faintly at GHSV of 4500 h^{-1}.

When the space velocity is increased, i.e., the amount of catalyst presence is decreased, the efficiency of the reforming is reduced. This means that less bio-oil hydrocarbons will be reformed into syngas and the concentrations of the unreformed bio-oil species will be elevated in the reactor [96]. Among those components, the bio-oil oxygenates are abundant [46]. These species are precursor for carbon formation and coke deposition over the catalyst surface which eventually lead to its partial deactivation and a drop of its efficiency [12].

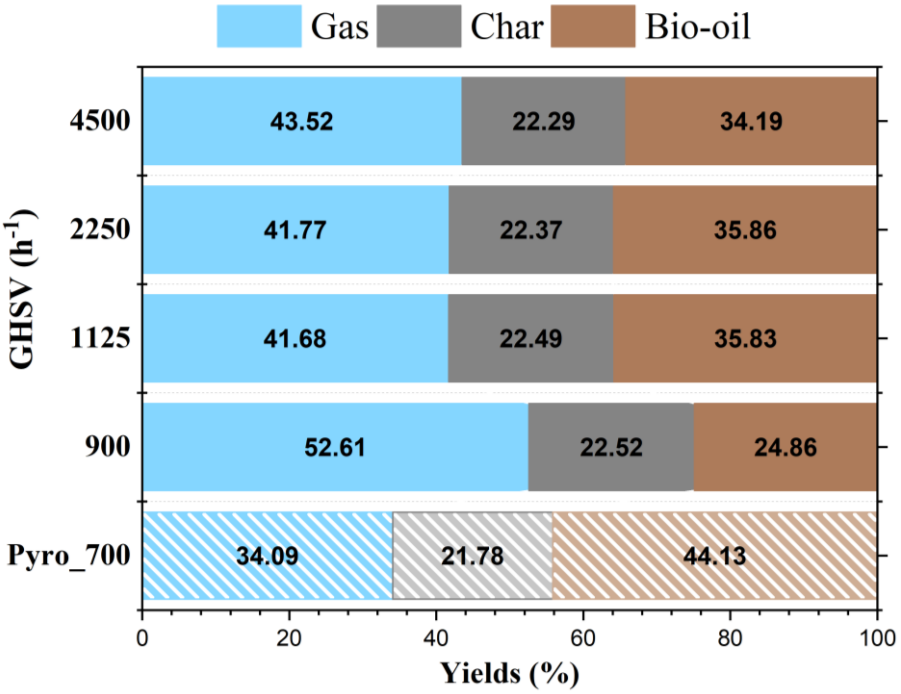

Figure 4.15 Effect of GHSV on the distribution of the products derived from the pyrolysis-reforming process realized with the Ni/Al_2O_3 beads. The pyrolysis and the reforming were both realized at 700°C. A one-stage pyrolysis was realized alone under the same conditions (temperature: 700°C, heating rate: 80°C/min and 25 mL_n/min nitrogen flowrate)

4.4.6.2. Major gases' concentrations

The variation of the major gases' concentrations with the GHSV under the same conditions described previously is given in **Figure 4.16**. GHSV had a different impact on the four major gases studied. The CO had a monotone dropping tendency while CH_4 had a constantly increasing trend when the GHSV was varied from 900 to 4500 h^{-1}. On the other hand, H_2 started by increasing to reach a maximum of 42.79 vol.% at a GHSV of 1125 h^{-1} after which it declined as the GHSV reached 4500 h^{-1}. The CO_2 followed an opposite tendency where it reached a trough at GHSV of 1125 h^{-1} followed by an increase until the GHSV attained 4500 h^{-1}.

The lower the GHSV, the bigger the volatiles residence time is, which thereby increases the contact time between the volatiles and the catalyst. This amplifies the intensity of the catalytic reforming reactions and therefore multiplies the products formed such as the gases, in particular H_2 and CO, and leads to a higher consumption of the reactants among which CO_2, CH_4 and the heavy bio-oil hydrocarbons.

The drop in the H_2 concentration observed as the space velocity was increased can be associated with the catalyst deactivation as well as the WGS reaction (equation **(4.8)**) which are higher as the GHSV is augmented. In addition, due to the higher presence of the bio-oil oxygenates in the reaction medium, their cracking reaction (equation **(4.13)**) intensifies, as the catalyst deactivates [96]. Subsequently, the concentrations of CO_2, CH_4 and other light hydrocarbons augment with the increase in the GHSV.

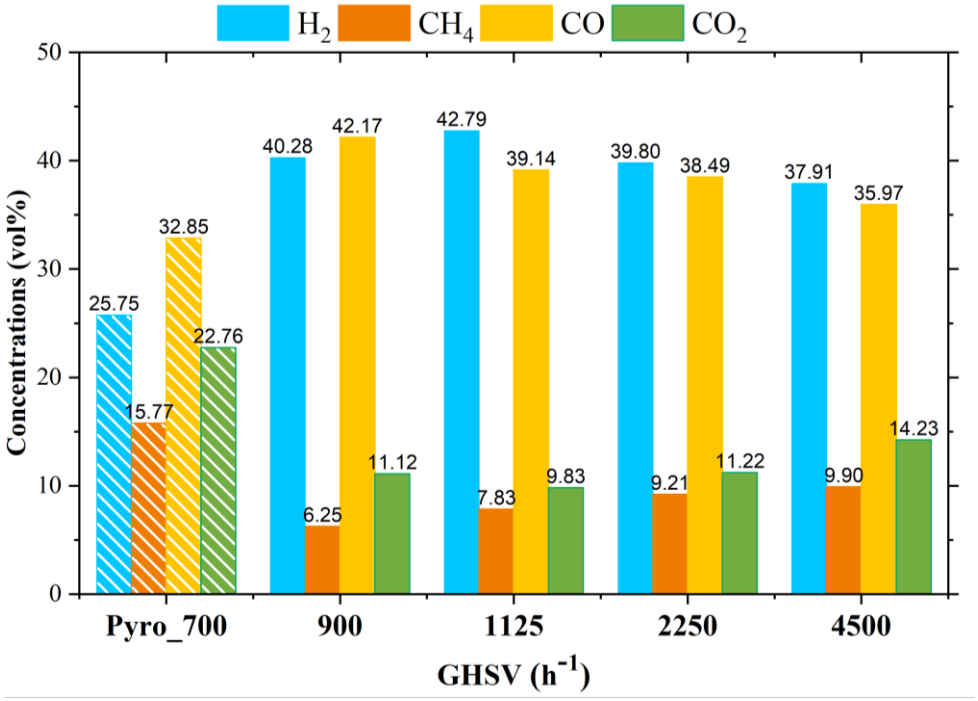

Figure 4.16 Effect of GHSV on the concentrations of major gases produced by the pyrolysis-reforming process realized with the Ni/Al_2O_3 beads. The pyrolysis and the reforming were both realized at 700°C

4.4.6.3. Main reactants' conversion rates

The impact of the GHSV over the conversion rates of the main reforming reactants is depicted in **Figure 4.17**. At a GSHV of 900 h^{-1}, the bio-oil conversion rate was the highest with 43.66%. Once it reached 1125 h^{-1}, the bio-oil conversion rate dropped to 18.82%, stabilized at 2250 h^{-1} and then faintly increased at 4500 h^{-1}. The CO_2 conversion rate peaked at 1125 h^{-1} above which it dropped. Whereas the CH_4 conversion had a single decreasing tendency from 60.36% to 37.21% as the GHSV increased from 900 h^{-1} to 4500 h^{-1}.

The values of GHSV found in the literature can be relatively small and comparable to those applied here. For instance, Khzouz *et al.* [85] applied GHSV of 1067.4 h^{-1} and 1388.9 h^{-1} for the methane steam reforming over $10\%Ni/Al_2O_3$ while Fernandez *et al.* [97] used GHSV of 3100 h^{-1} for the steam reforming of volatiles from pinewood sawdust fast pyrolysis. Nonetheless, larger GHSV values can be also applied as in the works of Angeli *et al.* [98] who applied a GHSV of 58,000 h^{-1}, 61,000 h^{-1} and 70,000 h^{-1} for the propane, ethane and methane steam reforming respectively. Remiro *et al.* [96] used a GHSV range between 8,000 h^{-1} and

155,000 h^{-1} for the steam reforming of raw bio-oil on a Ni/La_2O_3-αAl_2O_3. Although they observed different tendencies of the products evolution than in this work, given the higher GHSV values, but some trends remain similar. For example, the increase of the space velocity from 8,000 h^{-1} to 155,000 h^{-1} resulted in higher CH_4 and light hydrocarbons yields, and lower H_2 yields and bio-oil conversions [96].

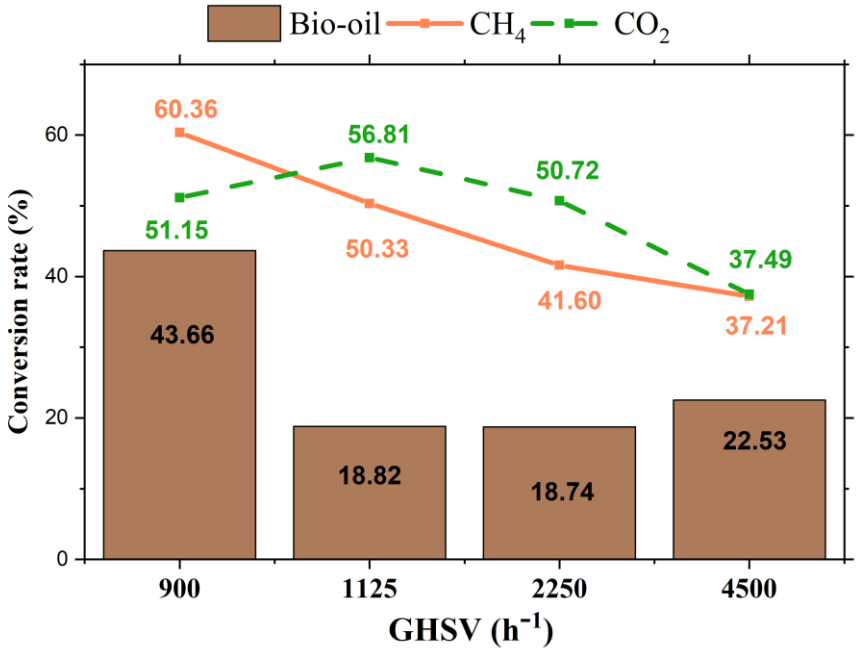

Figure 4.17 Effect of GHSV on the conversion rates of the main reactants involved in the pyrolysis-reforming process realized with the Ni/Al_2O_3 beads. The pyrolysis and the reforming were both realized at 700°C

4.4.6.4. Syngas production

Figure 4.18 displays the influence of the GHSV on the syngas production and the H_2/CO obtained from the pyrolysis-reforming process. The syngas production was the biggest at a GHSV of 900 h^{-1} with 23.12 mmol/g dry biomass then it decreased to 16.37 mmol/g dry biomass as the GHSV was raised to 4500 h^{-1}. On the other hand, the H_2/CO ratio was the lowest (0.95) at 900 h^{-1} and the highest (1.09) at 1125 h^{-1} then it fluctuated around 1.04.

Applying a low GHSV requires large amounts of catalysts which can be costly at an industrial scale. Therefore, in general higher GHSV values are more attractive if they are efficient. In our case, *it was noticed that the best catalytic performance was obtained with a very low GHSV of 900 h^{-1}*. Even though the catalytic activity dropped by increasing the GHSV from 900 h^{-1} to 1125 h^{-1}, an improvement was observed in the bio-oil conversion and the total gases formation when the GHSV reached 4500 h^{-1}. *Thereby, a GHSV of 4500 h^{-1} is considered to be a compromise for a relatively efficient catalytic reforming and will be applied for the catalyst aging test realized hereafter.*

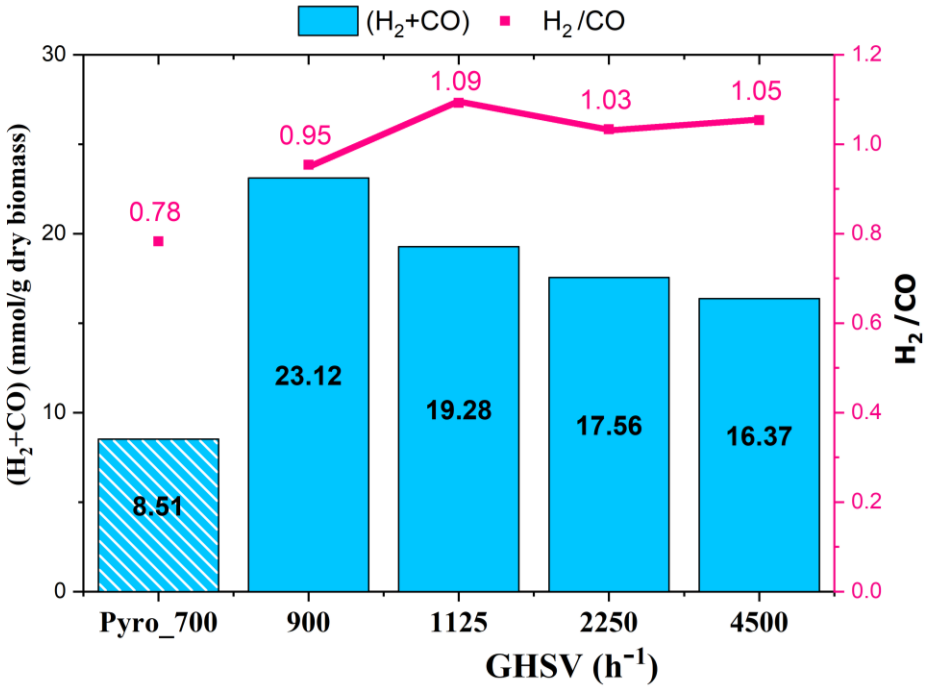

Figure 4.18 Effect of GHSV on syngas concentration and H_2/CO ratio produced by the pyrolysis-reforming process realized with the Ni/Al_2O_3 beads. The pyrolysis and the reforming were both realized at 700°C

4.4.7. Catalyst aging test

4.4.7.1. Main products concentrations

The evolution of the major products of the pyrolysis-reforming process produced during the aging test of the 20%Ni/Al_2O_3 beads (GHSV of 4500h^{-1}) over five cycles is represented in **Figure 4.19**. The pyrolysis was realized at 700°C while the reforming was at 750°C. The gas yield is the highest and the bio-oil yield the lowest after the first cycle. Starting by the second cycle, the gas yield began to decrease by around 10% and the bio-oil to increase by 20%. The strongest gas drop and bio-oil surge were observed after the third cycle. Nevertheless, the gas concentration started increasing and the bio-oil decreasing once the fourth cycle was realized to reach values close to that of cycle 2. The fifth cycle witnessed a stabilization in the values as the fourth cycle.

This might suggest that the partial deactivation of the catalyst caused by some carbon deposition started taking place at the end of the first cycle and was amplified at the end of the second cycles. But during the initial start-up of the fourth cycle, the catalyst seemed to be partially regenerated and it restored some of its activity, after which it stabilized. This can be due to the presence of residual oxidizing gases such as water vapor after the reforming or oxygen from air during switching on/off which can oxidize the carbon deposited over the catalyst surface, transforming it into carbonaceous volatiles (CO or CO_2) [99,100] and therefore removing it. It can also be associated with the presence of some remaining H_2 in the system which can reduce and reactivate the catalyst [38].

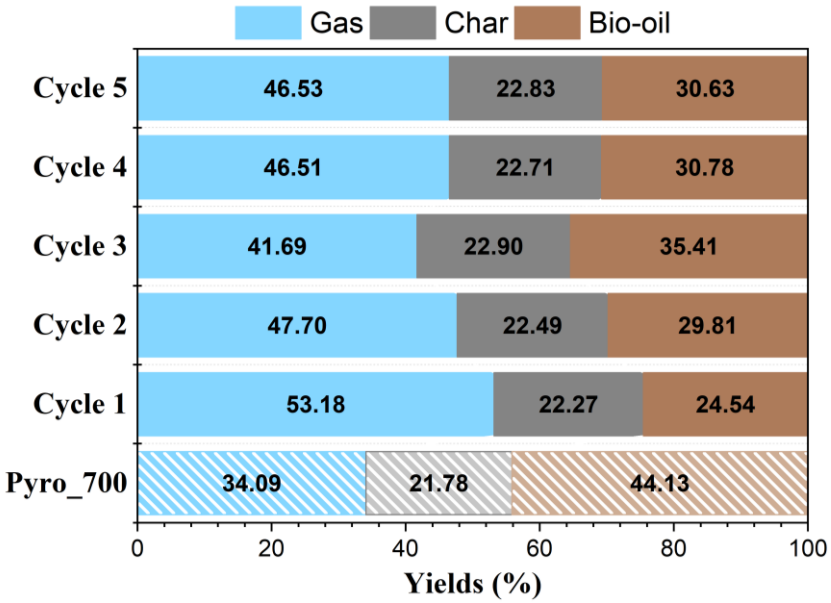

Figure 4.19 Distribution of the products derived from the pyrolysis at 700°C coupled to catalytic reforming at 750°C, over 20%Ni/Al_2O_3 beads (GHSV=4500h^{-1}) during its aging test over five cycles

4.4.7.2. Major gases' concentrations

The variation of the major gases produced during the five cycles of the aging test of the 20%Ni/Al_2O_3 beads is depicted in **Figure 4.20**. The largest H_2 and CO and smallest CO_2 and CH_4 concentrations are observed after cycle 1. Passing the first cycle, the H_2 started decreasing down to cycle 4 after which it stabilized. CO on the other hand dropped and CO_2 increased, and both remained constant after cycle 3. CH_4 started by increasing, peaked after cycle 3 then it decreased after cycle 4 and was stabilized. These observations are in accordance with the ones realized for the gases and bio-oil evolution during the five cycles, where a decrease in the total efficiency of the process is observed from cycle 1 to 3 after which it is relatively maintained constant.

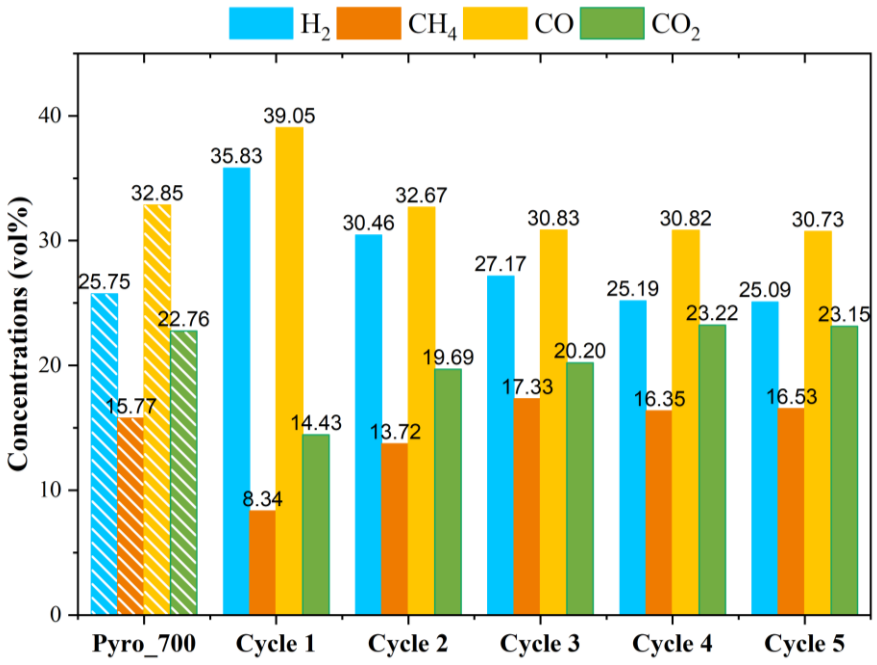

Figure 4.20 Variation of the volume concentrations of the major gases derived from the pyrolysis at 700°C coupled to catalytic reforming at 750°C, over 20%Ni/Al_2O_3 beads (GHSV=4500h^{-1}) during its aging test over five cycles

4.4.7.3. Main reactants' conversion rates

Figure 4.21 illustrates the conversion rates of the main reactants involved in the pyrolysis-reforming process for the aging test of the 20%Ni/Al_2O_3 beads. It can be noticed that the bio-oil conversion decreased from cycle 1 and reached a minimum after cycle 3 but was then risen back after cycle 4 and stabilized. The CH_4 conversion rate had a similar behavior but with negative conversion rate after cycle 3 which indicates a lack of CH_4 reaction and suggests that cracking reactions are favored over the methane reforming reactions. The CO_2 conversion rate experienced a constant decrease over the five cycles.

Khzouz *et al*. [85] performed the methane steam reforming using 10% Ni/Al_2O_3 catalyst at reforming temperatures between 500°C and 700°C. They also realized an on-off catalytic stability test for 20 hours over 3 days by running on and off campaigns. The reforming temperature was set at 700°C and the steam to carbon ratio was fixed at 2. They observed a drop from 87% to 75% of the methane conversion over the first day of operation, explained by the carbon formation on their catalyst. The methane conversion increased at the second day which they attributed to the reactivation of the catalyst by the steam which remained in the reactor during the shutting down and turning on of their process as well as for the hydrogen remaining in the cooling phase. After the third day, the methane conversion dropped again.

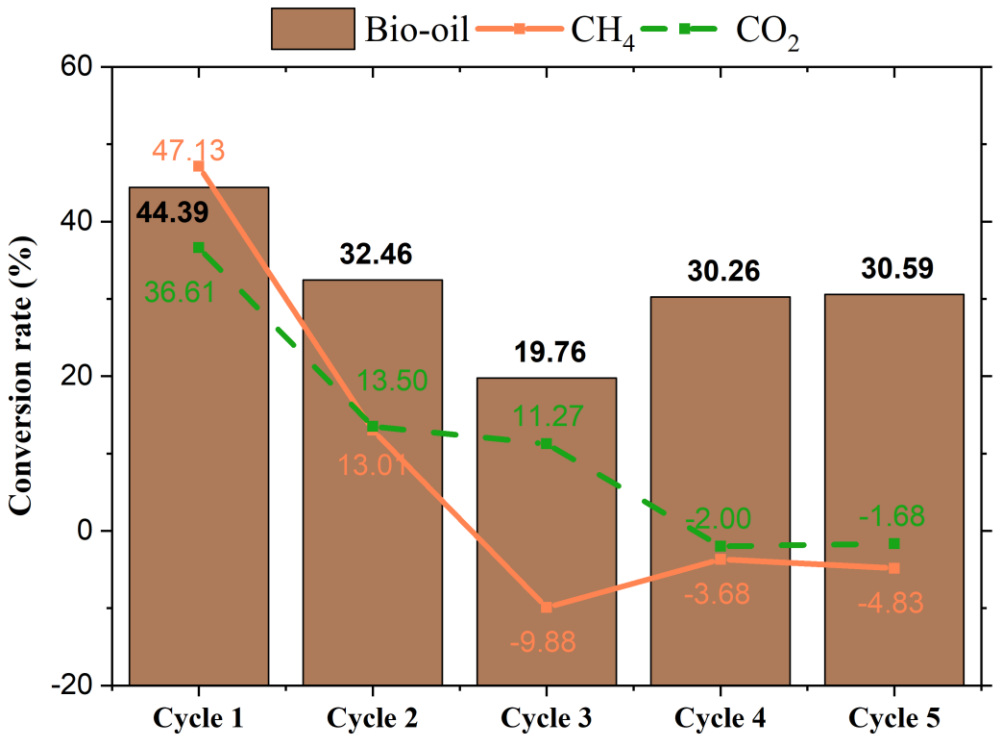

Figure 4.21 Variation of the conversion rates of the main reactants involved in the pyrolysis-reforming process realized with the pyrolysis at 700°C coupled to catalytic reforming at 750°C, over 20%Ni/Al_2O_3 beads (GHSV=4500h^{-1}) during its aging test over five cycles

4.4.7.4. Syngas production

The syngas concentrations and the H_2/CO ratio obtained after the aging test of the 20%Ni/Al_2O_3 beads during the pyrolysis-reforming process are represented in **Figure 4.22**. The syngas production had a remarkable decline between cycle 1 and cycle 3 after which it was stabilized. The H_2/CO ratio was almost the same for cycles 1 and 2 but it experienced a drop after cycles 3 and 4 above which it was constant.

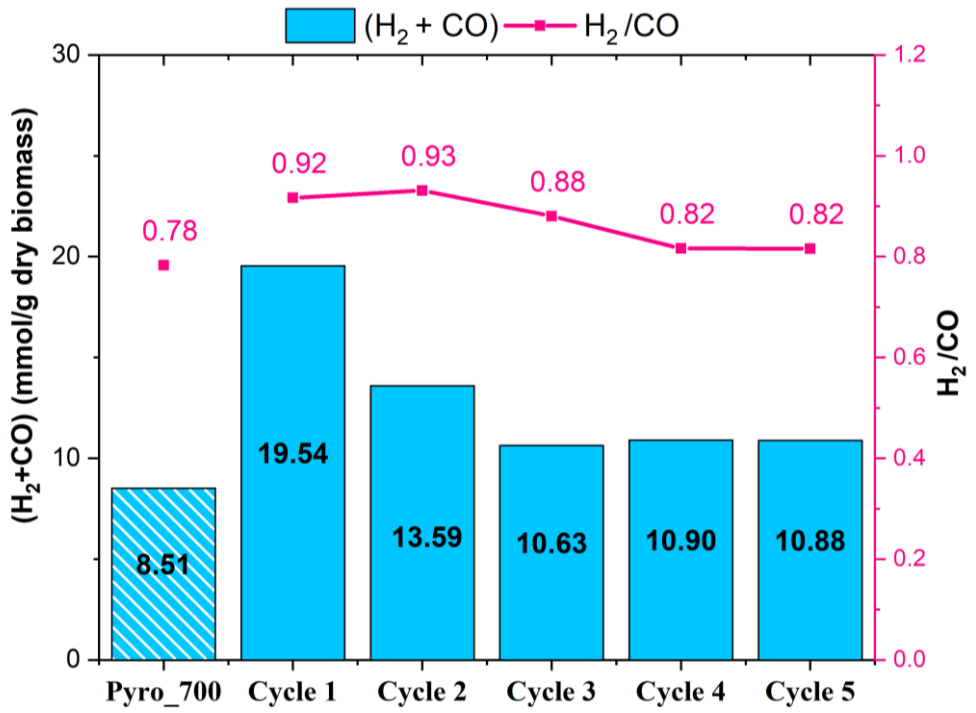

Figure 4.22 Evolution of syngas concentration and H_2/CO ratio produced by in the pyrolysis-reforming process realized with the pyrolysis at 700°C coupled to catalytic reforming at 750°C, over 20%Ni/Al_2O_3 beads (GHSV=4500h^{-1}) during its aging test over five cycles

All these previous observations lead to presuming that the *catalyst becomes partially deactivated after every reforming operation and after 3 cycles of operation it becomes almost completely deactivated. It therefore requires some external intervention to restore its activity.* This could be done through some pretreatment steps involving oxidation using an oxidizing agent such as air (or oxygen) and reduction using reduction agents like hydrogen which can regenerate and reactivate the catalyst [35,39]. The regeneration of the catalyst by an oxidation pre-step was realized in chapter 3 with the bulk catalysts and was proven to be efficient were the catalyst' activity was restored and maintained with time.

4.4.8. Characterization of the spent catalysts

4.4.8.1. Porosity and BET surface area

Table 4.5 summarizes the physical properties of the fresh and some of the spent catalysts after the reforming at different temperatures. The fresh catalysts with 10% metal loading have relatively close BET surface area, total pore volume and pore diameter. Doubling the Ni loading from 10 to 20%, lowered the surface area by 15% from 166.67 to 141.42 m^2/g, reduced the pore volume by 18% from 0.434 to 0.358 cm^3/g, and decreased the pore size by 20% from 8.83 to 7.09 nm. This is related to the presence of higher amounts of Ni which are more spread over the alumina support surface.

Examining the physical properties of the catalyst fresh before and spent after the reforming, for the same initial metal loading, reveals around 10% drop in the surface area and an average 15% drop in the total volume pore for the three types of active phase. It was accompanied by an increase in the pore diameter of around 22% for Ni and Co-Ni, except for the Co which had a slight drop in the pore diameter of around 4%. All these observations suggest the deposition of carbon over the catalyst surface which forms an additional layer around the catalyst support and

increases the pore diameter, thereby reducing the total volume of pores. It can also indicate the occurrence of the catalyst sintering phenomenon which causes a clustering of the metal particles and reduces the total surface area. This shall be confirmed by the SEM images hereafter.

The influence of temperature was evaluated also on the spent catalyst for the 20% Ni after reforming at 650°C and 800°C. It can be remarked that increasing the reforming temperature reduces the catalyst surface area by around 7% while increasing the pores diameter by almost 13%, whereas the total pore volume was only slightly reduced. This indicates the formation of carbon deposit over the catalyst surface, which is to be proven by the SEM, EDX and TGA analyses hereafter.

Table 4.5 Physical properties of the fresh and spent catalysts after reforming at different temperatures

Catalyst	Reforming temperature	Surface area (BET) (m^2/g)	Total pore volume (cm^3/g)	Pore diameter (BJH) (nm)
10% Cobalt – fresh	Not applicable	156.14	0.430	8.83
10% Cobalt-Nickel – fresh	Not applicable	165.04	0.436	7.30
10% Nickel – fresh	Not applicable	166.67	0.434	8.83
20% Nickel – fresh	Not applicable	141.42	0.358	7.09
10% Cobalt – spent	800°C	139.54	0.358	8.50
10% Cobalt-Nickel – spent	800°C	148.48	0.371	8.96
20% Nickel – spent	650°C	126.79	0.312	8.57
20% Nickel – spent	800°C	118.38	0.309	9.66

4.4.8.2. Scanning Electron Microscopy and Energy-dispersive X-ray spectroscopy

The SEM images for the fresh 20% Ni/Al_2O_3 catalyst are provided for two magnifications: ×10,000 and ×50,000 in **Figure 4.23 (a)** and **(b)**, respectively at a working distance of 4 mm, along with the EDX graphs where the elements presents were identified **Figure 4.23 (c)**. From **Figure 4.23 (a)** and **(b)**, the bead's structure can be observed with the Ni particles deposited over the alumina support, with an average diameter approximated to be between 30 and 40 nm. This is confirmed by the EDX graph presented in **Figure 4.23 (c)**, where the elements O, Ni and Al are detected along with small traces of C. The pores between the Ni particles can also be remarked in **Figure 4.23 (c**) with a diameter falling between 5 and 15 nm on average, as was reported previously in **Table 4.5** for the fresh 20% Ni catalyst with an average pore diameter of 7.09 nm. Note also the presence of large pores (about 1µm diameter) randomly dispersed on the catalyst surface, corresponding to the initial pores present in the alumina bead's structure that were poorly filled by the Ni particles.

The SEM images of the 20% Nickel catalyst after the reforming at 700°C are given in **Figure 4.24 (a)** and its magnification in **Figure 4.24 (b)** along with the EDX plot in **Figure 4.24 (c)**. It can be observed the presence of large white spots on **Figure 4.24 (a)** and **(b)** which were analyzed by the EDX and identified to be Ni particles over the alumina support. It indicates the presence of a cluster of Ni particles over the catalyst surface of an approximate diameter of 100 nm, which is way larger than the Ni particles observed in **Figure 4.23 (b)**, of an average diameter lower than 40 nm. *This reveals the occurring of the sintering phenomenon over the catalyst surface.* Sintering consists of the enlarging of the metallic particles during the reaction due to two main mechanisms. The first one relies on the metallic particles migrating over the support and coalescing with neighboring particles. The second one is based on the atoms migrating from one crystallite over the support to another one nearby [72]. Sintering influences badly the catalytic activity by reducing the amount of active sites therefore dropping the catalyst activity and the incitation of carbon formation by the larger metal particles [101].

Moreover, the presence of carbon filaments can be remarked more clearly from the magnification SEM image in **Figure 4.24 (b)**. The average diameter of these carbon filaments is approximated to be 50nm. These were analyzed and recognized as carbon filaments as remarked in the EDX plots in **Figure 4.24 (c)** where the element C is the by far the most abundant. *The filamentous carbon, also known as whisker carbon, is the type of carbon that is the most devastating on the performance of the catalyst*. It behaves like a shell on the catalyst and covers the Ni active sites layer by layer [101]. The formation of carbonous filaments can result if the Boudouard reaction is predominant during the methane reforming, mainly at high temperatures and low water content [103]. It is highly impacted by the presence of aromatics [95], which is valid in our process where the volatiles deriving from the pyrolysis and which are reformed over the catalyst surface, are rich in aromatics [46].

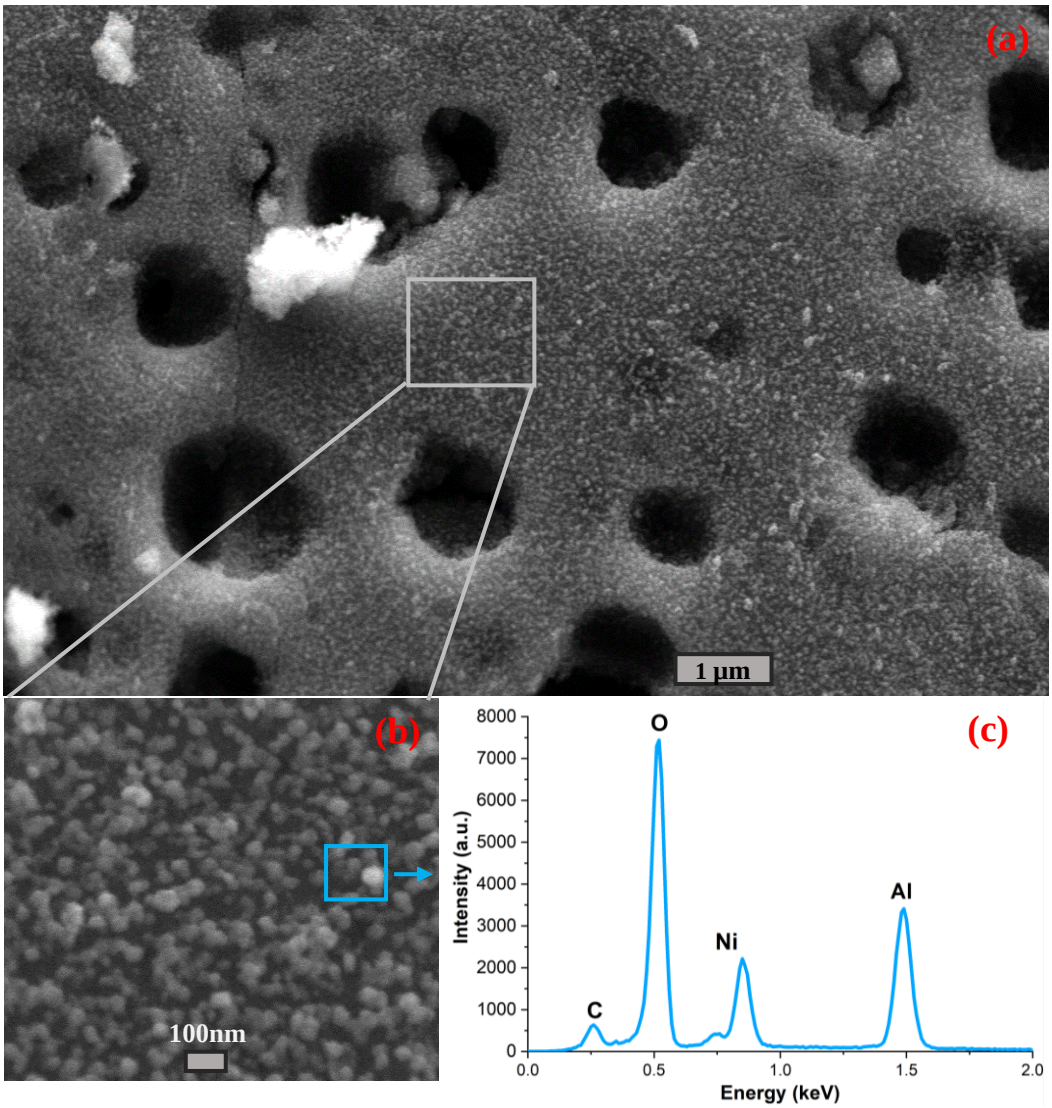

Figure 4.23 SEM images for the fresh 20% Ni/Al_2O_3 catalyst provided for two magnifications: 10,000 (a) and 50,000 (b) along with the SEM graphs (c) realized on the selected area in blue with the elements identified

The carbon formed by the methane cracking (equation **(4.21)**) and other hydrocarbons cracking reaction (equation **(4.12)**) and Boudouard reaction (equation **(4.10)**), spreads into the Ni crystal and nucleates on the opposite unexposed side [73]. This generates a strong filament which develops with a Ni crystal on its edge until it extracts the Ni crystal from the catalyst structure, and thereby destroys it [104]. The work of Artetxe *el al.* [16] also demonstrated the formation of filamentous carbon over their Ni/Al_2O_3 catalysts employed for the reforming of several biomass tar compounds after their reforming at 700°C. Similarly, Alvarez *el al.* [26] showed the presence of whiskers over their spent Ni/Al_2O_3 catalysts used for the pyrolysis/gasification of biomass and plastics.

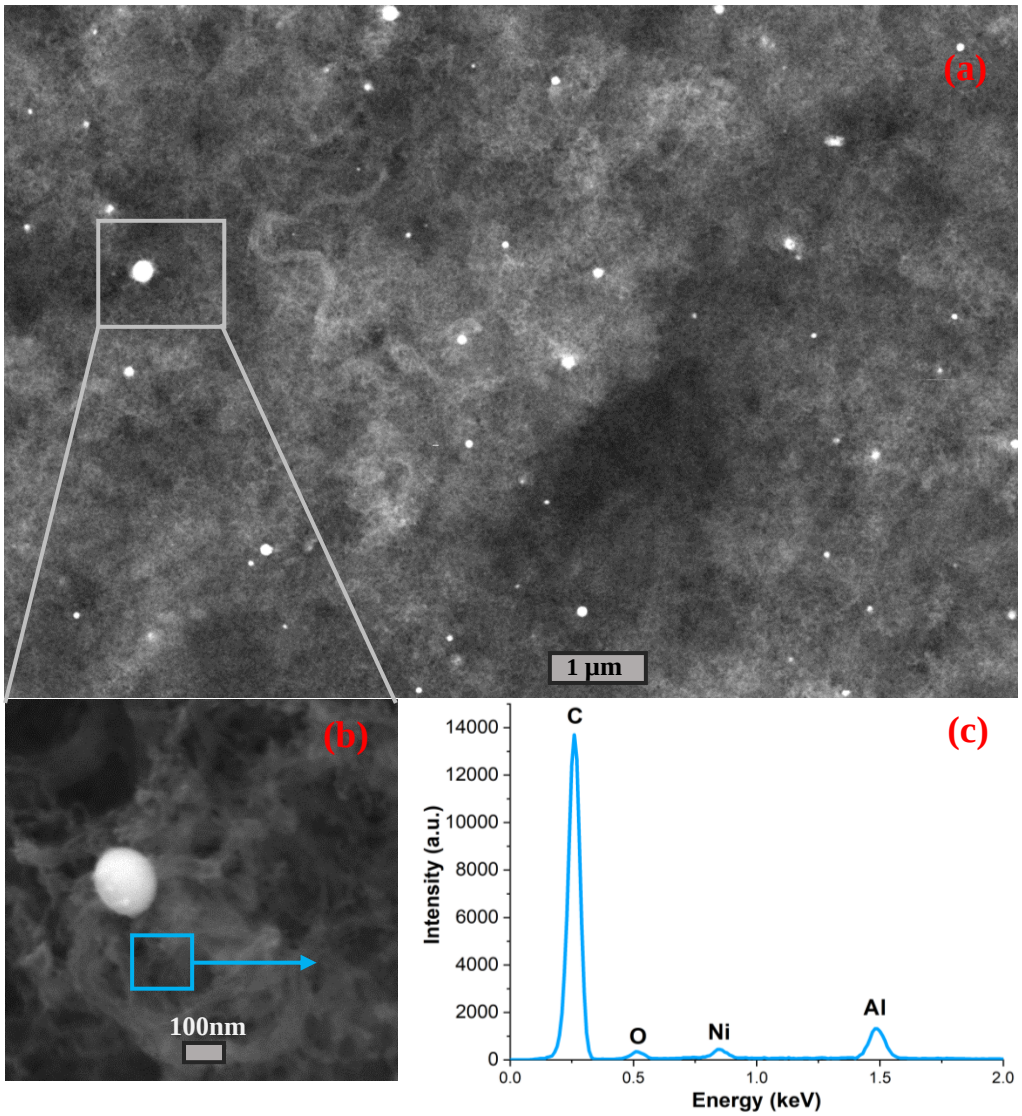

Figure 4.24 The SEM images for the spent 20% Ni/Al_2O_3 catalyst after reforming at 700°C, provided for two magnifications: 10,000 (a) and 50,000 (b) along with the SEM graphs (c) realized on the selected area in blue with the elements identified

The SEM images of the 20% Nickel catalyst after the reforming at 800°C are given in **Figure 4.25** (a) and its magnification in **Figure 4.25** (b) along with the EDX plot in **Figure 4.25** (c). More white spots can be observed for the 20% Ni catalyst after reforming at 800°C than after reforming at 700°C exposing the sintering of more Ni active sites as the reforming temperature is increased. On the other hand, the filamentous morphology of the carbon is less present for the catalyst after reforming at 800°C than after the reforming at 700°C, implying smaller amounts of carbon deposition by the reforming temperature increase, which shall be demonstrated by the TGA graphs as well.

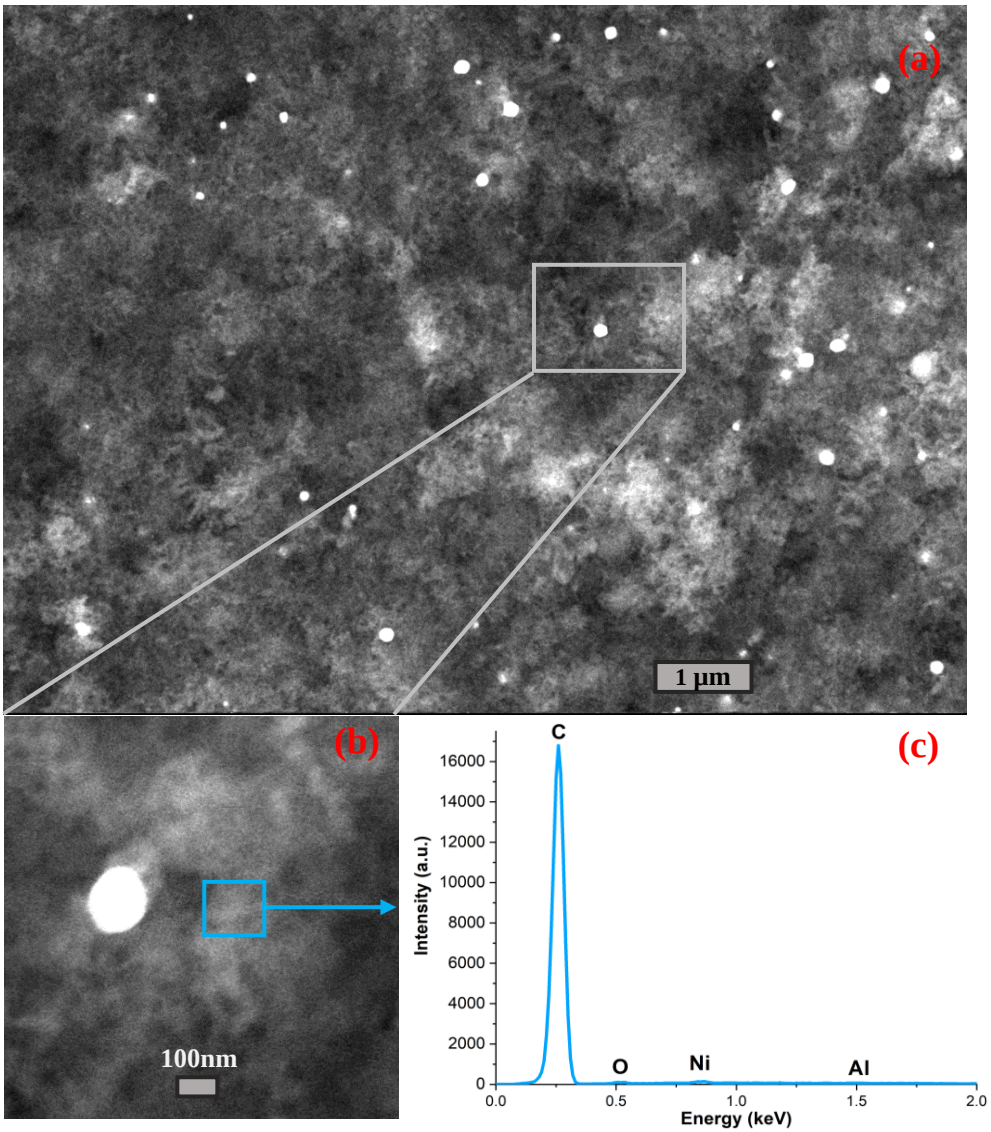

Figure 4.25 The SEM images for the spent 20% Ni/Al_2O_3 catalyst after reforming at 800°C, provided for two magnifications: 10,000 (a) and 50,000 (b) along with the SEM graphs (c) realized on the selected area in blue with the elements identified

The approximative diameter of the catalyst bead was determined for the three catalysts tested here and are reported in **Table 4.6.** This allowed the estimation of the thickness of the carbon layer formed over the spent catalysts' surfaces. The average diameter of the fresh Ni catalyst over the alumina bead is around 1492 µm or 1.492 mm which is in accordance with the average diameter of the alumina beads given by the supplier (around 1.6 mm). As can be remarked the average diameter of the catalyst is higher after the reforming than before it, leading to predict that the presence of a carbon layer. The thickness of this carbon layer was estimated to be 37.5 µm for the Ni catalyst after reforming at 700°C while that after reforming at 800°C was around 22.65 µm. This leads to the conclusion that *the amount of carbon deposited over the catalyst surface is considerable at a low reforming temperature and is lowered by the increase of the reforming temperature*, which will be confirmed by the TGA plots hereafter.

Table 4.6 Estimation of the average diameter of the catalysts and the thickness of the carbon layer over the spent nickel catalyst

Catalyst	*Average bead diameter (µm)*	*Carbon layer thickness (µm)*
20 % Ni-Fresh	1492,2	-
20% Ni-after reforming at 700°C	1567,2	37,5
20% Ni-after reforming at 800°C	1521,9	22,65

4.4.8.3. Thermogravimetry analysis

The high temperatures required for the dry reforming reactions lean to form carbons in addition to the side reactions occurring in parallel to the main reforming reactions such as the Boudouard reactions (equation **(4.10)**), and the methane decomposition reaction (equation **(4.21)**). The thermogravimetric analyses under air flow of the spent 20% Ni catalyst after the reforming at 700, 750 and 800°C are compared in the plots of **Figure 4.26**.

Considering the curve of the spent Ni catalyst after the reforming at 800°C, it can be noticed similarly a first weight loss of around 4% under 250°C corresponding to the evaporation of physiosorbed and coordinated water molecules [105]. It thereby represents the moisture content of the catalyst [106]. Between 300°C and 450°C, a weight gain of around 1.9% can be observed. It can be associated with the oxidation of the Ni metal active sites leading to the formation of metal oxides NiO, heavier than the metal particles, resulting in a weight gain. This reveals the presence of Ni active sites remaining over the spent catalyst surface even after reforming, meaning that the catalyst is not completely drained and can still be used for supplementary reforming reactions. A second weight loss of around 6% is observed which can be correlated to the oxidation of the carbon formed over the catalyst surface into CO or CO_2, which are volatiles leaving the catalyst and thereby leading to its weight loss [99,100,107]. This confirms the deposition of carbon over the catalyst surface as shown by the SEM images (**Figure 4.24 and Figure 4.25)**.

Looking at **Figure 4.26**, the TGA plots of the spent 20%Ni/Al_2O_3 catalysts after reforming at 700, 750 and 800°C show similar behavior consisting of a first weight loss below 300°C, followed by as small weight gain between 300 and 450°C and then a second major weight loss above 450°C. The first weight loss of between 4 and 5% is common for the three catalysts. The weight gain for the catalyst after reforming at 800°C (1.90%) is the highest, followed by that for the reforming at 700°C (1.2%) and then for the reforming at 700°C (0.96%). This means that the catalyst after reforming at 800°C has the highest remaining Ni active sites, which decrease as the reforming temperature is lowered. This confirms the results obtained with the reforming where the conversion rates were improved and syngas production increased with the increase of the reforming temperature as observed in **Figure 4.13** and **Figure 4.14**, respectively.

The major weight loss occurring above 450°C is the largest after the reforming at 700°C (9.2%). It then decreases to 8.6% for the reforming at 750°C and drops to 6% for the reforming at 800°C. *This implies that higher carbon amounts are deposited over the catalyst surface for lower reforming temperatures.* This conclusion was also retained from the SEM images (**Figure 4.24 and Figure 4.25)**, where less filamentous carbon was formed after the reforming at 800°C than at 700°C. The carbon formed blocks the pores as it was noticed by the reduction of the

pore sizes proven previously in **Table 4.5**, and it covers the active sites as demonstrated by the SEM images (**Figure 4.24 and Figure 4.25)**. This reduces the catalyst's activity and subsequently the hydrogen production. The drop in the carbon formation with the increase of the temperature was also proven by several other studies [74,101].

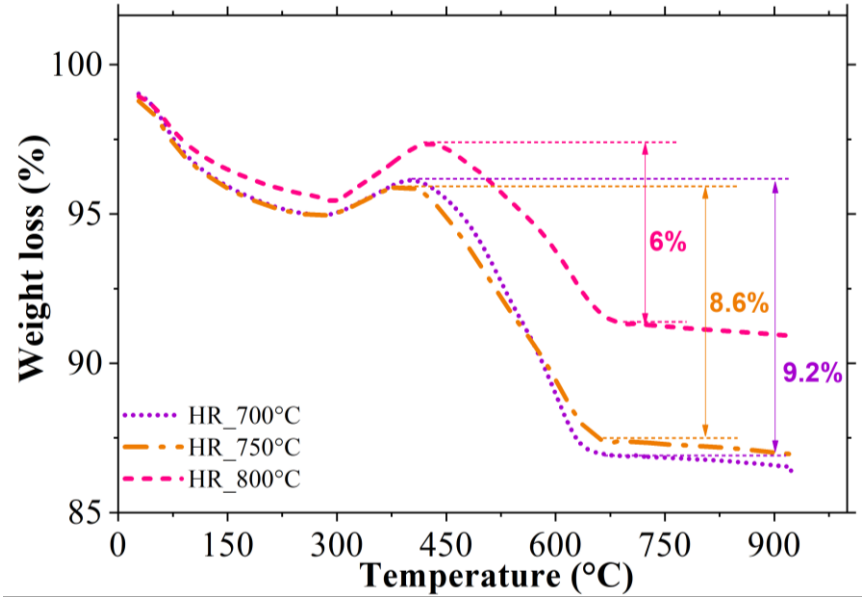

Figure 4.26 TGA plots for the spent 20% Nickel catalyst supported on alumina beads after the hybrid reforming at 700°C (in purple dots), 750°C (in orange dash dots) and 800°C (in pink dashes)

4.5. Conclusion

In this work, the coupling of the biomass pyrolysis to the catalytic reforming of the pyrolysis volatiles in a two-stage reactor was evaluated for the syngas production. In that purpose, flax shives were tested as biomass, and catalysts supported on alumina beads were used as catalysts. A single step of flax shives pyrolysis was realized separately at 700°C to analyze its products and determine the concentration of volatiles produced which will be fed to the reforming reactor when applied in the two-stage process. Numerous operating conditions were varied, and their effects were investigated over the major products, the main gases concentrations and syngas, in particular. The reforming is termed "hybrid" since both the dry and steam reforming occurs, at different extent, where the CO_2 and H_2O vapors produced by the pyrolysis are consumed as reactants for the reforming of the pyrolysis volatiles. Thanks to the analysis of the bio-oil composition pre- and post-reforming, it was demonstrated that the catalytic reforming is an efficient approach which transforms the heavy hydrocarbons in the pyrolysis bio-oil into lighter compounds and synthetic gases. Thereby, it can be regarded as an up-grading method which improves the bio-oil quality and favors its industrial applications.

First, three types of the catalysts' active phase were tested: Cobalt, Nickel and Cobalt-Nickel to realize the reforming at 800°C. The Ni-based catalyst was the most performant among the three catalysts for its selectivity towards syngas production and the methane conversion. However, only one metal loading of 10% for Co and Co-Ni catalysts and one ratio between Co and Ni (Co/Ni of 1) were tested. It therefore appears important to vary the metal loading of the Co relative to the Ni in the Co-Ni catalyst in order to improve its selectivity for the conversion of the main reactants: bio-oil, methane and carbon dioxide. However, this was out of the scope of this work, therefore Nickel was adopted for the other experiments.

Then, the metal loading of Ni over the alumina beads was varied from 0 to 25%. Increasing the metal loading to 20%, considerably improved the gases formation, syngas particularly, enhanced the bio-oil conversion and reduced the CH_4 and CO_2 emissions. However, surpassing the 20% Ni loading had opposing effects and therefore the 20% Ni loading was considered the optimal metal loading for an efficient catalytic bio-oil reforming.

Next, the reforming temperature was modified from 650°C to 800°C while fixing the pyrolysis temperature at 700°C. In general, increasing the temperature leads to a boost in the gases production, with the H_2 and CO markedly increasing, along with a strong improvement in the bio-oil, CH_4, and CO_2 conversions. The syngas reached its maximum amount of 22.55 mmol/g dry biomass with the 20%Ni and the reforming at 800°C. Nevertheless, an 800°C temperature can be considered energy intensive with a large economic impact and thereby a 750°C would be more appropriate with a satisfactory efficiency.

After that, the impact of the gas hourly space velocity (GHSV) was studied by changing the catalyst bed height which led to a GHSV variation from 900 to 4500 h^{-1}. Increasing the GHSV from 1125 to 4500 h^{-1} had a positive but relatively small impact on the products distribution where the gases were increased, and the bio-oil decreased. However, the syngas concentrations and the CH_4 and CO_2 conversions were dropped. Remarkably, the lowest GHSV value of 900 h^{-1}, had the most pronounced impact where the highest gases and syngas concentrations and reactants conversions were reached. Nonetheless, working at such a low GHSV implies consuming a large amount of the catalyst which can be economically inconvenient at larger scales. Therefore, a GHSV value around 4500 h^{-1} was adopted for the other experiments as it was considered relatively adequate for the reforming efficiencies.

Finally, a catalyst aging test was performed on the 20% Ni catalyst with the reforming at 750°C over five consecutive cycles. It revealed a drop in the catalyst activity from cycle 1 to cycle 3, with a decrease in the gases formation and conversion rates. Interestingly, the catalyst activity was restored at the end of the third cycle where an improvement in the gases' concentrations and the bio-oil conversion was obtained on the fourth cycle followed by a stabilization over the fifth cycle.

A summary of the different parameters studied with the values range tested, the optimal conditions, the corresponding products distribution, the main reactants conversion rates as well as the syngas concentrations and the H_2/CO ratios obtained is given in

Table 4.7.

Analytical tests were run on the fresh and spent catalysts to characterize them. They included the determination of the catalysts surface area, total pore volume and pore's diameter as well as SEM images with EDX mapping and TGA plots. They demonstrated that a carbon layer is deposited over the catalyst surface noticed by an increase in the pores' diameter and a decrease in the surface area and the pores volume which can also be associated to the catalyst's sintering. The SEM images also showed the formation of filamentous carbon which is one of the most adverse carbon types which significantly reduces the catalyst's performance. The TGA graphs confirmed these observations and helped quantify the amount of carbon deposited which was 9% over the 20%Ni catalyst after reforming at 700°C and was reduced to 6% as the reforming temperature was increased to 800°C.

Carbon deposition can be prevented by two approaches. The first one is to use carbon precursors which increase the steam adsorption on the catalyst surface [70]. The second one is to modify the catalyst by adding other metal additives like La_2O_3, MgO, CaO and K_2O which are basic promoters that aid in the adsorption and dissociation of CO_2, being of an acidic nature. Additionally, the carbon can be oxidized through the addition of some oxygen carriers such as ZrO_2 and CeO_2 reducing the carbon formation [75]. Moreover, a regeneration of the spent catalyst can be applied as a pre-treatment step, to remove the carbon deposited over its surface by realizing an oxidation under an air flow at 800°C. This will help restoring the catalyst activity and ensures its continuous use and stability with time.

Table 4.7 Summary of the parameters tested, the optimal conditions and the relative products distribution, conversion rates and syngas production

Parameter	**Values range tested**	**Optimal condition**	**Products distribution (wt.%)**	**Conversion rates (%)**	**Syngas (mmol/g dry biomass) and H_2/CO ratio**
Active phase	10% Co 10% Ni 10% Co-Ni	**10% Co-Ni**	**Gas:** ***51.12*** **Bio-oil:** ***26.52*** **Char:** 22.37	**Bio-oil:** ***39.92*** **CH_4:** -3.51 **CO_2:** 15.02	**Syngas:** 14.38 **H_2/CO ratio**: 0.91
		10% Ni	**Gas:** 42.89 **Bio-oil:** 34.65 **Char:** 22.46	**Bio-oil:** 21.49 **CH_4:** ***39.45*** **CO_2:** ***46.47***	**Syngas:** ***16.92*** **H_2/CO ratio:** ***0.95***
Nickel loading	[0%−25%]	**20%**	**Gas:** 52.99 **Bio-oil:** 24.33 **Char:** 22.68	**Bio-oil:** 44.87 **CH_4:** 62.57 **CO_2:** 48.27	**Syngas:** 22.55 **H_2/CO ratio**: 0.98
Temperature	[650°C−800°C]	**800°C**	**Gas:** 52.99 **Bio-oil:** 24.33 **Char:** 22.68	**Bio-oil:** 44.87 **CH_4:** 62.57 **CO_2:** 48.27	**Syngas:** 22.55 **H_2/CO ratio:** 0.98
GHSV	[900h^{-1}−4500h^{-1}]	**900 h^{-1}**	**Gas:** 52.61 **Bio-oil:** 24.86 **Char:** 22.52	**Bio-oil:** 43.66 **CH_4:** 60.36 **CO_2:** 51.15	**Syngas:** 23.12 **H_2/CO ratio:** 0.95

References

[1] V.N. Nguyen, L. Blum, Syngas and Synfuels from H2O and CO2: Current Status, Chem. Ing. Tech. 87 (2015) 354–375. https://doi.org/10.1002/cite.201400090.

[2] J.R. Rostrup-Nielsen, New aspects of syngas production and use, Catal. Today. 63 (2000) 159–164. https://doi.org/10.1016/S0920-5861(00)00455-7.

[3] S. Chu, S. Fan, Y. Wang, D. Rossouw, Y. Wang, G.A. Botton, Z. Mi, Tunable Syngas Production from CO2 and H2O in an Aqueous Photoelectrochemical Cell, Angew. Chem. Int. Ed. 55 (2016) 14262–14266. https://doi.org/10.1002/anie.201606424.
[4] N. Meng, W. Zhou, Y. Yu, Y. Liu, B. Zhang, Superficial Hydroxyl and Amino Groups Synergistically Active Polymeric Carbon Nitride for CO2 Electroreduction, ACS Catal. 9 (2019) 10983–10989. https://doi.org/10.1021/acscatal.9b03895.
[5] B. Sørensen, ed., Chapter 2 - Hydrogen, in: Hydrog. Fuel Cells Second Ed., Academic Press, Boston, 2012: pp. 5–94. https://doi.org/10.1016/B978-0-12-387709-3.50002-4.
[6] A. Velazquez Abad, P.E. Dodds, Green hydrogen characterisation initiatives: Definitions, standards, guarantees of origin, and challenges, Energy Policy. 138 (2020) 111300. https://doi.org/10.1016/j.enpol.2020.111300.
[7] J.M. Bermudez, I. Hannula, Hydrogen – Analysis, IEA. (2021). https://www.iea.org/reports/hydrogen (accessed February 21, 2022).
[8] A. Serrano-Lotina, A.J. Martin, M.A. Folgado, L. Daza, Dry reforming of methane to syngas over La-promoted hydrotalcite clay-derived catalysts, Int. J. Hydrog. Energy. 37 (2012) 12342–12350. https://doi.org/10.1016/j.ijhydene.2012.06.041.
[9] H. Balat, E. Kırtay, Hydrogen from biomass – Present scenario and future prospects, Int. J. Hydrog. Energy. 35 (2010) 7416–7426. https://doi.org/10.1016/j.ijhydene.2010.04.137.
[10] F. Dawood, M. Anda, G.M. Shafiullah, Hydrogen production for energy: An overview, Int. J. Hydrog. Energy. 45 (2020) 3847–3869. https://doi.org/10.1016/j.ijhydene.2019.12.059.
[11] M. Abou Rjeily, C. Gennequin, H. Pron, E. Abi-Aad, J.H. Randrianalisoa, Pyrolysis-catalytic upgrading of bio-oil and pyrolysis-catalytic steam reforming of biogas: a review, Environ. Chem. Lett. (2021) 48. https://doi.org/10.1007/s10311-021-01190-2.
[12] M. Abou Rjeily, C. Gennequin, H. Pron, E. Abi-Aad, J.H. Randrianalisoa, Chapter 9 - Catalysts for steam reforming of biomass tar and their effects on the products, in: M.R. Cesario, D.A. de Macedo (Eds.), Heterog. Catal., Elsevier, 2022: pp. 249–295. https://doi.org/10.1016/B978-0-323-85612-6.00009-7.
[13] M.I. Jahirul, M.G. Rasul, A.A. Chowdhury, N. Ashwath, Biofuels Production through Biomass Pyrolysis —A Technological Review, Energies. 5 (2012) 4952–5001. https://doi.org/10.3390/en5124952.
[14] G. Guan, M. Kaewpanha, X. Hao, A. Abudula, Catalytic steam reforming of biomass tar: Prospects and challenges, Renew. Sustain. Energy Rev. 58 (2016) 450–461. https://doi.org/10.1016/j.rser.2015.12.316.
[15] N. Gao, S. Liu, Y. Han, C. Xing, A. Li, Steam reforming of biomass tar for hydrogen production over NiO/ceramic foam catalyst, Int. J. Hydrog. Energy. 40 (2015) 7983–7990. https://doi.org/10.1016/j.ijhydene.2015.04.050.
[16] M. Artetxe, J. Alvarez, M.A. Nahil, M. Olazar, P.T. Williams, Steam reforming of different biomass tar model compounds over Ni/Al2O3 catalysts, Energy Convers. Manag. 136 (2017) 119–126. https://doi.org/10.1016/j.enconman.2016.12.092.
[17] Y. Shen, K. Yoshikawa, Recent progresses in catalytic tar elimination during biomass gasification or pyrolysis—A review, Renew. Sustain. Energy Rev. 21 (2013) 371–392. https://doi.org/10.1016/j.rser.2012.12.062.
[18] J. Ashok, Y. Kathiraser, M.L. Ang, S. Kawi, Bi-functional hydrotalcite-derived NiO–CaO–Al2O3 catalysts for steam reforming of biomass and/or tar model compound at low steam-to-carbon conditions, Appl. Catal. B Environ. 172–173 (2015) 116–128. https://doi.org/10.1016/j.apcatb.2015.02.017.
[19] X. Xu, E. Jiang, M. Wang, Y. Xu, Dry and steam reforming of biomass pyrolysis gas for rich hydrogen gas, Biomass Bioenergy. 78 (2015) 6–16. https://doi.org/10.1016/j.biombioe.2015.03.015.

[20] M. Balajii, S. Niju, Biochar-derived heterogeneous catalysts for biodiesel production, Environ. Chem. Lett. 17 (2019) 1447–1469. https://doi.org/10.1007/s10311-019-00885-x.
[21] S.A. Salaudeen, P. Arku, A. Dutta, 10 - Gasification of Plastic Solid Waste and Competitive Technologies, in: S.M. Al-Salem (Ed.), Plast. Energy, William Andrew Publishing, 2019: pp. 269–293. https://doi.org/10.1016/B978-0-12-813140-4.00010-8.
[22] O.C.N. Ndoung, C.C. de Figueiredo, M.L.G. Ramos, A scoping review on biochar-based fertilizers: enrichment techniques and agro-environmental application, Heliyon. 7 (2021) e08473. https://doi.org/10.1016/j.heliyon.2021.e08473.
[23] Y. Shen, Y. Fu, Advances in in situ and ex situ tar reforming with biochar catalysts for clean energy production, Sustain. Energy Fuels. 2 (2018) 326–344. https://doi.org/10.1039/C7SE00553A.
[24] N. Gao, Y. Han, C. Quan, Study on steam reforming of coal tar over NiCo/ceramic foam catalyst for hydrogen production: Effect of Ni/Co ratio, Int. J. Hydrog. Energy. 43 (2018) 22170–22186. https://doi.org/10.1016/j.ijhydene.2018.10.119.
[25] M.M. Barroso-Quiroga, A.E. Castro-Luna, Catalytic activity and effect of modifiers on Ni-based catalysts for the dry reforming of methane, Int. J. Hydrog. Energy. 35 (2010) 6052–6056. https://doi.org/10.1016/j.ijhydene.2009.12.073.
[26] J. Alvarez, S. Kumagai, C. Wu, T. Yoshioka, J. Bilbao, M. Olazar, P.T. Williams, Hydrogen production from biomass and plastic mixtures by pyrolysis-gasification, Int. J. Hydrog. Energy. 39 (2014) 10883–10891. https://doi.org/10.1016/j.ijhydene.2014.04.189.
[27] J. Ashok, N. Dewangan, S. Das, P. Hongmanorom, M.H. Wai, K. Tomishige, S. Kawi, Recent progress in the development of catalysts for steam reforming of biomass tar model reaction, Fuel Process. Technol. 199 (2020) 106252. https://doi.org/10.1016/j.fuproc.2019.106252.
[28] X. He, Y. Chen, Y. Liu, L. Fang, Z. Chen, H. Ji, Distribution of Products from Catalytic Conversion of Cellulose Over Metal-Modified Hierarchical H-ZSM-5 in Aqueous Media, Catal. Lett. 149 (2019) 2078–2088. https://doi.org/10.1007/s10562-019-02795-7.
[29] A.M. Fidalgo, L.M. Ilharco, Tailoring the structure and hydrophobic properties of amorphous silica by silylation, Microporous Mesoporous Mater. 158 (2012) 39–46. https://doi.org/10.1016/j.micromeso.2012.03.009.
[30] L. Santamaria, G. Lopez, E. Fernandez, M. Cortazar, A. Arregi, M. Olazar, J. Bilbao, Progress on Catalyst Development for the Steam Reforming of Biomass and Waste Plastics Pyrolysis Volatiles: A Review, Energy Fuels. 35 (2021) 17051–17084. https://doi.org/10.1021/acs.energyfuels.1c01666.
[31] B. Valle, A. Remiro, A.T. Aguayo, J. Bilbao, A.G. Gayubo, Catalysts of Ni/α-Al2O3 and Ni/La2O3-αAl2O3 for hydrogen production by steam reforming of bio-oil aqueous fraction with pyrolytic lignin retention, Int. J. Hydrog. Energy. 38 (2013) 1307–1318. https://doi.org/10.1016/j.ijhydene.2012.11.014.
[32] S. Wang, X. Li, F. Zhang, Q. Cai, Y. Wang, Z. Luo, Bio-oil catalytic reforming without steam addition: Application to hydrogen production and studies on its mechanism, Int. J. Hydrog. Energy. 38 (2013) 16038–16047. https://doi.org/10.1016/j.ijhydene.2013.10.032.
[33] M. Artetxe, M.A. Nahil, M. Olazar, P.T. Williams, Steam reforming of phenol as biomass tar model compound over Ni/Al2O3 catalyst, Fuel. 184 (2016) 629–636. https://doi.org/10.1016/j.fuel.2016.07.036.
[34] D. Li, M. Tamura, Y. Nakagawa, K. Tomishige, Metal catalysts for steam reforming of tar derived from the gasification of lignocellulosic biomass, Bioresour. Technol. 178 (2015) 53–64. https://doi.org/10.1016/j.biortech.2014.10.010.
[35] S.H. Kim, S.-W. Nam, T.-H. Lim, H.-I. Lee, Effect of pretreatment on the activity of Ni catalyst for CO removal reaction by water–gas shift and methanation, Appl. Catal. B Environ. 81 (2008) 97–104. https://doi.org/10.1016/j.apcatb.2007.12.009.

[36] J. Yang, J. Guo, Y. Wang, T. Wang, J. Gu, L. Peng, N. Xue, Y. Zhu, X. Guo, W. Ding, Reduction-oxidation pretreatment enhanced catalytic performance of Co3O4/Al2O3 over CO oxidation, Appl. Surf. Sci. 453 (2018) 330–335. https://doi.org/10.1016/j.apsusc.2018.05.103.

[37] Y.-Z. Wang, Y.-X. Zhao, C.-G. Gao, D.-S. Liu, Preparation and Catalytic Performance of Co3O4 Catalysts for Low-Temperature CO Oxidation, Catal. Lett. 116 (2007) 136–142. https://doi.org/10.1007/s10562-007-9099-4.

[38] P. Destro, S. Marras, L. Manna, M. Colombo, D. Zanchet, AuCu alloy nanoparticles supported on SiO2: Impact of redox pretreatments in the catalyst performance in CO oxidation, Catal. Today. 282 (2017) 105–110. https://doi.org/10.1016/j.cattod.2016.08.003.

[39] J. Lu, Y. Zhang, C. Jiao, S.K. Megarajan, D. Gu, G. Yang, H. Jiang, C. Jia, F. Schüth, Effect of reduction–oxidation treatment on structure and catalytic properties of ordered mesoporous Cu–Mg–Al composite oxides, Sci. Bull. 60 (2015) 1108–1113. https://doi.org/10.1007/s11434-015-0805-0.

[40] J. Leboucher, P. Bazin, D. Goux, H. El Siblani, A. Travert, A. Barbulée, J. Bréard, B. Duchemin, High-yield cellulose hydrolysis by HCl vapor: co-crystallization, deuterium accessibility and high-temperature thermal stability, Cellulose. 27 (2020) 3085–3105. https://doi.org/10.1007/s10570-020-03002-2.

[41] J.C. del Río, J. Rencoret, A. Gutiérrez, L. Nieto, J. Jiménez-Barbero, Á.T. Martínez, Structural Characterization of Guaiacyl-rich Lignins in Flax (Linum usitatissimum) Fibers and Shives, J. Agric. Food Chem. 59 (2011) 11088–11099. https://doi.org/10.1021/jf201222r.

[42] M. Sain, D. Fortier, Flax shives refining, chemical modification and hydrophobisation for paper production, Ind. Crops Prod. 15 (2002) 1–13. https://doi.org/10.1016/S0926-6690(01)00090-5.

[43] J.-W. Kim, G. Mazza, Optimization of Extraction of Phenolic Compounds from Flax Shives by Pressurized Low-Polarity Water, J. Agric. Food Chem. 54 (2006) 7575–84. https://doi.org/10.1021/jf0608221.

[44] W. Hu, M. Zhang, M.-T. Ton-That, T. Ngo, A comparison of flax shive and extracted flax shive reinforced PP composites, Fibers Polym. 15 (2014) 1722–1728. https://doi.org/10.1007/s12221-014-1722-6.

[45] A. Day, K. Ruel, G. Neutelings, D. Crônier, H. David, S. Hawkins, B. Chabbert, Lignification in the flax stem: evidence for an unusual lignin in bast fibers, Planta. 222 (2005) 234–245. https://doi.org/10.1007/s00425-005-1537-1.

[46] M. Abou Rjeily, F. Cazier, C. Gennequin, J.H. Randrianalisoa, Detailed Analysis of Gas, Char and Bio-oil Products of Oak Wood Pyrolysis at Different Operating Conditions, Waste Biomass Valorization. (2022). https://doi.org/10.1007/s12649-022-01848-0.

[47] A. Demirbaş, Gaseous products from biomass by pyrolysis and gasification: effects of catalyst on hydrogen yield, Energy Convers. Manag. 43 (2002) 897–909. https://doi.org/10.1016/S0196-8904(01)00080-2.

[48] P. Parthasarathy, K.S. Narayanan, Hydrogen production from steam gasification of biomass: Influence of process parameters on hydrogen yield – A review, Renew. Energy. 66 (2014) 570–579. https://doi.org/10.1016/j.renene.2013.12.025.

[49] M. Abou Rjeily, M. Chaghouri, C. Gennequin, E. Abi Aad, H. Pron, J.H. Randrianalisoa, Biomass Pyrolysis Followed by Catalytic Hybrid Reforming for Syngas Production, Waste Biomass Valorization. (2023) 29. https://doi.org/10.1007/s12649-022-02012-4.

[50] L. Li, J.S. Rowbotham, H. Christopher Greenwell, P.W. Dyer, Chapter 8 - An Introduction to Pyrolysis and Catalytic Pyrolysis: Versatile Techniques for Biomass

Conversion, in: S.L. Suib (Ed.), New Future Dev. Catal., Elsevier, Amsterdam, 2013: pp. 173–208. https://doi.org/10.1016/B978-0-444-53878-9.00009-6.

[51] E. Ranzi, A. Cuoci, T. Faravelli, A. Frassoldati, G. Migliavacca, S. Pierucci, S. Sommariva, Chemical Kinetics of Biomass Pyrolysis, Energy Fuels. 22 (2008) 4292–4300. https://doi.org/10.1021/ef800551t.

[52] C. Branca, C. Di Blasi, Kinetics of the isothermal degradation of wood in the temperature range 528–708 K, J. Anal. Appl. Pyrolysis. 67 (2003) 207–219. https://doi.org/10.1016/S0165-2370(02)00062-1.

[53] C. Di Blasi, Modeling chemical and physical processes of wood and biomass pyrolysis, Prog. Energy Combust. Sci. 34 (2008) 47–90. https://doi.org/10.1016/j.pecs.2006.12.001.

[54] L. Dong, C. Wu, H. Ling, J. Shi, P.T. Williams, J. Huang, Promoting hydrogen production and minimizing catalyst deactivation from the pyrolysis-catalytic steam reforming of biomass on nanosized NiZnAlOx catalysts, Fuel. 188 (2017) 610–620. https://doi.org/10.1016/j.fuel.2016.10.072.

[55] H.-G. Park, S. Han, K.-W. Jun, Y. Woo, M.-J. Park, S. Kim, Bench-Scale Steam Reforming of Methane for Hydrogen Production, Catalysts. 9 (2019) 615. https://doi.org/10.3390/catal9070615.

[56] Z. Qin, J. Chen, X. Xie, X. Luo, T. Su, H. Ji, CO2 reforming of CH4 to syngas over nickel-based catalysts, Environ. Chem. Lett. 18 (2020) 997–1017. https://doi.org/10.1007/s10311-020-00996-w.

[57] S.K. Chauhan, S. Gangopadhyay, N. Singh, Environmental aspects of biofuels in road transportation, Environ. Chem. Lett. 7 (2009) 289–299. https://doi.org/10.1007/s10311-008-0185-7.

[58] S. Sumrunronnasak, S. Tantayanon, S. Kiatgamolchai, T. Sukonket, Improved hydrogen production from dry reforming reaction using a catalytic packed-bed membrane reactor with Ni-based catalyst and dense PdAgCu alloy membrane, Int. J. Hydrog. Energy. 41 (2016). https://doi.org/10.1016/j.ijhydene.2015.10.129.

[59] M.A. Soria, C. Mateos-Pedrero, A. Guerrero-Ruiz, I. Rodríguez-Ramos, Thermodynamic and experimental study of combined dry and steam reforming of methane on Ru/ ZrO2-La2O3 catalyst at low temperature, Int. J. Hydrog. Energy. 36 (2011) 15212–15220. https://doi.org/10.1016/j.ijhydene.2011.08.117.

[60] M. Negri, M. Wilhelm, C. Hendrich, N. Wingborg, L. Gediminas, L. Adelöw, C. Maleix, P. Chabernaud, R. Brahmi, R. Beauchet, Y. Batonneau, C. Kappenstein, R.-J. Koopmans, S. Schuh, T. Bartok, C. Scharlemann, U. Gotzig, M. Schwentenwein, New technologies for ammonium dinitramide based monopropellant thrusters – The project RHEFORM, Acta Astronaut. 143 (2017). https://doi.org/10.1016/j.actaastro.2017.11.016.

[61] N. Gao, L. Baoling, A. Li, L. Juanjuan, Continuous pyrolysis of pine sawdust at different pyrolysis temperatures and solid residence times, J. Anal. Appl. Pyrolysis. 114 (2015). https://doi.org/10.1016/j.jaap.2015.05.011.

[62] M. Van de Velden, J. Baeyens, A. Brems, B. Janssens, R. Dewil, Fundamentals, kinetics and endothermicity of the biomass pyrolysis reaction, Renew. Energy. 35 (2010) 232–242. https://doi.org/10.1016/j.renene.2009.04.019.

[63] P. Morf, P. Hasler, T. Nussbaumer, Mechanisms and kinetics of homogeneous secondary reactions of tar from continuous pyrolysis of wood chips, Fuel. 81 (2002) 843–853. https://doi.org/10.1016/S0016-2361(01)00216-2.

[64] C. Wu, P.T. Williams, Hydrogen production by steam gasification of polypropylene with various nickel catalysts, Appl. Catal. B Environ. 87 (2009) 152–161. https://doi.org/10.1016/j.apcatb.2008.09.003.

[65] Y. Li, D. Li, G. Wang, Methane decomposition to COx-free hydrogen and nano-carbon material on group 8–10 base metal catalysts: A review, Catal. Today. 162 (2011) 1–48. https://doi.org/10.1016/j.cattod.2010.12.042.
[66] C. Quan, N. Gao, C. Wu, Utilization of NiO/porous ceramic monolithic catalyst for upgrading biomass fuel gas, J. Energy Inst. 91 (2018) 331–338. https://doi.org/10.1016/j.joei.2017.02.008.
[67] M. Kong, J. Fei, S. Wang, W. Lu, X. Zheng, Influence of supports on catalytic behavior of nickel catalysts in carbon dioxide reforming of toluene as a model compound of tar from biomass gasification, Bioresour. Technol. 102 (2011) 2004–2008. https://doi.org/10.1016/j.biortech.2010.09.054.
[68] N.D. Charisiou, A. Iordanidis, K. Polychronopoulou, I.V. Yentekakis, M.A. Goula, Studying the stability of Ni supported on modified with CeO2 alumina catalysts for the biogas dry reforming reaction, Mater. Today Proc. 5 (2018) 27607–27616. https://doi.org/10.1016/j.matpr.2018.09.081.
[69] N. Gao, X. Wang, A. Li, C. Wu, Z. Yin, Hydrogen production from catalytic steam reforming of benzene as tar model compound of biomass gasification, Fuel Process. Technol. 148 (2016) 380–387. https://doi.org/10.1016/j.fuproc.2016.03.019.
[70] D. Swierczynski, C. Courson, A. Kiennemann, Study of steam reforming of toluene used as model compound of tar produced by biomass gasification, Chem. Eng. Process. Process Intensif. 47 (2008) 508–513. https://doi.org/10.1016/j.cep.2007.01.012.
[71] J. Ashok, S. Kawi, Steam reforming of toluene as a biomass tar model compound over CeO2 promoted Ni/CaO–Al2O3 catalytic systems, Int. J. Hydrog. Energy. 38 (2013) 13938–13949. https://doi.org/10.1016/j.ijhydene.2013.08.029.
[72] J. Sehested, Four challenges for nickel steam-reforming catalysts, Catal. Today. 111 (2006) 103–110. https://doi.org/10.1016/j.cattod.2005.10.002.
[73] J.R. Rostrup-Nielsen, Production of synthesis gas, Catal. Today. 18 (1993) 305–324. https://doi.org/10.1016/0920-5861(93)80059-A.
[74] M. Chaghouri, S. Hany, H.L. Tidahy, F. Cazier, C. Gennequin, E. Abi-Aad, Chapter 8 - Dry reforming of methane for catalytic valorization of biogas, in: M.R. Cesario, D.A. de Macedo (Eds.), Heterog. Catal., Elsevier, 2022: pp. 207–248. https://doi.org/10.1016/B978-0-323-85612-6.00008-5.
[75] S. Aouad, M. Labaki, S. Ojala, P.K. Seelam, E. Turpeinen, C. Gennequin, J. Estephane, E. Abi-Aad, A Review on the Dry Reforming Processes for Hydrogen Production: Catalytic Materials and Technologies, in: 2018: pp. 60–128. https://doi.org/10.2174/9781681087580118020007.
[76] J. Zieliński, Morphology of coprecipitated nickel/alumina catalysts with low alumina content, Appl. Catal. Gen. 94 (1993) 107–115. https://doi.org/10.1016/0926-860X(93)85001-6.
[77] R. Lamber, G. Schulzekloff, On the Microstructure of the Coprecipitated Ni-Al2O3 Catalysts, J. Catal. 146 (1994) 601–607. https://doi.org/10.1006/jcat.1994.1102.
[78] L. Znak, J. Zieliński, The effect of potassium on Ni/Al2O3 catalyst in relation to CO/H2 reaction, Appl. Catal. Gen. 413–414 (2012) 132–139. https://doi.org/10.1016/j.apcata.2011.10.048.
[79] T. Borowiecki, A. Denis, M. Rawski, A. Gołębiowski, K. Stołecki, J. Dmytrzyk, A. Kotarba, Studies of potassium-promoted nickel catalysts for methane steam reforming: Effect of surface potassium location, Appl. Surf. Sci. 300 (2014) 191–200. https://doi.org/10.1016/j.apsusc.2014.02.053.
[80] M. Zhang, S. Ji, L. Hu, F. Yin, C. Li, H. Liu, Structural Characterization of Highly Stable Ni/SBA-15 Catalyst and Its Catalytic Performance for Methane Reforming with CO2, Chin. J. Catal. 27 (2006) 777–781. https://doi.org/10.1016/S1872-2067(06)60043-0.

[81] F. Yin, S. Ji, P. Wu, F. Zhao, C. Li, Deactivation behavior of Pd-based SBA-15 mesoporous silica catalysts for the catalytic combustion of methane, J. Catal. 257 (2008) 108–116. https://doi.org/10.1016/j.jcat.2008.04.010.

[82] A. Carrero, J.A. Calles, A.J. Vizcaíno, Hydrogen production by ethanol steam reforming over Cu-Ni/SBA-15 supported catalysts prepared by direct synthesis and impregnation, Appl. Catal. Gen. 327 (2007) 82–94. https://doi.org/10.1016/j.apcata.2007.04.030.

[83] P. Wu, X. Li, S. Ji, B. Lang, F. Habimana, C. Li, Steam reforming of methane to hydrogen over Ni-based metal monolith catalysts, Catal. Today. 146 (2009) 82–86. https://doi.org/10.1016/j.cattod.2009.01.031.

[84] P.O. Sharma, M.A. Abraham, S. Chattopadhyay, Development of a Novel Metal Monolith Catalyst for Natural Gas Steam Reforming, Ind. Eng. Chem. Res. 46 (2007) 9053–9060. https://doi.org/10.1021/ie070373+.

[85] M. Khzouz, E. Gkanas, Experimental and Numerical Study of Low Temperature Methane Steam Reforming for Hydrogen Production, Catalysts. 8 (2017) 5. https://doi.org/10.3390/catal8010005.

[86] J.R. Rostrupnielsen, J.H.B. Hansen, CO2-Reforming of Methane over Transition Metals, J. Catal. 144 (1993) 38–49. https://doi.org/10.1006/jcat.1993.1312.

[87] T.E. McMinn, F.C. Moates, J.T. Richardson, Catalytic steam reforming of chlorocarbons: catalyst deactivation, Appl. Catal. B Environ. 31 (2001) 93–105. https://doi.org/10.1016/S0926-3373(00)00274-5.

[88] D.K. Liguras, D.I. Kondarides, X.E. Verykios, Production of hydrogen for fuel cells by steam reforming of ethanol over supported noble metal catalysts, Appl. Catal. B Environ. 43 (2003) 345–354. https://doi.org/10.1016/S0926-3373(02)00327-2.

[89] A. Younis, J. Estephane, C. Gennequin, L. Tidahy, B. El Khoury, S. Aouad, E. Abi Aad, Influence of promoting Ni-based catalysts with ruthenium in the dry reforming of polypropylene plastics for syngas production, Int. J. Hydrog. Energy. (2022). https://doi.org/10.1016/j.ijhydene.2022.07.156.

[90] J. Xu, W. Zhou, Z. Li, J. Wang, J. Ma, Biogas reforming for hydrogen production over a Ni–Co bimetallic catalyst: Effect of operating conditions, Int. J. Hydrog. Energy. 35 (2010) 13013–13020. https://doi.org/10.1016/j.ijhydene.2010.04.075.

[91] C. Tanios, C. Gennequin, H.L. Tidahy, A. Aboukaïs, E. Abi-Aad, F. Cazier, C. Tanios, M. Labaki, C. Tanios, B. Nsouli, H2 production by dry reforming of biogas over Ni-Co-Mg-Al mixed oxides prepared via hydrotalcite route, in: 2016 7th Int. Renew. Energy Congr. IREC, 2016: pp. 1–6. https://doi.org/10.1109/IREC.2016.7478866.

[92] C. Tanios, S. Bsaibes, M. Nawfal, C. Gennequin, H.L. Tidahy, A. Aboukais, E. Abi-aad, M. Labaki, B. Nsouli, Preparation and characterization of Ni-Co-Mg-Al mixed oxides derived from layered double hydroxides and their performance in the dry reforming of methane, 2016 3rd Int. Conf. Renew. Energ. Dev. Ctries. REDEC. (2016). https://doi.org/10.1109/REDEC.2016.7577544.

[93] C. Tanios, S. Bsaibes, C. Gennequin, M. Labaki, F. Cazier, S. Billet, H. Tidahy, B. Nsouli, A. Aboukaïs, E. Abi-Aad, Syngas production by the CO2 reforming of CH4 over Ni–Co–Mg–Al catalysts obtained from hydrotalcite precursors, Int. J. Hydrog. Energy. (2017). https://doi.org/10.1016/j.ijhydene.2017.01.120.

[94] D. Kunii, T. Chisaki, 3 - Conversion of Solids with Gaseous Reactant, in: D. Kunii, T. Chisaki (Eds.), Rotary React. Eng., Elsevier, Amsterdam, 2008: pp. 27–46. https://doi.org/10.1016/B978-044453026-4.50005-0.

[95] J. Remón, F. Broust, J. Valette, Y. Chhiti, I. Alava, A.R. Fernandez-Akarregi, J. Arauzo, L. Garcia, Production of a hydrogen-rich gas from fast pyrolysis bio-oils: Comparison between homogeneous and catalytic steam reforming routes, Int. J. Hydrog. Energy. 39 (2014) 171–182. https://doi.org/10.1016/j.ijhydene.2013.10.025.

[96] A. Remiro, B. Valle, A.T. Aguayo, J. Bilbao, A.G. Gayubo, Steam Reforming of Raw Bio-oil in a Fluidized Bed Reactor with Prior Separation of Pyrolytic Lignin, Energy Fuels. 27 (2013) 7549–7559. https://doi.org/10.1021/ef401835s.

[97] E. Fernandez, L. Santamaria, M. Artetxe, M. Amutio, A. Arregi, G. Lopez, J. Bilbao, M. Olazar, Conditioning the volatile stream from biomass fast pyrolysis for the attenuation of steam reforming catalyst deactivation, Fuel. 312 (2022) 122910. https://doi.org/10.1016/j.fuel.2021.122910.

[98] S.D. Angeli, F.G. Pilitsis, A.A. Lemonidou, Methane steam reforming at low temperature: Effect of light alkanes' presence on coke formation, Catal. Today. 242 (2015) 119–128. https://doi.org/10.1016/j.cattod.2014.05.043.

[99] S.-J. Park, M.-K. Seo, Chapter 7 - Types of Composites, in: S.-J. Park, M.-K. Seo (Eds.), Interface Sci. Technol., Elsevier, 2011: pp. 501–629. https://doi.org/10.1016/B978-0-12-375049-5.00007-4.

[100] Y. Cui, J. Liang, Z. Wang, X. Zhang, C. Fan, D. Liang, X. Wang, Forward and reverse combustion gasification of coal with production of high-quality syngas in a simulated pilot system for in situ gasification, Appl. Energy. 131 (2014) 9–19. https://doi.org/10.1016/j.apenergy.2014.06.001.

[101] N. Charisiou, S. Douvartzides, G.I. Siakavelas, L. Tzounis, V. Sebastian, V. Stolojan, S. Hinder, M. Baker, K. Polychronopoulou, M. Goula, The Relationship between Reaction Temperature and Carbon Deposition on Nickel Catalysts Based on Al2O3, ZrO2 or SiO2 Supports during the Biogas Dry Reforming Reaction, Catalysts. 9 (2019) 676. https://doi.org/10.3390/catal9080676.

[102] J. Snoeck, G. Froment, Steam/CO2 Reforming of Methane. Carbon Formation and Gasification on Catalysts with Various Potassium Contents, Ind. Eng. Chem. Res. - IND ENG CHEM RES. 41 (2002). https://doi.org/10.1021/ie010665p.

[103] C.H. Bartholomew, Mechanisms of catalyst deactivation, Appl. Catal. Gen. 212 (2001) 17–60. https://doi.org/10.1016/S0926-860X(00)00843-7.

[104] N.A.K. Aramouni, J.G. Touma, B.A. Tarboush, J. Zeaiter, M.N. Ahmad, Catalyst design for dry reforming of methane: Analysis review, Renew. Sustain. Energy Rev. 82 (2018) 2570–2585. https://doi.org/10.1016/j.rser.2017.09.076.

[105] L. Chmielarz, M. Rutkowska, P. Kuśtrowski, M. Drozdek, Z. Piwowarska, B. Dudek, R. Dziembaj, M. Michalik, An influence of thermal treatment conditions of hydrotalcite-like materials on their catalytic activity in the process of N 2 O decomposition, J. Therm. Anal. Calorim. - J THERM ANAL CALORIM. 105 (2011) 161–170. https://doi.org/10.1007/s10973-011-1284-4.

[106] A. Awad, Md.A. Salam, B. Abdullah, Thermocatalytic decomposition of methane/methanol mixture for hydrogen production: Effect of nickel loadings on alumina support, in: 2017: p. 020030. https://doi.org/10.1063/1.5005363.

[107] L. Zhou, Chapter 3 - Fundamentals of Combustion Theory, in: L. Zhou (Ed.), Theory Model. Dispersed Multiph. Turbul. React. Flows, Butterworth-Heinemann, 2018: pp. 15–70. https://doi.org/10.1016/B978-0-12-813465-8.00003-X.

Chapter 5: Hydrogen production routes and their technico-economical evaluation

Résumé

Ce chapitre est issu dans son intégralité du chapitre d'ouvrage qui sera soumis en mai 2023 pour publication par « *Elsevier* » dans le livre intitulé « *Hydrogen Technology : Fundamentals and Applications* ».

Ce chapitre constitue la continuité du chapitre précédent en termes de couplage de la pyrolyse et du reformage pour la production de gaz de synthèse d'une part et d'autre part, et une ouverture vers l'intensification de la production d'hydrogène.

Tout d'abord, le reformage à la vapeur d'eau des composés volatils issus de la pyrolyse de la biomasse a été réalisé, sous différents rapports vapeur d'eau/biomasse (S/B pour Steam to Biomass ratio) et à plusieurs températures. Ensuite, l'environnement réactionnel a été modifié en changeant le gaz vecteur de l'azote (inerte) à l'air (oxydant) et à la vapeur d'eau pour évaluer son impact sur la pyrolyse de la biomasse seule et sur le couplage de la pyrolyse au reformage. Les effets de ces conditions opératoires ont été étudiés sur les produits majeurs et les principaux gaz formés ainsi que sur les taux de conversion des réactifs et les concentrations en gaz de synthèse.

En ce qui concerne la partie expérimentale, la même biomasse (anas de lin) et le même catalyseur (20% nickel supporté par des billes d'alumine) qui ont été testés dans le chapitre précédent ont été utilisés. De même, les mêmes fours de pyrolyse et de reformage ont été employés mais des modifications au montage expérimental ont été apportées pour permettre la réalisation du reformage à la vapeur d'eau (couramment appelé « vaporeformage »). Pour cela, une partie supplémentaire a été rajoutée au montage expérimental pour alimenter le reformeur en vapeur d'eau. Par conséquent, seules les modifications apportées au dispositif expérimental sont détaillées dans ce chapitre.

Concernant la série d'expériences de vaporeformage réalisées avec l'azote comme gaz vecteur, le rapport S/B a d'abord été augmenté de 0,29 à 3, ce qui a légèrement amélioré la production de gaz et réduit celle de la bio-huile. Par rapport au reformage à sec, le vaporeformage produit des concentrations de H_2 nettement supérieures, mais des quantités de CO inférieures. Il consomme également beaucoup moins de CO_2 et de CH_4, surtout lorsque le rapport S/B augmente. En réalité, le vaporeformage et le reformage à sec ont généralement lieu simultanément dans notre procédé de reformage hybride. Sans alimentation externe en vapeur, le reformage à la vapeur est moins important, comme le montre le rapport H_2/CO fluctuant autour de 1, et donc le procédé a plutôt été catégorisé comme un reformage à sec. Ainsi, une alimentation externe en vapeur d'eau est nécessaire pour accentuer l'effet du vaporeformage. Le vaporeformage permet de produire des quantités de H_2 supérieures à celles de CO, selon la

stœchiométrie de la réaction de vaporeformage, ce qui se traduit par un ratio H_2/CO supérieur à 1. Ceci a été observé lors de nos expériences où le ratio H_2/CO a atteint 1.65 quand un ratio S/B égal à 3 a été appliqué, à l'opposé d'un ratio H_2/CO de 1.26 pour un ratio S/B de 0.29. Néanmoins, la production totale de gaz de synthèse a été maintenue pour les différents rapports S/B. L'augmentation de la température de reformage de 700°C à 800°C pour un rapport S/B fixe a nettement amélioré la formation de gaz, y compris le gaz de synthèse, et a réduit celle du CO_2, du CH_4 et de la bio-huile.

L'utilisation de l'air comme gaz vecteur a eu un impact important sur la pyrolyse et le reformage. Pour la pyrolyse seule, la présence d'air a fortement augmenté la formation de gaz et réduit le rendement en charbon. La réalisation d'une étape de reformage postérieure à la pyrolyse a remarquablement intensifié la production de gaz pour atteindre presque 70 % en masse des produits totaux, la plus élevée parmi les différentes méthodes appliquées. Néanmoins, la formation d'hydrogène a été médiocre. Inversement, la pyrolyse à la vapeur a non seulement amélioré la production de gaz, mais a également produit les concentrations de gaz de synthèse et le rapport H_2/CO les plus élevés parmi les différents essais de pyrolyse réalisés sous air ou sous azote. Ces résultats ont été amplifiés lors du couplage du reformage à la vapeur à la pyrolyse à la vapeur avec un S/B de 3, où les plus importantes concentrations de gaz de synthèse ont été produites.

La seconde partie de ce chapitre a été dédié à une étude technique, environnementale et économique des voies de production d'hydrogène les plus couramment décrites dans la littérature. Il a été constaté que les principales voies de production d'hydrogène reposent sur les combustibles fossiles, la biomasse, l'eau, les sources biologiques et les flux de gaz résiduaires, par l'application de méthodes thermochimiques, biologiques et physiques ainsi que par la thermolyse et l'électrolyse. En ce qui concerne l'impact environnemental, il a été déduit que les voies de production d'hydrogène les plus respectueuses de l'environnement sont celles basées sur des sources d'énergie renouvelables telles que l'énergie solaire et éolienne. Toutefois, leur rapport coût-efficacité est inférieur à celui des autres technologies, ce qui rend difficile leur application à grande échelle.

Les décompositions thermochimiques des combustibles fossiles par gazéification du charbon et par reformage du gaz naturel présentent un rendement élevé de production d'hydrogène et sont commercialement développés mais elles entraînent non seulement de la pollution atmosphérique mais également contribuent significativement au réchauffement climatique par leur émission de gaz à effets de serre. Leurs applications à long terme nécessiteraient la mise en place d'un système de séquestration du carbone, ce qui augmenterait considérablement leur coût d'investissement. L'utilisation de la biomasse pour la production d'hydrogène semble être une solution appropriée à court et moyen termes, étant donné le bilan "neutre en carbone" de la biomasse. La combinaison de la pyrolyse de la biomasse en ligne avec le reformage catalytique à la vapeur se présente donc comme une solution viable pour la production d'hydrogène en raison de sa bonne efficacité et de son coût compétitif, comme cela a été démontré dans ce travail. En outre, étant donné la capacité du procédé à réduire les émissions de dioxyde de carbone et de méthane, il réduira la nécessité d'un système de séquestration du carbone en aval.

Pour permettre un meilleur référencement, les équations des réactions de pyrolyse et de reformage sont rementionnées aussi dans ce chapitre puisqu'elles sont cruciales pour les interprétations et les explications des résultats.

5.1. Introduction

Energy is regarded as one of the most crucial needs for the maintenance and the development of the everyday human life. The chief energy use is the power consumption used in several applications like building and accounts for 51% of the total energy consumption [1]. Thereby, energy became a key word in the worldwide discussions and considerations for the sustainability. A 50% increase in the global energy demand is predicted by 2023, as reported by the International Energy Agency [2]. Fossil fuels (coal, oil and natural gas) have been the main source of energy for more than a century now supplying 81% of the total energy and responsible for the generation of 66% of electricity [3]. Nevertheless, the reserves of oil, natural gas and coal are estimated to last for around 40, 60 and 200 years, respectively, following the current consumption rates [4]. Currently, the worldwide concern is mainly concentrated on the global warming caused by the greenhouse gases (GHG) emissions, deriving from their combustion and processing [5]. Thereby, the fossil fuels limited nature, their continuous depletion as well as their negative impact on the environment led the scientific community to search for alternative and sustainable sources of energy [6,7]. A "sustainable energy source" is regarded as an energy source that is not considerably drained by its continuous use and does not lead to major health hazards, pollutant emissions, social injustices or other environmental issues [8].

The renewable sources of energy such as wind, tides, waves, and solar energies are regarded as eco-friendly sources. Hydrogen has been considered as an alternative independent clean energy carrier which can be generated from green energy sources [9].The use of hydrogen as an alternative of fossil fuels is not a novel subject. Some studies dating from the 70s and the 80s can be found [10,11]. However, it is now experiencing a remarkably increasing interest due to the urging of the global problems accompanying the fossil fuel depletion, the rising carbon emissions and the climate change [12–14]. Hydrogen fuel energy can be used for transportation and electricity production. It has a low environmental impact and long storage duration [15]. Its conversion to mechanical energy such as combustion or electricity in fuel cells, contrarily to fossil fuels, produces only water vapor as by-product and leads to the production of almost three times more energy than other fuels with a higher efficiency [16]. For instance, the hydrogen energy content is 120 MJ/kg while that of liquefied natural gas is 54.4 MJ/kg and that of dry wood is 16.2 MJ/kg [16].

Despite being the most abundant element in the universe, dihydrogen (H_2) is only found in traces on the surface of the Earth (0.14%), and it is barley present in its atmosphere (0.07%). Hydrogen is mostly encountered combined with other elements [17]. With the continuous increase in the Earth's temperature, the use of hydrogen as fuel is urgently growing. This requires its production at large scales while using small quantities of fossil reserves [13] and mostly relying on biomass based feedstocks. The key which enables the hydrogen production would be developing and deploying processes capable of producing hydrogen while meeting the requirements of sustainability. This includes securing the energy supply, protecting the environment and competing economically [18].

In spite of the fact that multiple technologies have been developed at several scales for the use of hydrogen gas as an energy carrier, its major application is currently as chemical industrial feedstock [13]. In the automobile industry, hydrogen is used to produce lubricants and gasoline [19], whereas in the fertilizer industry, it is a staple feedstock for the ammonia synthesis [20]. Presently, the production of hydrogen was mainly realized by partial oxidation, gasification,

and steam reforming processes relying on fossil fuels as feedstock. They are considered as mature and commercial technologies which can be applied at lower production costs and higher efficiencies. The partial oxidation of natural gas has a 50% efficiency. The steam reforming of methane, major natural gas component, is vastly employed for the hydrogen production with 65 to 75 % efficiency [13]. Hydrogen can be also produced through biomass pyrolysis and gasification processes [21–26]. Theses thermal methods are appropriate for the production of hydrogen from biomass derivative products such as bio sourced gas [26] and oil [27]. Nevertheless, these methods still face some major drawbacks including the strong energy requirement and the high carbon emissions [2].

Moreover, hydrogen can be produced from water through numerous methods such as photolysis [28], electrolysis [29], thermolysis [30] and thermochemical splitting processes [31]. Recently, an emerging technology had been investigated for a non-fossil hydrogen production method based on ammonia NH_3 using plasma with and without a catalyst [32,33]. It has a 28.3% efficiency and can produce hydrogen with a 99.99% purity [2]. But this technology is novel and still under evaluation. Several review papers and studies exist on the hydrogen, its sources, applications [2,13], production methods from methane [34,35], coal [36,37], water [9,38], biological sources [39,40] and from biomass [27,24], its production costs and environmental effect [18,41,42,12].

The combination of the biomass pyrolysis to the steam reforming of the volatiles produced appears to be a viable approach for the hydrogen production [6], while consuming the methane (GHG) and valorizing the biomass simultaneously [7,43,44]. It is regarded as a potential technology for the small scale hydrogen production despite the rare studies on the subject [45]. Moreover, the pyrolysis step alone produces char, a solid valuable by-product [14], which can be recuperated at the end of the process from the pyrolysis reactor. The pyrolysis reaction environment strongly influences its products. It is conventionally realized in an inert atmosphere [43,46]. It would be of great interest to test the pyrolysis under an oxidative environment provided by air or steam [47], or other gases such as H_2 and CO_2, on which the studies are scarce [23]. Extrapolating to the industrial large scale requires a deep study of the operational cost since it would demand escalating the production capacity on several aspects, in order to adopt hydrogen as an energy currency [13].

This study focuses on three major axes. In this part, the steam reforming of the biomass pyrolysis' volatiles is evaluated while studying the effect of the steam to biomass ratio and the reforming temperature on the products distribution and gases concentrations. In the second part, the reaction environment was changed from nitrogen to air and steam for both the pyrolysis alone and the pyrolysis coupled to the reforming processes with an assessment of its effect on the products formation. The third part is dedicated to technical, environmental, and economic aspects of different hydrogen production routes.

5.2. Materials and methods

5.2.1. Biomass and catalyst used

The biomass investigated in this study was also flax shives. Details on its physical characteristics can be found in **chapter 4 in subsection 4.2.1.** The catalyst employed is the nickel supported on alumina 20% Ni/Al_2O_3 beads, as it was proven the most convenient for the syngas production according to the results obtained in **chapter 4 subsection 4.4.3.** Its synthesis and characterization were previously realized and described in **chapter 4 subsection 4.2.2**.

5.2.2. Reforming of pyrolysis volatiles *under different reaction environments*

The experimental set up designed for the previous pyrolysis/catalytic reforming experiments was also adopted for the experiments here with the scheme represented in **Figure 5.1** (a) and (b). It represents a first stage biomass pyrolysis reactor, a second stage volatiles' reforming reactor, and a steam generator. These three compartments can be operated simultaneously, interconnected, or used separately, by applying the appropriate connections, depending on the desired experiment. A condensate trap is used to remove the condensable volatiles forming the bio-oil which can plug the downstream pipelines. The gases produced are analyzed using a micro–Gas Chromatography/Mass Spectrometry gas analyzer previously calibrated to determine the concentrations of the main gases.

To push the steam reforming reactions further, an external feed of water vapor was injected into the reforming reactor in combination with the pyrolysis volatiles inlet flow. A controlled evaporator mixer (CEV, Bronkhorst) was used to generate steam from a water tank and to mix it with the desired nitrogen flow. Different water flow rates were injected resulting in several steam to biomass ratios, with details given in **section 3.2.3.**

To determine the influence of the carrier gas, two set of experiments were performed in this work. In the first one, pyrolysis took place in an inert environment guaranteed by the nitrogen stream. The reforming was tested with a steam input ensured by the steam generator system. In a second set, air (O_2) and steam were employed successively to realize pyrolysis experiments alone as well as a pyrolysis coupled to reforming experiments.

Figure 5.1 (a) represents the set up used for the experiments of pyrolysis and pyrolysis-reforming realized with nitrogen or air as carrier gas and for the steam reforming while the pyrolysis was realized under nitrogen. **Figure 5.1** (b) illustrated the experimental set up for the pyrolysis and pyrolysis-reforming realized with steam mixed with nitrogen as carrier gas.

For the experiments with air, the pyrolysis alone was realized at 700°C with an 80°C/min heating rate under 25 mL_n/min of air for 2 hours. For the coupled pyrolysis-reforming process, the pyrolysis was realized under the same conditions whereas the reforming was realized at 800°C. For the experiments with steam, a 25 mL_n/min of nitrogen carrying 5.25g/h of water steam at 105°C equivalent to a steam to biomass ratio (S/B) of 3 was used. Similarly, the reforming of the pyrolysis volatiles was done at 800°C. The average carrier gas flow rates applied imposed an average volatiles residence time in the pyrolysis reactor to be around 400s while in the reforming reactor it was 128s.

For all the experiments, the 3.5g of flax shives were first dried at 100°C for 1 h under 50 mL_n/min of nitrogen flow rate. For the reforming, the catalyst employed was 20% Ni supported on Al_2O_3 beads with a GHSV of 4500 h^{-1}, unless stated differently. The catalyst was first subject to oxidation at 800°C for 1 h under 30 mL_n/min air flowrate, then purge for 0.5 h under 50 mL_n/min of nitrogen and finally reduction for 1.5 h under 50 mL_n/min of a gas mixture of 10% H_2 and 90% N_2.

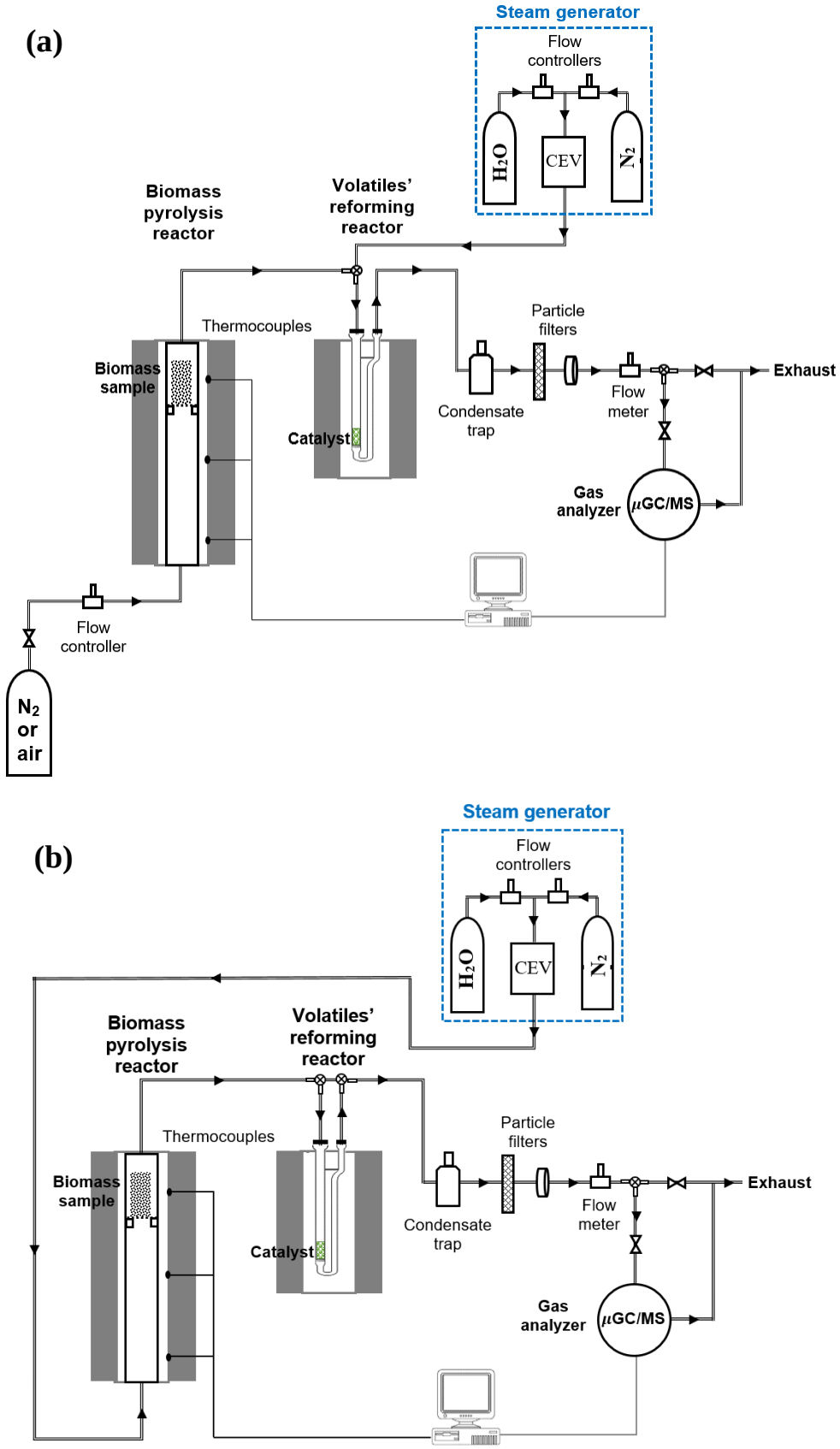

Figure 5.1 Schematic of the experimental set up used for the pyrolysis coupled in-line with the catalytic reforming. It consists of a two-stage reactor with the first one devoted to the biomass pyrolysis and the second one is for the catalytic reforming of the pyrolysis volatiles. CEV (Controlled evaporator mixer) is used for steam generation. Configuration (a) corresponds to the experiments realized with nitrogen or air as carrier gas for the pyrolysis and reforming as well as for the steam reforming with pyrolysis under nitrogen. Configuration (b) corresponds to the pyrolysis and reforming realized with steam mixed with nitrogen

5.3. Theory/Calculation

5.3.1. Pyrolysis and reforming reactions

The details on the pyrolysis and reforming reactions are described in the previous chapters with only the main reactions cited here. The global pyrolysis reaction simplifying the whole pyrolysis process is given in equation **(5.1**) [48]:

Biomass pyrolysis: $\text{Biomass} \rightarrow \text{char} + \text{hydrocarbon volatiles} + H_2 + CO + CO_2 + H_2O$ **(5.1)**

Numerous are the reactions of the steam and dry reforming of methane and tar involved in the process of syngas production and they are listed in equations **(5.2)** to **(5.7)** [48–51]:

Steam tar reforming: $C_xH_yO_z(\text{tar}) + (x-z)H_2O \rightarrow \left(x + \frac{y}{2} - z\right)H_2 + xCO \qquad \Delta H > 0$ **(5.2)**

Hydrocarbon volatiles steam reforming: $C_mH_n + mH_2O \rightarrow (m + \frac{n}{2})H_2 + mCO \qquad \Delta H > 0$ **(5.3)**

Steam reforming of methane SRM: $CH_4 + H_2O \leftrightarrow 3H_2 + CO \quad \Delta H°_{298K} = +205.9\ \text{kJ/mol}$ **(5.4)**

Dry tar reforming: $C_xH_yO_z(\text{tar}) + (x-z)CO_2 \rightarrow \frac{y}{2}H_2 + (2x-z)CO \qquad \Delta H > 0$ **(5.5)**

Hydrocarbon volatiles dry reforming: $C_mH_n + mCO_2 \rightarrow \frac{n}{2}H_2 + 2mCO \qquad \Delta H > 0$ **(5.6)**

Dry reforming of methane: $CH_4 + CO_2 \leftrightarrow 2H_2 + 2CO \qquad \Delta H°_{298K} = +247\ \text{kJ/mol}$ **(5.7)**

The endothermic nature of the reforming reactions leads to the occurrence of multiple secondary reactions (equations **(5.8**) to **(5.14**)) which can take place simultaneously as the main reforming reactions [48–51].

Water-gas shift reaction WGSR: $CO + H_2O \leftrightarrow H_2 + CO_2 \qquad \Delta H°_{298K} = -41.1\text{kJ/mol}$ **(5.8)**

Reverse WGSR: $H_2 + CO_2 \leftrightarrow CO + H_2O \qquad \Delta H°_{298K} = +41.1\text{kJ/mol}$ **(5.9)**

Boudouard reaction: $2CO \leftrightarrow CO_2 + C \qquad \Delta H°_{298K} = -172\ \text{kJ/mol}$ **(5.10)**

Reverse water-gas reaction: $CO + H_2 \rightarrow H_2O + C \qquad \Delta H°_{298K} = -131\text{kJ/mol}$ **(5.11)**

Thermal tar cracking: $pC_nH_x(\text{tar}) \rightarrow qC_mH_y(\text{smaller tar}) + rH_2 \qquad \Delta H > 0$ **(5.12)**

Tar decomposition: $C_nH_x(\text{tar}) \rightarrow \text{coke precursors (aromatics + olefins)} \rightarrow nC + (\frac{x}{2})H_2 \qquad \Delta H > 0$ **(5.13)**

Hydrocarbons (HC) steam reforming: $HC + H_2O \rightarrow H_2 + CO + CO_2 \qquad \Delta H > 0$ **(5.14)**

5.3.2. Characteristic parameters

5.3.2.1. Global mass balance, conversion rates and syngas concentration

The global mass balance is realized around the designated process to determine the mass concentrations of the gas, bio-oil and char. The conversion rates of the main reactants involved in the pyrolysis/reforming process are defined by equations **(5.15)-(5.17)**, with X attributed for the conversion rate. "Pyrolysis" is for the pyrolysis products entering the reforming process whereas "pyrolysis-reforming" refers to the volatiles exiting the reforming reactor.

$$\text{Conversion rate of bio} - \text{oil } (X_{bio-oil})\ (\%) = \frac{\text{moles of bio} - \text{oil(pyrolysis)} - \text{moles of bio} - \text{oil (pyrolysis/reforming)}}{\text{moles of bio} - \text{oil(pyrolysis)}} \times 100 \quad \textbf{(5.15)}$$

$$\text{Conversion rate of } CH_4\ (X_{CH_4})\ (\%) = \frac{\text{moles of } CH_4\text{(pyrolysis)} - \text{moles of } CH_4\text{(pyrolysis/reforming)}}{\text{moles of } CH_4\text{(pyrolysis)}} \times 100 \quad \textbf{(5.16)}$$

$$\text{Conversion rate of } CO_2\ (X_{CO_2})\ (\%) = \frac{\text{moles of } CO_2\text{(pyrolysis)} - \text{moles of } CO_2\text{(pyrolysis/reforming)}}{\text{moles of } CO_2\text{(pyrolysis)}} \times 100 \quad \textbf{(5.17)}$$

The syngas concentration was evaluated in terms of mmol/g of dry biomass by equation **(5.18)** while the hydrogen to carbon monoxide ratio is determined by equation **(5.19)**.

$$\text{Syngas concentration } (H_2 + CO)\ (\text{mmol/g dry biomass}) = \frac{\text{number of moles of } H_2 + \text{number of moles of CO}}{\text{dry weight of biomass}} \quad \textbf{(5.18)}$$

$$\text{Ratio } H_2/CO = \frac{\text{number of moles of } H_2}{\text{number of moles of CO}} \quad \textbf{(5.19)}$$

5.3.2.2. GHSV

The gas hourly space velocity was determined for the supported beads catalysts by applying the equation **(5.20)**:

$$\text{GHSV } (h^{-1}) = \frac{N_2 \text{ flow rate}}{\text{Volume of catalytic bed}} = \frac{N_2 \text{ flow rate}}{\text{Height of catalytic bed} \times \text{Reactor's surface} \times \text{void fraction}} \quad \textbf{(5.20)}$$

The N_2 carrier gas flow rate was fixed at 25 mL_n/min for all the experiments. The internal diameter of the reactor was 0.022m. The height of the catalytic bed was varied 1.6 mm, corresponding to a catalyst weight of 0.32 g. The void fraction between the catalyst beads was assumed to be 0.55 maximum [52]. Therefore, the GHSV was determined to be 4500 h^{-1}.

5.3.2.3. Steam to biomass ratio

The steam to biomass ratio is defined as follows by equation **(5.21)**:

$$\text{Steam to biomass ratio: } S/B = \frac{\text{Water vapor flow rate}}{\text{biomass flow rate}} \quad \textbf{(5.21)}$$

Thus, the carbon in the volatiles can be determined by equation **(5.22)** and was found to be around 0.96 g and the carbon flow rate is thereby 0.48 $g.h^{-1}$. Therefore, the steam to carbon ratio calculated following equation **(5.23)**.

$$\text{Carbon weight in pyrolysis volatiles} = [\%C_{biomass}] \times m_{biomass} - [\%C_{char}] \times m_{char} \quad \textbf{(5.22)}$$

$$\text{Steam to carbon ratio: } S/C = \frac{\text{Water vapor flow rate}}{\text{carbon flow rate in pyrolysis volatiles}} \quad \textbf{(5.23)}$$

Where $\%C_{biomass}$ stands for the Carbon percentage in the biomass, $m_{biomass}$ is for the weight of the biomass, $\%C_{char}$ refers to the Carbon percentage in the char determined from a previous elemental analysis and m_{char} is for the weight of the char. A summary of the steam feeds, the S/B and S/C ratios applied for the steam reforming process is delivered in the **Table 5.1**.

Table 5.1 List of the steam feeds, the S/B and S/C ratios applied for the steam reforming process

Steam feed ($g.h^{-1}$)	**0.5**	**1**	**1.75**	**3.5**	**5.25**
S/B ratio	0.29	0.57	1	2	3
S/C ratio	1.04	2.08	3.63	7.27	10.90

5.4. Results and discussion

5.4.1. Steam reforming of pyrolysis volatiles over supported catalysts

5.4.1.1. Effect of Steam/Biomass ratio

The steam reforming is known to produce higher amounts of hydrogen than the dry reforming [6]. In this perspective, an external steam feed was added to the main pyrolysis volatiles stream with different steam to biomass S/B ratios as detailed in **Table 5.1.** The impact of the S/B ratio was studied over the pyrolysis-reforming process with the 20% Ni/Al_2O_3 beads and a GHSV of $4500h^{-1}$ with the pyrolysis temperature set at 700°C and that of reforming at 800°C.

To present the effect of the S/B ratio over the different products, the steam enriched reforming experiments with the different S/B ratios are identified with "S/B=x" with x being the value of the S/B ratio going from 0.29 to 3. The results obtained previously with the hybrid dry reforming (i.e., without an external steam feed) are displayed as well for the comparison purpose with the pyrolysis realized at 700°C and the reforming at 800°C and is labeled "DR_700-800".

5.4.1.1.1. Main products concentrations

The pyrolysis-reforming process produces different products that can be categorized into three major categories: char (solid), bio-oil (condensable vapors) and gas (incondensable vapors). The impact of the S/B ratio on the major products distribution is illustrated in **Figure 5.2**. For the hybrid steam enriched reforming, at a low S/B ratio of 0.29, the gases yield was lower, and the bio-oil was higher than with the hybrid dry reforming. It reflects that a S/B ratio of 0.29 is fairly low and insufficient to trigger the steam reforming reactions.

However, when the S/B ratio is increased to 0.57, the gas yields increased while the bio-oil yield dropped and became relatively close to that obtained with the hybrid dry reforming. This means that the addition of an external steam feed pushes the reforming reactions towards the steam reforming. *Nonetheless, increasing the S/B ratio above 0.57 had a low impact on the overall gas production, whereas it significantly affects the gaseous composition,* as it will be remarked hereafter.

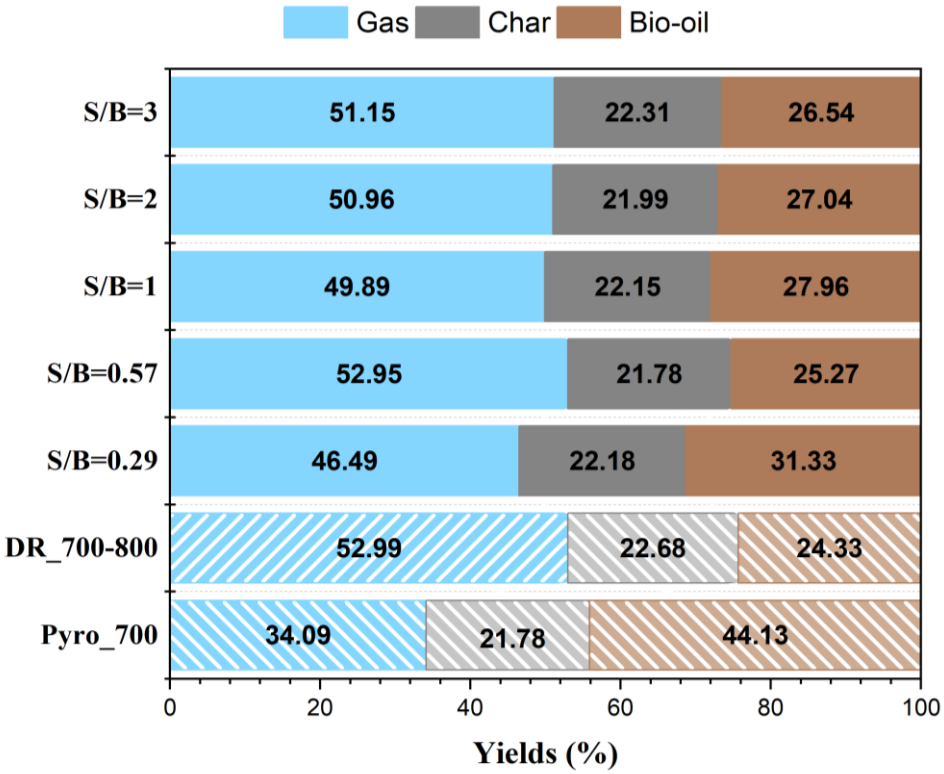

Figure 5.2 Effect of S/B ratio on the distribution of the products derived from the pyrolysis coupled to the hybrid steam enriched reforming process realized with the 20% Ni/Al_2O_3 beads ($GHSV=4500h^{-1}$). The pyrolysis was realized at 700°C while the reforming was at 800°C. The results obtained previously with the hybrid dry reforming are shown as well and labeled "DR_700-800" referring to the Dry Reforming (without an external water vapor feed)

5.4.1.1.2. Major gases' concentrations

Similarly, the effect of the S/B ratio on the major gases' concentrations derived from the hybrid reforming with the external steam feed is illustrated in **Figure 5.3**. The major gases produced are divided into two groups: the syngas comprising the H_2 and CO, and the greenhouse gases GHG including the CH_4 and CO_2. It can be noticed that in contrast to the hybrid dry reforming, *as the S/B ratio increases from 0.29 to 3 with the hybrid steam enriched reforming, the H_2 production markedly enhances while that of CO drops*, contrarily to the dry reforming where both H_2 and CO increased. Simultaneously, the CO_2 concentrations were also increased with the augmentation of the S/B ratio relative to the hybrid dry reforming. The CH_4 concentrations were also higher with the steam reforming than with the dry reforming but remained almost steady with the increase of the S/B ratio. In fact, as the S/B ratio is raised, the steam partial pressure is also increased thus improving the kinetics of the steam reforming reactions (equations **(5.2)-(5.4)**) and displacing the equilibrium of the WGSR (equation **(5.8)**) towards the hydrogen production.

Similar conclusions were driven by Arregi *et al.* [43] who realized a two-stage process aiming the hydrogen production from biomass. The first stage is a conical spouted bed reactor reserved for fast pyrolysis of pinewood waste while the second stage is a fluidized bed reactor for the catalytic steam reforming in the presence of 14%NiO supported on alumina. They studied the effect of the S/B ratio by varying it from 2 to 5 and found that increasing the S/B ratio led to an increase in the H_2 and CO_2 yields and a reduction in those of CO and CH_4. The changes were minimal when the S/B ratio was increased from 3 to 5 and therefore they deduced that a low S/B ratio can be efficient and sufficiently convenient.

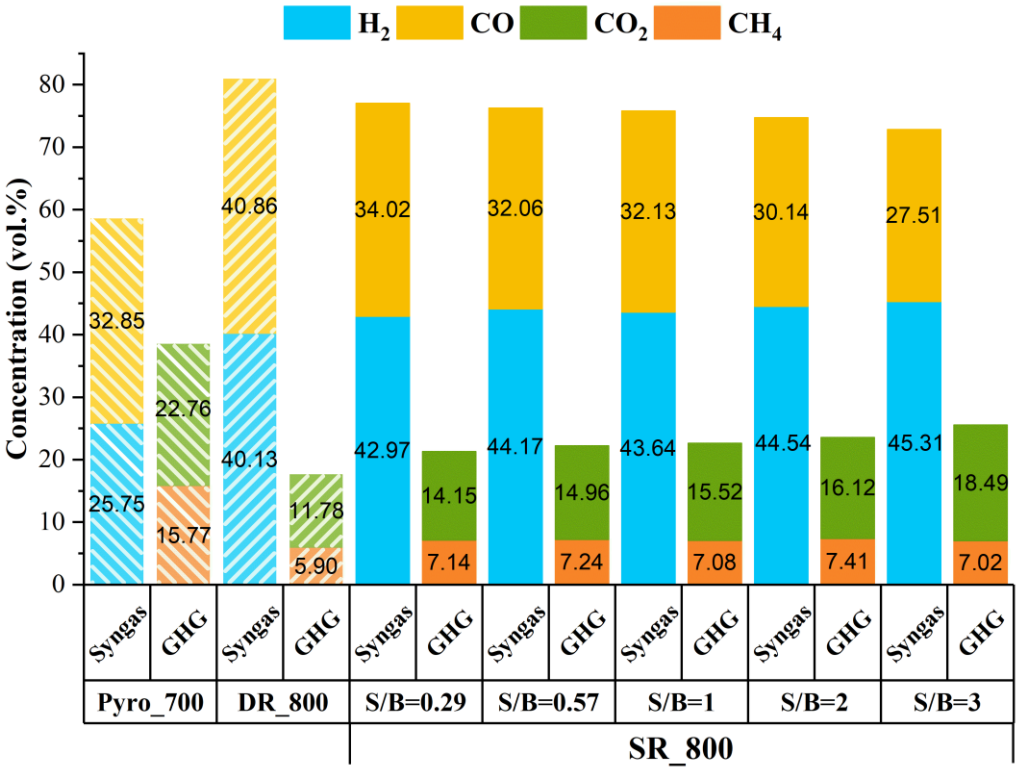

Figure 5.3 Effect of S/B ratio on the concentrations of major gases produced by the pyrolysis coupled to the hybrid steam enriched reforming process realized with the 20% Ni/Al_2O_3 beads (GHSV=4500h^{-1}). The gases are divided into syngas and greenhouse gases GHG

A potential explanation of the results could be as follows. During the steam reforming of the pyrolysis volatiles, the bio-oil hydrocarbons are adsorbed on the Ni active sites resulting in the occurrence of the cracking and dehydrogenation reactions. This liberates H_2 molecules along with lighter hydrocarbon molecules which can be re-adsorbed on the catalyst. These smaller hydrocarbon fragments can be polymerized into unwanted intermediate molecules leading to the formation of coke. These reactions are in competition with the ones involving the water compounds. The catalyst must thereby supply enough adsorbed water species to overcome the coke forming reactions [7,53]. One of the possible solutions to reduce the coke deposition is to add other metals such as Mg in the structure of the catalyst's support which will generate basic oxides. These latter induce the chemisorption of oxidants such as H_2O and CO_2 by the catalyst, which reduces the coke formation [54].

5.4.1.1.3. Main reactants' conversion rates

Figure 5.4 demonstrates the impact of an external steam feed with several S/B ratios on the conversion rates of the main reactants consumed by the pyrolysis-reforming process. The observations made on the bio-oil and the gases concentrations are translated on their conversion rates. For instance, the bio-oil conversion was the lowest (29%) with the steam enriched reforming at S/B ratio of 0.29. It then increased with an S/B ratio equals 0.57 and continued fluctuating around 38% as the S/B ratio was elevated, remaining nevertheless always inferior to the conversion rate obtained with the dry reforming (around 45%).

The CH_4 conversion rate with the steam enriched reforming was almost stable around 54% and remained lower than that with the dry reforming (62.6%). The CO_2 conversion drastically decreased from 37.85% to 18.8% as the S/B ratio was risen and was significantly lower than

that with hybrid dry reforming (48.27%). This observation is expected since with the steam enriched reforming, the bio-oil hydrocarbons are more likely to react with the water vapor molecules injected externally than with the CO_2 molecules produced by the biomass pyrolysis (equations **(5.2)-(5.4)** and equation **(5.14)**). Moreover, secondary reactions can also take place such as the reverse WGSR (equation **(5.9)**).

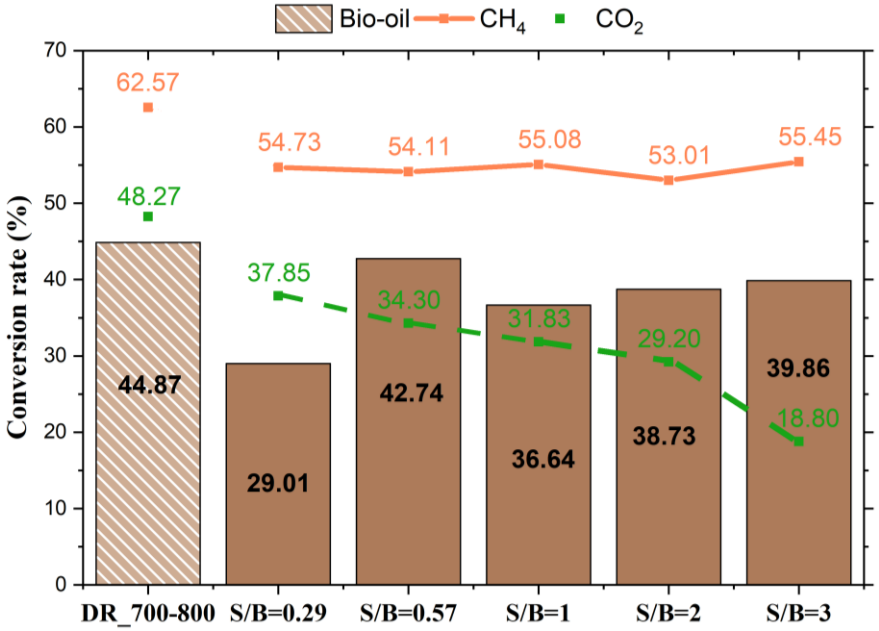

Figure 5.4 Effect of S/B ratio on the conversion rates of the main reactants involved in the pyrolysis coupled to the hybrid steam enriched reforming process realized with the 20% Ni/Al_2O_3 bead (GHSV=4500h^{-1})

5.4.1.1.4. Syngas production

The influence of the S/B ratio over the syngas production and the H_2/CO ratio derived from the pyrolysis-reforming process realized with an external steam feed is illustrated in **Figure 5.5**. Even though the H_2 concentration increased while that of CO decreased with the S/B increase, the syngas concentration was less impacted and was shockingly lower than that obtained with the dry reforming. It reached a maximum of 21.93 mmol/g dry biomass at a S/B ratio of 0.57. Nonetheless, the H_2/CO ratio conserved an increasing trend from 1.26 at S/B ratio of 0.29 to 1.65 at S/B ratio of 3, surpassing the traditional H_2/CO ratio equaling 1 with the dry reforming. In fact, as the S/B ratio is raised, the steam partial pressure is also increased thus improving the kinetics of the steam reforming reactions (equations **(5.2)-(5.4)**) and displacing the equilibrium of the WGSR (equation **(5.8**)) towards the hydrogen production.

Although high S/B improves the hydrogen production, the process would require an important steam generation which can be energy and cost extensive. Moreover, the remaining part of the steam that had not reacted might condense on both the outlet of the reforming reactor as well as on the downstream pipelines. The process energy efficiency will be negatively impacted. Thereby, the S/B ratio should be reasonably chosen and optimized. *Given that the gases' overall yield was minimally impacted with the S/B ratio, adopting a small S/B ratio, between 0.5 and 1 for instance, can be considered adequate for a satisfying reforming efficiency*. Therefore, the elevated energy consumption and the high associated operating expenses can be avoided [6].

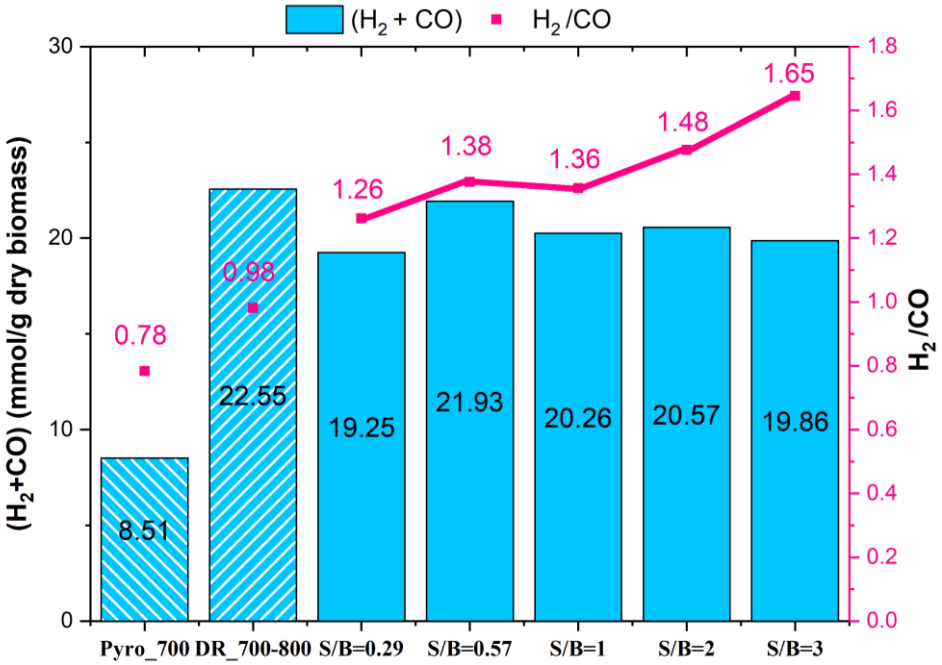

Figure 5.5 Effect of S/B ratio on syngas concentration and H_2/CO ratio produced by the pyrolysis coupled to the hybrid steam enriched reforming process realized with the 20% Ni/Al_2O_3 beads (GHSV=4500h^{-1})

5.4.1.2. Effect of steam reforming temperature

5.4.1.2.1. Main products concentrations

The effect of temperature on the hybrid steam enriched reforming was studied by varying the reforming temperature from 700°C to 800°C while considering two intermediate S/B ratio (0.57 and 2). The products distribution resulting from these experiments are given in **Figure 5.6.**

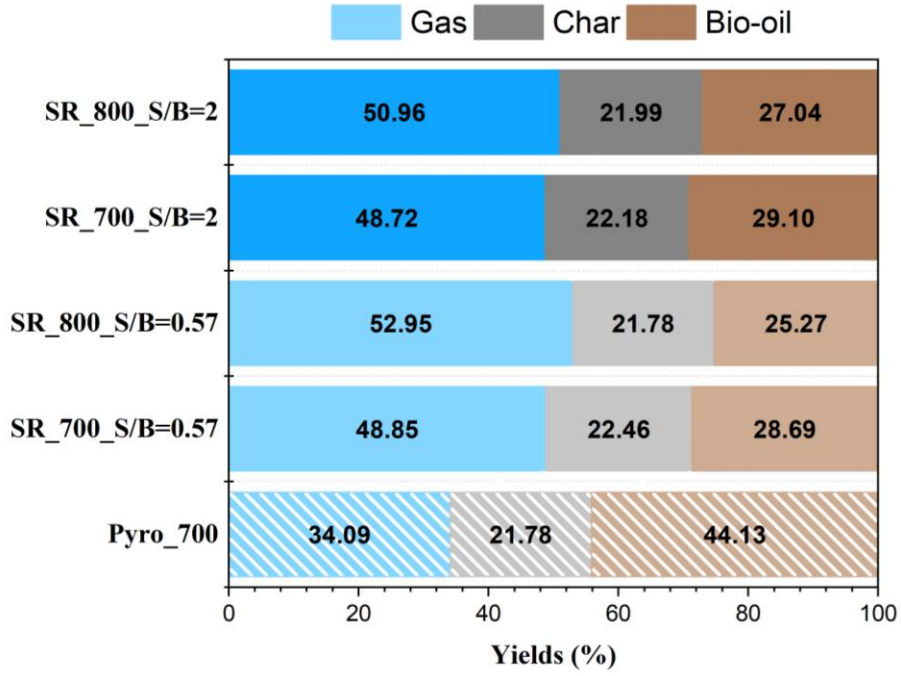

Figure 5.6 Effect of temperature on products distribution derived from the pyrolysis coupled to the hybrid steam enriched reforming at two S/B ratios (0.57 and 2) labelled as "SR_YYY_S/B=x" with SR short for steam reforming, YYY referring to the reforming temperature and x is for the value of the S/B ratio. The catalyst used was 20% Ni/Al_2O_3 beads (GHSV=4500h^{-1})

The steam enriched reforming experiments are labelled as "SR_YYY_S/B=x" with SR short for steam reforming, YYY referring to the reforming temperature and x is for the value of the S/B ratio. For a fixed S/B ratio, it can be remarked that the increasing the steam reforming temperature from 700°C to 800°C, leads to a slight improvement in the gases' formation and a reduction in the bio-oil production. Similar tendencies are observed for both S/B ratio but with the lower S/B ratio, at 800°C the gas yield is higher, and the bio-oil yield smaller than at 700°C.

5.4.1.2.2. Major gases' concentrations

Figure 5.7 depicts the evolution of the major gases' concentrations with the increase of the steam reforming temperature at two S/B ratios. *Increasing the steam reforming temperature from 700°C to 800°C while fixing the S/B ratio, strongly enhances the H_2 production and reduces the formation of both CH_4 and CO_2.* CO slightly dropped with the temperature increase when the S/B ratio was 0.57 but augmented when the S/B ratio was risen to 2. Moreover, at 700°C, increasing the S/B ratio had a higher impact on the H_2 concentration than at 800°C. This implies that the steam reforming reaction 700°C is not totally complete and is thereby improved with the augmentation of the steam feed. However, at 800°C, the steam reforming reaction produced almost equal amounts of H_2 at both S/B ratio which leads to deduce that at 800°C, the steam reforming reaction reaches its almost full potential and is poorly affected by the S/B ratio.

Being of an endothermic nature, the equilibrium of steam reforming reactions (equation **(5.2)** to **(5.4)**) is shifted towards the products formation with the temperature increase, given the Le Chatelier's principle. This increases the H_2 and CO formation and leads to the consumption and thus reduction of the CH_4 and CO_2 concentrations. The CO_2 decrease can also be related to the WGS reaction (equation **(5.8)**) which is disfavored with the temperature increase and thereby enhances the CO formation. The hydrocarbons concentrations, including CH_4, are diminished by the increase of the reforming temperature since these compounds are more effectively reformed at higher temperatures [55].

Similar gases' concentrations evolution tendencies with the temperature were obtained in the works of Remiro *et al.* [55] who performed the steam reforming of raw bio-fuel produced by the flash pyrolysis of pine sawdust. The flash pyrolysis was realized at 480°C and the steam to carbon ratio was set at 9 with a space velocity of 155,000 h^{-1}. The temperature was varied from 600 to 800°C where the tar conversion was also increased. In addition, the H_2 and CO yields were improved and the CO_2 and CH_4 yields reduced when the temperature was increased from 700°C to 800°C. They explained it by the fact that the WGS reaction (equation **(5.8**)), being exothermic, would be disfavored with the temperature increase which increases the CO formation and decreases that of CO_2 in addition to the thermal decomposition reactions. Moreover, their catalysts might have been deactivated due to coke formation which is reduced by the temperature increase where the coke and its precursors are gasified (reverse Boudouard reaction (equation **(5.10)**) and reverse tar decomposition reaction (equation **(5.13)**).

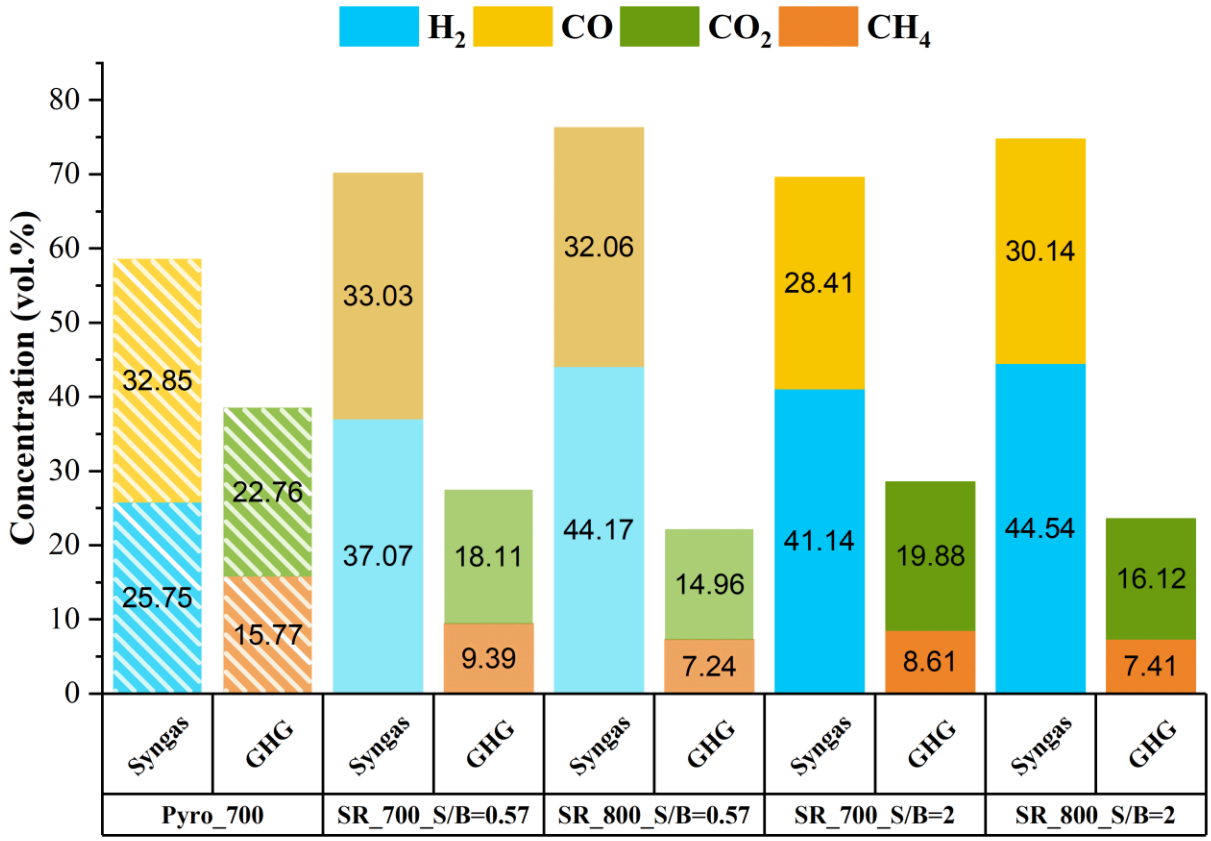

Figure 5.7 Effect of temperature on the concentrations of major gases (divided into syngas and greenhouse gases GHG) produced by the pyrolysis coupled to the hybrid steam enriched reforming at two S/B ratios (0.57 and 2)

5.4.1.2.3. Main reactants' conversion rates

The variation of the conversion rates of the main reforming reactants in function of the temperature and the S/B ratio is demonstrated in **Figure 5.8**. The augmentation of the steam reforming temperature strongly enhances the conversion rates of the different reactants for both S/B ratio considered. It is in conformity with the endothermic nature of the steam reforming reaction enhanced by higher temperatures which effectively activate the breaking of the C−H bond. Nevertheless, the differences between the conversion rates at 700°C and at 800°C are more significant when the S/B ratio is lower for the bio-oil and the methane conversion. In addition, at a fixed temperature, the conversion rates of CO_2 and bio-oil are higher for the lower S/B ratio, which was observed earlier.

This confirms the conclusion made on the effect of temperature which is more pronounced at lower S/B ratios. Remarkably, the CH_4 conversions rates are significantly higher than those of CO_2 for the different S/B ratios and reforming temperature. In fact, with the presence of an external steam feed, the steam reforming reactions (equations **(5.2)-(5.4)**) are favored over the dry reforming reactions (equations **(5.5)-(5.7)**). This leads to a CH_4 consumption higher than that of CO_2 since CH_4 is involved in both the dry and steam reforming reactions whereas the CO_2 is mainly consumed in the dry reforming reactions.

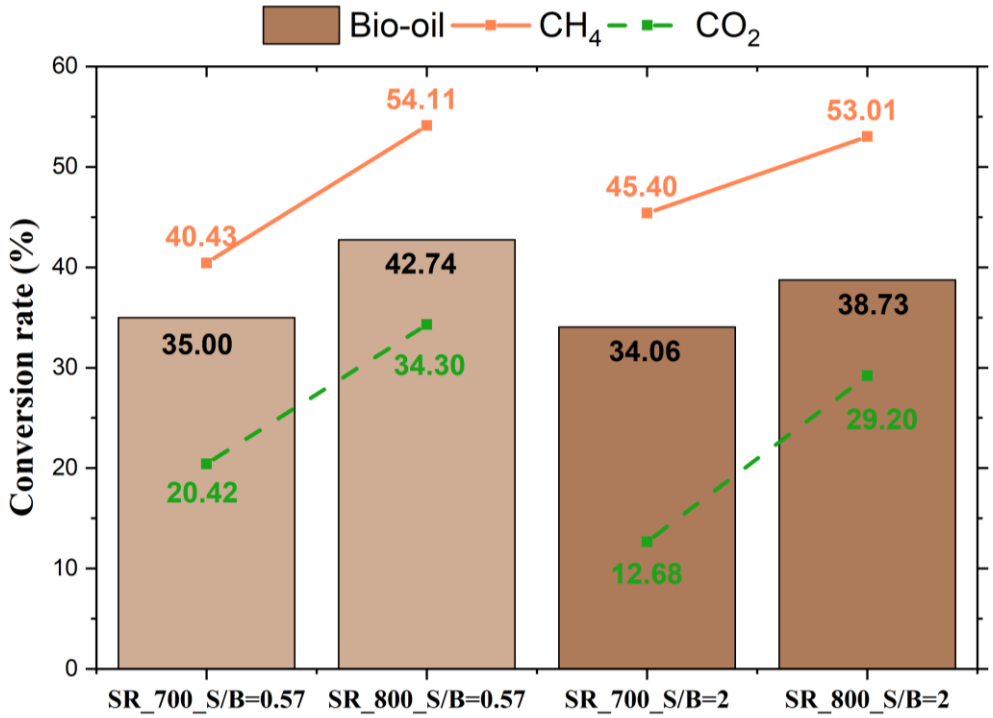

Figure 5.8 Effect of temperature on the conversion rates of the main reactants involved in the pyrolysis coupled to the hybrid steam enriched reforming at two S/B ratios (0.57 and 2)

5.4.1.2.4. Syngas production

Figure 5.9 demonstrates the influence of the temperature and S/B ratio on the syngas concentration and the H_2/CO ratio produced by the hybrid steam enriched reforming. As the steam reforming temperature is elevated from 700°C to 800°C, the syngas production is markedly ameliorated for both S/B ratios with similar values obtained at both temperatures for a given S/B ratio value.

On the other hand, even though the increase of the temperature enhances the H_2/CO ratio, the impact of the temperature was more explicit when the S/B ratio was smaller where the H_2/CO ratio surges from 1.12 at 700°C to 1.38 at 800°C at S/B ratio equals 0.57, whereas it passes from 1.45 to 1.48 at S/B ratio of 2. This confirms the previous observations made due to the promotion of the steam reforming (equations **(5.2)-(5.4)**), reverse WGS reactions (equation **(5.9)**) and thermal tar cracking (equation **(5.12**)) with the temperature surpassing 700°C, which is advantageous for the reduction of bio-oil.

This again demonstrates the importance of the temperature when the S/B ratio is low. *Therefore, it can be concluded that to obtain similar results with high efficiency and good syngas production, in particular H_2, if a lower operating temperature is preferred, the S/B should be increased but to a reasonable extent in order to maintain a good economic efficiency.*

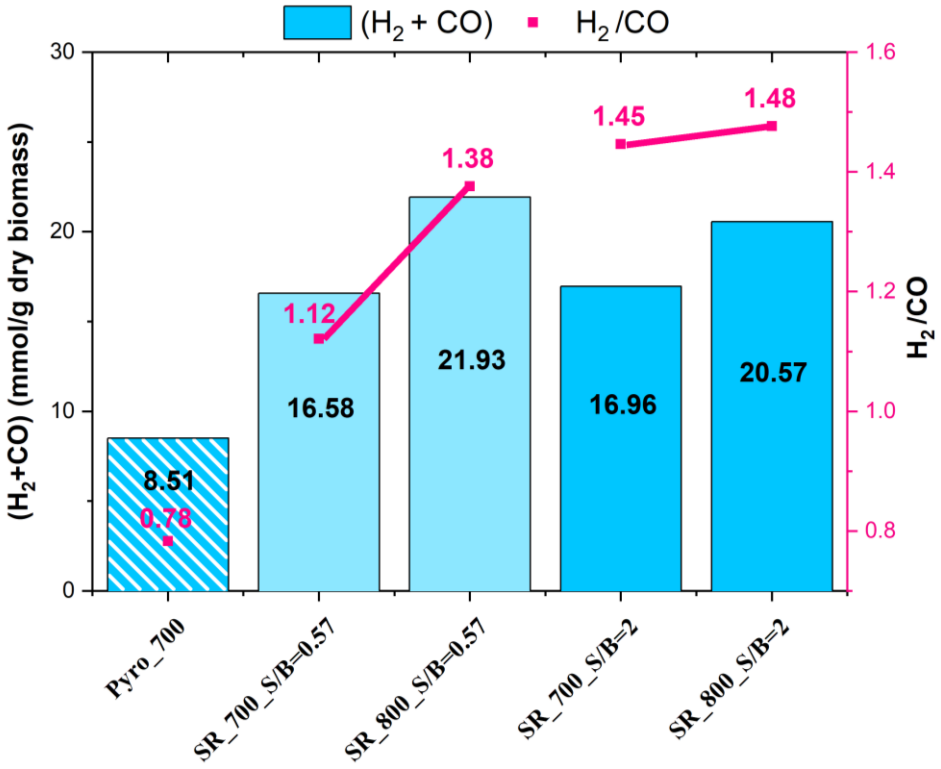

Figure 5.9 Effect of temperature on syngas concentration and H_2/CO ratio produced by the pyrolysis coupled to the hybrid steam enriched reforming at two S/B ratios (0.57 and 2)

5.4.2. Reforming of pyrolysis volatiles under different reaction environments

5.4.2.1. Main products concentrations

Figure 5.10 reports the effect of the carrier gas (N_2, air or steam) on the products distribution derived from a pyrolysis alone (700°C) labelled as "Pyro" and a pyrolysis (700°C) coupled to catalytic reforming (800°C) with 20%Ni/Al_2O_3 (GHSV=4500h^{-1}) labelled as "Ref". The gas flow rate was fixed at 25mL_n/min. For the steam reforming, the S/B was set to 3, the largest S/B ratio previously tested, to push the steam reforming reactions to the highest extent.

It can be noticed that realizing a reforming step strongly enhances the gases production while converting the bio-oil, which is applicable for the three different gases. Comparing the pyrolysis experiments alone, it can be remarked that *the presence of an oxidizing environment supplied by the air or the water vapor leads to the high production of gases* which was increased by around 40% in contrast to the pyrolysis realized in an inert atmosphere. This implies that the bio-oil hydrocarbons strongly react with oxygen and are transformed into volatiles accounted for in the gases part of the products. Similar results are observed for the pyrolysis coupled to the reforming where the presence of oxygen with steam or air led to a 20% and 30% increase in the gases yield, respectively, in contrast to the nitrogen. Nevertheless, the highest gases yields are obtained with the air among both the pyrolysis (47.49 wt.%) and reforming (68.75 wt.%) experiments.

These values largely exceed the ones previously obtained with the pyrolysis under an inert atmosphere followed by the catalytic reforming. For instance, the gas yield obtained by the pyrolysis realized under nitrogen coupled to the reforming under steam with S/B ratio of 3 was 51.15 wt.% (**Figure 5.2**), which is significantly lower than the one obtained by a pyrolysis coupled to a reforming both realized under steam (63.22 wt.%) (**Figure 5.10**). This is due to

the higher concentrations of volatiles produced in the first stage of pyrolysis in the steam environment (82.67 wt.% of volatiles, composed of 45.08 wt.% gas and 37.59 wt.% bio-oil) than in the inert atmosphere (78.22 wt.% of volatiles with 34.09 wt.% of gas and 44.13 wt.% of bio-oil) which pushes further the hydrocarbon reforming and the gases production in the second stage.

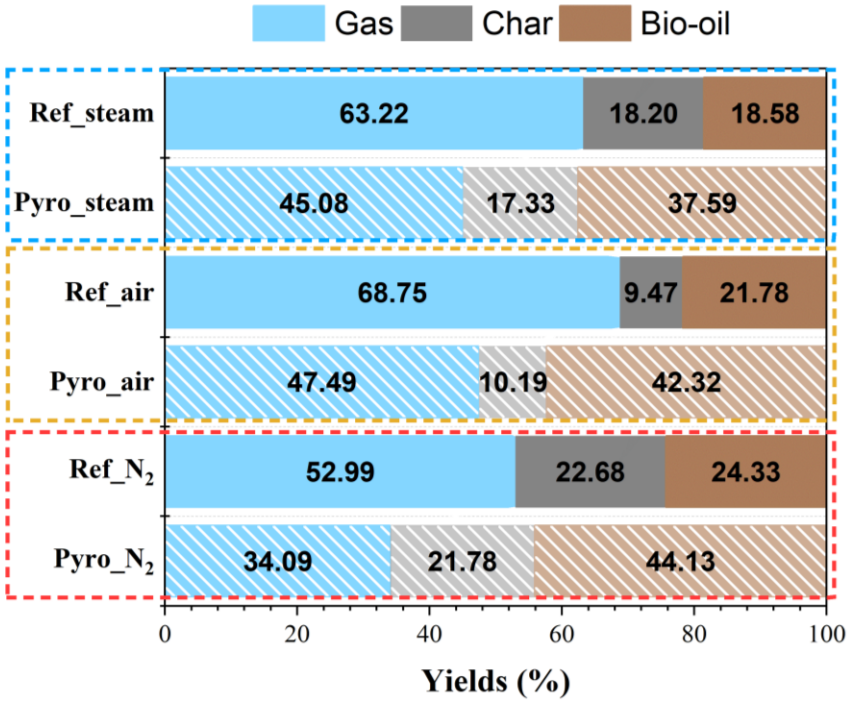

Figure 5.10 Effect of carrier gas (N_2, air and steam) on the products distribution derived from a pyrolysis alone (700°C) labelled as "Pyro" and a pyrolysis (700°C) coupled to catalytic reforming (800°C) with 20% Ni/Al_2O_3 (GHSV=4500h^{-1}) labelled as "Ref". The gas flow rate was fixed at 25mL_n/min. For the steam reforming, the S/B was 3. Experiments with N_2 are grouped in a red dashed box, with air in a yellow dashed box and with steam in bleu dashed box

5.4.2.2. Major gases' concentrations

The volume concentrations of the gases produced by the pyrolysis alone and the pyrolysis/reforming processes realized under different carrier gases are illustrated in **Figure 5.11**. It can be observed that the pyrolysis with air produces the lowest H_2 (15.93 vol.%) and the highest CO_2 concentrations (36.97 vol.%). This could lead to consider the pyrolysis in presence of air to be rather close to a combustion reaction (equation **(5.24)**) [56].

$$\text{Combustion: } CH_yO_x + (1 + \frac{y}{2} - \frac{x}{4})O_2 \rightarrow \frac{y}{2}H_2O + CO_2 \quad \textbf{(5.24)}$$

Nonetheless, realizing a subsequent reforming step under air strongly enhances the H_2 and CO production while reducing that of CH_4 and CO_2. Comparing the pyrolysis results with the three carrier gases, it can be remarked that the steam pyrolysis produced the lowest CH_4 concentration and the highest H_2 concentration of 40.6 vol.%, remarkably higher than the H_2 concentrations obtained with the reforming under nitrogen or air. On the other hand, the largest CO concentration and lowest CO_2 concentration was obtained with the pyrolysis under nitrogen.

The steam during the pyrolysis of biomass can be consumed as an agent which converts the pyrolysis hydrocarbons into CO and H_2 following equations **(5.2)** to **(5.4)** and equation **(5.25)**.

Moreover, the CO formed can further react with the water vapor to produce CO_2 and additional H_2 as in the water-gas shift reaction (equation **(5.8)**) [57–59].

$$C + H_2O \rightarrow H_2 + CO \qquad \Delta H°_{298K} = +131.3\ MJ/kmol \qquad \textbf{(5.25)}$$

Comparing the pyrolysis under N_2 and H_2O (steam), it can be noted that steam pyrolysis markedly enhanced the production of H_2 and slightly that of CO_2 while strongly lowering that of CH_4 and CO. These trends were similarly obtained by the work of Mellin *et al.* [60]. They studied the effect of the reaction's atmosphere on the products of biomass pyrolysis experimentally and compared it to a model they developed. For the experimental part, they realized a fluidized bed pyrolysis at 500°C in presence of N_2 and H_2O as fluidizing agents. They also found an increase in the H_2 and CO_2 production and a drop in that of CH_4 and Co by changing the carrier gas from N_2 to H_2O for the pyrolysis. It can be explained by the fact that a less dense gas (N_2) reduces the density of the whole vapor mixture which will drop the outlet temperature and the residence time. Subsequently, the condensable vapors yield, thus the bio-oil will be higher and thereby the gases lower, as it was also observed in **Figure 5.10**.

Now looking at the pyrolysis/reforming experiments, it can be noticed that the reforming in general enhances the production of H_2 and CO and reduces that of CH_4 and CO_2, which is conforming with the reforming reactions (equations **(5.2)** to **(5.7)**). Interestingly, *the steam reforming led to the largest formation of H_2* (43.24 vol.%), *the reforming under air resulted in the strongest CO production* (42.82 vol.%) *and the poorest CH_4 concentration* (5.11 vol.%) *while the reforming under nitrogen produced the lowest CO_2 amounts* (11.78 vol.%).

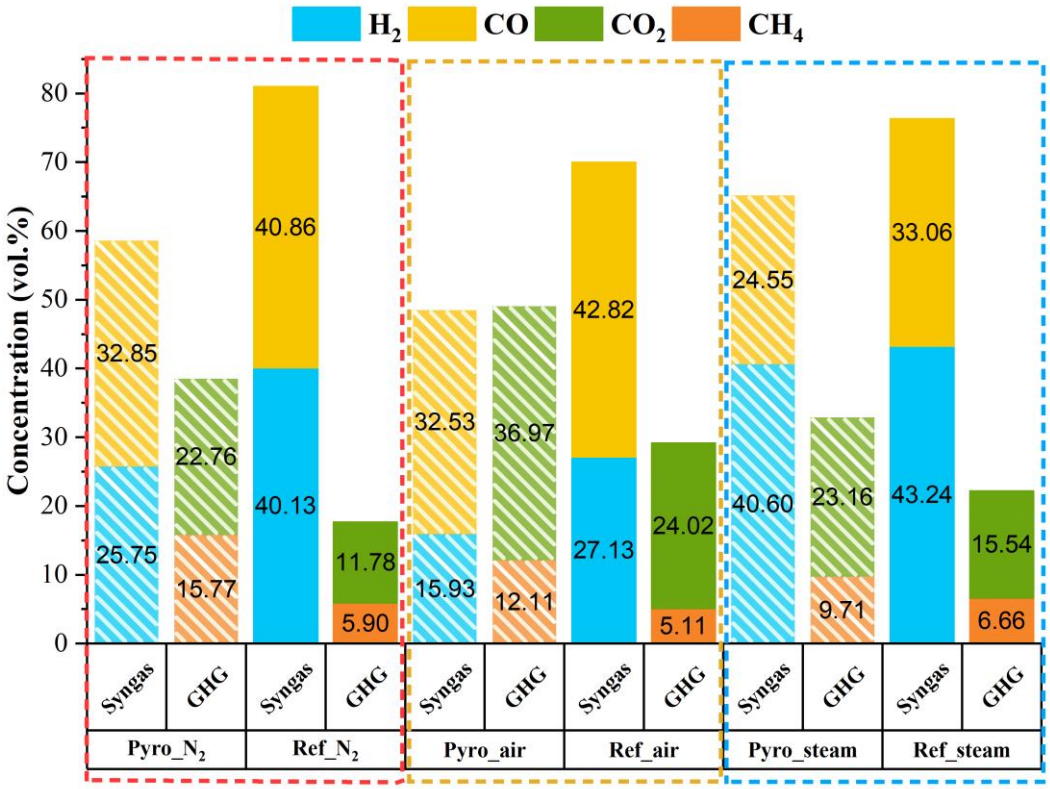

Figure 5.11 Effect of carrier gas (N_2, air and steam) on the volume concentrations of the major gases derived from a pyrolysis alone (700°C) labelled as "Pyro" and a pyrolysis (700°C) coupled to catalytic reforming (800°C) with 20% Ni/Al_2O_3 (GHSV=4500h^{-1}) labelled as "Ref". For the steam reforming, the S/B was 3

5.4.2.3. Main reactants' conversion rates

The conversion rates of the main reactants involved in the reforming of the pyrolysis volatiles realized under different reaction environments are depicted in **Figure 5.12**. Even though the steam reforming led to the strongest bio-oil conversion (50.57%), it had the weakest CH_4 and CO_2 conversion rates of 31.4% and 32.93%, respectively. On the other hand, the highest CH_4 conversion rate (62.57%) and that of CO_2 (48.27%) were obtained by the reforming realized in an inert atmosphere however it resulted in the lowest bio-oil conversion rate (44.87%). The conversion performance of the reforming with air was intermediary between the reforming with nitrogen and steam. These observations are in accordance with the ones made in the previous subsections where the *lowest bio-oil yield and thus highest conversion were obtained for the reforming under steam* since the steam reforming strongly decomposes and cracks the bio-oil hydrocarbons (equations **(5.2)-(5.4)** and equation **(5.14)**). On the other hand, *the dry reforming consumes more CO_2 and CH_4 than the steam reforming* thereby leading to higher conversion rates as explained previously (**Figure 5.4**).

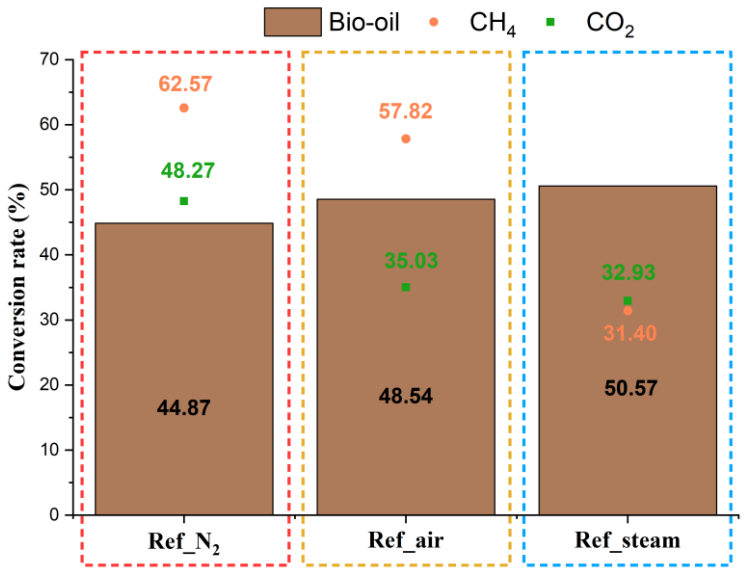

Figure 5.12 Effect of carrier gas (N_2, air and steam) the conversion rates of the main reactants involved in the pyrolysis (700°C) coupled to catalytic reforming (800°C) with 20% Ni/Al_2O_3 (GHSV=4500h^{-1})

5.4.2.4. Syngas production

The syngas production determined in terms of mmol/g dry biomass along with the H_2/CO ratios are represented in **Figure 5.13**. It can be remarked that the pyrolysis and the reforming under air had the poorest selectivity towards the syngas production. Moreover, the H_2/CO ratio values were even lower than those obtained with the experiments under an inert atmosphere. In fact, the process would be closer to a combustion than to a pyrolysis when realized under air, which produces more CO_2 and H_2O than CO and H_2, as previously discussed (equation **(5.24)**). Remarkably, the *largest syngas quantity of 25.64 mmol/g dry biomass was produced by the steam reforming* with an H_2/CO ratio of 1.31, since the steam reforming is known for its high syngas production capacity as demonstrated previously (**Figure 5.5**). Nonetheless, *the highest H_2/CO ratio of 1.65 was reached with the steam pyrolysis*. This can be due to secondary reactions occurring during the pyrolysis in the presence of steam, an oxidizing agent, which reacts with bio-oil hydrocarbons and decomposes them, releasing lighter molecules such as H_2 (equations **(5.12)** and **(5.13)**).

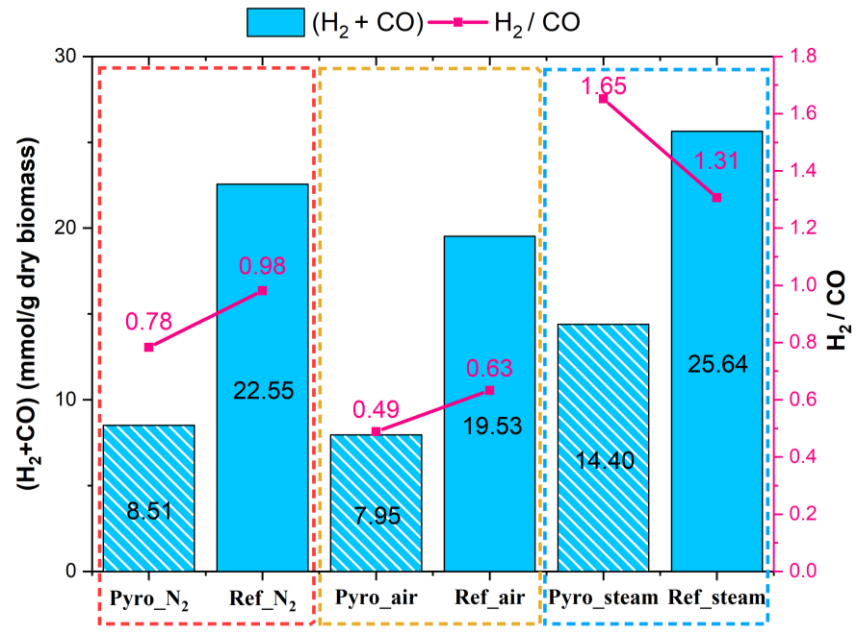

Figure 5.13 Effect of carrier gas (N_2, air and steam) on the syngas concentration and the H_2/CO ratios derived from a pyrolysis alone (700°C) labelled as "Pyro" and a pyrolysis (700°C) coupled to catalytic reforming (800°C) with 20% Ni/Al_2O_3 ($GHSV=4500h^{-1}$) labelled as "Ref"

Applying a steam environment for thermally converting the hydrocarbons present multiple technological and environmental benefits. It helps neutralizing harmful species produced in the gas-steam mixture [61,62], and ameliorates the quality of the liquid formed by the condensable hydrocarbons by reducing the ash and sulfur content and changing the molecular weight of the light hydrocarbons [59,63]. Moreover, the steam biomass pyrolysis is considered in the literature as an efficient approach to simultaneously produce chemicals, activated carbon and liquid fuels [47]. It has been the subject of several research works for the production of biochar and activated carbon, mostly in fixed bed reactors [64–66].

5.5. Graphical summary

A graphical summary resuming the main hydrogen production methods adopted in this work is illustrated in **Figure 5.14**. Beginning from the biomass, three major processes were applied: pyrolysis under air, inert and steam environments. The air pyrolysis of biomass realized at 700°C produces the highest gas yield (48 wt.%) among the different pyrolysis processes. Realizing a reforming at 800°C under air following the air pyrolysis further amplifies the gas production resulting in a gas yield of 69 wt.%, the largest among the other reforming processes.

The inert pyrolysis was realized under different operating conditions. For instance, a low biomass pyrolysis temperature of 400°C generates mainly bio-oil, followed by char then the gases to a lesser extent. Applying a small nitrogen flow rate of 25 mL/min at 400°C results in a high volatiles residence time and thereby the largest bio-oil yield (56 wt.%) amongst the different inert pyrolysis experiments. Whereas increasing the nitrogen flow rate to 300 mL/min for the pyrolysis at 400°C, thereby minimizing the volatiles residence time leads to the highest char yield of 32 wt.%. *Applying a higher biomass temperature of 700°C strongly improves the gases production and reduces that of bio-oil and char*. Aiming a higher syngas formation, this latter pyrolysis condition was adopted as a base for the following reforming processes, where two approaches were applied: hybrid and steam reforming.

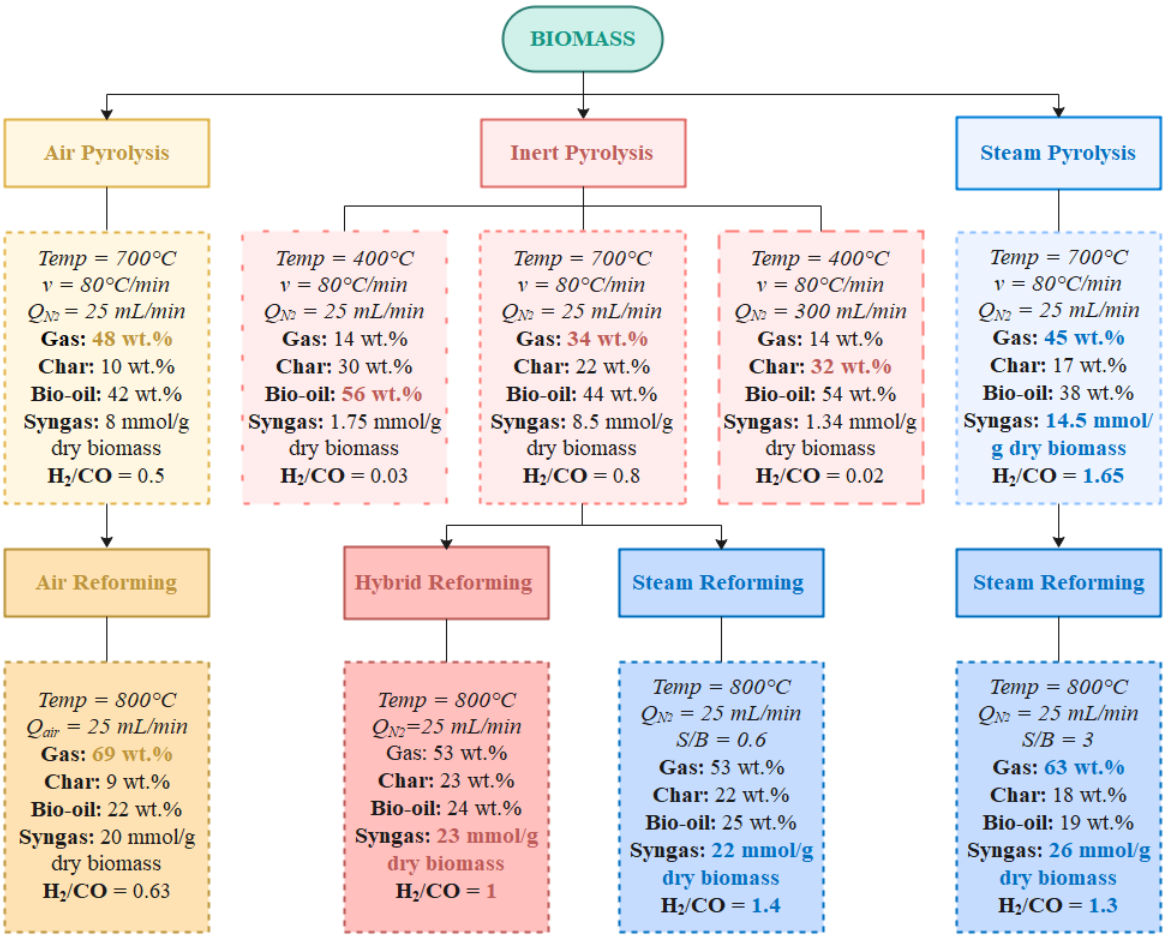

Figure 5.14 Graphical summary of the different routes of hydrogen production adopted in this work. The main operating conditions are given in italic, the products in bold with the main product of interest for each process represented in color and in bold

Comparing these two processes, it can be noticed that they both significantly ameliorate the gases formation and drop that of bio-oil, with reasonably close yields. While the hybrid reforming is realized without an external steam nor CO_2 feed, it consists basically of consuming the pyrolysis gases and hydrocarbons and reforms them into syngas with a concentration of 23 mmol/g dry biomass but with an H_2/CO ratio equaling 1, a characteristic value for the dry methane reforming. On the other hand, the steam reforming realized with an additional steam feed and an optimized S/B ratio of 0.6, markedly enhances the H_2 production relative to the CO with a H_2/CO ratio of 1.4. This confirms the fact that *steam reforming is the principal producer of hydrogen.*

Interestingly, realizing a steam pyrolysis amazingly produced not only a large amount of gas (45 wt.%) with a considerable amount of syngas of 14.5 mmol/g dry biomass comparingly to the other pyrolysis methods performed, but also the highest H_2/CO ratio of 1.65. *Coupling the steam pyrolysis to a subsequent steam reforming step further improved the gases production to 63 wt.% with particularly a syngas concentration of 26 mmol/g dry biomass, the highest among the other processes, with a H_2/CO ratio equaling to 1.3. Steam reforming and steam gasification of biomass has been proven to be the highest hydrogen producer.* The hydrogen yield is strongly influenced by multiple parameters with the major ones being the process, temperature, the steam to biomass ratio, the catalyst's nature, the biomass types and biomass particle size among others [67].

5.6. Technical and Environmental study

The anthropogenic emissions of the greenhouse gases strongly impacted the climate, as highlighted by the sixth assessment report of the intergovernmental panel on climate change (IPCC) [68]. Carbon-neutral processes are needed in the energy sector to reduce the greenhouse gases emissions and mitigate global warming. Hydrogen, as an energy vector, has been attracting an escalating attention for its potential to applied in the transportation and industrial sectors given its decarbonization ability [69]. According to the International Energy Agency (IEA), in 2018, the global hydrogen demand was approximated to 73.9 MT among which 31.5 MT (42.6%) were consumed by the ammonia synthesis processes and 38.2 MT (51.6%) were used in the petroleum refineries [70]. In the future, it is expected that 40 MT of H_2 will be required if hydrogen is to be used in transport field [71]. It is characterized by having a fast combustion rate, a large energy density and a high-octane number as well as a null damaging potential. All of these will allow hydrogen to be, in the near future, the most favored fuel. Visioned as the future elixir of human life, hydrogen presents a clean, inexhaustible, effective, and inexpensive energy carrier. Multiple national governmental agencies world-wide have raised funded programs for promoting hydrogen as the future fuel [72].

Hydrogen can be produced from several divers technologies than can be categorized into five main classes: hydrogen form fossil fuels, water splitting, biomass, biological sources and recovery from waste gas stream, with each class grouping multiple processes [42,73]. These methods will be described briefly hereafter.

5.6.1. Hydrogen from fossil fuels

In the fossil fuels involved processes, hydrocarbons are combined with steam, oxygen or air and heated in a reactor which leads to the decomposition of these reactants into H_2, along with CO and CO_2. Another approach consists in decomposing the hydrocarbons under heat in the absence of air or steam resulting in the hydrogen formation. The hydrogen production therefore relies on the use of other primary energy sources. Natural gas ensures about 50% of the worldwide hydrogen production through mainly the steam reforming of methane (major natural gas). It is followed by 30% of oil where the hydrogen is formed via the oil partial oxidation and is mostly consumed in the petroleum refineries through the hydro-processing. Coal accounts for 19% of the hydrogen sources by coal gasification with the hydrogen produced involved in the ammonia synthesis [73].

When highly heated under limited oxygen amounts (inferior to necessity for a complete combustion), the biomass undergoes partial oxidation resulting in the formation of gas and coal [74]. The efficiency of the partial oxidation is generally very low compared to that of steam reforming. Moreover, it requires large amounts of pure oxygen which considerably increases the operating cost. The hydrogen produced by the partial oxidation is fed to a water-gas shift reactor followed by a purification step [75]. Adding catalysts to the hydrocarbon partial oxidation allows the use of the hydrogen produced in automobile fuel cells and several commercial applications [76–78]. The partial oxidation of hydrocarbons is an exothermic reaction as given in equation **(5.26)**.

$$\text{Partial oxidation: } C_nH_m + \frac{n}{2}O_2 \rightarrow \frac{m}{2}H_2 + nCO \qquad \Delta H < 0 \qquad \textbf{(5.26)}$$

During coal gasification, coal is subject to intense heating (above 900°C) which results in its transformation into a gas state to which oxygen and steam are added. They react to produce H_2,

CO and CO_2 following equation **(5.27**) [74]. The gasification can be realize without or with a catalyst (in general a nickel-based catalyst), in a fixed or fluidized bed reactor [79,80].

Coal gasification: $2C + H_2O + O_2 \rightarrow H_2 + CO + CO_2$ + ash **(5.27)**

Nonetheless, the gasification faces some challenges. Besides producing the syngas, which is a highly flammable gas mixture, the coal gasification forms some residues of ash and slag mineral, causing air pollution. In addition, one of the major issues associated with the biomass gasification is the tar formation, which can form tar aerosols with a complex composition. It might also lead to polymerization which can oppose the hydrogen formation by steam reforming [81]. Therefore, this method is generally less appealing, in addition to its strongly elevated heat requirements.

Nonetheless, the gasification of carbonaceous raw materials remains a well-developed and advanced methods for the hydrogen and syngas production, that has been applied for the last two hundred years [82]. It takes place in high pressure and temperature reactors and on a large-scale. Pure hydrogen production can be attained by adopting some subsequent steps. They include adding steam to the syngas mixture leading to their reaction following the water-gas-shift reaction which produces CO_2 and more H_2 (equation **(5.8)**) or realizing a Fischer-Tropsch [83]. The high purity hydrogen formed can be separated from the mixture by using a pressure swing adsorption (PSA) process, a membrane shift reactor or a membrane gasification reactor with shift reactor [84]. Moreover, to prevent its emission into the atmosphere, CO_2 can be captured from the syngas and either used in the chemical, food and pharmaceutical industries, petroleum recovery or stored underground [85].

5.6.2. Hydrogen from water splitting

Knowing that water covers around 70% of the Earth's surface and that hydrogen represents 11.2% of the water mass, it is logical to consider water as an abundant hydrogen source. To produce hydrogen form water three methods can be applied namely thermal decomposition or thermolysis thermochemical approach, and electrolysis.

Thermolysis consists in thermally cracking the water molecules at considerably high temperature (1400°C and above). The water vapor molecules break down into oxygen and hydrogen gases. Unfortunately, to produce hydrogen to be used at an industrial level, the temperature must be extremely high (in the order of 2500°C to 3000°C) [86]. The thermochemical decomposition of the water involves the chemical transformation of water and one or more reactants into hydrogen at relatively elevated temperatures (500-2000°C). The chemicals used can be repeatedly re-utilized, forming a closed loop which produces H_2 and O_2 and only consumes H_2O. It generally occurs in three steps: production of oxygen, production of hydrogen and recycling of consumed materials. The process is based on three stages where first the electricity and heat are produced, then the water is thermochemically decomposed and finally the oxygen and hydrogen produced are purified [87].

Among the water splitting methods, electrolysis is a very well-established technology and the most efficient method for water splitting [88]. Being an endothermic process, electricity mainly provides the required energy [89], where an electrical current splits the water into hydrogen and oxygen molecules in an electrolyte (equation **(5.28)**) [90]. The benefit of using hydrogen as a fuel is that during its combustion, the hydrogen combines with the oxygen from air and releases

heat and only water as by-products. Thereby, the water electrolyzed to generate hydrogen is regenerated as a result of its burning [73].

Water electrolysis: $2H_2O \rightarrow 2H_2 + O_2$ **(5.28)**

The power required for the electrolysis and the thermal decomposition of water can be provided by high temperature reactors powered by nuclear energy. In fact, the heat generated by the nuclear plants can be directly used or can be converted to electricity to produce hydrogen [91]. United States, Korea, France, and Japan are four of the top leaders in the world for the hydrogen production from nuclear energy [92]. France, for instance, has carried out several research and development programs for the large productions of hydrogen relying on advanced high temperature technologies such as nuclear plants [93]. Nonetheless, the nuclear route for hydrogen production cannot be totally regarded as sustainable due to its high risks (explosion in the Fukushima Nuclear power plant in Japan in 2011) [92].

5.6.3. Hydrogen from biomass

Renewable sources of energy such as lignocellulosic biomass can be used to produce hydrogen through thermochemical processes [94,95]. The biomass can be obtained from a large selection of resources such as agricultural residues and wastes, energy plants (wood, herbaceous, industrial water plants), forest wastes and residues as well as urban and industrial wastes. Hydrogen can be obtained by applying thermochemical processes such as pyrolysis followed by steam reforming or gasification [73]. In fact, first a pyrolysis or a gasification of the biomass is realized which produces a gas mixture consisting mainly of H_2, CO, CO_2 and CH_4. Then, steam is added to the gases where it reacts with CH_4 to be reformed into H_2 and CO. The H_2 yield is further improved through the WGS reaction (equation **(5.8)**) [48]. CO_2 is the gas by-product emitted from the biomass thermochemical processing. Nevertheless, this CO_2 is considered "neutral" relative to GHG since the CO_2 emitted during these processes is absorbed by the biomass during its growth. Therefore, the CO_2 total concentration does not increase in the atmosphere. Moreover, the hydrogen and carbon dioxide mixture may be utilized in fuel cells to produce electricity [96]. Contrary to the gasification, the pyrolysis takes place in an oxygen-free environment and aims mostly to the formation of bio-oil and char while the gasification aims towards the formation of gases [74].

The hydrogen efficiency of the thermochemical processes is between 35 and 50% [97], or less if the aim of the plant was not the maximization of the hydrogen generation. These processes yield multiple products with the possibility to recover the excess of heat generated by the process to be fed to another heat network. With all these energy products taken into consideration, the total energy efficiency of these thermochemical process can increase up to 70 to 80% [95]. Given the feedstock nature, small operating units were considered to rely on local supplies, reduce the distance of transport and decrease the concentration of trucks around the plant. At small-scale, the economic feasibility of these processes remains their major problem [2].

5.6.4. Hydrogen from biological sources

Bio-hydrogen is the biological hydrogen produced from biomass, organic wastes or water in the presence of bacteria and microalgae through biological or photobiological methods. Since 1920s, bacteria have been studied for the hydrogen production while the algae use was initiated in the 1940s. These technologies gained attention specially after the oil crisis in the 1970s.

Nonetheless, these methods are still studied on the lab-scale and their industrial applications are under investigation [98]. Hydrogen production can be reached through dark fermentation of anaerobic bacteria, photo-fermentation of green algae and cyanobacteria in the light and through a two-stage dark/fermentative process [99–101]. The dark fermentation converts the carbohydrates in the presence of water into H_2 and other products [102]. During the photo-fermentation, the photosynthetic bacteria consumes alcohols and organic acids as substrates and generate hydrogen during its metabolism [103]. The biological technologies for hydrogen production have been found to yield significant production efficiencies of hydrogen and minimal environmental impact [104]. Nonetheless, their hydrogen production capacity remains relatively low in comparison to their high unit capital cost, which is considered their chief limitation [105].

5.6.5. Hydrogen via recovery from waste gas stream

The petrochemical industries and refineries emit waste gas streams rich in hydrogen. These streams are used as fuel gas and in cycle gases of methanol and ammonia synthesis plants. Hydrogen can be produced from these gas streams without returning them to the reactors or using them as fuels by applying several different processes. They include membrane separation, adsorption, absorption, and cryogenic distillation.

Membranes are generally used as a post-treatment step following numerous conversion processes. A 90% H_2 efficiency is attained when the gas produced by partial oxidation, autothermal or steam conversion goes through a selective membrane. In the ammonia industry, since 1979, polymeric (organic) membranes have been involved in retrieving H_2 from the waste gases [106].

The most common adsorption processes are temperature swing adsorption (TSA) and pressure swing adsorption (PSA). PSA process relies on the fact that the unwanted gas components of a mixture are preferably adsorbed at a high pressure over a porous adsorbent. The components are released at low pressure and recovered. The most commonly used materials are zeolites and activated carbon having good adsorption and desorption capacities. This process separates a single gas component from a gas mixture [107]. TSA is based on heating with a hot gas an adsorbent charged with impurities allowing its regeneration. It is considered as an efficient purification method but suffers from long heating and cooling durations [73].

The absorption process is a separation technique using a solvent which withdraws hydrogen from a gas mixture containing methane and other heavy hydrocarbons. Polyethylene glycol is used as solvent and water is used for cleaning. For hydrogen derived from biomass, alkaline solution is used to absorb CO_2 and separated from H_2, which is one of the most appropriate way to obtain a purified hydrogen stream (95% purity of hydrogen) [108].

The cryogenic process is a separation method realized at low temperatures where the gas mixture is condensed and distilled by benefiting from the differences in the temperatures of condensation of different components. Hydrogen compared to hydrocarbons is extremely volatile which facilitates its separation from a hydrocarbon gases mixture. The partial condensation is the simplest and most vastly employed cryogenic process. The compression of the condensed hydrocarbons provides the required cooling to the process (Joule-Thomson cooling). However, the cooling step is very energy intensive [109].

5.6.6. Comparison of the environmental impact

The carbon dioxide emissions are regarded as the main greenhouse gases sources because of their devastating effect in the human health and the environment. To mitigate the CO_2 emissions, several methods were developed including Carbon Capture and Storage (CCS) or using CO_2 as a product or a waste in another facility [110,111]. One of the most intensively investigated research subjects is the mitigation towards a carbon neutral economy supplied by reliable energy. Hydrogen possesses a great capacity to reduce the CO_2 emissions if it is produced from renewable feedstock and sustainable and clean energy sources [42].

In the case of electrolysis of water, the problems related to the carbon dioxide emissions are conveyed towards the production of the electricity. For instance, the carbon dioxide content of the electric mix in France in 2021 was 36 gCO_2/kWh [112]. The electrolysis process is not free from CO_2 content but rather involves between 48 and 85 gCO_2/kWh due to its low energetic efficiency (between 40 to 70%). In contrast, the CO_2 content is much higher for the other processes with 410 gCO_2/kWh with the coal gasification and 560 gCO_2/kWh for the methane reforming [113]. Thereby, the electrolytic hydrogen is far from being the best option to drop the greenhouse gases emission in countries where the electric mix is rich in carbon with more than 300 gCO_2/kWh [97].

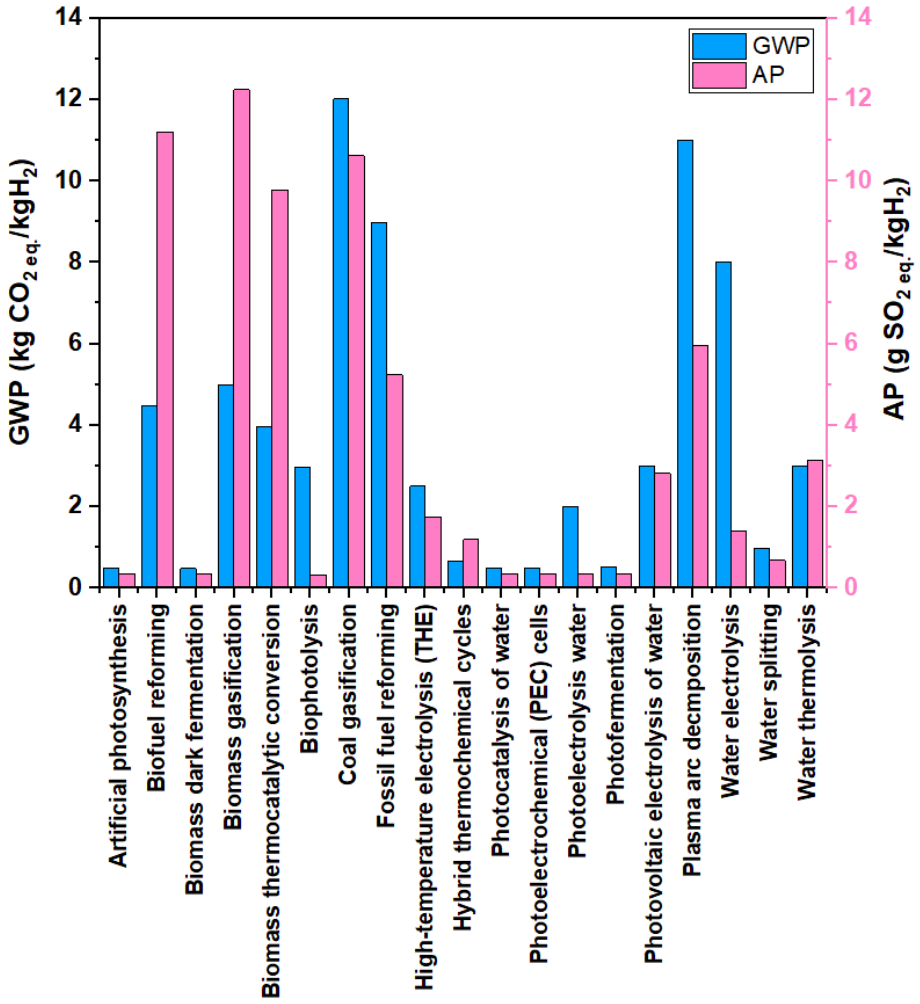

Figure 5.15. Comparison of some hydrogen production methods in terms of Global Warming Potential (GWP) measured in kg $CO_{2eq.}/kgH_2$ and Acidification Potential (AP) in g $SO_{2\ eq.}/kgH_2$ (adapted from [38,116]

A life cycle assessment (LCA) is essential to completely evaluate and comprehend the carbon dioxide emissions of a certain process. ISO standards define the LCA procedures published as "Operational Guide to the ISO standards" by the center of Environmental Science of Leiden University [114]. Two environmental impact categories are used to evaluate the hydrogen production methods described in this work, referring to the operational guide: global warming potential (GWP) and acidification potential (AP). Global warming potential determines the CO_2 emissions in kg CO_{2eq}./kgH_2, while the acidification potential measures the SO_2 ejection into the water and soil and evaluates the variation in the degree of acidity in g $SO_{2\ eq}$./kgH_2. [115]. The comparison of the environmental impact of the different hydrogen production methods are based on the studies realized by Bhandari *et al.* [38] and Ozbilen *et al.* [116]. The results are represented in **Figure 5.15**.

The most environmentally damaging methods are the ones relying on fossil fuel for hydrogen production such as coal gasification and fossil fuel reforming. Even though the GWP of the biomass gasification is low, its AP is the highest among the remaining methods. *The most environmentally benign processes in terms of acidification and global warming potentials are the ones relying on the hybrid thermochemical cycle and photonic energy.*

5.7. Economic study

After evaluating multiple hydrogen production routes, it appears of great importance to assess their cost to have an integral comparison among the different methods and verify their feasibility. Although the pyrolysis and the reforming processes are separately well-established mature processes, their coupling remains an innovative and relatively recent approach for the syngas production and the biomass valorization [6]. The purpose of the work realized was the optimization of the process and its operating conditions at a lab-scale, in order to maximize the production of syngas, hydrogen in particular. Its projection to the industrial scale is a promising technology and is potentially feasible. Therefore, an economical study will be performed on the process at a large-scale rather than on the lab-scale experimental set up.

It appears rather complicated to determine a precise production hydrogen cost since it relies on several uncertainties. It depends on the price of the feedstock, the nature of the process, its level of advancement and maturity, the infrastructure presence and availability, and the post-treatment methods applied to retrieve the hydrogen at a pure state [73]. It also involves the costs of operation and maintenance along with the capital costs [117]. The most appropriate unit to evaluate the hydrogen cost would be "per kilogram of hydrogen" because the energy content of hydrogen (119.9 MJ), on a lower heating value (LHV) basis, is almost equal to that of a gallon of gasoline (121.7 MJ). This makes easier the comparison of the amounts produced and the costs for hydrogen relative to gasoline. Knowing that the volume depends on the pressure and temperature of the gas, volume measurements are not usually used [41].

Table 5.2 provides a list of the hydrogen production methods along with the hydrogen production cost estimated in $/kg of hydrogen, the process efficiency, the production scale size, its development state as well as its main advantages and drawbacks [101,118–120]. The efficiency is determined by dividing the lower heating value of H_2 in gas product by the total energy supplied to the procedure applied.

According to **Table 5.2**, it can be noticed that the *most financially profitable hydrogen producing process is the steam methane reforming, followed by the coal gasification and biomass pyrolysis and gasification, without a carbon capture system*. The partial oxidation, autothermal reforming and thermo-chemical processes cost a bit higher but their prices are still cost-competitive. The water electrolysis has an intermediary economical cost, only if nuclear energy is used for the power generation required for the process. If electricity is generated from renewable source of energy (solar, wind, waves…), the cost of electricity would reach unattractive commercial prices. *The highest production costs are obtained by the photocatalytic and biological technologies for hydrogen production*. The newest hydrogen production technics such as dark and photo fermentations as well as the algae bio-photolysis of water are still under research and development and therefore their costs are still considered significantly high but could be decreased with future advancement in their implementations.

In future cases, the costs of hydrogen production of every process evaluated will be correlated with the specific emissions of CO_2. For instance, the costs of CO_2 emissions, lowered by employing renewable energy sources such as biomass as well as by carbon capture and storage (CCS) systems, are around 10 €/GJ_{H_2} [121]. Biomass by nature is a neutral source which can be declared as a carbon negative emitter if coupled to CCS [122]. *Therefore, biomass-derived hydrogen is considered sufficient for the present and future demands for hydrogen* [67].

From a techno-economic point of view, the most preferred technology is natural gas steam reforming. However, the rise in the price of natural gas is becoming a main concern. Currently, coal gasification might be cost-competitive, but is reasonable only if followed by a carbon capture step. To the best of our knowledge, up to the present moment, the commercial applications of biomass gasification at large scale for the hydrogen production are scarce with very few dedicated for the syngas production. *Realizing a two-stage process combining the biomass pyrolysis in-line with the catalytic reforming is a very attractive and quite novel approach which allows not only the hydrogen production, but also the reduction of the CO_2 and CH_4 emissions while valorizing waste residues and biomass.* Therefore, it can minimize the need for a CCS system, which increases its attractiveness and feasibility for an industrial scale projection.

Coupling the biomass pyrolysis to the catalytic reforming would have a hydrogen production cost falling between 1.96 and 2.94 $/kg H_2, which can be further reduced by optimization of the process, and by subtracting the bio-oil transport cost since the bio-oil will be generated on-site by the pyrolysis and the volatiles will be fed in-line to the reformer. A complete environmental and economic study of the hydrogen production chain would involve additional costs including the hydrogen storage, transport and final use [41].

Table 5.2 Hydrogen production routes listed by increasing production cost with the energy efficiency, the production scale and development state as well as the main advantages and drawbacks given [101,118–120]

Technology	H_2 production cost ($/kg H_2)	Energy efficiency	Size of production scale	State of development	Main advantages	Main drawbacks
Steam methane reforming (SMR)	0.75 (Without CO_2 capture)	83%	Large	Currently available	- High efficiency - Validated technic - Cost-effective	- Fossil fuel dependency - Methane supply limitation - CO_2 as by-product - Global warming
Coal gasification	0.92 (Without CO_2 capture)	63%	Large	Currently available	- Well-established - Economical	- Low quality H_2 - CO_2 as by-product
Biomass pyrolysis	1.21 – 2.19	56%	Mid-size	Currently available	- Renewable feedstock - Local sources - Sustainable energy source - Reduction of dependency on fossil fuels - Drop in GHG emissions - Increase in agricultural products' value - Decrease in residues of municipal and agricultural waste	- Char and tar formation - Varying H_2 content - Seasonal feedstock variability - Operation challenges (collection and handling) - Transportation issues - Low energy density
Biomass gasification	1.21 – 2.42	40-50%	Mid-size	Currently available	- Renewable feedstock - Local sources - Sustainable energy source - Reduction of dependency on fossil fuels - Drop in GHG emissions - Increase in agricultural products' value - Decrease in residues of municipal and agricultural waste	- Char and tar formation - Varying H_2 content - Seasonal feedstock variability - Operation challenges (collection and handling) - Transportation issues - Low energy density

Partial oxidation	1.39 (Residual oil)	70-80%	Large	Currently available	- Well-established - Economical	- Lower efficiency than SMR - CO_2 as by-product - Global warming
Autothermal reforming	1.93	71-84%	Large	Currently available	- Validated technic - Low capital cost	- Lower efficiency than SMR - Methane supply limitation - CO_2 as by-product
Thermo-chemical	2.01 (Sulphur – Iodine cycle)	42% (850°C)	-	Under research	- Alternative source - Emission free	- High corrosivity - Extreme operational parameters - Large capital costs
Electrolysis	2.56 – 2.97 (Nuclear source)	25% (electrical efficiency included)	Small	Currently available	- Validated technic - Emission free	- Electricity dependent - Expensive - Low overall efficiency
Photocatalytic	4.98	10-14% (theoretical)	-	Under research	- Renewable and alternative feedstock	- Costly - Low productivity
Biological	5.52	24 % (theoretical)	-	Under research	- Renewable and alternative feedstock	- Pricey - Low output
Dark fermentation	-	-	-	Under research	- Renewable - H_2 production and waste treatment simultaneously	- Small efficiency in energy conversion
Photo fermentation	-	-	-	Under research	- Elevated theoretical conversions - Absence of oxygen decreasing the inhibition potential	- Small efficiency in solar energy conversion - Large surfaces requirements for anaerobic photobioreactors - Needs nitrogenase enzyme demanding large energy
Bio-photolysis of water by algae	-	-	-	Under research	- Sustainable and renewable energy sources - Consumption of CO_2	- Low H_2 formation - High inhibition impact of produced O_2 on hydrogenase enzyme

5.8. Conclusion

Hydrogen, as a clean and effective energy carrier, has been attracting increasing attention given its potential application in the energy and transport sectors. In this chapter, hydrogen production was studied according to different experimental scenarios. First, the steam reforming of the biomass pyrolysis volatiles was realized, under different steam to biomass (S/B) ratios and several temperatures. Next, the reaction environment was changed by varying the carrier gas from nitrogen (inert) to air (oxidizing) and water vapor to evaluate its impact on the biomass pyrolysis alone and on the coupling of the pyrolysis to the reforming. The effects of these operating conditions were studied on the major products and the main gases formed as well as on the conversion rates of the reactants and the syngas concentrations.

Concerning the steam reforming series of experiments realized with nitrogen as a carrier gas, first the S/B ratio was increased from 0.29 to 3 which slightly improved the gases production and reduced that of bio-oil. Compared to a dry reforming, the steam reforming produces significantly higher H_2 concentrations, but lower CO amounts. It also consumes much less CO_2 and CH_4, especially as the S/B ratio was increased. In fact, the steam and dry reforming usually take place simultaneously during our hybrid reforming process. Without an external steam feed, the steam reforming is less pronounced as revealed by the H_2/CO ratio fluctuating around 1 and therefore, the process would rather be considered as a dry reforming. Thereby, an external water vapor feed is necessary to accentuate the effect of the steam reforming. The steam reforming produces H_2 amounts higher than those of CO, according to the stoichiometry of the steam reforming reaction, which is traduced by an H_2/CO ratio superior to 1. This was observed during our experiments where the H_2/CO ratio reached 1.65 when an S/B ratio equal 3 was applied, in opposite to an H_2/CO ratio of 1.26 for a S/B ratio of 0.29. Nevertheless, the total syngas production was maintained almost constant for the different S/B ratios. Increasing the reforming temperature from 700°C to 800°C for a fixed S/B ratio, markedly enhanced the gases formation, including syngas, and reduced that of the CO_2, CH_4, and bio-oil.

Changing the carrier gas to air had a great impact on both the pyrolysis and the reforming. For the pyrolysis alone, the presence of air led to a steep increment in the gases' formation and a drop in the char yield. Realizing a subsequent reforming step to the pyrolysis, remarkably increased the gases production to reach almost 70 wt.% of the total products, the highest among the different methods applied. Nevertheless, the hydrogen formation was mediocre. On the other hand, realizing steam pyrolysis not only improved the gases formation, but also produced the highest syngas concentrations and H_2/CO ratio, among the different pyrolysis tests realized under air or nitrogen. The results were extrapolated during the coupling of the steam reforming to the steam pyrolysis with a S/B of 3, where the largest syngas concentrations were produced.

The next part of this work was dedicated to a technical, environmental and economic study of the most common hydrogen production routes described in the literature. It was found that the main production routes of hydrogen rely on fossil fuels, biomass, water, biological sources and waste gas streams through the application of thermochemical, biological and physical methods as well as thermolysis and electrolysis. Regarding the environmental impact, it was deduced that the most eco-friendly hydrogen production routes are the ones based on renewable sources of energy such as solar and wind. However, their cost-effectiveness is lower than the other technologies which renders their applications on a large-scale challenging.

The thermochemical decompositions of fossil fuels through coal gasification and natural gas reforming have high hydrogen production efficiency and are commercially feasible but lead to severe atmospheric pollution and current global warming. Their applications would require the implementation of a carbon sequestration system which would significantly increase their capital cost. The use of biomass for hydrogen production appears to be a suitable solution in the short and mid-term given the biomass "carbon neutral" nature. Joining the biomass pyrolysis in-line to the catalytic steam reforming presents itself as a viable solution for the hydrogen production given its good efficiency and competitive cost, as it was demonstrated in this work. In addition, given the process capacity to lessen the carbon dioxide and methane emissions, it will reduce the need for a downstream CCS system.

References

[1] Distributed Energy Systems Flexible and Efficient Power for the New Energy Era - Arup, (n.d.). https://www.arup.com/en/perspectives/publications/research/section/distributed-energy-systems-flexible-and-efficient-power-for-the-new-energy-era (accessed August 26, 2022).
[2] M.I. El-Shafie, S. Kambara, Y. Hayakawa, Hydrogen Production Technologies Overview, J. Power Energy Eng. 7 (2019) 107–154. https://doi.org/10.4236/jpee.2019.71007.
[3] World Energy Outlook 2017 – Analysis, IEA. (n.d.). https://www.iea.org/reports/world-energy-outlook-2017 (accessed August 29, 2022).
[4] Statistical Review of World Energy | Energy economics | Home, Bp Glob. (n.d.). https://www.bp.com/en/global/corporate/energy-economics/statistical-review-of-world-energy.html (accessed August 29, 2022).
[5] R.E. Kopp, B.K. Mignone, The U.S. Government's Social Cost of Carbon Estimates after Their First Two Years: Pathways for Improvement, Economics. 6 (2012). https://doi.org/10.5018/economics-ejournal.ja.2012-15.
[6] M. Abou Rjeily, C. Gennequin, H. Pron, E. Abi-Aad, J.H. Randrianalisoa, Pyrolysis-catalytic upgrading of bio-oil and pyrolysis-catalytic steam reforming of biogas: a review, Environ. Chem. Lett. (2021) 48. https://doi.org/10.1007/s10311-021-01190-2.
[7] M. Abou Rjeily, C. Gennequin, H. Pron, E. Abi-Aad, J.H. Randrianalisoa, Chapter 9 - Catalysts for steam reforming of biomass tar and their effects on the products, in: M.R. Cesario, D.A. de Macedo (Eds.), Heterog. Catal., Elsevier, 2022: pp. 249–295. https://doi.org/10.1016/B978-0-323-85612-6.00009-7.
[8] G. Boyle, Renewable Energy: Power for a Sustainable Future, Oxford University Press, 1996.
[9] K. Zeng, D. Zhang, Recent progress in alkaline water electrolysis for hydrogen production and applications, Prog. Energy Combust. Sci. 36 (2010) 307–326. https://doi.org/10.1016/j.pecs.2009.11.002.
[10] T.N. Veziroglu, S. Kakaç, Ö. Başar, N. Forouzanmehr, Fossil/hydrogen energy mix and population control, Int. J. Hydrog. Energy. 1 (1976) 205–217. https://doi.org/10.1016/0360-3199(76)90072-0.
[11] T.N. Veziroğlu, I. Gürkan, M.M. Padki, Remediation of greenhouse problem through replacement of fossil fuels by hydrogen, Int. J. Hydrog. Energy. 14 (1989) 257–266. https://doi.org/10.1016/0360-3199(89)90062-1.
[12] T. Sinigaglia, F. Lewiski, M.E. Santos Martins, J.C. Mairesse Siluk, Production, storage, fuel stations of hydrogen and its utilization in automotive applications-a review, Int. J. Hydrog. Energy. 42 (2017) 24597–24611. https://doi.org/10.1016/j.ijhydene.2017.08.063.
[13] S.Z. Baykara, Hydrogen: A brief overview on its sources, production and environmental impact, Int. J. Hydrog. Energy. 43 (2018) 10605–10614. https://doi.org/10.1016/j.ijhydene.2018.02.022.
[14] L. Santamaria, G. Lopez, E. Fernandez, M. Cortazar, A. Arregi, M. Olazar, J. Bilbao, Progress on Catalyst Development for the Steam Reforming of Biomass and Waste Plastics Pyrolysis Volatiles:

A Review, Energy Fuels. 35 (2021) 17051–17084. https://doi.org/10.1021/acs.energyfuels.1c01666.
[15] I. Dincer, C. Acar, Smart energy solutions with hydrogen options, Int. J. Hydrog. Energy. 43 (2018) 8579–8599. https://doi.org/10.1016/j.ijhydene.2018.03.120.
[16] S. Satyapal, J. Petrovic, C. Read, G. Thomas, G. Ordaz, The U.S. Department of Energy's National Hydrogen Storage Project: Progress towards meeting hydrogen-powered vehicle requirements, Catal. Today. 120 (2007) 246–256. https://doi.org/10.1016/j.cattod.2006.09.022.
[17] E.D. GOEBEL, R.M. COVENEY, E.E. ANGINO, E.J. ZELLER, G.A.M. DRESCHHOFF, Geology, composition, isotopes of naturally occurring rich gas from wells near Junction City, Kans, Geol. Compos. Isot. Nat. Occur. Rich Gas Wells Junction City Kans. 82 (1984) 215–222.
[18] F. Mueller-Langer, E. Tzimas, M. Kaltschmitt, S. Peteves, Techno-economic assessment of hydrogen production processes for the hydrogen economy for the short and medium term, Int. J. Hydrog. Energy. 32 (2007) 3797–3810. https://doi.org/10.1016/j.ijhydene.2007.05.027.
[19] H. Goyal, D. Seal, R. Saxena, Thermochemical Conversion of Biomass to Liquids and Gaseous Fuels, in: 2008: pp. 29–44. https://doi.org/10.1201/9780789038746.ch3.
[20] M.F. Hordeski, Alternative Fuels—The Future of Hydrogen: The Future of Hydrogen, Third Edition, 3rd ed., River Publishers, New York, 2020. https://doi.org/10.1201/9781003151753.
[21] Y. Kalinci, A. Hepbasli, I. Dincer, Biomass-based hydrogen production: A review and analysis, Int. J. Hydrog. Energy. 34 (2009) 8799–8817. https://doi.org/10.1016/j.ijhydene.2009.08.078.
[22] D. Chen, L. He, Towards an Efficient Hydrogen Production from Biomass: A Review of Processes and Materials, ChemCatChem. 3 (2011) 490–511. https://doi.org/10.1002/cctc.201000345.
[23] Md. Nasir Uddin, W.M.A.W. Daud, H.F. Abbas, Potential hydrogen and non-condensable gases production from biomass pyrolysis: Insights into the process variables, Renew. Sustain. Energy Rev. 27 (2013) 204–224. https://doi.org/10.1016/j.rser.2013.06.031.
[24] C. He, C.-L. Chen, A. Giannis, Y. Yang, J.-Y. Wang, Hydrothermal gasification of sewage sludge and model compounds for renewable hydrogen production: A review, Renew. Sustain. Energy Rev. 39 (2014) 1127–1142. https://doi.org/10.1016/j.rser.2014.07.141.
[25] M.A. Hossain, J. Jewaratnam, P. Ganesan, Prospect of hydrogen production from oil palm biomass by thermochemical process – A review, Int. J. Hydrog. Energy. 41 (2016) 16637–16655. https://doi.org/10.1016/j.ijhydene.2016.07.104.
[26] G. Nahar, D. Mote, V. Dupont, Hydrogen production from reforming of biogas: Review of technological advances and an Indian perspective, Renew. Sustain. Energy Rev. 76 (2017) 1032–1052. https://doi.org/10.1016/j.rser.2017.02.031.
[27] S. Ayalur Chattanathan, S. Adhikari, N. Abdoulmoumine, A review on current status of hydrogen production from bio-oil, Renew. Sustain. Energy Rev. 16 (2012) 2366–2372. https://doi.org/10.1016/j.rser.2012.01.051.
[28] P. Sharma, M.L. Kolhe, Review of sustainable solar hydrogen production using photon fuel on artificial leaf, Int. J. Hydrog. Energy. 42 (2017) 22704–22712. https://doi.org/10.1016/j.ijhydene.2017.07.115.
[29] M. Wang, Z. Wang, X. Gong, Z. Guo, The intensification technologies to water electrolysis for hydrogen production – A review, Renew. Sustain. Energy Rev. 29 (2014) 573–588. https://doi.org/10.1016/j.rser.2013.08.090.
[30] S.Z. Baykara, Hydrogen production by direct solar thermal decomposition of water, possibilities for improvement of process efficiency, Int. J. Hydrog. Energy. 29 (2004) 1451–1458. https://doi.org/10.1016/j.ijhydene.2004.02.014.
[31] L. D'Souza, Thermochemical hydrogen production from water using reducible oxide materials: a critical review, Mater. Renew. Sustain. Energy. 2 (2013). https://doi.org/10.1007/s40243-013-0007-0.
[32] C. Liu, G. Xu, T. Wang, Non-thermal plasma approaches in CO2 utilization, Fuel Process. Technol. 58 (1999) 119–134. https://doi.org/10.1016/S0378-3820(98)00091-5.
[33] C. Du, J. Mo, H. Li, Renewable Hydrogen Production by Alcohols Reforming Using Plasma and Plasma-Catalytic Technologies: Challenges and Opportunities, Chem. Rev. 115 (2015) 1503–1542. https://doi.org/10.1021/cr5003744.

[34] C. Agrafiotis, H. von Storch, M. Roeb, C. Sattler, Solar thermal reforming of methane feedstocks for hydrogen and syngas production—A review, Renew. Sustain. Energy Rev. 29 (2014) 656–682. https://doi.org/10.1016/j.rser.2013.08.050.
[35] H.E. Figen, S.Z. Baykara, Effect of ruthenium addition on molybdenum catalysts for syngas production via catalytic partial oxidation of methane in a monolithic reactor, Int. J. Hydrog. Energy. 43 (2018) 1129–1138. https://doi.org/10.1016/j.ijhydene.2017.10.173.
[36] K. Damen, M. van Troost, A. Faaij, W. Turkenburg, A comparison of electricity and hydrogen production systems with CO2 capture and storage. Part A: Review and selection of promising conversion and capture technologies, Prog. Energy Combust. Sci. 32 (2006) 215–246. https://doi.org/10.1016/j.pecs.2005.11.005.
[37] K. Zeng, D. Gauthier, J. Soria, G. Mazza, G. Flamant, Solar pyrolysis of carbonaceous feedstocks: A review, Sol. Energy. 156 (2017) 73–92. https://doi.org/10.1016/j.solener.2017.05.033.
[38] R. Bhandari, C.A. Trudewind, P. Zapp, Life cycle assessment of hydrogen production via electrolysis – a review, J. Clean. Prod. 85 (2014) 151–163. https://doi.org/10.1016/j.jclepro.2013.07.048.
[39] P.C. Hallenbeck, M. Abo-Hashesh, D. Ghosh, Strategies for improving biological hydrogen production, Bioresour. Technol. 110 (2012) 1–9. https://doi.org/10.1016/j.biortech.2012.01.103.
[40] Z. Zhang, X. Zhou, J. Hu, T. Zhang, S. Zhu, Q. Zhang, Photo-bioreactor structure and light-heat-mass transfer properties in photo-fermentative bio-hydrogen production system: A mini review, Int. J. Hydrog. Energy. 42 (2017) 12143–12152. https://doi.org/10.1016/j.ijhydene.2017.03.111.
[41] J.R. Bartels, M.B. Pate, N.K. Olson, An economic survey of hydrogen production from conventional and alternative energy sources, Int. J. Hydrog. Energy. 35 (2010) 8371–8384. https://doi.org/10.1016/j.ijhydene.2010.04.035.
[42] I. Dincer, C. Acar, Review and evaluation of hydrogen production methods for better sustainability, Int. J. Hydrog. Energy. 40 (2015) 11094–11111. https://doi.org/10.1016/j.ijhydene.2014.12.035.
[43] A. Arregi, G. Lopez, M. Amutio, I. Barbarias, J. Bilbao, M. Olazar, Hydrogen production from biomass by continuous fast pyrolysis and in-line steam reforming, RSC Adv. 6 (2016) 25975–25985. https://doi.org/10.1039/C6RA01657J.
[44] G. Lopez, L. Santamaria, A. Lemonidou, S. Zhang, C. Wu, A.T. Sipra, N. Gao, Hydrogen generation from biomass by pyrolysis, Nat. Rev. Methods Primer. 2 (2022) 1–13. https://doi.org/10.1038/s43586-022-00097-8.
[45] T. Namioka, A. Saito, Y. Inoue, Y. Park, T. Min, S. Roh, K. Yoshikawa, Hydrogen-rich gas production from waste plastics by pyrolysis and low-temperature steam reforming over a ruthenium catalyst, Appl. Energy. 88 (2011) 2019–2026. https://doi.org/10.1016/j.apenergy.2010.12.053.
[46] M.N. Uddin, K. Techato, J. Taweekun, M.M. Rahman, M.G. Rasul, T.M.I. Mahlia, S.M. Ashrafur, An Overview of Recent Developments in Biomass Pyrolysis Technologies, Energies. 11 (2018) 3115. https://doi.org/10.3390/en11113115.
[47] E.P. Önal, B.B. Uzun, A.E. Pütün, Steam pyrolysis of an industrial waste for bio-oil production, Fuel Process. Technol. 92 (2011) 879–885. https://doi.org/10.1016/j.fuproc.2010.12.006.
[48] L. Dong, C. Wu, H. Ling, J. Shi, P.T. Williams, J. Huang, Promoting hydrogen production and minimizing catalyst deactivation from the pyrolysis-catalytic steam reforming of biomass on nanosized NiZnAlOx catalysts, Fuel. 188 (2017) 610–620. https://doi.org/10.1016/j.fuel.2016.10.072.
[49] N. Gao, S. Liu, Y. Han, C. Xing, A. Li, Steam reforming of biomass tar for hydrogen production over NiO/ceramic foam catalyst, Int. J. Hydrog. Energy. 40 (2015) 7983–7990. https://doi.org/10.1016/j.ijhydene.2015.04.050.
[50] G. Guan, M. Kaewpanha, X. Hao, A. Abudula, Catalytic steam reforming of biomass tar: Prospects and challenges, Renew. Sustain. Energy Rev. 58 (2016) 450–461. https://doi.org/10.1016/j.rser.2015.12.316.
[51] H.-G. Park, S. Han, K.-W. Jun, Y. Woo, M.-J. Park, S. Kim, Bench-Scale Steam Reforming of Methane for Hydrogen Production, Catalysts. 9 (2019) 615. https://doi.org/10.3390/catal9070615.
[52] M. Negri, M. Wilhelm, C. Hendrich, N. Wingborg, L. Gediminas, L. Adelöw, C. Maleix, P. Chabernaud, R. Brahmi, R. Beauchet, Y. Batonneau, C. Kappenstein, R.-J. Koopmans, S. Schuh, T. Bartok, C. Scharlemann, U. Gotzig, M. Schwentenwein, New technologies for ammonium

dinitramide based monopropellant thrusters – The project RHEFORM, Acta Astronaut. 143 (2017). https://doi.org/10.1016/j.actaastro.2017.11.016.
[53] B. Balagurumurthy, R. Singh, T. Bhaskar, Chapter 4 - Catalysts for Thermochemical Conversion of Biomass, in: A. Pandey, T. Bhaskar, M. Stöcker, R.K. Sukumaran (Eds.), Recent Adv. Thermo-Chem. Convers. Biomass, Elsevier, Boston, 2015: pp. 109–132. https://doi.org/10.1016/B978-0-444-63289-0.00004-1.
[54] C. Gennequin, S. Hany, H. Tidahy, S. Aouad, J. Estephane, A. Aboukaïs, E. Abi-Aad, Influence of the presence of ruthenium on the activity and stability of Co–Mg–Al-based catalysts in CO2 reforming of methane for syngas production, Environ. Sci. Pollut. Res. 23 (2016). https://doi.org/10.1007/s11356-016-7453-z.
[55] A. Remiro, B. Valle, A.T. Aguayo, J. Bilbao, A.G. Gayubo, Steam Reforming of Raw Bio-oil in a Fluidized Bed Reactor with Prior Separation of Pyrolytic Lignin, Energy Fuels. 27 (2013) 7549–7559. https://doi.org/10.1021/ef401835s.
[56] G.T. Marangwanda, D.M. Madyira, T.O. Babarinde, Combustion models for biomass: A review, Energy Rep. 6 (2020) 664–672. https://doi.org/10.1016/j.egyr.2019.11.135.
[57] S. Chimpae, S. Wongsakulphasatch, S. Vivanpatarakij, T. Glinrun, F. Wiwatwongwana, W. Maneeprakorn, S. Assabumrungrat, Syngas Production from Combined Steam Gasification of Biochar and a Sorption-Enhanced Water–Gas Shift Reaction with the Utilization of CO2, Processes. 7 (2019) 349. https://doi.org/10.3390/pr7060349.
[58] Z. Mei, D. Chen, J. Zhang, L. Yin, Z. Huang, Q. Xin, Sewage sludge pyrolysis coupled with self-supplied steam reforming for high quality syngas production and the influence of initial moisture content, Waste Manag. 106 (2020) 77–87. https://doi.org/10.1016/j.wasman.2020.03.012.
[59] K. Larionov, A. Kaltaev, K. Slyusarsky, D. Gvozdyakov, A. Zenkov, M. Kirgina, I. Bogdanov, V. Gubin, Steam Pyrolysis of Oil Sludge for Energy-Valuable Products, Appl. Sci. 12 (2022) 1012. https://doi.org/10.3390/app12031012.
[60] P. Mellin, Pyrolysis of biomass in fluidized beds: in-situ formation of products and their applications for ironmaking, 2015. https://doi.org/10.13140/RG.2.1.3048.3685.
[61] L. Moulin, S. Da Silva, A. Bounaceur, M. Herblot, Y. Soudais, Assessment of Recovered Carbon Black Obtained by Waste Tires Steam Water Thermolysis: An Industrial Application, Waste Biomass Valorization. 8 (2017) 2757–2770. https://doi.org/10.1007/s12649-016-9822-8.
[62] Q. Li, F. Li, A. Meng, Z. Tan, Y. Zhang, Thermolysis of scrap tire and rubber in sub/super-critical water, Waste Manag. 71 (2018) 311–319. https://doi.org/10.1016/j.wasman.2017.10.017.
[63] K.B. Larionov, K.V. Slyusarskiy, M.V. Kirgina, D.V. Gvozdyakov, I.A. Bogdanov, A.V. Zenkov, S.A. Yankovsky, V.E. Gubin, Liquid Hydrocarbons Production by the Steam Pyrolysis of Used Tires: Energy Characteristics and Environmental Sustainability, Waste Biomass Valorization. 13 (2022) 2233–2251. https://doi.org/10.1007/s12649-021-01628-2.
[64] M.F. Tennant, D.W. Mazyck, Steam-pyrolysis activation of wood char for superior odorant removal, Carbon. 41 (2003) 2195–2202. https://doi.org/10.1016/S0008-6223(03)00211-2.
[65] N. Ozbay, A. Putun, Characterization of Chars from Steam Pyrolysis of Apricot Pulp, Energy Sources. 33 (2011). https://doi.org/10.1080/15567030903397958.
[66] I. Hapazari, V. Ntuli, W. Parawira, Evaluation of single-step steam pyrolysis-activated carbons from lesotho agro-forestry residues, Tanzan. J. Sci. 37 (2011).
[67] P. Parthasarathy, K.S. Narayanan, Hydrogen production from steam gasification of biomass: Influence of process parameters on hydrogen yield – A review, Renew. Energy. 66 (2014) 570–579. https://doi.org/10.1016/j.renene.2013.12.025.
[68] V. Masson-Delmotte, P. Zhai, A. Pirani, S.L. Connors, C. Péan, S. Berger, N. Caud, Y. Chen, L. Goldfarb, M.I. Gomis, M. Huang, K. Leitzell, E. Lonnoy, J.B.R. Matthews, T.K. Maycock, T. Waterfield, Ö. Yelekçi, R. Yu, B. Zhou, eds., Climate Change 2021: The Physical Science Basis. Contribution of Working Group I to the Sixth Assessment Report of the Intergovernmental Panel on Climate Change, Cambridge University Press, Cambridge, United Kingdom and New York, NY, USA, 2021. https://doi.org/10.1017/9781009157896.
[69] The Future of Hydrogen – Analysis, IEA. (2019). https://www.iea.org/reports/the-future-of-hydrogen (accessed September 12, 2022).
[70] The Future of Hydrogen – Analysis, IEA. (n.d.). https://www.iea.org/reports/the-future-of-hydrogen (accessed February 21, 2022).

[71] D.B. Levin, R. Chahine, Challenges for renewable hydrogen production from biomass, Int. J. Hydrog. Energy. 35 (2010) 4962–4969. https://doi.org/10.1016/j.ijhydene.2009.08.067.
[72] R.C. Saxena, D. Seal, S. Kumar, H.B. Goyal, Thermo-chemical routes for hydrogen rich gas from biomass: A review, Renew. Sustain. Energy Rev. 12 (2008) 1909–1927. https://doi.org/10.1016/j.rser.2007.03.005.
[73] M. Kayfeci, A. Keçebaş, M. Bayat, Chapter 3 - Hydrogen production, in: F. Calise, M.D. D'Accadia, M. Santarelli, A. Lanzini, D. Ferrero (Eds.), Sol. Hydrog. Prod., Academic Press, 2019: pp. 45–83. https://doi.org/10.1016/B978-0-12-814853-2.00003-5.
[74] A. Demirbaş, Hydrogen Production from Biomass by the Gasification Process, Energy Sources. 24 (2002) 59–68. https://doi.org/10.1080/00908310252712307.
[75] S.D. Angeli, G. Monteleone, A. Giaconia, A.A. Lemonidou, State-of-the-art catalysts for CH4 steam reforming at low temperature, Int. J. Hydrog. Energy. 39 (2014) 1979–1997. https://doi.org/10.1016/j.ijhydene.2013.12.001.
[76] D. Trimm, Z. Önsan, Onboard Fuel Conversion for Hydrogen-Fuel-Cell-Driven Vehicles, Catal. Rev.-Sci. Eng. - CATAL REV-SCI ENG. 43 (2001) 31–84. https://doi.org/10.1081/CR-100104386.
[77] K.L. Hohn, L.D. Schmidt, Partial oxidation of methane to syngas at high space velocities over Rh-coated spheres, Appl. Catal. Gen. 211 (2001) 53–68. https://doi.org/10.1016/S0926-860X(00)00835-8.
[78] L. Pino, V. Recupero, S. Beninati, A.K. Shukla, M.S. Hegde, P. Bera, Catalytic partial-oxidation of methane on a ceria-supported platinum catalyst for application in fuel cell electric vehicles, Appl. Catal. Gen. 225 (2002) 63–75. https://doi.org/10.1016/S0926-860X(01)00734-7.
[79] G. Chen, Q. Li, X. Lv, N. Deng, L. Jiao, Production of Hydrogen-Rich Gas Through Pyrolysis of Biomass in a Two-Stage Reactor, 2004. https://doi.org/10.1115/GT2004-53582.
[80] A. DEMİRBAŞ, Biomass and Wastes: Upgrading Alternative Fuels, Energy Sources - ENERG SOURCE. 25 (2003) 317–329. https://doi.org/10.1080/00908310390142352.
[81] T.A. Milne, R.J. Evans, N. Abatzaglou, Biomass Gasifier "'Tars'": Their Nature, Formation, and Conversion, National Renewable Energy Laboratory, Golden, CO (US), 1998. https://doi.org/10.2172/3726.
[82] A. Midilli, H. Kucuk, M.E. Topal, U. Akbulut, I. Dincer, A comprehensive review on hydrogen production from coal gasification: Challenges and Opportunities, Int. J. Hydrog. Energy. 46 (2021) 25385–25412. https://doi.org/10.1016/j.ijhydene.2021.05.088.
[83] M. Asadullah, S. Ito, K. Kunimori, M. Yamada, K. Tomishige, Energy Efficient Production of Hydrogen and Syngas from Biomass: Development of Low-Temperature Catalytic Process for Cellulose Gasification, Environ. Sci. Technol. 36 (2002) 4476–81. https://doi.org/10.1021/es020575r.
[84] M.S. Casper, Hydrogen manufacture by electrolysis, thermal decomposition and unusual techniques, 1978, (1978). https://www.osti.gov/biblio/6467442 (accessed September 14, 2022).
[85] U. Arachchige, S. Sandupama, What To Do With CO2? Storage Vs. EOR Vs. CO2 As A Chemical Feedstock, 3 (2019) 104–109.
[86] J.W. Warner, R. Stephen Berry, Hydrogen separation and the direct high-temperature splitting of water, Int. J. Hydrog. Energy. 11 (1986) 91–100. https://doi.org/10.1016/0360-3199(86)90046-7.
[87] M.B. Gorensek, C. Corgnale, J.A. Staser, J.W. Weidner, Chapter 3 - Thermochemical hydrogen processes, in: T. Smolinka, J. Garche (Eds.), Electrochem. Power Sources Fundam. Syst. Appl., Elsevier, 2022: pp. 63–82. https://doi.org/10.1016/B978-0-12-819424-9.00001-X.
[88] C.E. Bamberger, D.M. Richardson, Hydrogen production from water by thermochemical cycles, Cryogenics. 16 (1976) 197–208. https://doi.org/10.1016/0011-2275(76)90260-5.
[89] J. Rossmeisl, A. Logadottir, J.K. Nørskov, Electrolysis of water on (oxidized) metal surfaces, Chem. Phys. 319 (2005) 178–184. https://doi.org/10.1016/j.chemphys.2005.05.038.
[90] J.I. Levene, M.K. Mann, R.M. Margolis, A. Milbrandt, An analysis of hydrogen production from renewable electricity sources, Sol. Energy. 81 (2007) 773–780. https://doi.org/10.1016/j.solener.2006.10.005.
[91] P. Moriarty, D. Honnery, Intermittent renewable energy: The only future source of hydrogen?, Int. J. Hydrog. Energy. 32 (2007) 1616–1624. https://doi.org/10.1016/j.ijhydene.2006.12.008.
[92] H. Dagdougui, R. Sacile, C. Bersani, A. Ouammi, Chapter 2 - Hydrogen Production and Current Technologies, in: H. Dagdougui, R. Sacile, C. Bersani, A. Ouammi (Eds.), Hydrog. Infrastruct.

Energy Appl., Academic Press, 2018: pp. 7–21. https://doi.org/10.1016/B978-0-12-812036-1.00002-0.
[93] Nuclear stands out for clean hydrogen, says French parliamentary report : Energy & Environment - World Nuclear News, (n.d.). https://world-nuclear-news.org/Articles/Nuclear-stands-out-for-clean-hydrogen-says-French (accessed September 20, 2022).
[94] S. PL, A. Aden, T. Eggeman, M. Ringer, B. Wallace, J. Jechura, Biomass to Hydrogen Production Detailed Design and Economics Utilizing the Battelle Columbus Laboratory Indirectly-Heated Gasifier, (2005). https://doi.org/10.2172/15016221.
[95] R. Demol, A. Dufour, Y. Rogaume, G. Mauviel, Production of Purified H2, Heat, and Biochar from Wood: Comparison between Gasification and Autothermal Pyrolysis Based on Advanced Process Modeling, Energy Fuels. 36 (2022) 488–501. https://doi.org/10.1021/acs.energyfuels.1c03528.
[96] S. Matsuda, Y. Niitsuma, Y. Yoshida, M. Umeda, H2-CO2 polymer electrolyte fuel cell that generates power while evolving CH4 at the Pt0.8Ru0.2/C cathode, Sci. Rep. 11 (2021) 8382. https://doi.org/10.1038/s41598-021-87841-4.
[97] M. David, C. Ocampo-Martínez, R. Sánchez-Peña, Advances in alkaline water electrolyzers: A review, J. Energy Storage. 23 (2019) 392–403. https://doi.org/10.1016/j.est.2019.03.001.
[98] A. Tanksale, J.N. Beltramini, G.M. Lu, A review of catalytic hydrogen production processes from biomass, Renew. Sustain. Energy Rev. 14 (2010) 166–182. https://doi.org/10.1016/j.rser.2009.08.010.
[99] D.B. Levin, L. Pitt, M. Love, Biohydrogen production: prospects and limitations to practical application, Int. J. Hydrog. Energy. 29 (2004) 173–185. https://doi.org/10.1016/S0360-3199(03)00094-6.
[100] K. Nath, D. Das, Biohydrogen production as a potential energy resource - Present state-of-art, J. Sci. Ind. Res. 63 (2004) 729–738.
[101] I.K. Kapdan, F. Kargi, Bio-hydrogen production from waste materials, Enzyme Microb. Technol. 38 (2006) 569–582. https://doi.org/10.1016/j.enzmictec.2005.09.015.
[102] J. Turner, G. Sverdrup, M.K. Mann, P.-C. Maness, B. Kroposki, M. Ghirardi, R.J. Evans, D. Blake, Renewable hydrogen production, Int. J. Energy Res. 32 (2008) 379–407. https://doi.org/10.1002/er.1372.
[103] P.C. Hallenbeck, J.R. Benemann, Biological hydrogen production; fundamentals and limiting processes, Int. J. Hydrog. Energy. 27 (2002) 1185–1193. https://doi.org/10.1016/S0360-3199(02)00131-3.
[104] R. Chaubey, S. Sahu, O.O. James, S. Maity, A review on development of industrial processes and emerging techniques for production of hydrogen from renewable and sustainable sources, Renew. Sustain. Energy Rev. 23 (2013) 443–462. https://doi.org/10.1016/j.rser.2013.02.019.
[105] I. Dincer, C. Acar, A review on clean energy solutions for better sustainability, Int. J. Energy Res. 39 (2015) 585–606. https://doi.org/10.1002/er.3329.
[106] G.Q. Lu, J.C. Diniz da Costa, M. Duke, S. Giessler, R. Socolow, R.H. Williams, T. Kreutz, Inorganic membranes for hydrogen production and purification: A critical review and perspective, J. Colloid Interface Sci. 314 (2007) 589–603. https://doi.org/10.1016/j.jcis.2007.05.067.
[107] A. Alonso-Vicario, J.R. Ochoa-Gómez, S. Gil-Río, O. Gómez-Jiménez-Aberasturi, C.A. Ramírez-López, J. Torrecilla-Soria, A. Domínguez, Purification and upgrading of biogas by pressure swing adsorption on synthetic and natural zeolites, Microporous Mesoporous Mater. 134 (2010) 100–107. https://doi.org/10.1016/j.micromeso.2010.05.014.
[108] Y. Fukushima, Y.-J. Huang, J.-W. Chen, H.-C. Lin, L.-M. Whang, H. Chu, Y.-C. Lo, J.-S. Chang, Material and energy balances of an integrated biological hydrogen production and purification system and their implications for its potential to reduce greenhouse gas emissions, Bioresour. Technol. 102 (2011) 8550–8556. https://doi.org/10.1016/j.biortech.2011.04.014.
[109] J.W. Sheffield, K.B. Martin, R. Folkson, 5 - Electricity and hydrogen as energy vectors for transportation vehicles, in: R. Folkson (Ed.), Altern. Fuels Adv. Veh. Technol. Improv. Environ. Perform., Woodhead Publishing, 2014: pp. 117–137. https://doi.org/10.1533/9780857097422.1.117.
[110] A.Ç. Köne, T. Büke, Forecasting of CO2 emissions from fuel combustion using trend analysis, Renew. Sustain. Energy Rev. 14 (2010) 2906–2915. https://doi.org/10.1016/j.rser.2010.06.006.

[111] A. Abánades, The challenge of Hydrogen production for the transition to a CO 2-free economy, Agron. Res. 10 (2012) 11–16.
[112] S. Rochain, Bilan électrique 2021 de la France : les chiffres de RTE, L'EnerGeek. (2022). https://lenergeek.com/2022/02/25/bilan-electrique-2021-rance/ (accessed September 12, 2022).
[113] R.W. Howarth, M.Z. Jacobson, How green is blue hydrogen?, Energy Sci. Eng. 9 (2021) 1676–1687. https://doi.org/10.1002/ese3.956.
[114] J.B. Guinée, M. Gorrée, R. Heijungs, G. Huppes, R. Kleijn, L. Oers, A. Wegener Sleeswijk, S. Suh, H.A. Haes, H. Bruijn, R. van Duin, M. Huijbregts, Life cycle assessment: An operational guide to ISO standards, Life Cycle Assess. Oper. Guide ISO Stand. 1 (2001).
[115] A. Ozbilen, I. Dincer, M.A. Rosen, A comparative life cycle analysis of hydrogen production via thermochemical water splitting using a Cu–Cl cycle, Int. J. Hydrog. Energy. 36 (2011) 11321–11327. https://doi.org/10.1016/j.ijhydene.2010.12.035.
[116] A. Ozbilen, I. Dincer, M.A. Rosen, Comparative environmental impact and efficiency assessment of selected hydrogen production methods, Environ. Impact Assess. Rev. 42 (2013) 1–9. https://doi.org/10.1016/j.eiar.2013.03.003.
[117] R. Kothari, D. Buddhi, R.L. Sawhney, Comparison of environmental and economic aspects of various hydrogen production methods, Renew. Sustain. Energy Rev. 12 (2008) 553–563. https://doi.org/10.1016/j.rser.2006.07.012.
[118] M. Mahishi, Theoretical and experimental investigation of hydrogen production by gasification of biomass, (2006).
[119] Z.M.A. Bundhoo, A. Mudhoo, R. Mobee, Biological processes for hydrogen production from biomass, JEnviron Sci Sustain. 1 (2013) 1–12.
[120] M. Balat, Thermochemical Routes for Biomass-based Hydrogen Production, Energy Sources Part Recovery Util. Environ. Eff. 32 (2010) 1388–1398. https://doi.org/10.1080/15567030802706796.
[121] K.D. Rose, R. Nelson, H. Hamje, S. Godwin, A. Reid, H. Maas, R. Edwards, L. Lonza, H. Hass, A. Krasenbrink, A. Huss, Well-to-wheels analysis of future automotive fuels and powertrains in the European context: tank to wheels report (TTW), version 4a, April 2014, Publications Office of the European Union, LU, 2014. https://data.europa.eu/doi/10.2790/95839 (accessed September 19, 2022).
[122] A.F. Kirkels, G.P.J. Verbong, Biomass gasification: Still promising? A 30-year global overview, Renew. Sustain. Energy Rev. 15 (2011) 471–481. https://doi.org/10.1016/j.rser.2010.09.046.

Conclusion générale

À l'heure où la demande mondiale en énergie ne fait qu'augmenter à cause de la croissance rapide de la population, et du fait de l'épuisement continue des combustibles fossiles et des émissions croissantes de carbone avec leurs effets néfastes sur l'environnement et le climat, des solutions renouvelables et décarbonées sont indispensables. Le couplage de la pyrolyse de la biomasse avec le reformage catalytique se présente comme une des solutions qui permet à la fois la valorisation de la biomasse et la production de gaz de synthèse et en particulier l'hydrogène, tout en limitant les émissions de dioxyde carbone. De plus, l'hydrogène vert issu des ressources renouvelables est identifié comme vecteur énergétique de l'avenir pour le transport et la génération d'électricité. Les travaux réalisés au cours de cette thèse s'inscrivent dans cette perspective.

L'étude bibliographique du chapitre 1 a permis de définir les procédés de pyrolyse et de reformage catalytique, d'identifier les paramètres principaux qui les impactent et de décrire les réacteurs qui y sont dédiés. Pour la pyrolyse, une description de la biomasse faite en premier lieu a révélé sa composition élémentaire en C, H et O ainsi que sa composition biochimique en cellulose, hémicellulose et lignine. Cette composition peut varier d'un type de biomasse à un autre ce qui impacte la répartition des produits de la pyrolyse. Le goudron, ou bio-huile pyrolytique, comprend plus de 300 composés organiques oxygénés qui sont des hydrocarbures légers, lourds, aromatiques, mono- et polycycliques, tels que des alcools, des acides, des furanes, des cétones, des aldéhydes, des phénols et des oléfines entre autres.

D'autre part, il a été montré que la pyrolyse est influencée par plusieurs paramètres, à savoir la température, la vitesse de chauffe et le temps de séjour des produits solides et volatils. Ces paramètres modifient la répartition des produits en charbon, bio-huile et gaz. Selon la vitesse de chauffe de la matière première, la pyrolyse peut être définie comme lente, intermédiaire, rapide et flash. Si un rendement élevé en charbon est recherché, les pyrolyses lentes ou intermédiaires sont appropriées. Cependant, si des hauts rendements en bio-huile et/ou gaz sont souhaités, la pyrolyse rapide voire flash est plus adaptée. Les réacteurs de pyrolyse jouent également un rôle important sur la distribution des différents produits. Les designs les plus courants concernent les réacteurs à lit fixe, à lit fluidisé et ceux employés pour les analyses thermogravimétriques, entre autres. En règle générale, les études de la littérature s'accordent sur les tendances qu'impactent ces paramètres sur la pyrolyse de la biomasse. En particulier, cette étude bibliographique montre que l'augmentation de la température de pyrolyse permet d'améliorer la production de gaz de réduire celle du charbon.

Le reformage catalytique, quant à lui, est fortement influencé par la température, le rapport de la vapeur d'eau/biomasse mais également par le catalyseur utilisé, sa nature, son support, sa charge en métal ainsi que par la vitesse spatiale horaire du gaz. L'étude des différents catalyseurs et leurs supports employés dans la littérature a dévoilé que les catalyseurs les plus couramment utilisés sont à base de métal de transition, surtout du nickel étant donné sa disponibilité, sa bonne activité catalytique, et son faible coût. Les supports de catalyseurs à base

d'alumine sont les plus courants du fait de leur bonne résistance aux hautes températures et de leur bonne compatibilité, permettant une dispersion homogène du catalyseur. Néanmoins, les catalyseurs de nickel sur support d'alumine souffrent du dépôt de carbone à leur surface menant à leur désactivation partielle. Dans la littérature, des études portant sur le reformage à la vapeur des gaz de la pyrolyse de biomasse ont montré qu'augmenter la température du reformage de 550°C à 900°C améliore la conversion du méthane et du dioxyde de carbone. La production d'hydrogène, quant à elle, atteint son maximum lorsque celle du monoxyde de carbone est à son minimum, à 700°C.

Ces deux procédés sont souvent étudiés séparément, à des échelles de laboratoire et même industrielles. Les études portant sur leur couplage pour la valorisation de la biomasse restent rares dans la littérature et sont toujours globalement à petite échelle. Pourtant, leur couplage présente des résultats prometteurs en termes de production de gaz de synthèse (H_2 et CO) comme cela a été montré au cours de cette thèse.

Dans le second chapitre, la pyrolyse de la biomasse seule a été réalisée pour former une base de données à laquelle les résultats de reformage catalytique pourront être confrontés. Pour cela, des copeaux de bois de chêne provenant d'une production locale ont été choisis comme biomasse à pyrolyser permettant, en outre, une comparaison avec les résultats de la littérature. Il a été montré que l'élévation de la température de pyrolyse de 400°C à 800°C contribue à l'augmentation de la production de gaz et la réduction de celle du charbon, tandis que la quantité de la bio-huile augmente jusqu'à une température de 500°C, au-delà de laquelle elle diminue. En détails, les concentrations de H_2, CO et CH_4 augmentent avec la température tandis que celle de CO_2 diminue. L'impact de la vitesse de chauffe en régime de pyrolyse intermédiaire est plus faible que celui de la température sur la distribution des produits. Le temps de séjour des volatils, quant à lui, a été modifié de deux façons : en changeant le débit du gaz vecteur et en modifiant le volume de la zone de réactions des composés volatils dans le réacteur de pyrolyse. Il a été remarqué que le temps de séjour influence de manière significative la répartition des gaz, avec des tendances opposées à celles obtenues avec le changement de la température.

L'étude de la composition de la bio-huile de pyrolyse a montré qu'elle était composée majoritairement de benzène, toluène, éthylbenzène, xylène, naphtalène et phénol. D'autre part, l'analyse élémentaire du charbon de pyrolyse a montré une baisse de la teneur en hydrogène et en oxygène et une augmentation de la proportion de carbone à la suite du processus de volatilisation, en comparaison à leur pourcentage respectif dans la biomasse initiale. Enfin, ce chapitre a permis d'identifier les paramètres opératoires menant à une production maximale de gaz de synthèse nécessaire (aux alentours de 58 vol.%) pour l'étape suivante, le reformage catalytique. Ces conditions sont dans notre cas : une température de 700°C, une vitesse de chauffe de 30°C/min et un temps de séjour de 140s.

Dans le chapitre 3, le couplage du reformage catalytique à la pyrolyse a été testé en premier lieu, avec la même biomasse (copeaux de chêne). Ce procédé a été réalisé en deux étapes avec, dans un premier temps la pyrolyse du bois de chêne à 700°C et dans un second temps, le reformage catalytique à une température variant entre 700 et 800°C. Le reformage est alors dit "hybride" car les reformages à sec et à la vapeur d'eau ont pu avoir lieu simultanément en consommant le dioxyde de carbone et la vapeur d'eau issus de la pyrolyse. Trois catalyseurs massiques à base de nickel Ni, de cobalt Co et de cobalt-nickel Co-Ni ont été étudiés.

Il a été montré que la température optimale de reformage favorisant la formation maximale de gaz de synthèse est de 750°C. Le reformage avec le Co-Ni a produit les plus grands rendements en gaz (43 % en masse) et les plus faibles rendements en bio-huile (32,4 % en masse). Le catalyseur à base de Ni a produit la plus grande concentration de gaz de synthèse (82,1 % en volume ou 16,8 mmol/g de biomasse sèche) avec les taux de conversions de CH_4 (68,2 %) et de CO_2 (52,65 %) les plus élevés. Le Co a été le moins efficace parmi les trois catalyseurs testés. Des analyses physico-chimiques ont montré la formation de dépôts de carbone sur les différentes surfaces des catalyseurs entraînant leur désactivation partielle. L'alliage du Cobalt au Nickel Ni-Co a permis de réduire cette formation de carbone. Un test de vieillissement du catalyseur a donc été réalisé sur 5 cycles consécutifs, révélant une baisse de son activité. La réactivation potentielle du catalyseur usé a été étudiée en réalisant des étapes de prétraitement de réduction, d'oxydation, et une combinaison des deux. L'oxydation sous air du catalyseur usé à 800°C a été la plus efficace pour rétablir son activité.

Le chapitre 4 a été consacré à l'application du couplage de la pyrolyse et du reformage catalytique avec une autre biomasse, des anas de lin et un autre type de catalyseur, des catalyseurs de Ni, Co et Co-Ni supportés sur des billes d'alumine. De nombreux paramètres opératoires, notamment la phase active du catalyseur, sa charge métallique, la température de reformage et la vitesse spatiale horaire du gaz (VSHG), ont été variés pour étudier leur impact sur l'efficacité du procédé et la formation de gaz de synthèse. Il a été constaté que le reformage à 750°C, avec 20% de nickel supporté sur des billes d'alumine et une VSHG au tour de 900 à 1125 h^{-1} sont les paramètres optimaux pour la production de gaz de synthèse (environ 75 vol.% ou 20 mmol/g biomasse sèche). Un test de vieillissement du catalyseur a également été réalisé pour étudier sa stabilité dans le temps. Les catalyseurs ont été caractérisés avant et après le reformage en réalisant des analyses de leurs propriétés physiques, des images MEB, des cartographies chimiques EDX et des analyses ATG. Elles ont révélé un dépôt de carbone filamenteux sur la surface du catalyseur. L'augmentation de la température de reformage a permis de réduire cette formation de carbone.

Enfin, le chapitre 5 a repris le procédé de couplage de pyrolyse et de reformage catalytique du chapitre 4 en conservant la même biomasse (anas de lin) et le catalyseur le mieux adapté (20%Ni sur billes de Al_2O_3) tout en ajoutant de la vapeur d'eau pour déclencher davantage de réactions de reformage à la vapeur et en remplaçant le gaz vecteur par de l'air. En ce qui concerne le reformage à la vapeur d'eau et la pyrolyse sous azote, il a été constaté que l'augmentation du ratio vapeur/biomasse de 0,29 à 3 améliore significativement la production de H_2 par rapport au CO où le H_2/CO passe de 1.26 à 1.65. L'élévation de la température de reformage augmente la formation de gaz, principalement H_2, et diminue celle de bio-huile, CO_2 et CH_4. Dans un deuxième temps, l'air a été utilisé comme gaz vecteur pour la pyrolyse et le reformage. Ceci a fortement augmenté la production de gaz (vers les 69 wt.% au lieu de 53 wt.% pour le reformage avec l'azote) mais a mené à des rendements en hydrogène plus faibles (27 vol.% pour le reformage à l'air par rapport à 40 vol.% avec l'azote). D'autre part, la pyrolyse à la vapeur d'eau et son couplage au reformage à la vapeur d'eau ont produit la plus forte concentration de gaz de synthèse (vers les 14.4 mmol/g biomasse sèche pour la pyrolyse et 25.6 mmol/g biomasse sèche pour le reformage à la vapeur) avec les plus grands rapports H_2/CO (1.65 pour la pyrolyse et 1.31 pour le reformage). Une étude technique, environnementale et économique a ensuite été réalisée pour explorer les différentes voies de production d'hydrogène. Elle a révélé que les méthodes reposant sur des sources renouvelables sont les plus respectueuses de l'environnement, mais qu'elles restent encore coûteuses. En même temps, les

carburants, et en particulier l'hydrogène, produits à partir de combustibles fossiles ont un impact négatif sur l'environnement et le climat. L'hydrogène dérivé de la biomasse permet donc un compromis en termes de neutralité carbone et de viabilité économique.

Bien que notre procédé ait montré de bonnes performances pour la production de gaz de synthèse, il présente tout de même plusieurs limitations. Premièrement, malgré les bonnes activités des catalyseurs et de l'efficacité du procédé, les conversions des réactifs principaux notamment la bio-huile, le CO_2 et le CH_4 ne sont pas totales. Cela peut s'expliquer par le fait que les catalyseurs utilisés sont normalement conçus pour le reformage d'un mélange de gaz simples (CH_4 et CO_2 ou CH_4 et H_2O). Les catalyseurs employés ne sont donc pas optimisés pour un mélange complexe d'hydrocarbures lourds issu de la pyrolyse de la biomasse. De plus, on a montré que les catalyseurs à base de cobalt et cobalt-nickel sont les plus sélectifs et efficaces pour la conversion de la bio-huile. Les catalyseurs à base de nickel étaient les plus performants vis-à-vis leur sélectivité pour la production de gaz de synthèse et la conversion du méthane. Néanmoins, dans le cadre de cette thèse, un seul ratio entre Co et Ni (Co/Ni de 1) dans le catalyseur cobalt-nickel a été testé. Par conséquent, il s'avère utile de faire varier le taux de Co dans le Ni afin d'optimiser la sélectivité du catalyseur vers la conversion des différents réactifs : bio-huile, méthane et dioxyde de carbone.

Il serait aussi intéressant de travailler sur la méthode de synthèse des catalyseurs afin de modifier leur structure et de les rendre plus sélectifs vers la production d'hydrogène et plus résistants au dépôt de carbone. Ceci pourrait se réaliser par l'alliage de diffèrent métaux tels Ni, Co, Fe, Cu, Mn voire même des métaux nobles comme Rh et Ru ou l'ajout d'agent promoteur tel que CaO, MgO et K_2O. Le carbone pourrait aussi être oxydé en ajoutant des porteurs d'oxygène comme La_2O_3, CeO_2 et ZrO_2.

Une autre approche serait de modifier le support du catalyseur en utilisant des particules de plus petite taille pour augmenter sa surface spécifique et par conséquent améliorer les transferts de chaleur et de masse. Par ailleurs, l'utilisation de mousses céramiques comme supports de catalyseurs pourrait améliorer la performance catalytique puisqu'elles sont connues pour leur grande porosité, leur bonne stabilité thermique à haute température, et leur perte de charge modérée par rapport aux supports de type bille ou aux catalyseurs massiques.

Deuxièmement, la pyrolyse de biomasse a requis des températures d'opération élevées (700°C) pour maximiser la production de gaz ce qui peut être énergivore surtout à l'échelle industrielle. Une solution serait l'utilisation du procédé de pyrolyse autothermique qui n'a besoin d'énergie qu'au début du processus pour augmenter la température du four et réaliser la pyrolyse. Passée cette étape, le processus s'auto-entretient si une partie du gaz produit est recyclé et oxydé pour chauffer le four. Une autre alternative serait de brûler une partie du charbon produit avec plus d'oxygène dans un réacteur séparé. Une solution plus propre que celles précédentes serait l'utilisation de source d'énergies renouvelables pour l'alimentation des fours de pyrolyse et de reformage comme des fours solaires ou se baser sur l'électricité d'origine nucléaire.

Troisièmement, les quantités de gaz de synthèse produites par notre procédé sont modérées. En effet, la durée du reformage (1 à 2 heures) est limitée par celle de la pyrolyse qui est imposée par la quantité et la nature de la biomasse initialement utilisée. Ce sont des limitations dues au fonctionnement discontinu du réacteur de pyrolyse. Une production d'hydrogène plus importante pourrait être obtenue en employant un réacteur de pyrolyse opérant en mode continu. Réaliser la pyrolyse avec une vitesse de chauffe plus élevée (supérieure à 100°C/min)

permettrait également de réduire la production de char et d'intensifier la production de l'huile, ce qui augmenterait la quantité de gaz produite par le reformage et le craquage des composés volatils de la bio-huile. De plus, le réacteur de reformage pourrait être changé de lit fixe à lit fluidisé pour améliorer les transferts massique et thermique entre le catalyseur et les composés volatils et déclencher davantage de réactions de reformage.

Quatrièmement, une pyrolyse à deux étages a été testée, dans laquelle le premier four est utilisé pour la pyrolyse de la biomasse et le second four est destiné à la pyrolyse des composés volatils (en absence de catalyseur) afin des craquer et décomposer les hydrocarbures lourds provenant de la pyrolyse de la biomasse. Deux paramètres opératoires ont été changés : les températures du premier et du second four de 400°C à 700°C mais aussi les temps de séjour des composés volatils en changeant le débit d'azote de 25 à 300 mL/min. Cependant, l'effet du temps de séjour sur les variations des produits est resté faible. Il serait alors intéressant d'approfondir l'étude en augmentant la plage des débits de gaz vecteur, et par conséquent les temps de séjour des composés volatils, afin d'améliorer le craquage des hydrocarbures de la bio-huile. Ensuite, un procédé à trois étages en série pourrait être réalisé. Il comprendrait un premier four de pyrolyse de la biomasse, un deuxième four de pyrolyse secondaire afin de craquer et décomposer les molécules lourdes et enfin, un troisième four de reformage des hydrocarbures légers pour la production des gaz de synthèse. Cette étape intermédiaire de pyrolyse secondaire pourrait améliorer la performance du reformage et réduire le dépôt de carbone sur la surface du catalyseur.

Cinquièmement, la biomasse utilisée dans notre procédé n'a pas été prétraitée. Une étape de prétraitement par ultrasons par exemple pourrait faciliter la dégradation des produits majeurs de la biomasse, à savoir la cellulose, l'hémicellulose et la lignine, pour produire plus de gaz. De même, d'autres matières premières pourraient être valorisées en gaz de synthèse dans notre procédé comme des déchets organiques et des déchets plastiques.

Enfin, l'hydrogène produit par ce procédé n'est pas pur mais il est mélangé avec les autres gaz. En conséquence, des étapes de séparation et de purification de l'hydrogène pourraient être utiles comme la séparation par membrane, l'adsorption, l'absorption ou la distillation cryogénique.

PRODUCTION DE GAZ DE SYNTHÈSE PAR PYROLYSE DE BIOMASSE ET REFORMAGE CATALYTIQUE DE VOLATILS

La demande massive en énergie et l'épuisement des combustibles fossiles nécessitent la production d'énergie « verte » pour répondre aux besoins globaux en électricité et en carburants. La biomasse, source d'énergie durable et renouvelable, est l'une des plus prometteuses pour atteindre ces objectifs. La pyrolyse de la biomasse produit majoritairement du monoxyde de carbone CO et du dioxyde de carbone CO_2 mais également du méthane CH_4 et de l'hydrogène H_2. Ce dernier est identifié comme vecteur énergétique de l'avenir pour le transport et la génération d'électricité. Il est donc nécessaire d'augmenter sa production. Traditionnellement, cela est réalisé à travers le reformage de gaz naturels.

Cette thèse vise à valoriser la biomasse en gaz de synthèse, et en hydrogène en particulier, tout en réduisant les émissions de CO_2. Un dispositif expérimental couplant la pyrolyse et le reformage catalytique a été développé. Dans le premier étage, la pyrolyse de biomasse (copeaux de chêne ou anas de lin) est réalisée. Dans le second, le reformage catalytique des hydrocarbures volatils et des gaz issus de la pyrolyse a lieu en présence d'un catalyseur**.** Les effets de divers paramètres ont été étudiés sur les produits de la pyrolyse (température, vitesse de chauffe et temps de séjour des composés volatils) et du reformage (température, phase active du catalyseur, sa charge métallique, vitesse horaire spatiale du gaz et le gaz vecteur). Les conditions opératoires favorisant respectivement la production de gaz biosourcés, de gaz de synthèse et d'hydrogène tout en réduisant les émissions de CO_2 par le biais du procédé couplé de pyrolyse et de reformage catalytique ont été révélées.

Mots-clés : Biomasse, Pyrolyse, Reformage catalytique, Gaz de synthèse, Hydrogène, Bio-huile, Charbon, Catalyseur, Énergie, Environnement, micro-Chromatographie en phase gazeuse/Spectrométrie de masse

SYNGAS PRODUCTION BY BIOMASS PYROLYSIS AND CATALYTIC REFORMING OF VOLATILES

The massive energy demand and the depletion of fossil fuels require the production of "green" energy to meet the global needs for electricity and fuels. Biomass, a renewable and sustainable energy source, is among the most promising resources to meet these objectives. Biomass pyrolysis mainly produces carbon monoxide CO and carbon dioxide CO_2, but also some methane CH_4 and hydrogen H_2. The latter has been identified as the energy carrier of the future for transportation and power generation. Therefore, it is of great importance to increase its production. Traditionally, H_2 is produced by natural gas reforming.

This thesis aims at valorizing biomass into syngas and hydrogen in particular, while reducing the CO_2 emissions. A two-stage experimental setup coupling the pyrolysis and the catalytic reforming processes has been developed. In the first stage, the pyrolysis of biomass (oak wood chips or flax shives) is performed. In the second one, the catalytic reforming of hydrocarbon volatiles and gases derived from biomass pyrolysis takes place in the presence of a catalyst. The effects of several parameters were studied on the products of pyrolysis (temperature, heating rate and residence time of volatile compounds) and the products of reforming (temperature, active phase of the catalyst, its metal loading, gas hourly space velocity and the nature of the carrier gas). The operating conditions favoring respectively the production of bio sourced gases, syngas, and hydrogen while reducing the CO_2 emissions via the process coupling the pyrolysis and the catalytic reforming were identified.

Key words: Biomass, Pyrolysis, Catalytic reforming, Syngas, Hydrogen, Bio-oil, Char, Catalyst, Energy, Environment, micro-Gas chromatography/mass spectrometry

Discipline : GENIE DES PROCEDES

Spécialité : Thermique et Énergétique

Université de Reims Champagne-Ardenne

ITheMM - EA 7548

UFR Sciences Exactes et Naturelles
Campus Moulin de la Housse – BP 1039
51687 Reims Cedex 2, FRANCE